UNIVERSITY OF SOUTHAMPTON

FACULTY OF NATURAL AND ENVIRONMENTAL SCIENCES

Chemistry

Interaction studies between the [FeFe]-hydrogenase maturation enzymes from *Thermoanaerobacter italicus*

by

BEATA MARTA MONFORT

Thesis for the degree of Doctor of Philosophy

December 2018

This thesis is dedicated to:

My parents, Eva & Walter

Le monde de la réalité a ses limites; le monde de l'imagination est sans frontières.

-Jean-Jacques Rousseau

University of Southampton

ABSTRACT

FACULTY OF NATURAL AND ENVIRONMENTAL SCIENCES

Chemistry

Thesis for the degree of Doctor of Philosophy

INTERACTION STUDIES BETWEEN THE [FEFE]-HYDROGENASE MATURATION ENZYMES FROM *THERMOANAEROBACTER ITALICUS*

BEATA MARTA MONFORT

The [FeFe]-hydrogenase enzyme is highly efficient at producing hydrogen under anaerobic conditions, hence a promising target to study in respect to scarce fossil energies and as an alternative zero-carbon energy source. The biosynthesis of the active [FeFe]-hydrogenase cofactor is a result of an interplay between three maturation enzymes named HydF, HydG and HydE. The unique diiron core and its surrounding CO and CN ligands, as well as the azadithiolate bridge form the H-cluster cofactor, responsible for hydrogen production. To understand the role of each maturation enzyme in context to the others, each maturation enzyme is produced *via* heterologous expression in *E. coli* and chemically reconstituted to ensure full activity. StrepHydF and StrepHydE expression vectors were generated and the pCDuet vector containing the T7 promoter resulted in a higher expression yield than initial expression studies with a pBAD expression vector. However, both HydE and HydF required chemical reconstitution despite several attempts to incorporate iron-sulfur cluster during expression and purification. The level of reconstitution is characterized by spectroscopic methods, including UV-Vis spectroscopy, electron paramagnetic resonance (EPR) and FT-IR (Fourier-transformed InfraRed) spectroscopy. Furthermore, FT-IR spectroscopy provided a tool to monitor the formation of the $[Fe(CO)_2(CN)]$-synthon by HydG after cleavage of L-tyrosine into p-cresol and dehydroglycine, which decomposes to CO and CN^- ligands. The presence of the synthon-iron was confirmed by EPR-spectroscopy and showed a characteristic S = 5/2 signal in the low magnetic field, if L-cysteine was added. HydG and HydE are radical SAM enzymes that are able to reductively cleave SAM into 5'-deoxyadenosyl and methionine which was confirmed by HPLC-based activity assays. Since the substrate of HydE is unknown the reductive SAM cleavage activity is significantly lower compared to HydG in the presence of its substrate L-tyrosine. Screening of compounds that might influence the activity of either HydG or HydE in the presence of all [FeFe]-hydrogenase maturation partner enzymes revealed that GTP has an enhancing effect on HydGs activity. However, alongside activity tests of the GTPase HydF, which has shown to hydrolyze GTP into GDP, HydG was found not to hydrolyze GTP. Suggesting HydG is not using GTP for energetic reasons. ATP and Pyro diphosphate also had a stimulating effect on HydGs activity, supporting the important role of the phosphates which might coordinate the synthon and initiate transport onto HydF. Attempts to study the interaction between the [FeFe]-hydrogenase maturation proteins confirmed the dimeric state of HydF and monomeric state of HydG in solution by gel-filtration. Moreover, binding studies using the pull-down assay method with HydF and HydG, revealed a crucial role of the pH and the presence of L-tyrosine for the complex formation between HydF and HydG.

Contents

List of Tables

List of Figures

List of Schemes

DECLARATION OF AUTHORSHIP

I, BEATA MARTA MONFORT, declare that the thesis entitled 'Interaction Studies between the [FeFe]-hydrogenase maturation enzymes from *Thermoanaerobacter italicus'* and the work presented in it is my own and has been generated by me as the result of my own original research.

I confirm that:

1. This work was done wholly or mainly while in candidature for a research degree at this University;
2. Where any part of this thesis has previously been submitted for a degree or any other qualification at this University or any other institution, this has been clearly stated;
3. Where I have consulted the published work of others, this is always clearly attributed;
4. Where I have quoted from work of others, the source is always given. With the exception of such quotations, this thesis is entirely my own work;
5. I have acknowledged all main sources of help;
6. Where the thesis is based on work done by myself jointly with others, I have made clear exactly what was done by others and what I have contributed myself;
7. None of this work has been published before submission.

Signature:……...

Date:……

Acknowledgments

First of all, I would like to thank all the people who guided and inspired me along my whole education.

Special thanks belong to my PhD supervisor Peter Roach, who always took the time to help, teach and support me during this rocky road. Especially motivating was his enthusiasm and passion for radical SAM enzymes and his humor. Thank you also for giving me this challenging and extremely interesting topic, I gained a lot of experiences that will give me a great foundation for the future.

Furthermore, endless thanks goes to my colleague Doctor Pedro Dinis, who introduced me to the lab, the equipment maintenance and the world of the [FeFe]-hydrogenases. Thank you for your continuous help and your funny stories. Big thanks go to Josh Prince for giving great ideas and being a huge help in the lab, Rachael Wilkinson for the practical and mental support, Mari Giurrandino for being understanding and providing solution strategies, Alice Parnell for always helping out when I struggled and giving advice. Moreover, Jessica Gusthart and Josh Prince for proof-reading and correcting my English, your help was truly essential to finish the thesis.

I would also like to thank my students for their motivation and endurance, Joanne Donnely, Ryan Squire, Francis Diomede, Chris Andric and especially Yiu Wai who brought this project a big step forward.

Very important contribution to this PhD thesis made Enrico Salvadori, John Wright and Maxie Roessler from the Queen Mary University London, by helping me carrying out EPR experiments and assist with analysis and simulation of spectra. Moreover, very crucial experiments on an FT-IR spectrometer were possible because of the help of Philip Ash and Kylie Vincent from the University of Oxford, who provided the time and equipment to carry out this special set-up experiment. Especially thanks to Philip Ash for arranging a last-minute FT-IR experiment and pre-analyzing the FT-IR data.

Also, I would like to thank Dave Kinnison for his support during my leg injury and giving assistance when in doubt of health and safety.

Big thanks to all people I met in Southampton, who created an international spirit, and let me discover many new things: Domenico and Julia (Italy), Damien, Thomas, Justine

and Clement (France), Ana and Marcos (Spain), Vaso (Greece), Janita and Costa (Latvia).

A special person who accompanied me during this time with all its up and downs, my husband. Tual, you managed to calm me in difficult times and enhance the good times by far. Thank you for being there and sharing your time to tackle every challenge.

Also, crucial to my life are my sister Alice and my brother-in-law Andi. Thank you for your guidance and really appreciative advice. Their kids Marina and Dana I would like to thank for their irresistible cuteness and cheerfulness.

I am the most thankful to my parents, Eva and Walter, who were immensely supportive in any imaginable way. From invalidating my doubts to encouragement and for making all this possible.

Abbreviations

(2*R*,4*R*)-TDA	(2*R*,4*R*)-1,3-thiazolidine-2,4-dicarboxylic acid
4HOB·	4-hydroxy benzyl radical
AdoCbl	5’-deoxyadenosylcobalamine
ACP	3-amino-2-carboxyl propyl
AdoMet	*S*-Adenosylmethionine
adt	azadithiolate
AlbA	Subtilosin maturase
anSME	anaerobic sulfatase maturating enzyme
ATR	Attenuated total reflection
BioB	Biotin synthase
BSA	Bovine serum albumin
BtrN	Butirosin biosynthesis pathway oxidoreductase
Ca	*Clostridium acetobutylicum*
CAP	catabolite activator protein
Cfr	Chloramphenicol-Florfenical resistance enzyme
CN^-	cyanide
CO	carbon monoxide
CpI	*Clostridium pasteurianum*
Cr	*Clamydomonas reinhardtii*
Cys	L-cysteine
dAdoH	5’-deoxyadenosine
DHG	Dehydroglycine
DFT	Density functional theory

DNA	Deoxyribonucleic acid
DOA	5’-Deoxyadenosine
DOIA	2-deoxy-scyllo-inosamine
Dph2	Diphthamide synthase
DTB	D-dethiobiotin
DTH	Dithionite
DTMA	Dithiomethylamine
DTT	Dithioreithol
ThitHydE1	ThitHydE1265
ThitHydE2	ThitHydE1675
E. coli	*Escherichia coli*
ENDOR	Electron nuclear double resonance
ESI	Electrospray ionization
EtOH	Ethanol
EPR	Electron Paramagnetic Resonance
EXAFS	Extended X-ray absorption fine structure
FAC	Ferric ammonium citrate
FeS	Iron-sulfur
FT	Fourier-transformed
GDP	Guanosine-5‘-diphosphate
GSH	Glutathione
GTP	Guanosine-5‘-triphosphate
H_4MPT	Tetrahydromethanopterin
HemN	oxygen-independent coproporphyrinogen III oxidase

HmdB	5,10-methyltetrahydromethanopterin hydrogenase cofactor biosynthesis protein
HOMO	highest occupied molecular orbital
HPLC	High pressure liquid chromatography
HYSCORE	Hyperfine sublevel correlation
IPTG	Isopropyl-*β*-D-1-thiogalactopyranoside
ITC	Isothermal calorimetry
ISC	Iron-sulfur cluster
IR	Infra-red
k_{cat}	catalytic constant/ turnover number
KCL	Potassium chloride
K_d	Dissociation equilibrium constant
K_M	Michaelis-Menten constant
LAM	Lysine 2,3-aminomutase
LipA	Lipoyl synthase
MALS	Multiangle light scattering
MCS	Multiple cloning site
Met	L-methionine
MftC	Mycofactocin system maturase
MIA	3-methyl-2-indolic acid
MM	Molecular Mechanics
MoaA	GTP 3’,8-cyclase
MST	Microscale thermophoresis
NaCl	Sodium chloride
NADPH	Nicotinamide adenine dinucleotide phosphate

NaOH	Sodium hydroxide
NMR	Nuclear magnetic resonance
NosL	Tryptophane lyase
NRVS	Nuclear resonance vibrational spectroscopy
OD	Optical density
PDB	Protein data bank
PELDOR	Pulsed electron-electron double resonance
PFL	Pyruvate-formate lyase
PLP	Pyridoxal phosphate
PQQ	Pyroloquinoline quinone
PqqE	PQQ biosynthesis
PylB	Methylornithin synthase
QM	Quantum mechanics
QueE	7-carboxy-7-deazaguanine (CDG) synthase
SAM	*S*-Adenosylmethionine
SAXS	Small-angle X-ray scattering
SDS-PAGE	Sodium dodecyl sulfate polyacrylamide gel electrophoresis
So	*Shewanella oneidensis*
SPASM	Subtilosin A, pyrroloquinoline quinone, anaerobic sulfatase mycofactocin maturation enzymes
SPR	Surface plasmon resonance
RlmN	23S rRNA methyltransferase
RNA	Ribonucleic acid
RNR	ribonucleotide reductase

RT	room temperature
ThiC	Thiamine biosynthetic enzyme
ThiH	Thiazole biosynthesis protein
Thit	*Thermoanaerobacter italicus*
TIM	Triose-phosphate isomerase
Tlet	*Thermotoga lettingae*
Tm	*Thermotoga maritima*
Tme	*Thermosipho melanesiensis*
Tn	*Thermotoga neapolitana*
Trp	L-tryptophan
Tyr	L-tyrosine
UV-Vis	Ultraviolet-Visible

Chapter 1

Introduction

1.1 Hydrogenases

1.1.1 Hydrogen – Impact for the future

Finding alternative energy sources that are clean and environmentally safe are one of the biggest challenges of our century, to reduce or stop climate change and global warming, and to sustain a future on the earth.(1) The importance of the environmental impact of transportation and of the urban, agricultural as well as industrial infrastructure that is powered by scarce fossil fuels causes global changes and urgently requires an alternative, cleaner energy source.(2)

A crucial non-polluting zero-carbon energy-carrier is hydrogen, the most abundant element on earth. Hydrogen can be generated from biomass, water, natural gas or coal.(3) Additionally, hydrogen possesses a high-energy content, which is advantageous for clean fuel applications.(4) Hydrogen generation from biomass (Bio-hydrogen) is a promising alternative because it does not require the use of primary energy sources.(5) Nonetheless, taking all the steps into account from production to end use, processes such as transportation, storage and distribution still place demands on primary carbon energy sources: hence the future technology will need to be optimized further.

With this in mind, hydrogen production from the microbial metabolism of anaerobic, aerobic, methylotrophs and photosynthetic bacteria as well as algae presents an interesting approach for the generation of hydrogen gas. Organisms carrying an active hydrogenase enzyme are a potential source for renewable bio-hydrogen.[6]

1.1.2 Hydrogenases

First discovered in colon bacteria in 1931 by Stephenson and Stickland[7], enzymes that catalyze the activation of dihydrogen were designated hydrogenases. Hydrogenases, which are anaerobic metalloenzymes, occur in all three domains of life;[8] however, the majority exist in microorganisms including archaea and bacteria and only a minority found in eukarya. Three phylogenetically unrelated types of hydrogenases are classified after their metal cluster composition, containing at least one central Fe^{II} ion and unusual diatomic ligands, the [Fe]-hydrogenases, the [NiFe]-hydrogenases and the [FeFe]-hydrogenases (Figure 1.1 and 1.2). All hydrogenases are responsible for hydrogen uptake and production in a reversible process (1-1), and their primary function is providing energy by hydrogen oxidation.[9]

$$2H^+ + 2e^- \rightleftharpoons H^+ + H^- \rightleftharpoons H_2 \qquad (1\text{-}1)$$

Equitation 1: Reversible hydrogen splitting catalyzed by Hydrogenases.

The [Fe]-hydrogenases only appear in methanogenic archaebacteria and carry a unique Fe ion coordinated by two CO ligands, a cysteine and by guanylylpyridinol, forming the Fe-GP cofactor[10] (Figure 1.1). Unlike the other hydrogenases, [Fe]-hydrogenases do not contain additional nickel or iron-sulfur clusters. [Fe]-hydrogenases catalyze the reversible reduction of the substrate 5,10-methenyltetrahydromethanopterin (methenyl-H_4MPT), transferring a hydride from molecular hydrogen, which splits to form methylene-H_4MPT and a proton as products.[11] Activation of H_2 is therefore dependent on the presence of the substrate.[12]

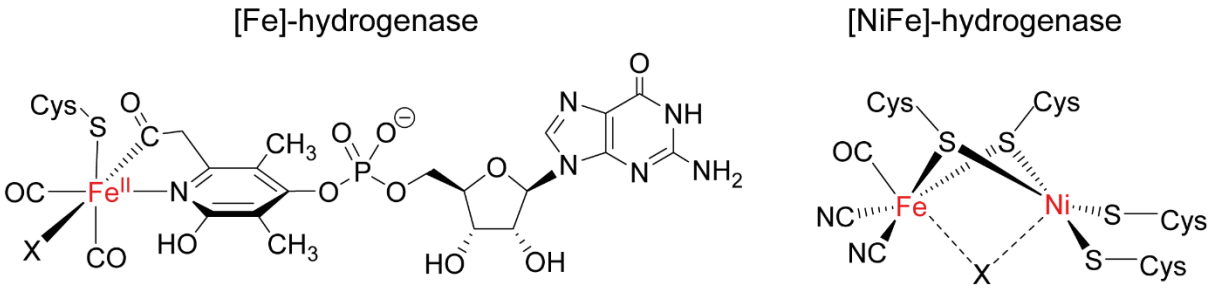

Figure 1.1: Molecular structure of [Fe]-hydrogenase and [NiFe]-hydrogenase cofactors. Metal ions are highlighted in red. X = potential hydride binding site. Adapted from [13].

The extensively studied [NiFe]-hydrogenases contain a characteristic sulfur-bridged bimetallic [NiFe]-center, which is coordinated by small inorganic ligands, one CO and two CN^-. As illustrated in Figure 1.1 the two thiolates forming the sulfur bridge originate from two cysteine residues in the polypeptide chain of the [NiFe]-hydrogenases.[14] Biosynthesis of the [NiFe]-cofactor has been thoroughly examined, and the function of six essential enzymes (HypA, HypB, HypC, HypD, HypE and HypF) determined.[15] The open coordination site at the Ni atom is proposed to be the site of hydrogen activation, but little or no direct experimental evidence has been reported. However, models of iron-centered proton reduction exist as well.[16] [NiFe]-hydrogenases and [FeFe]-hydrogenases contain additional iron-sulfur clusters, either [4Fe4S] and/or [2Fe2S] cluster that are responsible for electron-transfer from the protein surface to the active site.[17,18]

The catalytic activities of the [FeFe]-hydrogenases are the highest reported, with production rates of up to ~10^4 molecules of H_2 per enzyme per second at RT.[19] This potential for very efficient catalysis, coupled to the many remaining scientific questions to be answered regarding the biosynthesis of the [FeFe]-hydrogenase cofactor, have made the [FeFe]-hydrogenases our research topic and are discussed in more detail in the following paragraphs.

1.1.3 [FeFe]-hydrogenase

[FeFe]-hydrogenases exist in bacteria, unicellular algae as well as protozoa. Detailed information about the active site architecture of the [FeFe]-hydrogenases exists from high-resolution crystal structures of the enzyme from the soil-bacterium *Clostridium pasteurianum* (1.8 Å resolution)[20] and sulfate-reducing bacterium *Desulfovibrio desulfuricans* (1.6 Å resolution)[21].

A common feature in all oxygen sensitive [FeFe]-hydrogenases is the bimetallic [FeFe]-center (referred to as the $[2Fe]_H$ subcluster), which is attached to a $[4Fe4S]_H$-cluster through a shared cysteine ligand.[20] The $[2Fe]_H$ subcluster and $[4Fe4S]_H$-cluster together form the H-cluster, the active cofactor of the [FeFe]-hydrogenase.[22]

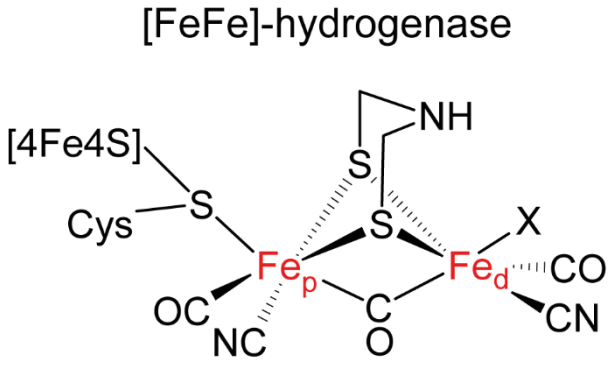

Figure 1.2: Molecular structure of [FeFe]-hydrogenase cofactor. Metal ions are highlighted in red. X = Hydride binding site. The Fe_p and Fe_d refer to the proximal and distal irons. Adapted from [23].

With the help of infrared-spectroscopy, the presence of one CO and one CN^- ligand per Fe atom as well as one bridging CO ligand between them, has been confirmed (Figure 1.2).[24,25] The composition of the sulfur-bridge has been elucidated with spectroscopic and chemical methods, and is suggested to be an azadithiolate (adt^{2-}) ligand of unknown biosynthetic origin.[26,27,28,29]

Nevertheless, [FeFe]-hydrogenases differ in aspects of their overall three-dimensional structures. The conserved H-domain (40 kDa) embeds the H-cluster by coordination via four conserved cysteines.[30,9,12] [FeFe]-hydrogenases found in green algae such as *Chlamydomonas reinhardtii*[31] or *Chlorella fusca*[32] consist of only the H-domain carrying the H-cluster and are classified as the simplest form of [FeFe]-hydrogenases.

In addition to the H-cluster, clostridial [FeFe]-hydrogenases contain binding sites for the accessory [4Fe4S] or [2Fe2S]-cluster responsible for electron-transfer from the active site to the protein surface, present in the F-domain (Figure 1.3).[33]

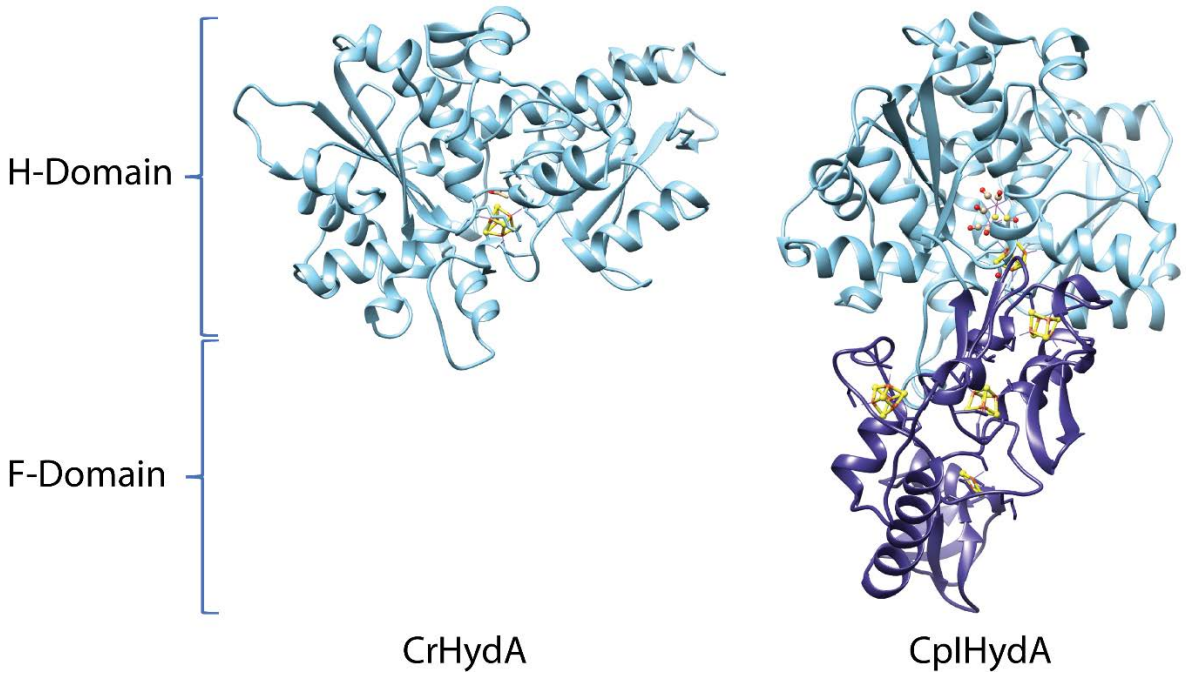

Figure 1.3: Crystal structures of [FeFe]-hydrogenases. Left: Crystal structure of *Chlamydomonas reinhardtii* HydA with missing diiron-subcluster of the H-cluster (left) (PDB: 3LX4)[31], right: Crystal structure of *Clostridium pasteurianeum* HydA with H-cluster and four additional iron-sulfur cluster in the F-domain (PDB: 1FEH).[20] H-domain illustrated in *sky blue* and F-domain in *dark slate blue*.

1.1.4 Maturation of the [FeFe]-hydrogenase

While the maturation process of the [NiFe]-hydrogenase is well studied, and characterized,[17] the mechanism for the [FeFe]-hydrogenase is only partly revealed[22] and requires further exploration.

Immediately after the ribosomal synthesis of the [FeFe]-hydrogenase polypeptide (HydA), encoded by the *hydA* gene, the resulting inactive HydA protein is loaded with the accessory electron transfer iron-sulfur cluster and the $[4Fe4S]_H$-cluster but lacks the active [2Fe]-cofactor of the H-cluster.[31,34,35] These prosthetic groups and cofactor are synthesized and loaded onto the HydA protein in a process that can be divided

into two parts; the first part is the synthesis and incorporation of the accessory [4Fe4S]- and/or [2Fe2S]-cluster and the second part is the biosynthesis and incorporation of the [2Fe]-subcluster onto $[4Fe4S]_H$ (H-cluster).

The first part of this process, synthesis of FeS-cluster, is likely accomplished by the host cell FeS-cluster assembly machinery system, either the ISC system present in bacteria (*Escherichia coli*) and eukarya or the SUF system present in bacteria, plastids and archaea.[36] Furthermore, the $[4Fe4S]_H$ component of the H-cluster is independently synthetized from the [2Fe]-subcluster component, because it is incorporated into the hydrogenasae even if the [2Fe]-subcluster maturation machinery is lacking. It has been proposed that the $[4Fe4S]_H$-cluster is also synthesized and incorporated by the ISC or SUF system.[35]

The second biologically challenging part of the maturation process is the synthesis of the bioinorganic $[2Fe]_H$ subcluster of the [FeFe]-hydrogenase metallocofactor. In this process, three different steps need to be taken into account: ligand synthesis of CO, CN^- and the adt^{2-} bridge; assembly of the ligated $[2Fe]_H$ subcluster; and incorporation of $[2Fe]_H$ subcluster into HydA containing the $[4Fe4S]_H$-cluster to give the completed H-cluster.[37,38] Moreover, due to the fact that the CO and CN^- ligands are toxic and the adt^{2-} bridge sensitive to hydrolysis, the chemistry of the assembly processes needs to take place in a shielded protein environment, presumably through protein-protein complexes.[37,39]

The *hyd* gene cluster responsible for the full maturation of the [FeFe]-hydrogenase was first discovered in 2004 in the eukaryotic green algae *C. reinhardtii* by Posewitz *et al.*.[40] Deletion of either the *hydEF* or *hydG* genes resulted in a dysfunctional full-length hydrogenase CrHydA1.[40,41] Heterologous expression of an active CrHydA1 protein in *Escherichia coli*, was only achieved if co-expressed with both the HydEF and HydG protein.[40] The necessity of at least two enzymes (HydEF and HydG) are essential for the H-cluster maturation which has been clearly demonstrated with mutants lacking one of these enzymes.[40,41]

Investigation of the *hydEF* gene in *C. reinhardtii*, revealed the presence of two distinct domains coding for the enzymes HydE and HydF, which appear either as a fusion or separate proteins (in prokaryotes) depending on the organism. All [FeFe]-hydrogenase gene clusters contain genes encoding for HydE, HydF and HydG.[40,42]

Studies on the selectivity of the [FeFe]-hydrogenase maturation proteins HydE, HydF and HydG have shown that: 1. CrHydA1 can be activated with the maturation enzymes of a different expression host containing the *hyd* gene cluster, for example *C. acetobutylicum (Ca)*[43] or *Shewanella oneidensis* (*So*)[44]. 2. Heterologous co-expression of CaHydE, CaHydF and CaHydG in *Escherichia coli* with HydA proteins from several algal and bacterial genes leads to a fully active holo-HydA protein.[42] 3. Incubation of an *E. coli* extract of CaHydA with *E. coli* extracts containing coexpressed CaHydE, CaHydF and CaHydG resulted in efficient *in vitro* activated [FeFe]-hydrogenases.[45] A cell-free activation of bacterial and algal [FeFe]-hydrogenases was also possible by addition of *E. coli* cell extracts of SoHydG, SoHydF and SoHydE proteins.[46]

Since it was evident that *E. coli* extracts of *Ca* or *So* maturation enzymes were sufficient to activate HydA *in vitro*,[45] it was used as a basis by Swartz *et al.* to screen small biological compounds and salts which might enhance the activation process.[47,48,49,50] Included in the list of compounds that increase the hydrogen production of the [FeFe]-hydrogenase CrHydA1 were the amino acids - cysteine and tyrosine, SAM,[47] and, critical for FeS-cluster formation, iron and sulfide (Figure 1.4).[48]

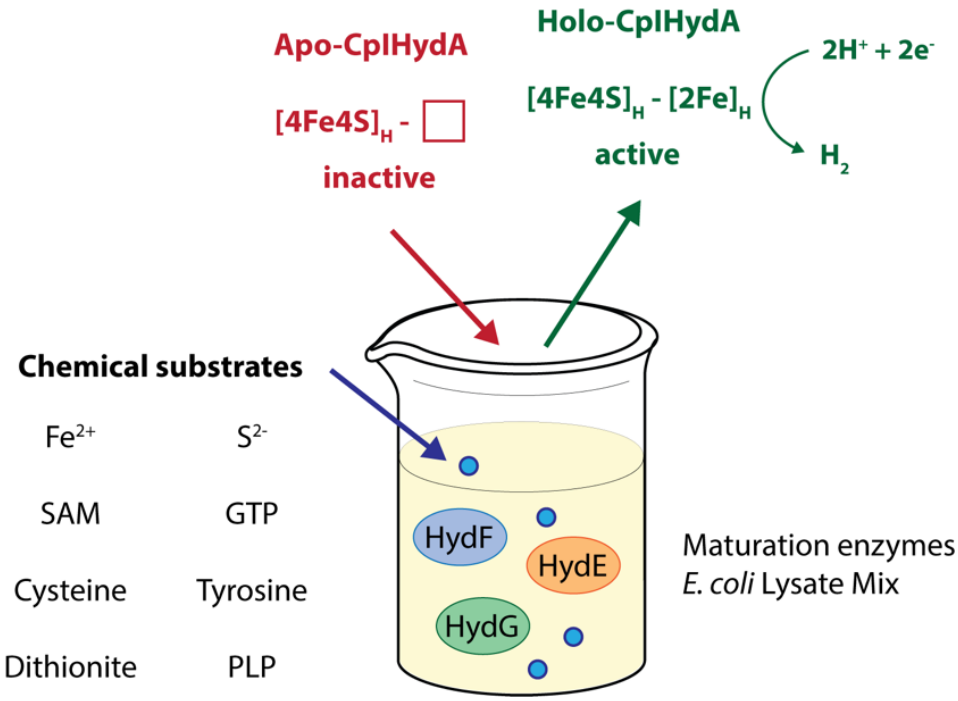

Figure 1.4: *In vitro* activation of the [FeFe]-hydrogenase. The *red* square indicates that no 2Fe subcluster is present. Adapted from [49].

To optimize the *in vitro* maturation process even further to achieve a fully active [FeFe]-hydrogenase with minimal efforts, the separate functions of the maturation enzymes HydE, HydF and HydG need to be studied further. By analyzing the appropriate amino acid sequences, HydE and HydG contain the characteristically conserved 'CX_3CX_2C' motif, classifying them as radical SAM enzymes, coordinating at least one [4Fe4S]-cluster.[40,42] Characteristic binding motifs for nucleotides (Walker-motifs) are found in the amino acid sequence of HydF, which was later characterized as GTPase.[42,51]

Surprisingly, isolated HydF, co-expressed in the background of HydE and HydG, was able to activate $[4Fe4S]_H$-cluster carrying CpIHydA, suggesting HydF's role as scaffold protein in the maturation reaction.[43]

The radical SAM enzymes HydE and HydG have been extensively studied with biochemical, spectroscopic and crystallographic techniques.[49,52-71] Both enzymes catalyze the reductive cleavage of SAM, as all members of the radical SAM family.[52] Nonetheless, HydG also catalyzes the cleavage of L-tyrosine into *p*-cresol, cyanide[55] and CO[56], which make up the small inorganic ligands for the [2Fe]-subcluster. On the other hand, the role of HydE in the maturation process is still unknown, despite intensive scientific investigation by several research groups.[52,53,58,65,70] It has been proposed that HydE might be responsible for the synthesis of the adt^{2-} bridge.[22,65] A summarizing scheme of the proposed maturation events[27,28,43,55,56,61,64-66] is shown in the following (Scheme 1.1):

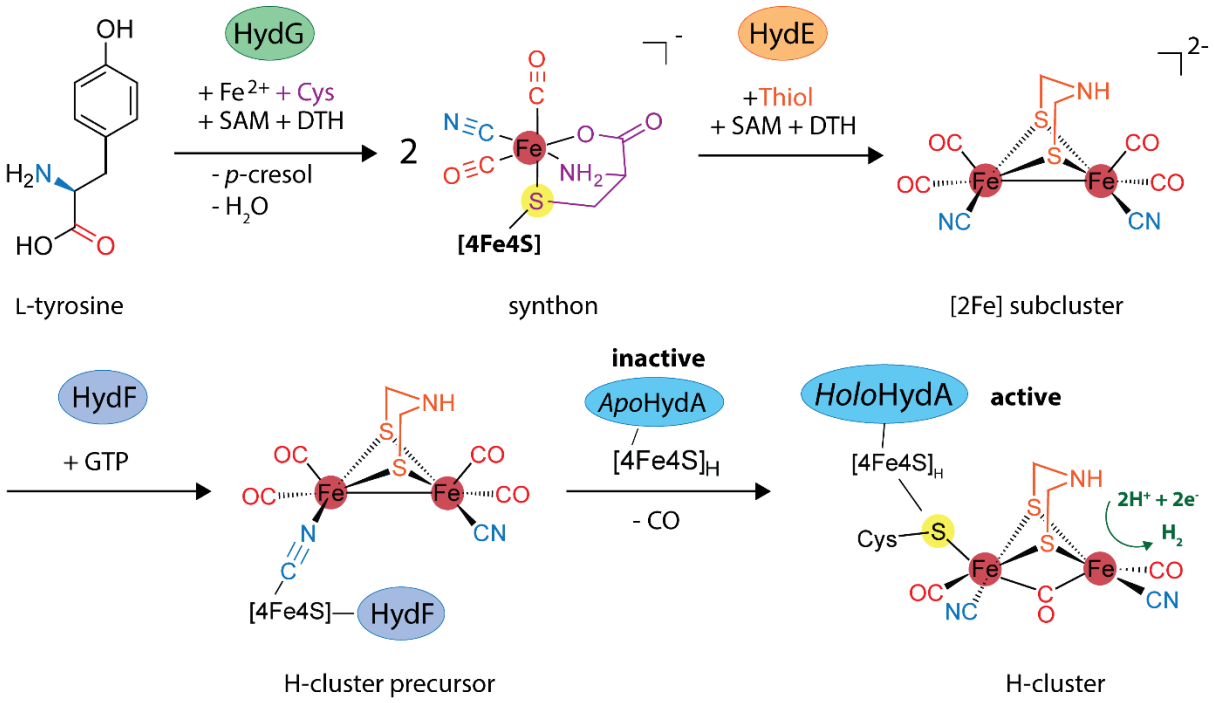

Scheme 1.1: Proposed maturation of the [FeFe]-hydrogenase. Biosynthesis of the H-cluster by the maturation enzymes HydG, which is forming the synthon after cleavage of SAM and tyrosine, HydE which is likely responsible for the dithiomethylamine synthesis and transfer of the resulting [2Fe] subcluster onto HydF which further transports the H-cluster precursor onto HydA resulting in an active HydA protein with the H-cluster.

The specific role of each maturation enzyme in the biosynthesis of the [FeFe]-hydrogenase cofactor is discussed in greater detail in sections 1.2.7, 1.2.8 and 1.3.2.

1.1.5 Activity of the [FeFe]-hydrogenase

As described earlier, the active H-cluster is composed of two coupled sub-clusters termed $[4Fe4S]_H$ and $[2Fe]_H$. The two Fe of the $[2Fe]_H$ subcluster are termed the proximal Fe_p (closest to $[4Fe4S]_H$) and distal Fe_d (Figure 1.2).[12] Both Fe atoms bind to a terminal CO and CN^- ligand and are connected via a μ-bridged CO ligand.[72,24,25] The CO and CN^- ligands are strong π-acid/acceptors, which stabilize low oxidation states (low-spin) of the Fe atoms (Fe^I/Fe^{II}) via back bonding.[9,25,73-77] By stabilizing the low oxidation states, the ligands promote fast and reversible Electron-Transfer (ET) and therefore the reversible heterolytic H_2 cleavage.[12]

The proposed site for hydrogen-binding is the free coordination site of the distal Fe_d atom.[78,79] This is supported by the observation that the adt-bridge conformation

directs the nitrogen towards the free coordination site of the distal iron, and evidence from EPR spectroscopic and theoretical studies support the hypothesis that the nitrogen is involved in proton transfer during H_2 activation .[80-82] The nitrogen of the adt-bridge serves as the Lewis base of the Lewis pair crucial for the H_2 conversion process, whereas the Fe_d is the Lewis acid.[83,84]

The H-cluster itself is embedded in a hydrophobic pocket of the [FeFe]-hydrogenase protein, coordinated by four highly conserved cysteines. The unique $[2Fe]_H$ subcluster possesses only one covalent bond to one of these cysteine sulfur atoms of the polypeptide chain.[85]

The proton transfer pathway has been studied by biochemical and QM/MM methods, which showed that the protons are transferred through the protein surface to the active site via two Glu residues, one Ser, one water molecule and one Cys residue (Cys-299, Glu-279, Ser-319, and Glu-282 in *Clostridium pasteurianum* HydA), which is in close proximity to the amine of the adt^{2-}-bridge.[86-89] In recent studies of the mechanism leading to H_2 formation this specific cysteine residue, Cys-299, plays a crucial part. *Via* steady-state kinetics, ATR-IR (attenuated total reflection infrared), FT-IR (fourier transform infrared), NRVS (^{57}Fe nuclear resonance vibrational spectroscopy), DFT (Density functional theory), EPR, Mössbauer and even NMR spectroscopy the terminal hydride state has been characterized as an iron-to-hydride bond interacting with amine base and with the conserved cysteine, which provides the proton at the end of the transfer chain.[90-93] The bound hydride accepts the proton, forms molecular hydrogen and leads to release of the hydrogen, forming the precursor H_{ox} for new hydride generation (Scheme 1.2).[6]

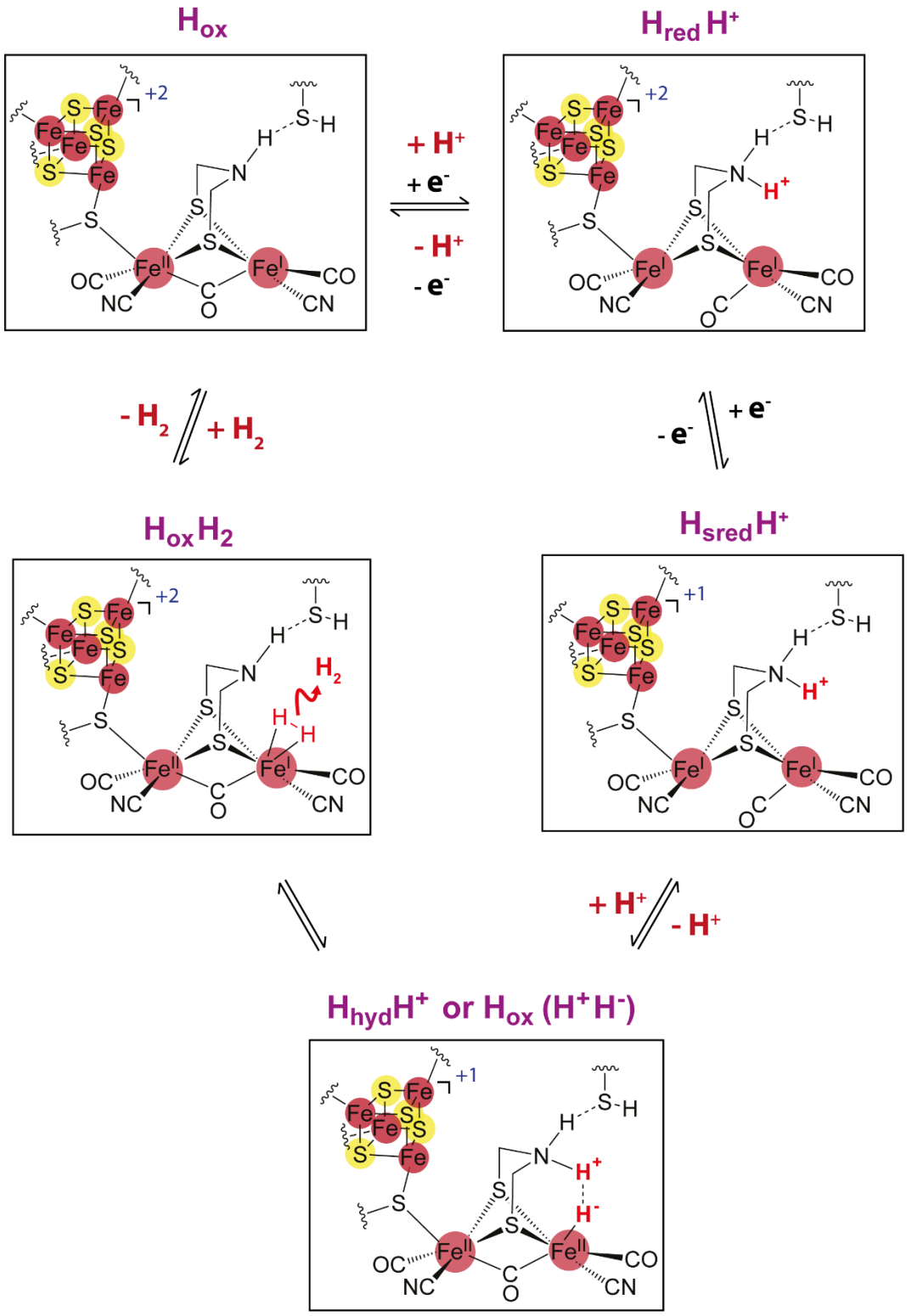

Scheme 1.2: Proposed catalytic mechanism of the [FeFe]-hydrogenase. First step: transition from H_{ox} to $H_{red}H^+$ state by proton transfer onto the amine of the adt-bridge and electron transfer onto the distal iron. Second step: formation of $H_{sred}H^+$ by accepting an electon at the [4Fe4S] cluster and releasing the bond between the proximal iron and μ-CO. Another proton is accepted and immediately accepts an electron from the distal iron to form the terminal hydride Fe-H^- ($H_{hyd}H^+$) or $H_{ox}(H^+H^-)$. The bound hydride accepts the proton and forms molecular hydrogen ($H_{ox}H_2$). Upon hydrogen release the precursor H_{ox} is reformed. Adapted from [6,92,94].

1.2. Radical SAM enzymes

The [FeFe]-hydrogenase maturation proteins HydE and HydG are radical SAM enzymes, and therefore belong to a group of enzymes that are extremely versatile and are involved in at least 85[95] different types of known biological transformations. To create a better overview and understand the different types of radical SAM enzymes a summary of the most important features are described in the following paragraphs, before focusing on HydE and HydG.

Radical SAM enzymes were classified as a superfamily for the first time in 2001 by Sofia *et al.*.[96] To date, the radical SAM superfamily consists of > 110 000 unique sequences.[97] Radical SAM enzymes catalyze the reductive cleavage of *S*-adenosylmethionine (SAM or AdoMet). A common feature of Radical SAM enzymes is the characteristic CX_3CX_2C binding motif for a redox active [4Fe4S] cluster, often observed in the *N*-terminal region of the protein.[98] However, there are exceptions to this, radical SAM enzymes that do not contain the classical CX_3CX_2C binding motif. Examples include ThiC from *Caulobacter crescentus* (modified cluster binding motif: CX_2CX_4C)[99], HmdB from *Methanococcus maripaludis* S2 (CX_5CX_2C)[100] and QueE from *Burkholderia multivorans* ($CX_{14}CX_2C$)[101]. In its active reduced state, the [4Fe4S]-cluster coordinates and cleaves SAM into L-methionine and a 5'-desoxyadenosyl (DOA or Ado) radical. The generated radical is responsible for a wide variety of downstream reactions including (but not limited to) sulfur insertion[102-104], rearrangements[105-107], dehydrations[108,109], decarboxylations[110-112], DNA and RNA modifications[113, 114] and maturation of complex metallocofactors[115,116].

1.2.1 SAM cleavage mechanism

Three conserved cysteine residues ligate three iron atoms of the $[4Fe4S]^{2+}$ cluster; the un-ligated iron (commonly termed the unique iron) is coordinated by the α-amino and α-carboxylate group of bound SAM forming a five-member chelate ring (Scheme 1.3).[117,118] The catalytically active [4Fe4S] cluster oxidation state is +1 (detailed $[Fe^{III}Fe^{II}_3S_4]^{+1}$) and conversion from the +2 to +1 state requires an external reducing system such as flavodoxin, flavodoxin reductase, NADPH or another single electron donor *in vivo*.[111] *In vitro* strong reducing agents like dithionite or 5-deazariboflavin provide electrons to reduce the enzyme.[119]

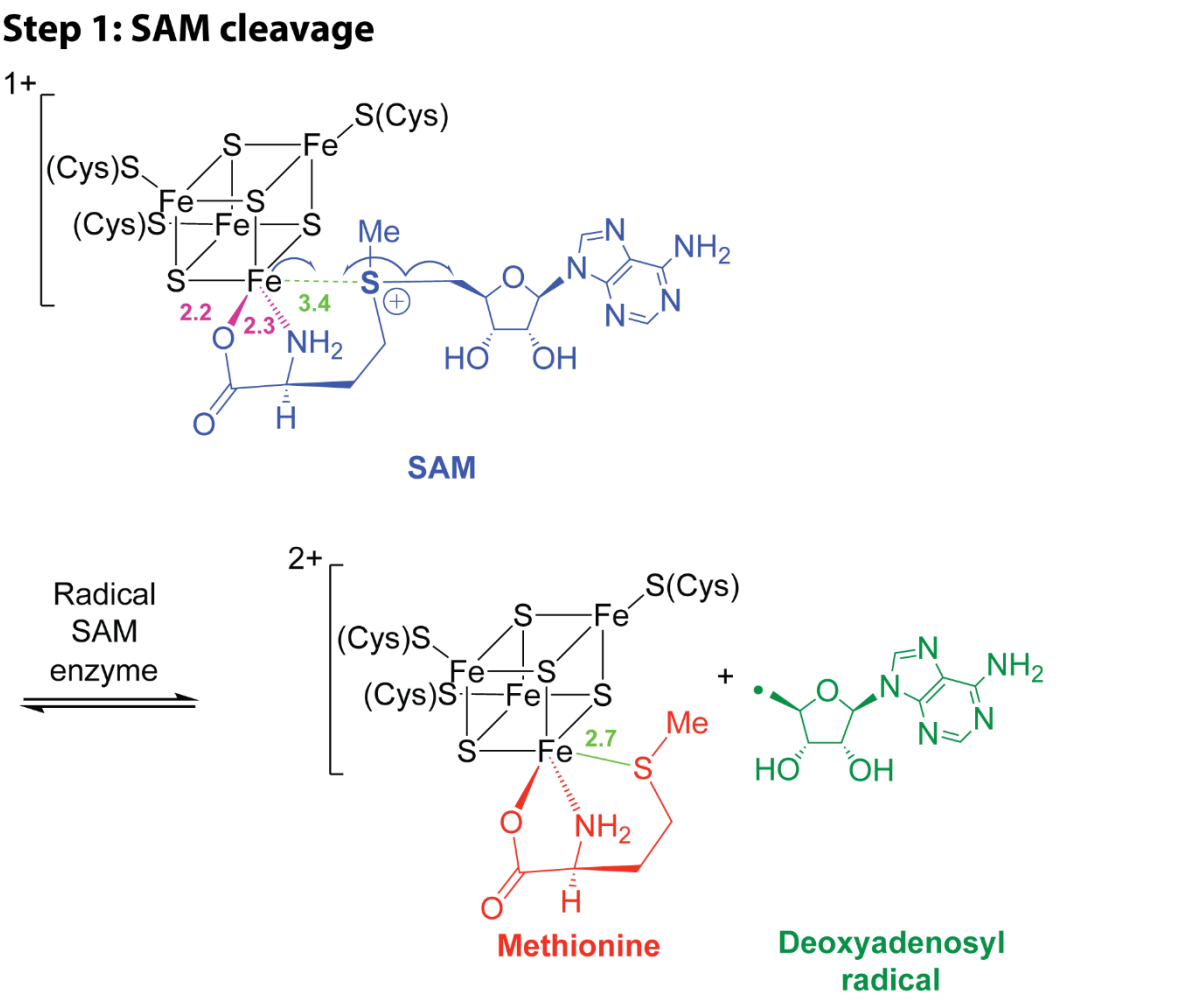

Scheme 1.3: The interaction of SAM (*blue*) and the [4Fe4S] cluster during SAM cleavage (Step 1). Reaction products are methionine (*red*) and the deoxyadenosyl radical (*green*). The [4Fe4S] cluster has been reduced before by an external electron donor/reducing agent. Distances are represented in Ångström between the unique iron and the sulfur of SAM or methionine (*light green*, Fe-S) and the Fe-O (2.2Å) and Fe-N (2.3Å) distances between the unique iron and the methionine moiety of SAM in *light purple*. The deoxyadenosyl radical initiates hydrogen abstraction from the substrate (Step 2).[53,120,121]

Through an inner-sphere one-electron transfer from the reduced [4Fe4S] cluster to the antibonding orbital of the sulfonium ion, SAM is homolytically cleaved.[118,120,122,123] This leaves the resulting L-methionine coordinated to the unique iron of the [4Fe4S] cluster and a free 5′- deoxyadenosyl radical (Scheme 1.3). This primary radical is highly reactive and rapidly abstracts a proton from either a protein moiety, substrate or from a solvent exchangeable position.[62,124] Addition of substrate, i.e. the compound from which a hydrogen atom will be abstracted (Scheme 1.3, Step 2), usually enhances the SAM cleavage activity of the radical SAM enzymes. For most enzymes, SAM is used in a stoichiometric manner as a co-substrate producing an equal ratio of the reaction products. However, some enzymes only use SAM catalytically, by producing a product radical intermediate that initiates H-atom abstraction from dAdoH, which in turn regenerates the dAdo-radical and forms SAM with methionine.[98]

The state of the oxygen sensitive [4Fe4S] cluster is crucial for the activity of the enzymes, even short periods of oxygen exposure can lead to the degradation of the cluster leading to a [3Fe4S] state for example.[125] Evidence for the [4Fe4S]-SAM complex shown in Scheme 1.3 has come from spectroscopic studies such as ENDOR[126,127] and Mössbauer[117], as well as by X-ray crystal structures[122,128] of radical SAM enzymes.

Convincing experimental data for direct observation of the highly reactive 5'-deoxyadenosyl radical intermediate has not been reported: however, a stabilized allylic delocalized radical analogue (anAdo·) has been generated with the radical SAM enzyme LAM during the reductive cleavage of *S*-3',4'-anhydroadenosyl-L-methionine (anSAM) (Scheme 1.4). This stabilized analogue radical anAdo· was detectable with EPR at a temperature of 77 K and 4.5 K, analysis of the hyperfine splitting parameters confirmed the conformation of the radical species.[129]

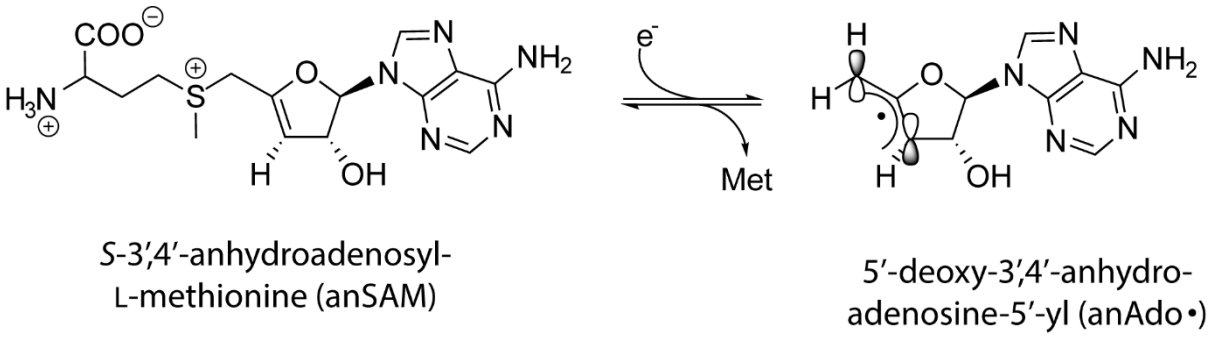

S-3′,4′-anhydroadenosyl-L-methionine (anSAM)

5′-deoxy-3′,4′-anhydro-adenosine-5′-yl (anAdo•)

Scheme 1.4: Reductive cleavage of *S*-3',4'-anhydroadenosyl-L-methionine (anSAM). The reaction results in generation of the stable allylic radical 5'-deoxy-3',4'-anhydroadenosine-5'-yl (anAdo·). Adapted from [98,129].

1.2.2 Classes of reactions catalyzed by radical SAM family

To introduce the variety of reactions catalyzed by radical SAM enzymes, an overview is represented in the following Schemes 1.5 and 1.6. The reactions illustrated are downstream reactions after the SAM cleavage event (Scheme 1.3, step 2) and are initiated by H-atom abstraction from either the substrate molecule or in a few cases from a specific polypeptide residue of the enzyme itself for example, Gly734 in pyruvate-formate lyase (PFL)[130] (Scheme 1.5B).

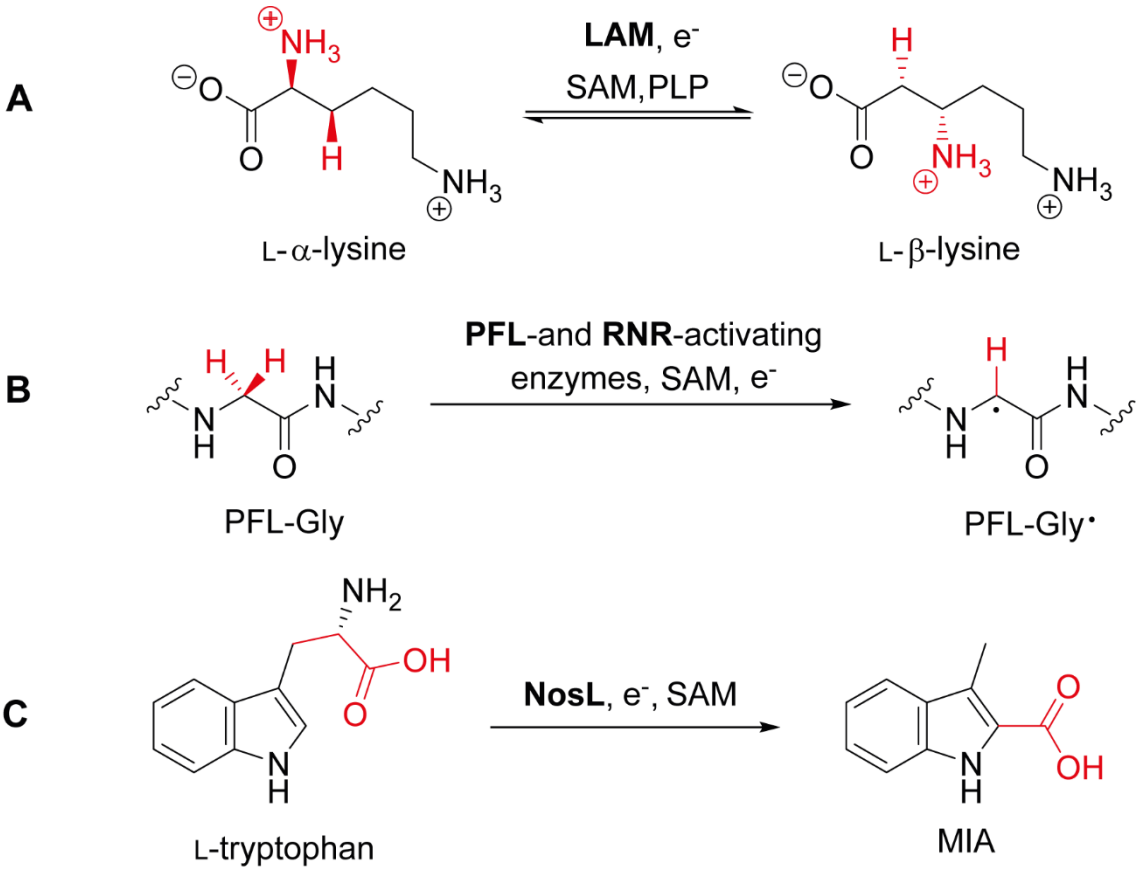

Scheme 1.5: Reactions catalyzed by radical SAM enzymes. (A) **Radical SAM Mutase**: Interconversion of L-α-lysine to L-β-lysine by lysine 2,3-aminomutase (LAM) with pyridoxal phosphate as a cofactor. (B) **Glycyl Radical Activating Enzymes**: activation of glycyl radical enzymes like pyruvate formate lyase (PFL) and ribonucleotide reductase (RNR). (C) **Enzymes catalysing complex rearrangements**: rearrangement of L-tryptophan to 3-methyl-2-indolic acid (MIA) catalysed by tryptophane lyase NosL. Adapted from [131,132,133].

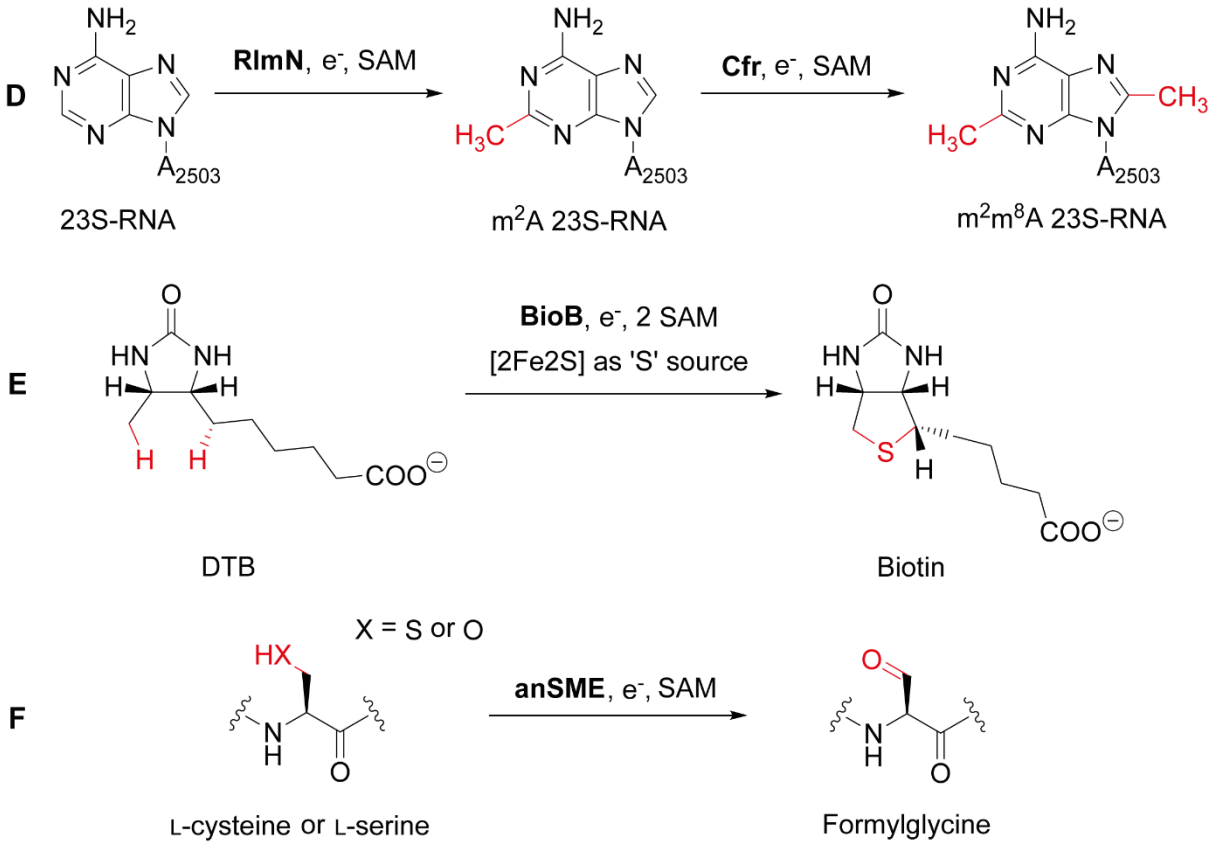

Scheme 1.6: Reactions catalyzed by radical SAM enzymes. (D) **Methyltransferases**: 23S-RNA modification catalysed by methyltransferase RlmN and Chloramphenicol-Florfenical resistance enzyme Cfr. RlmN methylates at the m^2A position followed by Cfr m^8A methylation. SAM also provides the methyl group in these reactions. (E) **Sulfur Insertion**: biotin synthase BioB sulfur insertion into D-desthiobiotin forming Biotin. (F) **Dehydrogenases**: anaerobic sulfatase maturating enzyme anSME oxidizes serine or cysteine residues to yield formylglycine sidechains. Adapted from [131,134, 135].

1.2.3 Energetics of the radical SAM reaction

A high-energy reaction is required to reduce the SAM sulfonium ion and homolytically cleave the carbon-sulfur bond of SAM. Thermodynamically the one electron-transfer to a trialkyl sulfonium ion in solution is estimated to have a half-wave reduction potential of -1.6 V, as described by Colichman and Love in 1953.[136] As the potential for a trimethylsulfonium ion was slightly lower at -1.85 V, the estimated potential for SAM in free solution is set to -1.8 V.[137] For the resting cysteine coordinated [4Fe4S]-cluster (in the absence of substrates), the reduction potential is -484 mV and upon SAM binding the potential increases to -430 mV for the cluster to be reduced to +1 (Figure 1.5). The binding of lysine decreases the reduction potential of the cluster to -600 mV.[138]

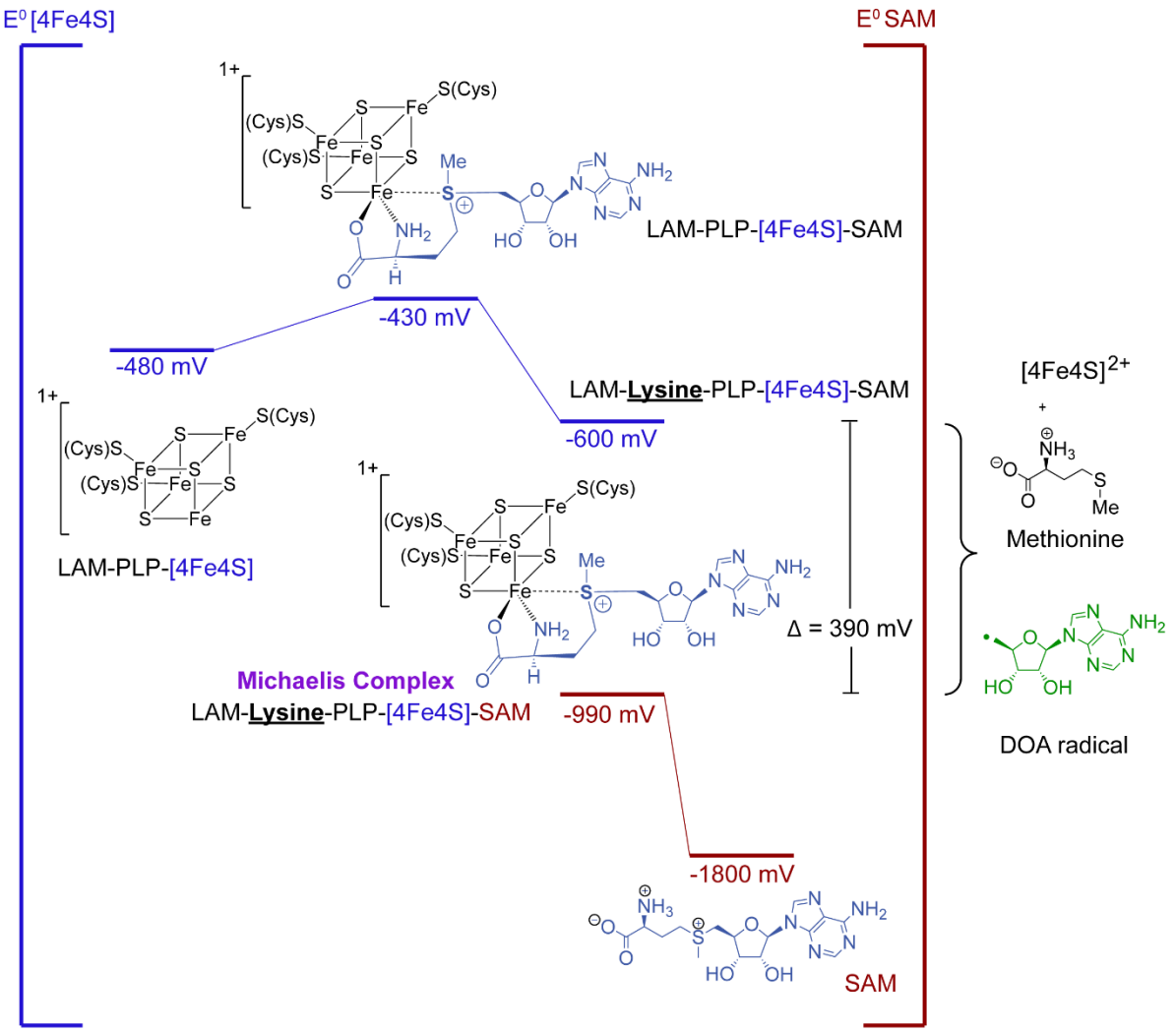

Figure 1.5: Energetic diagram of the one-electron reductive reversible SAM cleavage in the active site of LAM. The blue scale is representative for the midpoint reduction potentials of the [4Fe4S] cluster and the red one for the SAM reduction potentials. Adapted from [98,138]

As shown in Figure 1.5, the reduction potential for SAM increases drastically from -1800 mV to -990 mV with [4Fe4S] binding in the active site of LAM (Lysine 2,3-aminomutase) in the presence of PLP (pyridoxal phosphate), as proximity facilitates the electron transfer step. The potential difference in the Michaelis complex between the [4Fe4S] cluster and SAM is only 390 mV in the active site of LAM compared to a difference of 1400 mV in solution. Binding of the substrate lysine and co-substrate PLP results in decrease of the activation energy potential for reductive cleavage by about 170 mV and upon SAM binding to the [4Fe4S] cluster the barrier is 810 mV lower than in solution. Therefore, the reductive cleavage involving efficient electron-transfer from the iron-sulfur cluster to the sulfonium ion is able to occur and overcome the much narrower potential barrier of 390 mV.[98,138]

1.2.4 Electron Transfer during radical SAM cleavage

The main role of SAM in many biological reactions is methyl group donation by a substitution mechanism leading to heterolytic bond cleavage between the sulfonium-ion and the methyl-group. The methyl group reacts directly with a nucleophile *via* a S_N2 mechanism (however, without forming a carbocation intermediate), as it's the case for SAM-dependent methyltransferases[139]. For radical processes, there are three different types of homolytic bond cleavage of SAM, between the sulfonium-ion and each attached carbon i.e. 1. S-C(5') 2. S-C(γ) or 3. S-C(methyl) bond cleavage (Figure 1.6). The most common cleavage by radical SAM enzymes is the breakage of the S-C(5') bond following a nucleophilic mechanism leading to a 5'-deoxyadensoyl radical and methionine.[140,141]

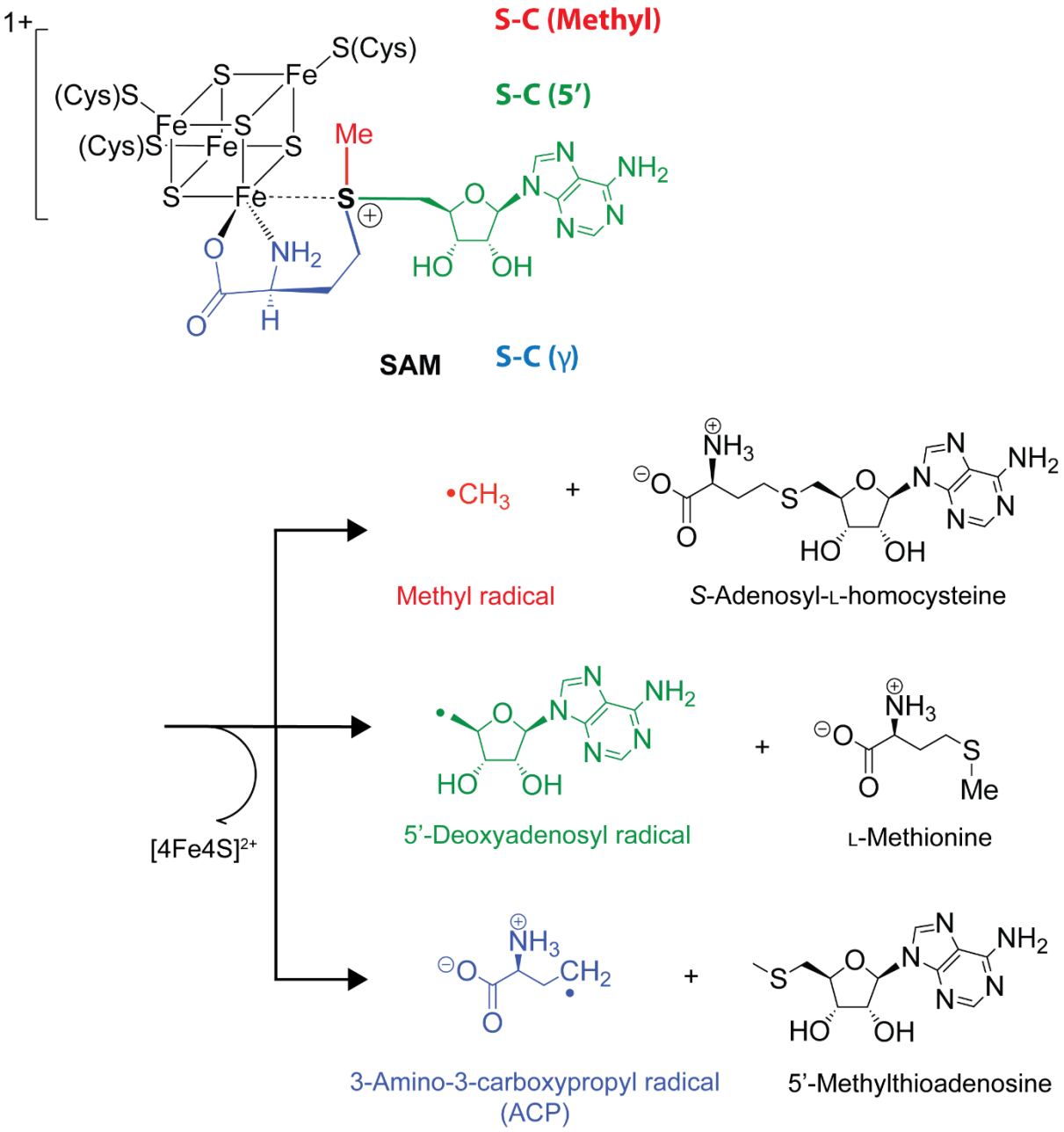

Figure 1.6: Representation of three different types of homolytic cleavage between the sulfonium-carbon bonds in SAM. Adapted from [98].

The position of bond cleavage is largely determined by the interactions between SAM, the substrate and [4Fe4S]. The reduced $[4Fe4S]^{+}$ cluster provides an electron for the reductive cleavage of SAM. Studies with seleno-SAM and the radical SAM enzyme LAM in presence of a substrate analogue showed a very short Se-Fe distance of 2.7 Å, which underlines a direct coordination of the sulfonium-ion of SAM and the unique iron of the [4Fe4S] cluster.[120] The result also supports the inner-sphere transfer from the unique iron to the sulfonium-ion. Spectroscopic investigations by ENDOR on PFL-AE

suggested a direct orbital overlap between the sulfonium sulfur and the [4Fe4S] cluster,[117,127] which was later confirmed by several X-ray structures[117,142,143] to derive from the unique site of the [4Fe4S] cluster. However other radical SAM enzymes exist that cleave the S-C(γ) bond in SAM, including for example, the B_{12}-independent glycerol dehydratase activating enzyme[144] and Dph2[145,146]. One effect that influences the increase of the activation energy potential for the S-C(5') bond cleavage is the coordination state of SAM to the iron sulfur cluster, and in almost all cases the S-C(5') is positioned *trans*- to the sulfonium-cluster interaction bond (Figure 1.7).[121,140,141] Moreover, the electronic environment of the active site is crucial, depending if the substrate is bound and the SAM is coordinated to the unique iron it induces perturbations in the cluster itself and the antibonding S-C(5') orbital and thus lowering the activation barrier to enable bond cleavage.[98]

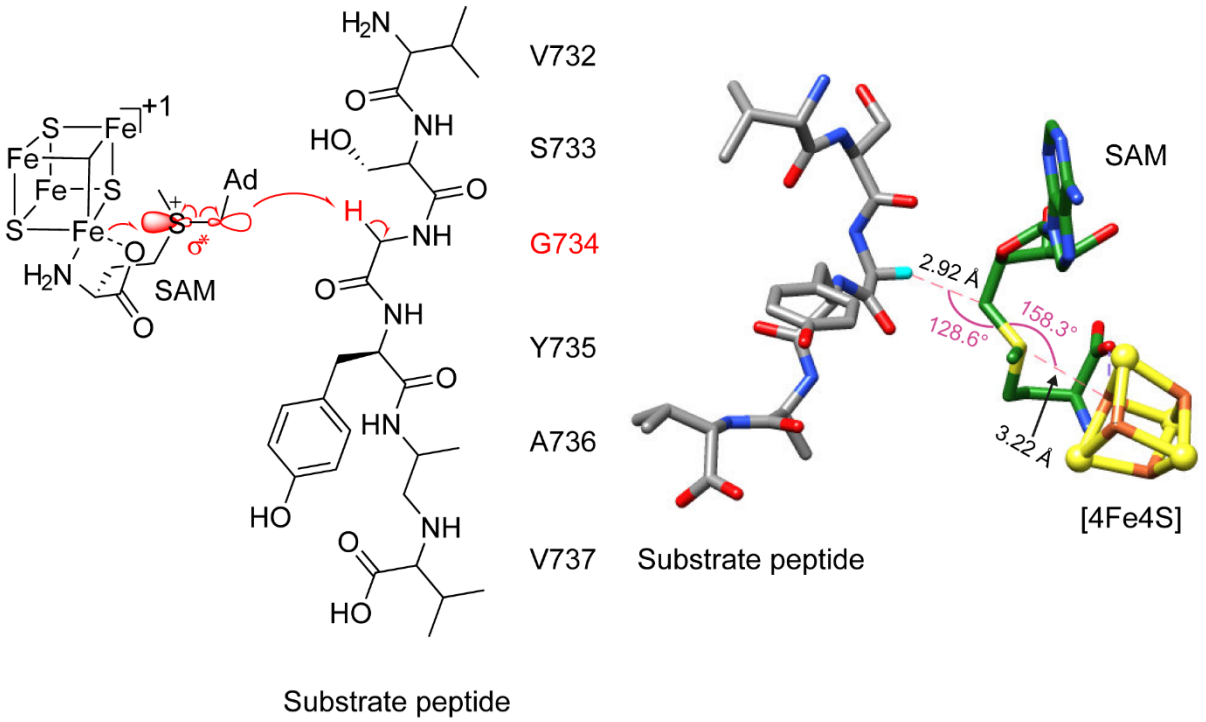

Figure 1.7: Left: H-atom abstraction from the substrate peptide in *trans*-position by PFL, showing the σ*-orbitalof the C(5')-S bond in SAM (*red*). Right: crystal structure of PFL (PDB: 3CB8) with peptide substrate. The FeS bond of [4Fe4S] aligns to the SAM (*gree*n) C-S bond that aligns to the cleaved C-H bond (hydrogen shown in *cyan*) showing corresponding bond distances and angles.[147]

Studies of the crystal structure of *Thermotoga maritima* HydE in its SAM and Met bound state using hybrid quantum mechanical/molecular mechanical (QM/MM) calculations provided further support for the hypothesis that the electron transfer

derives from the unique iron.[122] The [4Fe4S]-SAM bound transition state (TS) in HydE combines a HOMO (highest occupied molecular orbital) which is derived from the carbon-centred 5'-deoxyadenosyl radical, the methionine base Sδ and the site-differentiated unique iron. Another argument for direct fast electron transfer is the fact that the unique iron d-orbital and the SAM S-C bond σ^* orbital have the same energy level.[122] Furthermore, induced bond cleavage after electron transfer is facilitated by similar energies (difference 8.4 kJ/mol) of the transition state (TS) with 54.0 kJ/mol and the product DOA radical with 45.6 kJ/mol. Therefore the activation barrier for the C-S bond cleavage is relatively low[122]

1.2.5 Structural features of radical SAM enzymes

The crystal structure of over 30 unique Radical SAM enzymes have been determined[95] and they share some common structural features and patterns. A typical feature is the triose phosphate isomerase mutase (TIM) barrel. This fold can be divided into two subtypes: a $(\beta/\alpha)_6$ or a $(\beta/\alpha)_8$ fold type, each forming a barrel-like shape.[148] It is characterized by alternating inner parallel β-sheets and are surrounded by α-helices on the surface.[149]

Radical SAM enzymes that possess a full $(\beta/\alpha)_8$ fold are BioB from *E. coli*[143] (Figure 1.8a), HydE from *Thermotoga maritima*[53], HydG from *Thermoanaerobacter italicus*[64] and *Carboxydothermus hydrogenoformans*[63], NosL from *Streptomyces actuosus*[150] and PylB from *Methanosarcina barkeri*[151]. Examples for radical SAM enzymes with a $(\beta/\alpha)_6$ TIM-barrel fold are HemN from *Escherichia coli*[142], MoaA from *Staphylococcus aureus*[112](Figure 1.8b), LAM from *Clostridum subterminale*[152] and PFL-AE from *E. coli*[147] and for a (β_5/α_6) TIM barrel BtrN from *Bacillus circulans*[153]. Different TIM barrel types and their sizes are related to the substrate sizes of the appropriate enzyme.[154] For example, HemN which modifies the large substrate haemoglobin and LAM catalyses the small molecule lysine only when the larger cosubstrate PLP is present posess a broad $(\beta/\alpha)_6$ TIM-barrel fold. Instead, smaller substrates like DTB or L-tryptophan in the case of BioB and NosL, respectively, can be accommodated in the narrow $(\beta/\alpha)_8$ fold. Comparisons relating the substrate binding in radical SAM enzymes

revealed that they occur mainly inside the TIM-barrel and in close proximity to SAM.[148]

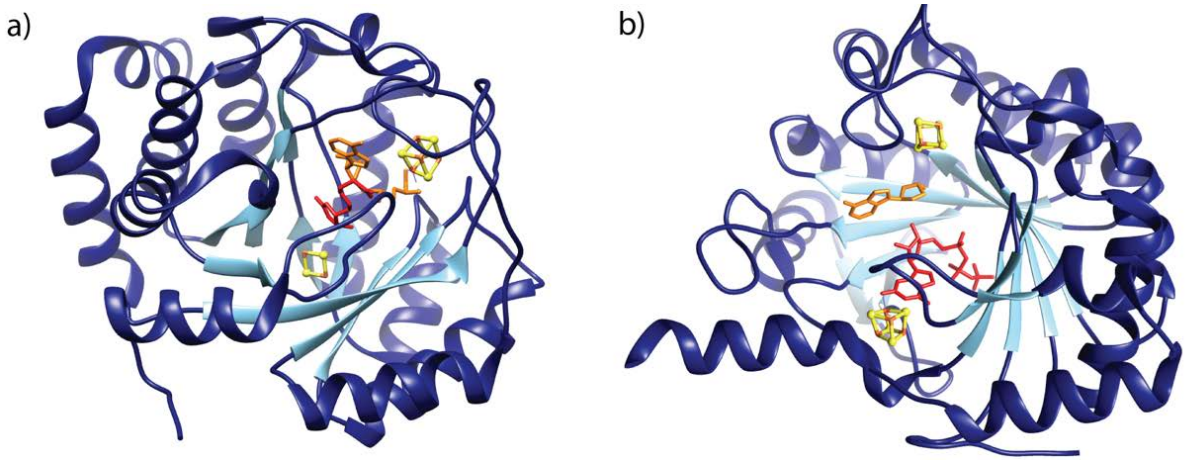

Figure 1.8: Two representative structures of typical radical SAM enzymes. a) Crystal structure of BioB from *E. coli* (PDB.ID: 1R30)[143] with SAM (*orange*) and the substrate DTB (*red*) as well as one [4Fe4S] and [2Fe2S]-cluster b) Crystal structure of MoaA from *Staphylococcus aureus* (PDB.ID: 2FB3)[115] with DOA (*orange*) and substrate GTP (*red*) and two [4Fe4S]-cluster. Beta-sheets of the TIM-barrel are shown in *sky blue*.

A typical folds have been observed in thiamine synthase ThiC from *Caulobacter crescentus*[99,155] (Figure 1.9a) and diphthamide synthase (Dph2) from *Pyrococcus horikoshii*[145,156] (Figure 1.9b). The ThiC cluster binding motif CX_2CX_4C differs from the canonical radical SAM superfamily motif and is situated in the *C*-terminal domain. The SAM molecule is coordinated to another additional transition metal site (either iron or zinc, depending on the preparation of the protein sample) and the cluster-binding domain moves upon substrate binding. In the *apo*-form the cluster is 25 Å away from the active site of the protein. The distorted cluster binding domain of the homodimeric structure folds into the active domain of the other homodimer.[155] The uncommon cluster binding domain ($CX_{103}CX_{123}C$) of Dph2 is extended over three different protein domains and the [4Fe4S]-cluster is situated in the center of the protein molecule.[145] Dph2 is a highly unusual radical SAM enzyme also in regard to its reaction, it cleaves the C_γ-S bond of SAM and the resultant ACP (3-amino-3-carboxy propyl) radical attacks the substrate, the side chain of residue His600 in the protein EF2 (Scheme 1.7).[156-159]

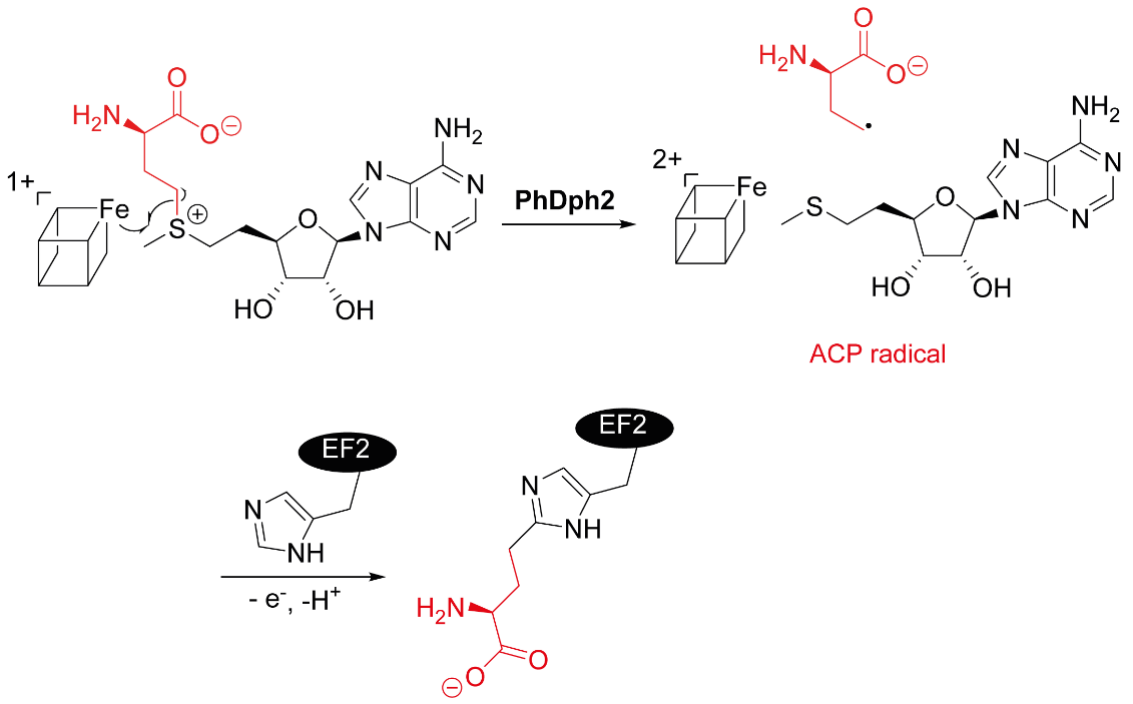

Scheme 1.7: Reaction catalyzed by radical SAM enzyme PhDph2. Adapted from [158,159].

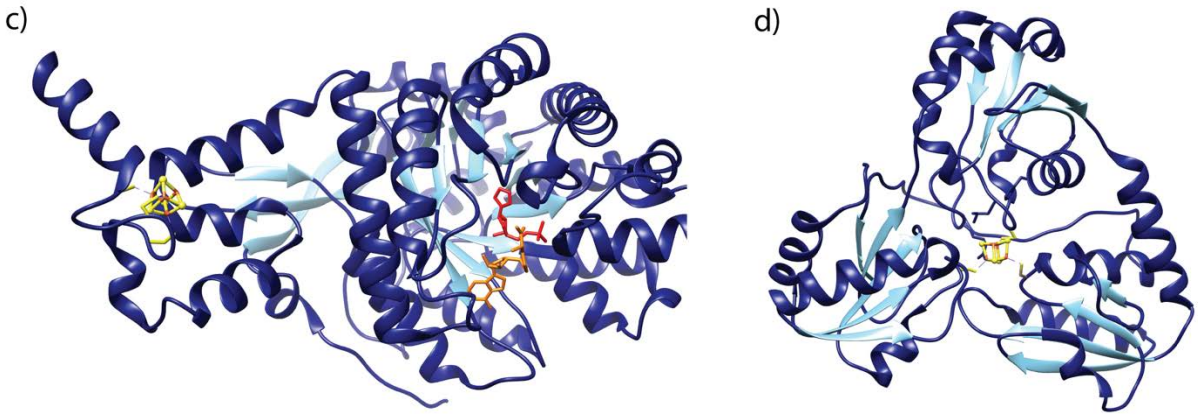

Figure 1.9: Unusual Radical SAM enzyme structures. c) Crystal structure of ThiC from *Arabidopsis thaliana* (PDB.ID: 4S25)[155] with SAM (orange) and substrate analogue imidazole ribonucleotide (IMR, red) and the C-terminal [4Fe4S]-cluster. d) Crystal structure of Dph2 from *Pyrococcus horikoshi* (PDB.ID: 3LZD)[145] with [4Fe4S]-cluster.

For most radical SAM enzymes, the conserved cluster binding motif is located inside the TIM-barrel 7-10 Å away from the protein surface and allows interactions with protein partners, like ISC (iron sulfur cluster) synthases or redox proteins like flavodoxin.[121] The actual [4Fe4S] cluster is shielded by loop regions on the top of the TIM-barrel followed by the first β-strand and SAM.[121] The carboxylic group of SAM is not oriented by a shared pattern; however, examples have been observed of forming

hydrogen bonds via arginine, lysine, histidine or serine and threonine.[121] A conserved 'GGE' motif builds hydrogen bonds to the SAM amino group and ensures the right methionine orientation. The adenine moiety is held by H-bonds from the partially conserved 'GxIxGxxE' motif.[121,160,161] The ribose hydroxyl groups are coordinated by charged or polar groups deriving from the β4 and β5 strands. [121,160-162]

Another radical SAM enzyme, which has an uncommon structure with a paired-down (β_6/α_3) fold is QueE, however the active site contains many of the canonical motifs described above, including conserved residues $CX_{14}CX_2C$ to stabilize the SAM-[4Fe4S]-complex (Figure 1.10).[101] Common binding patterns including 'GGE' motif interacting with the α-amino group of SAM, 'ribose' motif consisting of S133 and K135 on β4-strand and the adenine moiety coordinated by the β5-motif, with V151 and F48. Besides V151 and F48, two residues of β6-strand (D176 and Q173) are involved in forming hydrogen-bonds to the adenine part of SAM (Figure 1.10).[101]

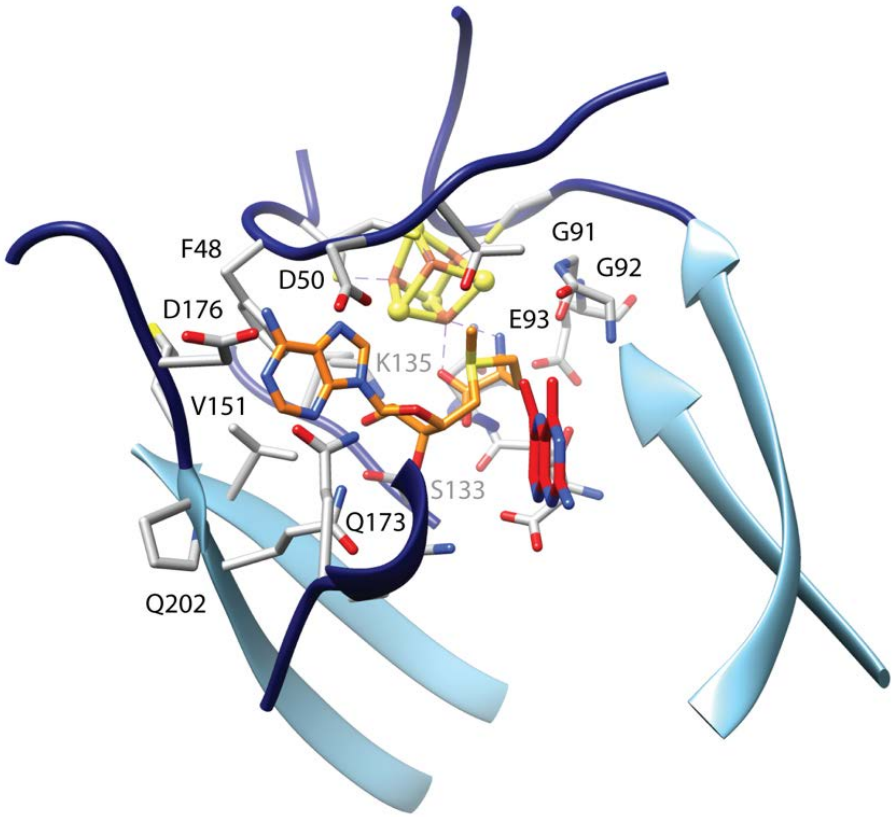

Figure 1.10: Residues involved in SAM coordination in the active site of QueE (crystal structure *Burkholderia multivorans* QueE (PDB.ID: 4NJG)[101]. SAM is shown in *orange* and the substrate CPH_4 in *red*.

QueE (7-Carboxy-7-deazaguanine synthase) catalyzes the ring contraction and following rearrangement of 6-carboxy-5,6,7,8-tetrahydropterin (CPH_4) into CDG in the presence of Mg^{2+} with ammonia as side product, and CDG forms the pyrrolopyrimidine base of 7-deazapurines (Scheme 1.8).[163-167]

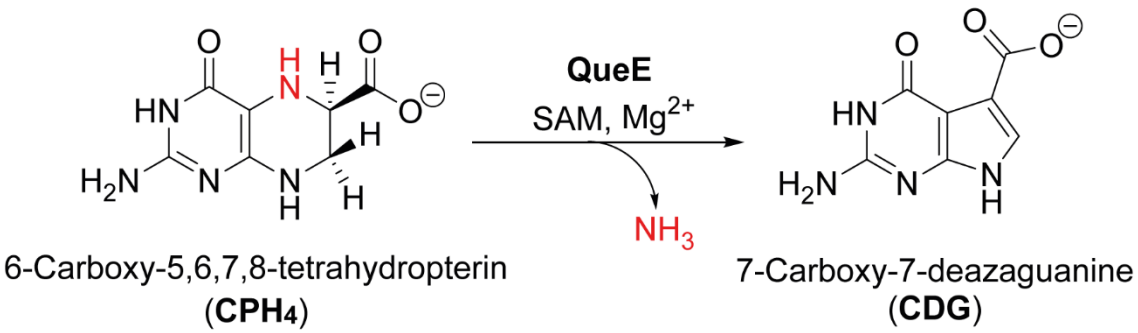

Scheme 1.8: Catalyzed reaction by the radical SAM enzyme QueE. Adapted from [167].

1.2.6 Radical SAM enzymes with an auxiliary cluster

Many radical SAM enzymes carry one or more auxiliary clusters in addition to the [4Fe4S] cluster required for SAM cleavage. The functions and compositions of these auxiliary clusters, as well as the reactions they initiate, vary among the radical SAM superfamily.[135] The auxiliary cluster binding motifs are not conserved and the distances between the iron sulfur clusters vary from 8 to 30 Å. The substrate is often embedded between the radical SAM and the auxiliary clusters.[168] The mechanistic role of these clusters is for the majority of enzymes unknown, but there are certain types that have been well studied and characterized (Table 1.1). An overview of these reaction types is given in the following paragraphs.

Table 1.1: Examples for radical SAM enzymes (RSE) carrying an auxiliary cluster.

RSE (PDB)	**Aux. cluster binding motif**	**SPASM/ Twitch**	**Function** ***(of cluster)***
BioB (1R30)	$CX_{30}CX_{59}CX_{71}R$[143] [2Fe2S]	-	Biotin synthesis *(Sulfur donation)*
LipA (4U0O)	$CX_4CX_5CX_{234}S$[169]	-	Lipoic acid synthesis *(Sulfur donation)*
anSME (4K39)	$CX_5CX_{14}C\text{-}X_n\text{-}C$ (I) $CX_2CX_5CX_{21}C$ (II)[170]	SPASM	Dehydrogenation *(oxidation o. deprotonation)*
AlbA (-)	$CX_5CX_2CX_{15}C$[171]	Twitch	Subtilosin A maturation *(substrate binding)*
MftC (-)	$CX_6CX_{10}C$ (I) $CX_2CX_5CX_3CX_{17}C$(II)[172]	SPASM	Mycofactocin maturation *(substrate binding)*
PqqE (6C8V)	$CX_{19}CX_{54}CX_1C$ (I) $CX_2CX_5DX_{21}C$ (II) [173]	SPASM	PQQ synthesis *(oxidation?)*
BtrN (4M7T)	$CX_{17}CX_{44}CX_2C$[153]	Twitch	Butirosin synthesis *(oxidation)*
MoaA (2FB3)	$CX_2CX_8GX_4C$[115]	Twitch	Molydopterin synthesis *(substrate binding)*
HydG (4WCX)	$HX_{114}CX_2CX_{22}C$[64]	-	H-cluster maturation *(synthon binding)*
HydE (3CIW)	CX_7CX_2C[58] [2Fe2S]	-	H-cluster maturation *(unknown)*

The radical SAM enzymes BioB and LipA are examples of enzymes containing auxiliary clusters that donate one or two sulfurs into their organic substrates. BioB contains an additional [2Fe2S] cluster and its function is to convert dethiobiotin (DTB) into biotin by inserting a sulfur atom between C6 and C9 of dethiobiotin (Scheme 1.9).[102,174,175] LipA inserts sulfur atoms at C6 and C8 position of a protein-bound *n*-octanoyl chain (Scheme 1.10).[103, 176-178]

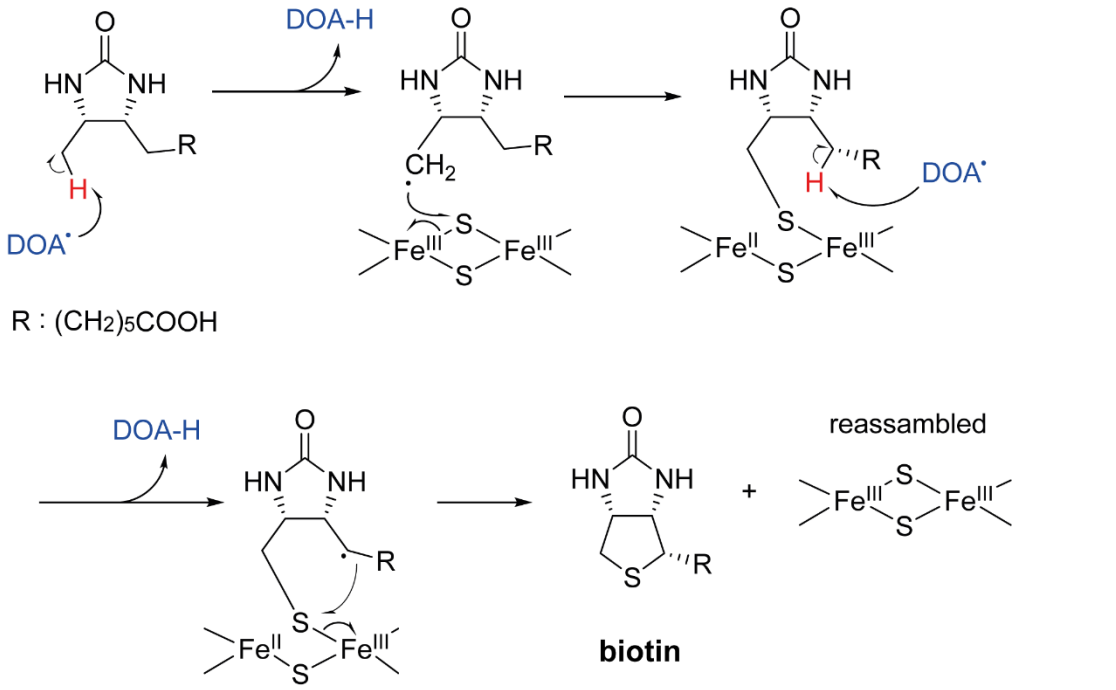

Scheme 1.9: Reaction mechanism of the radical SAM enzyme and biotin synthase BioB. Adapted from [132].

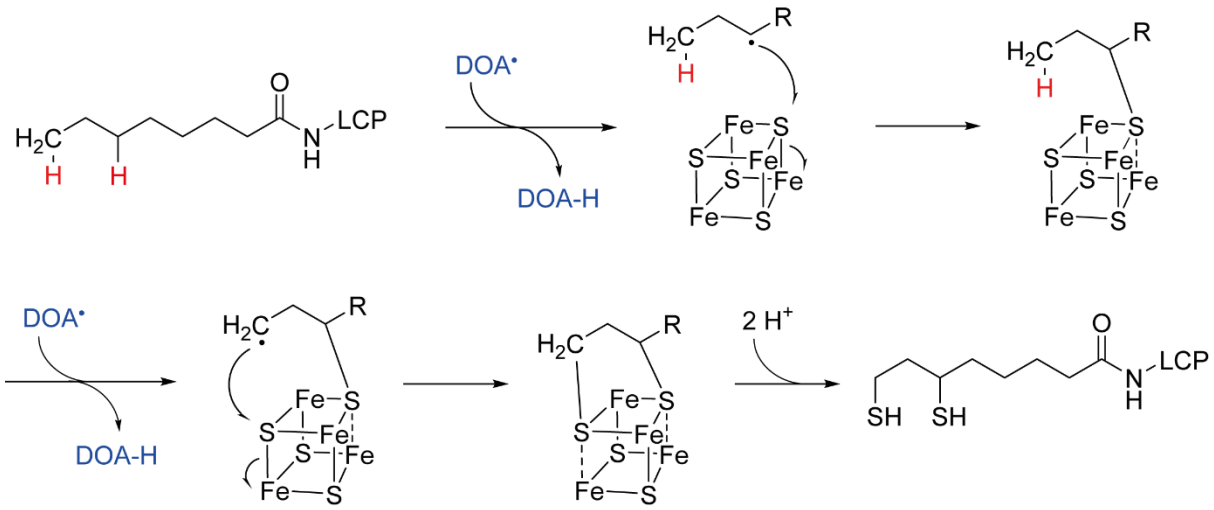

Scheme 1.10: Reaction mechanism of the radical SAM enzyme and lipoyl synthase LipA. Adapted from [135].

A subgroup of the radical SAM enzymes with *C*-terminal extensions are the SPASM domain-containing enzymes, they are named after the function of the first members: **s**ubtilosin A, **p**yrroloquinoline quinone (PQQ), **a**naerobic **s**ulfatase and **m**ycofactocin maturation enzymes.[95,179-181] They share a binding motif for two iron sulfur clusters ($CX_{9-15}GXC$-gap-$CX_2CX_5CX_3C$-gap-C).[110,171-173,179-182] Members lacking the

$CX_2CX_5CX_3C$ part are still included in the family, the truncated version of the SPASM domain is called the Twitch domain and these members contain only one auxiliary cluster (SPASM/Twitch subgroup).[181,153,170] Already more than 18000 putative members of the SPASM/Twitch subfamily have been assigned and they are still expanding.[95]

Two radical SAM dehydrogenases that belong to the SPASM/Twitch superfamily will be discussed in detail: anSME and BtrN. The anaerobic sulfatase maturating enzyme (anSME) carries two additional [4Fe4S] clusters which are 12.9 Å away from each other and the furthest distance between the radical SAM cluster and the auxiliary cluster is 26.7 Å.[170] After SAM cleavage, a hydrogen is abstracted from the β-carbon of a cysteine or serine residue and followed by deprotonation *via* aspartate acting as catalytic base and oxidation *via* the auxiliary cluster I.[170] This results in the generation of an aldehyde or thioaldehyde, which hydrolyses to form an aldehyde and H_2S (Scheme 1.6F).[170,182-184] The auxiliary clusters have been proposed to function as electron acceptors in several dehydrogenases.[181] The 2-Deoxy-scyllo-inosamine (DOIA) dehydrogenase BtrN, involved in biosynthesis of the antibiotic butirosin B, carries one auxiliary [4Fe4S] cluster and catalyzes the two-electron oxidation of DOIA to amino-dideoxy-*scyllo*-inosose (amino-DOI) (Scheme 1.11).[153, 185-187] The auxiliary cluster of BtrN is coordinated by four cysteines in the Twitch domain, which consists of a β-hairpin structure including the cysteines for ligation of the auxiliary cluster (Figure 1.11).[153]

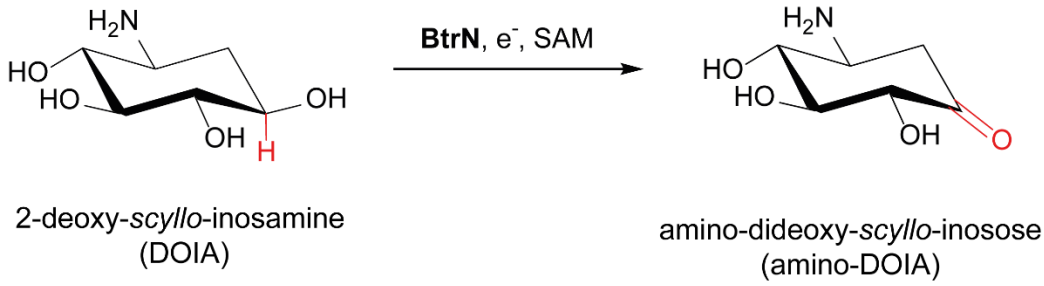

Scheme 1.11: Reaction catalyzed by the radical SAM enzyme BtrN. Adapted from [153].

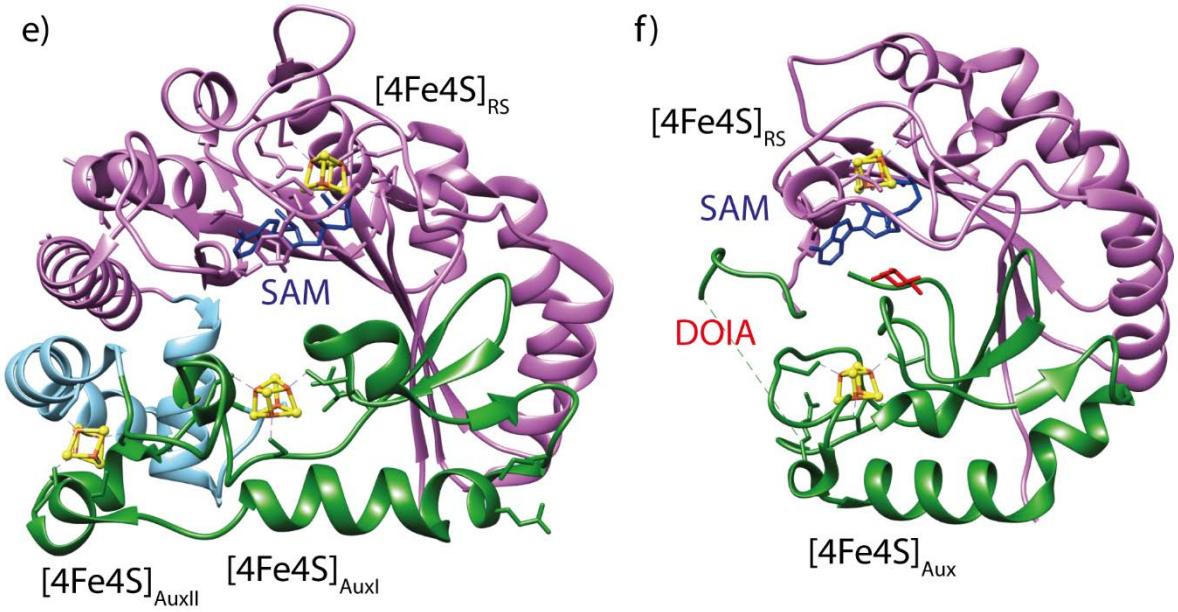

Figure 1.11: Two exemplary crystal structures of SPASM/Twitch enzymes. e) Anaerobic sulfatase maturating enzyme (anSME) from *Clostridium perfringens* (PDB: 4K37).[170] f) BtrN from *Bacillus circulans* (PDB: 4M7T).[153] SAM core is shown in *orchid,* the Twitch domain in *forest green* and two helices that are not part of either group in *sky blue*. SAM molecule is represented in *blue* and the DOIA substrate in BtrN in *red*. $[4Fe4S]_{RS}$: radical SAM cluster, $[4Fe4S]_{Aux}$: auxiliary cluster.

Furthermore, auxiliary iron sulfur clusters have an important role in the maturation of complex cofactors like molybdopterin or the H-cluster of the [FeFe] hydrogenase.[168] The enzyme MoaA is responsible for the first step of the synthesis of the molybdenum cofactor (Scheme 1.12).[115,188] MoaA together with the companion protein MoaC convert GTP into the precursor Z (cPMP), an oxygen-sensitive 6-alkyl-pterin product by the rearrangement of GTP.[115] Initial hydrogen abstraction is proposed to take place at the 3' hydrogen atom of the GTP ribose moiety.[189-192] The purine ring nitrogen of GTP is coordinated to the unique iron of the auxiliary [4Fe4S] cluster similar to an enol tautomer, which may influence substrate activation (Figure 1.12).[193,194]

The auxiliary [4Fe4S] cluster of the [FeFe] hydrogenase maturase HydG is involved in the formation of the CO and CN^- ligands of the H-cluster,[60] and will be described in detail in section 1.2.7. The role of HydE's additional iron sulfur cluster, which is a [2Fe2S] in the crystal structure of *Thermotoga maritima* HydE is still unknown.[53] Furthermore, it is suspected that the auxiliary cluster of HydE is not required for the maturation of the H-cluster, since not all HydE enzymes carry an auxiliary cluster.[53]

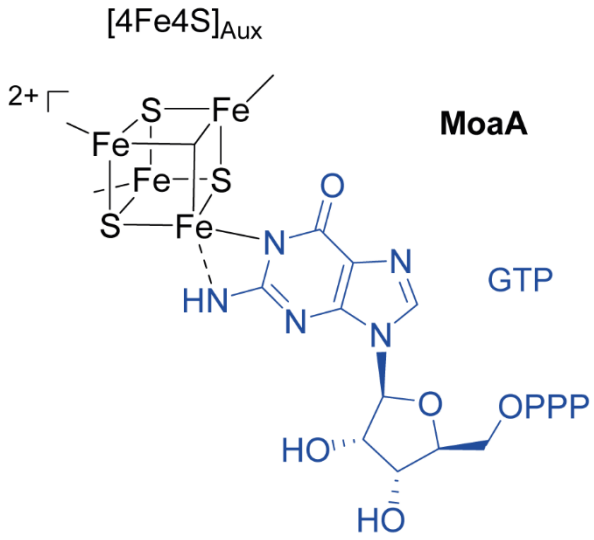

Figure 1.12: GTP binding to the unique iron of the auxiliary [4Fe4S]-cluster in MoaA.

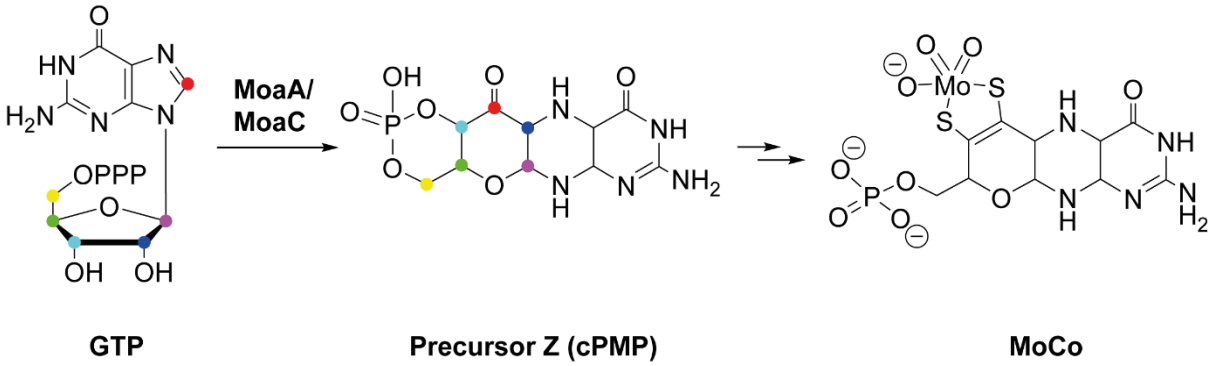

Scheme 1.12: Pathway for molybdenium cofactor (MoCo) synthesis. First step catalyzed by radical SAM enzyme MoaA and the MoaC enzyme. Adapted from [98].

Furthermore, auxiliary cluster containing radical SAM enzymes are relevant in activating glycyl residues[195-198] and in the biosynthesis of complex heterocycles like wybutosine.[199,200]

1.2.7 Radical SAM enzyme HydG

The [FeFe]-hydrogenase maturation enzyme HydG belongs to the radical SAM superfamily.[40] Early characterization of HydG's sequence revealed the presence of the typical CX_3CX_2C binding motif for the radical SAM [4Fe4S]-cluster ($[4Fe4S]_{RS}$)[40] as well as a second binding motive $CX_2CX_{22}C$ for an auxiliary [4Fe4S]-cluster ($[4Fe4S]_{Aux}$).[40,52] The reductive SAM cleavage activity of HydG has also been confirmed in an enzymatic assay.[52] All six cysteines are crucial for the resulting [FeFe]-hydrogenase enzyme activity, as shown by site-directed mutagenesis experiments with variants lacking one of the six cysteines.[42] Both clusters are required to achieve full HydG enzyme activity, which was shown by triple cysteine-to-alanine mutants of the ligating cysteines, resulting in variants that were missing either the radical SAM or the auxiliary [4Fe4S] cluster.[60]

Comparing the sequence of HydG with other radical SAM enzyme sequences, HydG has a sequence similiarity to aromatic amino acid lyases such as ThiH[54] and NosL[150]. HydG is most closely related to ThiH,[54] which is involved in thiazole biosynthesis and which catalyzes the cleavage of tyrosine into *para*-cresol and dehydroglycine (DHG).[201] Thus, due to the high homology it was likely that tyrosine is also the substrate of HydG, which was later proven to be the case.[54] Upon reductive SAM cleavage, the generated DOA-radical abstracts a hydrogen atom from L-tyrosine for HydG and ThiH catalyzed reactions.[54,201] The site of hydrogen abstraction is likely to be the α-nitrogen of the amino group, as has been observed in the crystal structure of the tryptophan lyase NosL.[150] As a result of the hydrogen abstraction, β-scission between the C_α-C_β bond is induced, following the formation of a 4-hydroxyl benzyl radical (4OB·)[59] as well as dehydroglycine (DHG)[54] (Scheme 1.13). The 4OB· radical was detected with freeze-quench EPR spectroscopy with tyrosine analogues and it is immediately reduced, forming *para*-cresol.[59]

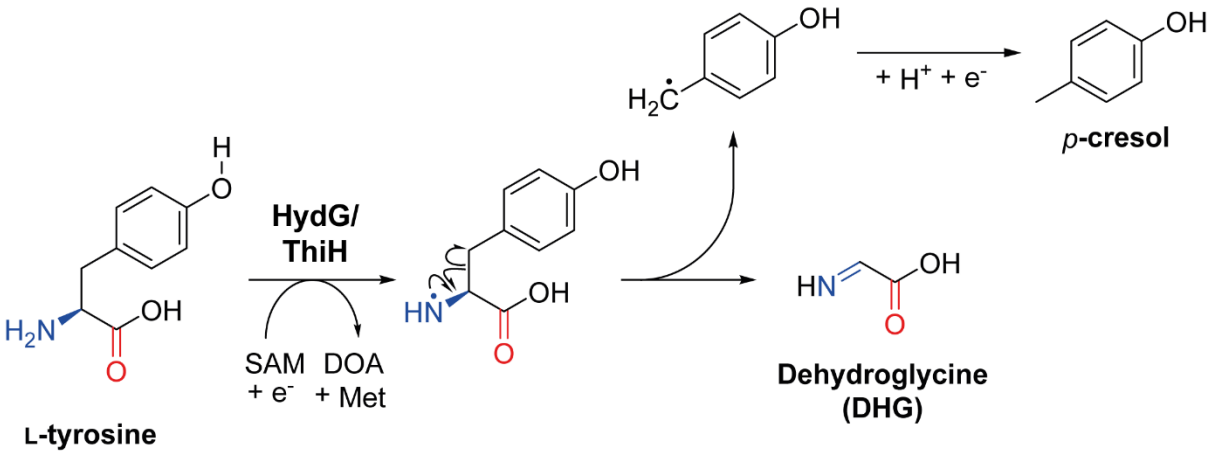

Scheme 1.13: Shared L-tyrosine cleavage mechanism of ThiH and HydG.

Dehydroglycine is a short-lived intermediate, which in HydG is broken down into diatomic CO (carbon monoxide)[56] and CN^- (cyanide)[55] molecules (Scheme 1.14). The second $[4Fe4S]_{Aux}$ cluster is proposed to be the site for generation of CO and CN^- ligands.[60] Biochemical characterization of the CO and CN^- formation showed that the auxiliary cluster is necessary for CO production, but CN^- formation was still observed for a variant missing the auxiliary cluster. However, removing the complete *C*-terminal domain of HydG completely abolished CO and CN^- production, whereas L-tyrosine cleavage was drastically reduced but still detectable.[60] EPR spectroscopic characterization of the auxiliary cluster of *Shewanella oneidensis* HydG revealed an uncommon high spin S = 5/2 signal for the reduced $[4Fe4S]_{Aux}$ cluster, which likely derived from a 5th iron attached to the $[4Fe4S]_{Aux}$ cluster. This was confirmed with the crystal structure of *Thermoanaerobacter italicus* HydG containing a [4Fe4S]·[FeS] cluster in monomer A (Figure 1.13).[64] Another crystal structure of HydG from *Carboxydothermus hydrogenoformans* has been published with a missing auxiliary cluster, possibly due to insufficient reconstitution, exhibiting typical structural features of a radical SAM enzyme.[68]

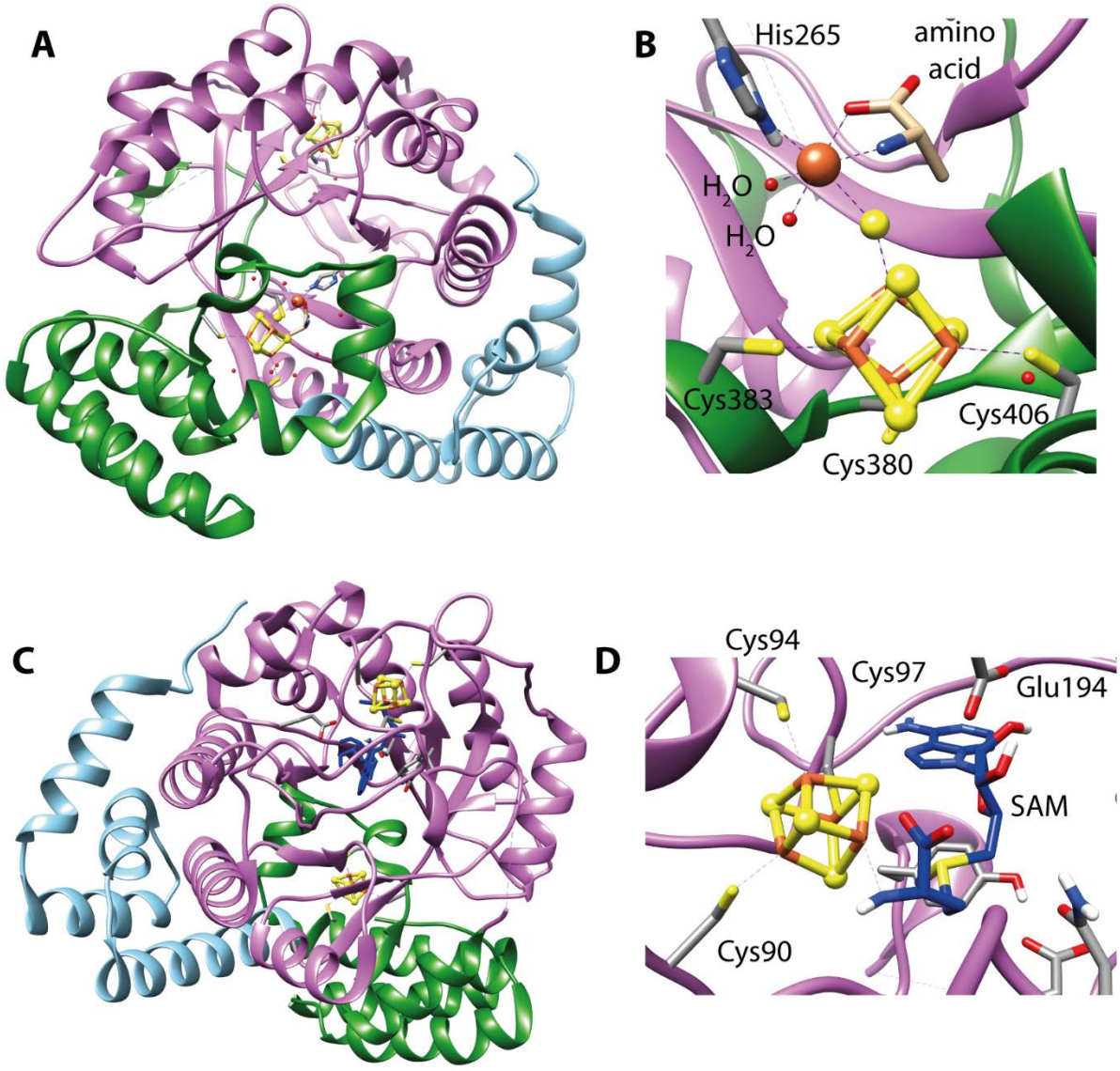

Figure 1.13: Crystal structure of *Thermoanaerobacter italicus* HydG (PDB: 4WCX)[61]. SAM core is shown in *orchid*, *N*-terminal extension in *sky blue* and the C-terminal extension in *forest green*. A: Monomer A with [5Fe5S] auxiliary cluster and with the [4Fe4S] radical SAM cluster. B: Monomer A close up on [4Fe4S]·[FeS] cluster, 5th iron is coordinated by two water molecules (*red*), histidine 265, an amino acid, and sulfide (possibly from a cysteine). C: Monomer B with SAM bound [4Fe4S] radical SAM cluster and [4Fe4S]·[S] cluster lacking the 5th iron. D: Monomer B close up on *N*/*O*-chelation by SAM with the unique iron of the [4Fe4S] cluster.

In the crystal structure of ThiHydG two monomers form an asymmetric unit with each containing a full TIM-barrel, typical of an enzyme utilizing a small substrate such as L-tyrosine. The $[4Fe4S]_{RS}$ cluster in monomer B does coordinate SAM through the free coordination site of the unique iron via *N*/*O*-chelation and demonstrates characteristic spectroscopic features as reported for other radical SAM enzymes (Figure 1.13).[64] The measured distance between the two iron-sulfur cluster at either end of the TIM-

barrel is more than 23 Å.[64] Dehydroglycine is proposed to migrate through the TIM-barrel tunnel to be transferred from cluster I to cluster II.[22] While monomer A is carrying the [4Fe4S]·[FeS] auxiliary cluster, monomer B is lacking the 5th iron containing a [4Fe4S]·[S] auxiliary cluster suggesting loose binding of the 5th iron.[64]

Time resolved FT-IR spectroscopy identified two different intermediate complexes which are presumed to be derivatives of the 5th iron with bound CO and CN ligands, called complex A and B. Complex A is formed first (30 s), followed by complex B (1200 s) (Scheme 1.14).[59] The second complex B is proposed to form the $Fe(CO)_2(CN)$ synthon upon release from HydG,[38,66,67,69,71] and is suggested to be transferred onto HydF to form the H-cluster precursor.[59,64]

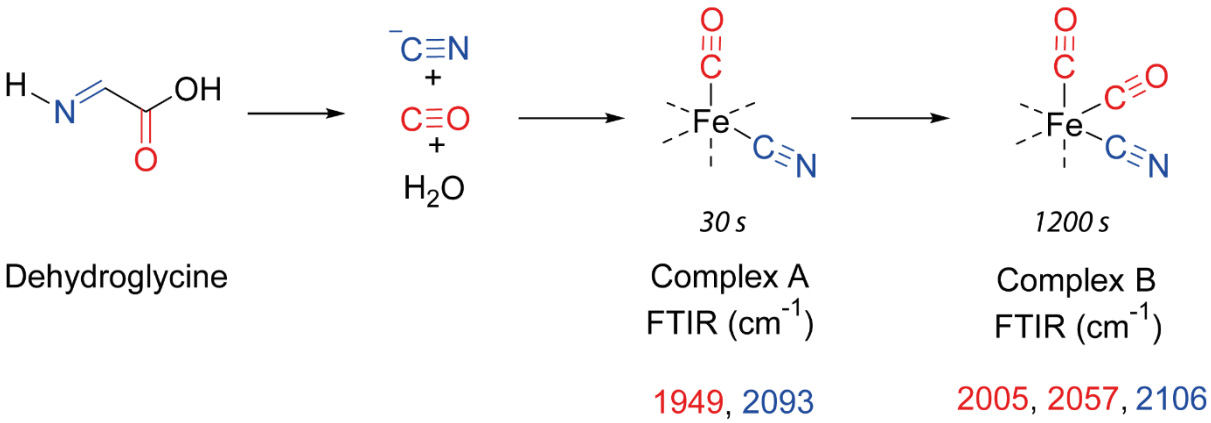

Scheme 1.14: Formation of complex A and complex B by HydG with corresponding wavenumbers detected by FT-IR spectroscopy. Adapted from [22].

However, Fontecilla-Camps and co-workers suggested a different mechanism for the decomposition of dehydroglycine, since they detected the production of formate (HCO_2H) during the production of CN^- and CO ligands (Scheme 1.15).[68]

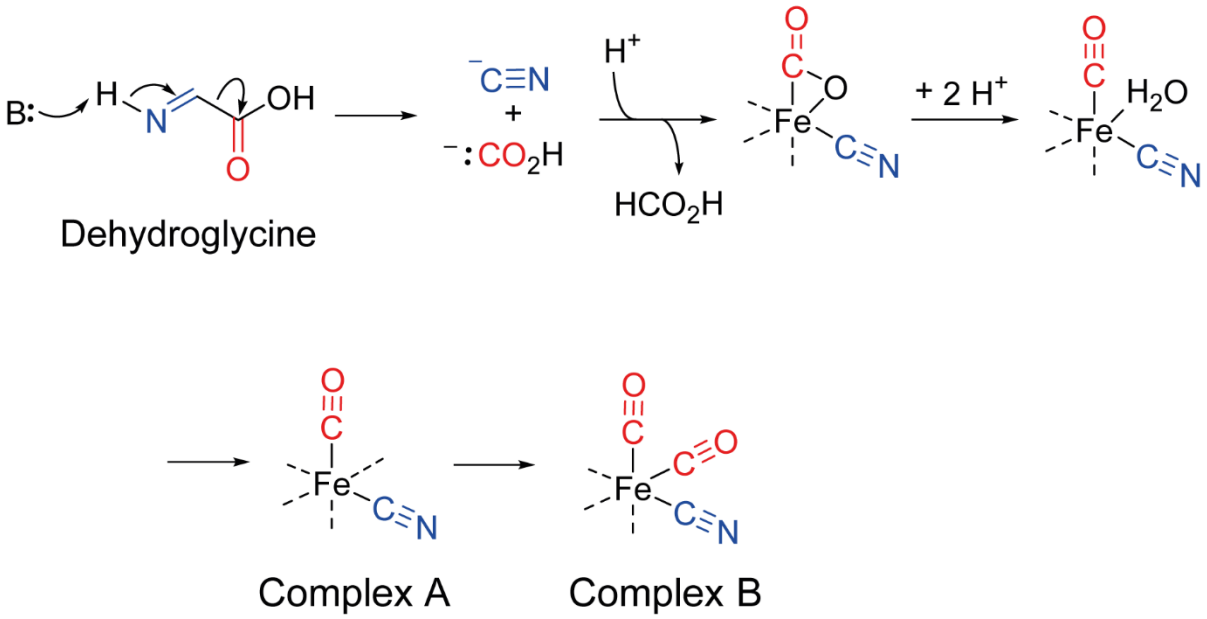

Scheme 1.15: Fontecilla-Camps *et al.*[68] proposed CO and CN^- production by HydG, following formation of complex A and complex B.

Since the coordination sphere around the 5th iron in the crystal structure of ThitHydG indicated the presence of an amino acid and sulfide ligating the iron,[64] EPR, ENDOR and FT-IR spectroscopic studies have been carried out to identify the amino acid coordinating the 5th iron.[66,69] L-cysteine has been shown to bind the auxiliary cluster 5th iron in HydG by observation of the characteristic high-spin signal in the EPR spectrum, whereas D-cysteine, L-homocysteine, L-serine or L-alanine plus sulfide did not show the corresponding signals.[66] Furthermore, in support of the EPR results FT-IR studies revealed that only in the presence of cysteine, the formation of complex A and complex B could be observed in the corresponding FT-IR spectra.[69] Just recently, complex A has been detected by EPR at 24 s after reaction initiation with 1 equivalent of L-tyrosine.[71] In comparison to the resting state high-spin S = 5/2 signal of the auxiliary cluster, complex A adopts a low spin S = ½ signal in the EPR spectrum.[71] After the formation of complex A, another equivalent of CO and CN^- is transferred onto the 5th iron resulting in the released synthon and a CN-bound [4Fe4S] cluster ([4Fe4S][CN]), which has been observed by EPR and ENDOR spectroscopy[66] and can be recycled to catalyse another HydG turnover by addition of Fe^{2+} and L-cysteine (Scheme 1.16).[71]

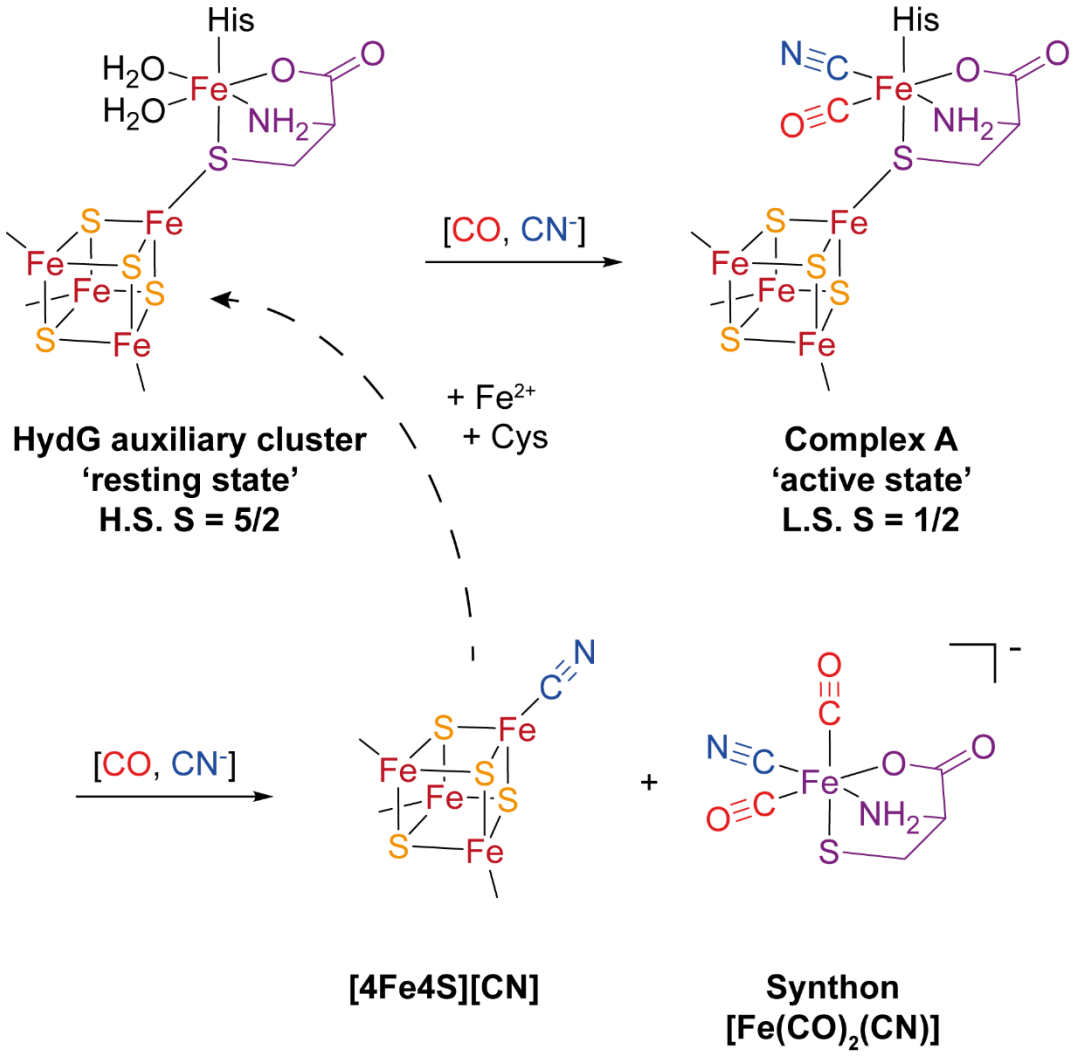

Scheme 1.16: The mechanism of HydG proposed by Britt *et al.*[38,66,67,69,71] to generate the synthon $[Fe(CO)_2(CN)]$ with complex A as an intermediate.

1.2.8 Radical SAM enzyme HydE

The HydE enzyme is a member of the radical SAM superfamily and is responsible for the maturation of the [FeFe]-hydrogenase.[40] The first identification was in the green alga *Chlamydomonas reinhardtii* and revealed the fusion protein HydEF1 as [FeFe]-hydrogenase maturase, which contains the sequence of the radical SAM enzyme HydE. Besides the typical CX_2CX_3C binding motif for radical SAM [4Fe4S] clusters, some HydE proteins possess another CX_7CX_2C binding domain for a potential second [4Fe4S] or [2Fe2S] cluster.[40,52] The reductive SAM cleavage activity of HydE has been confirmed and each cysteine of the radical SAM binding motif is crucial for the resulting [FeFe]-hydrogenase activity.[42]

The first crystal structure of the [FeFe]-hydrogenase enzyme HydE had already been published in 2008 by Fontecilla-Camps *et al.* (Figure 1.14). The structure shared the typical structural patterns of radical SAM enzymes with a complete TIM barrel.[53] A large active site cavity inside the TIM barrel is a possible binding site for an unknown substrate of HydE. The [2Fe2S] auxiliary cluster is positioned outside the TIM-barrel.[53]

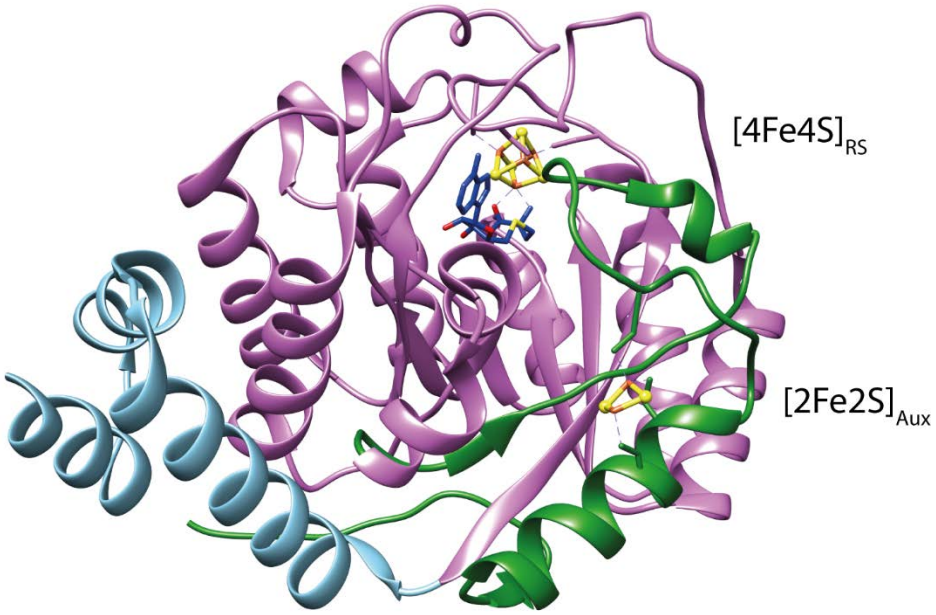

Figure 1.14: Crystal structure of TmHydE (PDB: 3CIX)[53]. SAM core shown in *orchid*, N-terminal extension in *sky blue* and C-terminal extension in *forest green*.

The auxiliary cluster of HydE is not required for the maturation of the [FeFe]-hydrogenase, since mutations of the cluster binding site resulted in CaHydE variants that were still able to activate the hydrogenase.[53] Furthermore replacing a HydE protein with two clusters (*Clostridium acetobutylicum*) with a HydE protein carrying only one iron-sulfur cluster (*Bacteroides thetaiotaomicron*) did yield an active hydrogenase for both samples.[53]

Sequence comparison of HydE with other radical SAM enzymes reveals- HydE shares a high degree of sequence similiarity to biotin synthase BioB and pyrrolysine biosynthesis protein PylB.[65] However, since the second cluster of HydE does not have an essential role for [FeFe]-hydrogenase maturation, a similar reaction as BioB, where the second cluster serves to donate sulfur,[102] is unlikely. But a similarity to the reaction catalyzed by PylB is possible (Scheme 1.17). PylB is catalyzing a carbon backbone rearrangement in α-L-lysine to form 3-methyl-D-ornithine.[98]

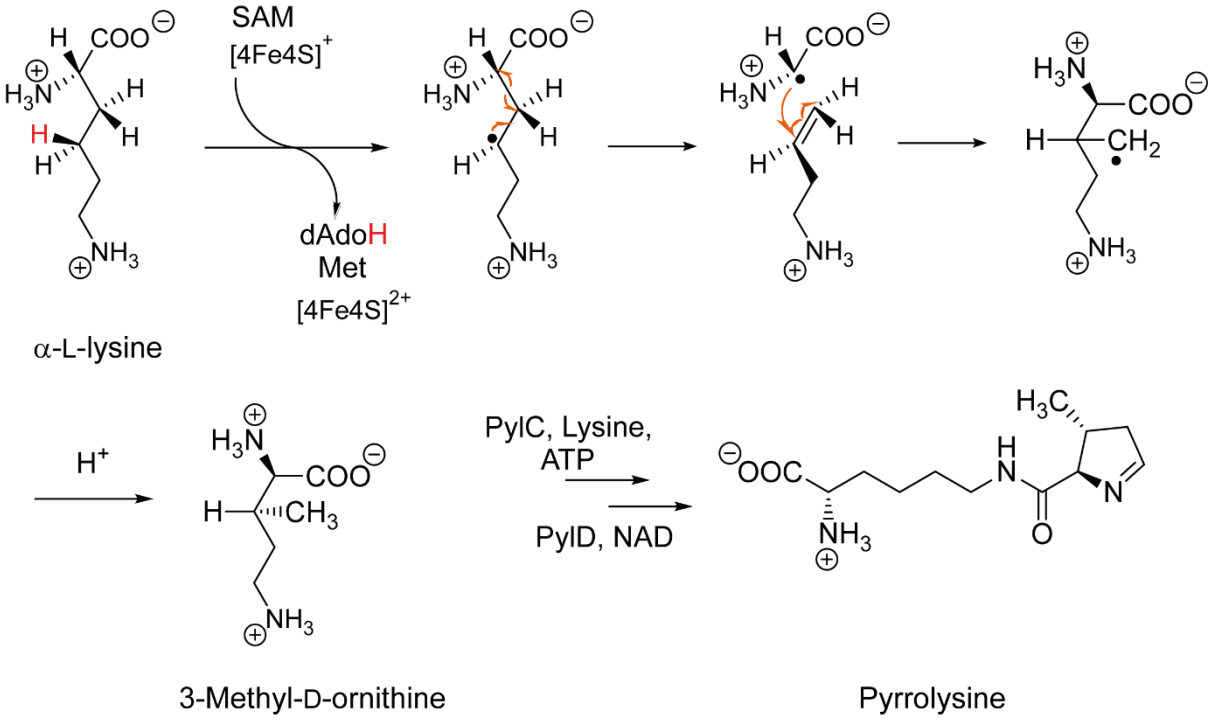

Scheme 1.17: Reaction catalyzed by radical SAM enzyme PylB. PylB catalyzes the rearrangement of α-L-lysine to 3-methyl-D-ornithine. Adapted from [98].

One of the biggest questions in [FeFe]-hydrogenase maturation remains the substrate of HydE, which is still unidentified. However, recent studies gave insights into which compounds stimulate the SAM cleavage activity of HydE, by screening different small amino acids and low molecular weight thiols. Besides L-cysteine, other thiol-group containing compounds such as mercaptopyruvate, coenzyme M and 3-mercaptopropionic acid induced an increase in DOA formation, suggesting that the substrate of HydE contains a thiol.[65] Furthermore, HydE has been crystallized with thiocyanide in the active site suggesting an affinity to this molecule.[53]

Another class of molecules, the 1,3-thiazolidines were shown to act as ligands and possible substrates for HydE. X-ray crystallographic studies with TmHydE were intended to yield crystals with bound L-cysteine, however addition of cystine resulted in crystals with 1,3-thiazolidines, which possibly derived from cystine decomposition in alkaline buffers to cysteine, pyruvate and hydrogen sulfide in presence of iron.[70] A solution of a 1:1 mixture of cysteine and pyruvate forms 1,3-thiazolidines. In the crystal structure the 5'-C of SAM is positioned close to the chalcogen S of the 1,3-thiazolidines, suggesting that the generated radical is directly interacting with the sulfur

and inducing bond breakage instead of abstracting a hydrogen atom. HydE activity studies with 1,3-thiazolidines did not show any enhancement of SAM cleavage, suggesting they do not act as substrates.[70]

Although no clear evidence has been reported yet, HydE is proposed to synthesize the azadithiolate bridge in the [FeFe] hydrogenase cofactor, the H-cluster.[22,53,65,70,98] Nevertheless, screening different labelled ^{15}N compounds as potential substrates, subsequent maturation of the [FeFe]-hydrogenase and analysis of the resulting active hydrogenase site by HYSCORE spectroscopy provides a route to identify the precursor of the azadithiolate bridge.[199]

1.3 GTPases

GTP hydrolysis is catalyzed by GTPases, a large family of hydrolase enzymes that can bind GTP and convert it into GDP.[203] GTPases are involved in numerous biological processes such as protein biosynthesis[204,205], growth control[206,207] and differentiation[208,209] as well as transport of vesicles within the cell[210,211]. A subgroup of GTPases are small GTPases which again divide into subfamilies including Ras, Rho, Rab, Ran and ARF (ADP ribosylation factor) GTPases.[212] These small GTPases are regulators for a number of functions central to the dynamics of the cell cytoplasm.[213] Another subclass of GTPases are called G proteins, which also include small GTPases, that function as intermediates in transmembrane signaling pathways[214] and are molecular switches that transfer from an activated GTP-bound state ‘on’ to an inactivate GDP-bound state ‘off’ after hydrolysis (Figure 1.15)[215-217].

In this following section the focus will be on small GTPases that are involved in metal transport or metallocofactor assembly.

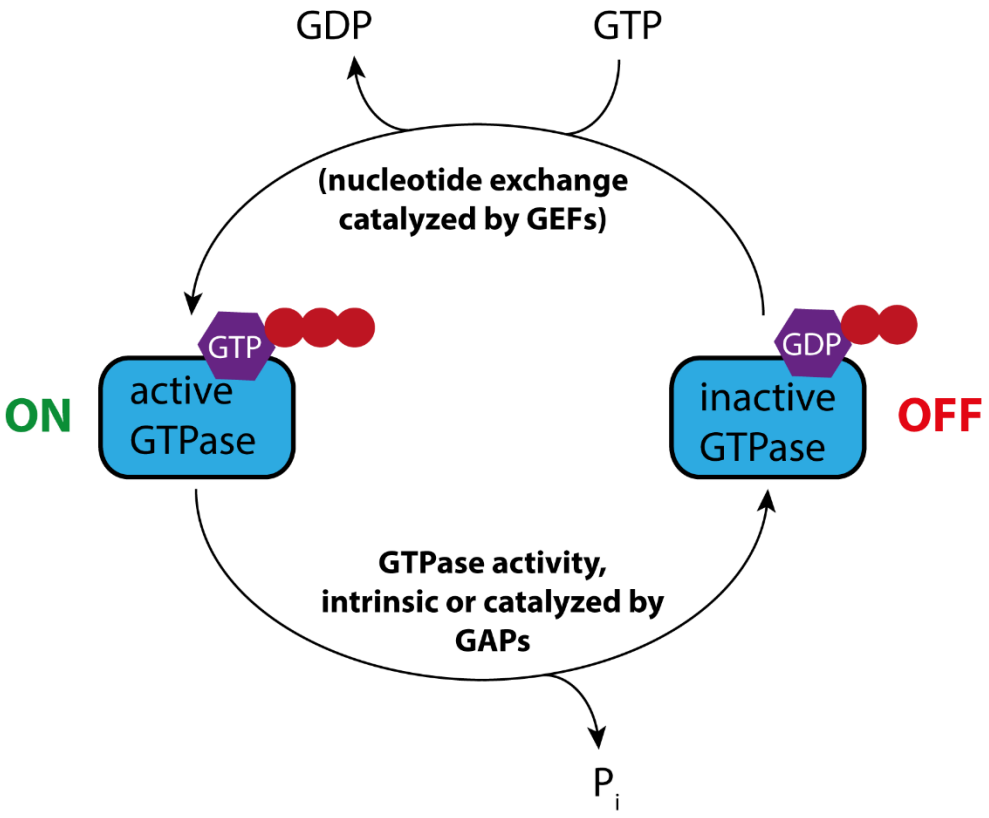

Figure 1.15: General GTPase cycle. GEF: Guanine nucleotide exchange factor, GAP: GTPase activating protein. GTPase might also exist as dimer with one nucleotide molecule per monomer and the cycle functions without GEFs and GAPs.

1.3.1 Metallo GTPases

The polytopic bacterial membrane protein FeoB (Ferrous iron transporter B) is essential for Fe(II) uptake in bacteria and is a G protein with GTPase activity.[218] Upon potassium addition, the GTPase activity of FeoB is accelerated by 20-fold, with an asparagine residue proposed to be responsible for K^+ binding and K^+-dependent activation.[219] This potassium mediated activation is also observed for other GTPases such as MnmE, which is involved in tRNA modification.[220] Despite the well-studied GTPase mechanism by FeoB, the mechanism of iron transport is still poorly understood.[221]

Another GTPase involved in metal transport and metallocofactor assembly is HypB, which is required for nickel incorporation into the [NiFe]-hydrogenase and urease (Figure 1.16).[222] The GTP hydrolysis is essential for the nickel incorporation and belongs to the maturation process.[223] A CXXCGC binding motif is responsible for the high-affinity binding to nickel in HypB another binding motif in the *C*-terminus binds Ni(II) with low affinity.[224] HypB is also able to bind Zn(II) with nanomolar affinity, however Zn(II) is found to lower the GTPase activity.[225] Furthermore, Ni(II) and GTP-binding induce the dimerization of HypB, whereas Zn(II) does not.[225] HypB interacts with the hydrogenase protein HypA in proximity to the Ni(II) binding site to facilitate nickel transfer. This process is accelerated by the presence of GDP.[226,227] Overall GTP hydrolysis is mediating both metal binding and protein-protein interaction in HypB.[228]

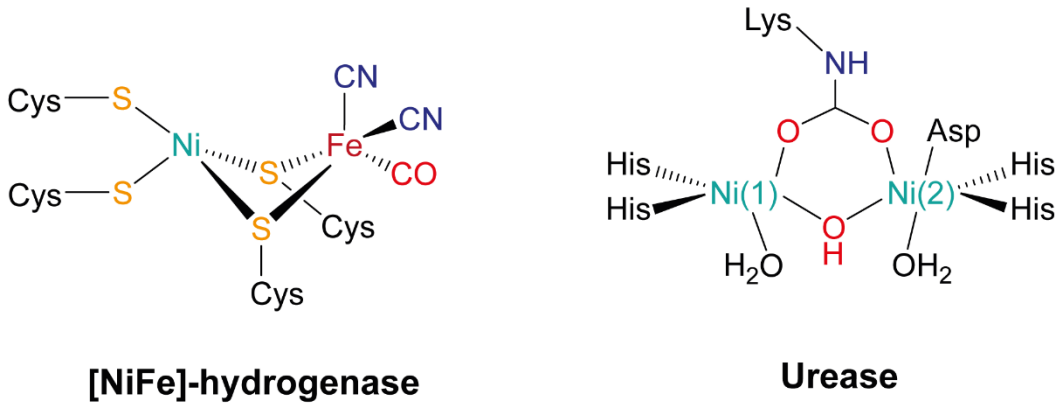

Figure 1.16: Molecular structures of the metallocofactors of [NiFe]-hydrogenase and urease.

Similar to HypB, the GTPase and metallochaperone UreG binds two nickel ions and transfers them onto the metallocofactor of urease (Figure 1.16).[229] Urease catalyzes the hydrolysis of urea, forming ammonia and carbon dioxide as reaction products.[230] Crucial for the activity of the urease is the binding of Ni(II) by a cysteine and histidine residue proposed to be involved in GTPase activity.[231] Additionally, binding of Zn(II) plays a direct role in the dimerization of UreG, however, no GTPase activity was observed if only Zn(II) was present.[232] UreG is the first discovered intrinsically disordered enzyme with a largely disordered tertiary structure.[233] Conformational changes induced by GTP binding and hydrolysis facilitating urease maturation.[234]

MeaB is a small GTP and metallochaperone involved in the maturation of the B_{12}-dependent methylmalonyl-CoA mutase (MCM) (Figure 1.17). GTPase activity of MeaB is enhanced by 100-fold when binding to the MCM.[235] Its function in the maturation process is assisting the loading of the active 5'-deoxyadenosylcobalamine cofactor onto MCM (Figure 1.17).[236] The *N*-terminal domain of MeaB serves as the protein-protein interaction with the mutase (blue circle, Figure 1.17) whereas the *C*-terminal domain is responsible for GTP binding (purple circle, Figure 1.17). Upon GTP hydrolysis, a large conformational change is suggested to gate the domain for signal transduction to the interaction surface with the mutase.[237]

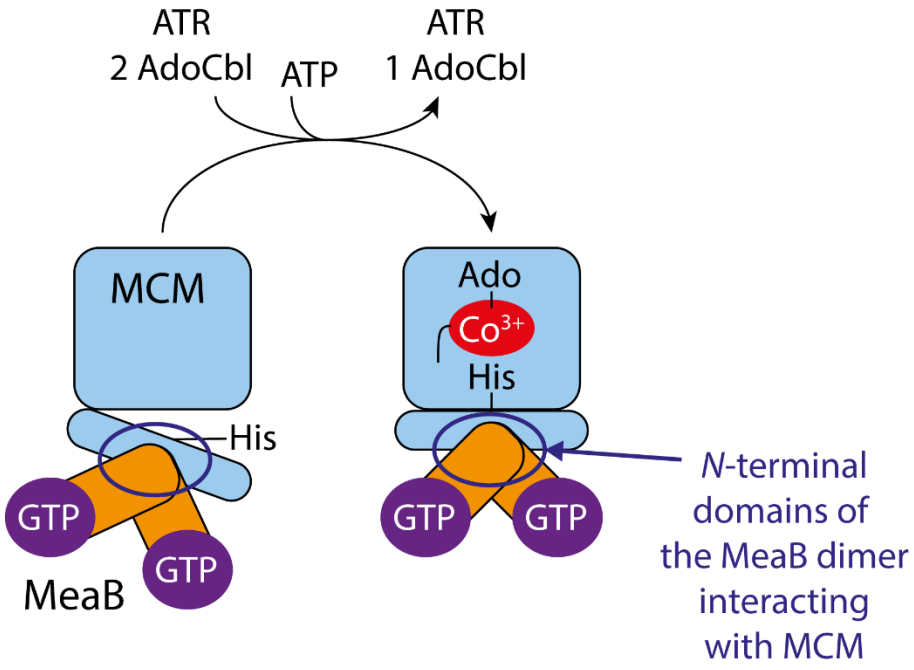

Figure 1.17: Nucleotide and MeaB-gated transfer of AdoCbl (5'-deoxyadenosylcobalamine) from ATR (adenosyltransferase) to MCM (methylmalonyl-CoA mutase). Adapted from [238]

1.3.2 Small GTPase HydF

The HydF enzyme was first reported as a fusion protein HydEF1 in green alga *Chlamydomonas reinhardtii* and was assigned as GTPase being responsible for the [FeFe]-hydrogenase maturation.[40-42] Spectroscopic characterization by UV-Vis and EPR spectroscopy of HydF from *Thermotoga maritima* confirmed the presence of a [4Fe4S] cluster with a $CX_{50}CX_2C$ binding motif.[51] Furthermore, primary sequence analysis revealed characteristic sequences for GTP-binding in small G-proteins.[51] These characteristic sequences include the P-loop/ Walker A $(G/A)X_4GK(T/S)$ motif for binding of the α- and β-phosphate groups, G2-loop (TTT) involved in Mg^{2+} binding, G3/ Walker B loop (DX_2G) for interaction with the γ-phosphate and Mg^{2+}, G4 loop (N/T)(K/Q)XD for interaction with the nucleotide and the G5 loop (T/G/C)(C/S)A for recognition of the guanine base.[51] GTP hydrolysis activity of reconstituted and as-isolated HydF has been confirmed with an enzymatic assay and the [4Fe4S] cluster is not required for GTPase activity.[51]

Spectroscopic studies were carried out to identify the fourth non-cysteine exchangeable ligand of the [4Fe4S] cluster in HydF.[51,239-242] A combination of EPR and HYSCORE spectroscopy showed that the fourth ligand of HydF is easily exchangeable with imidiazole.[51] The crystal structure of *apo*-HydF (i.e. without an iron-sulfur cluster bound) from *Thermotoga neapolitana* revealed that two conserved histidines close to the presumed cluster-binding cysteines, that could potentially bind the [4Fe4S] cluster of HydF.[243] All three cysteine residues of the binding motif are absolutely required for [4Fe4S] ligation, and the additional fourth ligand is proposed to be histidine.[239,240] HYSCORE spectroscopy confirmed the [4Fe4S] cluster ligation by a histidine from the protein backbone, but binding of histidine from a hexahistidine-affinity tag has been also detected.[241] However, since the fourth ligation position is an exchangeable site, it is very accessible to solvent, therefore a hydroxyl species was proposed to bind to the [4Fe4S] cluster.[242]

The first reported crystal structure of *holo*-HydF from *Thermosipho melanesiensis* (Tme) in 2017 represented the first crystal structure of HydF with [4Fe4S] cluster coordinated by a fourth labile non-cysteine ligand, glutamate (Figure 1.18).[244]

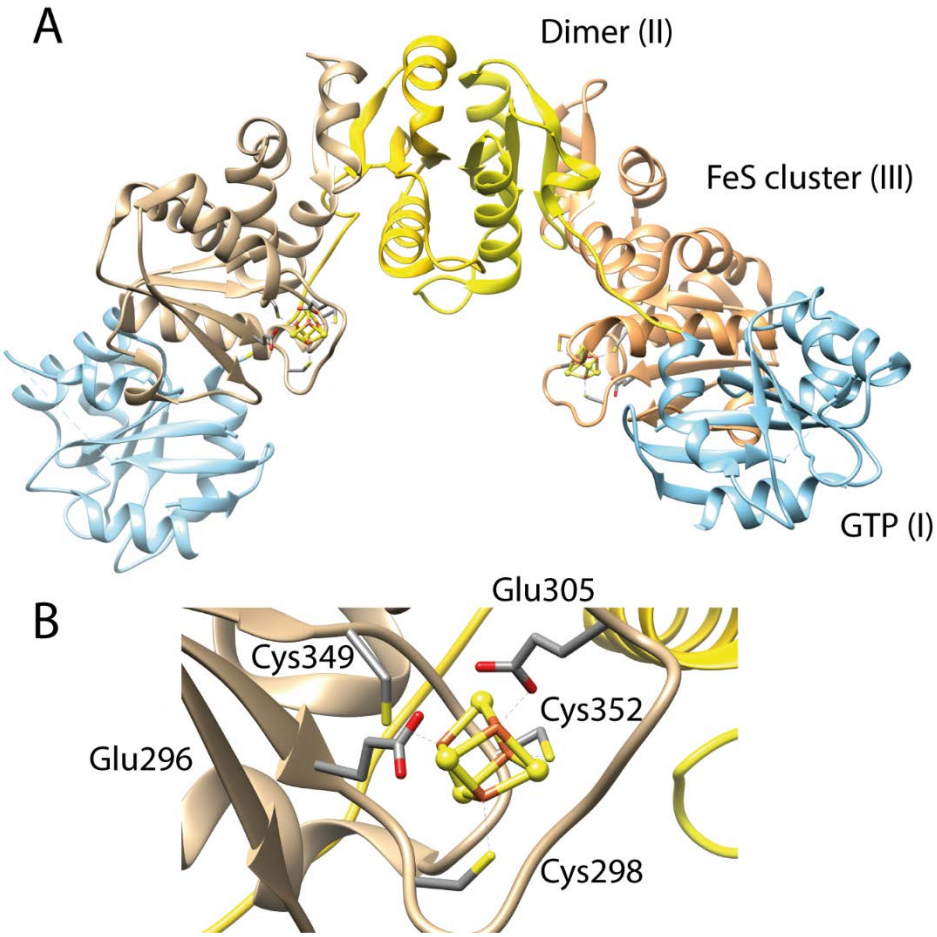

Figure 1.18: Crystal structure of TmeHydF with [4Fe4S] cluster (PDB: 5KH0)[244]. A: HydF dimer, with GTP-binding domain (I) in *blue*, dimerization domain (II) in *yellow* and FeS-cluster binding domain (III) in *beige*. B: Coordination sphere of the [4Fe4S] cluster with Glu305 as 4th ligand.[244]

The three domains observed in the TmeHydF monomer in the crystal structure are the *N*-terminal GTP-binding domain, the dimerization domain and the *C*-terminal iron-sulfur cluster binding domain (Figue 1.18). The TmeHydF structure consists of dimers, which have an open configuration, with a solvent exposed [4Fe4S] cluster.[243,244]

The fourth labile cluster ligand glutamate observed in this structure (Figure 1.18B) is proposed to bind an additional [2Fe] subcluster or a [2Fe2S] cluster as the precursor of the H-cluster.[245] In the maturation of the [FeFe]-hydrogenase HydF functions as a scaffold protein, transferring the H-cluster intermediate onto HydA leading to an active [FeFe] hydrogenase.[246] First evidence for an existing [2Fe] subcluster with CO and CN^- ligands in HydF, if coexpressed with HydG and HydE was given by Happe *et al.*[43] EPR and FTIR studies revealed similar signals for the [2Fe] subcluster to that of the active [FeFe]-hydrogenase, indicating the presence of a structurally related H-cluster

precursor in HydF and confirming the presence of CO and CN^- by FTIR.[43,246] Further evidence for the [2Fe] subcluster in HydF was given by X-ray absorption spectroscopy at the Fe K-edge of HydF showing repeatedly a similarity of the iron-iron and iron-sulfur distances of HydA with the di-iron cluster.[247] *Clostridium acetobutylicum* HydF is proposed to contain an additional [2Fe2S] cluster prior to interaction with HydG and HydE, which either serves as a scaffold or as a placeholder for the synthon $Fe(CO)_2CN$ synthesized by HydG.[248] Furthermore, spectroscopic studies with the additional [2Fe2S] accompanied with gel filtration experiments indicated an important role for the HydF dimer in the activation of the [FeFe]-hydrogenase.[249,250]

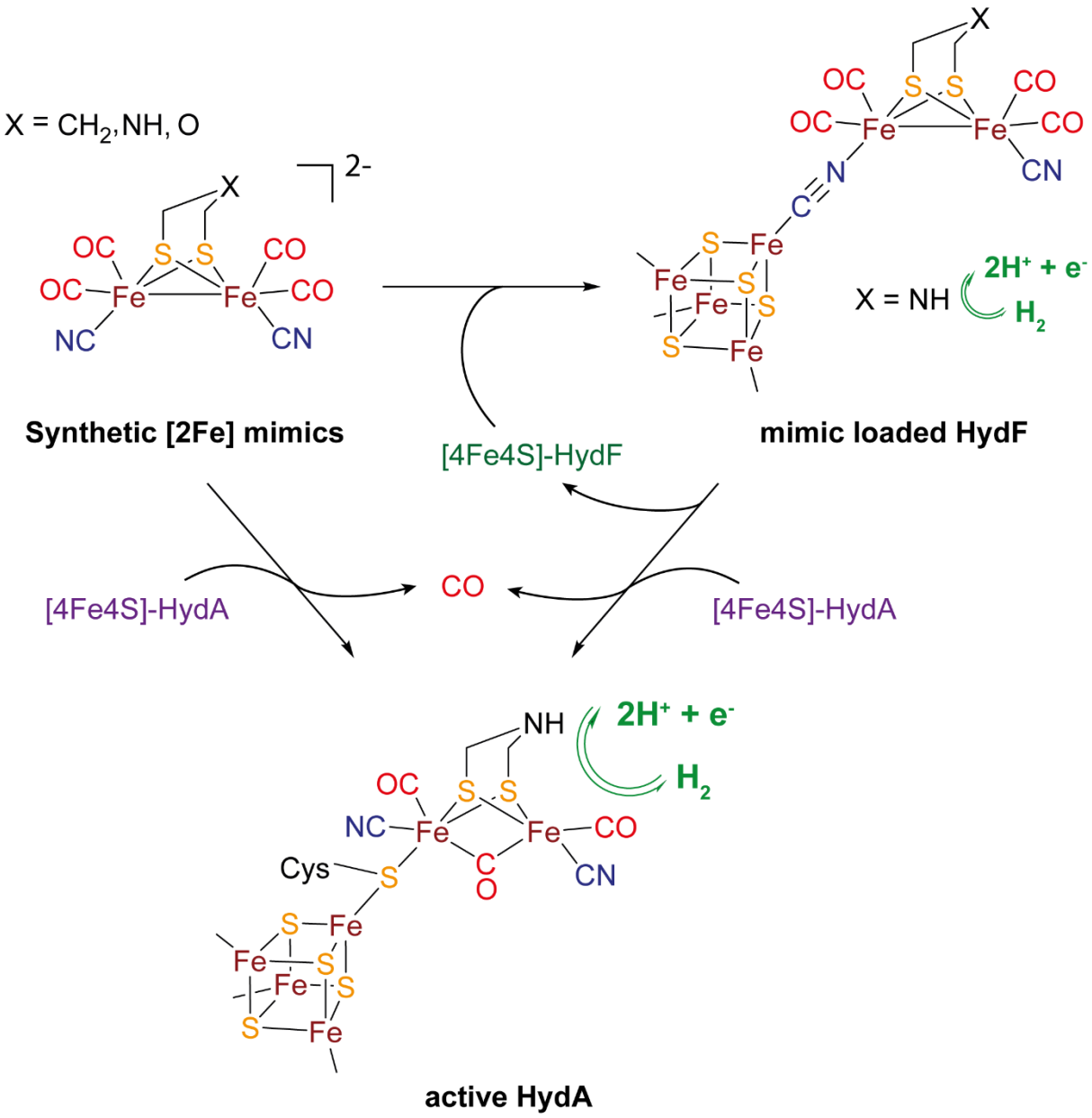

Scheme 1.18: Hydrogenase (HydA) and HydF activation for hydrogen production by using synthetic [2Fe] mimics. Adapted from [22].

An important contribution to understanding HydF's role in [FeFe]-hydrogenase was made by Fontecave *et al*. by using synthetic H-cluster mimics (with propanedithiolate (pdt), oxodithiolate (odt) or azadithiolate bridge (adt)) and loading them onto *Thermotoga maritima* HydF, which transfers the mimic onto *Chlamydomonas reinhardtii* apo-HydA1 (Scheme 1.18).[27] The resulting mimic-loaded HydA protein achieved full activation with the mimic containing the azadithiolate bridge. Moreover, HydF from *Thermotoga maritima* and *Thermosipho melanesiensis* loaded with the same adt-mimic also showed hydrogen evolution activity.[244] These observations confirmed HydFs role as a scaffold and transporter of the H-cluster precursor.

The function of GTP hydrolysis in [FeFe]-hydrogenase maturation is still unclear, GTP is not required for the transport of the [2Fe] precursor onto HydA.[27] Furthermore, HydF forms a dimer independent from the presence of GTP.[249] One known factor influencing GTPase activity of HydF are potassium cations, which increase GTP hydrolysis activity in HydF.[246] The effect of potassium has been thoroughly studied for the GTPase MnmE, which is hypothesized to stabilize the position of the attacking water molecule and thus the GTPase does not require a GTPase activating protein (GAP) to start the reaction.[251] Furthermore the presence of the maturation partners HydE and HydG enhanced HydFs GTPase activity by 50%.[246] Recent studies on the GTP-binding domain of HydF proposed its function to be a molecular switch upon GTP binding. By EPR/PELDOR spectroscopy, conformational changes are observed upon GTP-binding that suggest a similar mechanism to other small GTPases such as HypB[225] or UreG[234], where GTP activates the protein to carry out further reactions/interactions.[252]

Interaction studies between HydF and the partner [FeFe]-hydrogenase maturation enzymes HydG and HydE proposed a further role for GTP binding.[253] By using SPR and co-purification methods, the complex formation between HydF and either HydG or HydE has been characterized. Complex formation between the radical SAM enzymes HydG and HydE has not yet been observed. Moreover, HydF has been found to bind HydE with stronger affinity than HydG, but can not replace HydG in an already formed HydF:HydG complex.[253] Addition of GTP to a complex of HydF:HydE or HydF:HydG results in induced dissociation of these complexes, suggesting a mediating role for the maturase interactions. However, GTPase activity is not required for the interactions as variants of HydF lacking the important residues for GTP hydrolysis were still able to bind HydE and HydF with the similar affinity to wild-type HydF. Nevertheless, an important caveat should be applied to this study, as these experiments were carried out under aerobic conditions, which might have influenced the binding events between the maturases.[253] Further investigations are needed to resolve the role of GTP in the [FeFe]-hydrogenase maturation.

1.4. Aims of the thesis

The objectives of this thesis are to identify the mechanisms and interactions between the [FeFe]-hydrogenase maturation enzymes HydF, HydE and HydG from the anaerobic, thermophilic, spore-forming Gram-positive bacterium *Thermoanaerobacter italicus Ab9*. Some important questions needed to be answered to investigate the above-mentioned objectives:

- How to obtain a sufficiently reconstituted and concentrated homogenous HydF solution for crystallization?

- What is the coordination and ligand structure of ThitHydG's auxiliary cluster? Is cysteine contributing to the stabilization and formation of synthon iron complex?

- Which compounds are increasing the coupled activity of HydG, HydE and HydF? Which specific role might these compounds have?

- What kind of thiol-substrate is HydE using, is cysteine a potential substrate?

- What is the role of HydF's GTP hydrolysis in H-cluster maturation? Do the other maturation enzymes influence GTP hydrolysis?

- How tight does HydF bind to HydG or HydE under anaerobic conditions and with efficient reconstitution of the iron sulfur clusters? Which are the factors that influence binding or dissociation?

- What is the *holo*-structure of HydF? How does HydF bind the H-cluster precursor?

Chapter 2

Optimization of [FeFe]-hydrogenase maturation enzyme expression

2.1 Introduction

This chapter describes the experimental studies into a high-yield expression and purification system for reconstituted [FeFe]-hydrogenase maturation proteins HydE, HydG and HydF from *Thermoanaerobacter italicus*.

Obtaining fully reconstituted proteins after expression and purification facilitates the characterization of naturally bound substrates and/or cofactors.

The first identification of genes necessary for [FeFe]-hydrogenase activity was reported by Posewitz *et al.* in 2004[40] and revealed proteins responsible for the maturation of the [FeFe]-hydrogenase from *C. reinhardtii*: the fusion-protein HydEF and the HydG protein. The [FeFe]-hydrogenase protein HydA was co-expressed with either HydEF and/or HydG and tested for its hydrogen production activity. Full hydrogenase maturation and activity was achieved when co-expressed with HydEF and HydG.[40]

In following studies, the radical SAM enzymes HydE and HydG from *Thermotoga maritima* were separately expressed from an IPTG-inducible vector for characterization. After the anaerobic chemical reconstitution of their iron-sulfur clusters, the radical SAM enzymes were spectroscopically characterized.[52] Both enzymes have been shown to carry at least one [4Fe4S]-cluster. In the crystal structure of *Thermotoga maritima* HydE, besides the already spectroscopically observed [4Fe4S]-cluster, a second [2Fe2S]-cluster[53] is coordinated by three cysteines in the second binding site. The second cluster binding site **C**X_7**C**X_2**C** is not conserved across all HydE proteins (Figure 2.1) and the presence of a second [4Fe4S]- or [2Fe2S]-cluster is not required for [FeFe]-hydrogenase maturation and activity.[53]

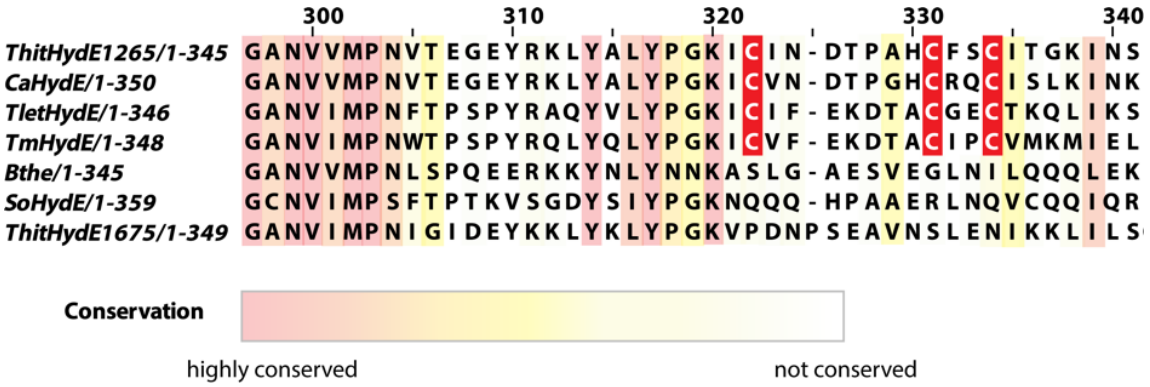

Figure 2.1: Alignment of the *C*-terminal domains in HydE proteins from different organisms. Cysteine binding motifs for a potential auxiliary [4Fe4S]- or [2Fe2S]-cluster are highlighted in *red*. The alignment was generated with ClustalW[254,255] and JalView[256].

HydG has been suspected to carry an auxiliary *C*-terminal [4Fe4S]-cluster in addition to the radical SAM [4Fe4S]-cluster (Figure 2.2).[56] The triple alanine sequence variant of the radical SAM cluster binding site cysteines in *Clostridium acetobutylicum* HydG confirmed the presence of an auxiliary [4Fe4S]-cluster, which is crucial for enzyme activity.[60] Upon crystal structure determination of *Themoanaerobacter italicus* HydG and spectroscopic studies on *Shewanella oneidensis* HydG, the auxiliary cluster was redefined as [4Fe4S][(Cys)Fe]-cluster, carrying an additional iron, which transforms into the synthon [(Cys)Fe(CO)$_2$CN] after tyrosine cleavage.[64,66]

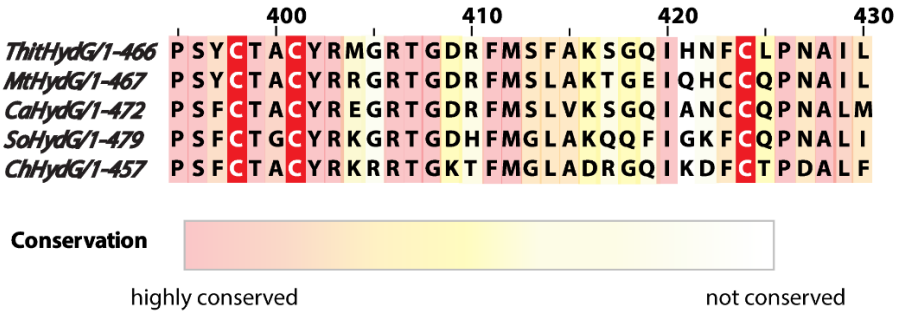

Figure 2.2: Alignment of the *C*-terminal domains in HydG proteins from different organisms. Cysteine binding motifs for auxiliary [4Fe4S]-cluster are highlighted in *red*. The alignment was generated with ClustalW[254,255] and JalView[256].

HydF from *Thermotoga maritima* has been expressed from an IPTG-inducible vector and classified as a GTPase carrying one [4Fe4S]-cluster after chemical reconstitution. Three conserved cysteine residues **C**X**H**X$_n$**HC**X$_2$**C** are involved in [4Fe4S]-cluster coordination and the coordination by a fourth histidine or water ligand is under investigation (Figure 2.3).[51,239]

The fourth ligand coordinating the [4Fe4S]-cluster in His_6-HydF is exchangeable and can be replaced with imidazole or histidine from the affinity tag. The recent crystal structure of *Thermosipho melanesiensis* HydF with bound [4Fe4S]-cluster (PDB: 5KH0) revealed a glutamate carboxylic group as a fourth ligand.[244] Almost all bacterial HydF proteins carry an acidic amino acid at this position (see Figure 2.3). Furthermore, the cluster is surrounded by highly conserved positive charged residues (R, H and K). The glutamate ligand is proposed to be crucial for H-cluster precursor binding.

Figure 2.3: Alignment of [4Fe4S]-cluster domains in HydF proteins from different organisms. Conserved amino acids involved in [4Fe4S]-cluster coordination are highlighted in *red*, wherease potential H-cluster precursor ligands are highlighted in *orange*. The alignment was generated with ClustalW[254,255] and JalView[256].

There are conflicting opinions about the existence of an additional [2Fe2S]-cluster bound to HydF. While the crystal structure of *Tme*HydF is clearly lacking any obvious binding site for a [2Fe2S], there has been spectroscopic evidence for a [2Fe2S]-cluster in *Ca*HydF, although the functional significance, if any, has yet to be demonstrated.[244,248-250]

Several strategies have been developed to improve the expression of HydF to increase the incorporation of cognate iron-sulfur clusters.[43,48-50,245-247] The first homologous expression and purification of a Strep-tagged HydF from *Clostridium acetobutylicum* has been carried out by Happe *et al.* under strict anaerobic conditions.[43] StrepHydF was expressed in the presence of HydE and HydG, isolated upon purification and subsequently spectroscopically characterized. The characterization with EPR, FT-IR and EXAFS supported the presence of a binuclear [2Fe2S]-cluster and confirmed bound CO and CN ligands.[43,247] Without chemical reconstitution, the protein only binds between 1.12 to 3.3 Fe equivalents per monomer.[244,50]

A second approach to improve expression of naturally reconstituted [FeFe]-hydrogenase maturation proteins, such as *holo*-HydF, used by our group, includes the full *E. coli* ISC machinery in the pBAD expression vector in an effort to improve the likelihood of iron-sulfur cluster incorporation during expression. The *Thermoanaerobacter italicus* HydG protein was successfully produced and characterized from this ISC machinery containing pBAD vector. We have chosen a Strep-Tag as affinity-tag for HydF and HydE expression to prevent additional ISC coordination from histidine residues of the His_6-Tag.[239] More importantly, the imidazole used in the His_6-Tag purification protocol can bind to and strip out labile iron-sulfur clusters, which does not occur with the Strep-Tag.

A similar approach by Fontecilla-Camps *et al.*[68] was to include the ISC operon in a separately supplemented vector and therefore improving incorporation of FeS cluster by co-expression with the vector that carries the ISC and MetK operon. The gene *metK* encodes for the *S*-adenosylmethionine synthetase and might increase the stability of the radical SAM proteins by overproducing SAM, which may bind to the cluster.

Another way to achieve reconstitution of the iron-sulfur cluster in HydF is the addition of iron and sulfide during lysis of the *E. coli* expression host cells, this method was used for the binding studies between the [FeFe]-hydrogenase maturases of *Clostridium acetobutylicum*.[253]

Alternatively adding an iron-source and the potential sulfide precursor, cysteine, to expression media alongside other additives also yielded in partially or fully reconstituted and active protein, as shown by Swartz *et al.*[50]

Cluster assembly for [FeFe]-hydrogenase maturases during (over-)expression can be enhanced by the use of an *E. coli* BL21 (DE3) strain mutated so that it lacks the regulator gene for the ISC machinery Δ*iscR*.[257] Since the regulator is knocked out, these cells cannot down-regulate the expression/production of iron-sulfur cluster biosynthetic machinery and the whole ISC pathway is overproduced. Overproduction of ISC leads to better incorporation of iron-sulfur cofactors in the heterogeneously expressed protein (schematically described in Figure 2.4).

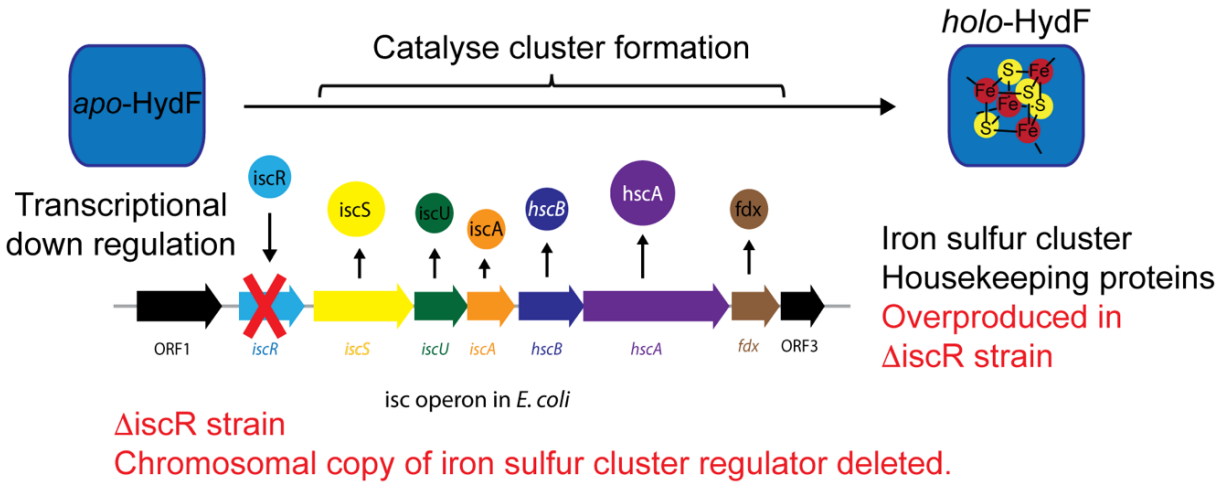

Figure 2.4: Schematic description of the ΔiscR *E. coli* strain and its possible effects on HydF expression.

2.2 pBAD expression systems

The promotor of the *E. coli* arabinose operon pBAD and its regulatory gene araC are incorporated into pBAD expression vectors.[258] The AraC protein also regulates the Pc promotor, which transcribes in the opposite direction as pBAD.[259] In the absence of arabinose, AraC binds to operator O_2 and I_1 sites as an elongated dimer. The distance between these operators is critical for AraC repression. The dimeric bound conformation of AraC prevents the binding of the catabolite activator protein (CAP) and the RNA polymerase and acts as a repressor. Upon arabinose binding to the regulatory sites of AraC, AraC changes to a compact dimer confirmation, releases the DNA loop and binds to the neighboring I_1 and I_2 operators, enabling CAP and RNA polymerase binding and therefore activating gene expression (Figure 2.5).[260- 262]

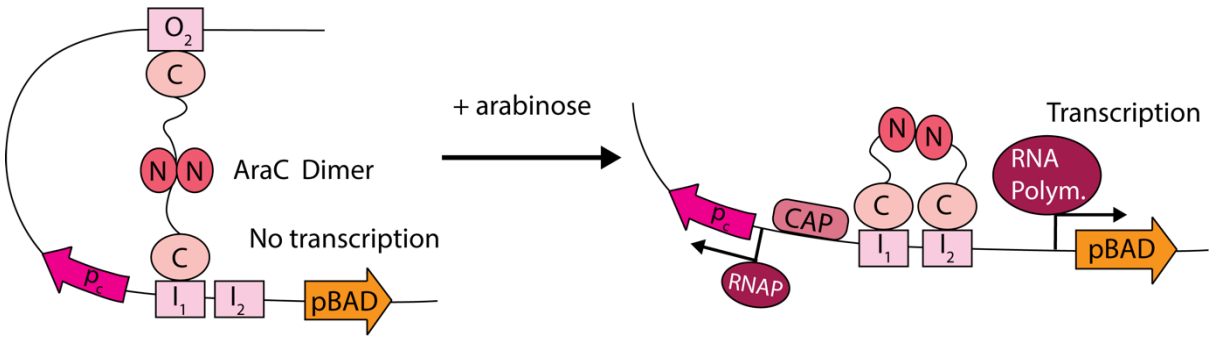

Figure 2.5: Schematic description of the arabinose operon.

The most important characteristics of the pBAD expression system is the dose-dependent induction that modulates different expression levels, which allows precise control for optimal yields. Tight control enables the expression of toxic proteins and optimization of protein solubility. A drawback of the pBAD expression system is the lack of cell homogeneity, since the population generated is a mixture of induced and un-induced cells. The potential for protein overexpression is also lower than for the stronger T7 promotor mediated expression.[263, 264]

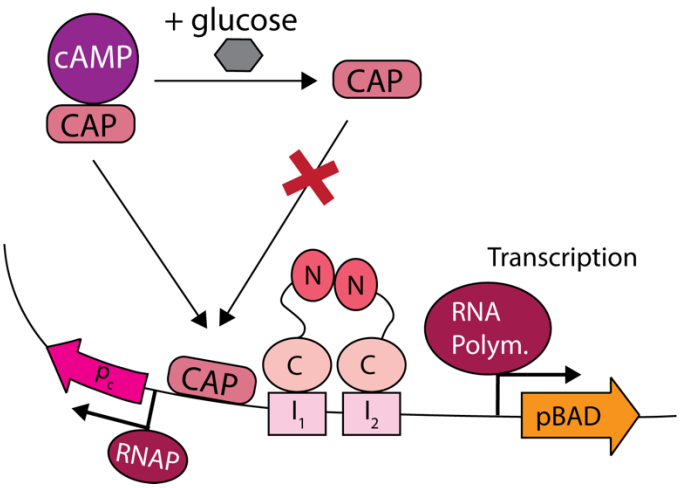

Figure 2.6: Schematic description on how high glucose concentrations result in reduced expression levels. Glucose is lowering cAMP levels, but cAMP is crucial for activation of CAP, which is binding to the DNA.

High glucose concentration in the growth medium (e.g. more than 0.2% (w/v) concentration) leads to repression of basal expression. Glucose indirectly lowers the concentration of the 'hunger signal' molecule cAMP, and cAMP is binding to and activating CAP prior to binding the DNA. Therefore, lower cAMP levels are linked to lower CAP binding and decreased transcriptional activation (Figure 2.6).[257,265]

2.2.1 Generation of pBAD expression vectors

Amino acid sequences from putative *Thermoanaerobacter italicus Ab9* HydF, HydE1265 and HydE1675 proteins were taken from the UniProt and NCBI database (accession codes D3T5I7, D3T2S6, D3T3X2, respectively).[266-268] There are two putative HydE proteins in *Thermoanaerobacter italicus*, which differ in iron-sulfur cluster binding sites, although the potential for different activities has not been reported. The corresponding genes *hydF*, *hydE1265* and *hydE1675* were codon optimized for heterologous expression in *Escherichia coli* with the Invitrogen GeneArt

Tool. Furthermore, genes were modified to include specific restriction sites for insertion into the desired vector and insertion or deletion of affinity tags. Finally, a StrepII-Tag was inserted into the *N*-terminal part of the *hydF*, *hydE1265* and *hydE1675* gene sequence and the open-reading-frame sequence was generated with the program pDraw32.

All final genes coding for StrepThitHydF, StrepThitHydE1265 and StrepThitHydE1675 were commercially synthesized by Invitrogen GeneArt and supplied in a GeneArt plasmid, specifically pMA-RQ_ThitStrepHydF2142, pMA-ThitStrepHydE1265 and pMA-ThitStrepHydE1675. To simplify the notation, StrepThitHydE1265 is called StrepThitHydE1 in the text and StrepThitHydE1675 notified as StrepThitHydE2, but in Figures and Tables the full numbering still persists. The abbreviation for the organism: Thit (*Thermoanaerobacter italicus*) is left out in the text, since all proteins mentioned in the following belong to this organism.

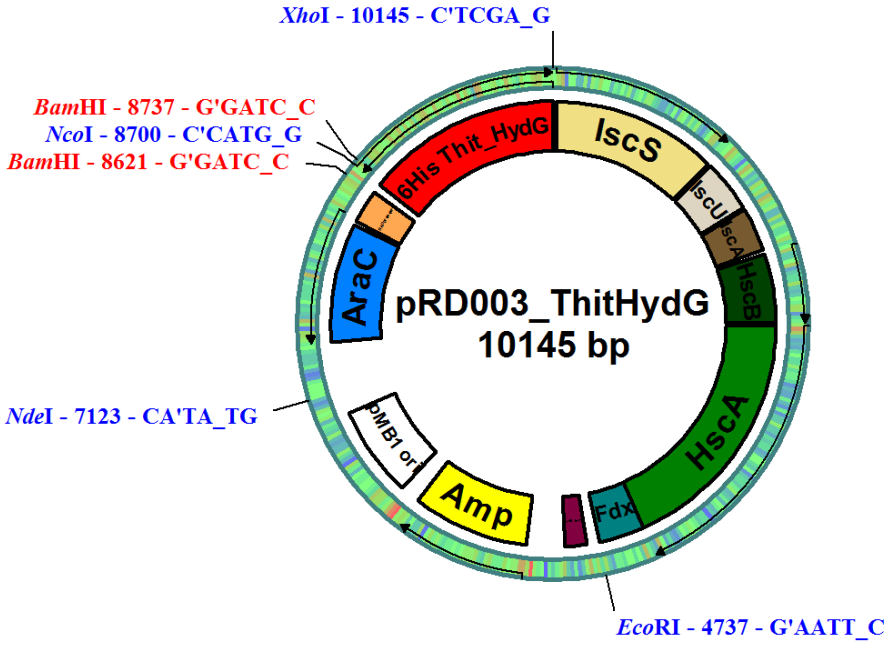

Figure 2.7: Plasmid map of pRD003_ThitHydG with ampicillin resistance and *E. coli* ISC operon.

The assembly of expression vectors builds on the work of Dr. R. C. Driesener[269] who assembled pRD003_ThitHydG, a pBAD derived plasmid encoding for His_6-tagged HydG followed by the downstream ISC operon. To clone each specific [FeFe]-hydrogenase maturase gene into the pRD003-backbone vector (Figure 2.7) the corresponding GeneArt plasmids were amplified and digested with restriction

enzymes NcoI and XhoI. The same enzymes were used to digest the pRD003 backbone as well. Digested fragments were separated and purified on agarose gels (see Figure 2.8).

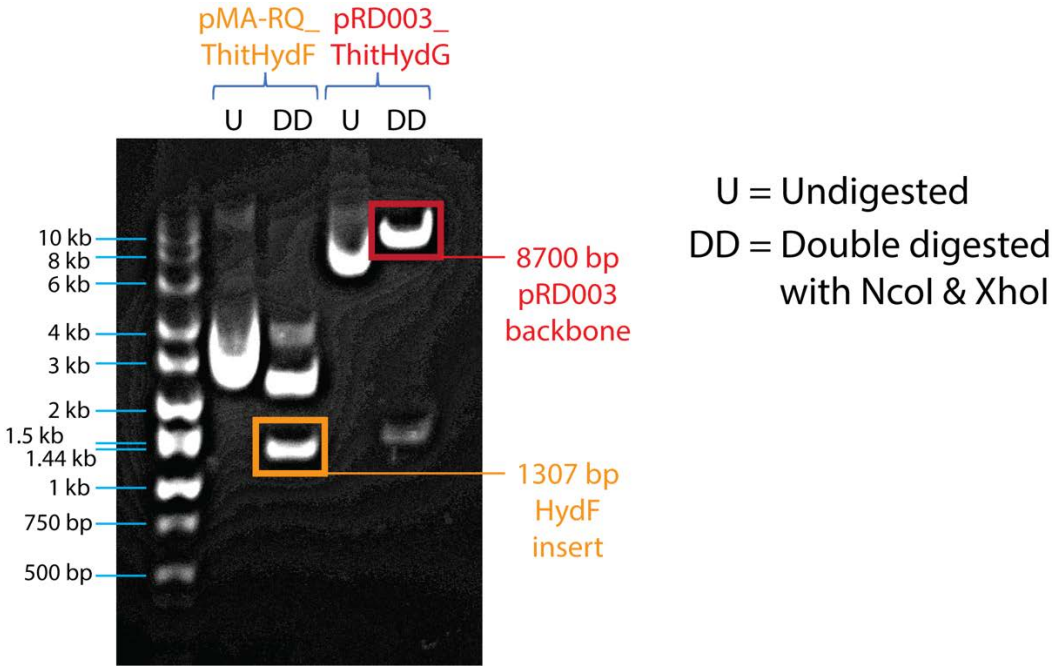

Figure 2.8: Agarose gel of preparative digest of pMA-RQ_HydF and pRD003_ThitHydG.

Table 2.1: Sizes of DNA fragments used to ligate [FeFe]-hydrogenase maturases with the pRD003 vector backbone.

Fragment	HydF insert	HydE1265 insert	HydE1675 insert	pRD003 vector backbone
Size (bp)	1307	1105	1117	8700

Gel extracted fragments (Table 2.1) were prepared for ligation reactions and the pRD003 vector backbone was ligated with either HydF, HydE1 or HydE2 inserts in a 1:3 insert to vector ratio. Ligation reactions (Method 7 and 9) were transformed into *E. coli* JM109 cells, grown on solid selective 2YT media (supplemented with 100 μg/mL ampicillin) and the resultant ligated plasmids isolated. These were subjected to analytical digests and analyzed *via* agarose gel electrophoresis (Figure 2.9). Positive ligated plasmids carrying fragments of the anticipated size, were re-transformed into *E. coli* JM109 and BL21(DE3) cells for expression studies.

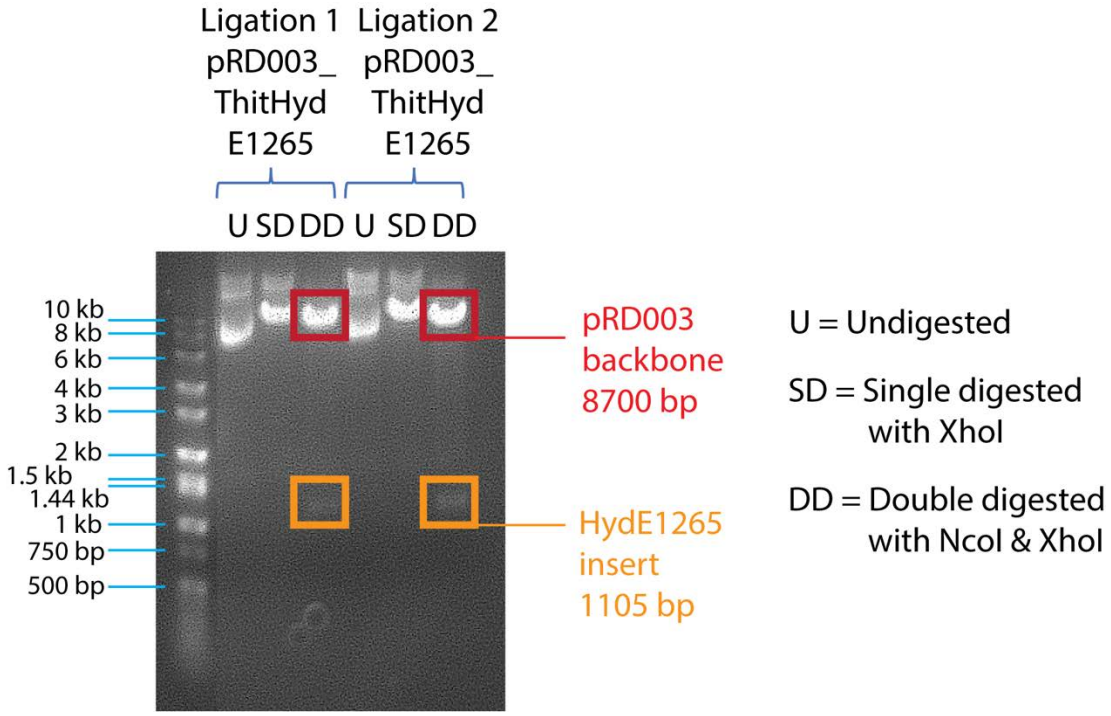

Figure 2.9: Analytical digest of ligated plasmids pRD003_ThitHydE1265 and pRD003_ThitHydE1675, to confirm the right sizes of inserted fragments. Two extracted plasmids from independent ligation colonies from pRD003 ligated with ThitHydE1265. The insert size of HydE1265 is 1105 bp, which corresponds to the DNA band seen on the gel. If the ligation would have been unsuccessful we would observe the HydG insert size of 1445 bp.

The characteristics of the newly generated pBAD derived plasmids for HydF and HydE expression are summarized in Table 2.2.

Table 2.2: Newly generated pRD003 derived plasmids, with characteristics of the corresponding inserted protein genes.

Plasmid Name	**pBMW001_ Strep*Thit*HydF**	**pBMW002_ Strep*Thit*HydE1265**	**pBMW003_ Strep*Thit*HydE1675**
Plasmid Size	10007 bp	9805 bp	9817 bp
Protein Name	Strep*Thit*HydF	Strep*Thit*HydE1265	Strep*Thit*HydE1675
Protein Size	47539.4 Da	41214.7 Da	41269.1 Da
Amino acids	426	362	366
pI	6.69	8.87	8.56
ε_{ox}	37025 1/cm·M	28350 1/cm·M	31330 1/cm·M

Proteins also encoded in the pBAD-derived newly generated vectors belonging to the ISC cluster machinery are listed in Table 2.3.

Table 2.3: Characteristics of *Escherichia coli* ISC machinery proteins.

Name	Protein Size/ kDa	Protein Function
IscS	45	*E. coli* cysteine desulfurase[270]
IscU	13.9	Scaffold Protein[271]
IscA	11.5	A-type cluster carrier protein[272]
HscA	65.7	DnaK-like chaperone[273]
HscB	20.1	DnaJ-like co-chaperone[274]
Fdx	12	Redox protein, electron source/acceptor[275]

2.2.2 Expression and purification of StrepHydF and StrepHydE

For initial protein expression trials, small scale expression studies with different sets of conditions have been carried out for the HydF and HydE proteins from the pBAD derived vector. Conditions were screened for optimization of protein yield and solubility. The general procedure of small scale expression and their analysis is described in Method 11.

Starting conditions were adapted from Dr. R. C. Driesener[269] and small scale expression cultures were grown at three different temperatures, each for a different time duration. The media was supplemented with 0.5% (w/v) glucose and with 50 mM K_2HPO_4 (pH 7.4) buffer.[246,269]

Three different growth conditions were tested after induction: the temperature was changed to 27°C for 4 h, 16°C for 18 h or to 4°C for 18 h.

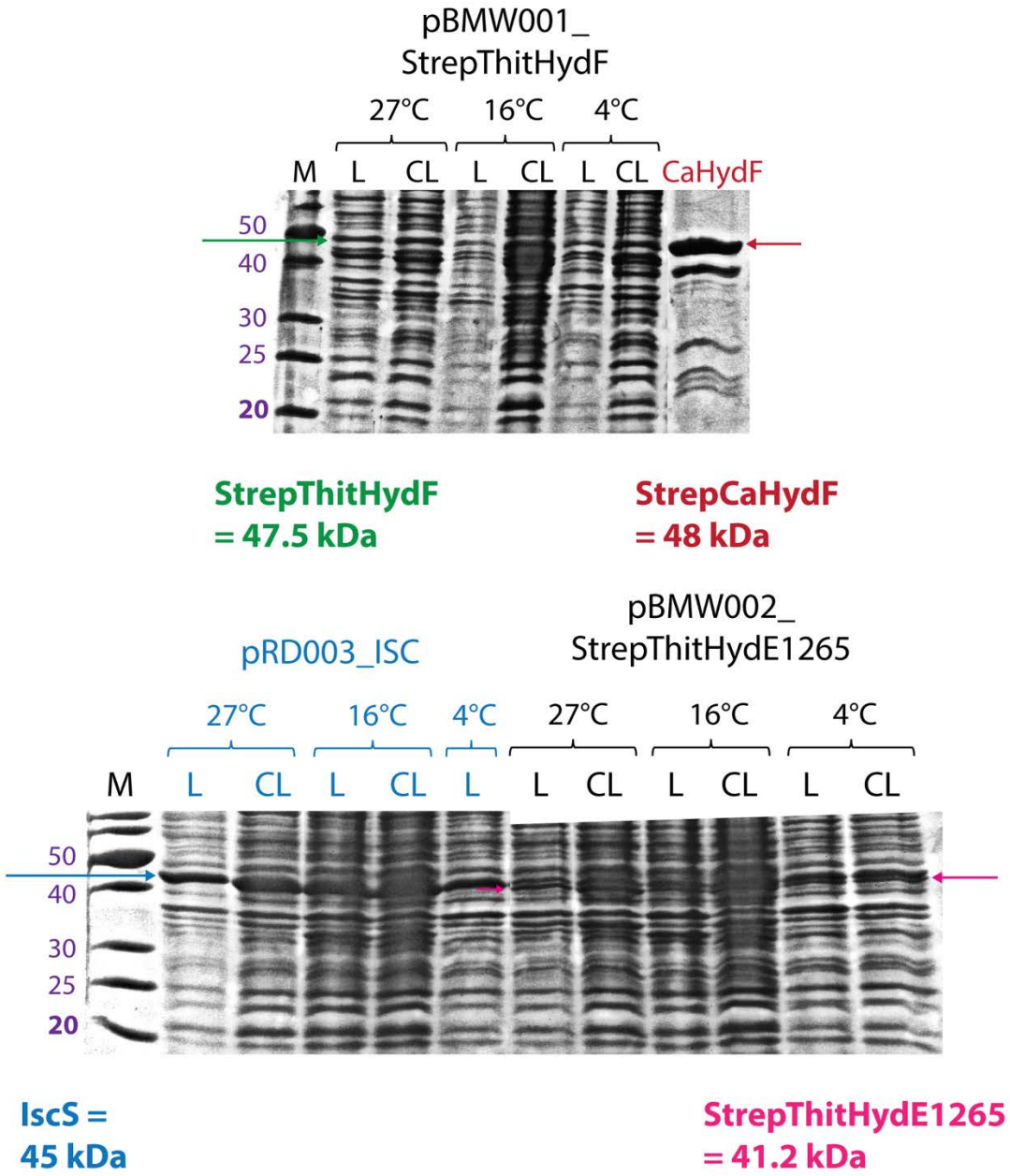

Figure 2.10: SDS-PAGES of small scale expressions of HydF, ISC and HydE1265. L: Lysate, CL: Clear Lysate/Supernatant. Top: Test expression of StrepThitHydF with a loaded reference of StrepCaHydF with similar molecular mass. Bottom: Test expression of StrepThitHydE1265 in comparison of the expression of an empty pRD003_ISC vector.

Analysis of resultant cell pellets and cleared lysate with SDS-PAGE clearly showed the expression of StrepThitHydF (47.5 kDa), if compared to a reference sample of StrepCaHydF (*Clostridium acetobutylicum* HydF) with a similar molecular mass of 48 kDa. An expression temperature of 27°C appears to give the highest yield of soluble protein as estimated by the strength and thickness of the protein bands in comparison to the other temperatures (Figure 2.10). However, the expression levels of

StrepHydE1 and StrepHydE2 were very low compared to HydF and it was difficult to confidently assign a HydE protein band on the SDS-PAGE based on the position of the 40 kDa standard. Only a very weak band was observed at ~ 40 kDa, one interpretation of which is that HydE proteins might be toxic for the cells. A very thick band at 45 kDa, corresponding to the ISC machinery protein IscS might have obscured the protein band of HydE as well.

Building on the expression observed in the small scale StrepHydF expression experiments, larger scale expression studies have been extensively optimized. Maximum protein yields in *E. coli* BL21 (DE3) cells with the same additives as in small scale expression experiments were 6 mg/L 2YT medium for the 27°C, 5 h expression (Table 2.4, Figure 2.11).

Transformation of the pBMW001_StrepThitHydF plasmid into the *E. coli* ΔiscR BL21 (DE3) strain improved the expression yields significantly. No extra glucose or phosphate buffer was added to the media and the arabinose concentration ranged from 5-10 mg/L. Supplementing the media with glucose > 0.2%, might have had a negative impact on the protein yield, as discussed in section 2.2. The best results were achieved with an overnight growth at 16°C. which yielded 12 mg HydF/L of culture after an anaerobic purification (Table 2.4, Figure 2.12).

Table 2.4: Data of two example expressions of pBMW001_StrepThitHydF aerobically and anaerobically purified. Highest yield expression and purifications of HydF protein are represented in the following two Figures 2.11 and 2.12.

	Aerobic	**Anaerobic**
Type of expression cells	*E. coli* BL21 (DE3)	*E. coli* ΔiscR BL21 (DE3)
Volume of culture	5 L	5 L
OD_{600}	0.8	1.0
Arabinose concentration (mg/mL)	10	5
Expression conditions	27°C, 5 h	16°C, on
Cell Mass (g)	72	108
Buffer	Tris (50 mM)	HEPES (25 mM)
Reducing agent (1 mM)	DTT	DTT
Protein yield (total in mg)	32	61
Protein yield (mg/L)	6	12

Purification of resultant cell pellets has been carried out aerobically for *E. coli* BL21 (DE3) cultures (Figure 2.11) and anaerobically for *E. coli* ΔiscR BL21 (DE3) expression cultures (Figure 2.12) with StrepTactin® high capacity resin (50 mL, XK26/50). Purification buffers were varied in the optimization process. Initially, a Tris-based buffer with KCl (150 mM) and DTT (1 mM) as reducing agent were used, but as the purified protein was unstable in this buffer upon concentration as well as reconstitution, conditions were modified to HEPES-based buffer with higher salt concentration (300 mM KCl) similar to that successfully used for ThitHydG[64]. To improve the iron-sulfur cluster/reconstitution state and solubility of HydF, trials with stronger reducing agent sodium dithionite containing buffers were made. After further chemical reconstitution in sodium dithionite-containing buffer, bound FeS colloids could not been removed by subsequent gel filtration chromatography, and sodium dithionite was consequently removed from the buffers.

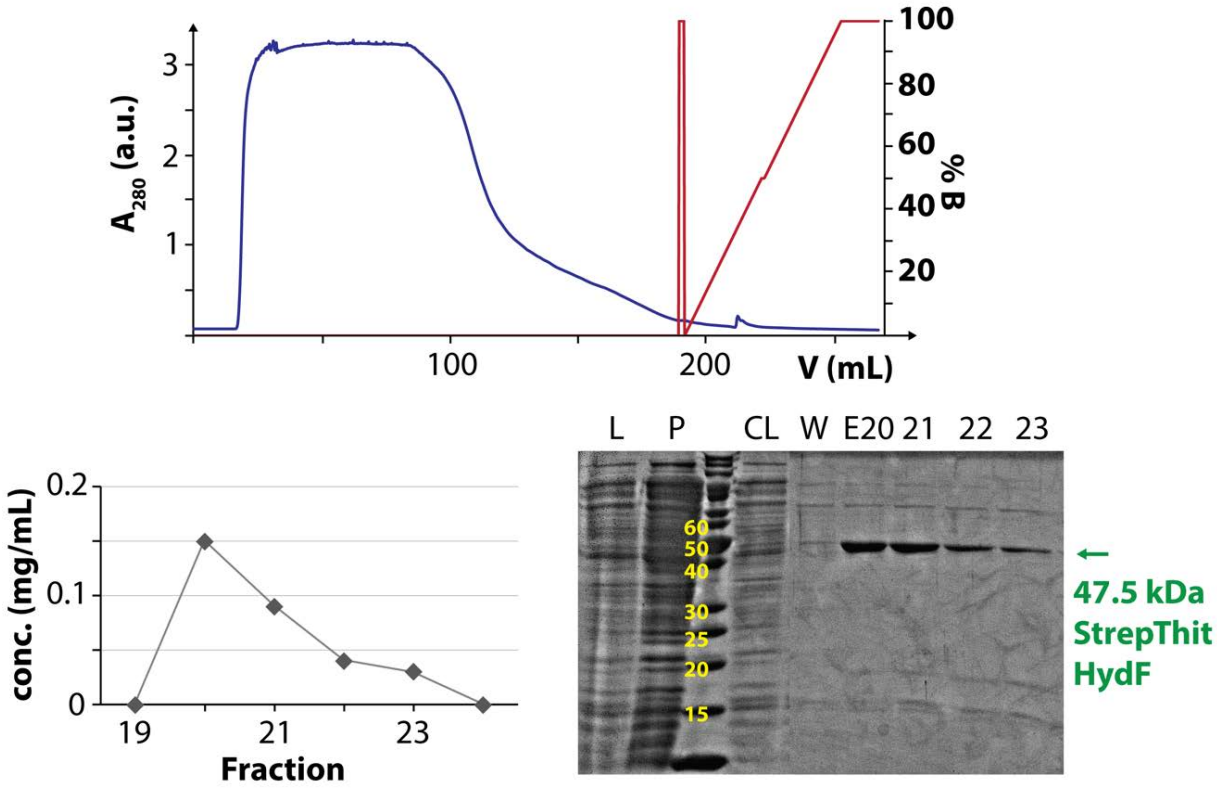

Figure 2.11: Selected example of a purification chromatogram of an aerobic StrepHydF purification from an *E. coli* BL21 (DE3) expression, the appropriate SDS-PAGE and results from the Bradford assay of the HydF fractions. The aerobic purification corresponds to the one described in Table 2.4. L: Lysate, P: Pellet, CL: Cleared Lysate, W: Wash fraction/Flow through, E20-23: Elution fractions.

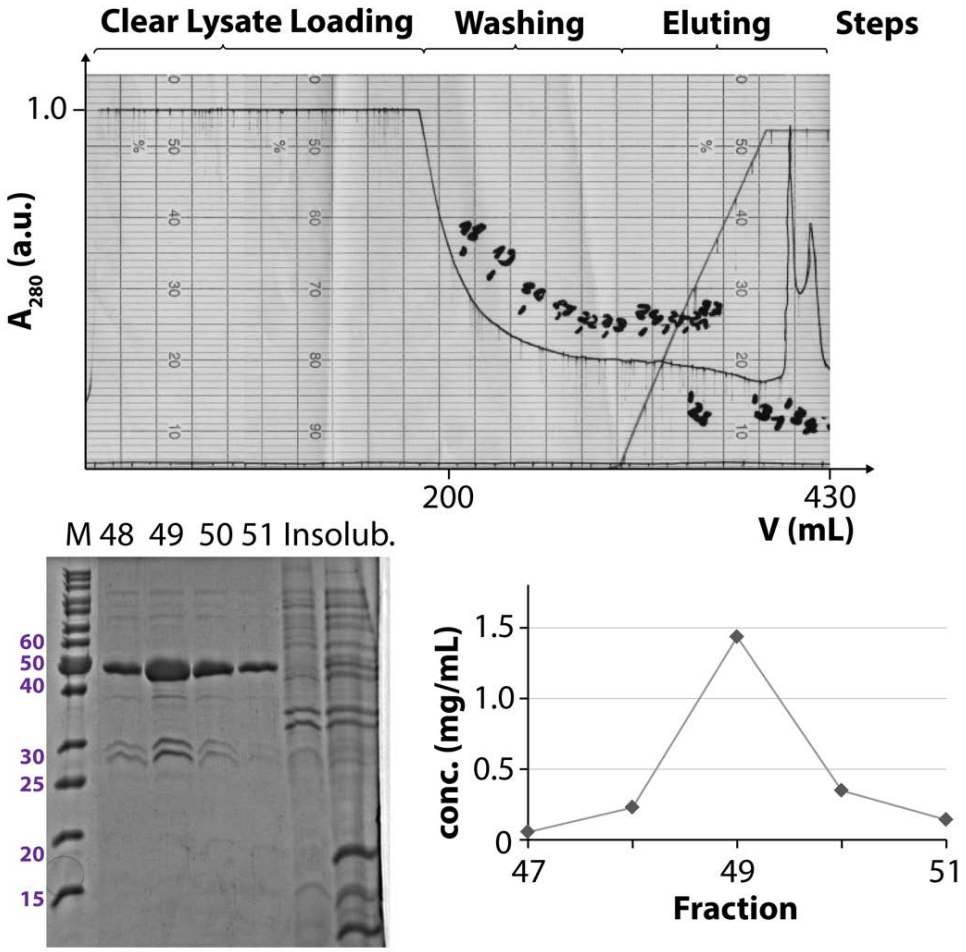

Figure 2.12: Selected example of a purification chromatogram of an anaerobic StrepHydF purification from an *E. coli* BL21 (DE3) ΔiscR expression and the appropriate SDS-PAGE and results from the Bradford assay of the HydF fractions. The anaerobic purification corresponds to the one described in Table 2.4.

Concerning the two HydE proteins, both expression vectors pBMW002_StrepThitHydE1265 and pBMW003_StrepThitHydE1675 were directly transformed into *E. coli* BL21 (DE3) and ΔiscR BL21 (DE3) cells for large scale expression. Large scale expressions experiments (5 L cultures) were carried out by R. Squire and were unsuccessful with pBMW002_StrepThitHydE1 for both cell strains, since the cells containing this plasmid did not grow. The expression and purification of StrepHydE2 yielded small amounts of protein (less than 1 mg) and had been cultured after induction at 37°C for 6 h. The resultant StrepThitHydE2 protein was assayed by HPLC using SAM and dithionite as substrates, but did not show the formation of DOA, which is indicative of uncoupled reductive SAM cleavage activity. The low expression

levels observed for HydE2 (Figure 2.13 and Table 2.5) suggests HydE2 production is very low, which might result from the HydE proteins being toxic for the cells.

Table 2.5: Data from expressions of pBMW002_StrepThitHydE1265 and pBMW003_StrepThitHydE1675 anaerobically purified. The purification of StrepThitHydE1675 is shown in Figure 2.13.

	pBMW002_StrepHydE1265	**pBMW003_StrepHydE1675**
Expression cells	*E. coli* ΔiscR BL21 (DE3)	*E. coli* BL21 (DE3)
Volume of culture (L)	5	5
OD_{600}	-	0.6
Arabinose (mg/mL)	-	10
Expression conditions	37°C, 6 h	37°C, 6 h
Cell Mass (g)	no growth	14.6
Buffer	-	Tris
Reducing agent	-	1 mM DTT
Protein yield (total)	-	Less than 1 mg
Protein yield (mg/L)	-	-

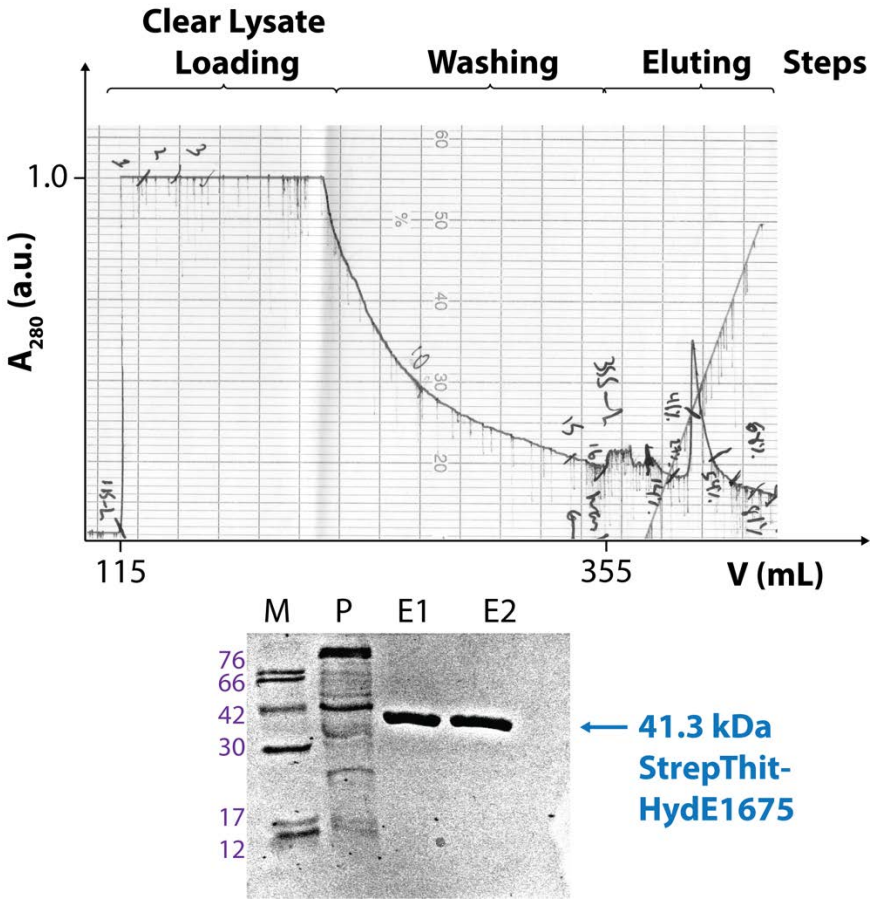

Figure 2.13: Chromatogram of an anaerobic purification of StrepThitHydE1675 and the corresponding SDS-PAGE. M: Marker, P: Pellet, E1-2: Elution fractions. The anaerobic purification corresponds to the one described in Table 2.5.

2.2.3 Expression and purification of His_6HydG

The heterologous expression and purification of His_6*Thit*HydG in *E. coli* BL21 (DE3) was optimized by Dr. P. Dinis[64,276] and the same protocol was used for the studies described herein (Figure 2.14, Flow Chart). HydG was produced under reduced oxygen levels in a fermenter (Method 13) in 2YT media. At an OD_{600} between 0.7-0.8 the 5 L 2 YT culture was induced with 250 mL 20% (w/v) arabinose (10 mg/mL final concentration). After a period of 5-6 h at 27°C in average 5-7g/L of cell pellet was collected by centrifugation.

The yield of protein after NiNTA affinity chromatography was on average 94 ± 11 mg/L of cultured media, with some loss of protein during buffer exchange (typically 100 mg from a total of 450 mg isolated), and some precipitation occurring during reconstitution and size exclusion chromatography (for example, 150 mg from a total of 350 mg isolated). The final yield after the last protein concentration step was approximately 200 mg at a concentration of 55 mg/mL. One of the critical steps to obtain an active HydG with auxiliary [Fe(κ^3-Cys)]·[4Fe4S]-cluster are careful slow reconstitution steps, addition of correct iron and sulfide equivalents (calculated as 10 and 5 equivalents relative to the protein concentration determined by the method of Bradford[277]). A second critical step was a well resolved separation between the high molecular weight FeS-colloid-bound HydG (observed as a black band on the column) (retention time 30 mins) and gold-brown colored reconstituted HydG (retention time 40 mins) using an S200 size exclusion column (volume 300 mL, internal diameter 26 mm). Moreover, the resultant HydG (Table 2.6) is very stable and can be stored at 1 mM concentrations at -80°C.

Table 2.6: Data from a typical fermenter expression of pRD003_His_6ThitHydG.

	pRD003_His_6ThitHydG
Expression cells	*E. coli* BL21 (DE3)
Volume of culture (L)	5
OD_{600}	0.7
Arabinose (mg/mL)	10
Expression conditions	27°C, 6 h
Cell Mass (g)	30
Buffer (20 mM)	HEPES
Reducing agent	1 mM DTT
Protein yield (total)	200
Protein yield (mg/L)	40

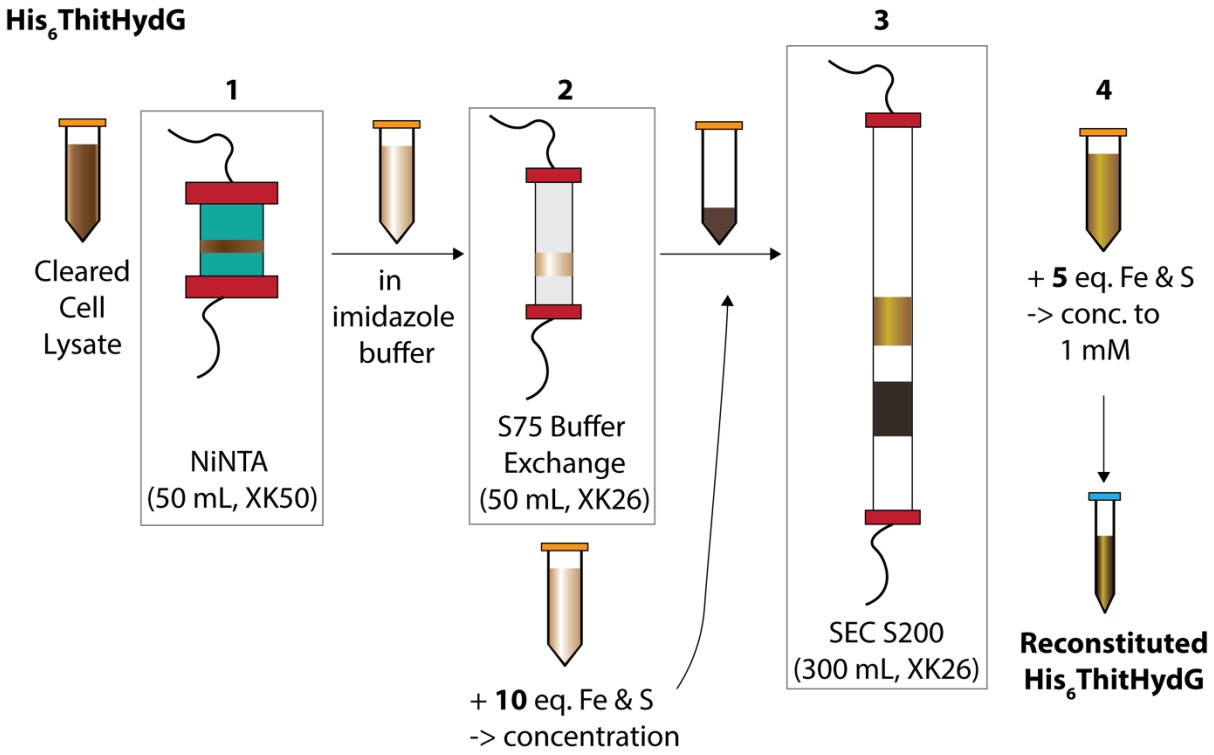

Figure 2.14: Purification flow chart for His_6ThitHydG. **1**: Cleared Lysate applied to NiNTA column, eluted brown fractions in high imidazole buffer. **2**: Brown fractions are buffer exchanged on S75 column, resultant protein fractions are combined and reconstituted with 10 equivalents of Fe and S and concentrated to 3 mL. **3**: Reconstituted protein applied to S200 size exclusion column to separate purified reconstituted protein (eluting second) from FeS-aggregated protein (eluting first). **4**: Gold brown fractions of His_6ThitHydG reconstituted with 5 eq. of Fe and S and subsequently concentrated to 1 mM, aliquoted and stored at -80°C. (Method 15).

HydG is typically reconstituted with 10 equivalents of iron and sulfide prior to SEC, since it is assumed[64,66] to carry up to 9 equivalents of iron and sulfide in its native state. The iron-sulfur clusters of HydG are delicate and readily break down, so that a fair amount of iron-sulfur cluster is lost (approximately 40% as estimated by UV-Vis) while passing through the S200 size exclusion column. The studies of Dr. P. Dinis[276] indicated that after SEC, a second reconstitution of HydG is required (Fig. 2.14, purification flow chart), this time with 5 equivalents of iron and sulfide.

The purification method of His_6*Thit*HydG was modified in preparation for FT-IR measurements carried out to measure the formation of CO and CN^- ligands. FT-IR measurements by Dr. P. Dinis showed, that fully reconstituted or unreconstituted HydG were unable to produce CO and CN^- ligands in a manner that was detectable by IR-spectroscopy. Therefore, in alteration to the previous purification method, HydG

was left unreconstituted until after the size-exclusion chromatography. Afterwards, HydG was reconstituted with only 5 mM DTT, 5 eq. of Fe and S, concentrated to 1 mM, separated into aliquots, flash frozen and kept at -80 °C until analysis. The protein yield was slight increased with 47 mg/L media.

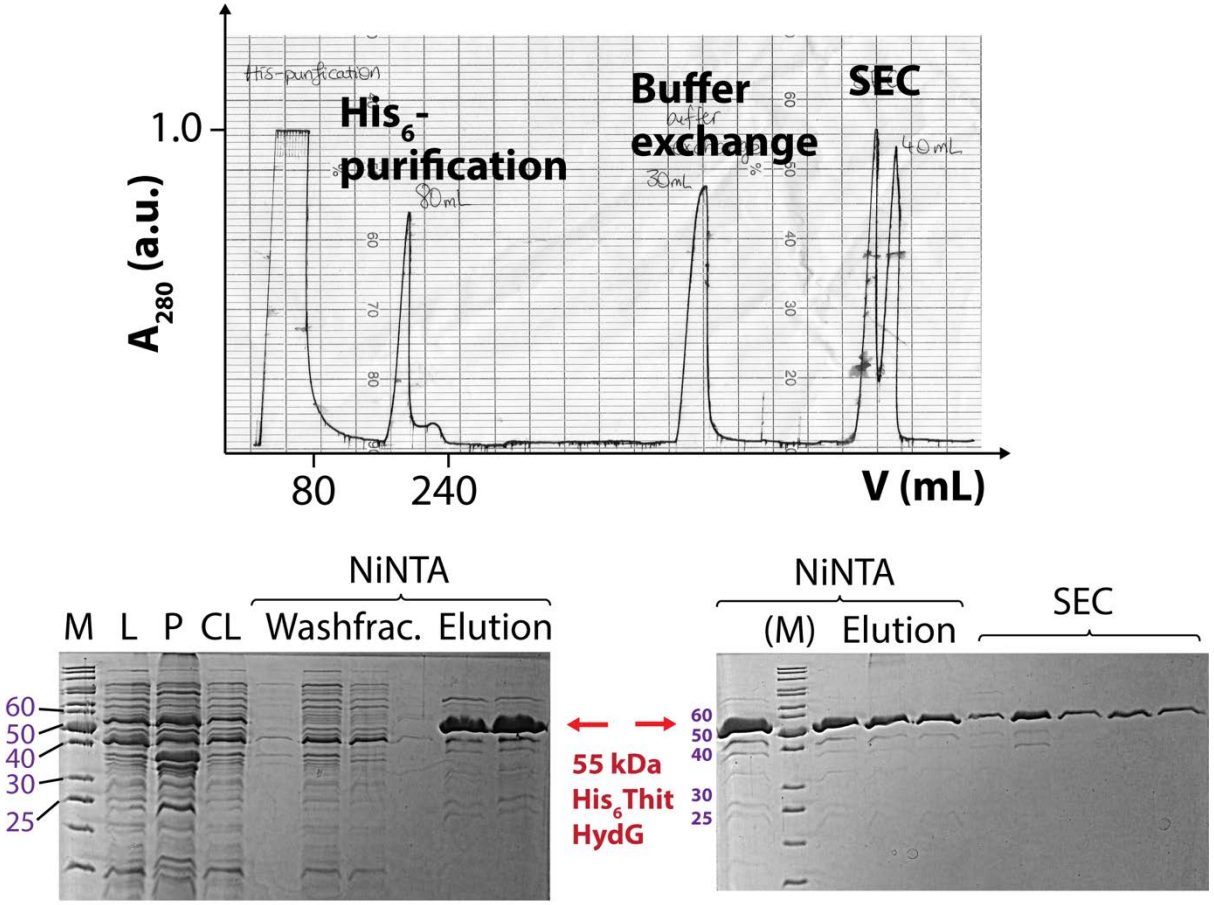

Figure 2.15: Chromotogram and SDS-PAGES of the His_6ThitHydG purification. (Method 15). M: Marker, L: Lysate, P: Pellet, CL: Cleared Lysate, Washfrac.: Flow through.

Table 2.7: Characteristics of the pRD003_His_6ThitHydG plasmid and the His_6ThitHydG protein.

Plasmid Name	**pRD003_ His_6*Thit*HydG**
Plasmid Size	10145 bp
Protein Name	His_6*Thit*HydG
Protein Size	55351.46 Da
Amino acids	482
pI	7.91
ε_{ox}	47220 1/cm·M

2.3 pCDuet expression systems

The pCDFDuet™-1 (Novagen, here named as pCDuet) expression vectors are optimized for co-expression and include two multiple cloning sites (MCS). Expression from the MCS is driven by the T7 promotor, *lac* operator and ribosome binding site (rbs). The *lac* promotor, *lac* operator and ribosome binding site are part of the *lac* operon present in *Escherichia coli* regulating lactose metabolism and transport.[278-280] The *lac* operon is an important tool for molecular biology; it enables controlled high yield expression of heterologous proteins by utilizing the strong T7 promotor from the T7 bacteriophage, which has an extremely high affinity for the T7 RNA polymerase.[281]

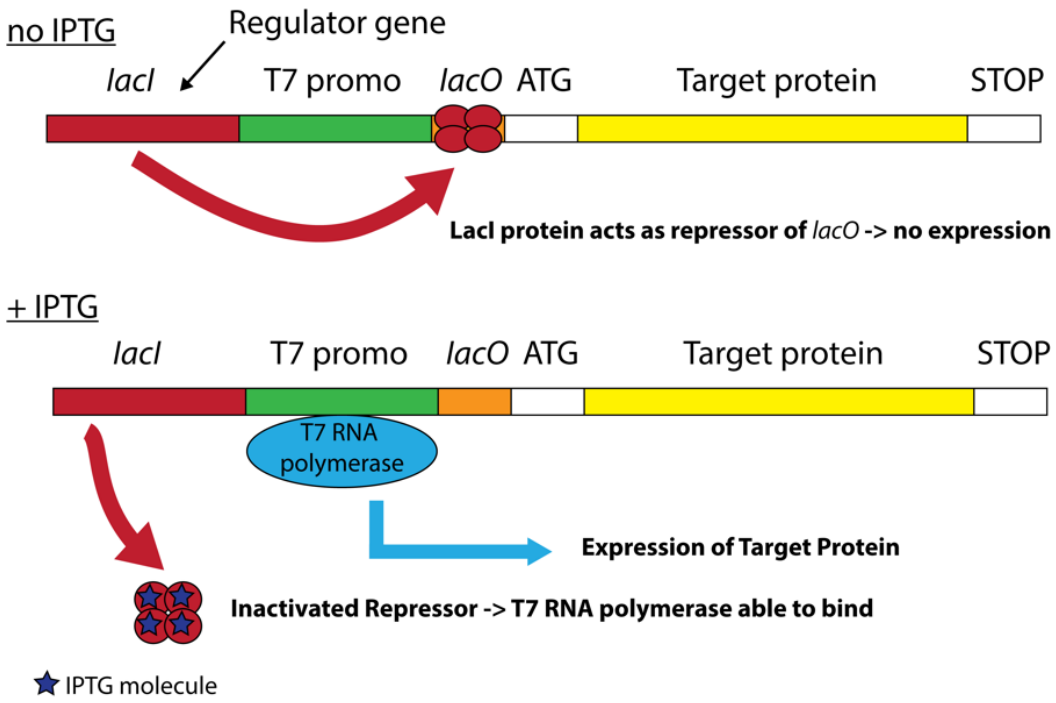

Figure 2.16: Schematic description of a *lac* operon for heterologous protein expression which contains the stronger T7 instead of the *lac* promotor.[279] LacI binds as repressor to *lacO* and prevents expression. As soon as IPTG binds to LacI the former repressor is inactivated and enabled the binding of the RNA polymerase to the T7 promotor and start the target protein expression.[282-284]

In the absence of IPTG or lactose/allolactose, the lac repressor LacI binds to the *lacO* operator, bends the DNA and prevents binding and transcription from the T7 promotor site by the T7 RNA polymerase.[282-284] When lactose/allolactose or IPTG bind to LacI the confirmation of LacI changes and it cannot bind to the (T7) operator anymore.[284] Subsequently the T7 RNA polymerase begins transcribing the protein of interest. Since IPTG is not involved in *E. coli* metabolism, the sugar remains stable over the whole process of induced protein expression.[285,286]

For this family of plasmids, an alternative to IPTG induction is autoinduction[287-290], which includes three carbon-sources in the cell culture media: glucose, which acts as an initial repressor and early phase energy source, lactose which acts as an inducer when glucose has all been metabolized and glycerol, which is a late phase energy source. In the early stages, the cells consume glucose first, which prevents lactose uptake by lactose permease LacY (as the Lac operon is repressed by glucose, due to catabolite repression of alternative carbon utilization pathways[289,291,292]). Once glucose runs out, lactose is taken up by tiny amounts of LacY from un-inducted cells. Afterwards, lactose is converted to allolactose by β-galactosidase. Allolactose therefore acts as an inducer, by binding to the LacI repressor, changing its conformation and preventing it from binding to the operator gene. The promotor region is free to bind the produced T7 RNA polymerase, which is present in the chromosome of *E. coli* BL21 (DE3) strains and the expression is induced. The mechanism is described in Figure 2.17. Advantage of the autoinduction is a tightly controlled gentle expression through defined nutrient requirements. Furthermore, expression of toxic proteins is facilitated.[288,293]

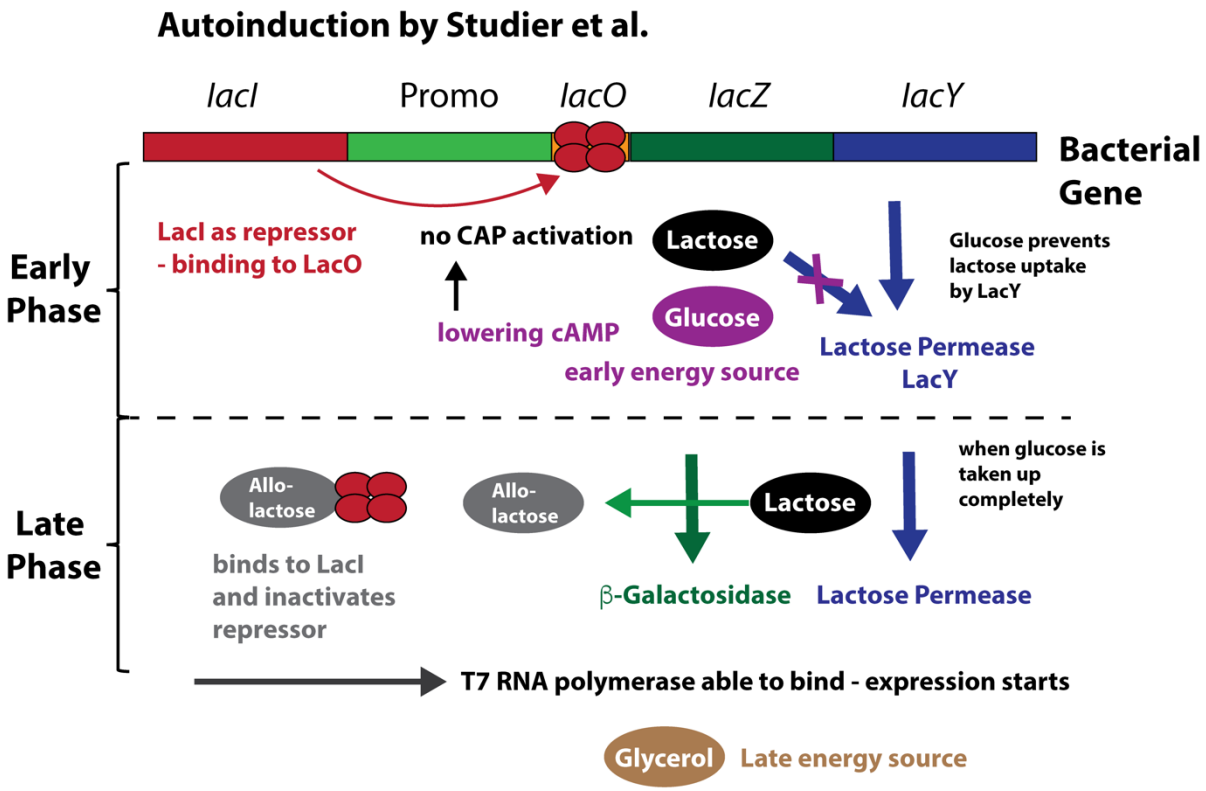

Figure 2.17: Principle of autoinduction. Addition of three carbon sources and their effects on the bacterial *lac* operon and plasmid *lacI* gene and promotor. Early phase: Glucose acts as early energy source and prevents lactose uptake by lacY. LacI is binding to the promotor unit and avoids expression. Late Phase: Upon depletion of glucose, lactose is uptaken by lactose permease and catabolized to alloloactose by β-galactosidase. Allolactase acts as inducer, binds to LacI and inactivates the repressor leading to a free promotor ready to bind the RNA polymerase and induce expression.

2.3.1 Generation of pCDuet expression vectors

An alternative expression system, to ensure high protein yield by utilizing the *lac* operon from *E. coli* and the strong T7 promotor, is the pET or pCDFDuet1 expression vector. In this study the pCDFDuet1 vector was used, as it allows the possibility of inserting two genes and carrying out protein co-expression. As described previously StrepHydF, StrepHydE1265 and StrepHydE1675 genes were commercially synthesized by GeneArt and provided in a GeneArt vector (section 2.2.1). The pCDFDuet1 vector used in this study[276] had the radical SAM enzyme Cfr in the first site and a 23S ribosomal RNA fragment in the second site (Figure 2.18), To assemble a plasmid expressing a single maturase, these genes were excised together by restriction with NcoI and XhoI and replaced with [FeFe]-hydrogenase maturase genes digested to give complementary sticky ends. To assemble plasmids bearing two maturase genes, the Duet plasmid is restricted with the enzymes NcoI and SalI to insert StrepHydF and NdeI and XhoI to insert an untagged HydE.

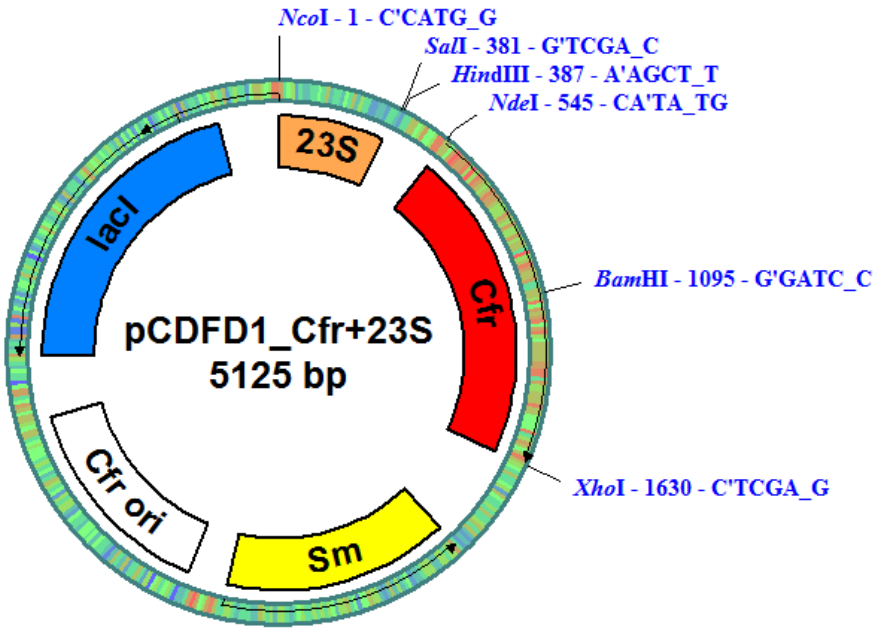

Figure 2.18: pCDFD1_Cfr+23S vector with *lacI* gene and streptomycin resistance.

To obtain the fragments required to assemble plasmid pCDFD1_StrepThitHydF (Figure 2.19), purified plasmids pCDFD1_Cfr+23S and pMA_RQ_StrepThitHydF were digested by the restriction enzymes NcoI and XhoI in a large scale (80 ng). The resultant digested fragments were isolated by separation on an agarose gel (see Table 2.7), extraction and purification (Method 6). Subsequently the purified fragments of the

HydF insert and the pCDFD1 backbone were ligated, catalyzed by the T4-DNA ligase at RT for 25 min and then the reaction mixture transformed into *E. coli* XL10 GOLD cells. After plating on appropriately selective agar, plasmid DNA was isolated from the observed colonies and characterized by restriction analysis to identify the successful assembly of plasmid pCDFD1_StrepThitHydF (Figure 2.20). Large scale digests and ligations of the HydE constructs pCDFD1_StrepThitHydE1 and pCDFD1_StrepThitHydE2 were completed by Dr. Pedro Dinis.

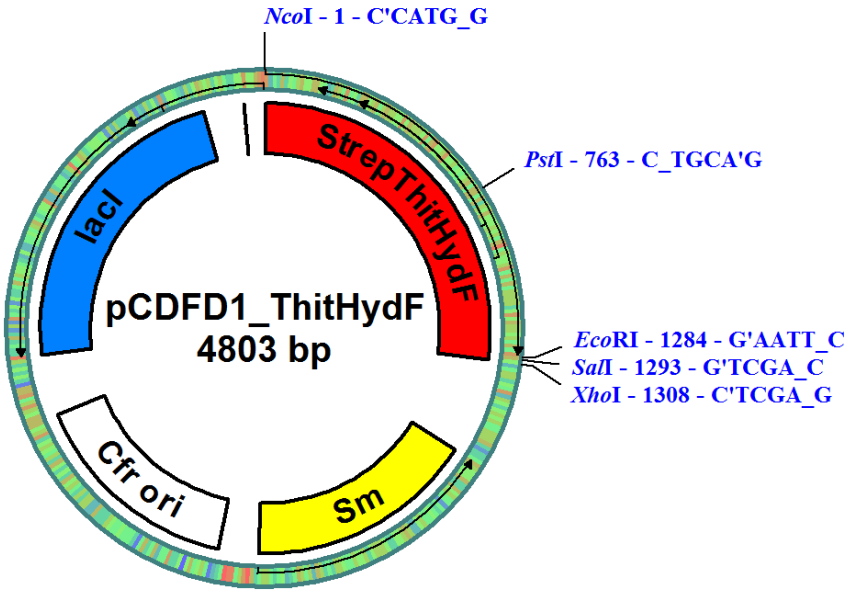

Figure 2.19: Plasmid map of newly generated pCDFD1_StrepThitHydF plasmid.

Table 2.8: Sizes of DNA fragments used to ligate [FeFe] hydrogenase maturases with the pCDFD1 vector backbone.

Fragment	HydF insert	HydE1265 insert	HydE1675 insert	pCDFD1_ vector backbone
Size (bp)	1307	1105	1117	3511

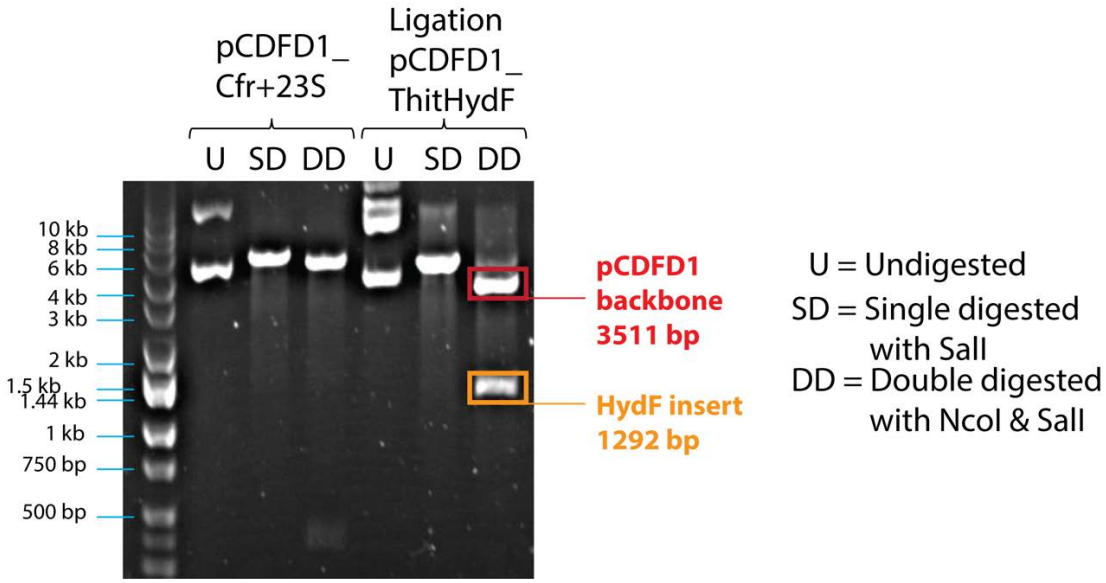

Figure 2.20: Analytical digest to confirm the right fragment sizes of ligated pCDFD1_StrepThitHydF.

For the generation of the co-expression plasmid carrying the StrepHydF gene and untagged HydE1265 gene, two separate steps of restriction plus ligation reactions were necessary, one for each inserted gene. Thus, NcoI and SalI restricted StrepHydF insert was ligated with pCDFD1_Cfr+23S plasmid backbone derived by a matching digest. The ligation to pCDFD1_StrepHydF+Cfr was successfully confirmed by an analytical digest. To insert the gene of untagged HydE1, the corresponding HydE plasmid was digested with the restriction enzymes NdeI and XhoI and the backbone generated by a matching digest of the newly generated pCDFD1_StrepHydF+Cfr plasmid. Then after ligation of the HydE1 fragment and the pCDFD1_StrepThitHydF backbone, the reactions were transformed into *E. coli* XL10GOLD and plasmid DNA isolated from resultant selected colonies. Restriction analysis of the resultant plasmids permitted the identification of the correctly assembled plasmid pCDFD1_StrepHydF+HydE1265 (see Figure 2.21 and 2.22, Table 2.9).

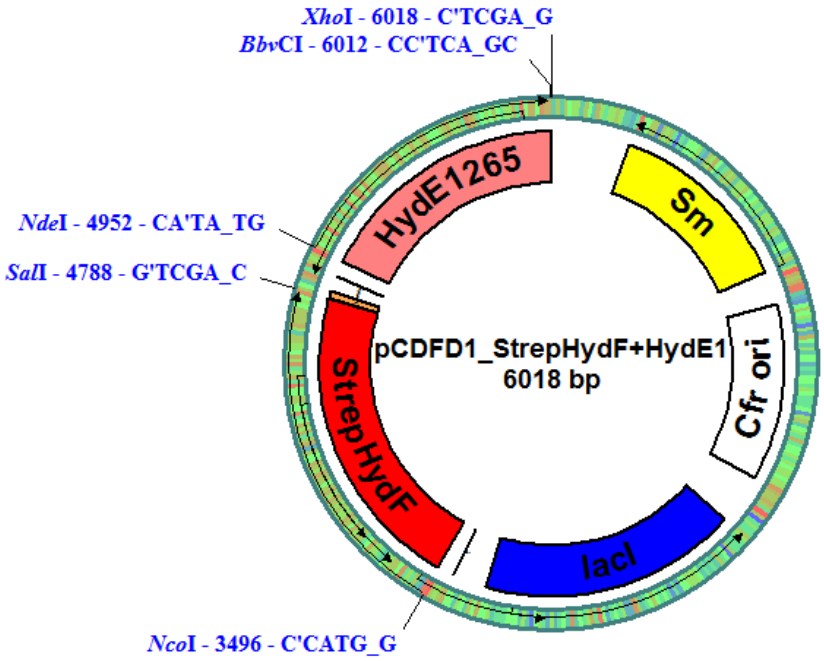

Figure 2.21: Plasmid map of newly generated pCDFD1_StrepThitHydF+ThitHydE1265.

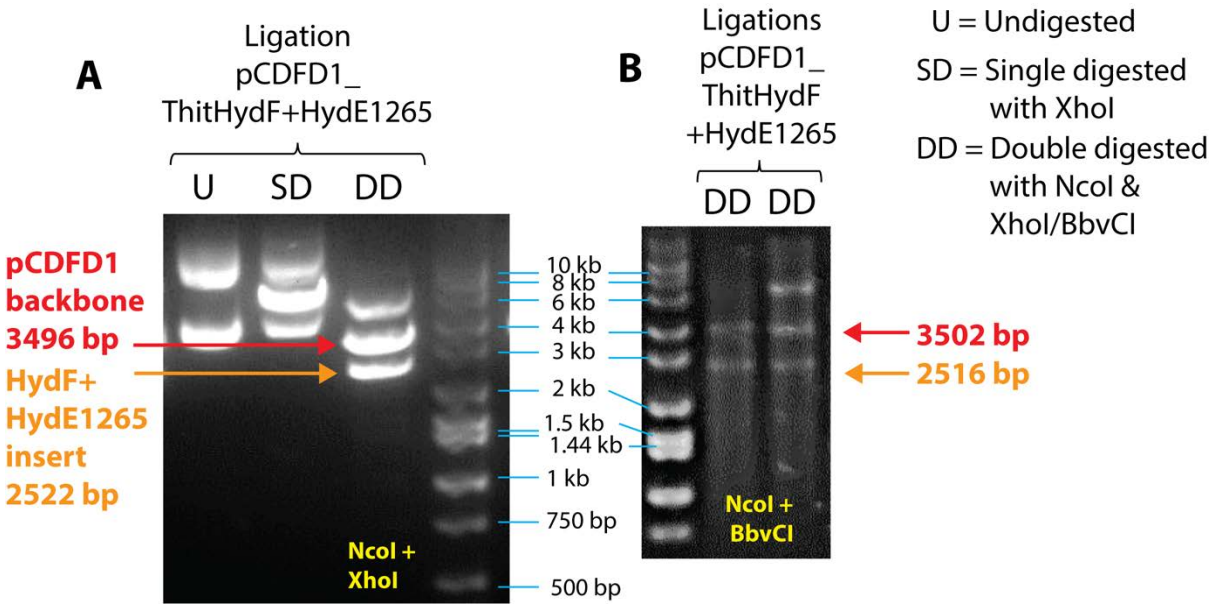

Figure 2.22: Analytical digest to confirm the right fragment sizes of ligated pCDFD1_StrepThiHydF+ThitHydE1265. Expected fragment sizes are summarized in Table 2.9. A: Analytical digest with NcoI & XhoI, B. Analytical digest with NcoI & BbvCI. BbvCI restriction site does not appear in the template vector pCDFD1_HydF+Cfr.

Table 2.9: Expected DNA fragment sizes for the restriction analysis with NcoI and XhoI (A) or NcoI and BbvCI (B) of the plasmid pCDFD1_StrepThitHydF+ThitHydE1265.

Fragment	StrepHydF+HydE1265 insert	pCDFD1 vector backbone
A Size (bp)	2522	3496
B Size (bp)	2516	3502

Newly generated plasmids of pCDFD1_StrepThitHydF, pCDFD1_Strep-ThitHydE1, pCDFD1_StrepThitHydE2 and pCDFD1_StrepThitHydF+ ThitHydE1 (Table 2.10) were transformed with *E. coli* BL21 (DE3 and Δ*iscR* BL21 (DE3) for expression studies.

Table 2.10: Characteristics of newly generated pCDuet constructs.

Plasmid Name	**pCDuet1_ StrepThitHydF**	**pCDuet1_ StrepThitHydE1265**	**pCDuet1_ StrepThitHydE1675**
Plasmid Size	4803 bp	4601 bp	4613 bp
Protein Name	ThitStrepHydF	ThitStrepHydE1265	ThitStrepHydE1675
Protein Size (Da)	47539.4	41214.7	41269.1
Amino acids	426	362	366
pI	6.69	8.87	8.56
ε_{ox}/ $cm^{-1}M^{-1}$	37025	28350	31330

2.3.2 Expression studies with pCDuet expression vectors

Initial expression studies with the pCDuet1_StrepThitHydF vector were made with two different BL21 (DE3) cell lines, at different temperatures after induction and with IPTG or lactose as inducer. Small scale 2YT media (100 mL) were inoculated with overnight cultures of the HydF plasmid transformed into either *E. coli* BL21 (DE3) or *E. coli* Δ*iscR* BL21 (DE3) cells and the culture was grown until OD_{600}=0.6. At this point, the cultures were induced with either 0.5 mM IPTG or 0.1% (w/v) lactose and the cultures continued at either 27°C or 37°C for 5 h or at 16°C overnight. Best results (shown on the SDS-PAGE as thick protein bands, Figure 2.23) were achieved with growth at 37°C with the BL21 (DE3) as well as Δ*iscR* BL21 (DE3) *E. coli* strain and with 0.5 mM IPTG as inducer. Large scale growth attempts of the same conditions and induction with 0.5 mM IPTG achieved very low yields of HydF (4 mg from 15 g of cell paste) after purification.

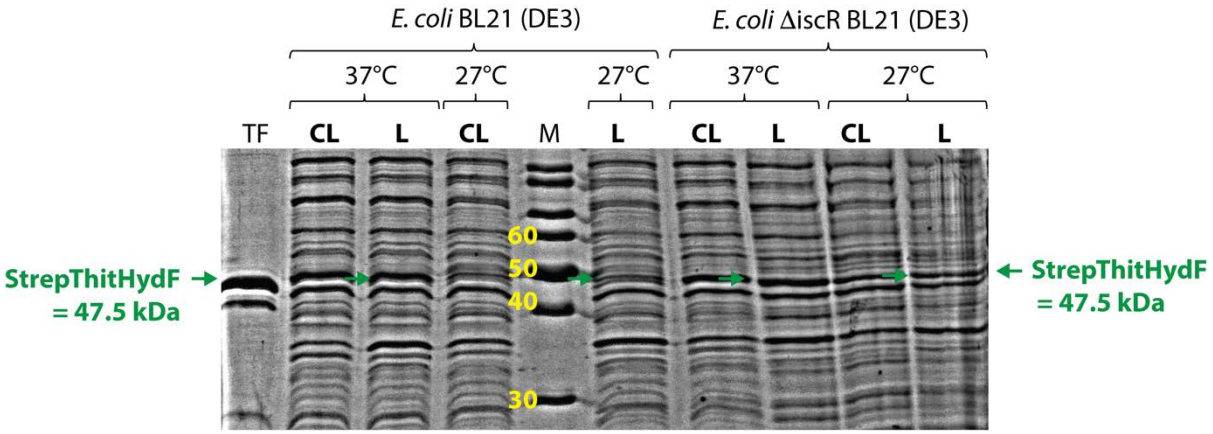

Figure 2.23: SDS-PAGE of small scale expressions of StrepThitHydF in *E. coli* BL21 (DE3) or *E. coli* ΔiscR BL21 (DE3) at two different temperatures 27 and 37°C. The cultures were induced with 0.5 mM IPTG. Previously purified StrepThitHydF (TF) serves as a reference. M: Marker, CL: Clear Lysate, L: Lysate. Protein bands of HydF were thicker at 37°C than at 27°C.

To circumvent this problem, medium scale expression cultures in 2YT or autoinduction media (1.25 L) have been analyzed by SDS PAGE (Figure 2.24) to evaluate autoinduction relative to IPTG induction on both pCDuet1_StrepThitHydE1 and pCDuet1_StrepThitHydE2 with overnight growth at 37°C.

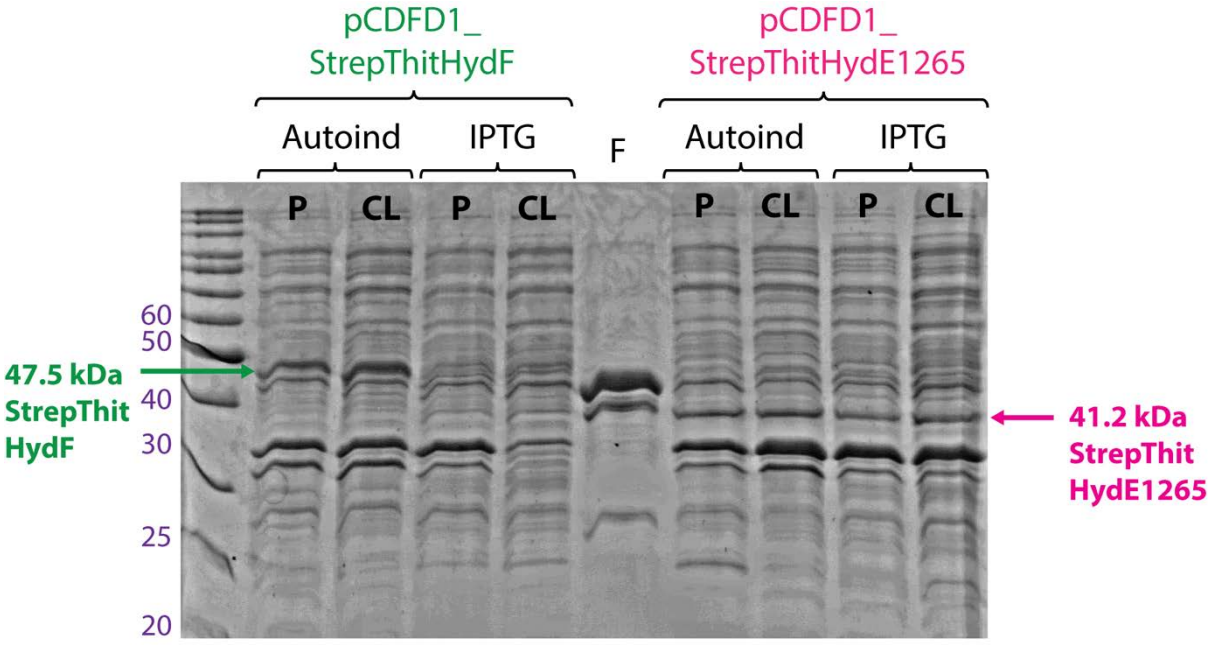

Figure 2.24: SDS-PAGE of small scale expression studies with StrepThitHydF and StrepThitHydE1265 from the pCDuet vector, either with IPTG as inducer or with autoinduction. F: StrepThitHydF as reference, P: Pellet, CL: Cleared Lysate.

The resultant SDS-PAGE of the medium scale expression cultures revealed clearly that autoinduction is the better induction system when considering higher protein yields of HydF, observed as thicker bands on the SDS-PAGE. In respect to HydE1 the protein band only appears slightly thicker for the autoinduction expression cultures. As a result, all subsequent pCDFD1 expression cultures where carried out using autoinduction.

2.3.3 Autoinduction expression and purification of HydF

Large scale autoinduction expression cultures of StrepHydF have been carried out in autoinduction media according to Studier *et al.*[287] in flasks (4 x 1.25 L). Autoinduction media was inoculated with an overnight culture of StrepHydF in Δ*iscR* BL21 (DE3) after being supplemented with antibiotic (100 μg/mL Streptomycin) and sugar mix (lactose, glucose and glycerol). The culture was left to grow at 37°C, 180 rpm overnight (Method 14). Average cell pellet yield the next day after spinning down the cell culture was 11 ± 1 g/L culture.

The resultant cell pellet was resuspended and lysed by sonication under anaerobic conditions in the glovebox. After removal of cell debris by centrifugation, the cleared cell lysate was applied to a StrepTactin® affinity column, then washed with HydF buffer SA and finally pure HydF was eluted with 60 mL HydF buffer SC (see Method 15, Figure 2.25). The average protein yield after purification was 31 ± 4 mg/L expression culture.

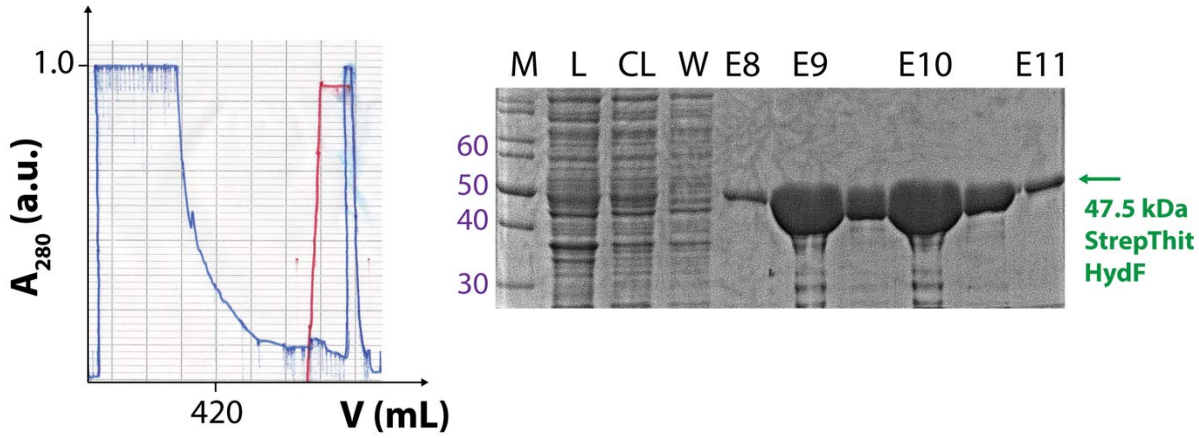

Figure 2.25: Chromatogram of the pCDuet1_StrepThitHydF purification and the corresponding SDS-PAGE. M: Protein Weight Marker, L: Lysate, CL: Cleared Lysate, W: Wash fraction/Flow through, E8-11: Elution fractions (corresponding to Table 2.11).

UV-Vis spectra of freshly purified StrepHydF did not seem to contain a high occupancy of [4Fe4S]-cluster(s), as measured from the characteristic absorption band of $[4Fe4S]^{2+}$ at around ~410 nm, with an extinction coefficient of ε_{410nm} = 16000 1/cm·M.[294] The background of the spectrum at 880 nm was subtracted from the absorption value used for the $[4Fe4S]^{2+}$-cluster concentration calculation at ~410 nm. The UV-Vis spectrum is shown in Figure 2.26 and the $[4Fe4S]^{2+}$-cluster concentration corresponds to 0.08 equiv. of [4Fe4S]-cluster per HydF.

In an effort to achieve a higher content of already incorporated [4Fe4S]-cluster, an iron and sulfur source was added to the autoinduction media. After reaching an OD_{600} = 0.6, iron(III)-ammnoniumcitrate (250 mg/L) and L-cysteine (1 mM final concentration) were added to the media. Following a similar culture protocol, the supplemented media yielded 10 g of cells/ L of medium (Table 2.11).

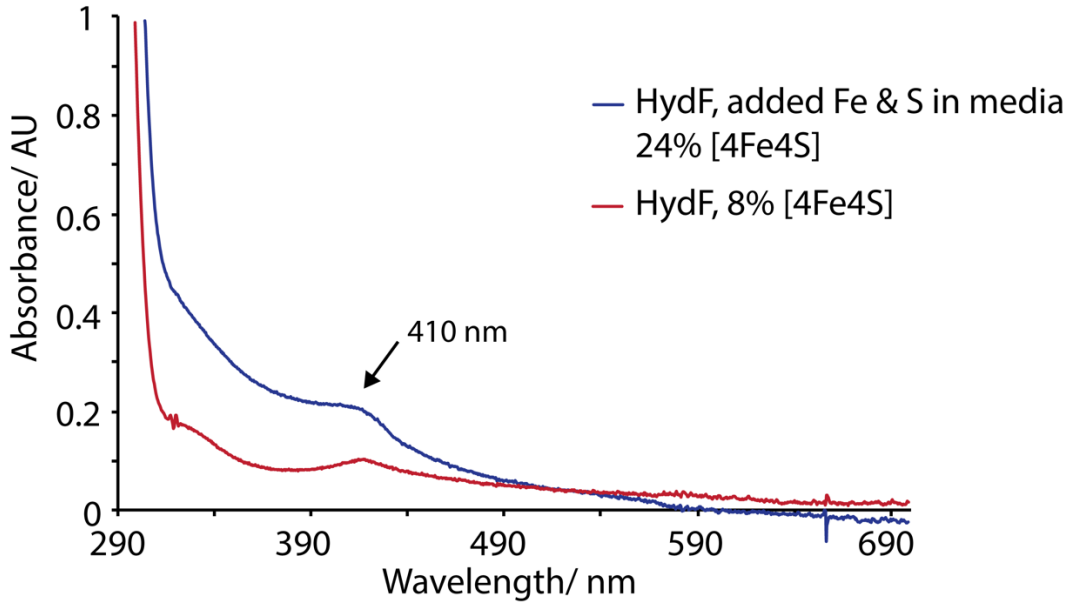

Figure 2.26: UV-Vis spectra of freshly purified StrepHydF. *Blue* (––): 69 μM HydF expressed from media containing additional Fe and S, *Red* (––): 74 μM HydF expressed from media without extra supplements.

The protein derived from cells grown on the Fe/Cys supplemented medium has an improved iron-sulfur cluster content, but only up to 24% of [4Fe4S]-cluster occupation in regard to protein concentration, according to the corresponding UV-Vis spectrum (Figure 2.26). Moreover, the yield of total protein was increased after purification to 38 ± 2 mg/L culture (corresponding SDS-PAGE Figure 2.27).

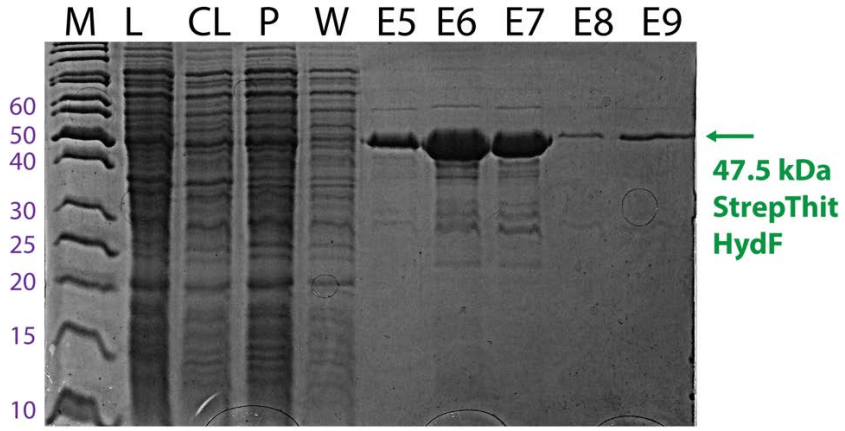

Figure 2.27: SDS-PAGE of StrepThitHydF purification fractions from an autoinduction expression with ferric ammonium citrate and L-cysteine supplemented media (Table 2.10). M: Protein Weight Marker, L: Lysate, CL: Cleared Lysate, W: Wash fraction/Flow through, E5-9: Elution fractions.

Table 2.11: Data from autoinduction expressions of pCDuet1_StrepThitHydF with standard conditions and supplemented media, which were anaerobically purified.

	Standard	**With supplements**
Type of expression cells	*E. coli* ΔiscR BL21 (DE3)	*E. coli* ΔiscR BL21 (DE3)
Volume of culture	5 L	5 L
Expression	Autoinduction	Autoinduction
Expression conditions	37°C, o/n	37°C, o/n
Supplements	-	Ferric ammonium citrate, L-cysteine
Cell Mass (g)	60	51
Buffer (25 mM)	HEPES	HEPES
Reducing agent (1 mM)	DTT	DTT
Protein yield (total in mg)	151	190
Protein yield (mg/L)	30	38
Equivalents of [4Fe4S]	0.08	0.24

2.3.4 Autoinduction expression and purification of HydE1265 and HydE1675

Since the HydF autoinduction expression gave excellent protein yields, the same approach was used for both pCDuet-HydE proteins. Same growth conditions were used as for HydF (Method 14) without exogenously added iron and sulfur sources.

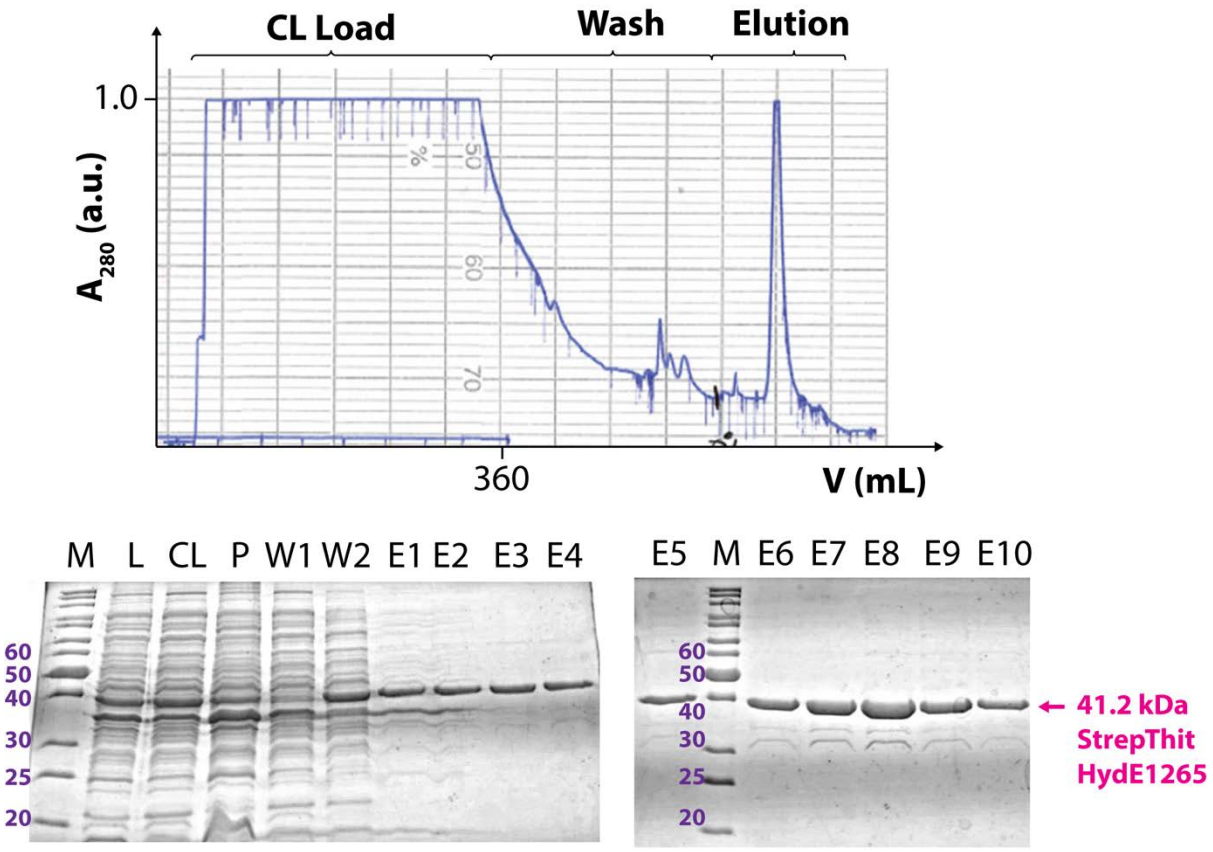

Figure 2.28: Strep-purification chromatogram of StrepThitHydE1265 and corresponding SDS-PAGES. M: Marker, L: Lysate, CL: Cleared Lysate, P: Pellet, W1-2: Wash fractions/Flow through, E1-10: Elution fractions.

The growth and purification of StrepHydE1 yielded 12 g cells/ L medium of cell paste and 10 mg/ L media of purified protein (Figure 2.28, Table 2.12). Surprisingly, the yield is significantly lower than for HydF, however without adding external iron and sulfur sources, the enzyme contains 0.21 equiv. [4Fe4S]-cluster per mol protein, perhaps indicating a relatively stable cluster(s) and a contribution from the presence of an auxiliary cluster.

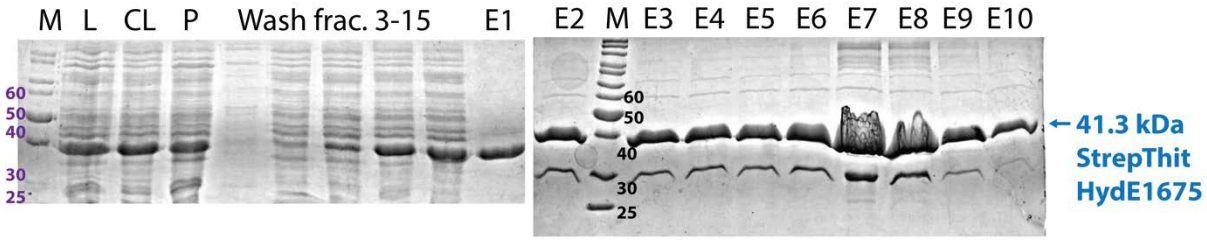

Figure 2.29: SDS-PAGES of the Strep-puriifcation of StrepThitHydE1675. M: Marker, L: Lysate, CL: Cleared Lysate, P: Pellet, W5-15: Wash fractions/Flow through, E1-10: Elution fractions.

Moreover, growth and purification of StrepHydE2 yielded 15 g/L media of cell paste and around 25 mg/ L media of purified protein (Figure 2.29, Table 2.12). In comparison, the overall protein yield is higher than for HydE1, nevertheless there is one additional protein or protein-complex eluting with HydE2, carrying a size of around 30 kDa. This co-eluting protein might be a truncated version of HydE2 from a potential second ribosomal binding site at M103 (leading to a protein size of 29.3 kDa). After purification 16% of HydE2 protein was occupied with [4Fe4S]-cluster suggesting a stable cluster conformation and carrying less iron-sulfur cluster than HydE1.

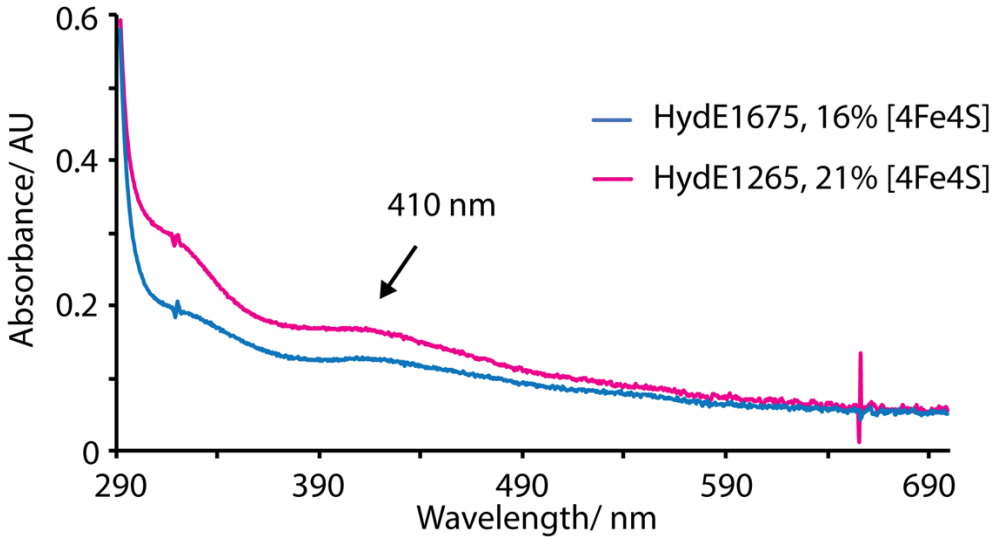

Figure 2.30: UV-Vis spectra of freshly purified StrepHydE1265 (––, 46 μM) and StrepHydE1675 (––, 45 μM). The arrow points to the characteristic absorbtion band of [4Fe4S]-cluster at 410 nm.

Table 2.12: Data from autoinduction expressions of pCDuet1_StrepThitHydE1265 and pCDuet1_StrepThitHydE1675, which were anaerobically purified.

	StrepThitHydE1265	**StrepThitHydE1265**
Type of expression cells	*E. coli* ΔiscR BL21 (DE3)	*E. coli* ΔiscR BL21 (DE3)
Volume of culture	5 L	5 L
Expression	Autoinduction	Autoinduction
Expression conditions	37°C, o/n	37°C, o/n
Cell Mass (g)	60	75
Buffer (50 mM)	Tris	Tris
Reducing agent (1 mM)	DTT	DTT
Protein yield (total in mg)	50	125
Protein yield (mg/L)	10	25
Equivalents of [4Fe4S]	0.21	0.16

2.3.5 Autoinduction coexpression and purification of HydF coexpressed with HydE1265

To investigate the effect of coexpression of HydF with HydE on the amount of HydF isolated and the level of cluster incorporation, the generated coexpression plasmid pCDuet1_StrepThitHydF+HydE1 was transformed with *E. coli* ΔiscR BL21 (DE3) cells. An overnight culture of the respective strain and plasmid were used to inoculated autoinduction media, containing the appropriate antibiotic and sugar mix. At an OD_{600}=0.6, a supplement of iron(III) ammonium citrate (0.5 mg/mL) was added. The expression culture was left to grow overnight at 37°C, 180 rpm.

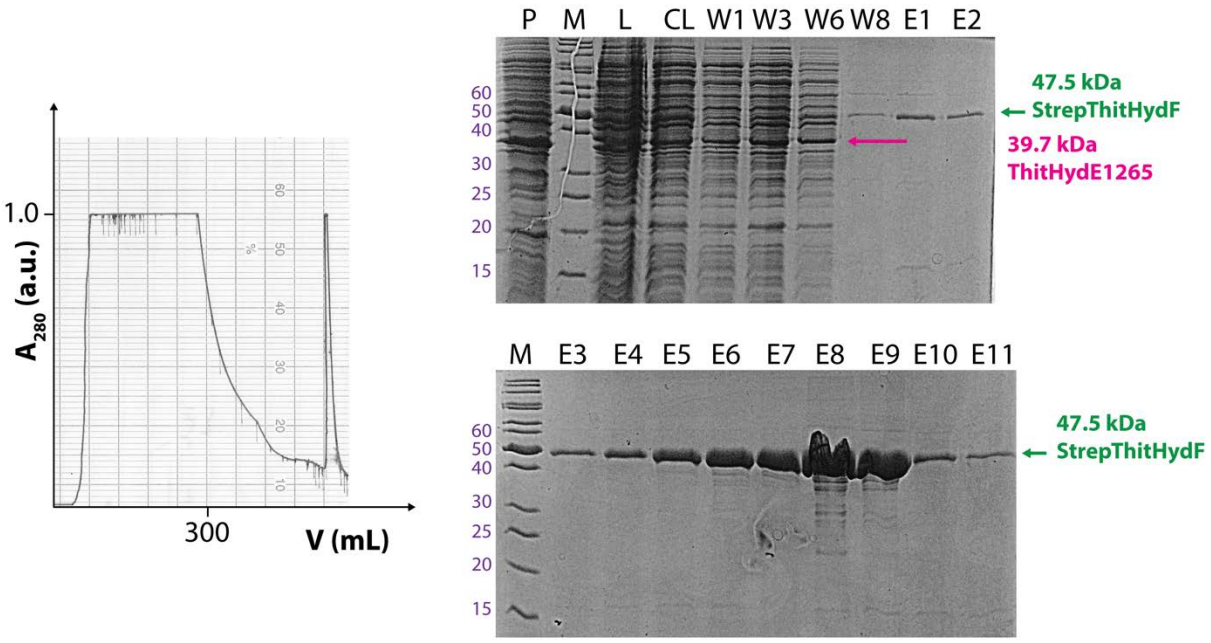

Figure 2.31: Anaerobic purification chromatogram of StrepHydF coexpressed with untagged HydE1265 and the corresponding SDS-PAGES. P: Pellet, M: Marker, L: Lysate, CL: Cleared Lysate, W1-8: Wash fractions, E1-11: Elution fractions.

Average cell pellet yield after autoinduction expression was 10 g/L medium and after purification the yield of purified HydF was in average 20 mg/ L media (Table 2.13).

Although HydE1 was clearly, as seen on the SDS-PAGE, expressed with HydF in the cleared lysate, it did not bind sufficiently tightly to HydF during the anaerobic Strep-purification (See Figure 2.31) to permit co-purification. Additionally, the UV-Vis spectrum of purified co-expressed HydF did not show any additional features or absorption bands (Figure 2.32).

Table 2.13: Data from the autoinduction expression of pCDuet1_StrepThitHydF+ThitHydE1265, which was anaerobically purified.

	StrepThitHydF + ThitHydE1265
Type of expression cells	*E. coli* ΔiscR BL21 (DE3)
Volume of culture	5 L
Expression	Autoinduction
Expression conditions	37°C, o/n
Cell Mass (g)	50
Buffer (25 mM)	HEPES
Reducing agent (1 mM)	DTT
Protein yield (total in mg)	100
Protein yield (mg/L)	20
Equivalents of [4Fe4S]	0.19

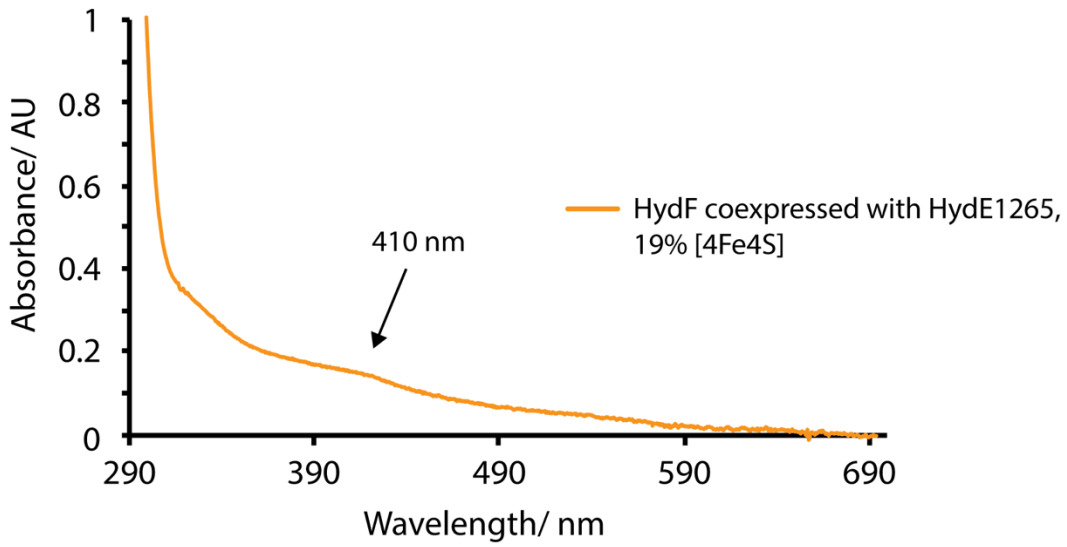

Figure 2.32: UV-Vis spectrum of freshly purified StrepHydF (58 μM) from coexpression with untagged HydE1265. The arrow points to the characteristic absorbtion band of [4Fe4S]-cluster at 410 nm.

2.4 Affinity-Tag mutation via SLIM

It was desirable to modify some of the affinity tags on the maturase proteins in the expression plasmids to facilitate planned biochemical experiments. This alteration of affinity-tags of His_6HydG and StrepHydE was achieved as a preliminary experiment in preparation of further expression and purification experiments. In particular, it was of interest to develop a very mild (StrepII) tag based purification system for pacification of HydG, so that a high proportion of the auxiliary cluster might be intact in the isolated protein, facilitating the analysis of the associated thiol ligand, which has been proposed by Britt *et al.* to be a cysteine (Figure 2.33).[38,66,69,71]

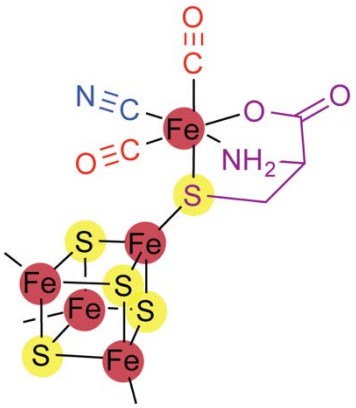

Figure 2.33: Current model for the auxiliary cluster of HydG after turnover of the substrates SAM and L-tyrosine in presence of L-cysteine and dithionite.[71]

In a further desirable modification, the tag of the HydE proteins was exchanged to a His_6-tag to permit orthogonal affinity pull-down studies with StrepHydF.

The experimental method of the site-directed-ligase-independent mutagenesis (SLIM) is described in the experimental section as Method 10. The principle of SLIM is schematically shown in Figure 2.34. Two sets of primers are designed; each set contains one short primer carrying the sequence before or after the sequence of interest (RP or FP) and one primer with overhang tail (RP_T or FP_T). The overhang contains the mutated sequence. Moreover, each set consists of one forward and one reverse primer. Two separate PCR reactions, each with one set of primers lead to two DNA probes with an overhang either on 3' or 5' position. Mixing the probes generates two-stranded DNA probes including the overhang on opposite sides of each single-strand. Through the hybridization reaction, the overlapping overhang sequences complementary to each other fuse, and the final ligation is catalyzed by the cellular ligase. A newly generated plasmid with the mutated sequence is the result (Figure 2.34).

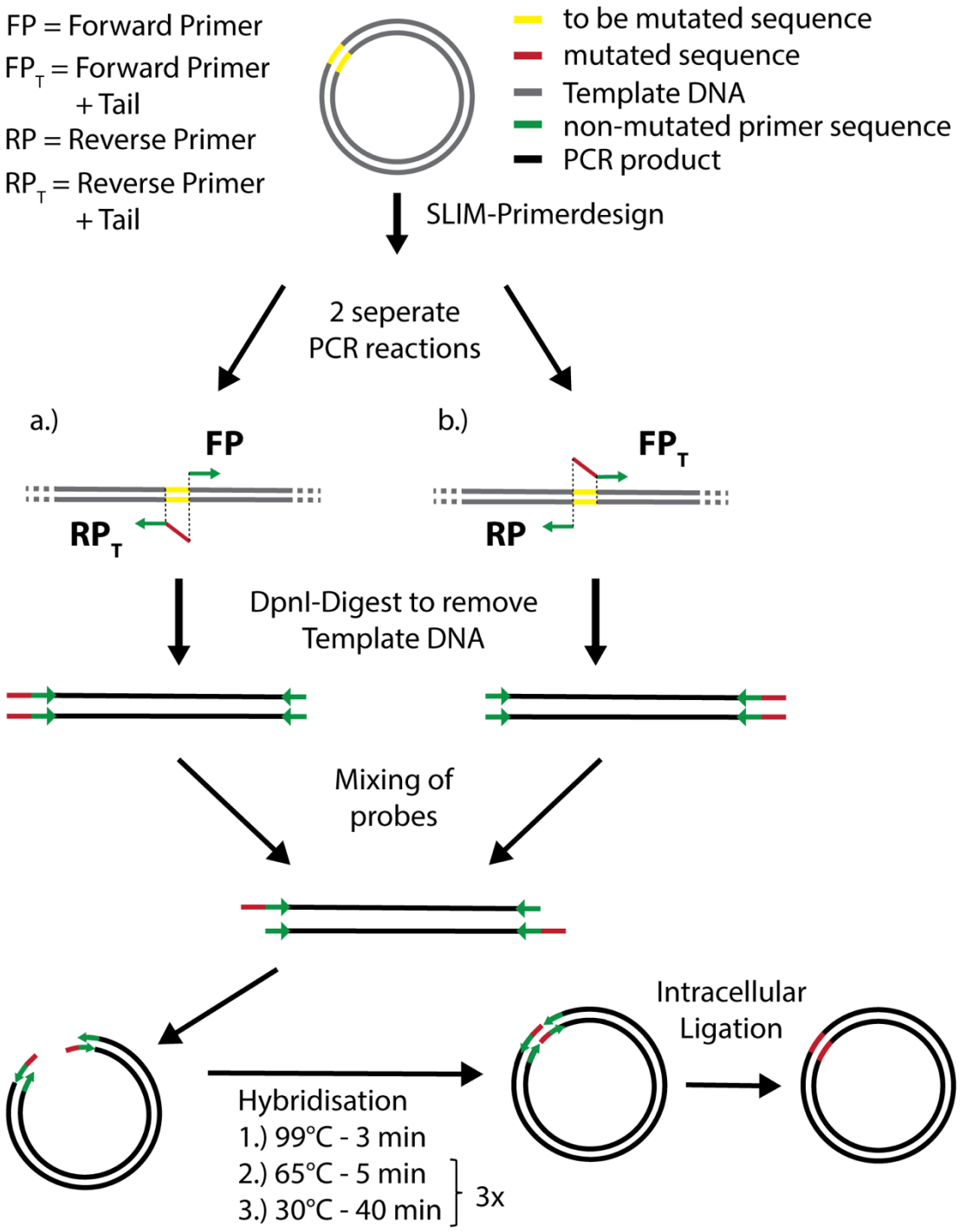

Figure 2.34: Workflow of the SLIM method.

2.4.1 Generation of His_6HydE and StrepHydG via SLIM

The first step towards an affinity-tag mutation via SLIM is the design of primers (Table 2.14). For each construct four primers were designed. The first set consists of a short forward primer FP and the reverse primer with tail RP_T, and the second set of RP and FP_T. The short primers are sequences just before (for RP) or after (for FP) the Tag-position and consist of 6 bp. The overhang/tail sequence contains the gene sequence of the newly inserted Tag, either His_6- or StrepII-Tag and can be up to 8 bp long.

Table 2.14: Gene sequences of SLIM primers.

StrepThitHydG	**Gene sequence**
FP	5’ AGC CAG GAT CCG ATG GTT 3’
FP_T	5’ TGG TCG CAT CCG CAG TTC GAG AAG AGC CAG GAT CCG ATG GTT 3’
RP	5’ GCT GCT GCC CAT GGT TAA 3’
RP_T	5’ CTT CTC GAA CTG CGG ATG CGA CCA GCT GCT GCC CAT GGT TAA 3’
His_6ThitHydE1265	
FP	5’ ATG TCG GGG GTG ATG CTG 3’
FP_T	5’ CAT CAC CAT CAT CAC CAC CAT ATG TCG GGG GTG ATG CTG 3’
RP	5’ CGA CCC GGC CAT GGT ATA 3’
RP_T	5’ ATG GTG GTG ATG ATG GTG ATG CGA CCC GGC CAT GGT ATA 3’
His_6ThitHydE1265	
FP	5’ ATG TCG GGG GTG ATG ATC 3’
FP_T	5’ CAT CAC CAT CAT CAC CAC CAT ATG TCG GGG GTG ATG ATC 3’
RP	5’ CGA CCC GGC CAT GGT ATA 3’
RP_T	5’ ATG GTG GTG ATG ATG GTG ATG CGA CCC GGC CAT GGT ATA 3’

The second and crucial step of the SLIM mutagenesis is separate PCR reactions with FP and RP_T as primers for the first PCR and RP and FP_T as primers for the second PCR. Depending on the melting temperatures of the primers, the annealing temperature is chosen and depending on the GC content of the primers the DMSO concentration is selected. Furthermore, to find the optimal conditions a temperature gradient PCR (from 55°C to 63°C) with 5 or 10% DMSO was carried out, to screen for best conditions. The SLIM mutagenesis was carried out by the master student Yiu Wai.[295]

The optimal conditions for the primer pair PCR reactions are summarized in the Table 2.15.

Table 2.15: Optimal SLIM PCR reaction conditions.

StrepThitHydG (10 145 bp)	Annealing Temperature	DMSO concentration
FP + RP_T	58	5
RP + FP_T	61	10
His_6ThitHydE1265 (4601 bp)		
FP + RP_T	57	10
RP + FP_T	57	10
His_6ThitHydE1265 (4613 bp)		
FP + RP_T	57	10
RP + FP_T	57	10

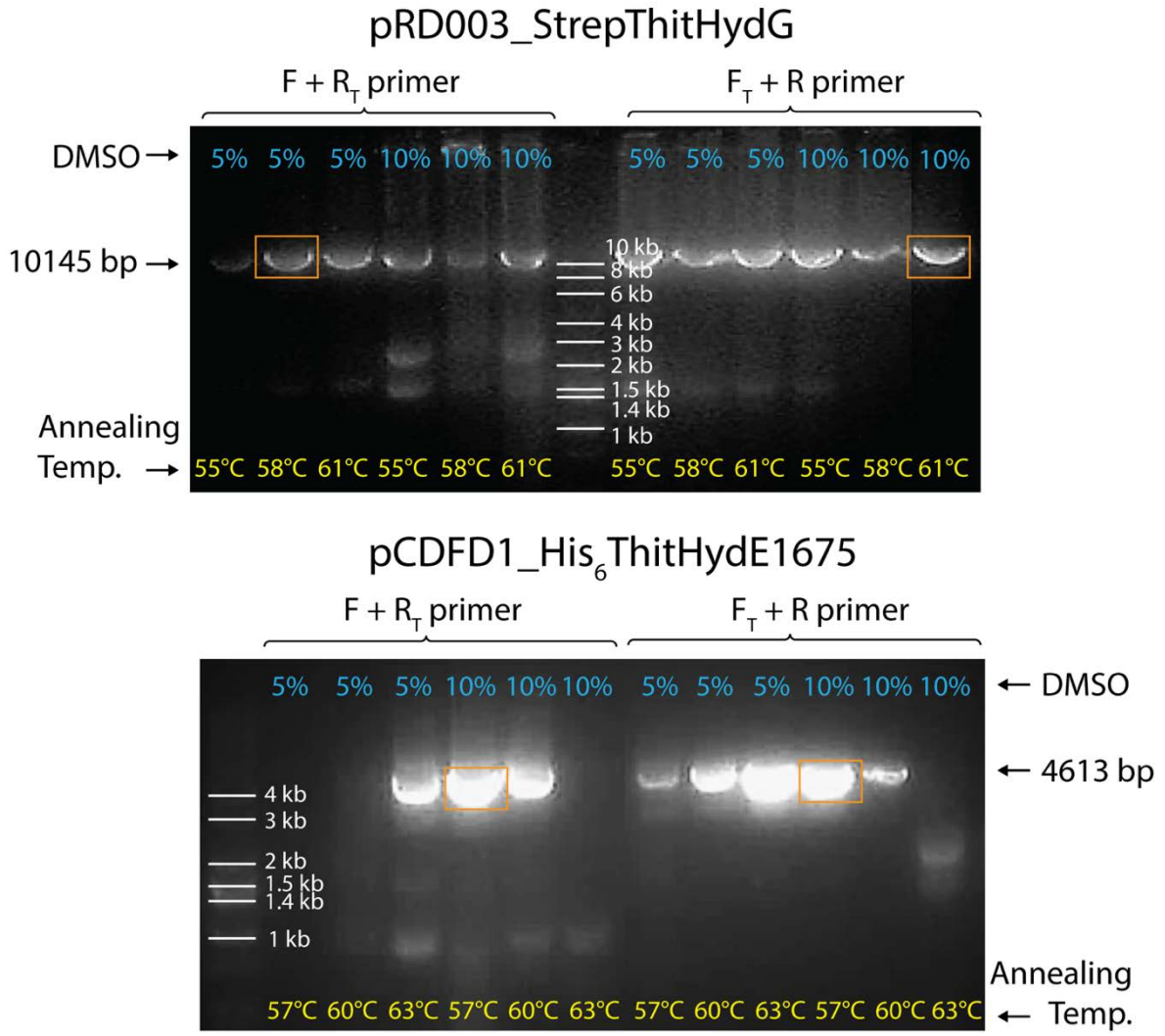

Figure 2.35: Exemplary 1% agarose gels of SLIM PCR products for pRD003_StrepThitHydG and pCDFD1_His_6ThitHydE1675 constructs. Highlighted with an orange box are PCR products with highest purity, that were selected for the hybridization reaction.

After obtaining the right DNA fragment sizes from the PCR reactions, as estimated by an analytical 1% agarose gel (Figure 2.35), a DpnI digest was carried out to remove template DNA. Reannealing and hybridisation was carried out by mixing the two PCR reactions and starting a hybridisation program (described in Method 10). Subsequently the resultant hybridisation product was directly transformed with *E. coli* XL10 GOLD cells. Four colonies for each mutant were picked, cultured overnight and the plasmid extracted and purified with a plasmid preparation kit (Method 4). The resultant plasmids were checked for the right size on an analytical 1% agarose gel and sequenced (sequencing data presented in appendix A 2.2). Plasmid samples in which the new affinity tag was confirmed by sequencing (2 out of 4 plasmids were sequenced, at least one plasmid of each had the right affinity tag) were directly transformed with *E. coli* ΔiscR BL21 (DE3) cells for expression studies.

Characteristics of newly generated protein genes are summarized in Table 2.16.

Table 2.16: Characteristics of newly generated plasmids with new affinity tags.

Plasmid Name	**pCDuet1_ His_6ThitHydE1265**	**pCDuet1_ His_6ThitHydE1675**	**pRD003_ StrepThitHydG**
Plasmid Size	4601 bp	4613 bp	10145 bp
Protein Name	His_6ThitHydE1265	His_6ThitHydE1675	StrepThitHydG
Protein Size (Da)	40997.5	41051.8	55351.5
Amino acids	360	364	482
pI	8.79	8.56	7.91
ε_{ox}/ cm^{-1} M^{-1}	22350	25330	47220

Plasmid maps for these are shown in the Appendix A 2.1.

2.4.2 Autoinduction expression and purification of His_6HydE proteins

The expression of His_6-tagged HydE protein was carried out with the standard autoinduction protocol without addition of external iron and sulfur sources. After supplementing the media with the appropriate antibiotic (100 μg/mL Streptomycin) and sugar mix, an overnight culture of pCDuet1_His_6ThitHydE1 or pCDuet1_His_6ThitHydE2 in *E. coli* BL21 ΔiscR (DE3) was added to the media and left to grow at 37°C (180 rpm) overnight. The cell pellet yield of His_6HydE1 was 8 g/ L medium and purified protein yield was 74 mg/L media. Autoinduction expression of

His_6HydE2 yielded 7.4 g of cell pellet per L medium and 100 mg/L media of purified protein (Table 2.17).

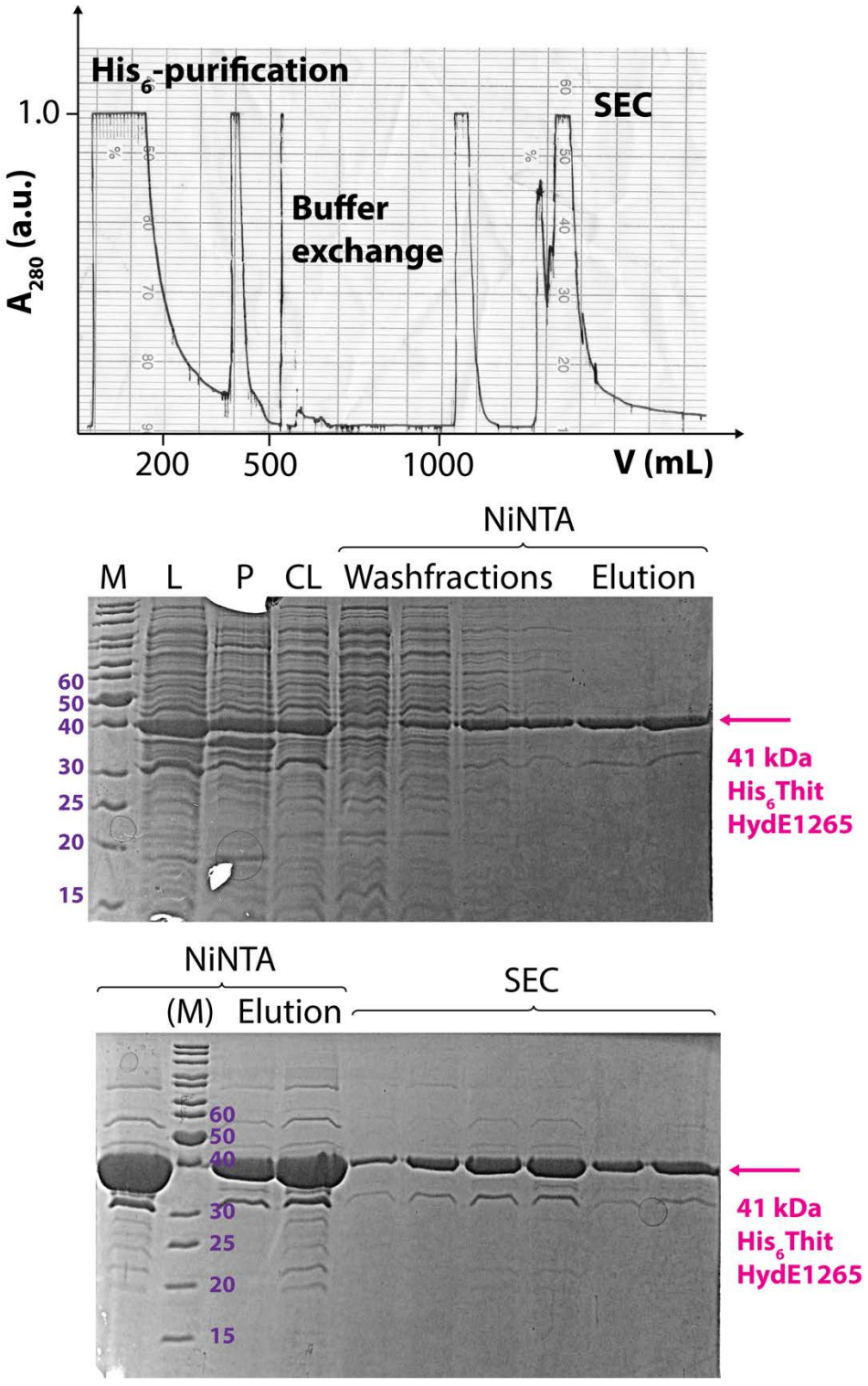

Figure 2.36: Purification chromatogram of His_6ThitHydE1265 and the corresponding SDS-PAGEs. M: Protein Ladder, L: Lysate, P: Pellet, CL: CL, SEC: Size-Exclusion fractions. Size of fractions: 13 mL.

Both HydE proteins were purified in three steps, similarly to the previously described method for the purification of His_6HydG (Figure 2.14, 2.36 and 2.37). The first step includes an NiNTA affinity purification and elution in high imidazole (500 mM) buffer. Subsequently, the high imidazole buffer is replaced with a buffer containing DTT by using a prompt S75 buffer exchange column (XK26, 50 mL). For reconstitution of the radical SAM and auxiliary [4Fe4S]-clusters, HydE1 was reconstituted with 10 eq. of Fe and S, whereas HydE2 was only reconstituted with 5 eq. of Fe and S, as the sequence suggested the absence of the second binding site for the auxiliary Fe-S cluster. After the first reconstitution, excess FeS colloids were removed by S200 size-exclusion chromatography. After SEC, for the final reconstitution step, HydE1 was incubated with 5 eq. and HydE2 with 3 eq. of Fe and S. Both proteins were then concentrated to about 1 mM and stored frozen in aliquots at -80°C.

Table 2.17: Data from autoinduction expressions of pCDuet1_His_6ThitHydE1265 and pCDuet1_His_6ThitHydE1675, which were anaerobically purified.

	His_6ThitHydE1265	**His_6ThitHydE1675**
Type of expression cells	*E. coli* ΔiscR BL21 (DE3)	*E. coli* ΔiscR BL21 (DE3)
Volume of culture	5 L	5 L
Expression	Autoinduction	Autoinduction
Expression conditions	37°C, o/n	37°C, o/n
Cell Mass (g)	40	37
Buffer (50 mM)	Tris	Tris
Reducing agent (1 mM)	DTT	DTT
Protein yield (total in mg)	370	500
Protein yield (mg/L)	74	100

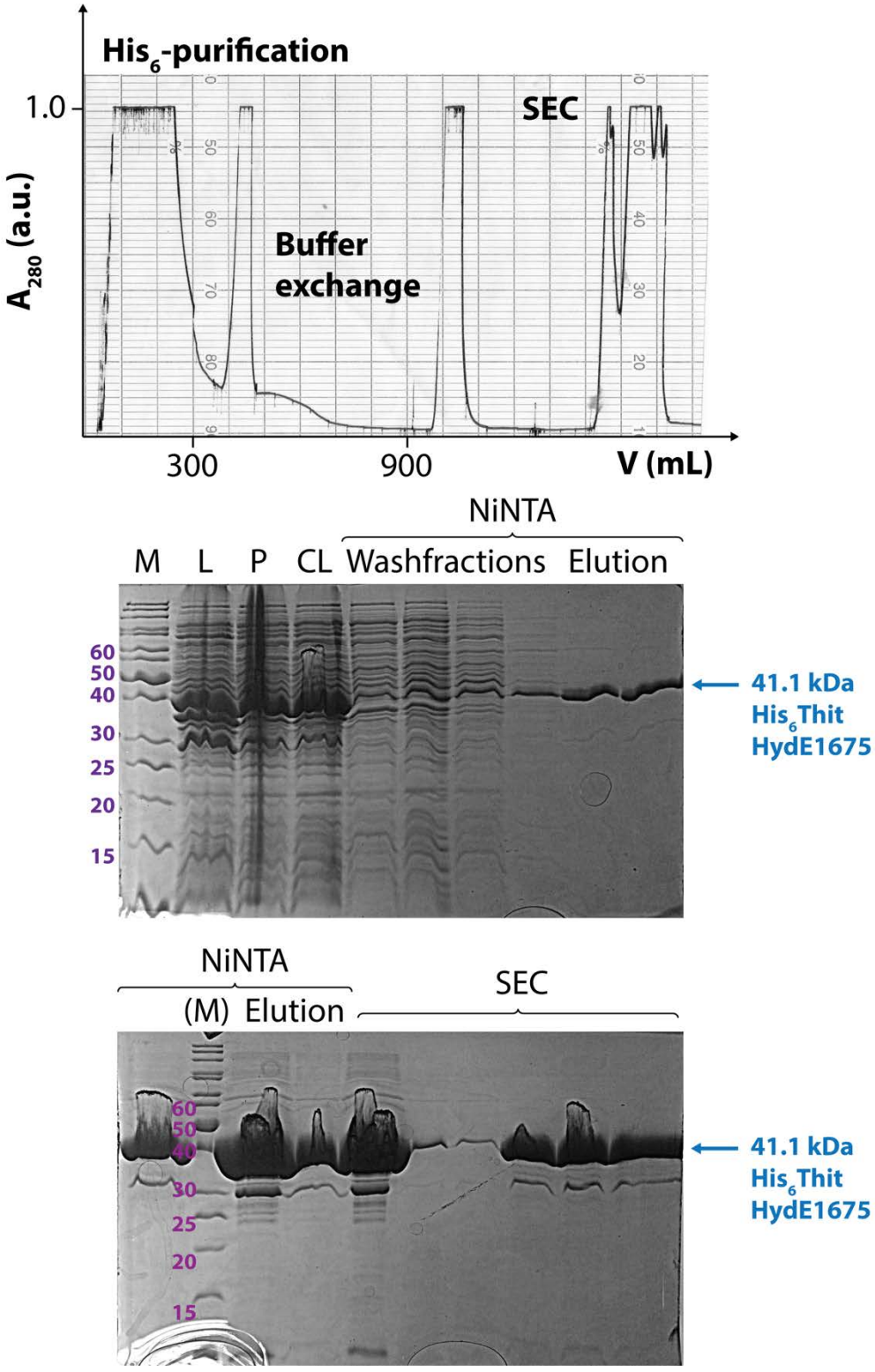

Figure 2.37: Purification chromatogram of His_6ThitHydE1675 and the corresponding SDS-PAGEs. M: Protein Ladder, L: Lysate, P: Pellet, CL: CL, SEC: Size-Exclusion fractions. Fraction size is 13 mL.

2.4.3 Expression and purification of StrepHydG

Expression of Strep-tagged HydG was carried out by Y. Wai[295] using a large-scale culture of pRD003_StrepThitHydG from a pBAD vector also containing the ISC machinery and was carried out in the fermenter and in flasks. For the fermenter and flask expression 2YT (5 L) media was supplemented with antibiotic (100 μg/L ampicillin) and inoculated with an overnight culture of pRD003_StrepThitHydG in *E. coli* BL21 ΔiscR (DE3). The culture was left to grow at 37°C for 2-3 h until an OD_{600} = 0.6. Subsequently, the media was further supplemented with 500 mg/L ferrous ammonium citrate and for induction 250 mL 20% (w/v) arabinose was added and the culture incubated at 27°C (180 rpm) for 5 h. Cell pellet yield from the fermenter expression was in average 7 g/L media, but much higher if carried out in flasks with 23 g/L media (Table 2.18). The difference in cell pellet yield might derive from the fact that in the fermenter the oxygen level was dropped to 40% compared to the outer atmosphere and the aeration was much greater in the shaking flasks, which may explain the greater *E. coli* cell growth rate.

After sonication and clearing the lysate, an anaerobic Strep purification with buffers containing 0.5-1 mM TCEP instead of DTT as reducing agent was carried out. TCEP was used to avoid any thiols binding to the auxiliary [4Fe4S]-cluster of HydG, potentially facilitating the characterization of naturally bound thiols. However, despite the fact of low or high cell pellet yield, for both cases fermenter or flasks the overall purified protein yield was considerably low with a maximum of 2 mg of protein. To increase the concentration of elution fractions, a step gradient to 100% buffer B containing 5 mM D-desthiobiotin has been applied (Figure 2.38).

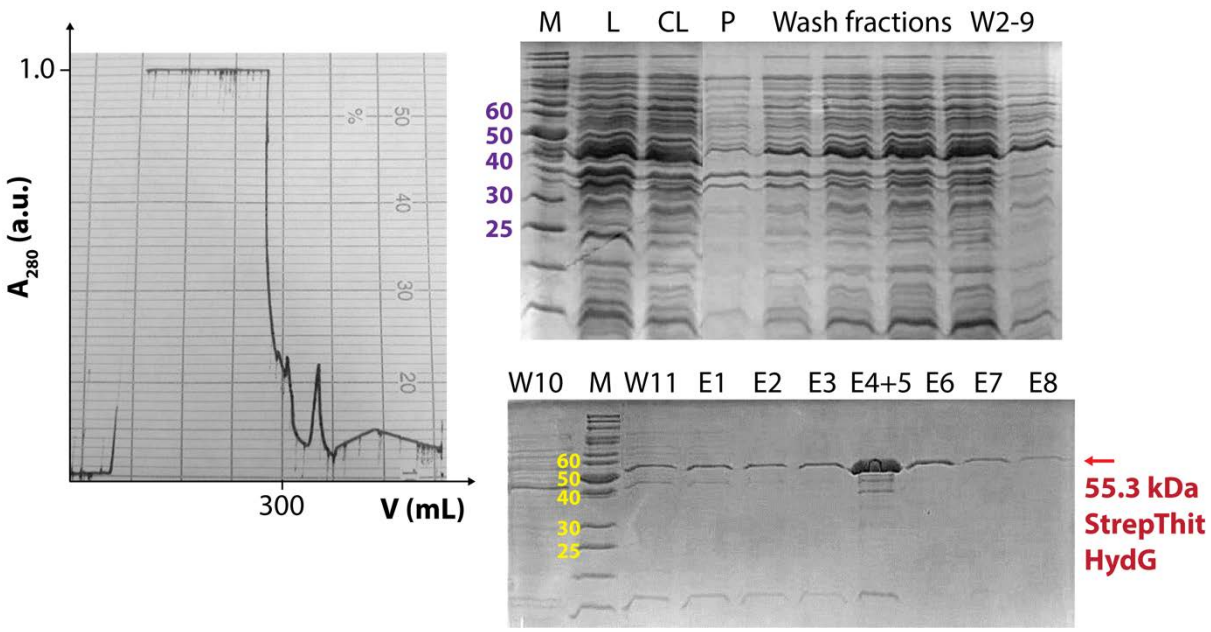

Figure 2.38: Anaerobic Strep-purification chromatogram of StrepThitHydG from an expression in the fermenter and step gradient to 100% buffer B and the corresponding SDS-PAGEs. M: Marker, L: Lysate, P: Pellet, E1-8: Elution fractions.

Obtained fractions with highest protein concentration were analyzed for [4Fe4S]-cluster content by UV-Vis spectroscopy (Figure 2.29).

The observed UV-Vis spectra of freshly purified StrepHydG did have a higher occupancy of [4Fe4S]-cluster(s), than StrepHydF in comparison (Section 2.3.3), up to 0.59 equivalents per mol of protein as measured from the characteristic absorption band of $[4Fe4S]^{2+}$ at around ~410 nm, with an extinction coefficient of ε_{410nm} = 16000 1/cm·M (Figure 2.39).[294] For the concentration measurement, the absorbance value at 410 nm was subtracted from the background value at 880 nm, where no absorption of the cluster should take place.

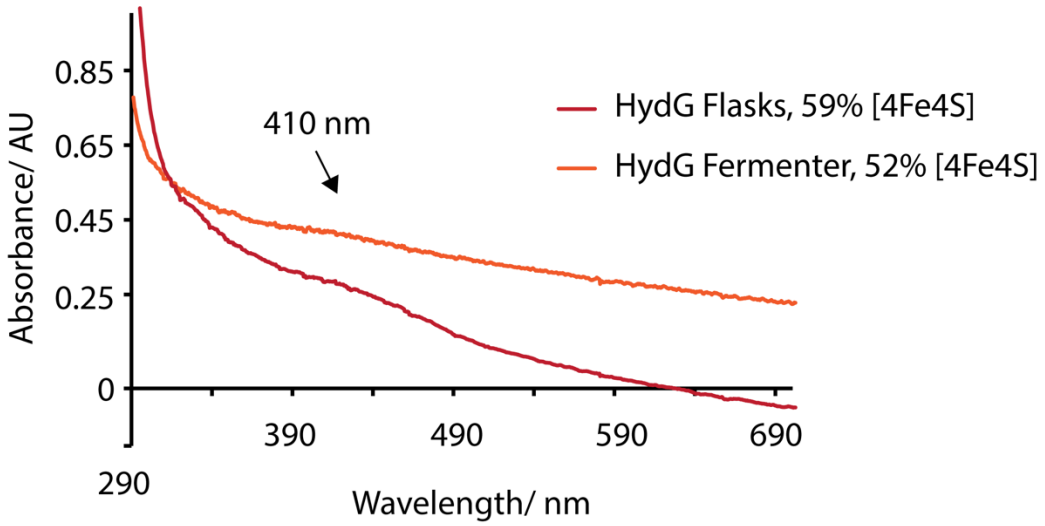

Figure 2.39: UV-Vis spectrum of StrepHydG from fermenter (––, 21 μM) and flask expression (––, 46 μM).

For the fermenter expression of StrepHydG, the protein concentration was twice as high and [4Fe4S]-cluster content was slightly lower, if compared with the flask expression (Table 2.18).

Table 2.18: Data from two different expressions of pRD003_StrepThitHydG in a fermenter and in flasks, which were anaerobically purified.

	StrepThitHydG	**StrepThitHydG**
Type of expression cells	*E. coli* ΔiscR BL21 (DE3)	*E. coli* ΔiscR BL21 (DE3)
Volume of culture	5 L	5 L
Expression carried out in	Fermenter	Flasks (4 x 1.25 L)
Expression	Arabinose induction	Arabinose induction
Expression conditions	27°C, 5 h	27°C, 5 h
Supplements	Ferrous ammonium citrate	Ferrous ammonium citrate
Arabinose concentration	10 mg/mL	10 mg/mL
Cell Mass (g)	31	114
Buffer (20 mM)	HEPES	HEPES
Reducing agent (1 mM)	TCEP	TCEP
Protein yield (total in mg)	2	1
Protein yield (mg/L)	0.4	0.2
Equivalents of [4Fe4S]	0.52	0.59

2.5 Summary and conclusions

By using the His_6ThitHydG protein expression and purification as a model system, newly synthesized genes of StrepThitHydF and StrepThitHydE (*Thermoanaerobacter italicus,* harbouring two putative HydE genes StrepThitHydE1265 and StrepThitHydE1675), were cloned into the same backbone vector as HydG pRD003, to take advantage of an already optimized process. The pRD003 vector is a pBAD vector carrying the *E. coli* ISC machinery genes to ensure the production of stable partly reconstituted proteins.

Expression of Strep-tagged [FeFe]-hydrogenase maturation protein constructs from the pBAD expression vector were produced in very low yields. Even copying the same conditions of the successfully overproduced and crystallized His_6-tagged HydG[64,276] from the same pBAD construct, did not provide the yields expected.

Reasons for this low expression level could derive from many different aspects, such as instability of the Strep-tagged proteins and their cofactors, which might be facilitated with the His_6-Tag, since histidine have been previously reported to be involved in iron-sulfur cluster coordination.[240, 241] One histidine residue in HydG has been shown to be crucial for the activity of the protein and the ligation of the auxiliary cluster.[64] Nevertheless, the Strep-tagged HydE proteins expressed from the pBAD expression were either unstable and inactive (HydE1675) or prevented the cells from growing well under the culture conditions (HydE1265). This might suggest a certain toxicity of the proteins for the cells.

Still, the pBAD expression of Strep-tagged HydF yielded a maximum of 55 mg purified protein per 5 L media. This amount was sufficient to carry out first characterization studies of HydF. However, upon reconstitution in DTT-containing buffer the protein precipitated quickly after reaching concentrations over 100 μM. A better stability of HydF in concentrated states was achieved with changing the reducing agent to sodium dithionite (NaDT). However, the main disadvantage of NaDT is its strong absorption band at 315 nm,[296] which partially overlaps the characteristic absorption band of [4Fe4S]-cluster at 410 nm and the fact that dithionite is a powerful reductant, so that the protein is already in its activated reduced state ($[4Fe4S]^{+1}$) during purification and reconstitution. After reconstitution of HydF in NaDT containing buffer, the formed FeS colloids could not be removed by SEC, leading to a high background in UV-Vis spectra

and black colored protein. Hence, NaDT was removed from purification and reconstitution buffers.

Another potential reason for low expression levels is the fact that pBAD expression systems have a weaker inducing system than T7/pET systems, containing the *lac* operon.[297-299] Therefore, as an alternative to the pBAD expression system, the Strep-tagged [FeFe]-hydrogenase maturation protein constructs were cloned into pCDuet (pCDFDuet1) vector containing the *lacI* gene and T7 promotor.

In the initial small scale expression studies with StrepHydF, using IPTG as inducer showed still very low expression levels. An alternative approach, using autoinduction to produce the HydF protein, yielded (after purification) an increase to about 150 mg per 5 L expression. Autoinduction leads to fully inducible cell cultures until autoinduction at late-log/lag phase; these cell cultures undergo a complete induction at saturation.[290] By optimal control of the growth and nutrient requirements with a gentle transition between autoinduction and saturation, high-density cultures are produced and a high yield of protein is expressed.[290] Adding ferrous ammonium citrate and cysteine in the mid-log phase increased the amount of [4Fe4S]-cluster bound after purification (from X to Y equivalents of [4Fe4S]-cluster/protein) and therefore had a positive impact on the protein stability, as observed by less precipitation occurring during chemical reconstitution and while concentrating to more than 1 mM. Using this purification and reconstitution protocol, StrepHydF could be concentrated to up to 1.5 mM.

A similar trend was observed for other maturases: higher amounts of purified StrepHydE proteins were obtained from autoinduction expressions leading to overall yields ranging from 50 mg for StrepHydE1 and 75 mg for StrepHydE2 for 5 L cell cultures. Without supplements of iron and sulfide in the expression culture, StrepHydE1 contained up to 0.21 equivalents of [4Fe4S]-cluster whereas StrepHydE2 carried 5% less [4Fe4S]-cluster, which might derive from the fact that HydE2 likely contains a single cluster, the Radical SAM cluster.

In anticipation of future pull-down interaction studies with StrepTactin®-Resin and StrepHydF, the affinity tags of the Strep-tagged HydE proteins in the pCDuet vector needed to be replaced with the His_6-Tag. Furthermore, to enable studies with naturally bound thiol-ligands that coordinate HydG's auxiliary [4Fe4S]-cluster, the [4Fe4S]-

cluster ligating His_6-Tag of HydG needed to be replaced with a Strep-Tag. By utilizing the SLIM mutagenesis method, sequences encoding the tags were replaced with the desired ones and the newly generated plasmids were transformed with the *E. coli* expression strain ΔiscR BL21 (DE3).

Following large scale cultures for protein expression, purification and reconstitution of the His_6-tagged HydE proteins using an optimized protocol, these produced excellent yields of purified reconstituted His_6HydE1 (300 mg) and His_6HydE2 (500 mg).

As described previously the expression of Strep-tagged [FeFe]-hydrogenase maturation protein constructs yielded in very low protein yields. This was also the case for the newly generated pRD003_StrepThitHydG, which did not yield more than 2 mg of protein from a 5 L expression. Even altering the expression conditions did not impact the overall yield. Nevertheless, a positive outcome was that the addition of ferrous ammonium citrate increase the [4Fe4S] incorporation to up to 59% (from 20%).[295]

The crucial steps in this optimization process were the usage of an alternative expression system, here the pCDuet vector containing the strong T7 promotor and furthermore taking advantage of autoinducting media (Figure 2.40). Enabled by the sugar composition of the autoinduction media is the diauxic growth of *E. coli* via self-regulation of the expression and induction at optimal cell density guided by the *lac* operon.

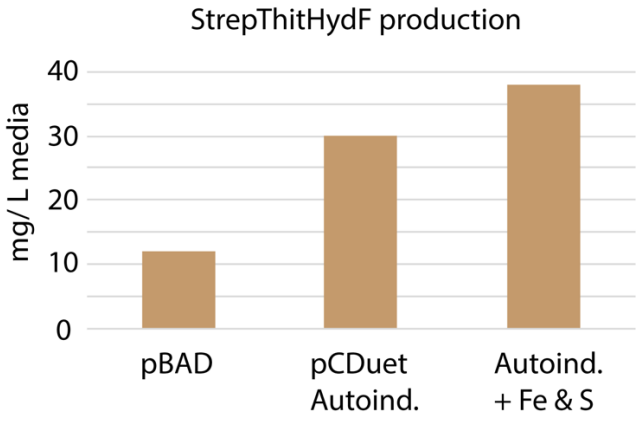

Figure 2.40: Bar-chart representing how the yield of purified StrepThitHydF changed over the expression optimization period. Autoind.: Autoinduction, Fe & S: Supplemented media with iron and sulfur.

Chapter 3

Spectroscopic characterization of [FeFe]-hydrogenase maturation enzymes

3.1 Introduction

This chapter describes the characterization of iron-sulfur cluster (ISC) states in the [FeFe]-hydrogenase maturation proteins HydG, HydE and HydF from *Thermoanaerobacter italicus* by UV-Vis, EPR and IR spectroscopy.

Iron-sulfur clusters play an important role in biological processes and are involved in catalysis[300,301], electron-transfer[302], redox chemistry[303,304] and oxygen sensing[305,306]. Processes that utilize ISCs include respiration[307], regulation of gene expression[308], nitrogen fixation[309], photosynthesis[310] and reversible oxidation of hydrogen[18], the latter being the focus of our study.

Iron-sulfur clusters are sometimes sensitive to oxidative degradation by molecular oxygen[311]. Consequently, in order to study iron-sulfur clusters of proteins, it is often necessary to partly or fully reconstitute the proteins with their organometallic Fe-S cluster cofactors. Reconstitution can be achieved by using one of two methods; either during expression and cell lysis (as described in Chapter 2), or by chemical reconstitution after protein purification which will be described in this chapter. The theoretical framework for the absorption spectroscopy used for characterization of the clusters is summarized in the following section.

3.2 UV-Vis spectroscopy

UV-Vis spectroscopy utilizes visible and ultraviolet light from the electromagnetic spectrum (200-900 nm) and measures which wavelengths of the input light are absorbed by the sample as well as the intensity of this absorption. The degree of absorption depends on the attributes of the sample. At a specific wavelength, each photon carries a defined amount of energy, causing electronic transitions within the

sample molecule. During the transition process electrons are excited from occupied bonding (σ or π) or non-bonding orbitals (n) to empty anti-bonding orbitals (σ^* or π^*).[312]

The relationship between light intensity, how strongly the sample absorbs light at a specific wavelength (termed the molar extinction coefficient), the sample concentration and the path length through the sample is summarized in the Lambert-Beer-Law (3-1):

$$A = -\log(T) = -\log\left(\frac{I}{I_0}\right) = \varepsilon_\lambda \cdot c \cdot d \qquad (3\text{-}1)$$

A: Absorption, *T*: Transmission, I_0 = Intensity of light source, *I* = Light intensity after passing the sample, ε_λ = Extinction coefficient specific for sample, *c* = sample concentration, *d* = path length through sample.

The basic set up of an UV-Vis spectrometer is shown in Figure 3.1. A light source, typically a deuterium and halogen lamp, provides UV-Vis light, which is passed through an entrance slit and hits a dispersion device, usually a prism. Subsequently, the dispersed light passes through an exit slit which only transmits a light of a certain wavelengths. The resulting monochromatic light is partially absorbed by the measured sample and the unabsorbed part of the light is received by the detector at the end, which converts it to a conventional UV-Vis absorption spectrum.[313]

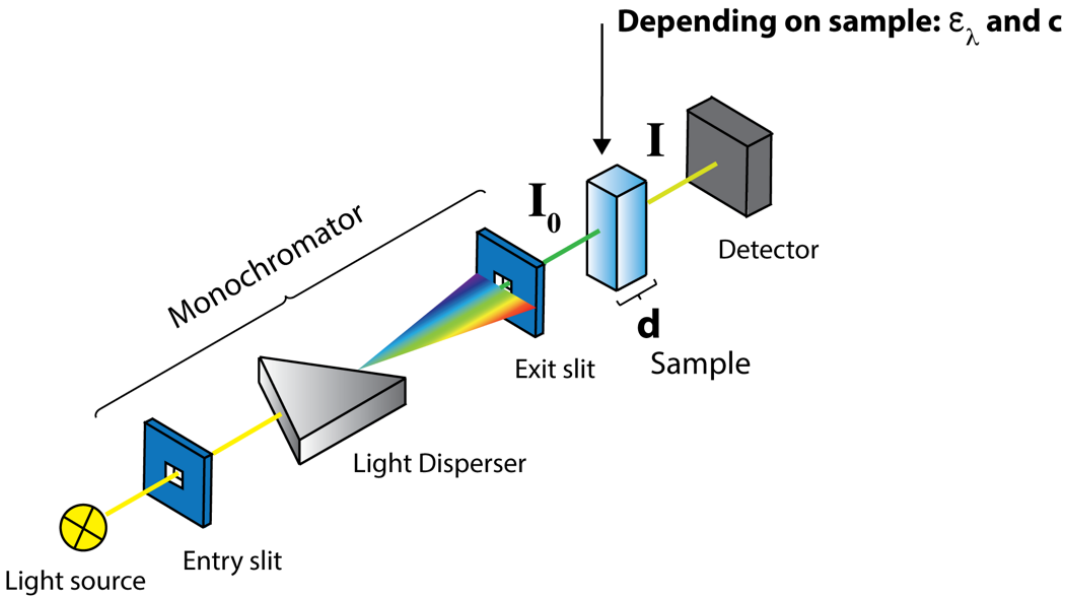

Figure 3.1: Basic setup of a UV-Vis spectrometer with a light absorbing sample. Adapted from [313].

UV-Vis spectroscopy is a useful tool to measure protein, DNA and RNA concentration and to study chromophore-containing cofactors of proteins. Protein concentrations are conveniently measured at 280 nm, the wavelength absorbed by the aromatic amino acids present in the protein.

In regard to iron-sulfur cluster proteins, UV-Vis spectroscopy is used to study the type of ISC bound by the protein, the nature of which can be deduced from the observed absorption band(s). In addition, UV-Vis is used to estimate the concentration of a certain type of FeS cluster from the intensity of the appropriate absorption band and the extinction coefficient (see Table 3.1).

Table 3.1: Characteristics of biologically relevant iron-sulfur clusters.

Iron Sulfur Cluster	Absorption band	Extinction coefficient
$[2Fe2S]^{2+}$	330, 420, 460, 550 nm[314]	ε_{460nm} = 13 200 1/M cm[315]
$[3Fe4S]^{1+}$	395, 420 nm[316]	ε_{420nm} = 14 000 1/M cm[316]
$[4Fe4S]^{2+}$	315, 410 nm[317]	ε_{410nm} = 16 000 1/M cm[294]

However, UV-Vis spectra of proteins carrying more than one FeS cluster can be misleading due to overlapping and very broad signals. Additionally, distinguishing between the UV-Vis spectra of $[3Fe4S]^{1+}$ and $[4Fe4S]^{2+}$ is very difficult since they are almost identical.[316] An alternative spectroscopic technique that can be used instead of UV-Vis is EPR (Electron paramagnetic resonance) spectroscopy which can be used in combination with mutagenesis of cluster binding residues in the binding sites to identify cluster types and their binding residues.

3.3 Reconstitution of [FeFe]-hydrogenase maturation enzymes

In this chapter, only [FeFe]-hydrogenase maturation enzymes from *Thermoanaerobacter italicus* are discussed and analyzed. These were produced in a high yield from the plasmids mentioned in Table 3.2 (for more details for expression conditions and outcomes, consult Chapter 2).

The bound iron content of each protein sample was determined using a colorimetric iron content assay[318] after reconstitution of Fe-S clusters. This was used to determine the amount of iron bound to the protein and is herein expressed as mole equivalents of iron per mole of protein (Method 22). From the iron equivalents, the amount and type of iron-sulfur cluster that is bound could be inferred. The number of iron and sulfur equivalents added during the reconstitution of [FeFe]-hydrogenase maturation enzymes was dependent on the Affinity-Tag and on the number of potential Fe-S cluster binding sites.

Table 3.2: Equivalents of iron and sulfide added and measured with the FISH assay[318]. Results for the reconstitution of [FeFe]-hydrogenase maturases from different expression vectors and with different affinity tags.

Expression from plasmid	Equiv. Fe[a] & S[b] First Reconst.	Equiv. Fe[a] & S[b] Second Reconst.	Fe-content/ Protein
pCDuet_StrepHydF	-	6.5	6.8 ± 0.5
pCDuet_StrepHydE1	-	8	6.0 ± 0.1
pCDuet_StrepHydE2	-	5	ND
pRD003_His_6HydG	10	5	9.2 ± 0.2
pCDuet_His_6ThitHydE1	10	5	10.0 ± 0.2
pCDuet_His_6ThitHydE2	5	3	5.4 ± 0.3

ND = not determined. [a] added as $FeCl_3$ (aq). [b] added as Na_2S (aq).

3.3.1 Reconstitution of StrepHydF

Before chemical reconstitution the iron content of StrepHydF was 1.3 ± 0.3 eq of Fe per protein and its [4Fe4S]-cluster content was no higher than 23% in regard to concentration as determined by the UV-Vis spectrum (Fig 2.26) using the extinction coefficients in Table 3.1 (see Chapter 2, section 2.3.3). The general procedure for the anaerobic reconstitution of HydF included ensuring the cysteine residue thiol groups were fully reduced by the addition of strong reducing agents such as DTT, GSH, L-cysteine or β-mercaptoethanol. With the exception of β-mercaptoethanol, all of the mentioned thiol reducing agents plus ferric ammonium citrate (FAC) were tested for their ability to stabilize the bound [4Fe4S]-cluster of HydF after gel filtration and for giving a low background signal in the corresponding UV-Vis spectrum of reconstituted HydF (Results in Figure 3.2 and 3.3). The cysteine-thiol reduction by ferric ammonium citrate might not be ensured since it is usually used as a reducing agent for gold nanoparticles[319], but not for thiols, whereby citrate acts as the mild reducing agent. In the context of iron-sulfur cluster reconstitution it has been more commonly utilized as an iron source.[112,171,320,321]

Intense and/or broad background absorption levels in the UV-Vis spectrum points towards the presence of high levels of iron and sulfide containing aggregates, the formation of FeS and unspecific binding of iron and/or sulfur to the protein. A general reconstitution protocol is described hereafter, although this could be adapted as noted for each protein. After the addition of the reducing agent and incubation for 30 mins,

iron(III) was added as a $FeCl_3$ solution and the protein solution turned red over circa 10 min, presumably as a result of the initial complexation of Fe^{3+} by the reducing agents. Over a period of approximately 1 h, the iron ions are incorporated into the protein and sulfide is then added as a Na_2S solution. Immediately upon addition of sulfide, the protein solution turned a brownish color, and gave rise to the absorption band at 410 nm over an incubation time of 2 h. To remove any black protein aggregates and precipitated FeS, the reconstituted protein mixture was briefly centrifuged (6000 rpm, 1 min, 18 °C) and the supernatant was applied onto a PD-10 column (2.5 mL, contains Sephadex G-25) for gel filtration. The brown protein containing fractions were collected, combined and analyzed by UV-Vis spectroscopy. The concentration of the [4Fe4S]-cluster was calculated from the background subtracted (880 nm) absorption band at 410 nm, using the known extinction coefficient in Table 3.1 and the Lambert-Beer-Law (3-1).

The most common reducing agent used for iron-sulfur cluster reconstitution has been dithiothreitol (DTT)[104,322-324], which has been shown to largely increase the FeS protein formation activity in mitochondrial extracts *in vitro* and protects the decomposition of Fe-S clusters.[325] Following the addition of the iron equivalents, DTT forms a red colored complex with the free Fe(III) ions which has an absorption band at around 470 nm.[326] Upon addition of sulfide, a new absorption band appears at 410 nm which corresponds to the formation of the [4Fe4S]-cluster.

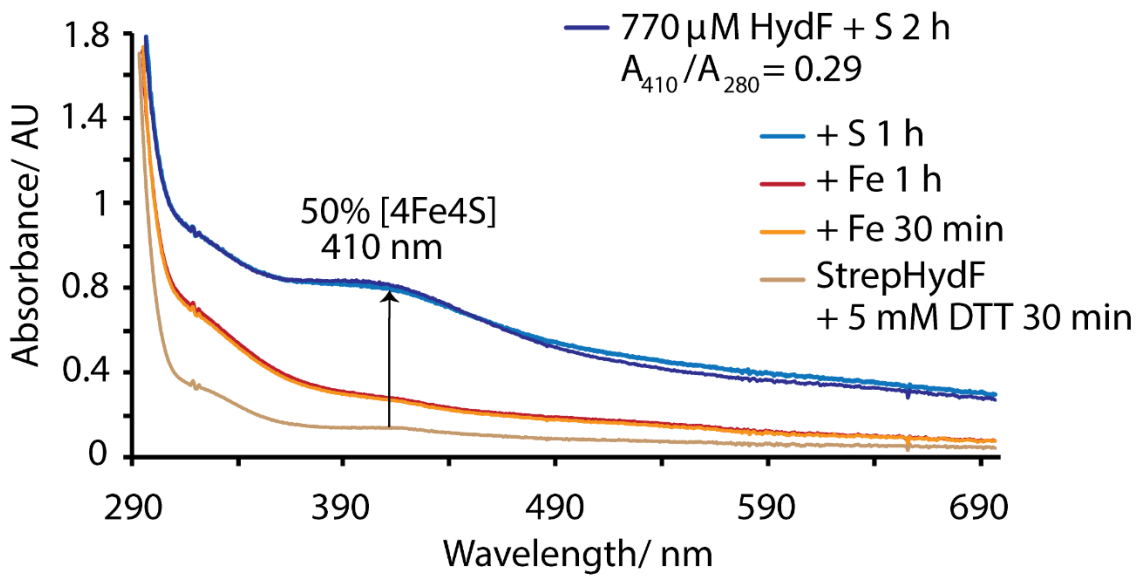

Figure 3.2: UV-Vis spectra of HydF [4Fe4S]-cluster reconstitution, measured in a 1 mm cuvette. First step: (—) reduction of cysteine thiols with 5 mM DTT for 30 min. Second step: Addition of 6.5 equivalents of Fe, UV-Vis after 30 min (– –) and 1 h (– –) incubation. Third step: Addition of 6.5 equivalents of S, UV-Vis after 1 h (– –) and 2 h (– –) incubation. The final concentration of [4Fe4S]-cluster is 385 µM as calculated from the absorption band at 410 nm (0.5 mol equivs., HydF 770 µM).

Using L-cysteine as an alternative reducing agent or ferric ammonium citrate for the preparation of [4Fe4S]-cluster *via* chemical reconstitution resulted in either a very broad absorption from 280-400 nm, in the case of ferric ammonium citrate, or a very high background absorption which was observed when L-cysteine was used (Figure 3.3).

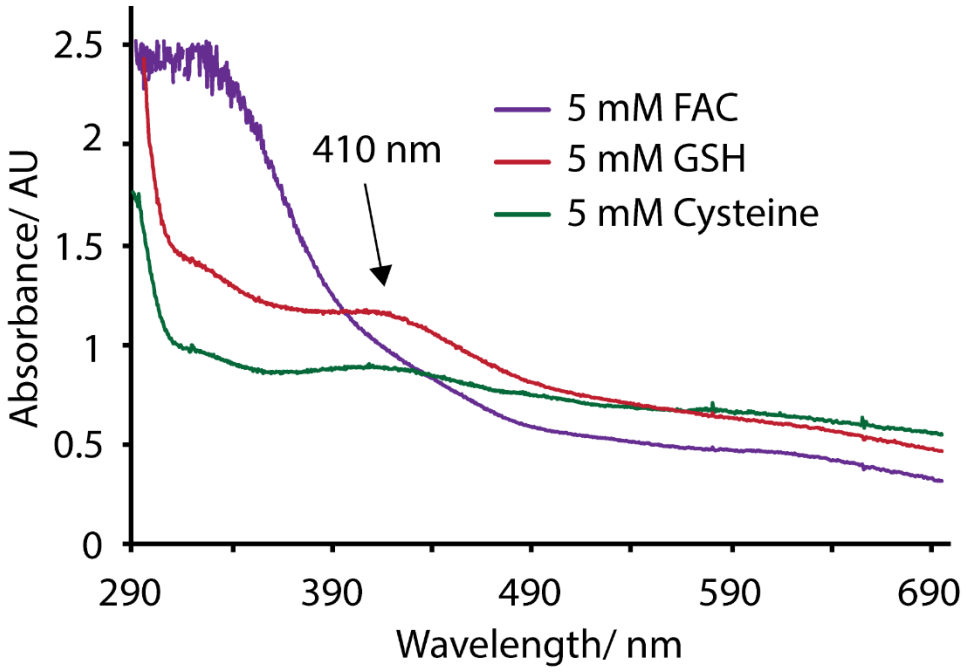

Figure 3.3: UV-Vis spectra of [4Fe4S]-cluster reconstitution of HydF (600 μM) with different reducing agents and additives (5 mM). For these reconstitutions 6.5 equivalents of Fe and S were added to HydF in respect to the protein concentration. FAC: ferrous ammonium citrate, GSH: reduced glutathione, Cysteine: L-cysteine.

However, reduction with reduced glutathione showed a distinct and defined band at 410 nm for reconstituted HydF, with little background. When compared with a UV-Vis spectrum of HydF reconstituted in the presence of DTT, it also shows more distinctive bands and a better uptake of the [4Fe4S]-cluster (Figure 3.4).

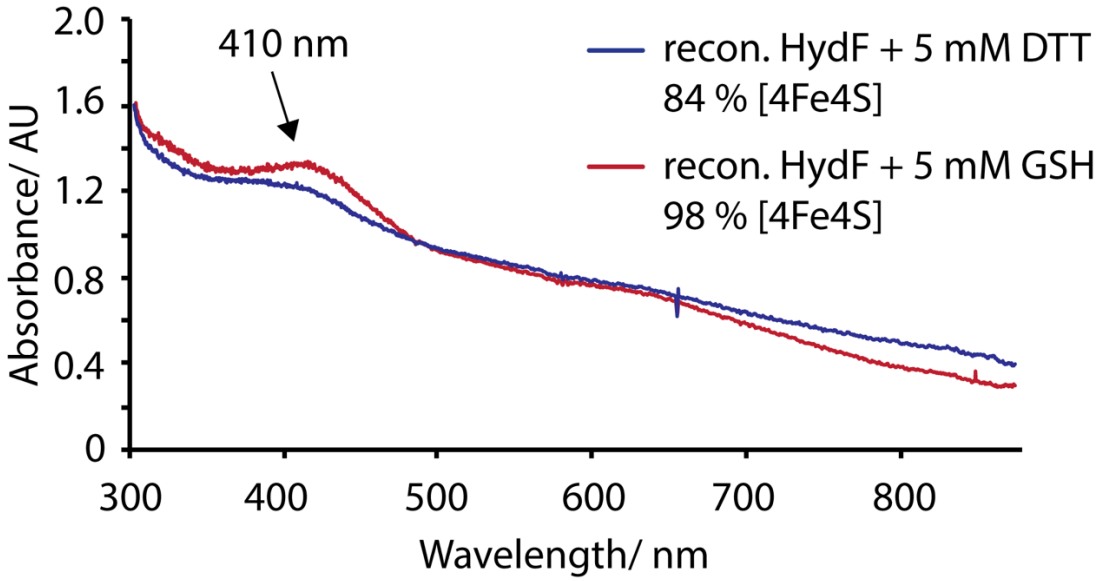

Figure 3.4: UV-Vis spectra of [4Fe4S]-cluster reconstitution of HydF either reduced with DTT (620 μM) or with GSH (660 μM), measured in a 1 mm cuvette. For these reconstitutions 6.5 equivalents of Fe and S were added to HydF in respect to the protein concentration.

After reconstitution, chromatography with a PD-10 gel filtration column removed excess and/or unbound iron, sulfide and any iron(II)sulfide colloids that may have formed. To differentiate high resolution size exclusion chromatography using S75 Superdex from buffer exchange with a PD-10 column, the latter will be referred to as 'PD-10 gel filtration' herein. After PD-10 gel filtration, another UV-Vis spectrum is recorded to check for the amount of [4Fe4S]-cluster remaining bound. Since the position of the [4Fe4S]-cluster in HydF is partly exposed to the solvent, according to the crystal structure of *Tn*HydF[243] and *Tme*HydF[244], it was regarded as likely to be very labile and therefore the addition of reagents to stabilize the cluster was investigated. A comparison of HydF reconstituted and gel filtered with either DTT or GSH as the reducing agent is shown in Figure 3.5. What becomes obvious is that the [4Fe4S]-cluster is less stable in the presence of DTT, as the [4Fe4S] cluster content significantly decreased (Fig 3.5B, by 29%) after gel filtration, but a better recovery of intact [4Fe4S]- cluster was achieved with GSH (Fig 3.5A, 97 % recovery). As GSH gave better [4Fe4S]-cluster stability and uptake, it was used as the reducing agent for all subsequent HydF reconstitutions (see for example Figure 3.6).

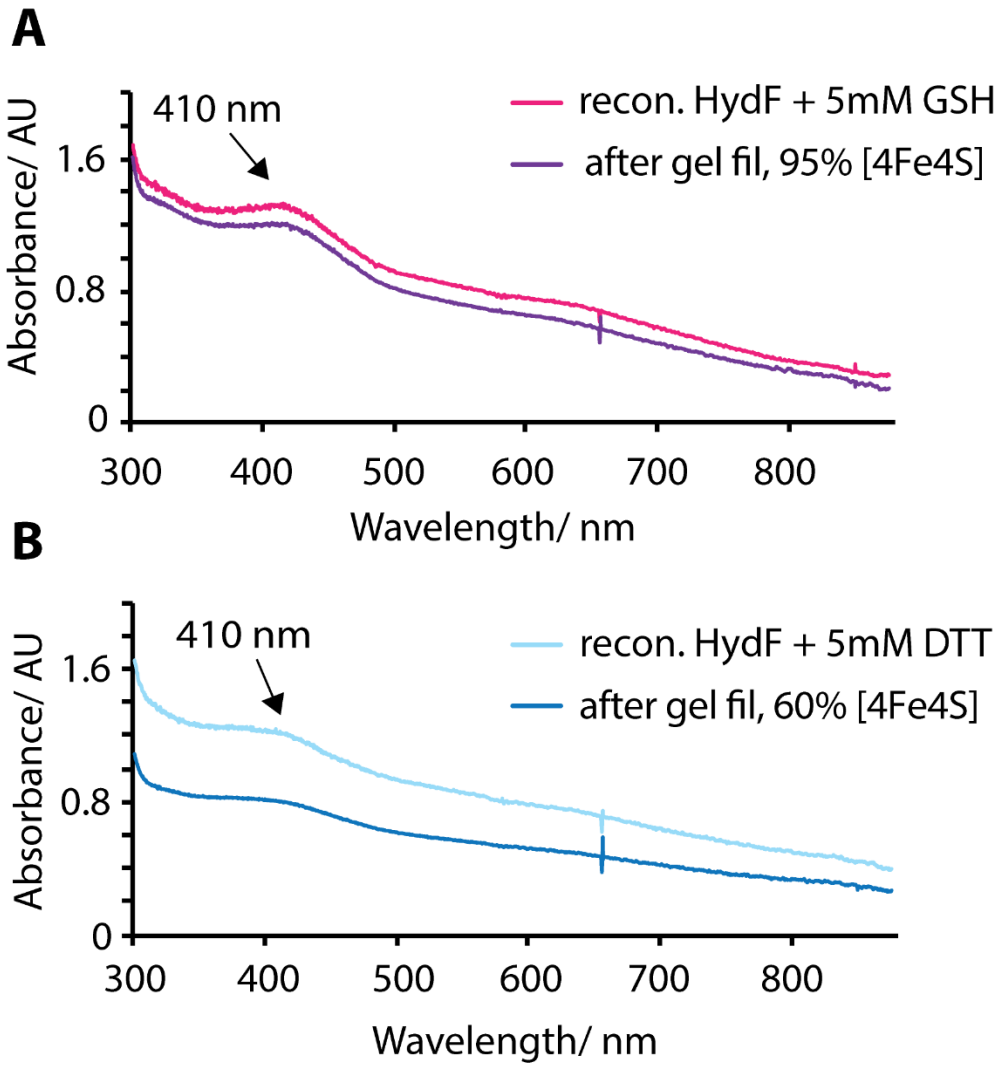

Figure 3.5: Comparison of UV-Vis spectra shown in Figure 3.4 with the UV-Vis spectrum of the appropiate sample before or after gel filtration using a PD-10 column. For these reconstitutions 6.5 equivalents of Fe and S were added to HydF in respect to the protein concentration. **A**. Gluthione sample before (–·–) and after (–··–) gel filtration. **B**. DTT sample before (—) and after (––) gel filtration. After the PD-10 gel filtration steps the concentrations were for HydF with 5 mM GSH: 650 μM and for HydF with 5 mM DTT: 562 μM. The spectra were measured in a 1 mm cuvette.

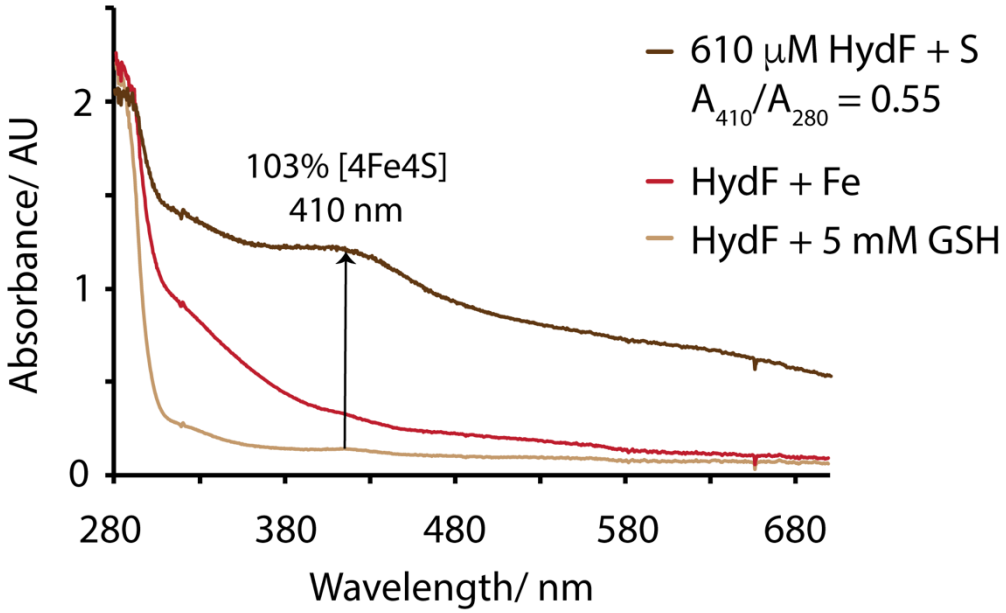

Figure 3.6: UV-Vis spectra of [4Fe4S]-cluster reconstitution of HydF (610 μM) measured in a 1 mm cuvette under optimized conditions (using glutathione as a reducing agent). For this reconstitution 6.5 equivalents of Fe and S were added to HydF in respect to the protein concentration.

3.3.2 Reconstitution of StrepHydF with H-cluster mimic

For envisaged future crystallization experiments and to provide a standard for FT-IR characterization, the HydF scaffold protein was reconstituted with an H-cluster precursor mimic. The dark-red mimic contains a pdt (propanedithiolate) group instead of an adt (azadithiolate) group, as found in the native H-cluster, as well as one additional CO ligand (Figure 3.7). The mimic was kindly provided by Prof. Chris Pickett (Chemistry Department, University of East Anglia). To characterize the pdt-mimic, an ESI (-) and ESI (+) mass spectrum was measured; in the ESI (+) spectrum the counter-ion tetraethylammonium could be observed, whilst in the ESI (-) spectrum the observed mass corresponded to the pdt-anion and peaks corresponding to the dissociation of one CO and one CN^- ligand, consistent with a degree of fragmentation during the measurement, which has been observed before for similar organometallic complexes[327,328]. The mass spectra are attached in the Appendix (A 3.1).

For reconstitution with the pdt-mimic, reconstituted HydF (~ 50 μM) was incubated with 10 eq. of the mimic (~ 500 μM) and left to incubate for 1 h or overnight. The nucleotide substrate of HydF, GTP (2 mM), was added for one reconstitution experiment, to check if it has an effect on the H-cluster binding. After the incubation period, unbound pdt-

mimic was removed by PD-10 gel filtration and a UV-Vis spectrum of the brown protein fraction was recorded (see Figure 3.8).

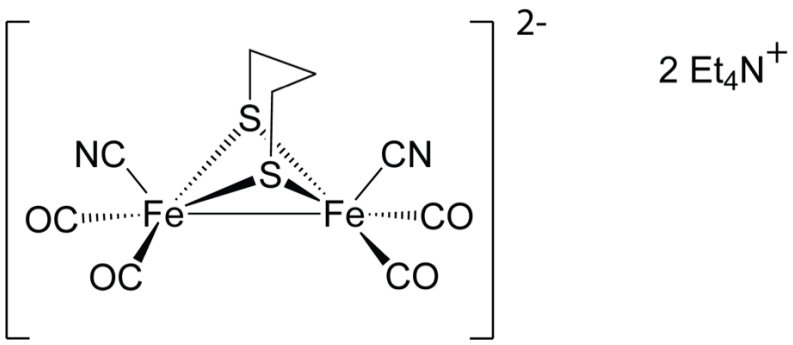

Figure 3.7: Molecular structure of the pdt-H-cluster mimic with tetraethylammonium counter-ion (kindly provided by Prof. C. Pickett).

Prior to the reconstitution, a 125 μM pdt-mimic stock in deionized water was analyzed by UV-Vis which showed a characteristic absorption band at 350 nm with an extinction coefficient of 7800 cm^{-1} M^{-1} (Figure 3.8).

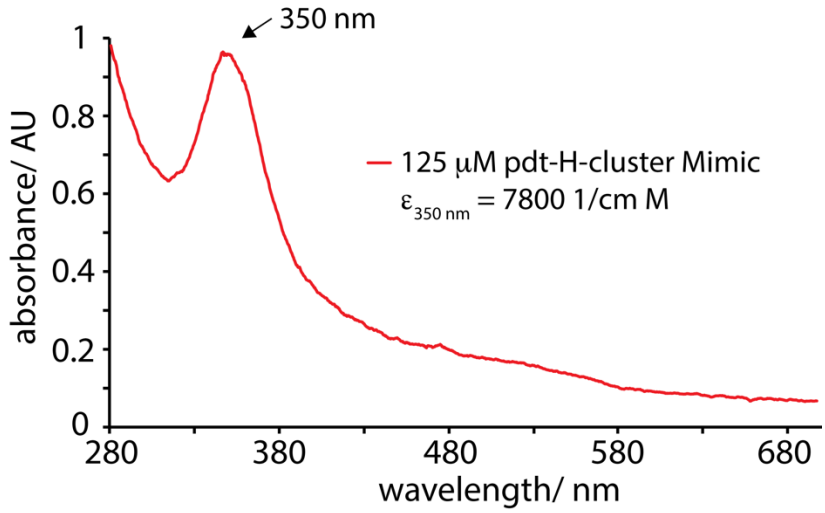

Figure 3.8: UV-Vis spectrum of the pdt-H-cluster mimic (125 μM) in a 1 cm cuvette.

The uptake of the pdt-mimic by reconstituted HydF was investigated by incubation together for either 1 h or overnight (Method 21). The concentrations were HydF (23-25 μM) and 10 equivalents pdt-mimic. Excess pdt-mimic was removed by PD-10 gel filtration. The uptake of pdt-mimic was estimated from the absorption at 350 nm in the UV-Vis spectra of the incubated protein samples (Fig 3.9).

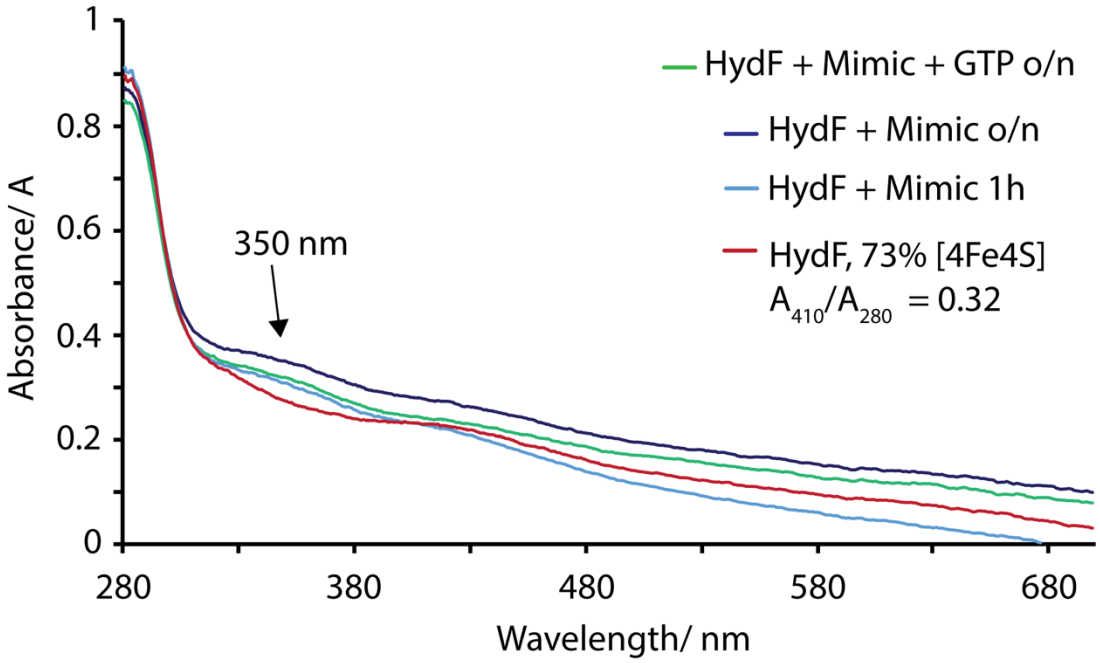

Figure 3.9: UV-Vis spectra of recon. HydF (23-25 μM) incubated in the absence (––) and in presence of pdt-mimic after PD-10 gel filtration. Incubation times with mimic were 1 h (––), overnight (––) and overnight in presence of GTP (––). Measured in a 1 cm cuvette. Data smoothed with Microsoft Excel exponential smoothing (0.9), due to high level of noise resulting from small sample concentration.

The iron content of each sample was measured and the mimic content estimated from the UV-Vis spectra (Table 3.3). In regard to the control iron content of HydF without mimic (6.8 eq.), the greatest degree of mimic incorporation was achieved either by incubation with GTP over 1 h or without GTP overnight. Nevertheless, the iron content obtained for the GTP (1 h) sample has a high error and could be misleading. By comparing the results from the UV-Vis spectra, the overnight incubation without GTP gave the highest amount of mimic binding. Both overnight incubation (± GTP) gave highest yields of mimic incorporation as estimated from the UV-Vis absorption. As interpreted from the UV-Vis spectra, GTP had a negative impact on the mimic incorporation. Overall, there has been no significant effect of GTP on improving the mimic incorporation, but overnight incubation versus 1 h incubation gave better yields of the mimic loaded HydF. The mimic content was less than 1 equivalent per mole HydF protein, which might derive from the fact that glutathione is coordinating the unique iron of the [4Fe4S]-cluster, which makes it inaccessible for mimic loading.

Table 3.3: Incorporation of pdt-H-cluster mimic onto HydF. Iron content measurements and the mimic content estimated from the absorbance at 350 nm and ε = 7800 cm^{-1} M^{-1} from the UV-Vis spectra in Figure 3.9. The background absorbance of the HydF control sample at 350 nm was subtracted from the absorbance value of the samples incubated with the mimic.

Sample	Iron Content	Mimic equiv. by UV-Vis
HydF control	6.80 ± 0.50	0
HydF + Mimic 1h	6.56 ± 0.15	0.11
HydF + Mimic + GTP 1h	9.42 ± 0.73	0.05
HydF + Mimic o/n	9.23 ± 0.26	0.40
HydF + Mimic + GTP o/n	8.81 ± 0.10	0.24

3.3.3 Reconstitution of StrepHydE and His_6HydE

The StrepHydE constructs required chemical reconstitution of their Fe-S cluster since the maximal [4Fe4S]-cluster content was only 0.21 equivalents per mole of HydE1 protein after purification (Chapter 2, Section 2.3.4). Consequently, the StrepHydE proteins were reconstituted with iron-sulfur cluster prior to EPR measurements. Due to the lack of a second binding site for [4Fe4S]- or [2Fe2S]-clusters, StrepHydE2 was reconstituted with 5 eq. of Fe and S, whereas HydE1, which contains potential ligand residues for an auxiliary cluster, was reconstituted with 8 eq.. Dithiothreitol (DTT) was used as a reducing agent for both reconstitutions, because the radical SAM [4Fe4S]-cluster is buried inside the TIM-barrel of the HydE proteins and is therefore more stable and less exposed in comparison to the cluster of HydF.

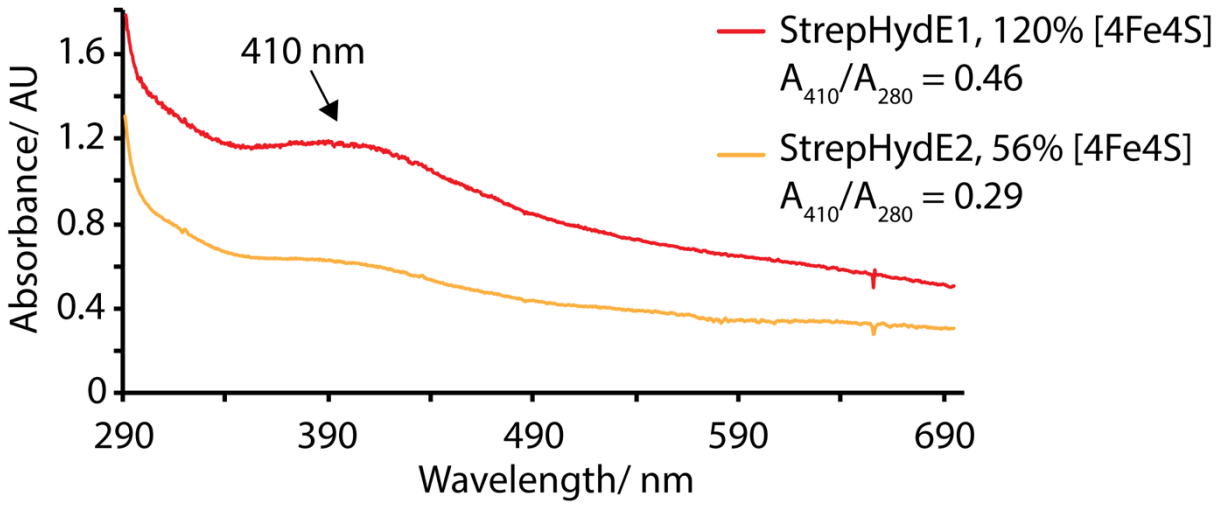

Figure 3.10: UV-Vis spectra of reconstituted StrepHydE1265 (448 μM, ––) and StrepHydE1675 (450 μM, ––), measured in a 1 mm cuvette.

UV-Vis spectra of reconstituted StrepHydE1 and HydE2 (Figure 3.10) showed as expected high amounts of [4Fe4S]-cluster for HydE1 (1.2 equivalents of [4Fe4S] per HydE1) and less for HydE2 (0.6 equivalents of [4Fe4S] per HydE2).

In preparation for pull-down studies, sequence variants bearing *N*-terminal affinity-tags on StrepHydE proteins have been generated, replacing the Strep with a His_6-Tag (Chapter 2, Section 2.4.1). For the His_6-tagged HydE proteins a similar reconstitution protocol to that of His_6HydG was applied. Directly after NiNTA purification and buffer exchange, HydE1 was reconstituted with 5 mM DTT and 10 equivalents of Fe and S (Method 20, or Chapter 2, Section 2.4.2). Subsequently, after further purification by high resolution size-exclusion chromatography a great loss of iron-sulfur cluster occurred (residual iron content was around 5 mol/mol HydE1) and the protein was further reconstituted with an additional 5 eq. of Fe and S. The same procedure was carried out for HydE2, but with fewer equivalents, 5 equivalents for the first reconstitution and 3 eq. for the second. The resulting UV-Vis spectrum of double reconstituted His_6HydE proteins is shown in Figure 3.11. The [4Fe4S]-cluster uptake was slightly less than that for the Strep-tagged proteins (Figure 3.10), but this could be caused by the fact that the auxiliary cluster of HydE1 might be a [2Fe2S] cluster, rather than a [4Fe4S]-cluster. Additionally, the difference of [4Fe4S]-cluster content between HydE1 and HydE2 are smaller when compared to the Strep-tagged version. This could derive from the impurities co-eluting with HydE after purification which lead to distorted protein concentration calculations (Chapter 2.4.2, Figure 2.36 and 2.37).

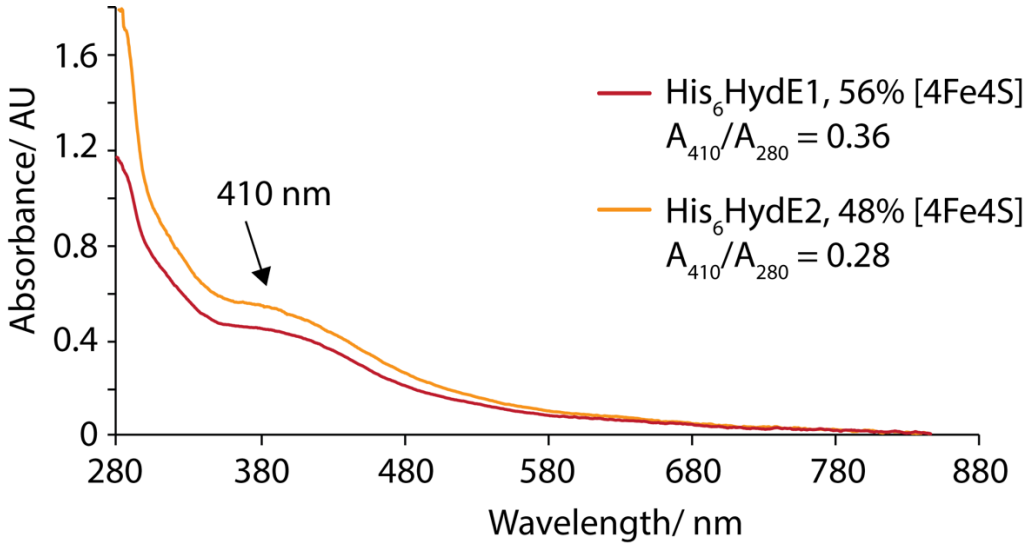

Figure 3.11: UV-Vis spectrum of reconstituted His_6HydE1265 (52 μM, ––) and His_6HydE1675 (71 μM, ––), measured in a 1 cm cuvette.

As observed in the UV-Vis spectra for both affinity-tag systems of reconstituted HydE proteins, the HydE2 protein contains a smaller amount of [4Fe4S]-cluster (Table 3.4) than HydE1, which was anticipated because of it appears to be missing a second cluster binding site.

Table 3.4: Comparison of [4Fe4S]-cluster equivalents. Results per mole of Strep/His_6HydE proteins and A_{410}/A_{280} values obtained from the respective UV-Vis spectra of reconstituted Strep/His_6HydE proteins.

Sample	Equivalents of [4Fe4S]	A_{410}/A_{280}
StrepHydE1265	1.20 ± 0.14	0.46 ± 0.05
His_6HydE1265	0.56 ± 0.19	0.36 ± 0.07
StrepHydE1675	0.56 ± 0.10	0.29 ± 0.01
His_6HydE1675	0.48 ± 0.12	0.28 ± 0.04

3.3.4 Reconstitution of His_6HydG

For the reconstitution of His_6HydG, the established protocol[64] was used, optimized by Dr. R. Driesener[269] and Dr. P. Dinis[276]. Similar to the described method for the His_6HydE proteins: after the nickel affinity chromatography step and desalting, HydG was reconstituted with 10 equivalents of Fe and S. After the second purification step, using S200 size-exclusion chromatography, HydG was further reconstituted with 5 eq. of Fe and S. The corresponding UV-Vis spectrum of HydG after the second reconstitution is shown in Figure 3.12 and the observed A_{410}/A_{280} value of 0.48 resembles the previously reported of 0.47[276].

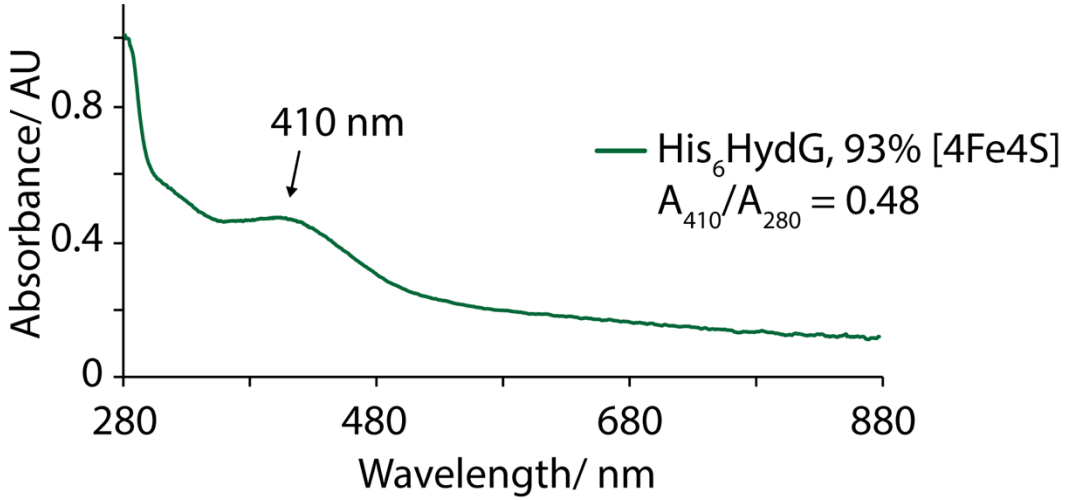

Figure 3.12: UV-Vis spectrum of reconstituted His_6HydG (52 μM), measured in a 1 cm cuvette. Data smoothed with Microsoft Excel exponential smoothing (0.9), due to high level of noise resulting from low sample concentration.

3.4 EPR spectroscopy

EPR (Electron Paramagnetic Resonance) spectroscopy is based on the absorption of electromagnetic radiation by a paramagnetic sample. It is a powerful tool to distinguish between different FeS cluster types. Not all oxidation states of the biologically relevant FeS cluster are EPR-active, because EPR requires unpaired electrons with spin of S = ½ due to their behavior in a strong magnetic field. Likewise, NMR (Nuclear Magnetic Resonance) spectroscopy works with nuclei that have a nuclear spin above zero, I > 0. In comparison, EPR needs resonance frequencies 300 times higher than those required for NMR and works with a constant magnetic field. Microwave/far-infrared frequencies are necessary to generate electron spin resonance.

Electrons possess an orbital and spin angular momentum in atoms and molecules, which give rise to a magnetic dipole moment μ.

$$\mu = h\gamma_e S = -g\beta_e S \tag{3-2}$$

$$\beta_e = e\hbar/2m_e \tag{3-3}$$

γ_e = magnetogyric ratio of the electron, β_e = Bohr magneton, g = g-factor, $\hbar$ = reduced Planck constant

If the electron is in a strong magnetic field B_0, conventionally in the z-direction, the energy levels of the spin states split depending on their magnetic quantum number, $m_S = \pm ½$, and the strength of B_0. This process is called the Zeeman effect.[329,330]

The difference in energy levels widens in the increasing magnetic field until the energy difference matches the energy of the irradiated microwaves resulting in absorption of photons.[331,332]

$$\Delta E = h\nu = g\beta_e B_0 \tag{3-4}$$

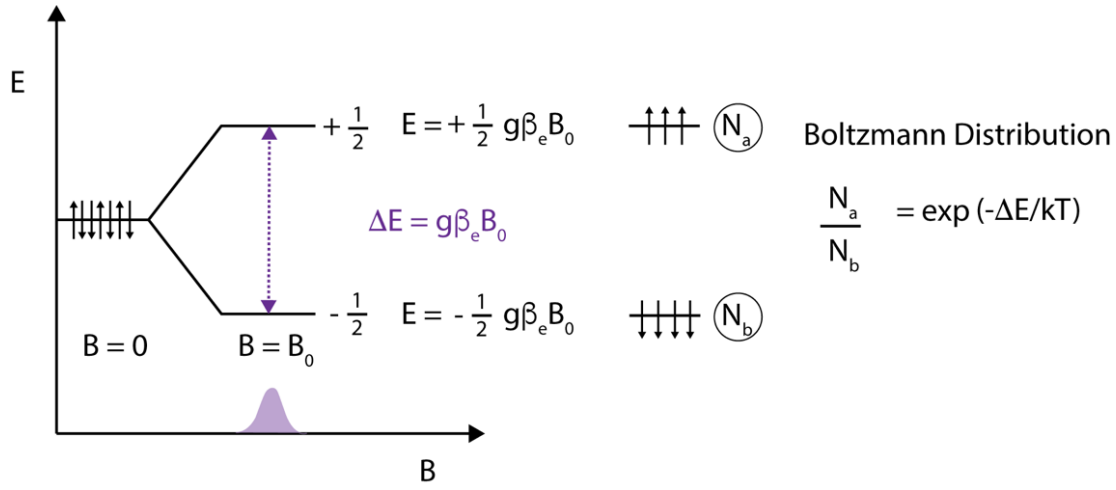

Figure 3.13: Energy levels as a function of the applied magnetic field and splitting of energy levels as a result of the Zeeman effect. ΔE is the required microwave energy to absorb and achieve electron resonance. Adapted from [333].

In the thermal equilibrium and in the presence of an external applied magnetic field, the spin population is split between the two Zeeman levels, following the Maxwell-Boltzmann law (Figure 3.13).[331] Absorption only occurs if the lower level is more highly populated (N_b) than or not equal to the higher level (N_a). To maintain the population excess in the lower level, the uneven number of electrons of the upper level need to lose energy by releasing a photon and returning to the lower level, according to the Maxwell-Boltzmann law. Release of energy occurs via a spin relaxation process, distinguishing between spin-lattice relaxation and spin-spin relaxation. At room temperature, the difference between the population levels is very small, and the net absorption increases as temperature decreases and magnetic field strength increases. The magnetic field strength is proportional to the microwave frequency.[329,332,334]

The basic set-up of an EPR-spectrometer is shown in Figure 3.14. The microwave bridge describes the part above the EPR magnets and is composed of the monochromatic microwave source, usually a Gunn-diode with a constant power output (200 mW). Also, part of the microwave bridge is a rectangular, hollow wave guide passing through an attenuator where the microwave power is reduced (usually to 2-4 mW) and transferred to a circulator which directs the microwaves into the resonator unit containing the sample. The transmitted/reflected radiation returns to the circulator and is directly transferred to the detector diode. A small fraction of the microwave source radiation is directed towards the reference arm, which includes an on/off switch and a phase shifter that are used to tune the resonator. The resonator role is to increase the sensitivity of the measurement. Moreover, the reference arm generates a

constant working current. For the EPR study of iron-sulfur cluster enzymes temperatures around 10 K are required and are created with a cryostat. The cryostat contains liquid and gaseous helium which flows through the system *via* a gas flow pump. A large storage Dewar serves as the liquid helium source and is connected to the spectrometer via a transfer line. The temperature of the helium is maintained and protected from the environment by a high vacuum applied by a turbomolecular pump.[335]

For the experiments mentioned in this chapter, continuous wave X-band frequencies (8-12 GHz) were used to record the EPR spectra, due to optimal sensitivities at this range.

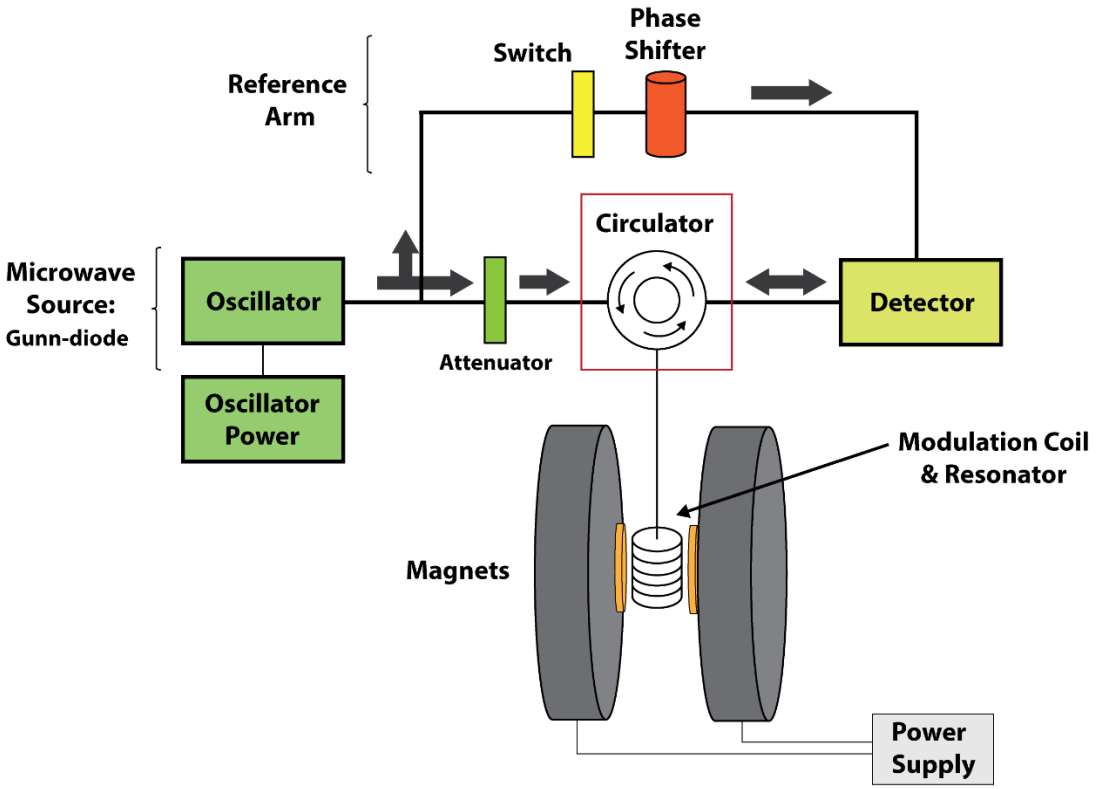

Figure 3.14: Set-up of an EPR spectrometer. Adapted from [336].

The signal as seen in an EPR spectrum arises from the absorption of microwaves by the unpaired electron/s in the sample and the shape and broadness of the peaks are dependent on many interactions. A major factor is the orientation of the electron spin, as well as the hyperfine or super-hyperfine interactions with the nuclear spin and nuclear Zeeman and quadrupole interaction. Additionally, zero field splitting (ZFS) is influencing the signal shapes and describes the interactions between more than one

unpaired electron within the sample.[337] Importantly, the electronic environment of the paramagnetic electron defines the signal shape.[338]

One parameter that is influenced by the electronic environment of the paramagnetic electron is the *g*-factor, which carries the chemical information used to determine the type of interaction between the electron and the electronic structure of the molecule. To determine *g*, a defined microwave frequency is needed (usually X-band: ~9 GHz) to irradiate the sample in a changing magnetic field strength to calculate ΔE and subsequently, *g*.[339,340] The *g*-value of EPR is similar to the chemical shift in NMR, a free electron in the vacuum has a *g*-value of 2.0023[341], whereas high spin *g*-values for transition metals in a complex are above 2.0 and low spin *g*-values are below, if the configuration is $d^{n>5}$. EPR signals of transition metals such as iron are strongly dependent on spin-orbit coupling and their *g*-anisotropy depends on the electronic configuration and the symmetry of the ligand field.[342]

The most common shapes of EPR signals relevant for biology are summarized in Figure 3.15. However, the conclusions drawn from the signal shapes in Figure 3.15 do not consider the contributions of hyperfine interactions or zero field splitting.[343] In order to consider hyperfine and zero-field splitting interactions of the obtained EPR signals, mathematical simulations of the spectra are required. Estimation of the hyperfine interaction constant A is important because it contains information about the number and identity of atoms in a molecule and their distance from the unpaired electron.[344] Furthermore, zero field splitting (ZFS) occurs even in the absence of an external magnetic field and it contains information about the distance and symmetry of at least two interacting unpaired electrons in the sample. The zero field splitting parameters are D and E, and depend on the average distance between two or more unpaired electrons and their deviation from the cubic symmetry, respectively.[345]

In the case of iron-sulfur clusters, the signal shape for EPR-active ([4Fe4S]- or [2Fe2S]-) clusters is usually rhombic, near axial, whereas the [3Fe4S] cluster possesses an isotropic shaped signal.[335]

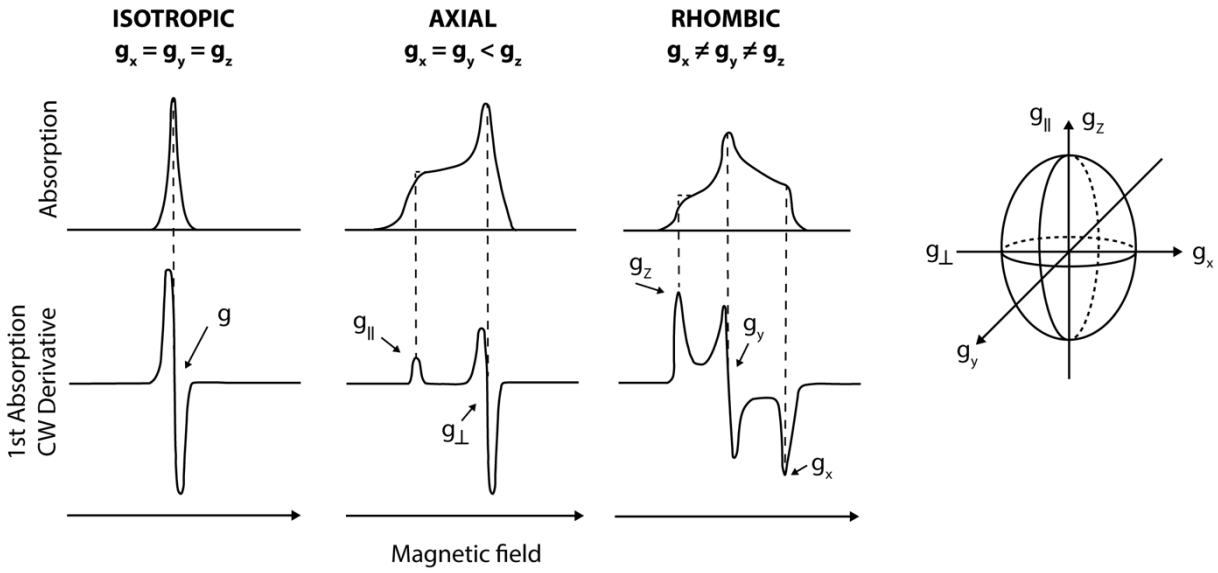

Figure 3.15: Schematic representation of the shape of the magnetic moment of a paramagnetic center with corresponding *g* values and the EPR spectral line shape. The line shapes are divided into three groups of anisotropy: isotropic, axial and rhombic. Adapted from [333].

To distinguish between different types of iron-sulfur cluster it is important to know the EPR-active redox states. For example, an oxidized sample that exhibits an EPR signal can only derive from a $[3Fe4S]^{+1}$ cluster or high-potential iron-sulfur protein (HiPIP) $[4Fe4S]^{+3}$-cluster that is stable in oxidation states of +2 and +3. For a sample prepared under strongly reducing conditions, the most likely possibilities are a $[2Fe2S]^{+1}$ or a $[4Fe4S]^{+1}$ -cluster.[335,346]

Another factor that needs to be taken into account is the temperature during the measurement, for example, the optimal temperature for detection of a $[4Fe4S]^{+1}$-cluster is 10 K, whereas for a $[2Fe2S]^{+1}$ -cluster it is 20-70 K.[346]

Characteristic EPR values for biologically relevant iron-sulfur clusters are summarized in Table 3.5.

Table 3.5: EPR characteristics of different iron-sulfur clusters in proteins.

Type of EPR active cluster		Spin	EPR active	*g*-values
	[2Fe2S]$^{2+}$	S = 0	No	-
	[2Fe2S]$^{1+}$	S = ½	Yes	2.01, 1.96, 1.92[347]
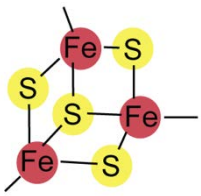	[3Fe4S]$^{1+}$	S = ½	Yes	2.03, 2.01, 2.00[348]
	[3Fe4S]	S = 0	No	-
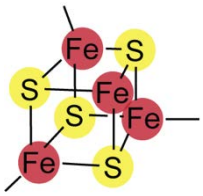	[4Fe4S]$^{+3}$	S = ½	Yes	2.12, 2.04, 2.04[349]
	[4Fe4S]$^{+2}$	S = 0	No	-
	[4Fe4S]$^{+1}$	S = ½	Yes	2.02, 1.94, 1.88[126]
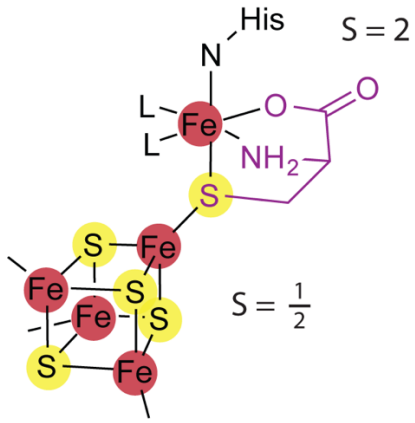	[5Fe5S]	S = 5/2	Yes	9.5, 4.7, 4.1, 3.8[64]

3.5 EPR studies on [FeFe]-hydrogenase maturation enzymes

The [FeFe]-hydrogenase maturation enzymes HydF, HydE and HydG have been extensively studied by using EPR spectroscopy. The EPR experiments carried out for this section are mainly to confirm that the enzymes from *Thermoanaerobacter italicus* contain the same features as the [FeFe]-hydrogenase maturation enzymes from other organisms and provide a foundation for future mechanistic studies. In particular, to confirm the presence of [4Fe4S]-cluster in all maturases, investigate if ThitHydE1265 can carry an auxiliary [4Fe4S]- or [2Fe2S]-cluster and to detect the HydG synthon high-spin iron in the [Fe(κ^3-Cys)]·[4Fe4S] complex.

3.5.1 EPR spectroscopy of HydE

Note: EPR spectra were recorded in collaboration with Dr. Enrico Salvadori and Dr. Maxie Roessler (Queen Mary University London, QMUL). Analysis of the spectra was assisted by Dr. Daniel Suess (UC Davis and MIT), Prof. David Britt (UC Davis) and Dr. Enrico Salvadori (QMUL). Their respective contribution to the studies described in this section is gratefully acknowledged.

Initial EPR studies were carried out with a smaller resonator (ER4118X-MS2) and with 2 mm OD Q-band tubes. Samples of StrepHydE1 (300 μM) were reduced with 10 mM DTH and subsequently frozen in liquid nitrogen for measurement in the EPR spectrometer.

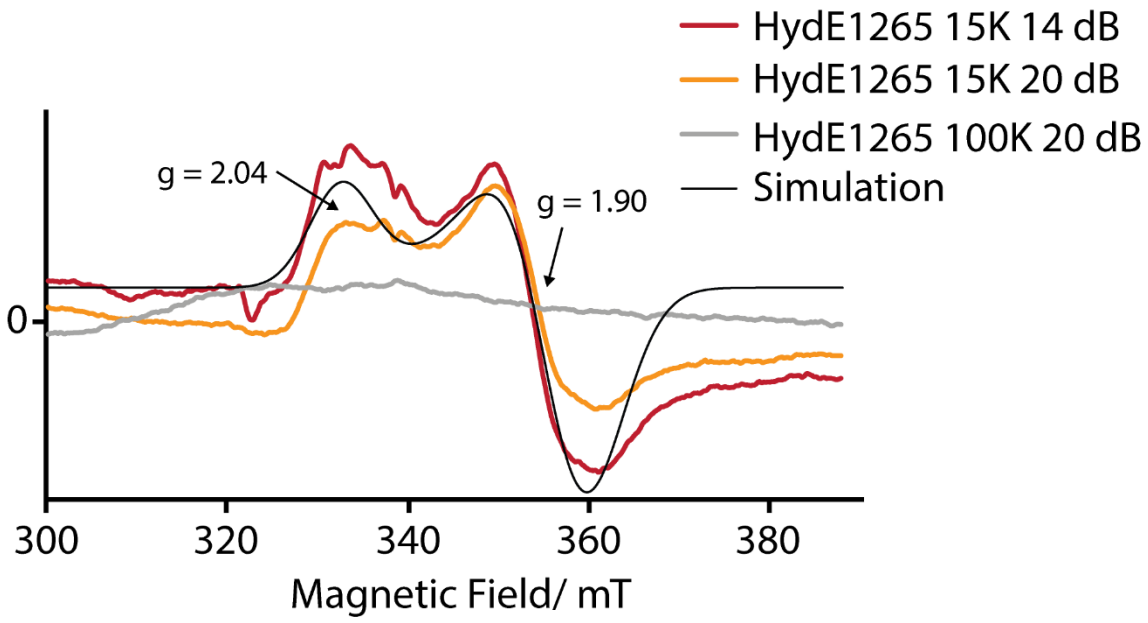

Figure 3.16: Background subtracted EPR spectra of 300 μM reduced StrepHydE1265 (HydE1) at different temperatures and powers using a small resonator. Data smoothed with Microsoft Excel exponential smoothing (0.9), because of noisy signals derived from small sample concentrations. Simulation of S = 1/2 signal was carried out with 'pepper' function of the program EasySpin[350] through MATLAB (Appendix 3.2).

The EPR spectrum at 15K of HydE1 showed the characteristic axial shape and *g*-values (*g* = 2.04, 1.90) typical of a [4Fe4S]-cluster (Figure 3.16). However, the presence of the EPR active $[2Fe2S]^{+1}$ cluster could not be confirmed, because no additional signal was detected at 15 K and no signal at a high temperature of 100 K. The little spikes at 330-335 mT might point toward the existence of a second [4Fe4S]-

cluster, a damaged [3Fe4S]-cluster or nonspecifically bound iron, however in a very low concentration.

Additionally, the EPR spectrum of HydE1 from a different batch (with 10 mM DTH added) obtained with a large resonator (ER4118X-MD5) and 4 mm OD Quartz tubes resulted in a different shaped signal and the sample in the presence of 3 mM SAM showed the typical axial shape upon SAM binding, giving EPR signals with *g*-values of 2.00, 1.88 and 1.83 (Figure 3.17) and a little signal at $g = 1.93$. However, in the absence of SAM the EPR spectrum of HydE was different, with a $g = 1.93$ signal and an extra signal appearing at around 365 mT, which might support the assumption that a second auxiliary [4Fe4S]-cluster is present and is overlapping with the signal of the radical SAM cluster.

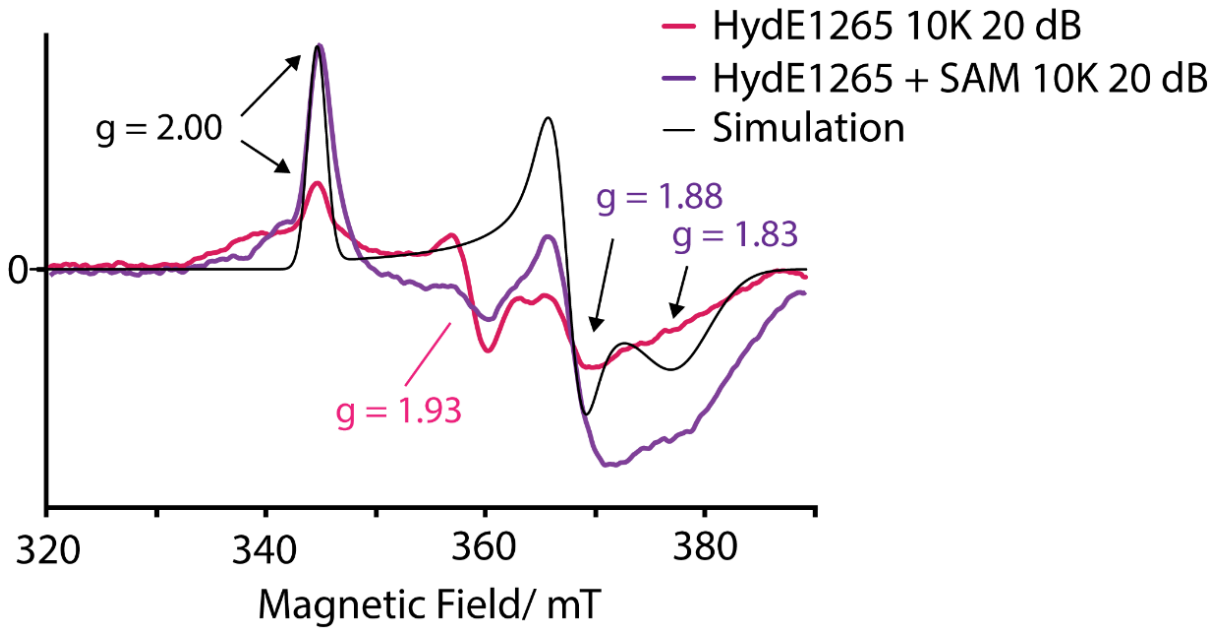

Figure 3.17: Background subtracted EPR spectrum of 300 μM reduced StrepHydE1265 at 10 K in absence and presence of 3 mM SAM using a large resonator. Data smoothed with Microsoft Excel exponential smoothing (0.9), due to high signal noise and low sample concentrations. Simulation of S = 1/2 signal was carried out with 'pepper' function of the program EasySpin[350] through MATLAB (Appendix 3.2).

The herein reported *g*-values for the [4Fe4S]-cluster of ThitHydE1 resemble the values stated for CaHydE and TmHydE (Table 3.6). The two [4Fe4S]-cluster in CaHydF were assigned as *N*- and *C*-terminal cluster by EPR simulations and by mixing with SAM, to observe the signal changes of the *N*-terminal radical SAM cluster.

Table 3.6: Comparison of EPR properties for HydE proteins from various organisms.

HydE from *Organism*	***g*-values (units)**
Thermoanaerobacter italicus HydE1265	+SAM : 2.00, 1.88, 1.83 No SAM : 2.04, 1.90
Clostridium acetobutylicum [4Fe4S]	 + SAM : 2.01, 1.88, 1.83 *N*-terminal: 2.04, 1.92, 1.90 *C*-terminal: 2.03, 1.91, 1.87[65]
[3Fe4S]	2.01
[2Fe2S]	2.00[65]
Thermotoga maritima	2.03, 2.02, (1.93)[52]

3.5.2 EPR spectroscopy of HydF

The EPR spectrum of reduced reconstituted HydF (300 μM HydF plus 20 mM DTH) showed the characteristic nearly axial shape corresponding to a [4Fe4S]-cluster with *g*-values of 2.05 and 1.86 (Figure 3.18). The *g*-values match the previously reported *g*-values for HydF proteins from other organisms (Table 3.7). There are low intensity spikes appearing at $g = 1.97$ and 1.93 in presence and absence of GTP which might correspond to nonspecifically bound iron or a degraded [4Fe4S]-cluster which would have resulted in a [3Fe4S] or [2Fe2S] cluster. To further clarify the cluster type present in HydF, it would be useful to record a relaxation profile with EPR recorded at different temperatures (for example, 10 to 100 K) during future studies. Nevertheless, there was no obvious change observed upon addition of GTP (10 mM), merely a very slight shift of the $g = 1.97$ signal, suggesting no direct interaction between GTP and the [4Fe4S]-cluster. A shift from $g = 2.00$ to $g = 2.01$ has been previously reported for CaHydF in the presence of bound GTP, but the GTP-influenced signal reported by Broderick *et al.* was much stronger and did correspond to a [2Fe2S] cluster.[246]

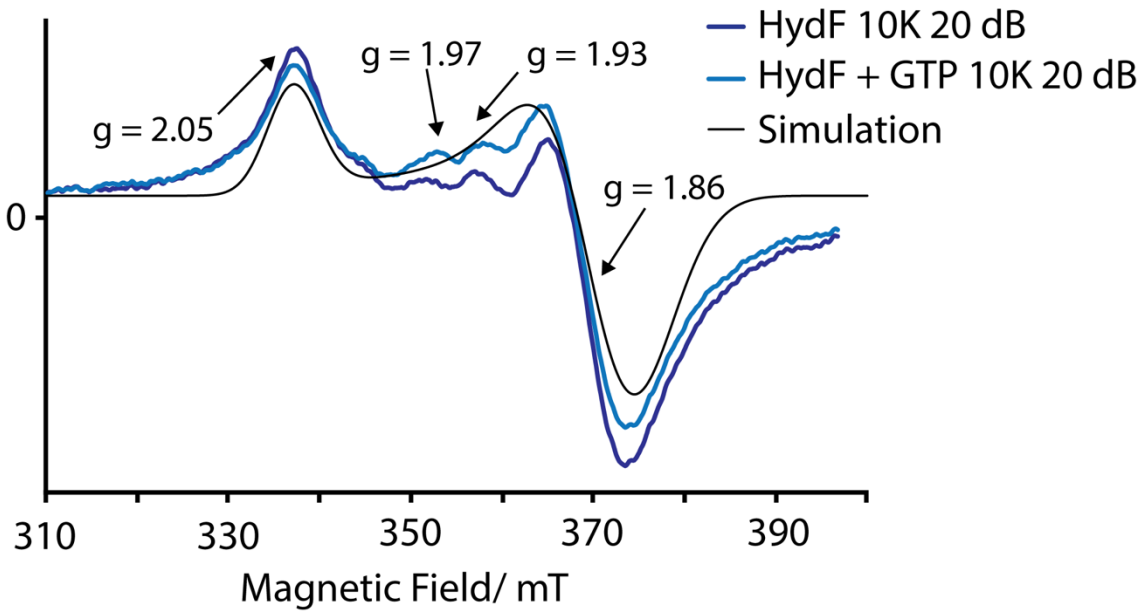

Figure 3.18: Background subtracted EPR spectrum of of 300 μM reduced StrepHydF at 10 K in absence and presence of 10 mM GTP using a large resonator. Data smoothed with Microsoft Excel exponential smoothing (0.9), due to a high signal to noise ratio. Simulation of S = 1/2 signal was carried out with 'pepper' function of the program EasySpin[350] through MATLAB (Appendix 3.2).

Table 3.7: EPR properties with *g*-values reported for HydF proteins from various organisms.

HydF from Organism	***g*-values (units)**
Thermoanaerobacter italicus	2.05, 1.86
Shewanella oneidensis	2.05, 1.93[50]
Thermotoga maritima	2.05, 1.90[51]
Thermosipho melanesiensis	2.05, 1.91, 1.87[244]
Thermotoga neapolitana	2.04, 1.90, 1.85[239]
Clostridium acetobutylicum [4Fe4S]	2.05, 1.89, 1.86[248]
[2Fe2S]	2.00, 1.96[248]

3.5.3 EPR spectroscopy of HydG

EPR spectra of His_6HydG (300 μM with 5 mM DTH) were initially measured with a smaller resonator for 2 mm OD Quartz tubes. Recorded spectra show either a characteristic rhombic shape for a [4Fe4S]-cluster with *g*-values 2.03, 1.91 and 1.87 and a split *g* = 2.03/2.06 peak or two clearly different clusters (radical SAM and auxiliary cluster, Figure 3.19) as reported previously for HydG from other organisms.[56,59] The resultant EPR-spectra with the large resonator (ER4118X-MD5) and another HydG batch are described in the following and allowed the assignment of the *C*- and *N*-terminal FeS-cluster of ThitHydG (Table 3.8, Figure 3.22 and 3.23).

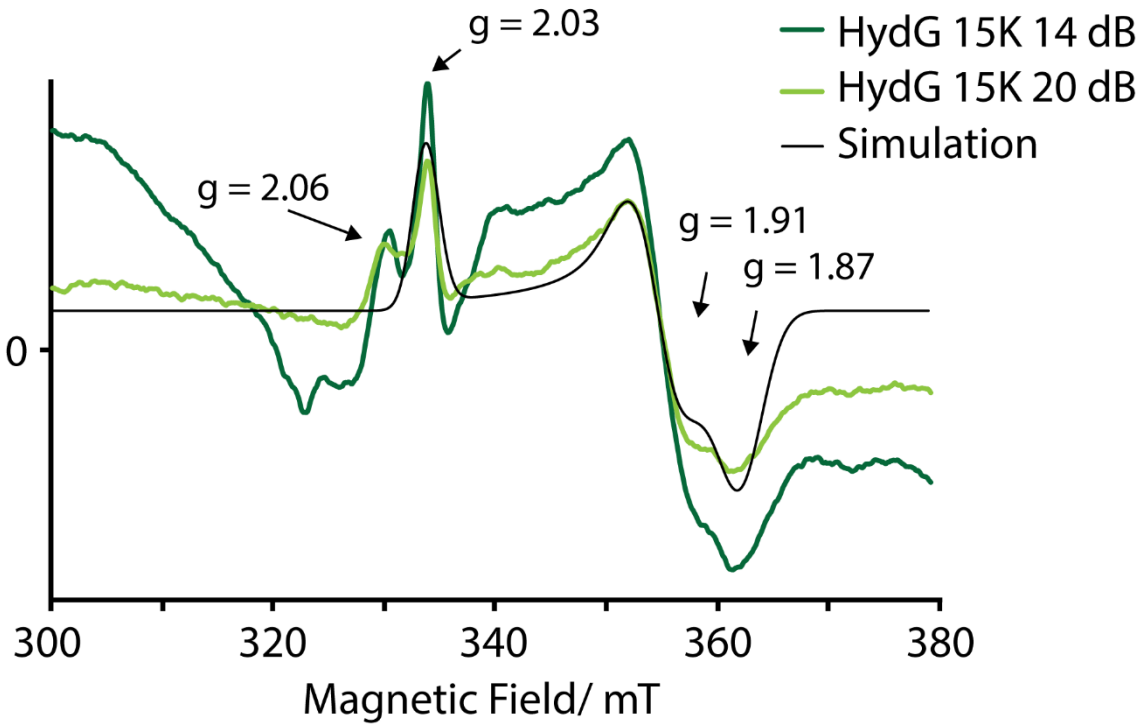

Figure 3.19: Background subtracted EPR spectrum of 300 μM reduced His_6ThitHydG at different microwave attenuations 14 dB and 20 dB, using a small resonator. Data smoothed with Microsoft Excel exponential smoothing (0.9). Simulation for an axial S = 1/2 signal was carried out with 'pepper' function of the program EasySpin[350] through MATLAB (Appendix 3.2).

Table 3.8: *g*-values reported for S = 1/2 signal of HydG proteins from various organisms.

HydG from Organism	***g*-values (units)**
Thermoanaerobacter italicus	2.04, 1.88 (*C*) / 2.00, 1.90, 1.86 (*N*)
Clostridium acetobutylicum	2.03, 1.92, 1.90 (both)[56] 2.02, 1.93, 1.91 (*C*-terminal)/ 2.00, 1.87, 1.83 (*N*-terminal)[56]
Shewanella oneidensis	2.05, 1.94, 1.91[59] 2.01, 1.88, 1.84 (SAM bound)[59] 2.06, 1.91, 1.88[59]

In good correspondence with the EPR results published for reduced SoHydG,[64,66] where in addition to the typical low-spin S = 1/2 signal of the $[4Fe4S]^{+}$ -cluster, a high-spin S = 5/2 signal was detected for the auxiliary FeS cluster in the low magnetic field region, a similar experimental strategy[66,69] was carried out to investigate ThitHydG. In order to detect the different forms of the auxiliary cluster, in the previous reported experimental conditions for SoHydG, a sequence variant lacking the *N*-terminal radical SAM cluster $SoHydG^{XN}$ was incubated with dithionite and different combinations of compounds influencing the auxiliary cluster compositions, Fe^{2+} (as $FeCl_2$), S^{2-} (as Na_2S) and L-cysteine. For studies reported in this thesis, the same approach was repeated for the wild-type ThitHydG protein (450 μM) to determine if it too can bind the $[Fe(\kappa^3\text{-Cys})]\cdot[4Fe4S]$ form of the auxiliary cluster. Results resembling the changes observed for SoHydG were obtained for the auxiliary cluster of ThitHydG; however, they were *g*-shifted compared to the signals of $SoHydG^{XN}$ (Fig. 3.20, Table 3.10). Table 3.9 summarizes all *g*-values obtained from the different experiments and Table 3.10 shows the *g*-values and detected signals for the incubation with DTH (10 mM), SAM (3 mM), Fe (3 mM) and Cys (3 mM) in comparison to the literature values of *Shewanella oneidensis* HydG. Figure 3.20, 3.22 and 3.23 highlight the obtained signals with HydG and different additives.

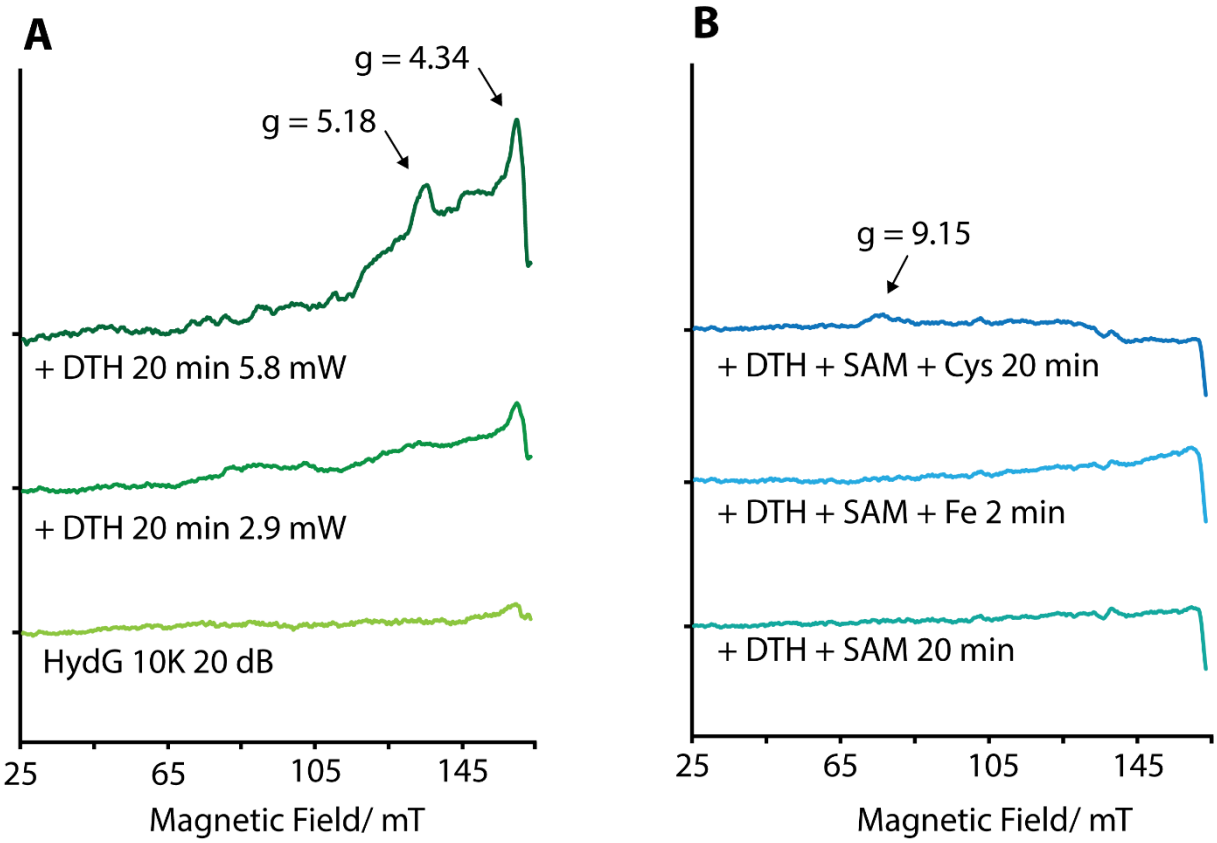

Figure 3.20: Low magnetic field signals of ThitHydG with different additives and time incubations. All spectra were recorded at 2.9 mW (low power) and 9.7 GHz (X-Band) and incubated for 20 min if not otherwise stated (5.8 mW high power). Data smoothed with Microsoft Excel exponential smoothing (0.9), due to high signal to noise ratio.

The low magnetic field EPR spectra in Figure 3.20A indicate that there are no signals with unreduced HydG, which means that there are no free Fe^{2+} ions present. Upon reduction with dithionite (DTH), signals with *g*-values of 5.18 and 4.34 at high power appear which may result from a [FeS]·[4Fe4S] form of the auxiliary cluster (Figure 3.21B), as observed in the crystal structure of ThitHydG.[64] However, the signal at 4.34 might not be real, since the background signal of the resonator overlaps with this region and the signal also could relate to adventitious Fe(III) which usually forms an isotropic signal at g = 4.3.[351] Furthermore, if reduced HydG is supplemented with SAM and L-cysteine a signal at g = 9.15 appears, already corresponding to the [Fe(κ^3-Cys)]·[4Fe4S] form of the auxiliary cluster (Figure 3.20B and Figure 3.21A), as observed for SoHydG[66].

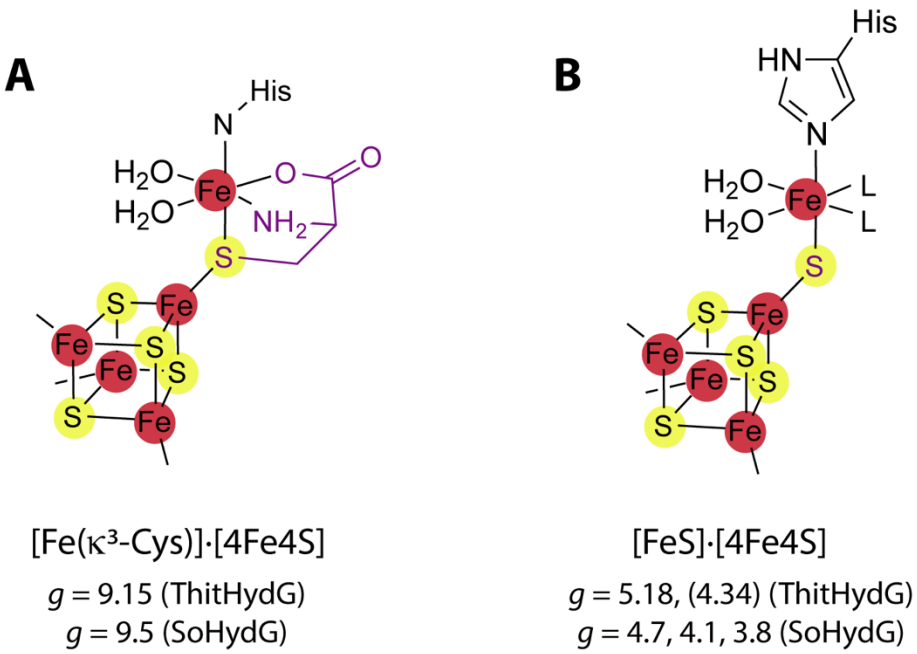

Figure 3.21: Molecular structures of HydGs auxiliary cluster forms in 'resting state' and possible corresponding EPR signals. A: [Fe(κ³-Cys)]·[4Fe4S], observed in the presence of L-cysteine, B: [FeS]·[4Fe4S], as observed in the crystal structure of ThitHydG. L = ligand.

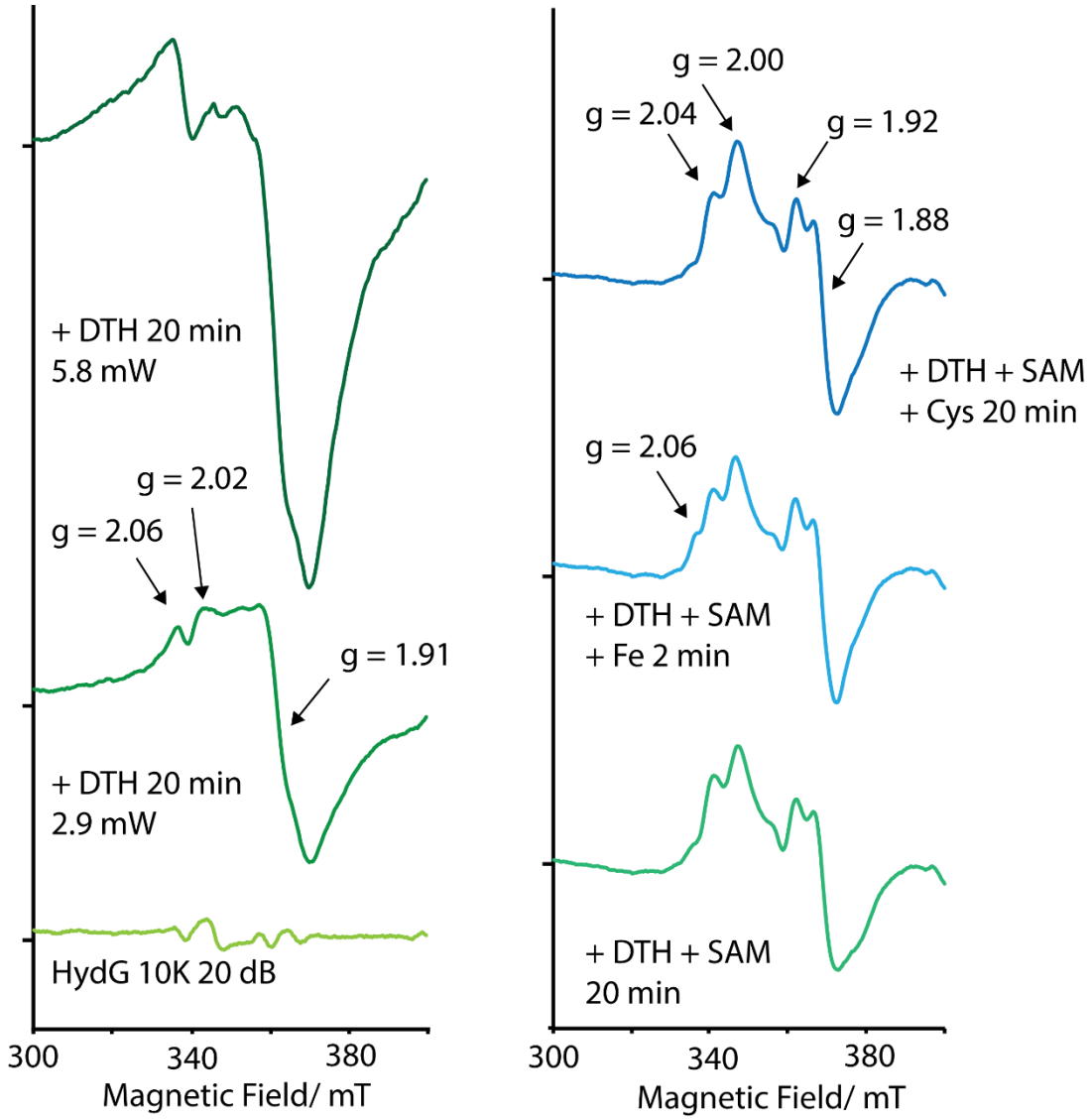

Figure 3.22: High magnetic field signals of ThitHydG with different additives and time incubations. All spectra were recorded at 2.9 mW and 9.7 GHz (X-Band) and incubated for 20 min if not otherwise stated. Data smoothed with Microsoft Excel exponential smoothing (0.9).

The richness of the high magnetic field [4Fe4S]-cluster signals in Figure 3.22 indicates the mixture of the radical SAM [4Fe4S]-cluster and the auxiliary [4Fe4S]-cluster. Signals appearing above 400 mT are most likely noise and out of the range where we would expect signals deriving from FeS cluster.

Table 3.9: Recorded *g*-values for EPR experiments carried out with His_6ThitHydG.

Experiment	*g*-values Low Field	*g*-values High Field
Ox. HydG	-	-
Red. HydG + DTH	5.18, 4.34	2.06, 2.02, 1.91
HydG + DTH + SAM	-	2.04, 2.00, 1.92, 1.88
HydG + DTH + SAM + Fe	-	2.06, 2.04, 2.00, 1.92, 1.88
HydG + DTH + SAM + Cys	9.15	2.04, 2.00, 1.92, 1.88
HydG + DTH + SAM + Fe + Cys	9.15, 5.38, 4.30	2.00, 1.90, 1.86

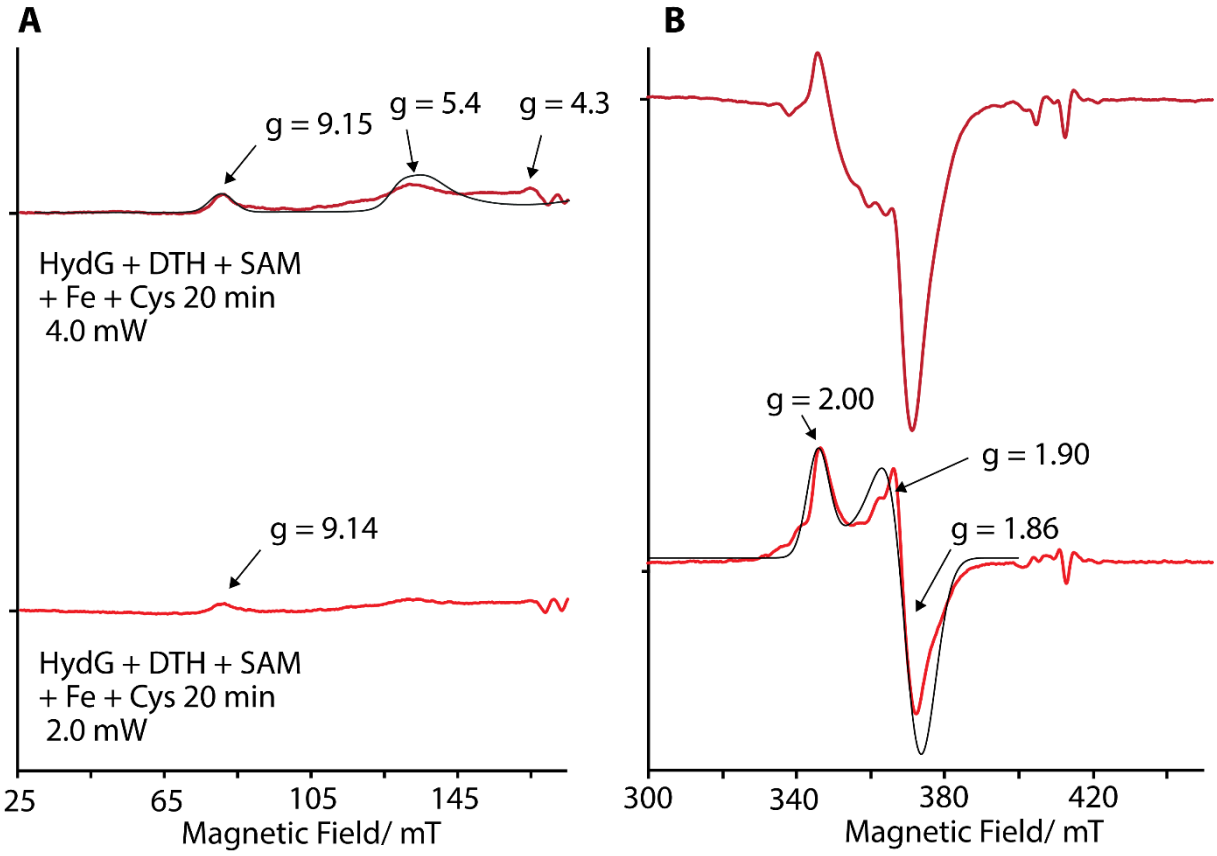

Figure 3.23: High (B) and low (A) magnetic field spectra of ThitHydG after incubation with DTH, SAM, Fe and Cys. Spectra were recorded at 2.9 mW or 4.0 mW and 9.7 GHz (X-Band) after an incubation time of 20 min. Data smoothed with Microsoft Excel exponential smoothing (0.9). Simulation were generated with the 'pepper' function in EasySpin[350] using MATLAB (Appendix 3.2).

Table 3.10: Reported *g*-values for HydGs reduced auxiliary cluster.

HydG	S =1/2 signals	S = 5/2 signals
So	2.06, 1.90, 1.87[66]	9.5, 4.7, 4.1, 3.8[66]
Thit	2.04, 1.92, 1.88	9.2, 5.4, 4.3

The resulting EPR spectra in Figure 3.23 give evidence of the binding mode of the auxiliary cluster. Since the resonator gave very strong background signal at around 170-200 mT, signals at *g*-values around *g* = 3-4.3 were impossible to be detected.
If SAM, Fe and L-cysteine are added to reduced HydG, the *g* = 9.14 becomes stronger with high power (Figure 3.23A), also signals at *g* = 5.4 and 4.3 appear which might derive from an S = 3/2 Fe-center due to antiferromagnetic coupling. Comparable S = 5/2 and S = 3/2 signals (*g* = 9.6 and 4.3) have been previously reported for the 'purple' aconitase enzyme which are rationalized as indicating a linear oxidized [3Fe4S] cluster[352] and a [Zn3Fe4S] cluster[335]. Nevertheless, this model does not fit accurately to the high-spin iron observed in the auxiliary cluster of HydG. The low power signals in Figure 3.23B (*g* = 2.00, 1.90 and 1.86) match the signals of the radical SAM cluster, since the low magnetic field S = 5/2 signal is a result of an exchange coupling of the S = 2 signal of the synthon Fe^{2+} and the S = 1/2 signal of the corresponding auxiliary $[4Fe4S]^{+}$-cluster (Figure 3.24A).

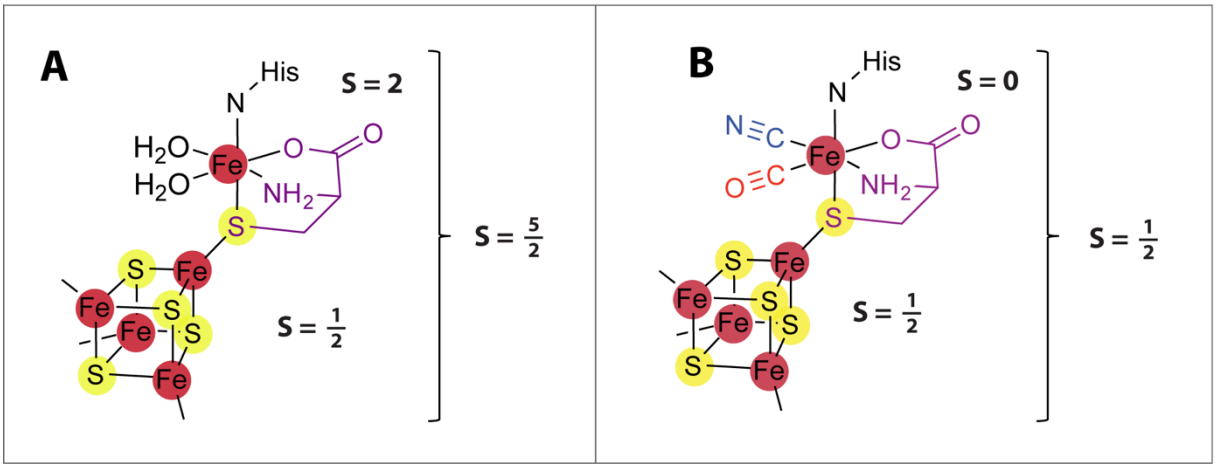

Figure 3.24: Resting state (A) of the auxiliary cluster of HydG described herein with contributions of the overall spin (S = 5/2 high spin), and active state or complex A (B) of the auxiliary cluster after HydG turnover in presence of 1 equivalent of L-tyrosine, 10 equivalents of SAM and dithionite in presence of L-cysteine with contributions to the overall spin (S = ½ low spin).

Most recent EPR studies on SoHydG[71] described the auxiliary cluster of HydG after turnover with its substrate L-tyrosine (1. Equiv.), SAM and dithionite in large excess freeze-quenched after 24s. By using a combination of ^{13}C-Mimis-ENDOR and ^{57}Fe-HYSCORE spectroscopy, the auxiliary cluster form was characterized as complex A [4Fe4S]-Fe(CO)(CN)-L-cysteine (Figure 3.24B) showing a low spin S = ½ signal in the corresponding EPR spectrum. The binding of strong π-acidic ligands CO and CN^- to the synthon iron results in a low spin Fe^{2+} S = ½ complex.[71]

The simulation of the low field signals has been difficult and future refinement of the parameters will likely lead to better simulations. The program EasySpin[350] on the MATLAB platform has been used and all simulations were generated with the 'solid-state cw' EPR function 'pepper'. For all S = 1/2 signals an axial or rhombic shaped simulation function with two or three *g*-values was generated with varying line broadening by the g-strain function.
In order to simulate the S = 5/2 and the S = 3/2 component of the auxiliary cluster signal from His_6ThitHydG two simulated functions were combined. One of these functions was generated for the S = 5/2 signal, with *g* = 2.0 using high *g*-strain values that induce line broadening. The zero-field splitting was also taken into account with similar values to the EPR study with SoHydG, where D stands for the axial zero field splitting parameter and E for the rhombic zero field splitting parameter (Figure 3.25 and Table 3.11). Since the hyperfine coupling constants were unknown, the H-strain broadening was also applied to the simulation. Nevertheless, the contribution from hyperfine coupling is not as relevant as the ZFS, since Fe and S basically have no nuclear spin (the magnetic active isotopes are in low abundance). The second function relates to the S = 3/2 signal, which gave the best overlap with the experiment if *g*-strain and H-strain broadening parameters were applied. However, the S = 3/2 signal around 4.3 could not be generated by simulation and in fact this was not definitely proven to be a real signal because of the proximity to a resonator background signal. For future experiments, to develop a better understanding of the auxiliary cluster and to obtain exact values for the zero-field splitting parameters, EPR spectra of a HydG sequence variant lacking the N-terminal radical SAM cluster should be recorded at different temperatures.

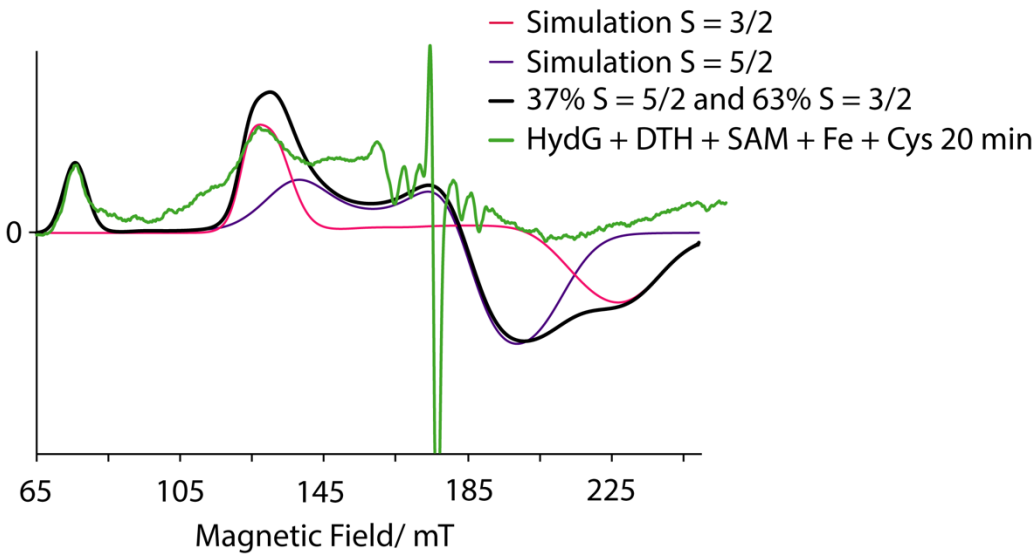

Figure 3.25: Simulation of high spin signals obtained with His_6ThitHydG in comparison with the real spectrum of His_6ThitHydGs auxiliary cluster in presence of L-cysteine.

Table 3.11: Parameters used to simulate the high-spin EPR signals of HydGs' auxiliary cluster.

OrganismHydG/Spin	D/ cm^{-1}	E/D	gStrain
SoHydG/ 3/2	>> hν	0.33	0.2 0.2 0.1[64]
SoHydG/ 5/2	+4.5	0.25	0.25 0.2 0.1[64]
ThitHydG/ 3/2	+4.2	0.29	0.25 0.2 0.1
ThitHydG/ 5/2	+4.5	0.20	0.2 0.2 0.3

3.6 FT-IR spectroscopy

FT-IR (Fourier-transform-Infrared) spectroscopy is a vibrational spectroscopy which, instead of using monochromatic light, uses a broad spectrum of mid-infra-red wavelengths in the range of 1-50 μm (wavenumbers 10 000 – 200 cm^{-1}). The wavelength range used in infra-red is similar to that of molecular vibrations. FT-IR signals provide information about the structure and interactions within the environments of molecules.

Under the assumption that a diatomic molecular (3-6) bond behaves as a spring where one atom does not change its position and the other atom behaves like a harmonic oscillator, then Hooke's Law is applied:(312)

$$\tilde{\nu} = \frac{1}{2\pi c}\sqrt{\frac{k}{\mu}} \tag{3-5}$$

μ = reduced mass, k = force constant, $\tilde{\nu}$ = vibration wavenumber.

The reduced mass μ of a diatomic molecule is given by the formula:

$$\mu = \frac{m_1 m_2}{m_1 + m_2} \tag{3-6}$$

The potential energy of a vibration is visually described with the anharmonic oscillator model (Figure 3.26) and in the formula (3-7) the values are approximated for a harmonic oscillator represented as discrete eigenvalues.(353)

$$E_{vib} = h\nu\left(\mathrm{v} + \frac{1}{2}\right) \tag{3-7}$$

(v = vibrational quantum number, with values of 0, 1, 2, 3, 4…)

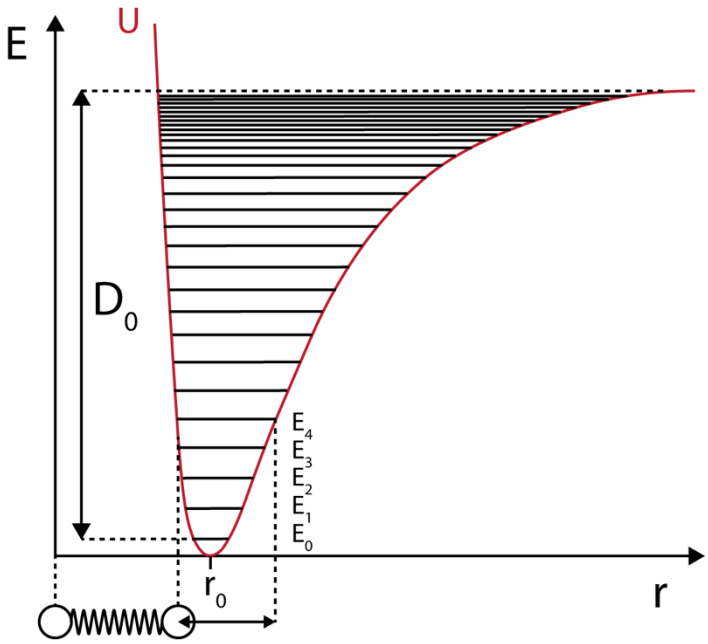

Figure 3.26: Diagram representing a diatomic molecule as an anharmonic oscillator, oscillating at energy level E_4. D_0: dissociation energy, U: potential energy, r_0: equilibrium bond length.[353]

Two main vibrational modes exist: stretching and bending. The stretching mode describes a motion that results in a change of bond length, which can be further divided into symmetric or anti-symmetric stretching if more than two atoms are involved. The bending mode is characterized by a change in bond angle between two atoms or a group of atoms.

Only if the irradiated IR frequency matches the vibrational frequency of the molecule, the radiation is absorbed and induces changes in the vibrational state. The resulting absorption of electromagnetic radiation is monitored as the IR spectrum.[312]

The set-up of an FT-IR spectrometer is based on a Michelson interferometer (Figure 3.27). A polychromatic infrared light source is directed to a beam splitter and 50% of the light is reflected towards the fixed mirror and 50% towards the moving mirror. Subsequently, the light is reflected back from the mirrors to the beam splitter and a selected part of the original light passes through the sample. While the sample is measured, the moving mirror constantly moves forward and backward changing the distance to the beam splitter. The change in distance of the optical path length between the two mirrors is called optical retardation (δ). For each mirror position the detector records a modulated power signal (as a function of retardation) and a plot of light intensity versus mirror position, which is known as an interferogram. The interferogram

is converted to a spectrum using the mathematical method called Fourier transformation.[354]

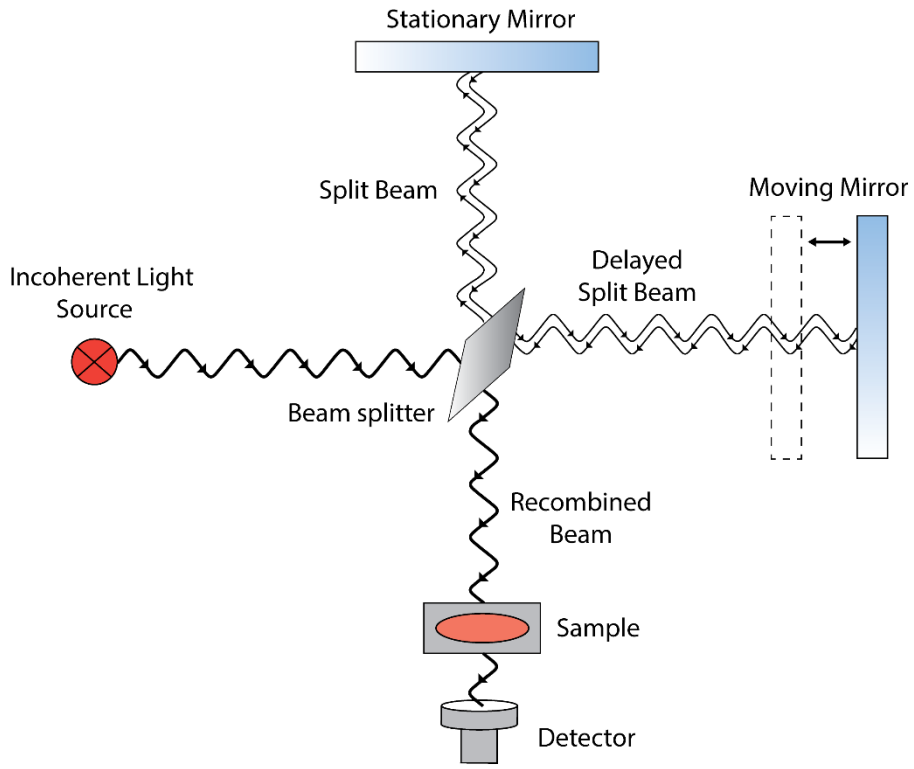

Figure 3.27: Set-Up of an Michaelson interferometer used for FT-IR spectroscopy.

The signal bands obtained in the FT-IR spectrum are given as wavenumbers $\tilde{\nu}$ in cm^{-1} and correspond to the infra-red radiation frequency absorbed by the sample, which is proportional to the energy of the vibration (3-6).

$$\Delta E = h\nu \tag{3-6}$$

All spectra mentioned in this chapter were measured in the transmission mode, where only the unabsorbed part of the radiation hits the detector. Because the unabsorbed radiation is very small and water produces a very strong and broad signal overlapping with our signals of interest, it is essential to measure a good background spectrum prior to the measurement.

In regard to the [FeFe]-hydrogenase maturation enzymes, FT-IR spectroscopy is used to define the binding mode and quantity of the CO and CN^- ligands that stabilize the low oxidation states of the H-cluster di-iron subcluster. The corresponding IR stretching vibrations of the diatomic ligand occur in a distinctive region, where no other vibrations take place, crucially in the 'transparent' window of solvent water. Interestingly, the wavenumber of free CO with $\tilde{\nu}_{CO}$ = 2155 cm^{-1} is shifted to lower wavenumbers upon

binding in complexes to wavenumber of 1800-2100 cm^{-1}, whereas bridging CO ligands show signals between 1770-1850 cm^{-1}. On the other hand, the wavenumber of free CN^- $\tilde{\nu}_{CN}$ = 2080 cm^{-1} is shifted towards higher wavenumbers of 2000-2200 cm^{-1}. Depending on the binding to iron, CN^- is a better σ-donor than CO, whereas CO is a better π-acceptor than CN^-.[355] This means CO is forming a stronger coordinative bond to iron than CN^-, which is usually supported by shorter bond lengths.[356] As a consequence, the wavenumbers of bound CN^- are higher than those of free CN^-, where, conversely, they are smaller for bound CO in comparison to free CO.

3.6.1 FT-IR analysis of HydF reconstituted with H-cluster mimic

Note: FT-IR spectra were recorded in collaboration with Dr. Philip Ash and Dr. Kylie Vincent (University of Oxford). Analysis of the spectra was assisted by Dr. Philip Ash Their respective contribution to the studies described in this section is gratefully acknowledged.

To confirm the incorporation of the H-cluster pdt-mimic into StrepThitHydF (Section 3.3.2), a concentrated sample of HydF plus mimic (500 μM) was measured with FT-IR spectroscopy. Adapting the experimental studies by Fontecave *et al.*[244], the HydF protein was incubated for 1h with the inorganic pdt-mimic and separated from unbound molecules *via* gel filtration with a PD-10 column. For the measurement, the resulting sample was simply thawed and applied to the FT-IR transmission sample cell. The corresponding spectrum is shown in Figure 3.28 with the solvent water background subtracted and in Figure 3.29 including the background.

Table 3.12: Previously reported FT-IR wavenumbers for HydF plus H-cluster mimic (pdt) and the results from the measurement with ThitHydF plus pdt-mimic.

Sample	CO ligands in cm^{-1}	CN ligands in cm^{-1}
ThitHydF + pdt-mimic	1967, 1944, 1906	2042, 2070, 2088
Pdt-Mimic alone	1981, 1950, 1914	2052
CaHydF	1967, 1943, 1907, 1877[27]	2044, 2069[27]
CaHydF + pdt-mimic	1968, 1943, 1897[27]	2038, 2055[27]
TmeHydF + pdt-mimic	1963, 1939, 1896, 1882[244]	2040. 2061[244]
TmeHydF + pdt-mimic + DTH	1968, 1945, 1902, 1883[244]	2040, 2064[244]

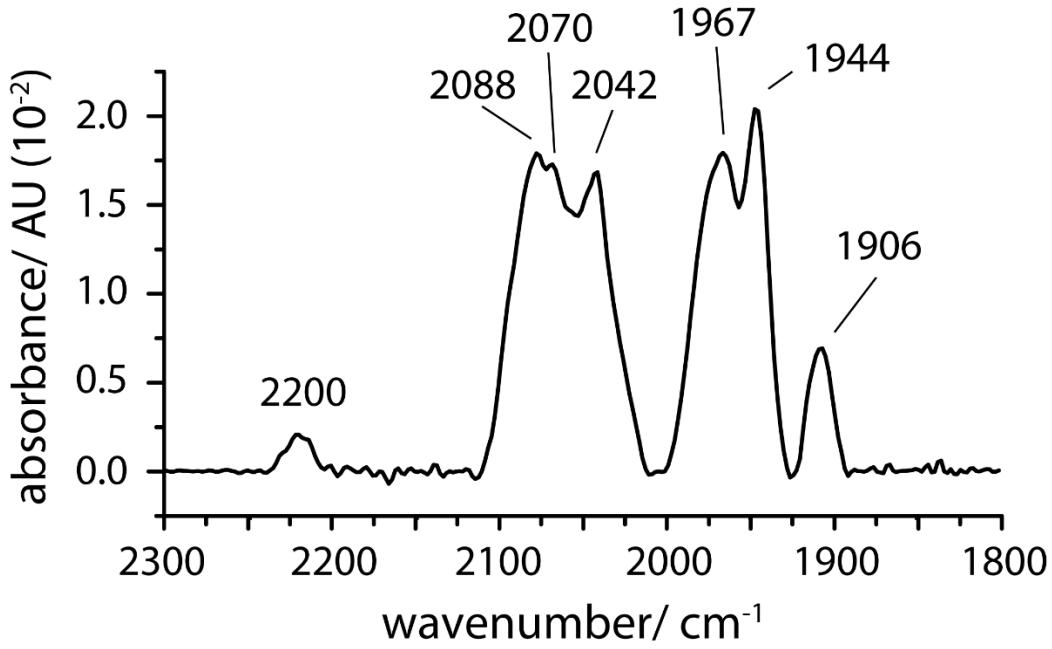

Figure 3.28: FT-IR spectrum of StrepThitHydF with pdt-mimic. Background subtracted.

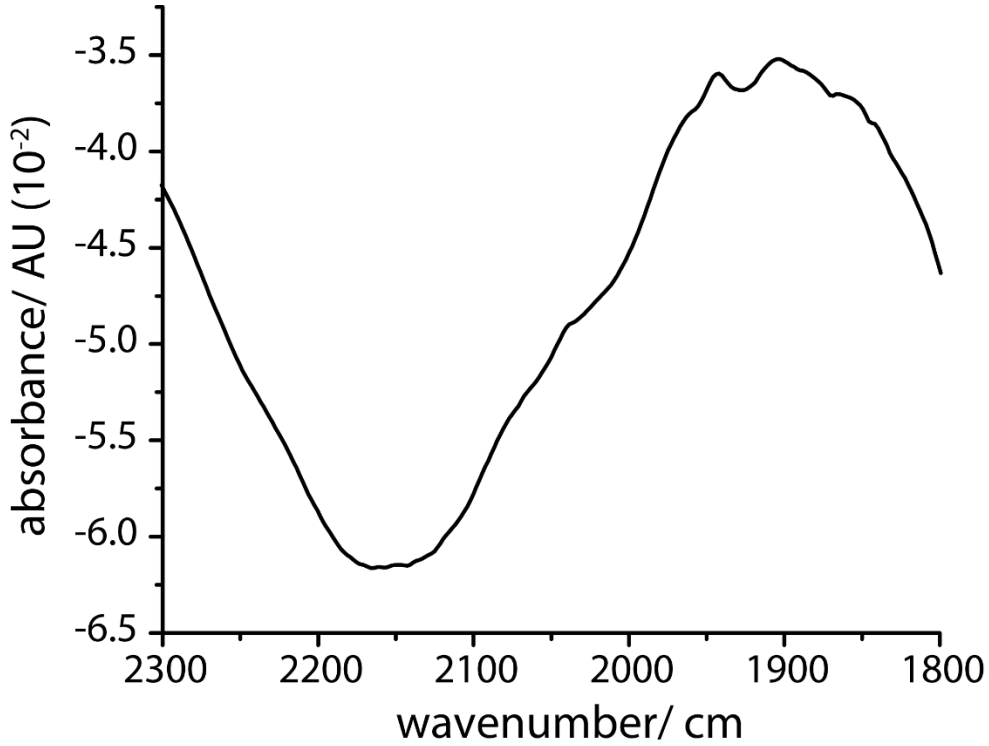

Figure 3.29: FT-IR spectrum of StrepThitHydF with pdt-mimic with background resulting from buffer/water.

FT-IR Signals reported for ThitHydF plus mimic are very similar to those reported for *Clostridium acetobutylicum* HydF (Table 3.12) and significantly shifted relative to the pdt ligand alone in solution. However, ThitHydF shows an additional signal for CN^- that results from a split peak, which might correspond to a non-specific 'FeCN' species.

Another difference is the peak at 2200 cm^{-1} which likely belongs to an artifact. What might have influenced the sample is the fact that it was stored on cardice for more than 24 h due to transportation, where it is possible some CO_2 diffused into the sample and changed the pH in solution.

3.6.2 Analysis of FT-IR studies with HydG

FT-IR studies have been applied to His_6ThitHydG to assay the formation of the [Fe-$(CO)_2$(CN)] synthon. The experimental part of this section was carried out by Dr. Pedro Dinis (reaction mixture) and Dr. Philip Ash (operation of the FT-IR spectrometer), who carried out a preliminary analysis of the data. Efforts to repeat the experiment were unsuccessful, possibly due to long term storage on cardice (more than 16 h on solid CO_2) which diffused into the sample as seen on the FT-IR spectra with background, followed by CO_2-induced pH changes that possibly inactivated ThitHydG. During the measurement, the CO_2 signal at 2200-2300 cm^{-1} was clearly present. A further detailed analysis of the peaks obtained and resolved over time from Dr. Pedro Dinis experiment, is provided in this section.

A premixed sample of reconstituted ThitHydG (500 μM, reconstituted with 5 equivalents of Fe and S, Chapter 2, Section 2.2.3), SAM, L-cysteine (both 3 mM final concentration) and 20 mM L-tyrosine was prepared for the FT-IR experiment. Subsequently, the reaction (volume 100 μL) to form the synthon complex was initiated by the addition of sodium dithionite (100 mM final concentration). Immediately after mixing, the reaction mixture was transferred into a FT-IR transmission cell and the spectra recorded. The time between the addition of dithionite and the start of the measurements was approximately 2 min.

After reductive SAM and L-tyrosine cleavage by HydG, the reaction intermediate dehydroglycine is decomposed to water, CO and CN^- ligands and subsequently complex A (Fe(CO)(CN)) is forming on the auxiliary cluster of HydG. After another turnover of SAM and L-tyrosine complex B/ synthon (Fe$(CO)_2$(CN)) is starting to form after approximately 1200 s. The mechanism is described in Scheme 3.1.

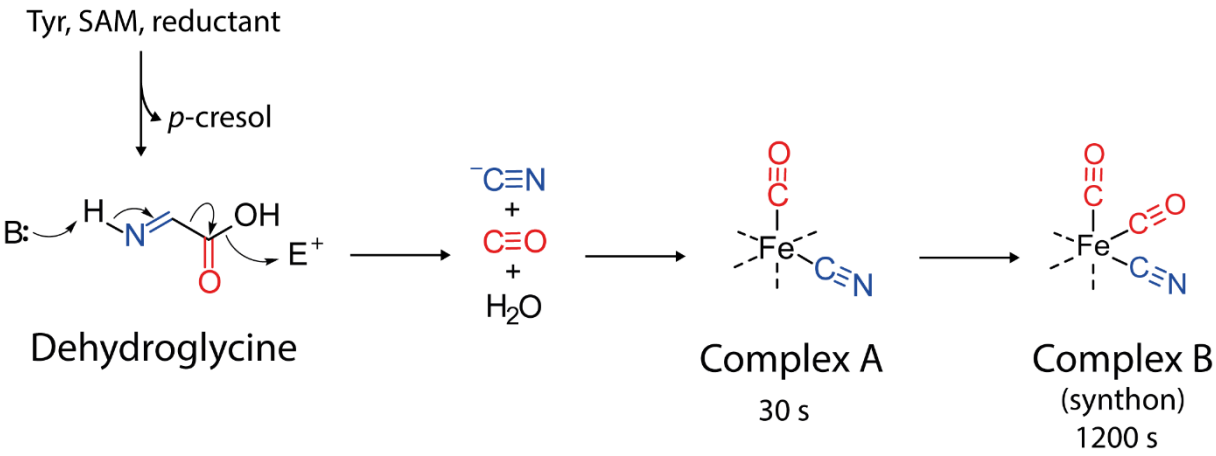

Scheme 3.1: Formation of complex A and complex B by HydG with the time by which the complex is formed, after reductive SAM and L-tyrosine cleavage initiation.

Resultant FT-IR spectra measured after the HydG reaction initiation are summarized in Figure 3.30. The spectra (10, 20, 30 ,40, 50, 60, 70, 80 min) were processed by subtraction from the initial spectrum at t ~ 2 min to visualize the changes.

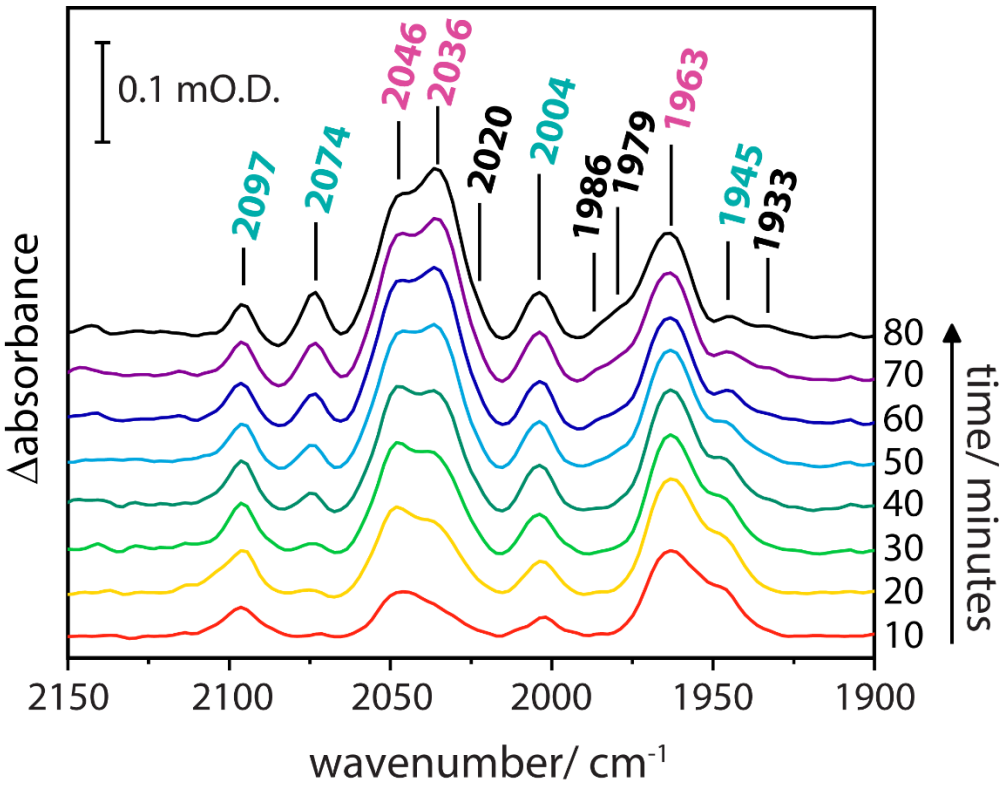

Figure 3.30: FT-IR spectra of ThitHydG after initiating the reaction with sodium dithionite, spectra measured over time and substraced from the start spectrum (t ~ 2 min). Pink coloured peaks: Large peaks summarized in Figure 3.32. Blue coloured peaks: Small peaks summarized in Figure 3.33.

The following detailed analysis of the resulting FT-IR spectra has been carried out on my own. By utilizing the peak analyzer tool of Origin, the peaks were picked manually and a Gaussian curve was fitted to the peaks with R^2 values above 0.995. Due to an uneven baseline, the standard error appeared to be bigger for the spectra measured at 30 min. An example for the fitted peaks of the 10 min FT-IR spectrum is shown in Figure 3.31.

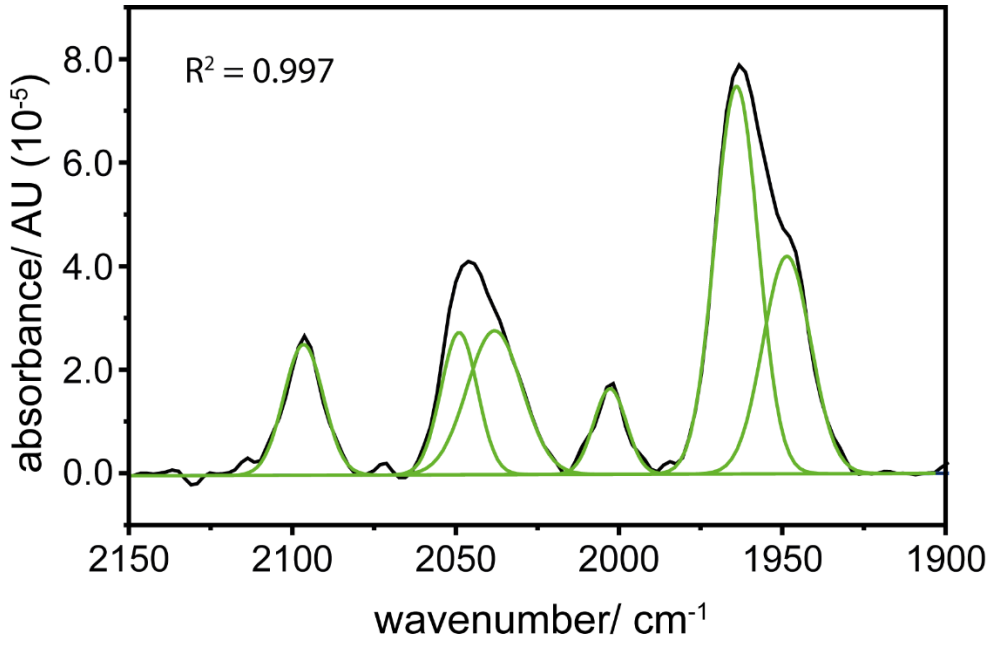

Figure 3.31: FT-IR spectrum at t ~ 12 min after reaction initiation with ThitHydG with fitted peaks (*green*).

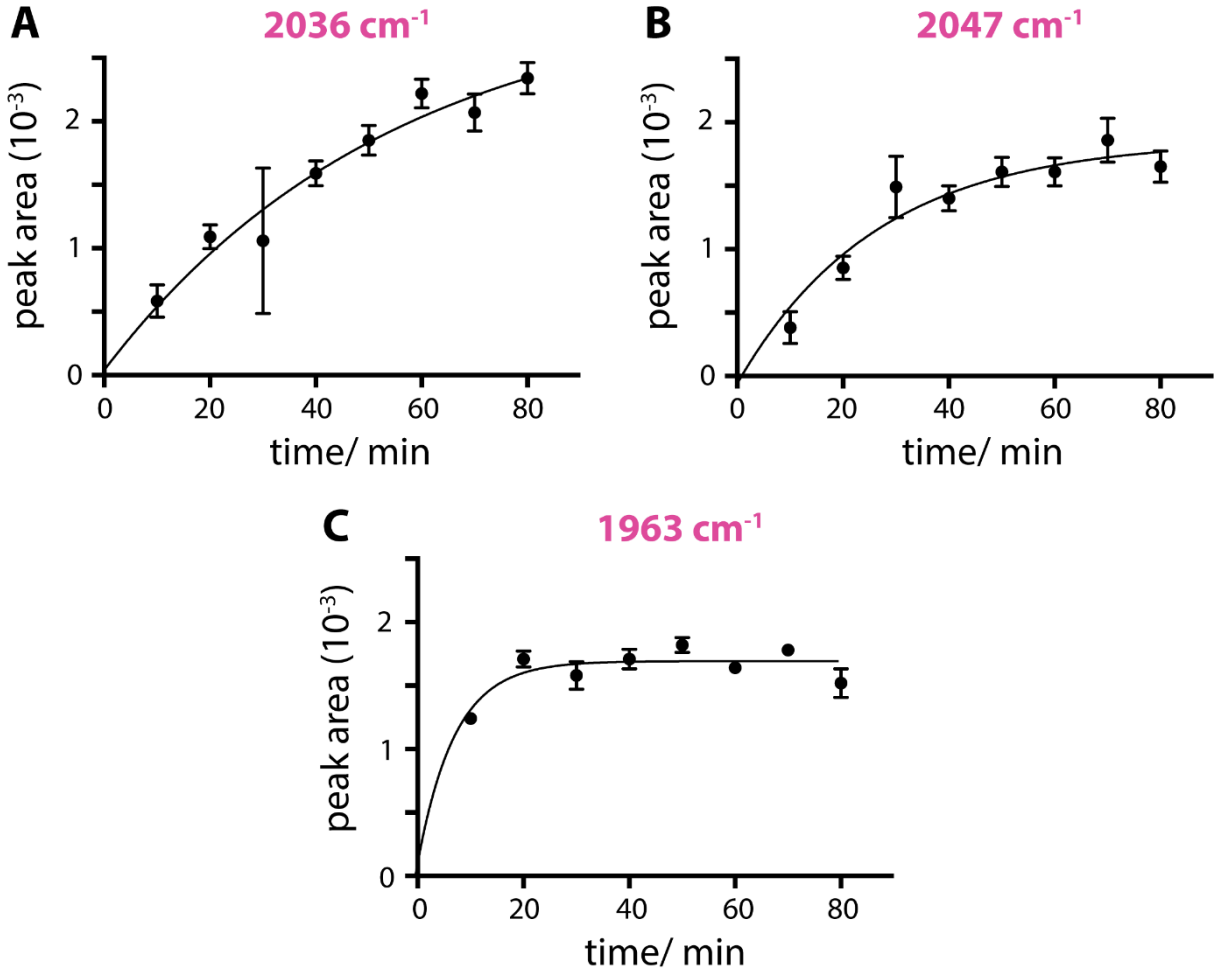

Figure 3.32: Progression of peak areas plotted against the time, from FT-IR spectra shown in Figure 3.30. Data points were fitted for an exponential, one phase association curve (for product formation kinetics) with GraphPad Prism.

Table 3.13: Rate constants resulting from the curve fitting and analysis of the FT-IR data.[b]

Wavenumber/ cm	Intensity Plateau (max.)	Equation	Rate constant, min^{-1}	Goodness of fit (R^2)
1963	(1.693 ± 0.048) x 10^{-3}	A[a]	0.142 ± 0.029	0.969
2004	(0.393 ± 0.015) x 10^{-3}	A[a]	0.084 ± 0.017	0.959
2036	(3.027 ± 0.541) x 10^{-3}	A[a]	0.018 ± 0.006	0.974
2047	(1.873 ± 0.163) x 10^{-3}	A[a]	0.038 ± 0.010	0.958

[a]Equations are: A, exponential, one phase association; [b]Unfitted (not suitable): 1945, 2074 and 2097 cm^{-1}.

It becomes clear when looking at the peak progression in Figure 3.32, that the peaks at a wavenumber of 2036 (A) and 2047 (B) cm^{-1} were forming much slower than the peak at 1963 (C) cm^{-1}. Assigning the peaks to either complex A or complex B gets difficult because the stoichiometry does not fit to the number of peaks observed. In the

study of the SoHydG, complex A forms very early at about 30 seconds after initiation, whereas the complex B forms after 15-20 min.[59] Nevertheless, the rate of peak progression could give a clue that the signal at 1963 cm^{-1} might belong to the CO ligand of complex A, whereas the signals at 2036 and 2047 might belong to two CO ligands in complex B. It is also possible that a mixture of 1:1 ratio of complex A: complex B co-exist in solution. A proper catalytic reaction rate was assigned by fitting the integrated peak areas to an exponential, one phase association curve and the corresponding rate constants are summarized in Table 3.13. Whereby the peak at 1963 cm^{-1} forms the fastest with a rate constant of 0.142 min^{-1}, assigned as complex A-CO and the 2036 cm^{-1} signal the slowest peak formation assigned as complex B-CO with 0.018 min^{-1}. A real assignment of peaks is only possible if accompanied by experiments with labelled ligands ^{13}CO and/or $C^{15}N$, confirmed through the shift in signal wavenumber.

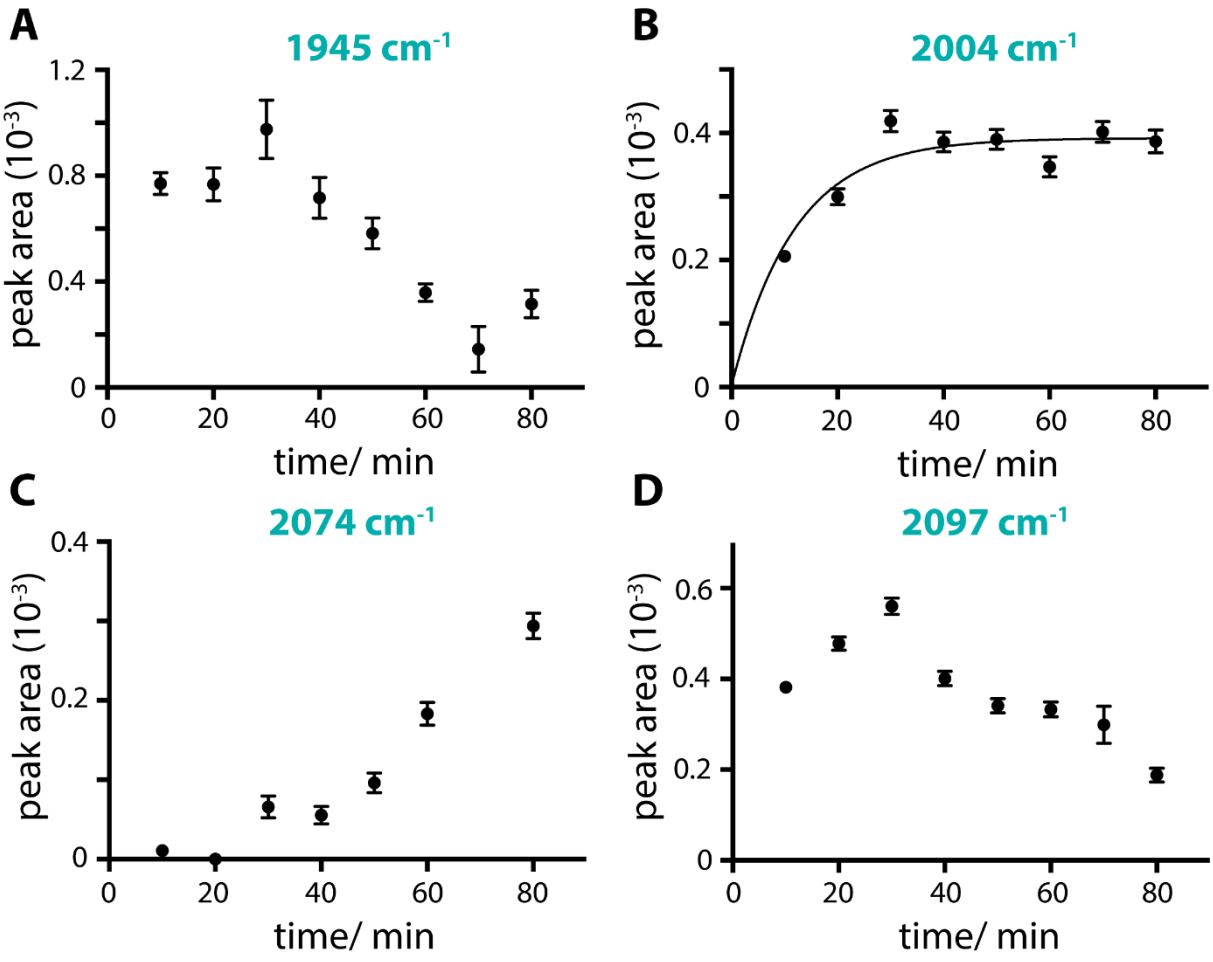

Figure 3.33: Progression of peak areas plotted against the time, from FT-IR spectra shown in Figure 3.30. Data points of 2004 cm^{-1} were fitted for an exponential, one phase association curve (for product formation kinetics) with GraphPad Prism.

The time progression of the smaller peaks, presented in Figure 3.33, was challenging to analyze, since the baseline fluctuated with every time point measurement. Nevertheless, some clear trends could be observed, with peaks at 1945 (A) and 2004 (B) cm^{-1} most likely belonging to a CO ligand. The 1945 (A) cm^{-1} peak forms very early and decreases with time which points toward a component of complex A. On the other hand, the peak at 2004 (B) cm^{-1} increased more slowly, which suggests it is likely to belong to complex B. Peaks at 2074 (C) and 2097 (D) cm^{-1} likely correspond to CN^- ligands, however there should be only a single CN^- ligand peak that appears in both complexes A and B. The peak at 2097 (D) cm^{-1} is formed early and is decreased slightly with time after reaching a maximum at 30 min. CN^- stretching usually exhibits lower peak intensities than CO, and the decrease might mean that the synthon is released from HydG by 80 min. If looking at the 2074 (C) cm^{-1} peak, it is starting to appear slowly and becomes stronger after 40 min which may mean it could derive from a non-specific 'FeCN' species. However, the observed peaks might not necessarily fit well to a reaction involving only complexes A and B. There could be non-productive side reactions (particularly with CN^-) that are visible with IR or other unknown intermediate states. To further investigate, isotopic substitution studies are required.

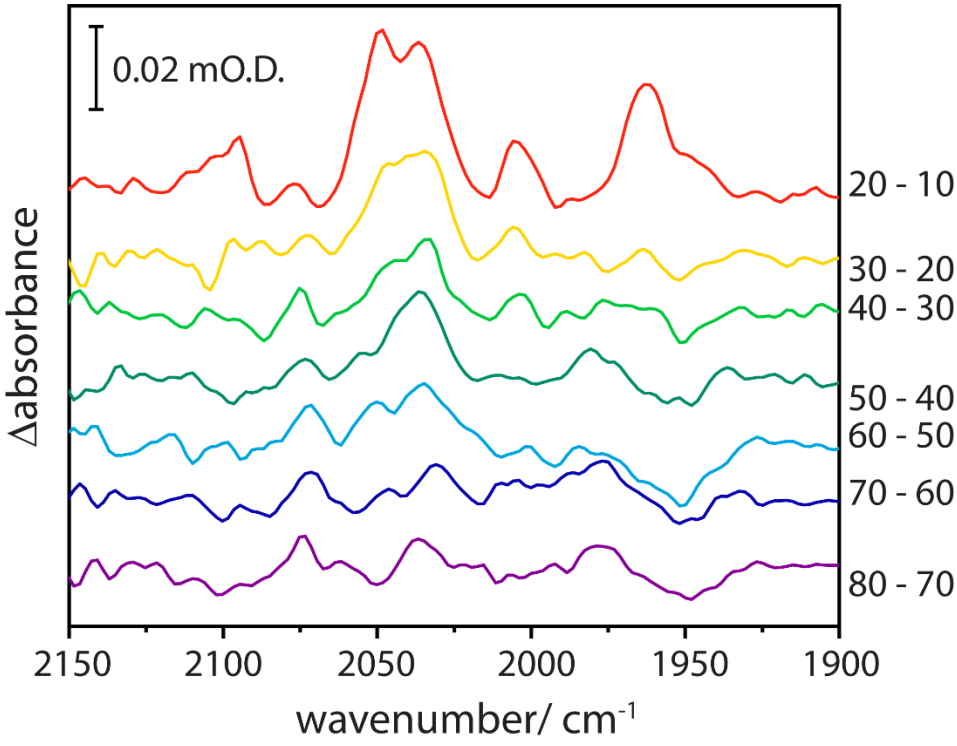

Figure 3.34: FT-IR spectra of ThitHydG after initiating the reaction with sodium dithionite. Spectra measured over time and substraced from the previous recorded spectrum (t ~ 2 min).

A good visualization of the changes in the FT-IR spectra happening over 80 min is shown as 'difference' spectra in Figure 3.34. These spectra confirm that intensity changes observed are real and not artefacts caused by the baseline correction. Interestingly, the biggest changes are happening in the first 20 min, since production formations are starting to saturate (Figure 3.32 and 3.33). Almost none are happening after 50 min (40-50 spectra), which is in line with the previous work on SoHydG, where the formation of complex B is completed after approximately 20 min.[59] The first two spectra (20-10 and 30-20) include the most important information of the observed species. Whereas in the first 20-10 spectrum five clear peaks are visible at 1963, 2004, 2036, 2047 and 2096 cm^{-1}, in the second 30-20 specta only two peaks at 2036 and 2047 cm^{-1} remain with an increased concentration. Therefore, the first species observed is likely to be a mixture of at least two different intermediate complexes. This suggests that the behaviour might be more complicated than just complex A and complex B. Nonetheless, the data obtained and the interpretation made from the peak progression analysis in Figure 3.32 and 3.33 allowed an approximate peak assignment to complex A and complex B, which is shown in Table 3.14.

Table 3.14: Previously reported FT-IR data on the formation of complex A (Fe(CO)(CN)) and complex B ($Fe(CO)_2(CN)$) by HydG in comparison with the obtained data herein.

	^{12}CO/ cm^{-1}	$^{12}C^{14}N$/ cm^{-1}
SoHydG-Complex A	1949	2093[61]
SoHydG-Complex B	2005, 2057	2106[61]
ThitHydG - potent. Cplx A	**1963**	**2097**
ThitHydG - potent. Cplx B	**2004**, **2036**, **2047**	**2074**, (**2097**)
ThitHydG - Cplx B2 Figure 3.35	(1903), 1957, 2045	2073, (2121)

A further analysis was carried out with the same data set as described before but processed in a slightly different way, in order to improve the steadiness of the baseline. The 'raw' data was subtracted by a collected bulk water reference spectrum and baseline corrected to give absolute peak heights and areas. If compared to the previous data processing, where the data were subtracted from the start spectrum, the outcome of the additional analysis shown in Figure 3.35 appears less rich in signals and the changes are not as significant as before. The signals are shifted in their

wavenumber compared to the previous data processing (Figure 3.30). Nevertheless, the peak progression was analyzed by fitting the peaks to a Gaussian curve and integration to calculate the peak area, using the Multiple Peak Fit tool of the program Origin. The results of the peak area progression over time is are presented in Figure 3.36.

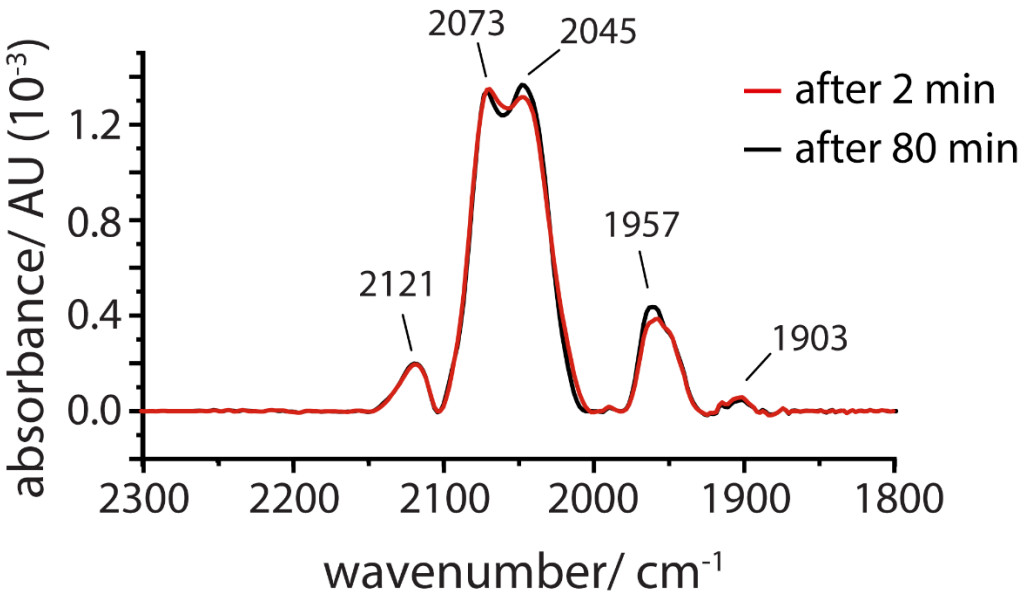

Figure 3.35: FT-IR raw data of ThitHydG for two timepoints (2 and 80 min) substracted from a water reference spectrum.

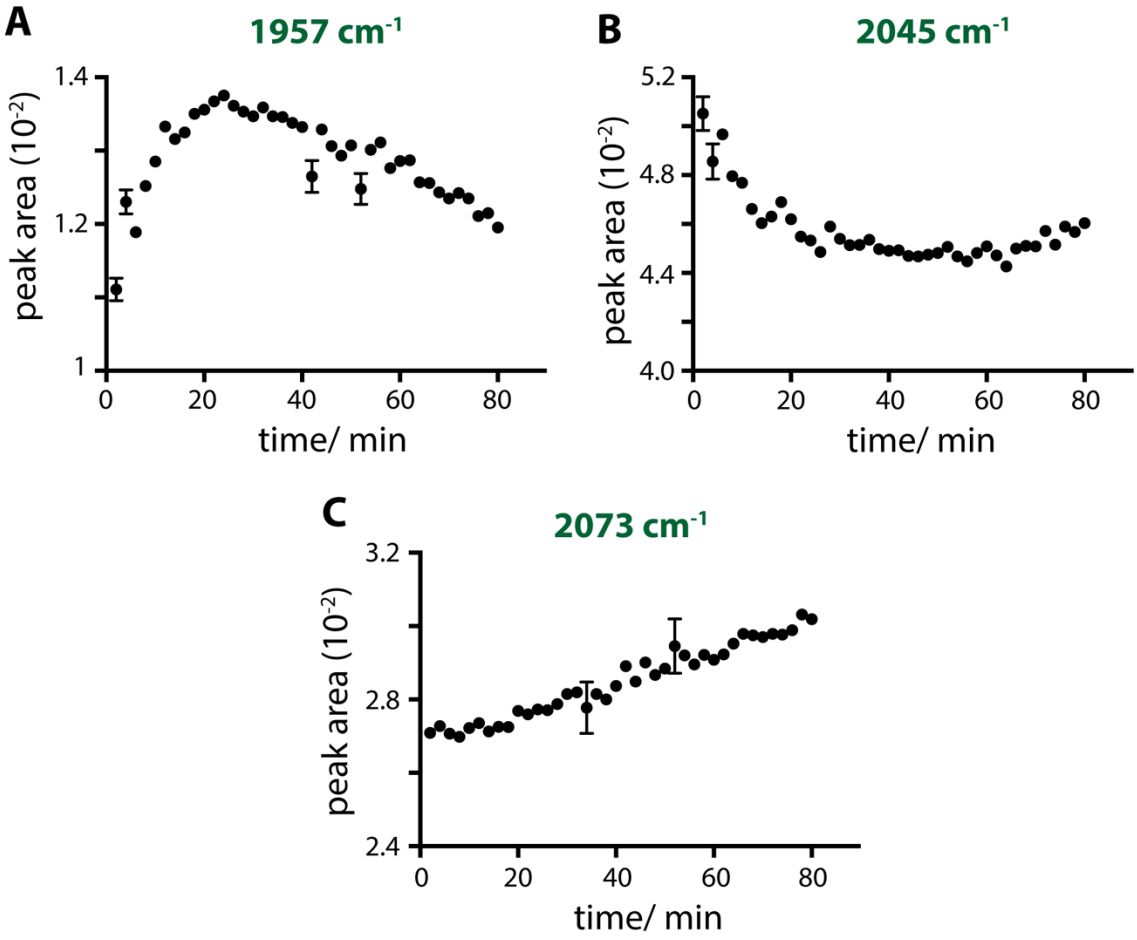

Figure 3.36: Progression of peak areas plotted against time, from representative FT-IR spectra shown in Figure 3.35. Error bars are not shown for every data point in order to provide a better overview, the ones shown exhibit the highest standard error observed.

As can be observed in Figure 3.35 for the smallest two outer peaks at 1903 and 2121 cm^{-1}, no change is happening over 80 min. The peak at 1903 cm^{-1} can be clearly assigned as CO, because CN^- peaks usually do not appear under 2000 cm^{-1}. The same applies to the 2121 cm^{-1} peak, because CO is not detected above 2100 cm^{-1} and therefore has to be CN^-. The peak at 1957 (A) cm^{-1}, most likely CO, quickly increases to a maximum at about 20 min, and then decreases to its initial intensity (Figure 3.36A). This is most similar to the previous data processing peak at 1963 cm^{-1} (Figure 3.33C), which was tentatively assigned to be the CO ligand present in complex A. Furthermore, the 2045 cm^{-1} peak could be assigned to another CO ligand when compared to literature values in Table 3.14 (2057 cm^{-1}) for complex B. However, the progression clearly shows a decreasing area of this peak with time, but the changes are marginal and towards the end, the peak becomes larger again. The bottom part of Figure 3.36C shows the time dependent progression of the peak at 2073 cm^{-1}, which is steadily increasing, suggesting either a ligand of complex B or, as previously described, the formation of free CO, which stretches at 2080 cm^{-1}.

3.7 Summary and conclusions

The spectroscopic studies based on absorption described in this chapter gave a significant insight into the type and state of the bioinorganic cofactors present in the [FeFe]-hydrogenase maturation proteins HydG, HydE and HydF from *Thermoanaerobacter italicus* as well as the activity of HydG to form an $[Fe(CO)_2(CN)]$ synthon.

UV-Vis spectroscopy provided a tool to determine [4Fe4S]-cluster concentration from the characteristic absorption band at 410 nm and to monitor and estimate the level of reconstitution. For the anaerobic reconstitution of HydF different reducing agents were tested for producing a stable [4Fe4S]-cluster and maintaining the cluster concentration after gel filtration. It is crucial to stabilize the [4Fe4S]-cluster of HydF, since it is partly exposed to solvent and easily degradable. Two reducing agents resulted in high [4Fe4S]-cluster uptake, dithiothreitol and glutathione. After gel filtration, the concentration of DTT-reduced [4Fe4S]-cluster dropped drastically (-40%), whereas the glutathione-reduced [4Fe4S]-cluster concentration remained almost constant. Thus, glutathione, which has been previously reported to complex iron-sulfur clusters,[357] had a stabilizing effect on the [4Fe4S]-cluster of HydF and was therefore used as a reducing agent for HydF reconstitutions. It is an interesting question whether the glutathione is directly bound to HydF, and in particular if it directly interacts with, or physically protects, the [4Fe4S]-cluster of HydF. This could be probed in future experiments by advanced EPR techniques such as ENDOR with labelled glutathione and with testing potential binding to HydF by ITC. Glutathione (Figure 3.37) could also potentially displace the glutamic acid (glu305) ligand in the crystal structure of *holo*-HydF by Fontecave *et al.* (Figure 3.38, PDB-code: 5KH0)[244].

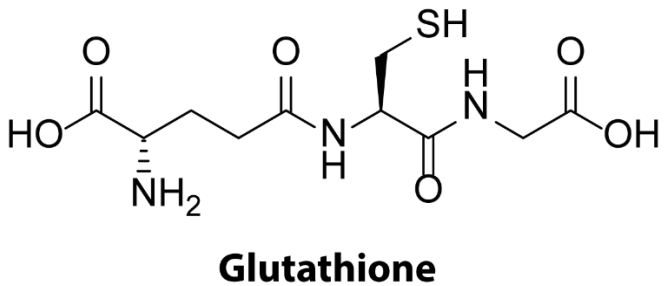

Glutathione

Figure 3.37: Molecular structure of glutathione.

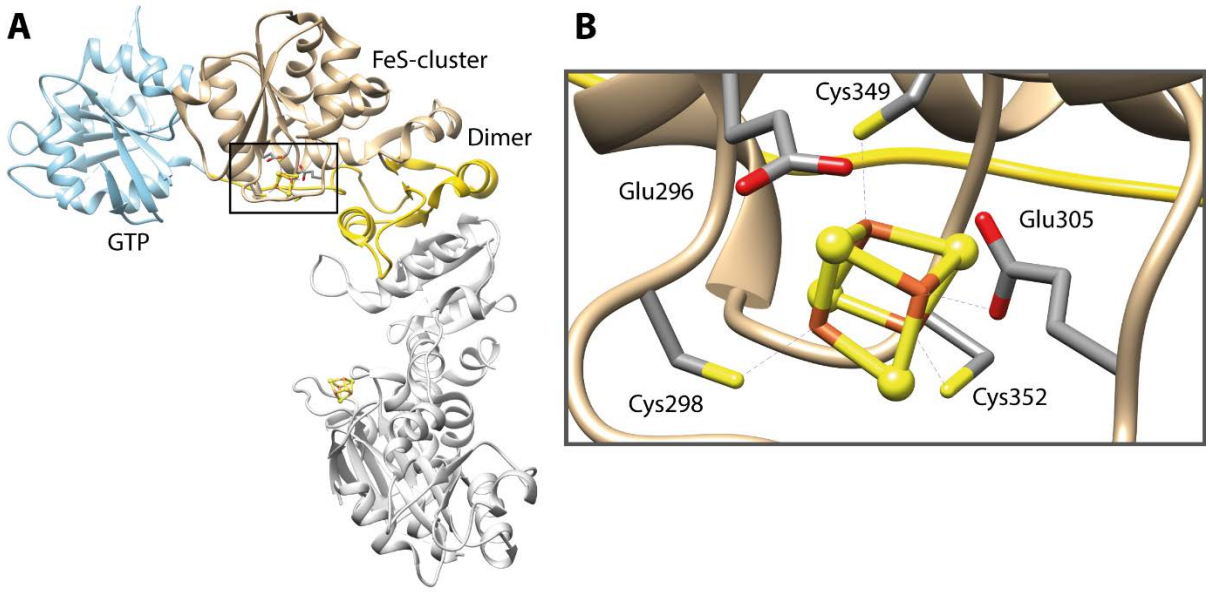

Figure 3.38: Crystal structure of TmeHydF. A: Dimer of TmeHydF with GTP-binding domain in *skyblue*, FeS-cluster binding domain in *tan* and the dimerization domain in *gold*. B: Zoom of the [4Fe4S]-cluster binding environment with amino acids coordinating the cluster Cys298, Cys349, Cys352 and Glu305.[244]

Additionally, HydF was reconstituted with 10 eq. of an H-cluster mimic, carrying a pdt-group instead of adt and incorporation of the mimic was quantified after gel filtration by measuring the intensity of the mimic absorption band at 350 nm. The mimic was successfully incorporated into HydF after an incubation time of 1 h-overnight at 18°C, however less than 1 equivalent of pdt-mimic remained bound. In future studies, a useful aim might be to improve the efficiency of this reconstitution step and examine the effect of varied conditions (for example concentrations of thiols, time and equivalents of the pdt-mimic) on the yield of cofactor bound to the HydF protein.

For the reconstitutions of Strep- and His_6HydE, as well as His_6HydG, DTT was used as a reducing agent, since the iron-sulfur clusters of radical SAM enzymes are usually buried inside the TIM-barrel and relatively shielded from solvent, which provides some degree of stability and protection. Both of these radical SAM enzymes bind [4Fe4S]-clusters. His_6HydG has been previously shown to bind two [4Fe4S]-clusters[60] and HydE1265 also likely binds two [4Fe4S]-clusters, as shown by the concentrations of [4Fe4S]-cluster determined by UV-Vis spectroscopy and the iron content assay. However, to ensure the existence of a second [4Fe4S]-cluster in HydE1265 for future studies a mutagenesis of the radical SAM cluster ligands (replacing cysteine with alanine for example) and following UV-Vis and EPR spectroscopic characterization of

the resulting HydG sequence variant would confirm the presence a second [4Fe4S]-cluster.

EPR spectroscopy serves as an additional tool to confirm the presence of [4Fe4S]-clusters and it can also detect other types of clusters like [3Fe4S]- or [2Fe2S]-clusters. All [FeFe] hydrogenase maturation proteins have been shown to carry at least one [4Fe4S]-cluster. EPR spectra of radical SAM [4Fe4S]-clusters have different shapes if in the presence or absence of the substrate SAM, which coordinates the radical SAM [4Fe4S]. The same has been observed for EPR spectra of HydE and HydG from *Thermoanaerobacter italicus*. Furthermore, the influence of GTP on the [4Fe4S]-cluster of HydF was tested but did not induce any changes to the EPR spectrum of [4Fe4S]-HydF.

Since HydG has been shown to carry an auxiliary [5Fe5S]-cluster, which was determined both by X-ray crystallography for ThitHydG and EPR spectroscopy for *Shewanella oneidensis* HydG, the missing EPR study of ThitHydG has been carried out in the context of this thesis. To confirm the presence of the synthon iron, both low and high power spectra have been recorded to obtain signals for the high-spin iron S = 5/2 reported for the auxiliary cluster of SoHydG. These appeared next to the typical signal for the S = 1/2 reduced $[4Fe4S]^{+}$-cluster, which were present if sodium dithionite (DTH), DTH plus SAM, DTH plus SAM and iron(II), DTH plus SAM, iron (II) and L-cysteine were added. For the last condition mentioned, high-power spectra revealed features in the spectra corresponding to S = 5/2 spins in the low magnetic field region, possibly deriving from the [Fe(κ^3-Cys)]·[4Fe4S] and [FeS]·[4Fe4S] forms of the auxiliary cluster (Figure 3.39). An additional S = 3/2 signal observed around g = 5.18 likely derives from an antiferromagnetic coupling of the 5th iron to the [4Fe4S]-cluster depending on the geometry of the cluster and other factors.(64)

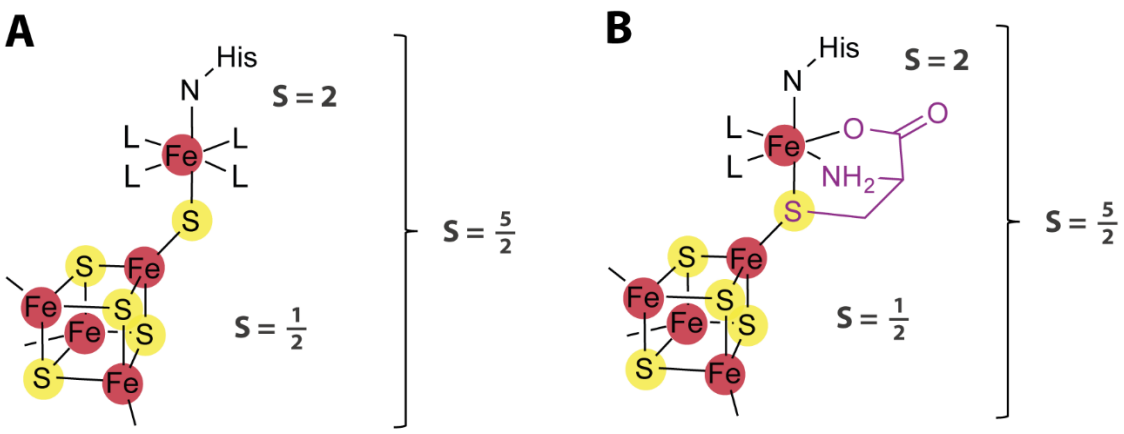

Figure 3.39: Two possible HydG auxiliary cluster forms that are responsible for an S = 5/2 spin signal in the corresponding EPR spectrum. A: Resting state of the auxiliary cluster [FeS]·[4Fe4S] form as observed in the crystal structure of ThitHydG. B: Resting state of the auxiliary cluster [Fe(κ^3-Cys)]·[4Fe4S] in the presence of L-cysteine as observed in the EPR spectrum for SoHydG.

To aid interpretation of the obtained data from the low-field experiments, a simulation was carried out, by taking Zero-Field parameters into account. However, it has been difficult to fit a function according to the signals from the experiment, which is why the simulation herein is a combination of two simulations, one for the 5/2 spin and the other for the 3/2 spin. Nonetheless, the signal at g = 4.3, close to the resonator background signal could not be fitted, due to limitations of the simulation program.

In contrast to the other spectroscopies, FT-IR spectroscopy is used to monitor the presence of free or bound CO and CN^- ligands, which become a part of the H-cluster. As CO and CN^- ligand stretching frequencies fit the frequencies of infra-red radiation, they are weak but detectable signals. To confirm the incorporation of the H-cluster pdt-mimic provided by Prof. C. Pickett, a concentrated HydF sample incubated with the mimic was measured by FT-IR. The resultant peaks were similar to those reported for *Clostridium acetobutylicum* HydF with pdt-mimic[27], but an additional signal appears for CN^-, most likely from a non-specific 'FeCN' species.

Mechanistic studies can also be carried out with FT-IR spectroscopy. Indeed, a published experiment from the Britt group[59] using SoHydG shows the formation of CO and CN^- ligands are interpreted as constituting the synthon complex A (Fe(CO)(CN)) after 30 seconds and complex B ($Fe(CO)_2(CN)$) after 15-20 min (Scheme 3.2).

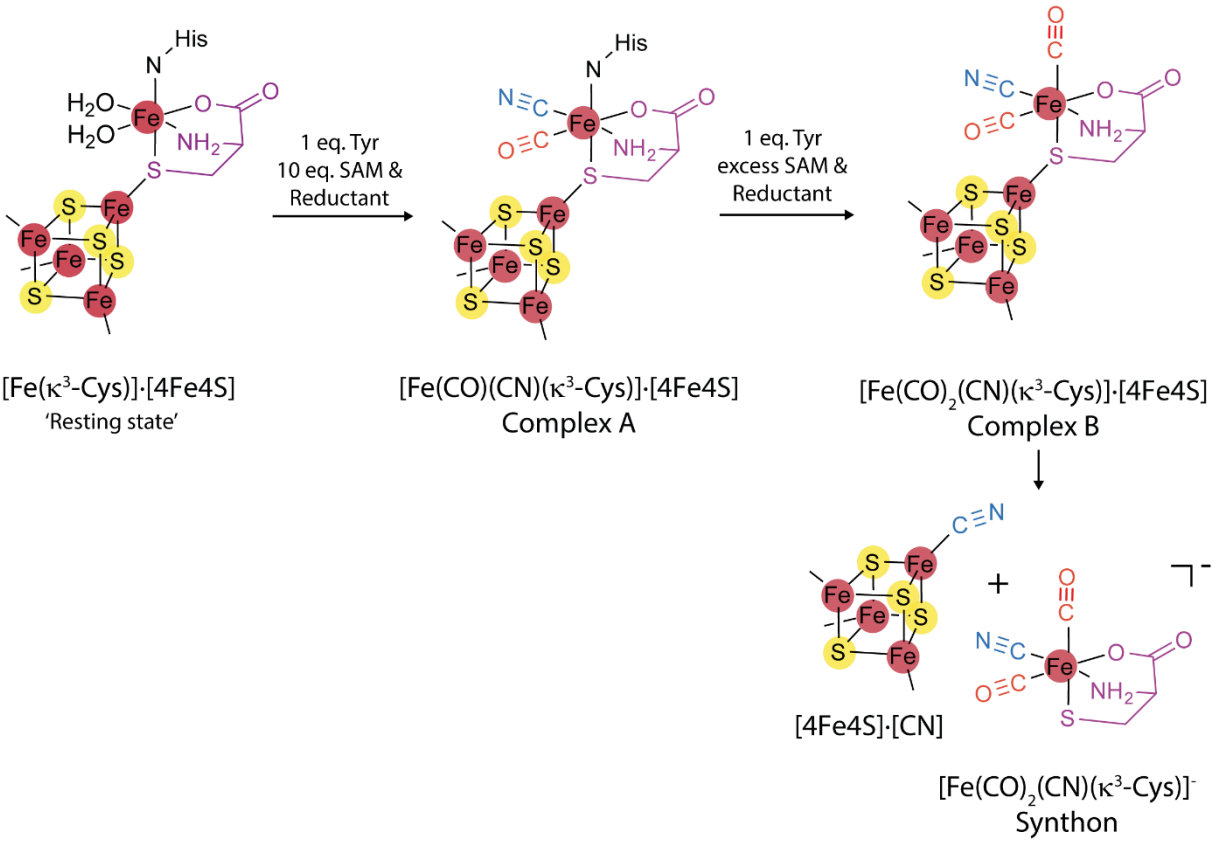

Scheme 3.2: Formation of complex A and complex B on the auxiliary cluster of HydG in presence of cysteine. Recent studies of D. Britt *et al.*[71] propose a reaction start from the resting state of the auxiliary cluster [Fe(κ^3-Cys)]·[4Fe4S], followed by reductive cleavage of SAM and L-tyrosine, whereby the CO and CN$^-$ ligands are produced which bind to the 5th iron and build the complex A [Fe(CO)(CN)(κ^3-Cys)]·[4Fe4S], after the cleavage of another equivalent of L-tyrosine the complex B [Fe(CO)$_2$(CN)(κ^3-Cys)]·[4Fe4S] is subsequently formed and released after as the synthon [Fe(CO)$_2$(CN)(κ^3-Cys)]$^-$.

The same type of experiment has been carried out by Dr. Pedro Dinis with ThitHydG, with the data collection by FT-IR and preliminary data analysis in collaboration with Dr. Philip Ash (ICL, University of Oxford). My contribution was the detailed analysis of the observed IR peaks. A time-resolved graph has been generated for each peak area progression. It becomes clear that some peaks are formed much slower than others, which are tentatively assigned to complex B (or similar complex). However, additional peaks have been observed that couldn't be classified to either complex A or complex B, but which might derive from artifacts or non-specific 'FeCN' species.

Future experiments for FT-IR spectroscopy might include the mechanistic studies whether HydG is transferring the synthon complex onto StrepHydF or StrepHydE, by carrying out the reaction and separating HydG from the reaction mixture (by NiNTA-affinity chromatography or size-exclusion chromatography) and measuring the FT-IR

as well as the EPR spectrum of the resulting HydF or HydE. The same experiment can be carried out in the presence of both His_6/StrepHydE and StrepHydF which can be separated either by affinity chromatography or size-exclusion chromatography if not forming a complex. Better characterization of the intermediates in ThitHydG would be possible with differently labelled tyrosine to distinguish the different peaks in the FT-IR, which has been done by Britt *et al.*[59,66]. Furthermore, factors could be tested that increase the rate of formation of the CO and CN ligands and monitoring by FT-IR.

Overall, UV-Vis, EPR and FT-IR spectroscopy provide comprehensive tools to characterize the [FeFe]-hydrogenase maturation proteins HydG, HydE and HydF from *Thermoanaerobacter italicus*.

Chapter 4

Activity of [FeFe]-hydrogenase maturation enzymes

4.1 Introduction

This chapter describes the individual enzyme activity of reconstituted [FeFe]-hydrogenase maturation proteins HydE, HydG and HydF from *Thermoanaerobacter italicus* in a coupled assay.

Since HydE and HydG belong to the radical SAM family of enzymes, their characteristic catalyzed enzymatic reaction is the reductive cleavage of *S*-adenoslymethionine into L-methionine and a 5'-deoxyadenosly radical (Scheme 4.1).[40]

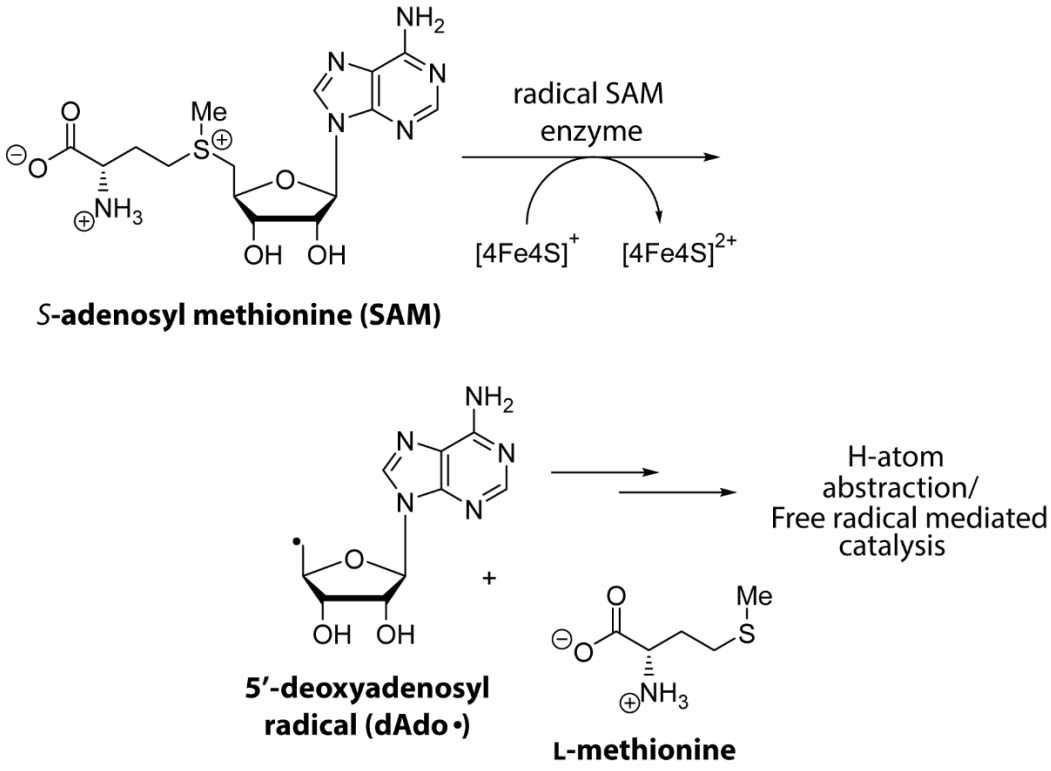

Scheme 4.1: Generalized reaction scheme for radical SAM enzymes showing the reductive SAM cleavage, adapted from [358].

In the absence of the second substrate, the generated radical is quenched by either abstracting a hydrogen atom from a C-H protein residue or from a weaker bond in a solute molecule such as S-H from a thiol (dithiothreitol or glutathione) and forms 5'-deoxyadenosine. The activity of both enzymes can be measured in an enzymatic SAM assay and by following HPLC analysis to track and quantify the reaction product 5'-deoxyadenosine through the absorbance at 254 nm.

Additionally, HydG also belongs to a subgroup of radical SAM enzymes which cleave the C_α-C_β bond of aromatic amino acids called C_α-C_β lyases. In particular, HydG cleaves L-tyrosine into *p*-cresol and dehydroglycine (DHG), which is further decomposed to CO and CN^- ligands (Scheme 4.2).[49] Therefore, HydG's co-substrate L-tyrosine, and its lysis product *p*-cresol can be analyzed via Fluorescence-HPLC in parallel in the coupled SAM-Tyr assay.[55,60]

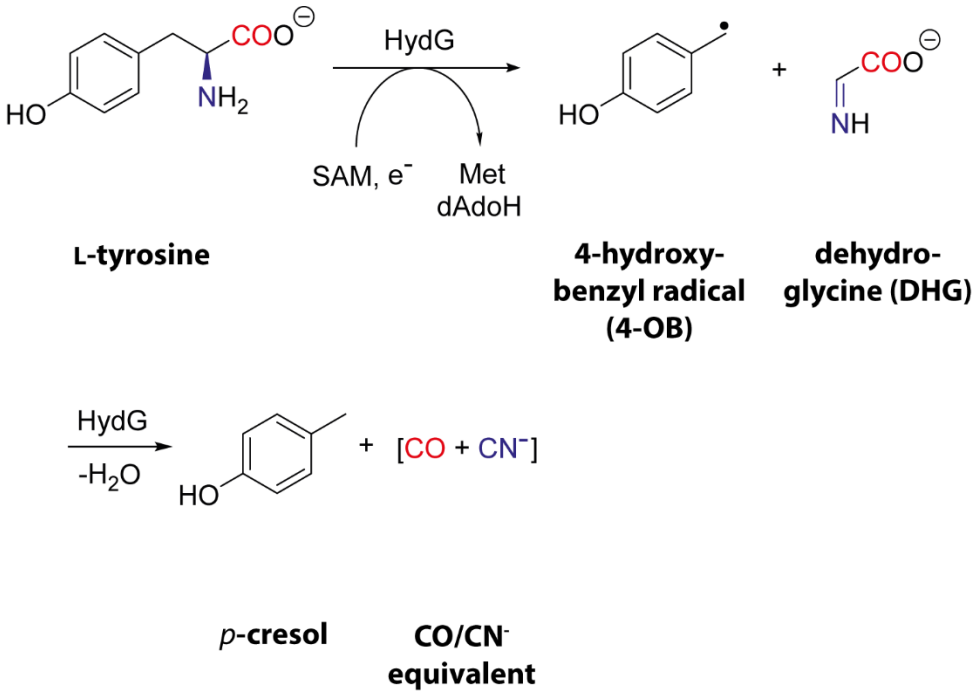

Scheme 4.2: Generalized reaction scheme for the radical SAM enzyme HydG showing the reductive cleavage of L-tyrosine, adapted from [71].

The HydF protein catalyzes the hydrolysis of GTP into GDP, and therefore belongs to the GTPase superfamily (Scheme 4.3).[51] One requirement for GTPase activity is the presence of Mg^{2+}, which coordinates to the phosphates of the nucleotide.[359,360] As described for the SAM assay, GTPase activity can also be measured in a biochemical HydF enzyme assay measuring the formation of GDP by HPLC analysis using an

optimized program[269] to separate GDP from GTP and quantify the generated amount of both nucleotides using the absorbance at 260 nm.

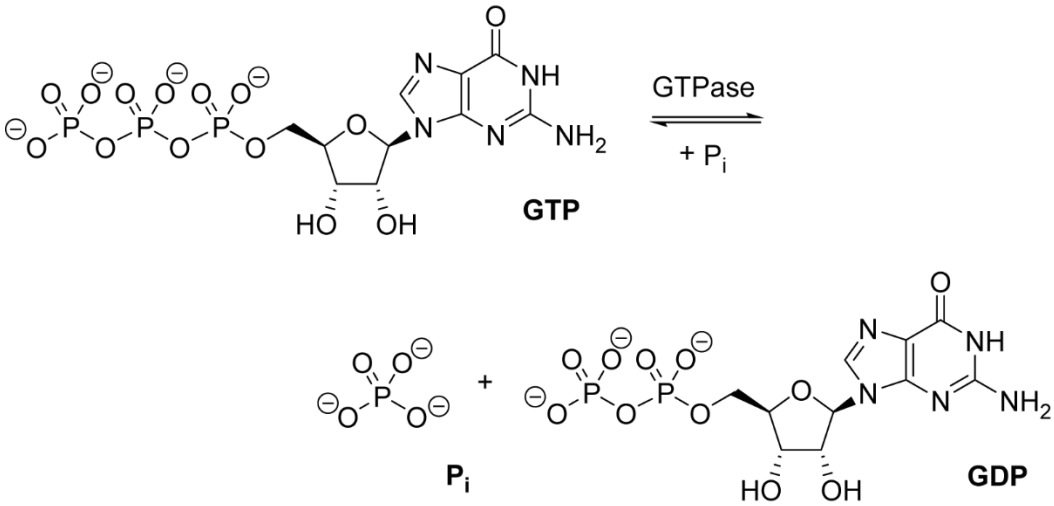

Scheme 4.3: Reaction scheme showing the reaction catalyzed by GTPases, the hydrolysis of GTP to GDP.

4.2 Basic Enzyme Kinetics

Experimental studies of enzyme kinetics are carried out by monitoring the initial rate of product formation in a solution and to simplify the kinetic models, it is convenient to follow reactions in which the relevant enzyme is at very low concentration with respect to the substrate.[361,362]

The basic features of enzyme-catalyzed reactions are: 1. With a given initial substrate concentration, [S], the initial rate of product formation (first few percent) is proportional to the total concentration of the enzyme, $[E]_0$; 2. For given $[E]_0$ and sufficiently low [S], the rate of product formation increases linearly with [S]; 3. For given $[E]_0$ and increased values of [S], the rate of product formation slows down and becomes independent of [S], and reaches at saturation of at a maximum value, known as the maximum velocity $V_{max.}$

An interpretation of these features was made by the Michaelis-Menten mechanism, which was proposed in 1913[363] and follows the scheme below:

$$E + S \overset{K_S}{\rightleftharpoons} ES \xrightarrow{k_{cat}} E + P \tag{4-1}$$

Two distinct processes are described for the catalytic reaction shown (4-1). In the first step an enzyme-substrate complex, ES, is formed which is assumed to be rapid and reversible, with no chemical modifications. In the second step the chemical modification occurs with a first order rate constant, k_{cat} (the turnover number).

The Michaelis-Menten equation describing enzyme kinetics (Figure 4.1) accounts quantitatively for the above-mentioned features:

$$v = \frac{[E]_0[S]k_{cat}}{K_M + [S]} \tag{4-2}$$

where

$$k_{cat}[E]_0 = V_{max} \tag{4-3}$$

v = rate of the reaction, $[E]_0$ = enzyme start concentration, [S] = substrate concentration, k_{cat} = catalytic constant, K_M = Michaelis-Menten constant, V_{max} = maximum reaction rate.

The Michaelis constant, K_M, is specific for a particular enzyme and its substrate and describes the concentration of substrate at which $v = \frac{1}{2} V_{max}$. In the case of $[S] \ll K_M$ the Michaelis-Menten equation becomes:

$$v = \frac{k_{cat}}{K_M} [E]_0[S] \tag{4-4}$$

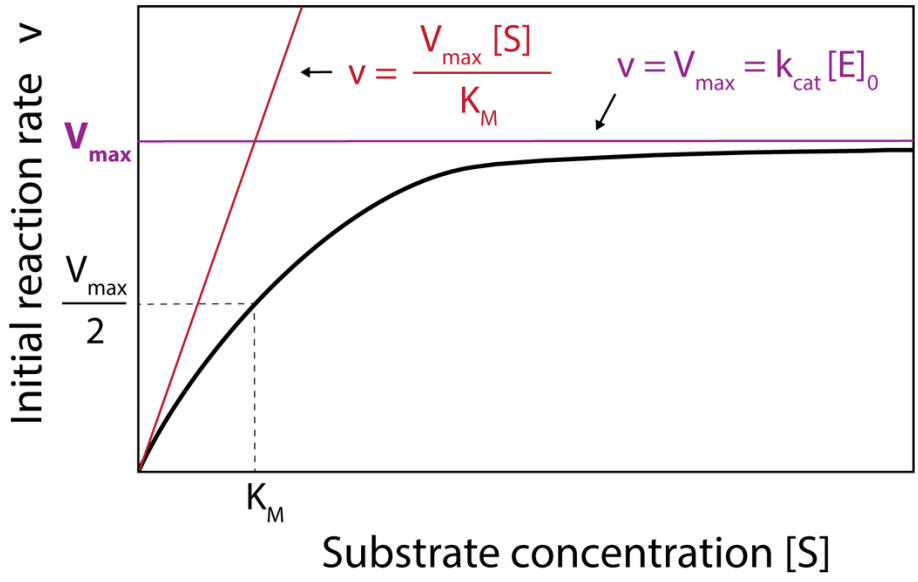

Figure 4.1: Graph describing enzyme reaction speed and the Michaelis-Menten kinetics.

From the reaction equation (4-1) the following can be derived:

$$\frac{[E][S]}{[ES]} = K_S \tag{4-5}$$

and

$$v = k_{cat}\,[ES] \tag{4-6}$$

If it is considered that the free enzyme concentration [E] is the total enzyme concentration $[E]_0$ minus the enzyme-substrate complex [ES] concentration, then the reaction rate becomes:

$$v = \frac{[E]_0[S]k_{cat}}{K_S + [S]} \tag{4-7}$$

For the enzyme-product complex EP, it is assumed that the dissociation is so fast that it can be taken out of the whole reaction process.

However, the Michaelis-Menten equation in (4-1) assumed in the Michaelis-Menten model that the ES-complex is on thermodynamic equilibrium with free enzyme and substrate. This is only the case if $k_2 \ll k_{-1}$ for:

$$E + S \underset{k_{-1}}{\overset{k_1}{\rightleftharpoons}} ES \xrightarrow{k_2} E + P \tag{4-8}$$

Analysis of this case was done by G. E. Briggs and J B. S. Haldane in 1925[364] and solution of this equation required a more complicated steady-state-kinetic differential equation, which resulted in following formula for the reaction rate:

$$v = \frac{[E]_0[S]k_2}{[S]+(k_2+ k_{-1})/k_1} \tag{4-9}$$

Which is similar to (4-1), where

$$K_M = \frac{k_2+ k_{-1}}{k_1} \tag{4-10}$$

K_s, the dissociation constant of the enzyme-substrate complex is equal to k_{-1}/k_1 and therefore (4-10) becomes:

$$K_M = K_s + \frac{k_2}{k_1} \tag{4-11}$$

and when $k_{-1} \gg k_2$, then it simplifies to $K_M = K_S$.

The catalytic constant, k_{cat} is the first-order rate constant for the chemical conversion of the ES complex to the EP complex. It refers to the properties and reactions of ES and EP complexes and is often also called turnover number representing the maximum number of substrate molecules converted to products per active site per unit of time.

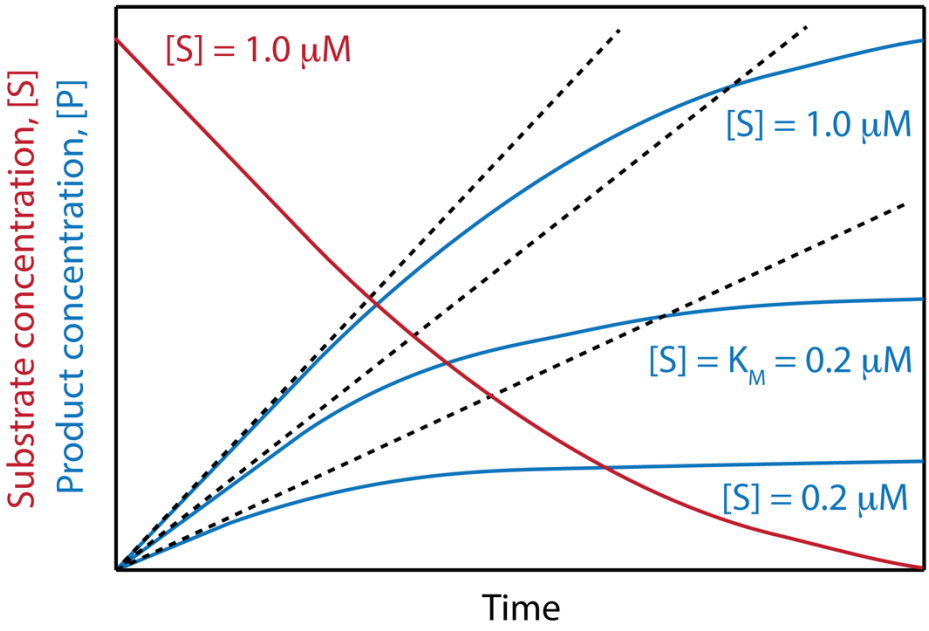

Figure 4.2: Exemplary time course of an enzyme with K_M = 0.2 μM, following the first order reaction profile for [S] >> K_M. The dotted lines represent initial rates.

In the context of this thesis, apparent turnover number values, termed k_{cat}^{app}, are estimated, for reactions following the first-order reaction profile:

$$[P] = [P]_{max} (1\text{-}e^{-kt}) \quad (4\text{-}12)$$

(shown in Figure 4.2), where [P] is the product formed at time t, $[P]_{max}$ is the final concentration of product, k is a first order rate constant and describing the rate of product formation per second where an endpoint is selected for the product with the apparent linear rate k = $[P]_{max}$/t or k = d[P]/t at constant enzyme concentration $[E]_0$.

For these first order reaction profiles, it is assumed that: 1. The progression of product formation is following the first order reaction profile; 2. The enzyme has only one active site; 3. That [S] >> K_M, generating a minimal error when calculating the initial apparent turnover rate (Figure 4.2). The corresponding apparent turnover number was k_{cat}^{app} calculated from the initial maximal velocity (dP/dt = k $[P_{max}]$ = V_{max}) divided by the enzyme concentration, similar to equitation (4-3):

$$k_{cat}^{app} = \frac{k[P]_{max}}{[E]_0} \quad (4\text{-}13)$$

The Michaelis-Menten constant, K_M, is an apparent dissociation constant, which gives a measure of how high the affinity of complex formation is between a substrate and a given enzyme, similar to binding affinity.[361]

All data presented herein are given in mean values with ± standard deviation error unless otherwise stated.

4.3 Enzyme activity of HydE and HydG

4.3.1 Enzyme activity of HydE

The natural substrate of HydE remains unknown (as of July 2018) although several research groups have investigated potential substrates. In general, the presence of the second substrate (from which the hydrogen is abstracted) often leads to much more efficient turnover of SAM by radical SAM enzymes. Evaluating compounds that enhance SAM cleavage activity represents one approach to identifying potential HydE substrates, leading to lists of substrate 'candidates'.[52,65,70]

HydE contains the typical radical SAM cluster binding motif CX_3CX_2C (Figure 4.3), which has been shown to be crucial for *C. acetobutylicum* [FeFe]-hydrogenase activation *via* generation of a CaHydE radical SAM cluster mutant.[42] *T. maritima* and *C. acetobutylicum* HydE have a relatively slow SAM turnover rate with 1 turnover per HydE per hour (but this is not unusual for uncoupled turnover, i.e. in the absence of the second substrate).[52,65] Small thiol-containing molecules, such as dithiothreitol (DTT), L-or D-cysteine, mercaptopyruvate, 3-mercaptopropionic acid and coenzyme M, stimulate the SAM cleavage activity of HydE and lead to the incorporation of deuterium from D_2O into the deoxyadenosine, which may potentially occur through exchange into the thiol group, which might be the crucial location for hydrogen abstraction by the generated DOA-radical.[65] These researchers[65] suggest a thiol-containing substrate is likely, which upon H-atom abstraction possibly gets converted into thioformaldehyde and the adt^{2-} bridge could be formed by condensation of two thioformaldehyde molecules in the presence of ammonia (Scheme 4.4), following the inorganic synthesis[365] of the dithiomethylamine bridge. However, the source of ammonia is unknown.

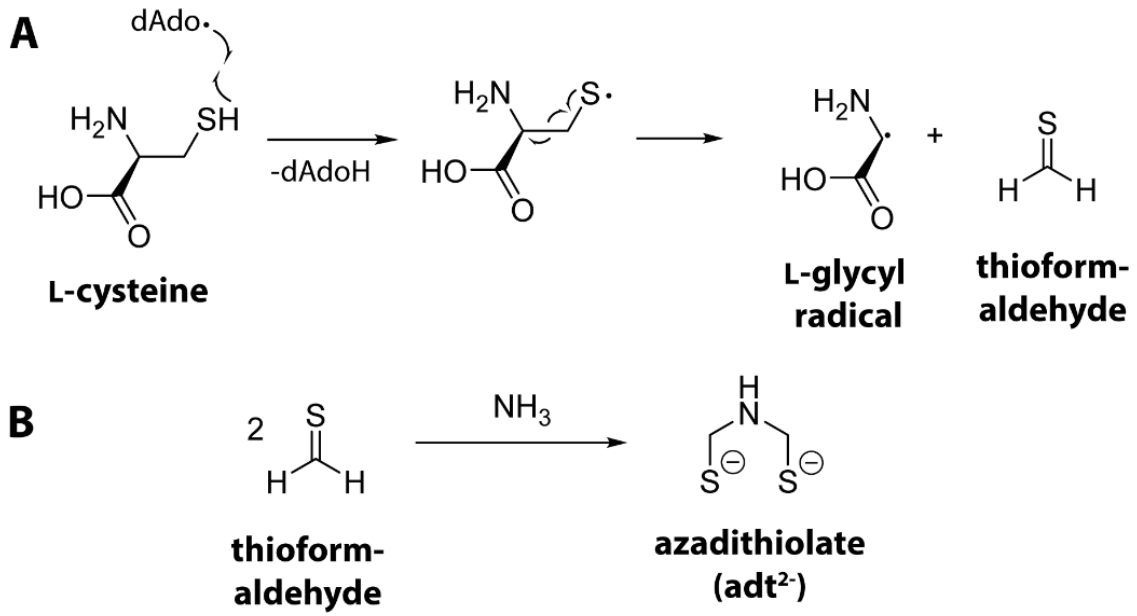

Scheme 4.4: A: Homolytic C_α-$C\beta$ bond cleavage in L-cysteine after H-atom abstraction by a DOA radical forming a glycyl radical and thioformaldehyde. B: Condensation of two thioaldehyde molecules in the presence of ammonia to form the azadithiolate bridge (adt^{2-}).

Another class of molecules, the 1,3-thiazolidines (MeTDA, Scheme 4.5), have been shown to act as ligands and substrates for HydE. However, they did not stimulate SAM cleavage activity to the same magnitude as DTT or coenzyme M.[70]

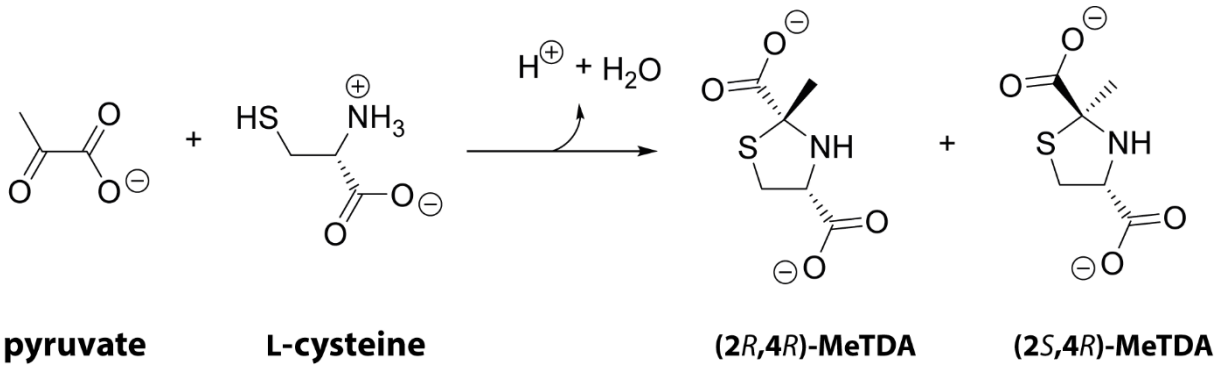

Scheme 4.5: Formation of the 1,3-thiazolidines (2*R*,4*R*)-2-methyl-1,3-thiazolidine-2,4-dicarboxylic acid (2*R*,4*R*)-MeTDA) and (2*S*,4*R*)- 2-methyl-1,3-thiazolidine-2,4-dicarboxylic acid (2*S*,4*R*)-MeTDA) from a 1:1 mixture of pyruvate and L-cysteine. Adapted from [70].

HydE proteins have a high sequence and structure homology to the radical SAM enzymes PylB and BioB (Figure 4.3). However, there are no kinetic data on SAM cleavage or final product formation data by PylB, which catalyzes the rearrangement of L-α-lysine to 3-methyl-D-ornithine (Scheme 4.6B).[151] BioB in contrast is well

characterized (Scheme 4.6A) and its SAM cleavage initial rate constant is 0.021 min^{-1} similar to that reported for the HydE rate of 0.017 min^{-1}.[366]

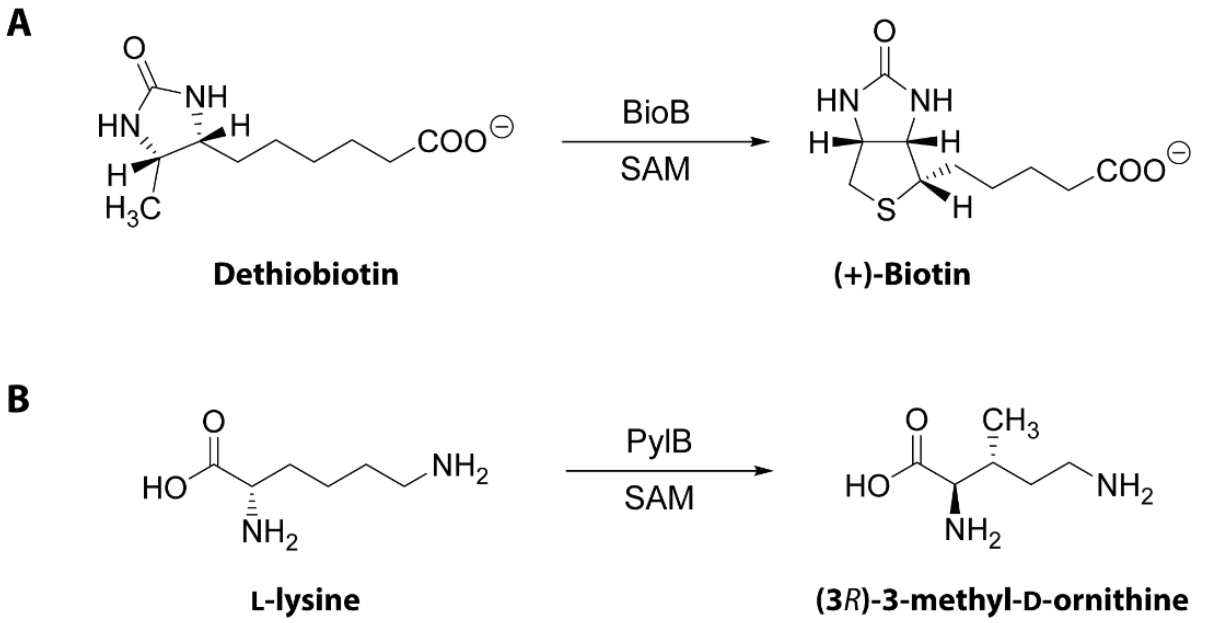

Scheme 4.6: A: Overall reaction of the radical SAM enzyme BioB converting dethiobiotin into biotin. B: Overall reaction of the radical SAM enzyme PylB converting L-lysine into (3*R*)-3-methyl-D-ornithine. Adapted from [151,367].

Figure 4.3: Sequence alignment of radical SAM binding motifs in HydEs studied in this thesis from *Thermoanaerobacter italicus* and in comparison to PylB from *Methanosarcina barkeri* and BioB from *Escherichia coli*. The Alignment was generated with ClustalW[254,255] and JalView[256]. The complete sequence alignment is in the Appendix 4.1.

The role of the auxiliary cluster, which is not present in all HydE enzyme sequences, is still mysterious.[22] Nevertheless, in work that replaced a HydE protein carrying both iron-sulfur clusters (*Clostridium acetobutylicum*) with a HydE protein with only the radical SAM cluster binding site (*Bacteroides thetaiotaomicron*), it was demonstrated that the additional cluster does not affect the maturation of the [FeFe]-hydrogenase.[53]

4.3.2 Enzyme activity of HydG

Reactions catalyzed by the radial SAM enzyme HydG include the reductive SAM cleavage and C_α-C_β scission of L-tyrosine into *p*-cresol and dehydroglycine (DHG). As is the case with almost all radical SAM enzymes, HydG contains the characteristic radical SAM cluster binding motif CX_3CX_2C (Figure 4.4). HydG shares a high homology to the tyrosine lyase ThiH, which catalyzes the same reaction as HydG: the conversion to *p*-cresol and dehydroglycine (DHG), a precursor for thiazole biosynthesis.[54] Moreover, the sequence of HydG also shares high homology with the tryptophan lyase NosL, for which recent crystallographic studies suggested the 5'-deoxyadenosyl radical initiated H-atom abstraction from the α-NH_2 group of tryptophan (Scheme 4.7).[150]

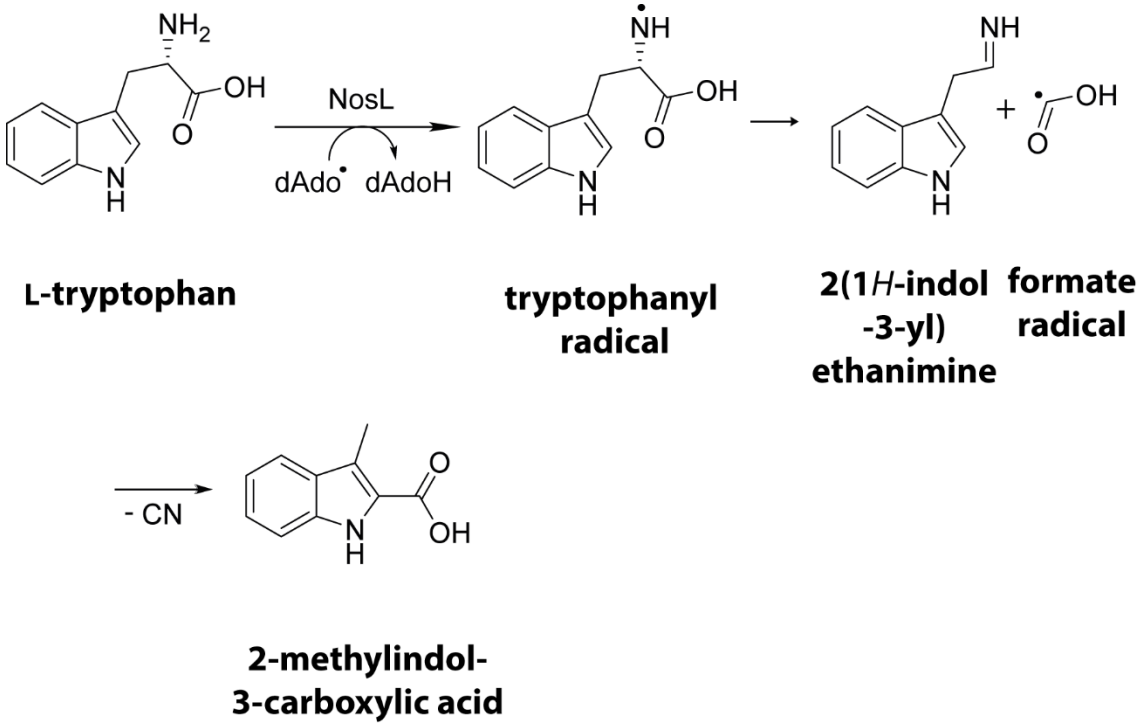

Scheme 4.7: Reaction of NosL with hydrogen abstraction at the amino-nitrogen α-NH_2, leading to a β-scission forming 2(1*H*-indol-3-yl) ethanimine and a formate radical. After rearrangement of the carboxylic group and formation of cyanide the 2-methylindol-3-carboxylic acid is formed.

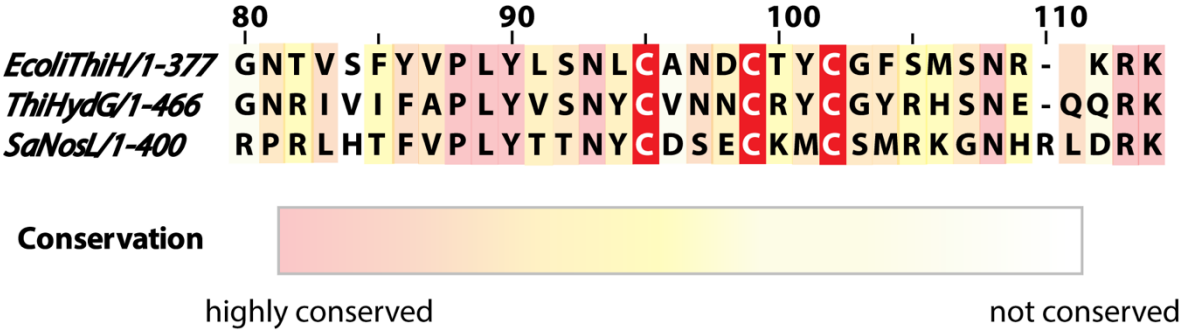

Figure 4.4: Sequence alignment of radical SAM binding motifs of HydG from *Thermoanaerobacter italicus* in comparison to ThiH from *Escherichia coli* and NosL from *Streptomyces actuosus*. The Alignment was generated with ClustalW[254,255] and JalView[256]. The complete sequence alignment is in the Appendix 4.1.

Remarkably, HydG synthesizes CO and CN^- ligands, which are derived from L-tyrosine, as shown in experiments with labelled L-tyrosine.[49] Just recently it was reported that NosL is able to produce cyanide as well (Scheme 4.8).[368]

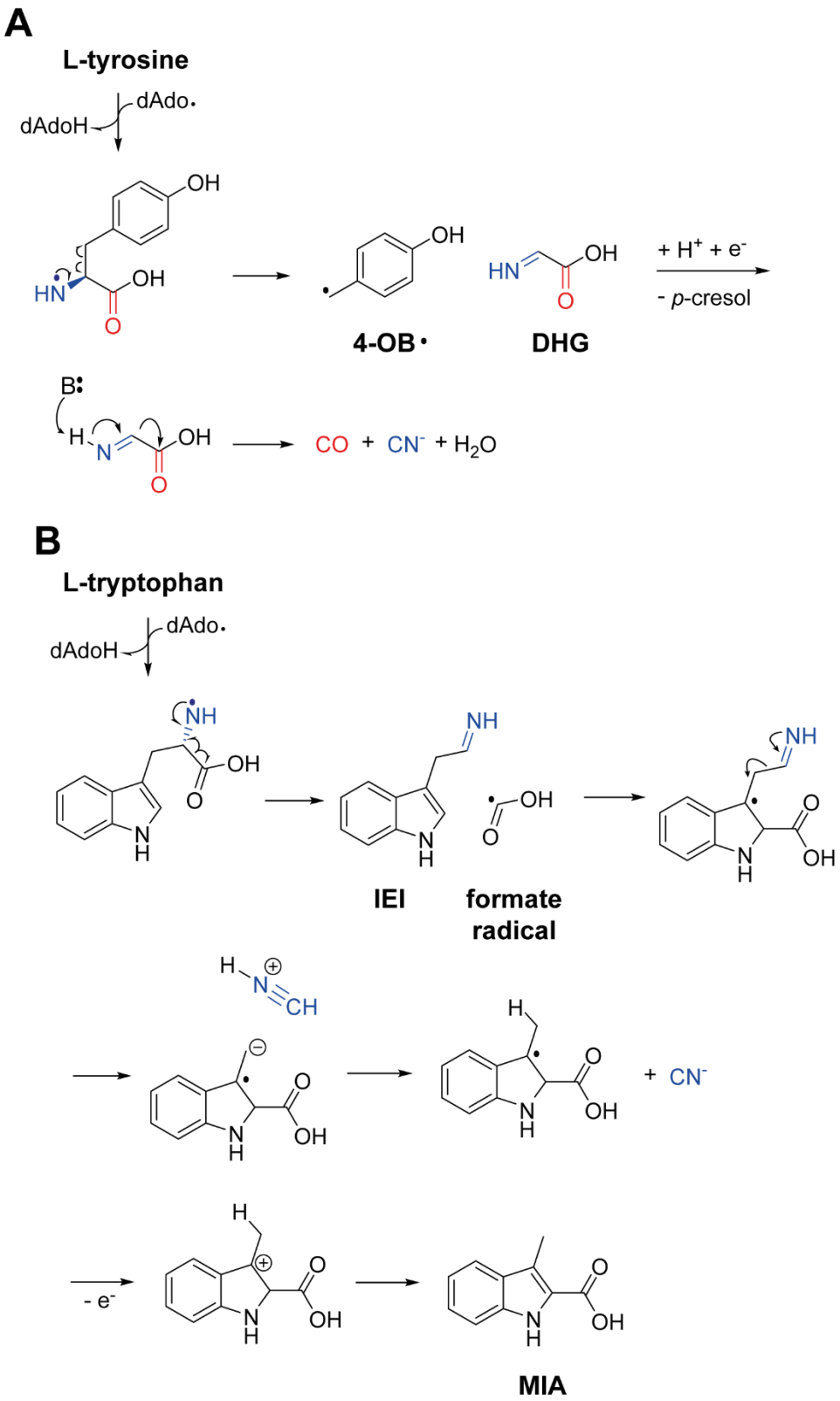

Scheme 4.8: Cyanide formation catalyzed by the radical SAM enzymes HydG (A) and NosL (B). After SAM cleavage the hydrogen is abstracted from the NH_2 group of either L-tyrosine (A) or L-tryptophan (B), following by a β-scission generating *p*-cresol and dehydroglycine for HydG (A) and IEI and a formate radical for NosL (B). Dehydroglycine is fragmented to CO, CN^- and water if a base is present for HydG (A). Whereas, for NosL IEI undergoes another β-scission forming H_2CN^+ and a methylindol carboxylic acid radical. The strongly acidic H_2CN^+ protonates the indol radical and forms cyanide. Rearrangement of the indolic cation leads to MIA.

EPR and ENDOR studies have been used for more detailed investigations of the HydG catalyzed reactions.[38,61,64,66,67,71] These studies revealed that the ligands are produced by activation of dehydroglycine and subsequent conversion into CO and CN^-.[59,61] The diatomic ligands then proposed to form the synthon complex $Fe(CO)_2(CN)$ with the 5th iron of the auxiliary cluster, which corresponds to the reactions observed via FT-IR spectroscopy.[61] Formation of CN^- can be quantified through derivatization with taurine and naphthalene-2,3-dicarboxyaldehyde (NDA), which forms the fluorescence probe 1-cyanobenz[f]isoindole (CBI), followed by analysis via HPLC (Scheme 4.9).[55] The initial reaction rate for cyanide formation in CaHydG was found to be 0.036 min^{-1}.[60] Formation of CO has thus been measured by two methods, *via* FT-IR[61,69] and *via* UV-Vis spectroscopy after reaction with hemoglobin.[56]

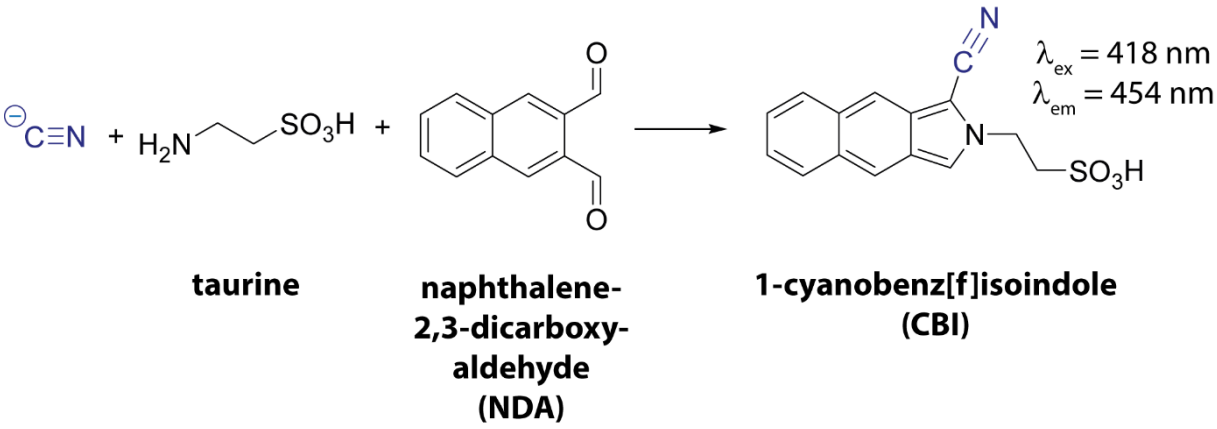

Scheme 4.9: Reaction of the cyanide assay. Cyanide is derivatized with taurine and naphthalene-2,3 dicarboylaldehyde (NDA) to form the fluorescent reaction product 1-cyanobenz[f]isoindole (CBI).

HydG from the mesophilic bacterium *Clostridium acetobutylicum* has an initial rate constant of 0.140 ± 0.017 min^{-1} for the SAM cleavage reaction and 0.110 ± 0.014 min^{-1} for the *p*-cresol formation, which was measured in a time-dependent HPLC-based assay.[60] The SAM cleavage product DOA was detected by UV-Vis absorbance at 254 nm and *p*-cresol was detected by a fluorescence detector set at λ_{ex} = 274 nm and λ_{em} = 312 nm.

Moreover, HydG carries an [5Fe5S] auxiliary cluster, as confirmed with X-Ray crystallography,[64] which is not directly involved in SAM cleavage, as was demonstrated with a HydG cysteine-mutant lacking the additional [5Fe5S]-cluster.[60]

However, without the *C*-terminal domain that carries the binding motif of the auxiliary cluster, the *p*-cresol formation is decreased (from 4.4 x 10^{-3} to 3.0 x 10^{-3} s^{-1} in turnover number k_{cat}) and CN^- production completely abolished, suggesting an important role of the auxiliary cluster for recognition/ interaction of tyrosine.(60)

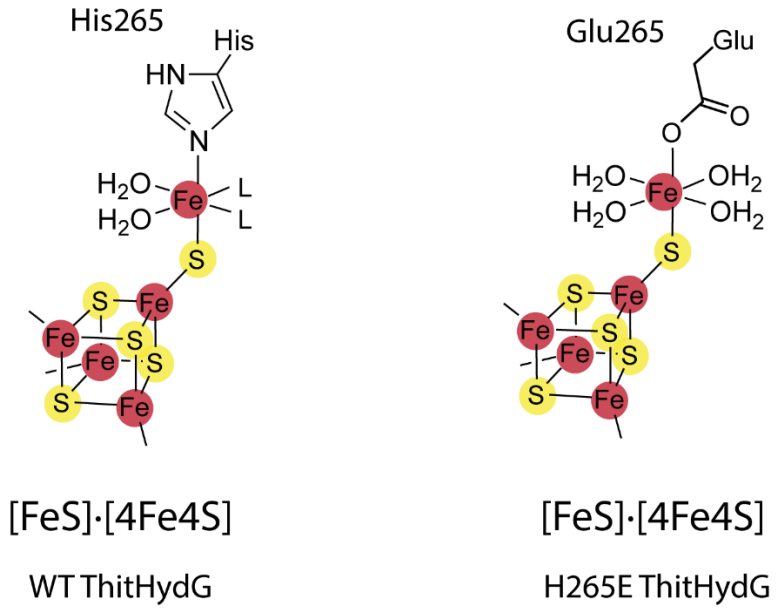

Figure 4.5: Auxiliary cluster of wild type ThitHydG (left) and the sequence variant H265E ThitHydG (right).

Another HydG sequence variant, which has been found to affect the activity of the enzyme was the replacement of the amino acid coordinating the 5th iron of the auxiliary cluster (Figure 4.5): histidine, by either glutamic acid or asparagine. The replacement of histidine showed increased turnover of CN^- for either glutamic acid and asparagine sequence variants, and increased DOA formation in the case of the Glu mutation, but no formation of CO if replaced with asparagine.(68,276)

Reasons for the change in activity of HydG caused by the replacement of histidine, may lie in the fact that the lability of the synthon iron is increased and it is therefore able to dissociate quicker.

Recent studies are consistent with a hypothesis that HydG transfers two equivalents of the synthon ($Fe(CO)_2CN$) onto HydF, which forms the H-cluster precursor (Scheme 4.10).(244)

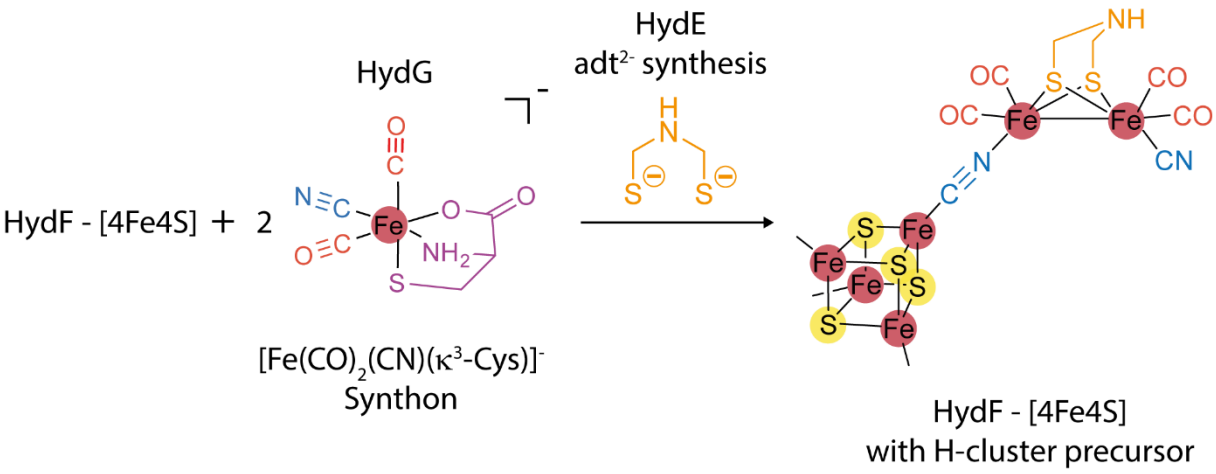

Scheme 4.10: Proposed reaction leading to the H-cluster precursor loaded HydF. Transfer of two synthons onto HydF by HydG and subsequent synthesis of the azadithiolate bridge by HydE.

4.3.3 Time-dependent activity of HydE and HydG

To determine if HydE is enhancing the activity of HydG and to estimate the turnover rates, a time-dependent activity assay measuring the conversion of SAM and tyrosine was carried out. The reaction containing all necessary and potential substrates (200 µM L-cysteine, 200 µM $FeCl_2$, 500 µM SAM, 1 mM L-tyrosine) as well as the appropriate enzyme (25 µM of His_6ThitHydG and/or His_6ThitHydE1265) were mixed together and 1 mM sodium dithionite was added last to initiate the reaction in HydG reaction buffer (50 mM HEPES, 500 mM KCl, pH 7.4). The assay was incubated at 37 °C and then stopped at 8 different time points (6, 8, 20, 25, 35, 65, 125 minutes). To stop the reaction, perchloric acid (20%) was added to precipitate the proteins. After the precipitated enzymes were removed by centrifugation, a portion of the assay (10 of 110 µL) was set aside to permit glyoxylate detection and the remaining portion (100 µL) was directly analyzed by reversed-phase HPLC for detection of the reaction products 5'-deoxyadenosine and *p*-cresol. An example of a typical HPLC-chromatogram trace of a coupled SAM-Tyr assay with HydG and HydE1 together in one reaction mix is shown in Figure 4.6.

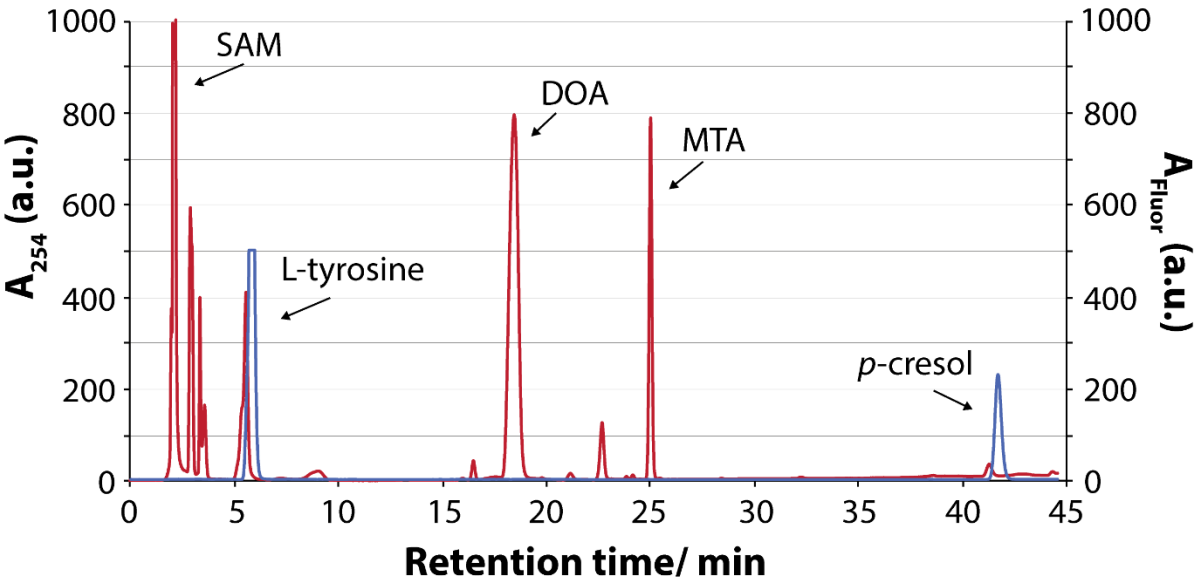

Figure 4.6: Typical chromatogram depicting the different reactions products of a SAM-Tyr assay with HydG and HydE1. The red trace is absorbance at 254 nm and the blue trace is fluorescence with excitation at 274 nm and detection at 312 nm, which detects both tyrosine and *p*-cresol.[276]

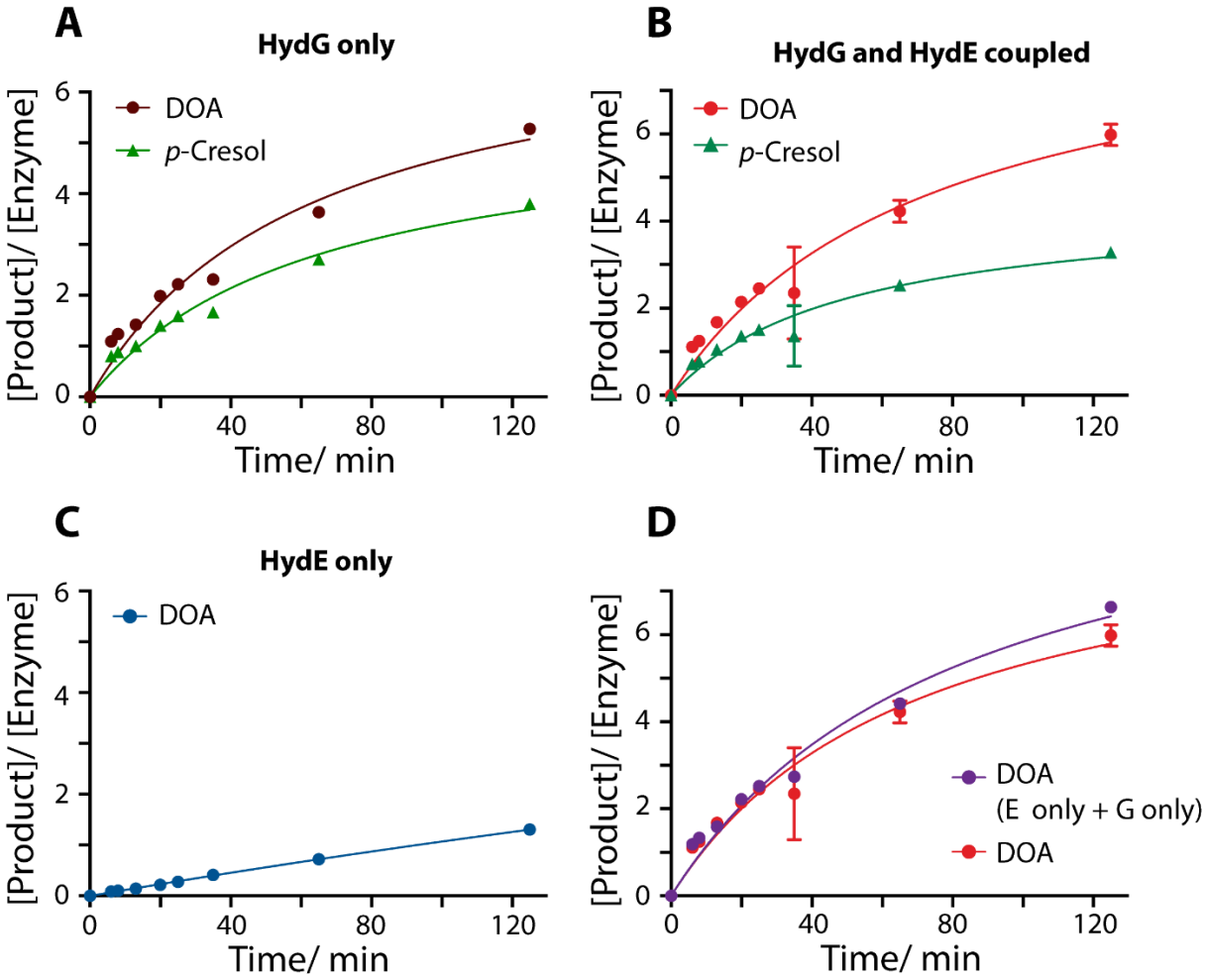

Figure 4.7: Formation of reaction products over time (time course). For **A**: HydG alone; **B**: HydE1 and HydG coupled activity; **C**: HydE1 alone and **D**: The acticity of HydG alone and HydE1 alone added up (E only + G only) in comparison to the coupled activity from **B**. Graphs are fitted to a first order exponential association curve (see equation 4-12). The concentration of each enzyme was 25 μM. Assays were carried out in duplicates.

Table 4.1: Rate constants obtained from the fitted exponential one phase association curve of the time-dependent activity assay shown in Figure 4.7. Endpoint is 125 min.

Assay – DOA (Graph in Figure)	**Intensity Plateau (max.)**	**Equation**	**Rate constant, 10^{-4} s^{-1}**	**Goodness of fit (R^2)**
HydG only (A)	(6.253 ± 0.554)	A[a]	2.275 ± 0.428	0.977
HydG & HydE (B)	(7.525 ± 1.377)	A[a]	1.983 ± 0.715	0.929
HydE only (C)	(5.632 ± 0.931)	A[a]	0.351 ± 0.049	0.999
HydG + HydE (D)	(8.357 ± 1.557)	A[a]	1.989 ± 0.697	0.972
Assay - *p*-cresol				
HydG only (A)	(4.466 ± 0.340)	A[a]	2.368 ± 0.388	0.981
HydG & HydE (B)	(3.720 ± 0.547)	A[a]	2.665 ± 0.897	0.903

[a]Equations are: A, exponential, one phase association.

Table 4.2: Kinetic parameters obtained and calculated from the experiments represented in Figure 4.7: Considered endpoint is 8 min to obtain initial linear rates.

DOA	**ΔC/ μM**	**k/ nM s^{-1}**	**k_{cat}^{app}/ 10^{-4} s^{-1}**
ThitHydG only	30.9 ± 0.9	64.4 ± 1.9	25.8 ± 0.8
ThitHydE1 only	2.5	5.2	2.1
ThitHydG & E1	31.1 ± 0.6	64.8 ± 1.3	25.9 ± 0.5
Sum of HydG and HydE1 only	33.4	69.2	27.7
p-cresol			
ThitHydG alone	22.1 ± 0.2	46.0 ± 0.4	18.4 ± 0.2
ThitHydG & E1	19.4 ± 0.5	40.4 ± 1.0	16.2 ± 0.4

Table 4.3: Kinetic parameters obtained and calculated from the experiments represented in Figure 4.7: Considered Endpoint is 65 min.

DOA	**ΔC/ μM**	**k/ nM s^{-1}**	**k_{cat}^{app}/ 10^{-4} s^{-1}**
ThitHydG alone	91.0 ± 1.9	23.3 ± 0.5	9.3 ± 0.2
ThitHydE1 alone	18.1 ± 0.7	4.6 ± 0.2	1.8 ± 0.1
ThitHydG & E1	105.7 ± 6.3	27.1 ± 1.6	10.8 ± 0.6
Sum of HydG and HydE1 only	109.1	28.0	11.2
p-cresol			
ThitHydG alone	67.7 ± 0.5	17.4 ± 0.1	7.0 ± 0.0
ThitHydG & E1	63.3 ± 2.4	16.2 ± 0.6	6.5 ± 0.2

Results of the His_6ThitHydE1 and His_6ThitHydG activity experiments (Figure 4.6, Table 4.1, Table 4.2 and Table 4.3) reveal that HydE1 is much less active than HydG, about 5-fold lower activity is observed. Reasons for the low activity of HydE1 might lie in the fact that the second substrate (target for H atom abstraction) is not present in the reaction mix, although the potential substrate L-cysteine is present. (L-cysteine has been shown to increase the activity of HydE 3-fold, although only when a large excess of 100 equivalents was added[65]). The low turnover rate of ThitHydE1 is comparable to HydE proteins of *T. maritima* and *C. acetobutylicum*, which is usually in the range of one equivalent of SAM per hour which is the case for ThitHydE1 in presence of cysteine (8 equivalents). Coupling HydG's activity to HydE did not have an enhancing effect on the production of DOA and *p*-cresol, which shows that the enzymes act independent from one another. Binding studies of the [FeFe]-hydrogenase maturation

proteins suggested that the two radical SAM enzymes HydG and HydE do not interact with each other[253] which is in accord with the results of the activity experiments reported here. The kinetic parameters obtained for using a 65 min endpoint in the assay of ThitHydGs SAM cleavage activity are similar to the kinetic studies carried out by Dr. P. Dinis[276] with ThitHydG, which were also measured after 60 min[276] (Table 4.4). However, the kinetic parameters for the initial 8 min of the ThitHydG SAM cleavage reaction are slightly decreased and closely resemble the values reported for CaHydG (k_{cat}^{app} = 27.7 s^{-1})[269] and EcoliThiH (k_{cat}^{app} = 27.0 s^{-1})[201] (Table 4.4). In addition, the turnover rates of L-tyrosine to *p*-cresol were reduced when compared to other studies of CaHydG, but comparable to those already demonstrated for ThitHydG.

Table 4.4: Comparison of kinetic parameters from this thesis with previously reported values for HydG proteins and for ThiH.

	DOA k_{cat}^{app}/ 10^{-4} s^{-1}	***p*-cresol k_{cat}^{app}/ 10^{-4} s^{-1}**
ThitHydG 8 min	25.8 ± 0.8	18.4 ± 0.2
ThitHydG 65 min	9.3 ± 0.2	7.0 ± 0.0
ThitHydG (from P. Dinis[267])	7.2 ± 0.1	6.8 ± 0.1
TletHydG (from P. Dinis[267])	9.6	2.6
CaHydG (initial, from R. Driesener[269])	27.7 ± 3.9	21.1 ± 2.7
EcoliThiH (initial[201])	27 ± 11	32 ± 11
EcoliThiH (steady state[201])	10.7 ± 1.0	5.9 ± 0.2

As well as the HPLC 'coupled' assay containing both Tyr and SAM, the formation of glyoxylate was measured in a parallel assay to test if the addition of HydE to HydG increases the formation of dehydroglycine, which is hydrolytically unstable and is readily converted to glyoxylate and ammonia. The glyoxylate assay employs a chemical derivatization with *o*-phenylene diamine prior to HPLC analysis using fluorescence detection (Scheme 4.11).[201,369]

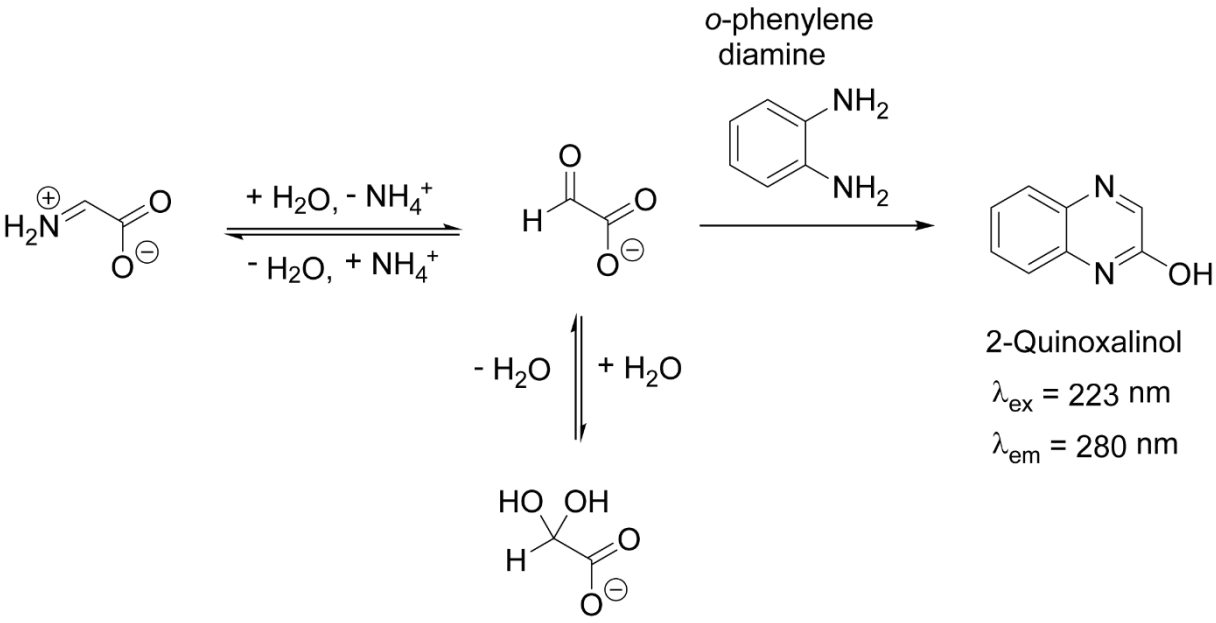

Scheme 4.11: Derivatization of glyoxylate by reaction with *p*-phenylene diamine forming the fluorescent 2-quinoxalinol. Adapted from [201].

The results of the time-dependent glyoxylate formation activity are summarized in Figure 4.9. As outlined by Dr. R. C. Driesener[269], dithionite causes a very high background signal in the glyoxylate assay if compared to the assay signals obtained with HydG, HydG & HydE1 coupled and HydE1 (time-dependent assay), thus causing difficulties in correctly quantifying the reaction products (Figure 4.8). To circumvent this problem, sodium dithionite was added to the calibration standards, facilitating the subtraction of the high background signals from the assay signals (Figure 4.8). However, the remaining amounts of glyoxylate detected were very small and ranged between around 0-15 μM.

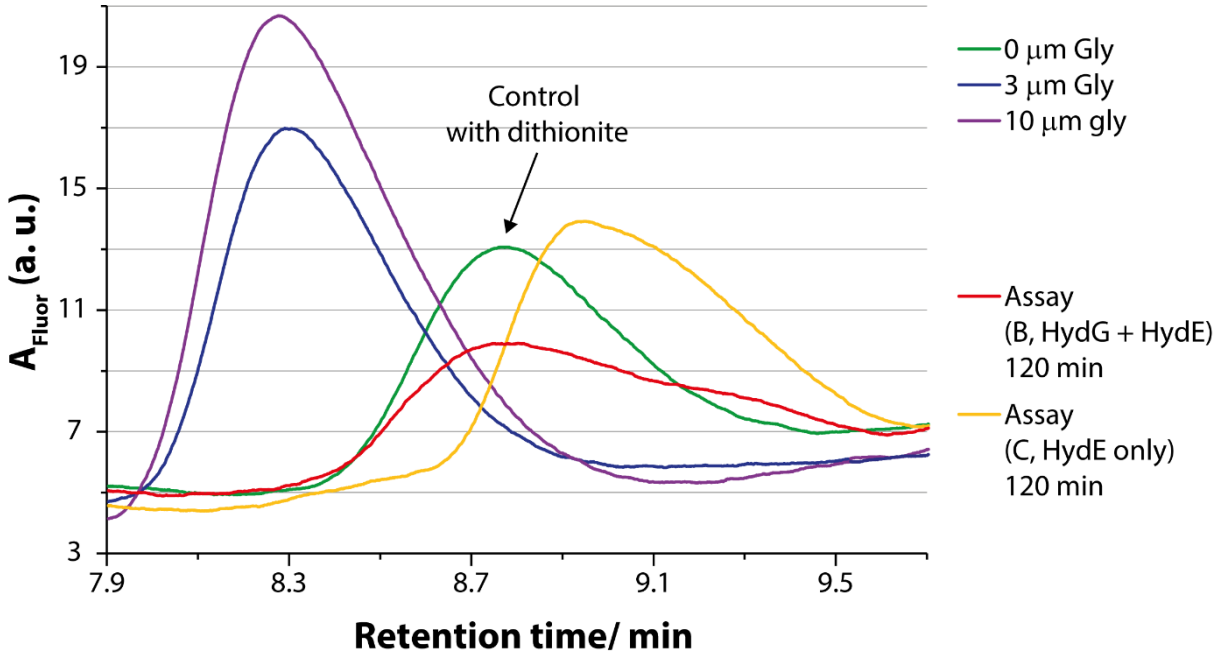

Figure 4.8: Exemplary chromatograms of calibration standards with glyoxylate (0, 3 and 10 mM) and dithionite (1 mM) as well as two time-dependent assay samples of B at 120 min (HydE1 and HydG coupled assay, Figure 4.9) and C at 120 min (HydE1 only assay, Figure 4.9)).

Another factor influencing the fluorescence of the derivatization product is time; previous studies[370] have shown that long incubation at room temperatures over 1 h decreases the fluorescence; however, the samples in this study were frozen upon preparation, stored at -80°C and then thawed shortly before analysis (1-10 min before). Despite these precautions, high fluctuation and substantial errors are observed and there is no real change in concentration of glyoxylate observed over time for all three assays that were carried out. Many peaks appear at a similar retention time as the 2-quinoxalinol peak, which impeded analysis. This led to interpretation of the data becoming very challenging and further optimization is needed in order to better resolve and separate the signal obtained. Storage times as well as temperature changes have a big impact on the fluorescence on the samples and these factors need to be taken into account. Furthermore, the amount of glyoxylate produced by HydG is expected to be very low, since the dehydroglycine is efficiently decomposed to CO and CN^- ligands and the glyoxylate is a minor 'shunt' product (Scheme 4.12).[55]

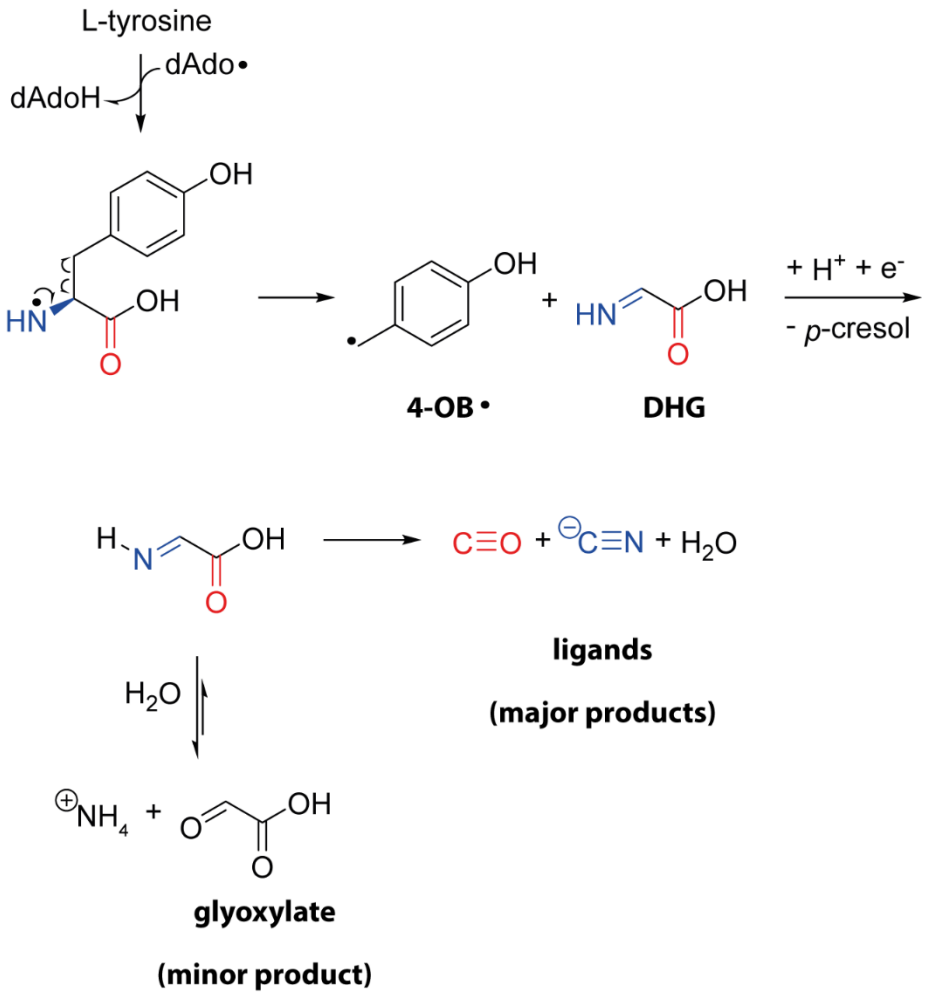

Scheme 4.12: Reaction scheme of HydG with glyoxylate as minor 'shunt' hydrolysis product. Formation of dehydroglycine and following decomposition to CO and CN^- ligands. Hydrolysis of DHG leads to glyoxylate (less than 10%)[9] and ammonia.

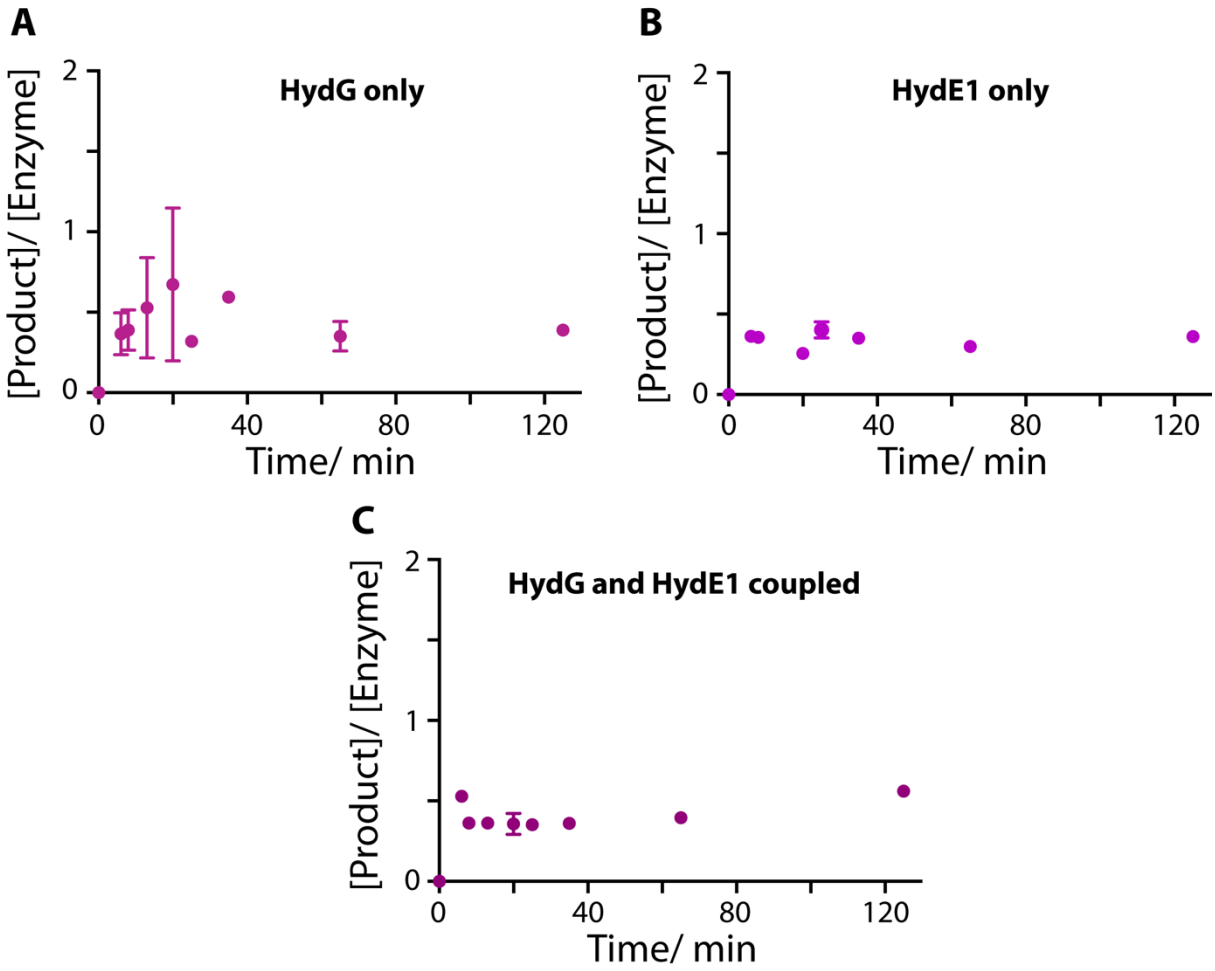

Figure 4.9: Time course of the glyoxylate formation in context of the time-dependent activity assays for HydG and HydE1. Formation of glyoxylate by A: HydG alone; B: HydE1 alone, C. HydG and HydE together. The concentration of each enzyme was 25 μM. Assays were carried out in duplicates.

4.3.4 Screening compounds which increase turnover rates of HydG and HydE

Kuchenreuther *et al.* investigated the influence of different compounds on the maturation of the [FeFe]-hydrogenase and its resultant activity[50] - and a similar approach was used herein. In this thesis the same compounds as previously reported,[50] as well as additional compounds not previously tested, were screened in an assay for increasing SAM and Tyr cleavage activity of His_6ThitHydG and His_6ThitHydE in the presence of the partner [FeFe]-hydrogenase maturation proteins. To investigate the activity change, the assay set-up was identical to the previous time-dependent activity test of His_6ThitHydE1 and His_6ThitHydG, though in this case the enzymes were mixed together with StrepThitHydF and His_6ThitHydE2 as well, to take interactions with these proteins into account. The core assay reactants were 25 μM

enzyme, 500 μM SAM, 200 μM L-cysteine, 200 μM Fe(II)Cl_2, 1 mM L-tyrosine and 1 mM DTH in HydG reaction buffer (50 mM HEPES, 500 mM KCl, pH 7.4)[267].

In two independent assay experiments, different combinations of [FeFe]-hydrogenase maturation proteins were tested for their activity resulting in the cleavage of SAM and Tyr to their detectable products, DOA and *p*-cresol respectively. Additionally, a mix of all [FeFe]-hydrogenase maturation proteins (GE1E2F) with core reagents was supplemented with one compound at a time to test their influence on the combined enzyme activities. For these activity assays, a single time point was selected (rather than the time courses used in earlier experiments, Figure 4.6 and 4.9). The selected reaction time was 65 min at 37°C, with the reagents being assembled inside the glovebox, then the reaction Eppendorf tubes (1.5 mL) were sealed and incubated at 37°C outside the glovebox.

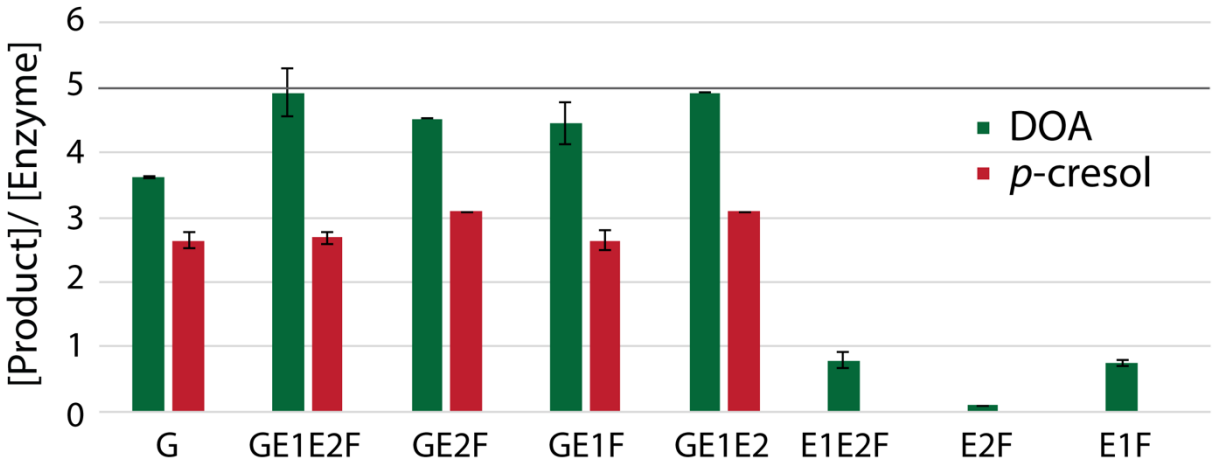

Figure 4.10: DOA and *p*-cresol product formation of different combinations of [FeFe]-hydrogenase maturases from *Thermoanaerobacter italicus*. Summary of two different experiments measured in duplicates. G = HydG, E1 = HydE1265, E2 = HydE1675, F = HydF.

As observed in the time dependent assay (Section 4.3.3), the total SAM cleavage activity of the mixtures GE1E2F (HydG + HydE1 + HydE2 + HydF), GE2F (HydG + HydE2 + HydF), GE1F (HydG + HydE1 + HydF), GE1E2 (HydG + HydE1 + HydE2) and E1E2F (HydE1 + HydE2 + HydF) represent approximately the sum of the single SAM cleavage activities of HydG (G), HydE1 (E1F) and HydE2 (E2F). Interestingly, the HydE2 protein has an even lower SAM turnover number than HydE1 (Table 4.5). Addition of HydF does not influence the SAM and L-tyrosine cleavage activity of HydG or the HydE proteins (Figure 4.9, Table 4.5 and 4.6) under these reaction conditions.

Table 4.5: Activity measurements of SAM turnover resulting from the experiments summarized in Figure 4.10.

DOA	**ΔC/ μM**	**k/ nM s^{-1}**	**k_{cat}^{app}/ 10^{-4} s^{-1}**
G	90.5 ± 0.5	23.2 ± 0.1	9.3 ± 0.1
GE1E2F	123.2 ± 9.5	31.6 ± 2.4	12.6 ± 1.0
GE2F	112.9	29.0	11.6
GE1F	111.4 ± 8.0	28.6 ± 2.1	11.4 ± 0.8
GE1E2	123.0	31.5	12.6
E1E2F	19.5 ± 3.1	5.0 ± 0.8	2.0 ± 0.3
E2F	2.5	0.6	0.3
E1F	18.8 ± 1.0	4.8 ± 0.3	1.9 ± 0.1

Table 4.6: Activity measurements of L-tyrosine turnover resulting from the experiments summarized in Figure 4.10.

p-cresol	**ΔC/ μM**	**k/ nM s^{-1}**	**k_{cat}^{app}/ 10^{-4} s^{-1}**
G	66.1 ± 3.0	16.9 ± 0.8	6.8 ± 0.3
GE1E2F	67.1 ± 2.3	17.2 ± 0.6	6.9 ± 0.2
GE2F	77.3	19.8	7.9
GE1F	66.1 ± 3.9	16.9 ± 1.0	6.8 ± 0.4
GE1E2	77.2	19.8	7.9

A set of metabolites have been assessed which were previously shown to be important for the full activation of the [FeFe]-hydrogenase,[50] and for enhancing the activity of the [FeFe]-hydrogenase maturation enzyme mix (GE1E2F). These compounds are GTP (2 mM), PLP (500 μM), DTT (300 μM), sulfide S^{2-} (200 μM), *E. coli* cleared lysate and desalted *E. coli* cleared lysate (4 mg total protein/ mL). Additionally, glutathione (200 μM) was tested, because it had been shown to be beneficial for iron-sulfur cluster incorporation in HydF (Chapter 3, section 3.3.1). In Figure 4.11 the DOA and *p*-cresol product formation from these activity assays is summarized.

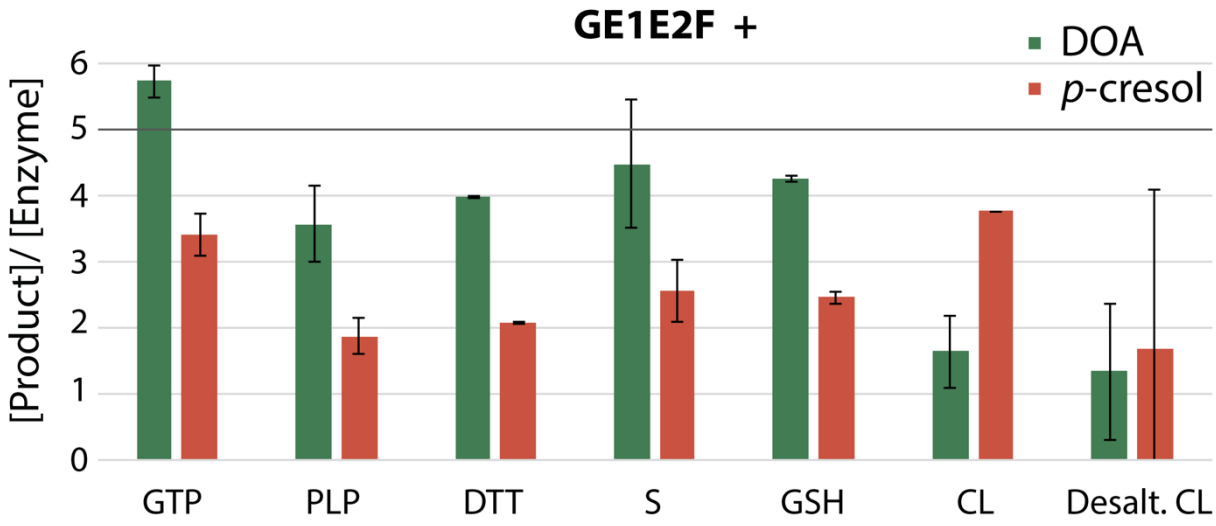

Figure 4.11: DOA and *p*-cresol product formation in a HydG assay containing all [FeFe]-hydrogenase maturases and additional components that might increase product turnover numbers. Summary of two different experiments measured in duplicates.

Table 4.7: Activity measurements of SAM and L-tyrosine turnover resulting from the experiments summarized in Figure 4.11.

DOA	**ΔC/ μM**	**k/ nM s^{-1}**	**k_{cat}^{app}/ 10^{-4} s^{-1}**
GE1E2F control	123.2 ± 9.5	31.6 ± 2.4	12.6 ± 1.0
+ GTP	143.3 ± 6.0	36.7 ± 1.5	14.7 ± 0.6
+ PLP	89.3 ± 14.6	22.9 ± 3.7	9.2 ± 1.5
+ DTT	100.0 ± 0.4	25.6 ± 0.1	10.3
+ S^{2-}	112.0 ± 24.2	28.7 ± 6.2	11.5 ± 2.5
+ GSH	106.7 ± 1.2	27.4 ± 0.3	10.9 ± 0.1
+ CL	41.0 ± 13.5	10.5 ± 3.5	4.2 ± 1.4
+ Desalt. CL	33.6 ± 59.7	8.6 ± 15.3	3.4 ± 2.6
p-cresol			
GE1E2F control	67.1 ± 2.3	17.2 ± 0.6	6.9 ± 0.2
+ GTP	85.5 ± 7.9	21.9 ± 2.0	8.8 ± 0.8
+ PLP	46.9 ± 6.8	12.0 ± 1.7	4.8 ± 0.7
+ DTT	52.0 ± 0.3	13.3 ± 0.1	5.3
+ S^{2-}	64.4 ± 11.7	16.5 ± 3.0	6.6 ± 1.2
+ GSH	61.6 ± 2.3	15.8 ± 0.6	6.3 ± 0.2
+ CL	94.2	24.1	9.7
+ Desalt. CL	42.2 ± 59.7	10.8 ± 15.3	4.3 ± 6.1

The only compound that seemed to have a stimulating effect on the DOA and *p*-cresol formation of the maturase mix (GE1E2F) was GTP (Figure 4.11 and Table 4.7). Since the *p*-cresol formation is increased, it seems likely that GTP acts to increase the turnover of HydG. Interestingly, there is a large increase of *p*-cresol formation if cleared *E. coli* lysate is added, which may be due to the presence of another tyrosine lyase ThiH, which is present in *E. coli*.

The hypothetical function of GTP might be the release and transport of the synthon from HydG to HydF, which is recognizing GTP as its substrate and accepts the synthon to build up the H-cluster precursor (Scheme 4.14). Release of the synthon of HydG, which is the reaction product of HydG could possibly increase HydG turnover numbers by regenerating the active site and therefore accelerating the formation of another synthon equivalent, after SAM and Tyr cleavage.

4.3.5 Activity of HydG and HydE in presence of GTP

To find out which enzymes of the three [FeFe]-hydrogenase maturases are influenced by GTP, 2 mM GTP was added to the core reagents and the activity was monitored after an incubation time of 65 min.

Table 4.8: Activity measurements of SAM and L-tyrosine turnover resulting from the experiments summarized in Figure 4.12, where GTP was added as core reagent.

+ GTP	DOA k_{cat}^{app} (10^{-4} s^{-1})	*p*-cresol k_{cat}^{app} (10^{-4} s^{-1})
G	15.7 ± 0.3	11.3 ± 4.5
GE1E2F	20.9 ± 2.5	10.6 ± 4.3
GE2F	17.5 ± 1.3	10.8 ± 4.3
GE1F	19.1 ± 0.3	10.3 ± 4.1
GE1E2F	17.8 ± 0.6	10.6 ± 4.3
E1E2F	2.8 ± 0.2	-
E2F	1.2 ± 1.3	-
E1F	2.3	-

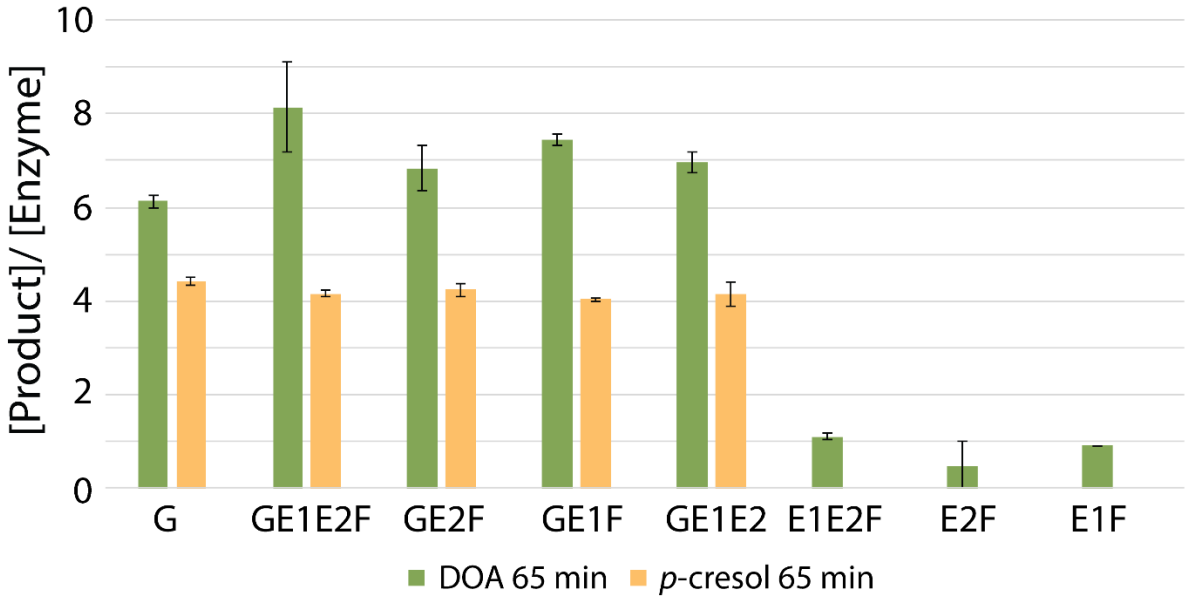

Figure 4.12: DOA and *p*-cresol product formation of different combinations of [FeFe]-hydrogenase maturases from *Thermoanaerobacter italicus*. GTP is added as a core reagent to each mixture. Summary of one experiment measured in duplicate.

When comparing the turnover rates (Table 4.9) represented in Figure 4.12 with the turnover rates from Figure 4.10, what is striking is that the activity of all HydG containing samples increased with presence of GTP, whilst the activity of the HydE proteins was not significantly affected by GTP.

Table 4.9: SAM and L-tyrosine turnover rates of HydG and a mixture of HydG, HydE1, HydE2 and HydF (GE1E2F) in absence and presence of GTP.

	DOA k_{cat}^{app}/ 10^{-4} s^{-1}	***p*-cresol k_{cat}^{app}/ 10^{-4} s^{-1}**
G	9.3 ± 0.1	6.8 ± 0.3
G + GTP	15.7 ± 0.3	11.3 ± 4.5
E1E2F	1.9 ± 0.1	-
E1E2F + GTP	2.8 ± 0.2	-
GE1E2F	12.6 ± 1.0	6.9 ± 0.2
GE1E2F + GTP	20.9 ± 2.5	10.6 ± 4.3

In order to confirm if GTP does have a direct effect on the activity of HydG, HydG reactions with and without GTP were incubated as stated before, but this time stopped at two time points, 35 and 65 min. The additional time point at 35 min was selected to

investigate if GTP is already influencing the initial product formation rate, or if it affects the activity from a later time point. This was repeated for the [FeFe]-hydrogenase maturation mix (GE1E2F) as well, both in the presence and absence of GTP.

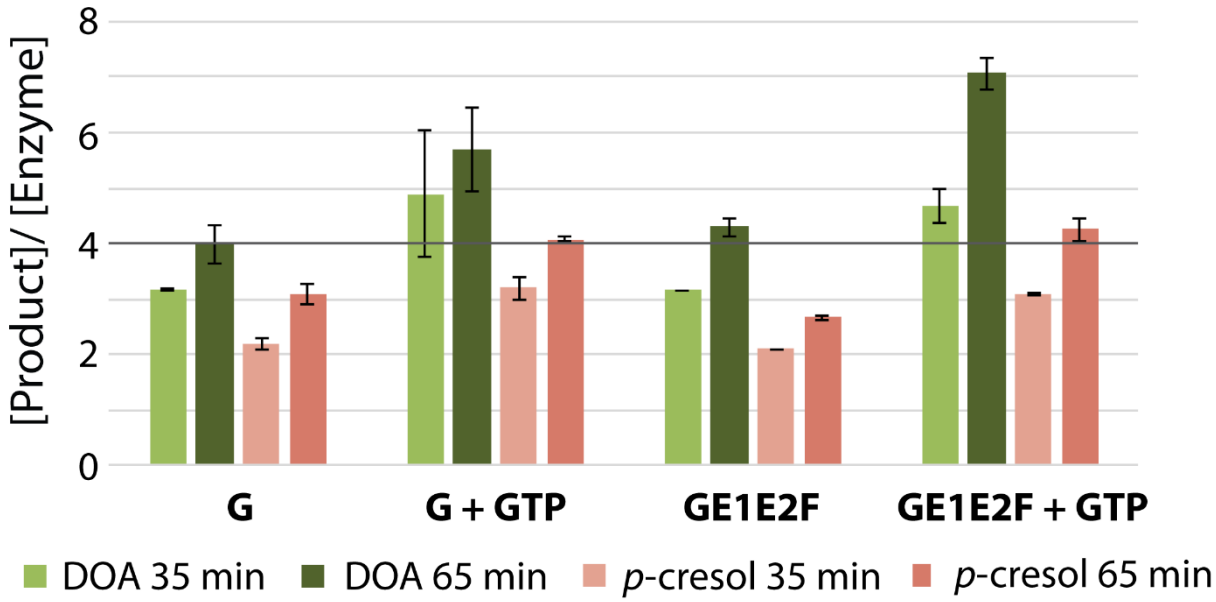

Figure 4.13: DOA and *p*-cresol product formation in the absence and presence of GTP of HydG and the [FeFe]-hydrogenase maturation proteins. The reaction was stopped at two timepoints 35 and 65 min. Results of one experiment measured in duplicate.

Table 4.10: SAM and L-tyrosine turnover rates of HydG and a mixture of HydG, HydE1, HydE2 and HydF (GE1E2F) in absence and presence of GTP stopped at two different time points (35 and 65 min).

	DOA k_{cat}^{app}/ 10^{-4} s^{-1}	***p*-cresol k_{cat}^{app}/ 10^{-4} s^{-1}**
G 35 min	15.1 ± 0.1	10.5 ± 0.5
G + GTP 35 min	23.3 ± 5.4	15.2 ± 0.9
G 65 min	10.2 ± 0.9	7.9 ± 0.5
G + GTP 65 min	14.6 ± 1.9	10.5 ± 0.1
all 35 min	15.1	10.0
All + GTP 35 min	22.3 ± 1.5	14.7 ± 0.1
all 65 min	11.0 ± 0.4	6.8 ± 0.1
All + GTP 65 min	18.1 ± 0.7	10.9 ± 0.5

Astonishingly, GTP has an effect on the activity of HydG for both the DOA and *p*-cresol formation (Figure 4.13 and Table 4.10). Addition of GTP clearly affects the initial product formation rate. The reason why GTP is increasing the activity of HydG,

however, is unclear. In order to evaluate if this stimulating effect is selective for GTP, or also appears in the presence of ATP, GDP or pyrophosphate (each 2 mM) another set of assays was prepared with these additives (and 2 mM magnesium(II)chloride included, to stabilize the phosphates) (Figure 4.14 and Figure 4.15).

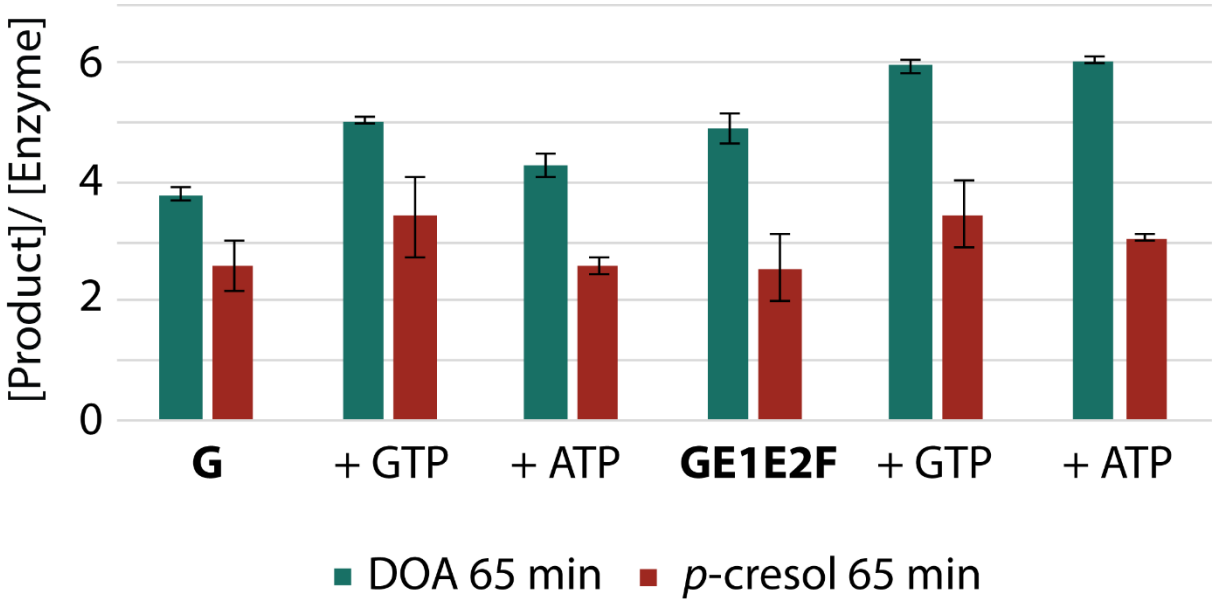

Figure 4.14: Equivalents of DOA and *p*-cresol produced by HydG in absence of nucleotides and either in presence of GTP or ATP as well by a mixture of all [FeFe]-hydrogenase maturation proteins in absence of nucleotides and either in presence of GTP or ATP over a time period of 65 min.

To understand which part of the nucleotide GTP (nucleoside or phosphates) is crucial for HydGs activity and if it selectively recognizes GTP, new experiments were designed that replaced GTP with ATP (Figure 4.14). The results obtained were not conclusive since it seemed that ATP did increase DOA formation slightly but not in the same magnitude as GTP. Formation of *p*-cresol by HydG was almost not affected by the presence of ATP. But, in context of all [FeFe]-hydrogenase maturation proteins, ATP had the same stimulating effect for DOA formation as GTP, however not for *p*-cresol. This results suggests that the nucleotide-HydG interaction is not strongly selective for the nitrogenous base of the nucleotide.

Table 4.11: SAM and L-tyrosine turnover rates of HydG and a mixture of HydG, HydE1, HydE2 and HydF (GE1E2F) in absence and presence of GTP or ATP stopped at 65 min.

	DOA k_{cat}^{app}/ 10^{-4} s^{-1}	*p*-cresol k_{cat}^{app}/ 10^{-4} s^{-1}
G	9.7 ± 0.3	6.5 ± 1.1
G + GTP	12.8 ± 0.1	8.7 ± 1.7
G + ATP	10.9 ± 0.5	6.6 ± 0.4
GE1E2F	12.5 ± 0.6	6.5 ± 1.4
GE1E2F + GTP	15.2 ± 0.3	8.8 ± 1.4
GE1E2F + ATP	15.4 ± 0.1	7.8 ± 0.1

Since the influence of ATP on HydG was not conclusive, further compounds which are similar to GTP were assessed; GDP and pyrophosphate. Moreover, the effect of cysteine in combination with GTP and pyrophosphate was studied by omitting cysteine from the reaction. The results are presented in Figure 4.15 and Table 4.12.

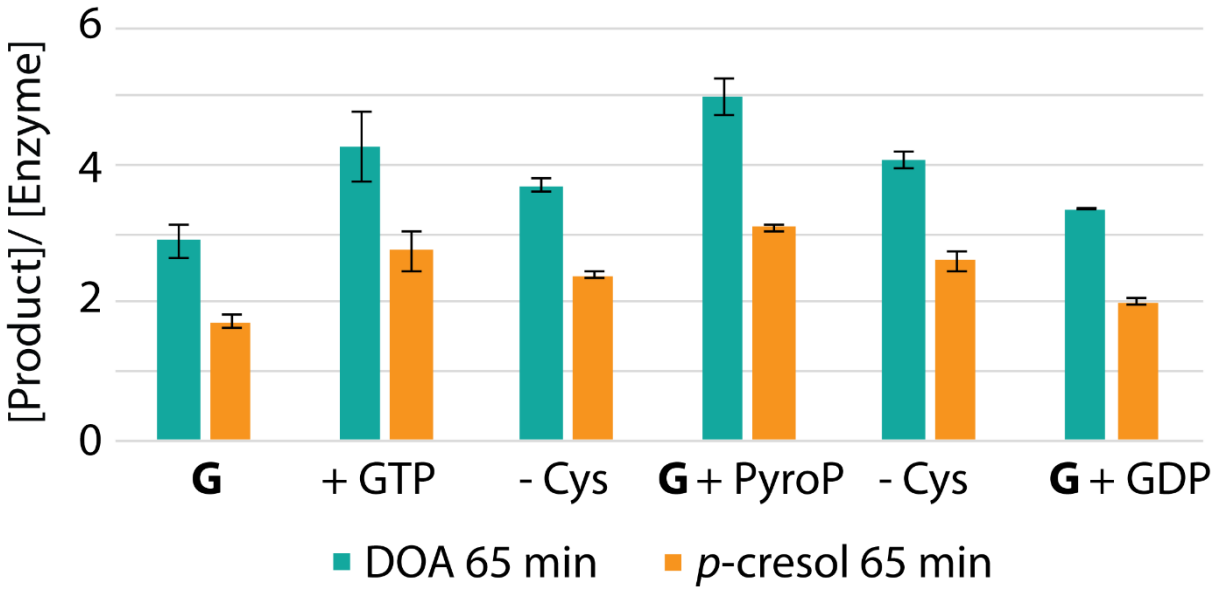

Figure 4.15: Equivalents of DOA and *p*-cresol produced by HydG in absence of nucleotides and in presence of GTP, pyrophosphate or GDP. For the samples in presence of GTP or pyrophosphate, a set without cysteine was tested. Reactions were stopped after 65 min.

Table 4.12: SAM and L-tyrosine turnover rates of HydG in absence and presence of GTP, pyro phosphate or GDP. For the GTP and pyro phosphate reaction cysteine was depleted for each of them separately in an experiment. Reactions were stopped at 65 min.

	DOA k_{cat}^{app}/ 10^{-4} s^{-1}	***p*-cresol k_{cat}^{app}/ 10^{-4} s^{-1}**
G	7.4 ± 0.7	4.4 ± 0.2
G + GTP	11.0 ± 1.3	7.1 ± 0.7
G + GTP - Cys	9.5 ± 0.2	6.2 ± 0.1
G + PyroP	12.8 ± 0.7	7.9 ± 0.1
G + PyroP - Cys	10.5 ± 0.3	6.7 ± 0.4
G + GDP	8.6	5.1 ± 0.1

Interestingly, pyro-phosphate had either the same or an even stronger effect than GTP on both the SAM and L-tyrosine cleavage activity of HydG. In both cases (GTP and pyrophosphate), the depletion of L-cysteine had a slightly negative influence on the activity of HydG. However, GDP changed the activity marginally towards higher turnover, suggesting it was having almost no control over the reaction. Because pyrophosphate increases the turnover rate in the same magnitude as GTP, the phosphates in GTP might play the crucial role in the interaction with HydG. One possibility is that the phosphates are coordinating the synthon iron and helping to transport it to HydF, making space for another turnover of SAM and L-tyrosine cleavage. Previous studies have reported Fe(II) or Fe(III) coordination by phosphates, as well as Fe(III)/Fe(II) ions complexed with GTP and ATP.[371-373] Furthermore, GTP is also required for iron-sulfur cluster biogenesis in mitochondria, however it is unclear which function it implements.[374]

In the speculative Scheme 4.13 a complex of pyrophosphate bound to the proposed synthon ($Fe^{II}(CO)_2CN$) is shown which might promote the release of the synthon from HydGs auxiliary cluster and transport to HydF.

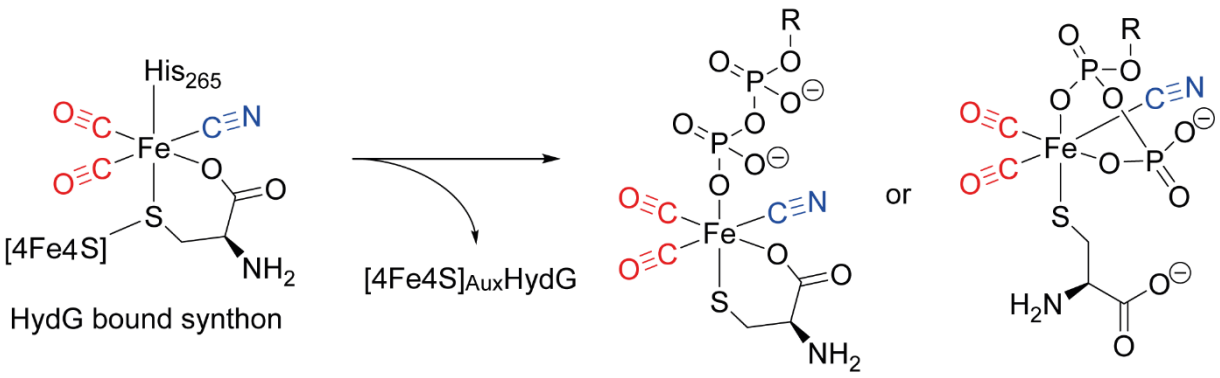

Scheme 4.13: Synthon release from the auxiliary cluster of HydG by complexation with a phosphoanhydride. Hypothetical roles for phosphoanhydrides in stabilizing the H-cluster synthon. R = nucleotide monophosphate or H.

The results with omitted cysteine indicate that the presence of cysteine, which coordinates the synthon iron, potentially *via* the thiolate group and also by the carboxylic and amine moieties, may be crucial for the stability of the synthon, and if it is absent, complexation or binding by GTP is not guaranteed.

Another interesting observation involves the histidine ligand (His265) of ThitHydG, which coordinates the 5th iron of the auxiliary [5Fe5S]. If His265 is replaced with glutamic acid that potentially coordinates the 5th iron by a carboxylic acid, it is believed that the lability of the synthon is increased, due to the observation that less 5th iron is present in the corresponding crystal structure of the H265E mutant.[267] Surprisingly, this mutant also increased turnover of DOA, *p*-cresol and cyanide by one equivalent.[267] In the case of GTP, addition to HydG possibly increases the dissociation of the synthon ($Fe^{II}(CO)_2CN$)).

Another potential function of GTP exists, which may include that HydG is using GTP or pyrophosphate (or ATP) for energetic reasons *via* hydrolysis of the phosphate bond and this is tested and discussed in a later section (4.4.2).

An additional observation that supports the role of GTP as a synthon transporter is the fact that, GTPase activity of HydF is not required for the transfer of the H-cluster onto HydA and following activation of the [FeFe]-hydrogenase.[246] On the other hand, GTP binding in HydF is essential for HydA activation, since mutations of the GTP binding site (Walker P-loop) lead to an inactive HydA protein[42], which promotes the function as synthon transporter (Scheme 4.14). The hydrolysis of GTP might play a role for the interaction and dissociation of the partner enzymes HydG and HydE from HydF after

enzymatic activity/transport of H-cluster precursors.[253] Furthermore, EPR results by Broderick *et al.*[246] suggested a communication between GTP and the cluster-binding site of HydF.

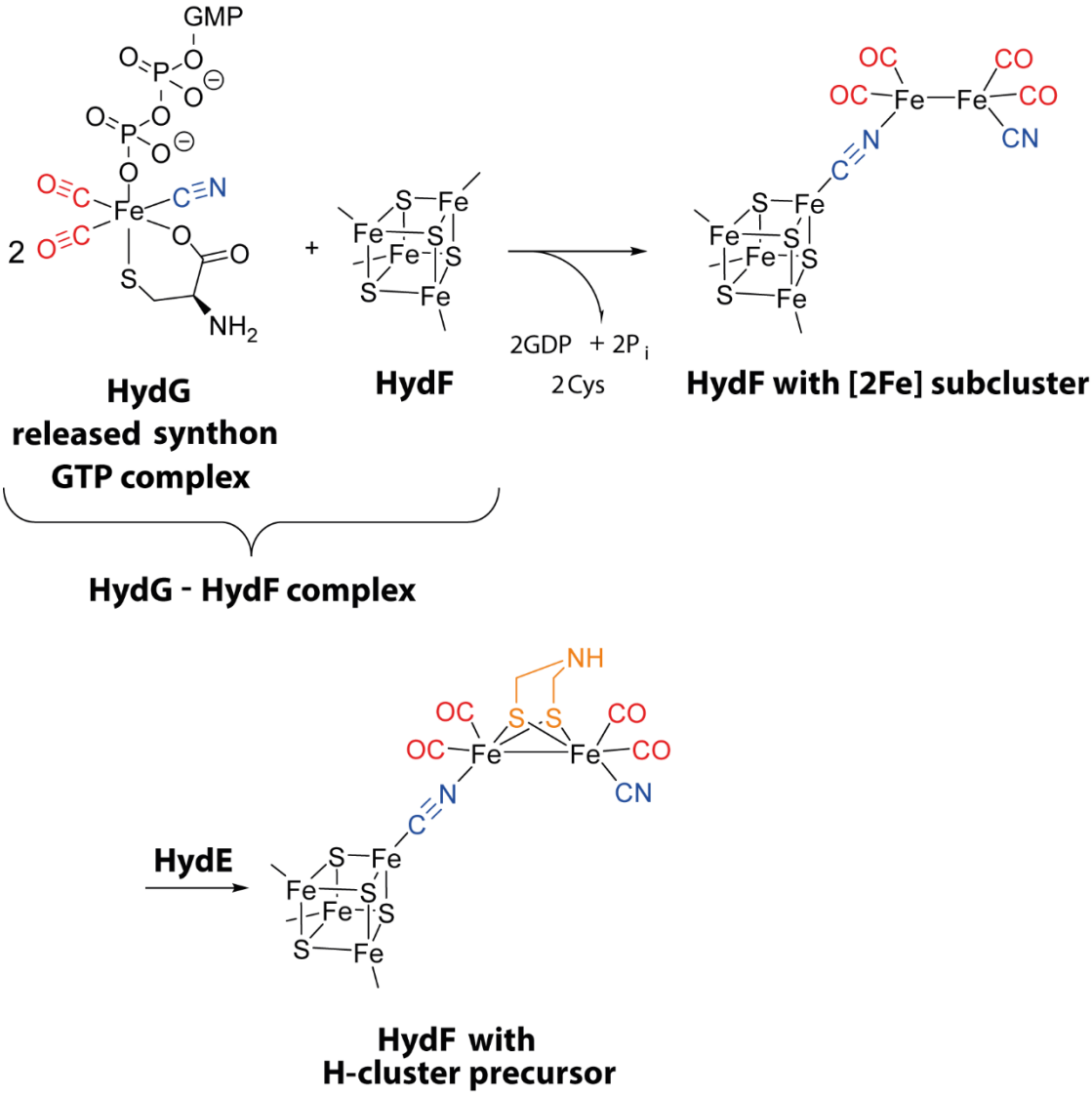

Scheme 4.14: Transfer of the synthon of HydG by complexation with GTP onto HydF, during hetero-complex formation between HydG and HydF. HydG is dissociating from HydF upon GTP hydrolysis and two equivalents of the synthon are transported onto HydF forming the [2Fe] subcluster. Possibly after interaction and reaction of HydE the azadithiolate bridge is transferred onto the [2Fe] subcluster forming the H-cluster precursor.

Since the activity of HydG varied somewhat with every experiment, a sample with and without GTP was measured for each independent experiment to ensure that GTP is consistently increasing the activity. The following Tables (4.13 and 4.14) summarize these comparisons between HydG and HydG + GTP in four different independent

experiments using HydG from the same batch purification. What is observed is that the overall activity of HydG decreases over time.

Table 4.13: SAM turnover rates of HydG in absence and presence of GTP from independent experiments. Reactions were stopped at 65 min.

		DOA formation (no GTP)		DOA formation (plus GTP)	
Date of Expt.	**Name**	**k_{cat}^{app}/ 10^{-4} s^{-1}**	**Normalized Activity/ %**	**k_{cat}^{app}/ 10^{-4} s^{-1}**	**Normalized Activity/ %**
21/07/17	**G 1**	10.2 ± 0.9	100	14.6 ± 1.9	143
28/07/17	**G 2**	9.7 ± 0.3	100	12.8 ± 0.1	132
08/08/17	**G 3**	10.8 ± 0.3	100	12.8 ± 0.5	119
17/08/17	**G 4**	7.4 ± 0.7	100	11.0 ± 1.3	149
Average	**-**	9.5 ± 1.5	100	12.8 ± 1.5	135 ± 13

Table 4.14: L-tyrosine turnover rates of HydG in absence and presence of GTP from independent experiments. Reactions were stopped at 65 min.

		***p*-cresol formation (no GTP)**		***p*-cresol formation (plus GTP)**	
Date of Expt.	**Name**	**k_{cat}^{app}/ 10^{-4} s^{-1}**	**Normalized Activity/ %**	**k_{cat}^{app}/ 10^{-4} s^{-1}**	**Normalized Activity/ %**
21/07/17	**G 1**	7.9 ± 0.5	100	10.5 ± 0.1	133
28/07/17	**G 2**	6.5 ± 1.1	100	8.7 ± 1.7	134
08/08/17	**G 3**	6.9 ± 0.3	100	7.1 ± 1.2	103
17/08/17	**G 4**	4.4 ± 0.2	100	7.1 ± 0.7	161
Average	**-**	6.4 ± 1.5	100	8.4 ± 1.6	133 ± 24

Although the activity of HydG changed slightly with each experiment, overall it is clear that GTP does have an influence on HydG's activity, by enhancing DOA and *p*-cresol formation. Even though large errors do appear for *p*-cresol formation, in two experiments (G1 and G4) with smaller error values, the difference between the experiments carried out in the absence and presence of GTP is very high (plus one equivalent of *p*-cresol).

4.4 Enzyme activity of HydF

A comparison of HydF protein sequences from different microorganisms revealed characteristic features of small G proteins binding guanine nucleotides (GTPases) in the *N*-terminal domain belonging to the Ras superfamily (Figure 4.16).[51] These features include the (G/A)X_4GK(T/S) sequence, which is named the P-loop and is responsible for the binding of the α- and β-phosphate groups of the nucleotide.[375] Furthermore, three conserved threonine residues (TTT) might belong to the G2 loop (Switch I) and be involved in Mg^{2+} binding. A third feature is the DX_2G motif, which makes up the G3 loop (Switch III) interacting with the γ-phosphate and Mg^{2+}.[376] Another loop, called G4 corresponds to the sequence (N/T)(K/Q)XD and may possibly coordinate the nucleotide.[257] The guanine base is probably recognized by the conserved residues valine, serine and alanine (VSA).[51] Mutation of the GK residues of the P-loop or the D residue of the G3 loop result in reduced GTP hydrolysis activity for HydF.[253] GTP binding has been verified and analyzed by fluorescence spectroscopy and isothermal calorimetry, giving K_d values of ~3 μM[51] and 1 μM[257] respectively.

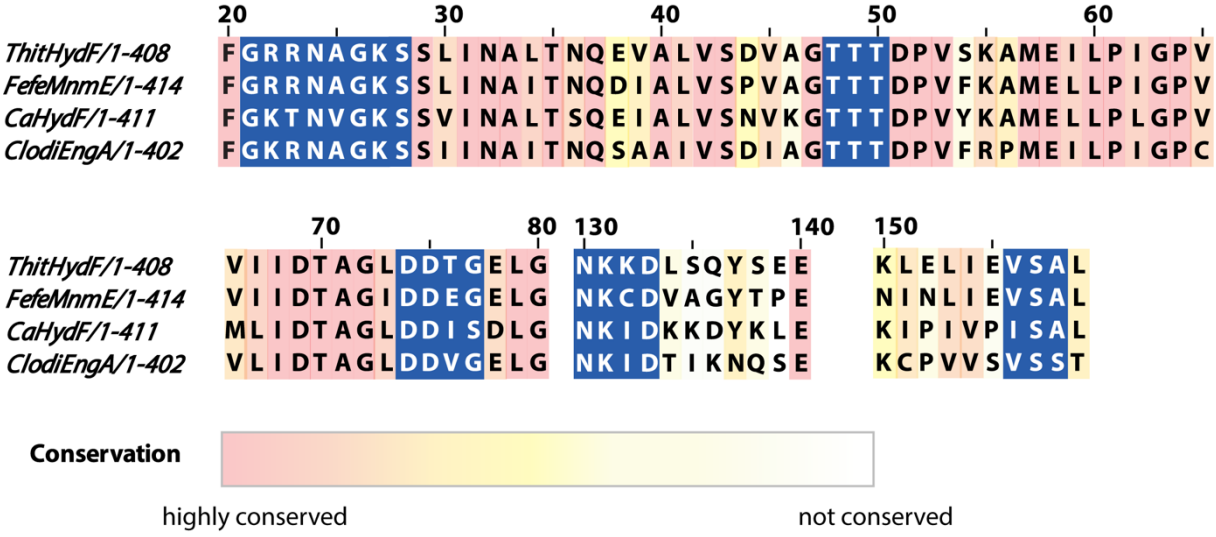

Figure 4.16: Sequence alignment of HydF from *Thermoanaerobacter italicus* and *Clostridium acetobutylicum*, as well as homologous GTPases MnmE from *Fervidicola ferrireducens* and EngA from *Clostridioides difficile*. The alignment was generated with ClustalW[254,255] and JalView[256].

HydF GTPase activity has been previously been studied in an enzyme assay, in the presence of excess GTP and Mg^{2+}.[246] The HydF enzyme from *T. maritima* slowly hydrolyzed GTP at the γ-phosphate position to give GDP with a production rate of 0.03 min^{-1}.[51] The iron sulfur cluster coordinated by the binding motif $CXHX_{46-58}HCX_2C$ has no effect on the HydF catalyzed hydrolysis of GTP.[246] Hydrolysis of ATP could not be observed with either HydF from *T. maritima* or from *C. acetobutylicum*.[51,246] The GTPase activity of *C. acetobutylicum* HydF was found to be influenced by the monovalent salt cation which is used in the reaction or purification buffer. The presence of K^+ or Rb^+ cations enhance the GTPase activity[378] of HydF to a production rate of 2.03 min^{-1} and 3.47 min^{-1} at 30 °C respectively, whereas Na^+ cations decrease the activity.[246] In another study of CaHydF, the protein exhibited a GTP turnover of 4.84 min^{-1} at a temperature of 95 °C.[253] Observations made for the monovalent cations suggest a binding pocket for these specific ions close to the active site. Mutations of the GTP binding motif of HydF, specifically the glycines or serine in the P-loop, resulted in inactive HydF and negatively affected the activation of HydA, thus GTP binding is involved in the activation of HydA.[42,246] Recent studies on the conformational changes occurring in HydF upon GTP binding suggest that the GTP binding domain acts as a molecular switch in gating the protein-protein interactions.[252]

Since GTP is not necessary for transfer of the H-cluster precursor from HydF to HydA, it has been suggested that the function of GTP is to serve in the interaction reactions between HydF and the partner maturation enzymes HydG and HydE.[244-246,253]

Furthermore, the addition of GTP results in an increase of the dissociation rates between the complexes HydE-HydF and HydG-HydF.[253]

Interestingly, although there are not many GTPases linked to metallocofactor assembly,[379,380,381] a comparable GTPase exists as HypB, which is involved in the maturation of the [NiFe]-hydrogenase. HypB is involved in the GTP-dependent insertion of a nickel atom into the cofactor of the [NiFe]-hydrogenase HypA, which already carries the $Fe(CO)(CN)_2$ sub-part of the active cluster.[227,228]

4.4.1 GTPase activity of ThitHydF

Initial HydF GTPase activity assays were carried out in order to monitor the GTPase activity of StrepThitHydF expressed from the pBAD derived vector, which had been purified in the presence of 1 mM sodium dithionite (Chapter 2, Section 2.2.2). The typical assay mixture contained 38 μM HydF, 2 mM GTP, 2 mM $MgCl_2$ and 5 mM DTT at pH 8.0. Additionally, the reaction buffer contained 300 mM KCl, which has previously been shown to increase GTP hydrolysis activity.[246] Assays were incubated for two different time periods at 37°C: 9 and 25 min. The hydrolysis product GDP was quantified using an optimized HPLC method described in Chapter 7 (Method 29). Exemplary HPLC traces of the GTP assay are shown in Figure 4.17.

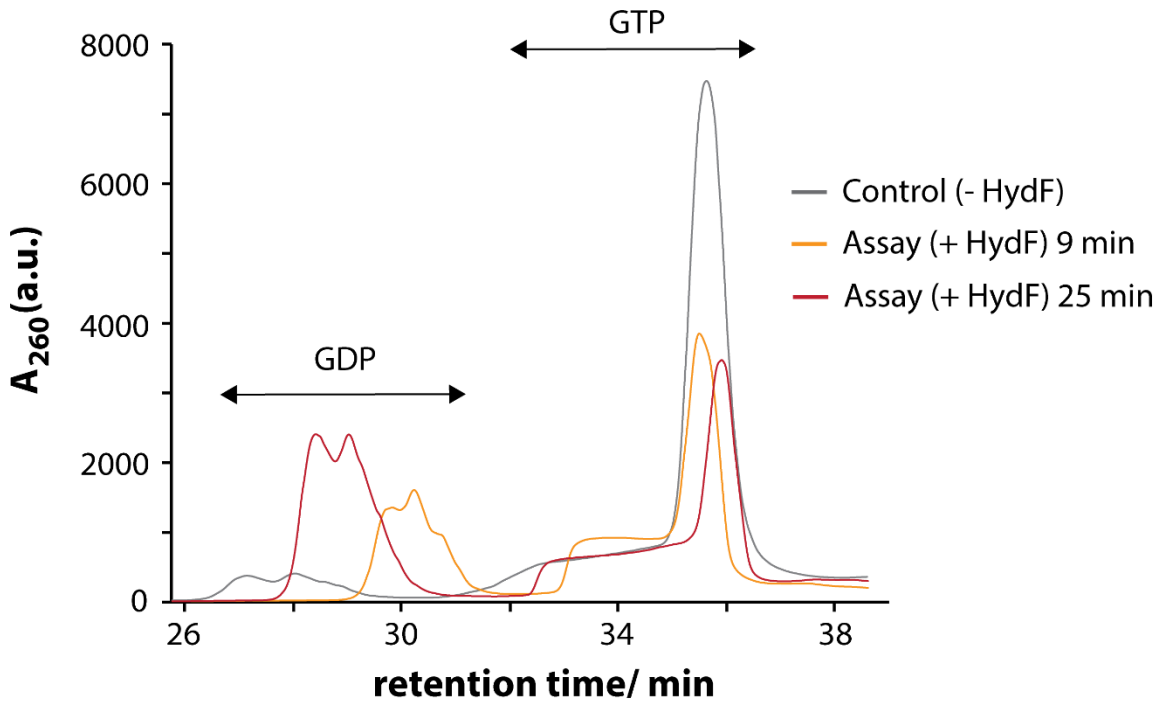

Figure 4.17: Representative chromatograms of the HydF GTP hydrolysis assay after 9 min and after 25 min of incubation and the control reaction assay without HydF.

As shown in the chromatogram in Figure 4.17, GTP eluted with a broad shoulder corresponding to an artefact which might derive from the change to the organic solvent MeOH, which is known to cause smearing, or from coordination of K^+ to the nucleotide. The whole peak, inclusive shoulder, was used to quantify GTP and it is clearly shown that GTP is hydrolyzed to GDP in the presence of HydF.

After analysis of the HPLC data (Figure 4.17 and 4.19) the kinetic parameters describing the GTP turnover were calculated (Table 4.15). The initial turnover rate of HydF calculated from the two time points (0 and 9 min), with k_{cat} = 1.15 ± 0.09 min^{-1}, was lower than reported for *C. acetobutylicum* HydF (~1.8 min^{-1}) but much greater than the *T. maritima* turnover rate (0.03 min^{-1}). When calculating the initial turnover rate, it was assumed that the first 9 minutes describe a linear reaction and that the K_M is much smaller than 2 mM (substrate concentration of GTP). It should be noted that, the protein was observed to precipitate quickly upon concentration (to 10 mg/mL) and a large background in the UV-Vis spectrum (Figure 4.18) suggested a large amount of colloidal iron-sulfide was bound to the protein. This might have influenced the activity by blocking the binding site of GTP for example.

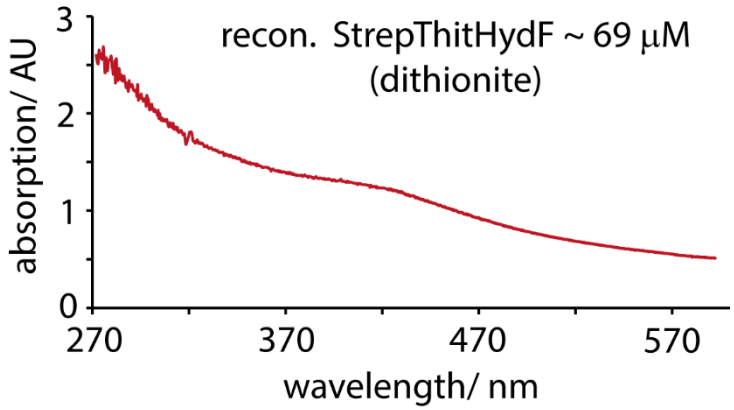

Figure 4.18: UV-Vis spectrum of reconstituted HydF in the presence of dithionite. This sample was used for the GTP assay in Figure 4.19.

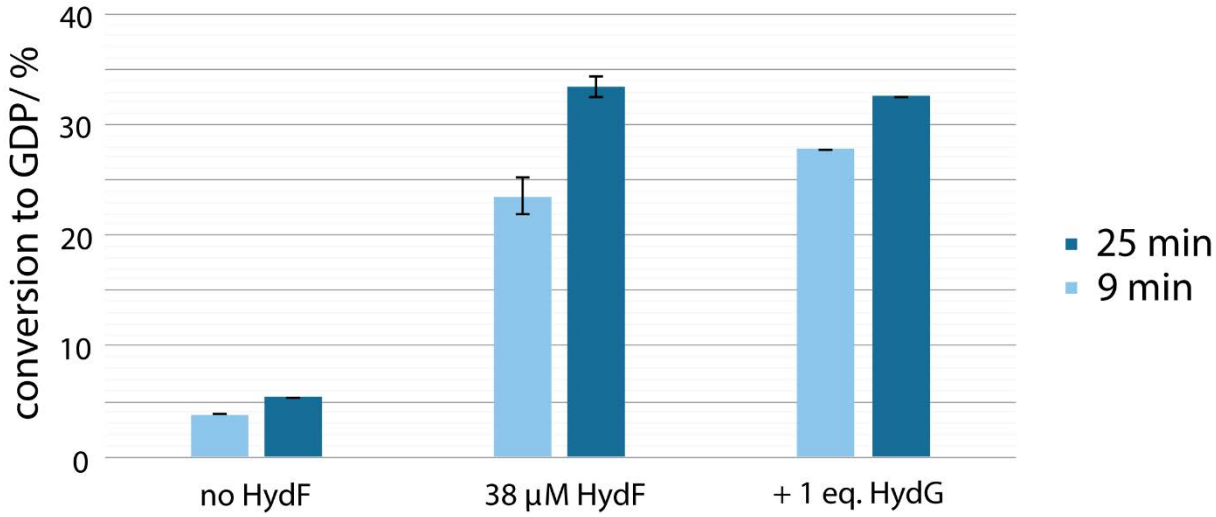

Figure 4.19: Bar-chart representing the GTP hydrolysis activity of HydF, comparing a control without HydF, a sample in presence of HydF and the another in the presence of HydF and HydG. Formation of GDP is represented as a percentage of the starting concentration of the substrate GTP (2 mM).

Table 4.15: Summary of kinetic parameters for GTP hydrolysis reactions presented in Figure 4.19. Exemplary HPLC traces are shown in Figure 4.17.

Sample	ΔC/ μM	k/ μM s^{-1}	k_{cat}^{app}/ min^{-1}
HydF (0-9 min)	394 ± 34	0.73 ± 0.06	1.15 ± 0.09
HydF (9-25 min)	275 ± 21	0.29 ± 0.02	0.45 ± 0.03
HydF (0-25 min)	593 ± 17	0.40 ± 0.01	0.62 ± 0.03
+ 1 eq. HydG (0-9 min)	480	0.89	1.40
+ 1 eq. HydG (9-25 min)	170	0.18	0.28
+ 1 eq. HydG (0-25 min)	575	0.38	0.61

Adding HydG to the reaction did not have a significant effect on the activity of HydF; the initial reaction rate was slightly increased to 1.40 min^{-1}, which could have been due to an early induced effect on HydF, but after 9 min the reaction rate slowed down remarkably. In the future, it should be possible with this assay to estimate a K_M of HydF for GTP, using time course data, at different initial substrate concentrations.

Another experiment using the GTP assay has been carried out with the stable StrepThitHydF protein obtained from the autoinduction of the pCDuet vector, which was purified in the presence of 1 mM DTT (Figure 4.20, Section 2.3.3). The basic assay mixture contained the same components as mentioned above, except that all protein concentrations were 40 μM.

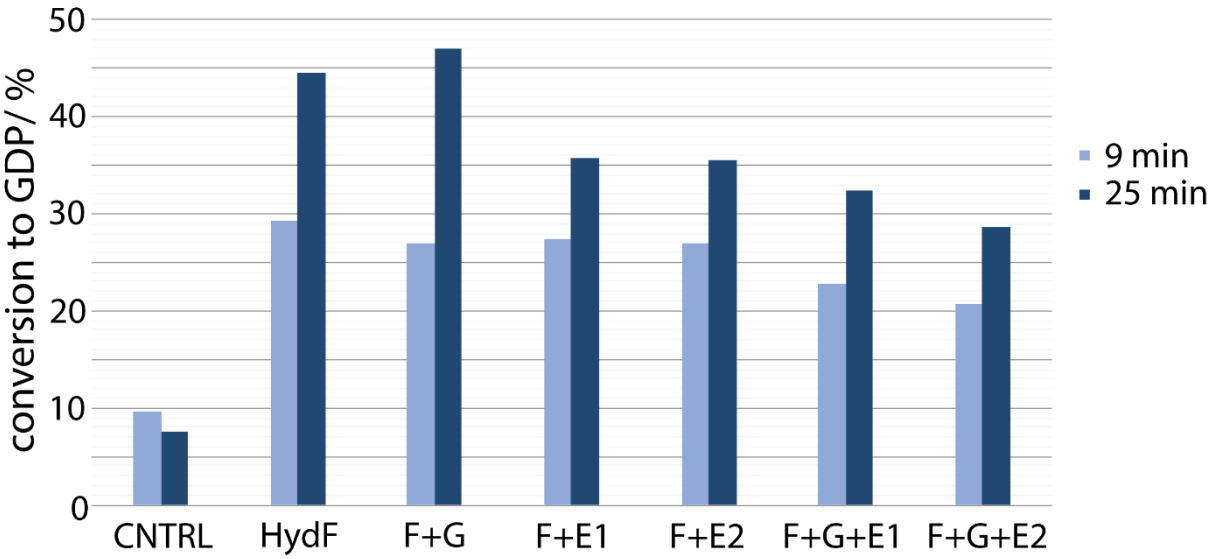

Figure 4.20: Bar-Chart of GTPase assay with HydF (from pCDuet expression, Section 2.3.3). Assays were measured in a single experiment. Formation of GDP is represented as a percentage of the starting concentration of the substrate GTP (2 mM).

Table 4.16: Initial rate constants/turnover numbers (k_{cat} in min^{-1}) corresponding to the bar-chart Figure 4.20. It is assumed that the reaction rate is linear for the time frame stated.

	Rate constant, k_{cat} in min^{-1}					
Time Frame	**F**	**+G**	**+E1**	**+E2**	**+GE1**	**+GE2**
0-9 min	1.20	1.08	1.09	1.08	0.84	0.73
9-25 min	0.48	0.63	0.27	0.27	0.30	0.25
0-25 min	1.18	1.26	0.90	0.90	0.79	0.67

As for the previous GTPase assays, the initial rate constant of the HydF catalyzed GTP hydrolysis is in the range of 1.20 min^{-1} (Figure 4.20 and Table 4.16). Adding two partner maturation enzymes appears to decrease the GDP formation rate, possibly the GTP binding site being inaccessible if the partner maturation enzymes are present and able to interact with HydF. Nevertheless, in the presence of HydG the production rate is almost the same as HydF alone, showing that HydG does not directly affect the GTP binding to HydF. On the other hand, if HydE is added to HydF, there is a clear decrease in GDP formation observed for later time points, which might be due to the fact that HydE is binding tighter to, or altering the conformation of HydF[253] and blocking the GTP binding site. In contrast, previous studies have reported a stimulating effect of HydG and HydE on the GTP hydrolysis by HydF.[246]

4.4.2 Is HydG hydrolyzing GTP?

The potential for GTPase activity from catalytically active HydG (i.e. during couple SAM and tyrosine turnover) was also investigated. This experiment used the same conditions as previous GTPase experiments (Section 4.4.1), except for the addition of 2 mM $MgCl_2$ (Section 4.3.5). One of the objectives of this experiment was to act as a control to assess whether HydG is hydrolyzing GTP during SAM/tyrosine turnover and also to estimate the influence of other compounds added to the reaction mix. The concentration of all enzymes was 25 μM.

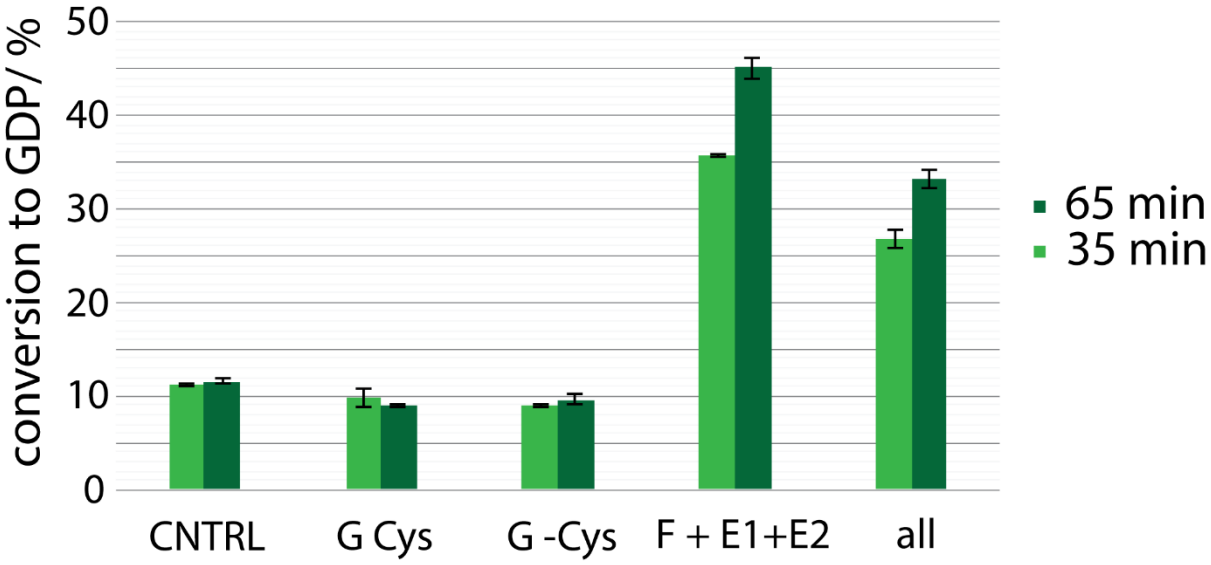

Figure 4.21: Bar-Chart of HydF GTP assay in context of the SAM-Tyr cleavage assay. The control reaction (CNTRL) is in the absence of any enzyme. Two reactions were carried out only in the presence of HydG with added or omitted L-cysteine. Additionally, GTP hydrolysis was assessed for a mixture of HydF, HydE1 and HydE2 (F+E1+E2) and a mixture of all maturases (all: HydG + HydF+ HydE1 + HydE2). Formation of GDP is represented as a percentage of the starting concentration of the substrate GTP (2 mM).

The results from the GTP-assay in context of the SAM-Tyr cleavage activity (Section 4.3.4, Figure 4.21) show that HydG definitely does not hydrolyze GTP into GDP. Nevertheless, if HydG is added to an assay where HydF and HydE and all its substrates are already present the GTPase activity of HydF slows down. This may tentatively be interpreted as HydG using GTP for a reaction other than hydrolysis. GTP could serve as an additional substrate or for coordination/ transportation purposes of the metalorganic synthon (Figure 4.22).

Table 4.17: Turnover numbers corresponding to the HydF GTPase-assays in Figure 4.21. Assumption that reaction rate is linear until endpoint.

Sample (Endpoint)	ΔC/ μM	k/ μM s^{-1}	k_{cat}^{app}/ min^{-1}
HydF + E1 + E2 (35 min)	538 ± 1	0.30	0.72
HydF + E1 + E2 (65 min)	725 ± 22	0.20	0.48
+ G (all) (35 min)	359 ± 19	0.20 ± 0.01	0.48 ± 0.03
+ G (all) (65 min)	495 ± 10	0.14	0.33

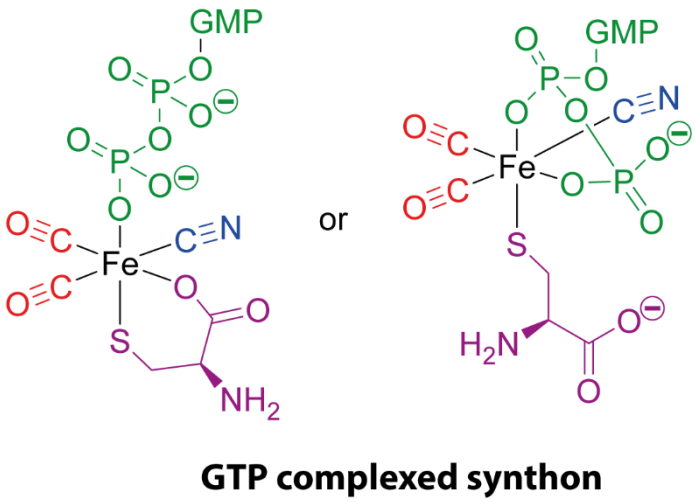

Figure 4.22: GTP complexed synthon. GTP shown in *green*, cysteine in *purple*, CO ligands in *red* and CN ligand in *blue*.

4.5 Summary and conclusions

In this chapter the activities of reconstituted [FeFe]-hydrogenase maturation proteins HydE, HydG and HydF from *Thermoanaerobacter italicus* have been characterized both individually and in the presence of their partner maturation proteins.

Firstly, the enzyme activity of HydG and HydE were analyzed in a time-dependent coupled SAM plus L-tyrosine cleavage assay by HPLC, separately and in combination. The amino acid L-cysteine was added to the assay to potentially stabilize the metalorganic synthon iron of HydG and as a potential substrate of HydE. Resulting from the time-dependant assay with HydG and HydE the SAM cleavage activities were independent from each other if assayed together, the SAM cleavage turnover rate simply added up to the sum of that of HydE and HydG (Figure 4.23). Resultant turnover rates were comparable to those previously reported for HydG from *Thermoanaerobacter italicus*[276] and for HydE from *Clostridium acetobutylicum*[65]. The amount of glyoxylate produced by HydG and HydE was measured alongside the SAM-L-tyrosine cleavage assay, but inconclusive results were obtained due to the large background produced by the reducing agent dithionite.

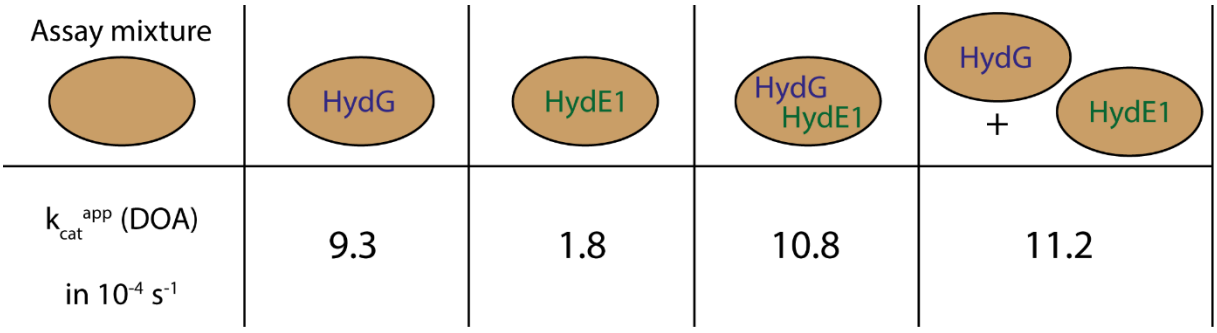

Figure 4.23: Apparent turnover numbers from the time-dependent SAM cleavage assay with HydG only, HydE1 only, a mixture of HydG and HydE1 and in comparison the sum of the single activities of HydG and HydE1.

Following this, HydF was added to the reaction mixture of HydE and HydG and different small molecules were evaluated for their effect on HydE or HydG's activity. The compounds selected for this study were based on studies conducted by Kuchenreuther *et al*. and addition of each of these compounds during maturation increased the hydrogen production activity of the [FeFe]-hydrogenase.[50] Only one of these compounds had a significant effect on the overall SAM-Tyr cleavage activity, this being GTP. Almost one new equivalent of DOA and *p*-cresol was generated over 65 min if GTP was added. Having increased the turnover of L-tyrosine to *p*-cresol, it was already suspected to have an effect on only HydG.

Building upon these results, all [FeFe]-hydrogenase maturation proteins were independently assessed for their change in activity if GTP was added to the reaction. The results have shown that GTP had a selective effect on HydG but not on HydE. To address the question as to how selectively HydG recognizes GTP, assays with similar compounds, ATP, GDP and pyrophosphate have been carried out. Despite inconclusive results for ATP, which did not significantly increase the activity of HydG alone, but the DOA formation of the [FeFe]-hydrogenase maturation proteins mix, it was observed that the compound pyro-phosphate had the same stimulating effect as GTP. Furthermore, GDP had no recognizable consequence on HydG's activity. Given these results, it can be suggested that the role of the phosphates might be an important factor for HydG's activity. Since coordination of iron by phosphates has been already reported[371-373] it stands to reason that GTP might coordinate the 5th iron of the auxiliary cluster of HydG or even the synthon complex containing the CO and CN ligands

(Scheme 4.15). However, it needed to be confirmed that HydG is not converting the GTP to GDP or any other product.

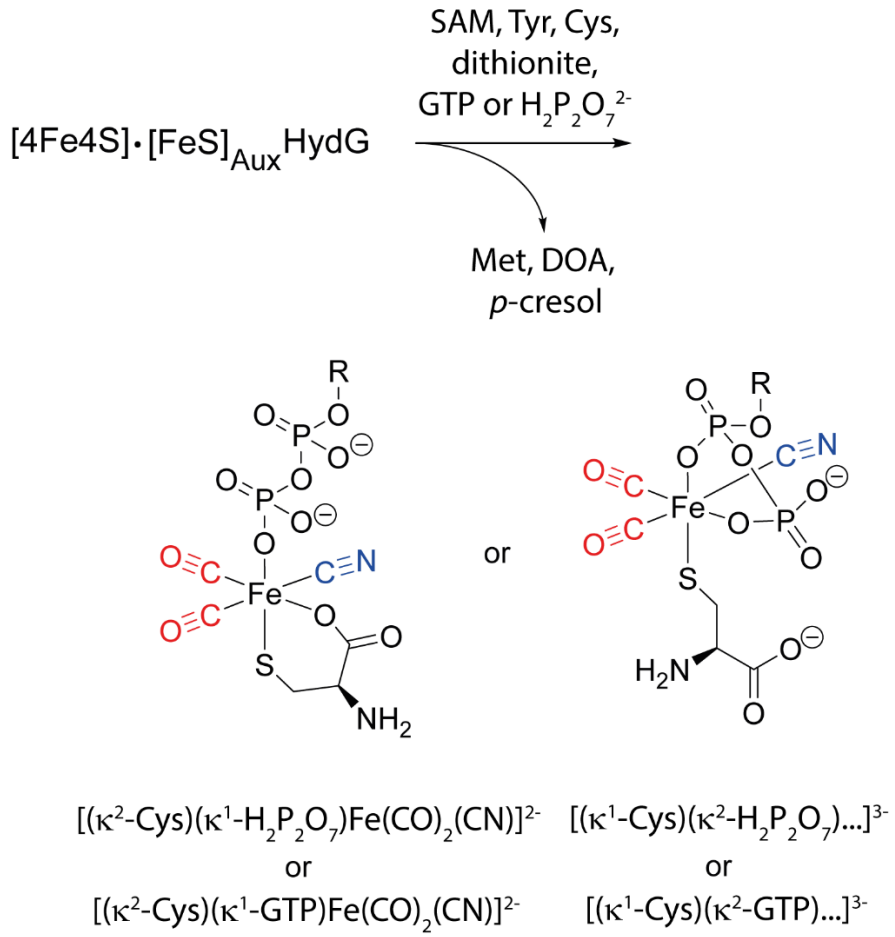

Scheme 4.15: Possible formation of pyro-phosphate- or GTP-synthon complexes during the activity assay of HydG.

GTP is the substrate of HydF, a GTPase that hydrolyses GTP, a characteristic that has been confirmed by HPLC analysis in this chapter. Initial studies with addition of the other [FeFe]-hydrogenase maturation proteins to HydF did not influence the hydrolysis of GTP by HydF, nonetheless, if HydF's activity was evaluated in a mix of [FeFe]-hydrogenase maturation proteins with the same conditions as in the SAM-Tyr cleavage assay including HydGs substrates, the activity was reduced when HydG was present. A potential future experiment could include measuring the GTPase activity of HydF in the presence of increasing concentrations of HydG, to find out if HydG sequesters the GTP.

Bearing in mind the effect of GTP on HydG's activity, it seemed appropriate to test if HydG is able to hydrolyze GTP. This was assayed, but no formation of GDP could be

detected, meaning HydG does not turnover GTP to GDP and does not require the energetic advantages. Another possible role of GTP could be the coordination of the synthon complex, recognition by HydF and transportation onto HydF, where two synthon equivalents could form the [2Fe]-subcluster, followed by DTMA synthesis by HydE to form the H-cluster precursor (Scheme 4.16).

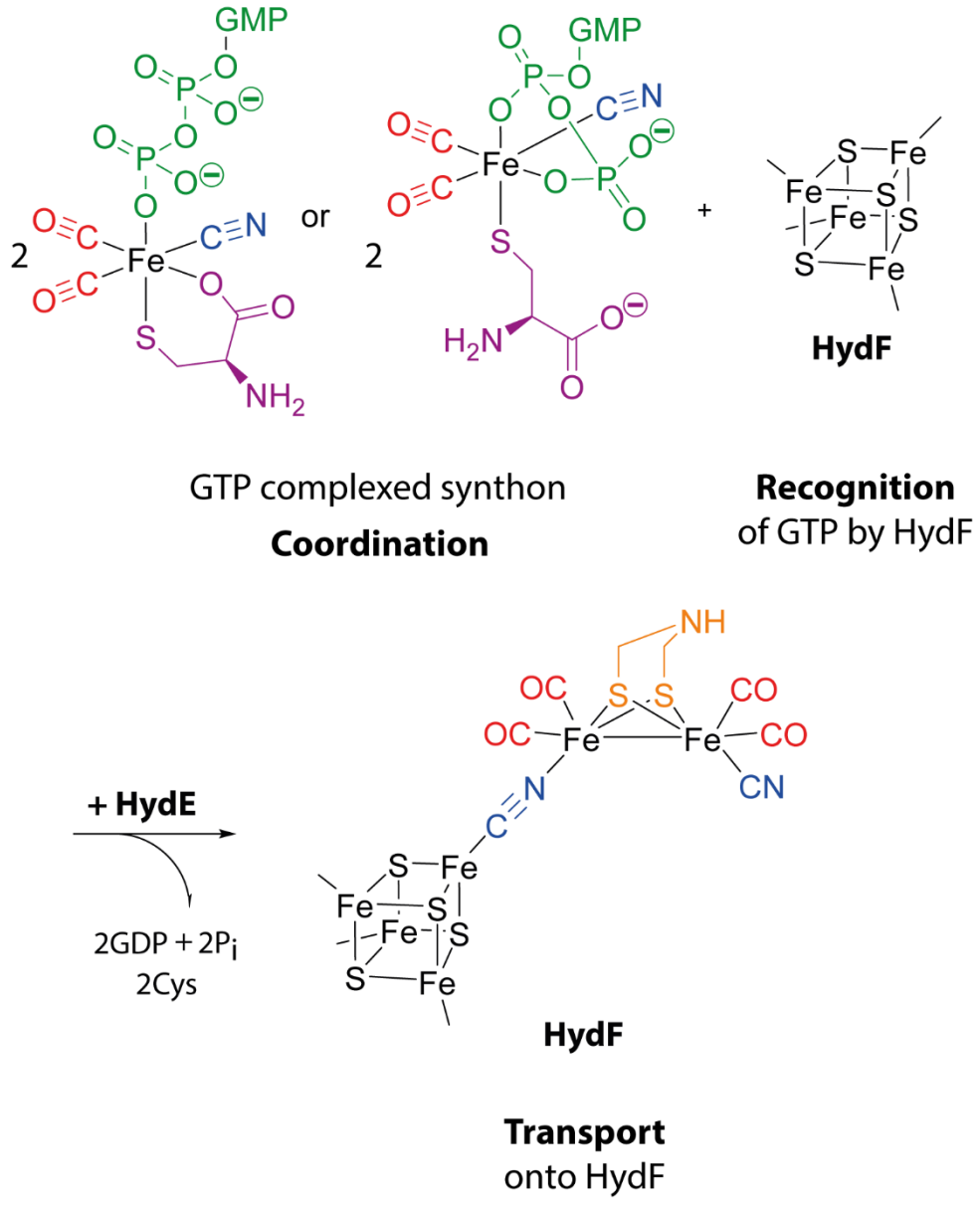

Scheme 4.16: Proposed mechanism for the function of GTP in H-cluster synthesis. GTP coordinates the synthon of HydG, it is recognized by HydF as its substrate followed by transport of two synthon equivalents onto HydF, GTP hydrolysis and adt^{2-} synthesis by HydE to form the H-cluster precursor.

Overall, the specific activity of each [FeFe]-hydrogenase maturation protein has been characterized in an enzymatic assay, with subsequent HPLC analysis. Additionally, the coupled activity of the mixture of [FeFe]-hydrogenase maturation proteins was studied, whereby an exciting new feature of HydG was discovered. It was shown that the addition of GTP to an activity assay with HydG had a stimulating effect on the turnover number of SAM and L-tyrosine. The nucleotide GTP might play a role in the coordination/transportation of the synthon $[(\kappa^3\text{-Cys})Fe^{II}(CO)_2(CN)]^-$.

Chapter 5

Insights into interactions between [FeFe]-hydrogenase maturation enzymes

5.1 Introduction

This chapter describes studies undertaken to characterize the binding events between the [FeFe]-hydrogenase maturation proteins HydE, HydG and HydF from *Thermoanaerobacter italicus*.

Studying binding events provides an important tool to predict and understand the [FeFe]-hydrogenase maturation mechanism, by investigating which protein-protein interactions exist, how tight the binding is and under which conditions the interactions take place. The results are crucial to the development of an H-cluster biosynthesis model including the order of maturation events.

A range of techniques are applicable to study these interaction. For example gel filtration/ size-exclusion experiments were carried out to estimate the multimeric state of the interaction partner enzymes HydF and HydG, as well as to check for spontaneous binding without substrates. Pull-down assays help to elucidate which substrates or factors influence binding events. ITC measurements served as a tool to quantify the strength of protein-substrate or protein-protein interactions.

5.2 Basic Thermodynamics of binding interactions

Protein-protein or protein-ligand interactions are non-covalent binding events, driven by electrostatic, hydrogen bonding, dipole-dipole or dipole-charge and hydrophobic forces. The study of these binding events includes determination of reversible equilibrium association or dissociation constants. The formation of the protein-protein complex can be described as an equilibrium (Scheme 5.1):[382]

$$A + B \underset{k_{off}}{\overset{k_{on}}{\rightleftharpoons}} AB$$

Scheme 5.1: Formation of a protein-protein complex. A: protein A, B: protein B, k_{on}: on-rate constant in M^{-1} s^{-1} , k_{off}: off-rate constant in s^{-1}.

In the equilibrium the formation of the protein-protein complex can be described with the equation:

$$k_{on}\,[A]\,[B] = k_{off}\,[AB] \tag{5-1}$$

The association equilibrium binding (in unit M^{-1}) constant is defined as:

$$K_a = \frac{k_{on}}{k_{off}} = \frac{[AB]}{[A]\,[B]} \tag{5-2}$$

Whereas, the dissociation equilibrium constant (in unit of M) results can be determined by the following equation:

$$K_d \equiv \frac{1}{K_a} \tag{5-3}$$

Furthermore, the occurring biological interactions can be very specific and binding with high affinity. The mechanism of interaction is based on molecular organization and recognition. Thermodynamically, the interaction process is split into the enthalpic (ΔH) component of the process, which accounts for the different types of interactions and into the entropic ($-T\Delta S$) component, where changes in dynamics (rotational and translational), conformation of the backbone and the arrangement of the solvents or counter-ions around the protein side chain are accounted for.[383]

The sum of the enthalphic and entropic term gives the free Gibbs energy ΔG, and the binding event or spontaneous process only occurs if the change in Gibbs' binding energy of the system is negative:[382,384]

$$\Delta G = \Delta H - T\Delta S \tag{5-4}$$

ΔG: free binding energy, ΔH: enthalpy, ΔS: entropy, T: temperature.

The strength of the interactions between two partner molecules is expressed by the enthalpy. Interactions types between proteins include electrostatic/ionic (Coulombic) and/or van der Waals interactions, hydrophobic as well as hydrogen bonds and their

energy ranges between 2-21 kJ/mol. Van der Waals interactions are usually weaker than hydrogen bonds, whereas hydrophobic bonds can be stronger than hydrogen bonds.[385]

Electrostatic/ionic interactions involve attractions between oppositely charged ions, dipoles, functional groups and/or amino acid residues or repulsions between similar charged groups. Whereas, van-der Waals interactions describe the weak attractive or repulsive forces between at least two induced dipoles. Non-polar amino acid residues are responsible for hydrophobic interactions, which are often driven by the hydrophobic effect. Generally the hydrophobic effect describes the tendency of nonpolar substances to aggregate in an aqueous solution under exclusion of water molecules which leads to a decrease in hydrophobic surface area and an increase of entropy. In the context of proteins, the hydrophobic effect accounts for non-polar amino acids accumulating together away from direct contact with water molecules or polar amino acid residues. Hydrogen bonds include dipole-dipole attractions between a partially positive hydrogen atom and a partially negative oxygen (carbonyl group), nitrogen (amine) or sulfur atom (thiol) and are often formed by amino acids.[383,385-387]

The entropy, a measure of uncertainty or disorder, is dependent on the dynamics of the overall system, describing the number of possible arrangements of atoms in a system. Increased rigidity or limited translational and rotational degrees of freedom resulting from the protein-protein complex formation changes the association entropy.[383,388]

The Gibbs' free energy is also described as:

$$\Delta G = -RT \ln K_d \qquad (5\text{-}5)$$

R: gas constant, K_d: binding constant.

The term (5-5) for the free Gibbs' binding energy includes the dissociation constant K_d, which can be determined by estimating the different thermodynamic components. With protein-protein complexes associated K_d values are in the range of 10^{-4}-10^{-14} M and therefore a ΔG range of 25-80 kJ/mol.[388]

A quantitative approach to study protein-protein interactions is calorimetry, specifically ITC (Isothermal titration calorimetry), measuring the heat taken up and/or released for a biomolecular interaction. The ITC experiment is usually carried out at constant temperature and constant pressure.

The relation between heat capacity (C_p) and the enthalpic and entropic term of the binding event is:[388]

$$\Delta C_p = \mathrm{d}\Delta H/\mathrm{d}T = T\,\mathrm{d}(\Delta S)/\mathrm{d}T \qquad (5\text{-}6)$$

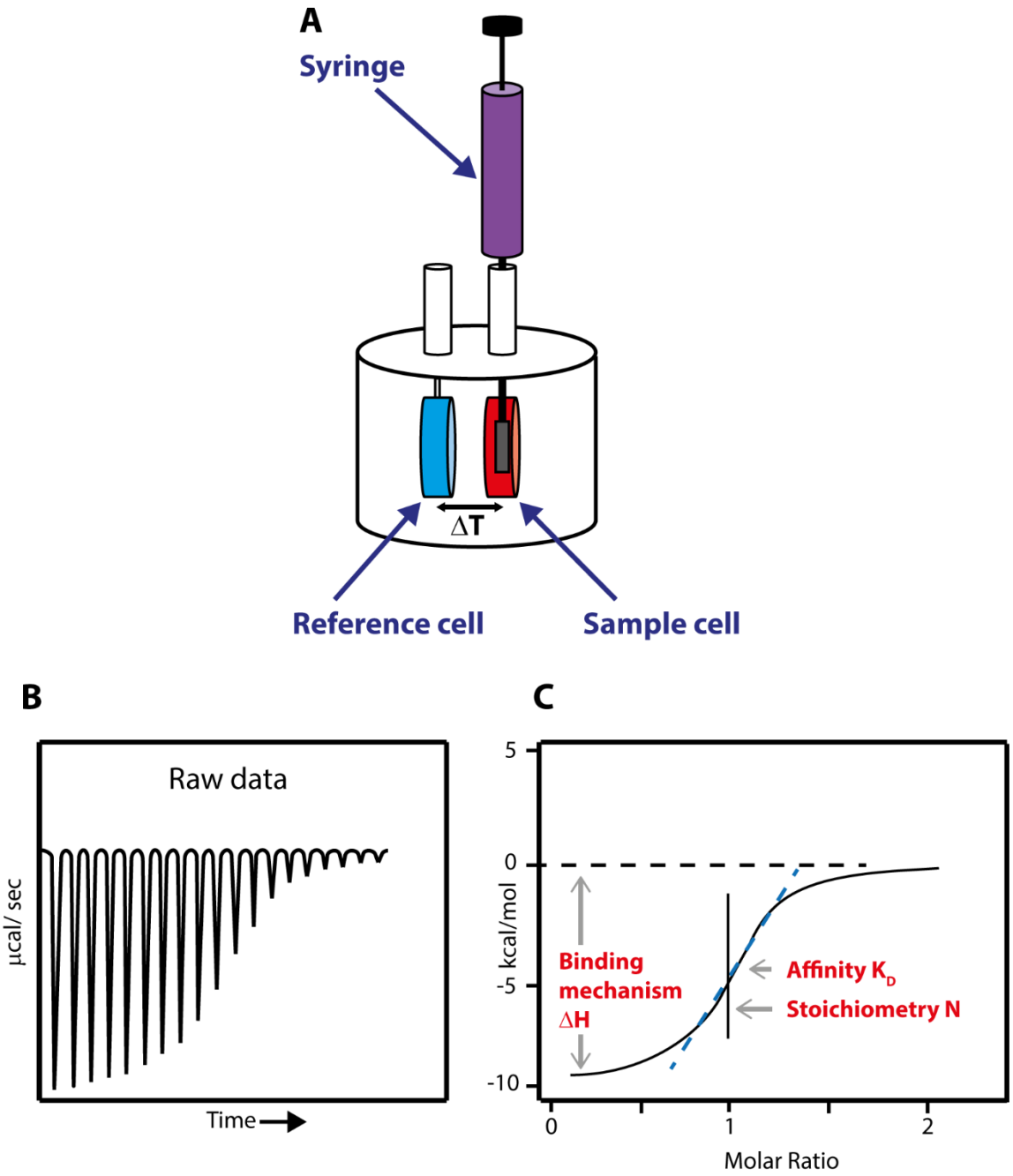

Figure 5.1: Schematic description of an ITC experiment with analysis. **A:** Experimental setup. Both reference and sample cell contain the same buffer and protein and the titrant is added in consecutive steps to the sample cell. **B:** Raw data output, each peak counts for one addition of titrant and the respective enthalpy is measured. **C:** Analysis of the data by fitting a sigmoidal curve to the released or consumed enthalpy per mol plotted against the molar ratio. Binding affinity and stoichiometry can be determined from the fitted curve. Adapted from [389].

In an ITC experiment, a consecutive addition (titration) of protein solution B into a solution of protein A in the reaction cell is produces a change in the heat/temperature of the cell, compared to the reference cell (Figure 5.1 A). For each addition, this energy change is measured and converted into the enthalpy per second, which relates to a specific number of protein-protein complexes formed. This allows the binding constant (K_d), enthalpy (ΔH), entropy (ΔS) and the exact stoichiometry (N) of the binding reaction to be estimated (Figure 5.1 C). A reference cell filled with the same protein A solution which remains unchanged during the experiment serves as temperature reference/control. Both reaction/sample and reference cells are enclosed in an adiabatic jacket.[382,e]

ITC is suitable to detect a broad range of binding affinities from nanomolar to millimolar range, however this method is limited for measuring binding affinities apart from this range.[382,390]

An alternative optical method to study protein-protein interactions which can measure a broader range of binding affinities, is surface plasmon resonance (SPR). One binding partner (protein or ligand) is immobilized on a gold sensor chip coated with an organic matrix polymer. The sensor chip forms the bottom of a microfluidic flow cell, through which an aqueous solution of the injected second binding partner (the analyte) can pass under constant flow rate. When the analyte binds to the immobilized partner protein/ligand on the sensor chip, the formation of protein-ligand complex on the surface inducing an increase of the refractive index (SPR response) is measured. SPR response is proportional to the mass bound to the surface, which is increased upon protein-protein or protein-ligand binding. Change in SPR response is measured and plotted as response units (RU) versus the time.[382,390]

The corresponding plot is divided into three parts (Figure 5.2), a baseline phase, before injection of the analyte, a binding phase during the injection of analyte and a dissociation phase, after injection of the analyte. If conducting the SPR experiments at different concentrations of the analyte, kinetic constants can be retrieved from the association and dissociation times as well as the change in response units during the experiment. Nevertheless, the immobilization of one binding partner results in restricted conformational and rotational freedom and therefore a reduction in entropy, which affects the association rates.[382,390]

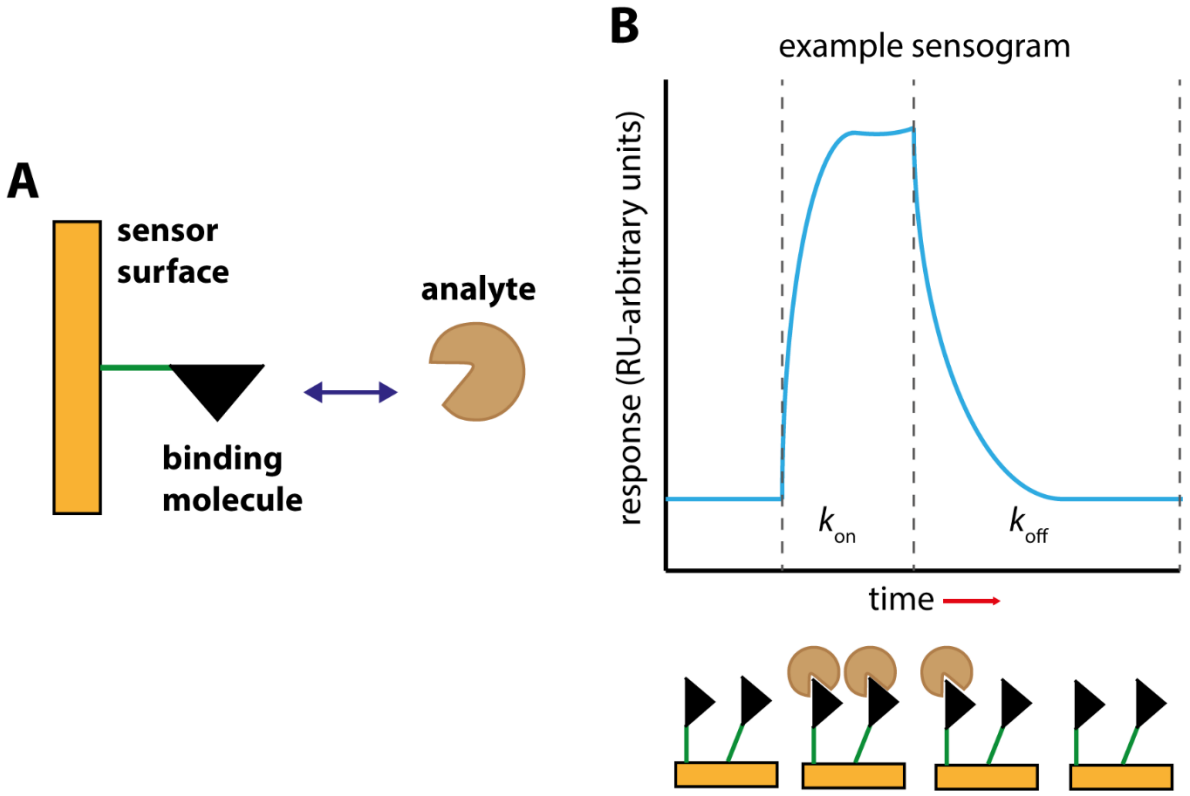

Figure 5.2: Schematic description of the surface plasmon resonance (SPR) method. **A:** Principle of immobilized binding molecule on the sensor surface and interaction with the analyte. **B:** Plot resulting from the SPR binding experiment, the baseline phase describes the buffer flow through, the second phase starts when the analyte is injected and binds to the immobilized molecule, the last phase corresponds to the dissociation of the analyte. Adapted from [390].

5.3 Brief introduction to protein crystallography

Protein crystallization describes the method to grow crystals in a supersaturated macromolecule (protein, nucleic acids, viruses or ribosomes) solution under precipitating conditions that ideally do not perturb the natural state of the molecule.[g] Two approaches to crystallization of proteins or protein-protein complexes are the sitting or hanging drop methods based on vapor diffusion or batch crystallization under oil. For the vapor diffusion methods, the protein solution is mixed with the precipitant solution in a shared sealed chamber, which also contains a reservoir of the mother liquor (the unmixed precipitant solution). Diffusion of water vapor from the protein-precipitant drop to the reservoir increases the concentration of the protein and precipitant in the drop which can potentially lead to supersaturation of the protein.

Crystallization proceeds in two distinct steps: nucleation and growth. Nucleation describes the process of initial crystal formation from a wholly disordered solution state to an ordered state of the crystalline macromolecule. Crystal growth follows when the mechanisms of dislocation and two-dimensional nucleation occur. The supersaturation of the protein solution is the critical factor that drives both process of nucleation and growth and determines the outcome and quality of the crystals (Figure 5.3). Very important factors for obtaining good quality protein crystals include homogenous and stable protein samples.[391,392]

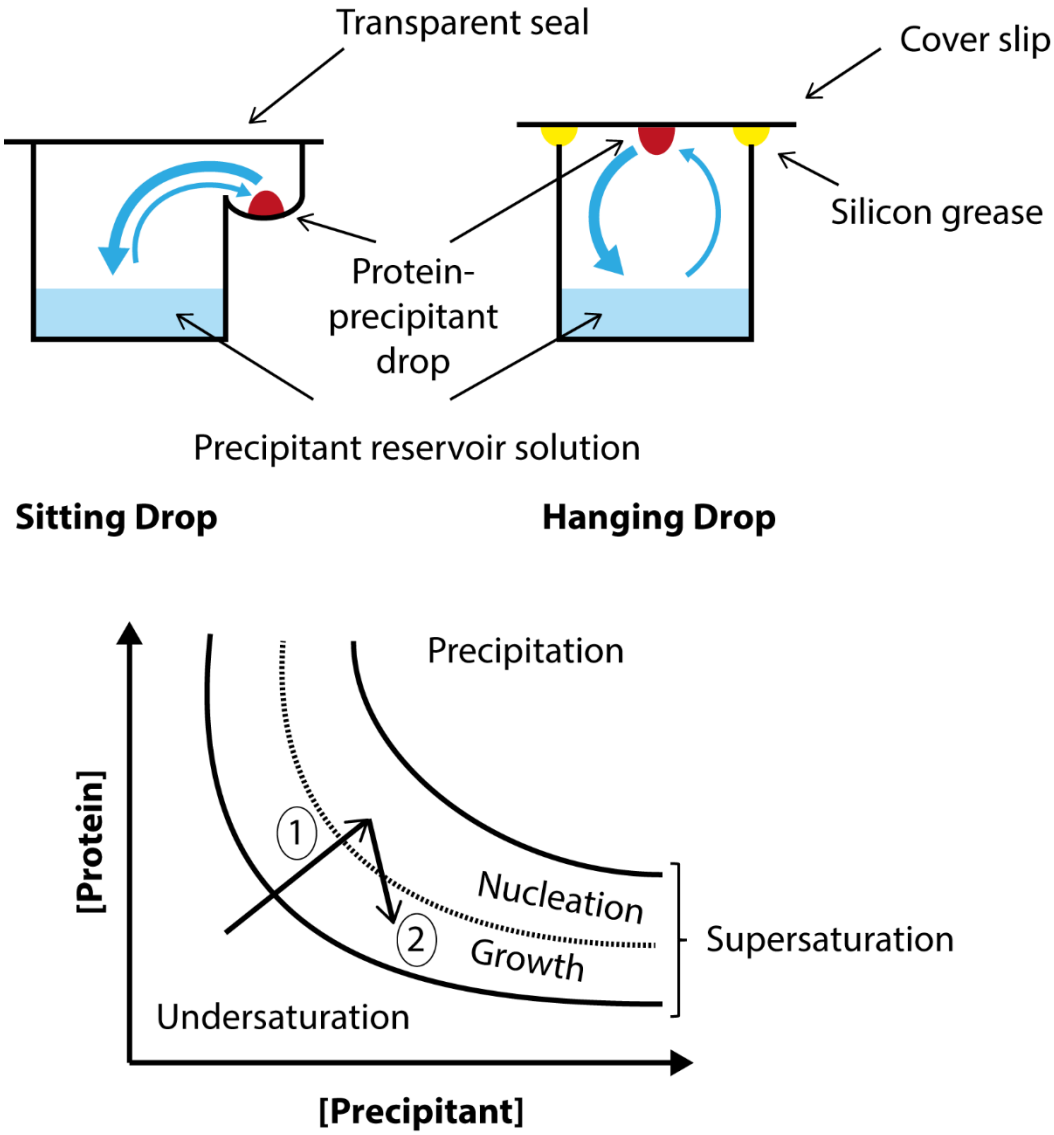

Figure 5.3: Techniques of protein crystallization and schematic principle of protein crystal growth. Top: Sitting drop and hanging drop vapor diffusion methods. The concentration of the protein and precipitant is rising due to vapor diffusion into the precipitant reservoir solution. Bottom: Schematic graph how the concentration of protein and precipitant is affecting crystal growth. First step for the formation of protein crystals is the dehydration of the protein-precipitant drop until the nucleation may occur (1) followed by a decrease of protein concentration and crystal growth (2) if still in the supersaturation zone. Adapted from [391,393].

5.4 Binding studies on [FeFe]-hydrogenase maturation enzymes

The proposed pathway for maturation of the [FeFe] hydrogenase cofactor is a multistep reaction with three enzymes HydG, HydE and HydF involved. The study of the protein-protein interaction mechanisms is important and facilitates the development of a model including the order of events that lead to a mature [FeFe]-hydrogenase, with its active cofactor the H-cluster. To measure interactions, the maturase HydF (StrepThitHydF) was mixed with one of the other two proteins (His_6ThitHydG, His_6ThitHydE1265 or His_6ThitHydE1675) and the complex solution was analyzed by either gel filtration, a pull-down assay, isothermal calorimetry or screening for co-crystallization conditions.

Based on the results of aerobic biochemical interaction studies from Costantini *et al.* with *Clostridium acetobutylicum* [FeFe] hydrogenase maturation proteins, HydE and HydG are thought to directly interact with HydF as demonstrated by co-expression and co-purification experiments.[253] The results obtained by surface plasmon resonance (SPR) analysis and pull-down assays (with detection by Western-Blot) suggested that there is no direct interaction between the radical SAM enzymes HydE and HydG. Moreover, the measured K_d for the HydE-HydF binding interaction is one magnitude lower and therefore slightly tighter than that between HydG and HydF (Table 5.1). It is hypothesized[253] that HydG and HydE are likely to interact with domain III of HydF, which is known to bind the partly assembled FeS cluster intermediates. For an already bound complex of HydF:HydE the exchange of HydE for HydG and *vice versa* could not be achieved.[253]

The GTPase activity of HydF has been shown to be affected by the presence of HydG and HydE resulting in an increase of the GTPase activity by HydF of 50%.[246] However, this was not confirmed by the experiments carried out herein (Chapter 4, Section 4.7.1). Mutants of HydF lacking important residues for GTPase activity still interact with similar K_d's, with HydE and HydG compared to the wild-type constructs, suggesting no direct interaction with the GTPase domain. SPR experiments with a non-hydrolyzable analog of GTP (GTPγC) resulted in comparable binding affinities to those reported without addition of GTPγC. Nevertheless, if GTP was added to an already formed complex of HydF:HydG or HydF:HydE it increased the dissociation rate of the binding partners.[253]

Table 5.1: Binding constants obtained from SPR experiments carried out by Constantini *et al*. with *Clostridium acetobutylicum* HydF and HydF mutant.[253]

	His_6HydG K_d (M)	**His_6HydE K_d (M)**
StrepHydF	$1.31 \cdot 10^{-6}$	$9.19 \cdot 10^{-8}$
StrepHydF_G24A/K25A	$9.47 \cdot 10^{-7}$	$8.20 \cdot 10^{-8}$
StrepHydF + GTPγC	$4.21 \cdot 10^{-7}$	$2.26 \cdot 10^{-8}$

5.5 Gel filtration of [FeFe]-hydrogenase maturation enzymes

Gel filtration chromatography separates proteins or protein complexes on the basis of their hydrodynamic volume, which is in turn related to the molecular size. As an analytical tool, it serves to estimate the molecular size of a protein and/or its multimeric state in solution (after determining a column calibration with suitable proteins of known size). The principle of separation is achieved by the column material, an adsorbent resin which is able to trap smaller molecules into pores, whereas larger molecules are excluded from the adsorbent matrix. Thus, the larger molecules are eluted first and the following molecules are eluted in a decreasing order of size.[394-396]

For the studies described herein gel filtration was used to determine the multimeric state of StrepThitHydF and His_6ThitHydG. Furthermore, StrepThitHydF was mixed with His_6ThitHydG, incubated and applied to the S200 analytical gel filtration column (1.5 cm x 50 cm, 150 mL), in order to find out if they form a protein-protein complex in the absence of their substrates. Prior to analysis, the analytical gel filtration column was calibrated with protein solutions of known molecular weights, which eluted in sharp peaks with no shoulders. The elution times were reported and based on the retention volumes a calibration slope generated (Table 5.2, Chapter 7, Method 17, Figure 7.1).

Table 5.2: Molecular mass and elution volumes of protein used to calibrate the analytical gel filtration column. V_0 is 18 mL. Corresponding Figure (7.1) in Chapter 7.

Enzyme	**M/kDa**	**V_e/mL**	**V_e/V_0**
β-Amylase	200	21.5	1.19
Alcohol dehydrogenase	150	23.5	1.31
Bovine Albumine	66	26	1.44
Carbonic anhydrase	29	29.6	1.64
Cytochrome C	12.4	32.3	1.79

5.5.1 Analysis of the multimeric state of HydF and HydG in solution

To analyze the multimeric state of purified and reconstituted StrepThitHydF, 300 μL of purified HydF (210 μM) and reconstituted HydF (210 μM) in HydF buffer SA (25 mM HEPES, 300 mM KCl, 5% glycerol, 1 mM DTT, pH 8.0) were applied to the calibrated analytical gel filtration column (1.5 cm x 50 cm, 150 mL) equilibrated with the same buffer with a flow rate of 0.5 mL/min. The elution of the HydF protein was monitored by UV-Vis absorption at 280 nm (Figure 5.4).

For the estimation of the multimeric state of His_6ThitHydG, 300 μL of reconstituted HydG (~ 300 μM) diluted in HydF buffer SA was injected onto the analytical gel filtration column and the retention volumes recorded by monitoring absorbance at 280 nm. No chromatogram could be obtained since the plotter was defective.

The multimeric states of the proteins were determined by calculating the molecular weight with the calibration graph obtained for the analytical gel filtration column (Method 17, Table 5.3).

Table 5.3: Retention volumes V_e, theoretical molecular weights and calculated molecular weights of the analyzed HydF and HydG proteins.

Enzyme	V_e/mL	V_e/V_0	M/kDa	calc. M/ kDa
As purified HydF	24.2	1.34	47.5	111
Recon. HydF	24.1	1.34	47.5	111
Recon. HydG	27.1	1.51	55	50

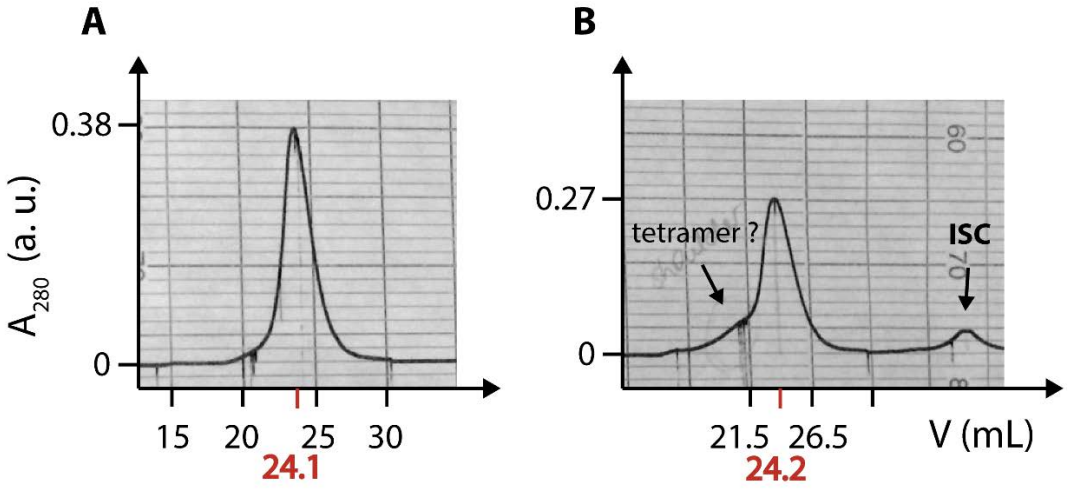

Figure 5.4: Gel filtration chromatogram of 300 μL of 210 μM unreconstituted (A) and reconstituted HydF (B).

It was found that purified HydF forms an apparent dimer in solution, as observed in the elution profile from the gel filtration (Figure 5.4 A), and as calculated by using the calibration slope (Table 5.2). However, the resulting molecular weight corresponding to the retention time is higher than expected with 111 kDa for a HydF dimer, compared to the 95 kDa calculated. In the elution profile of reconstituted HydF, which is also shown to form a dimer, an earlier elution shoulder can be seen (Figure 5.1 B), which might correspond to the tetrameric form of HydF and might have shifted the retention volume to higher molecular size. Additionally, a small peak is eluted after reconstituted HydF which possibly corresponds to dissociated iron-sulfur cluster aggregates or a bound ISC machinery protein like IscA (11.5 kDa)[272] (with V_e ~ 33.7 mL which corresponds to a molecular mass of 9.3 kDa, an [4Fe4S] cluster weights 351 Da, labelled ISC in Figure 5.4).

The calculated molecular weight of reconstituted HydG of 50 kDa matches the monomeric molecular weight observed by gel filtration chromatography of 55 kDa, and suggests HydG exists as a monomer in solution.

5.5.2 Test for complex formation

In order to assess if HydF dimer forms a complex with HydG, both enzymes (200 μM HydF + 200 μM HydG final concentration) were mixed together in HydF buffer SA and incubated for 1 h before being analyzed on the analytical gel filtration column (Figure 5.5 B). Moreover, a reference sample of reconstituted HydF (400 μM) was been analyzed immediately beforehand (Figure 5.5 A).

The elution profile of reconstituted HydF (Figure 5.5 A) corresponds to a dimeric form (Table 5.4), with a tiny shoulder eluting earlier which might correspond to the tetrameric form of the protein. Interestingly, the elution profile of the HydF and HydG mixture contains a large shoulder eluting after the HydF peak, likely belonging to HydG (Figure 5.5 B).

To evaluate if the shoulder in Figure 5.5 B belongs to HydG, 0.5 mL fractions were collected from the eluted peaks and analyzed by SDS-PAGE (Figure 5.6).

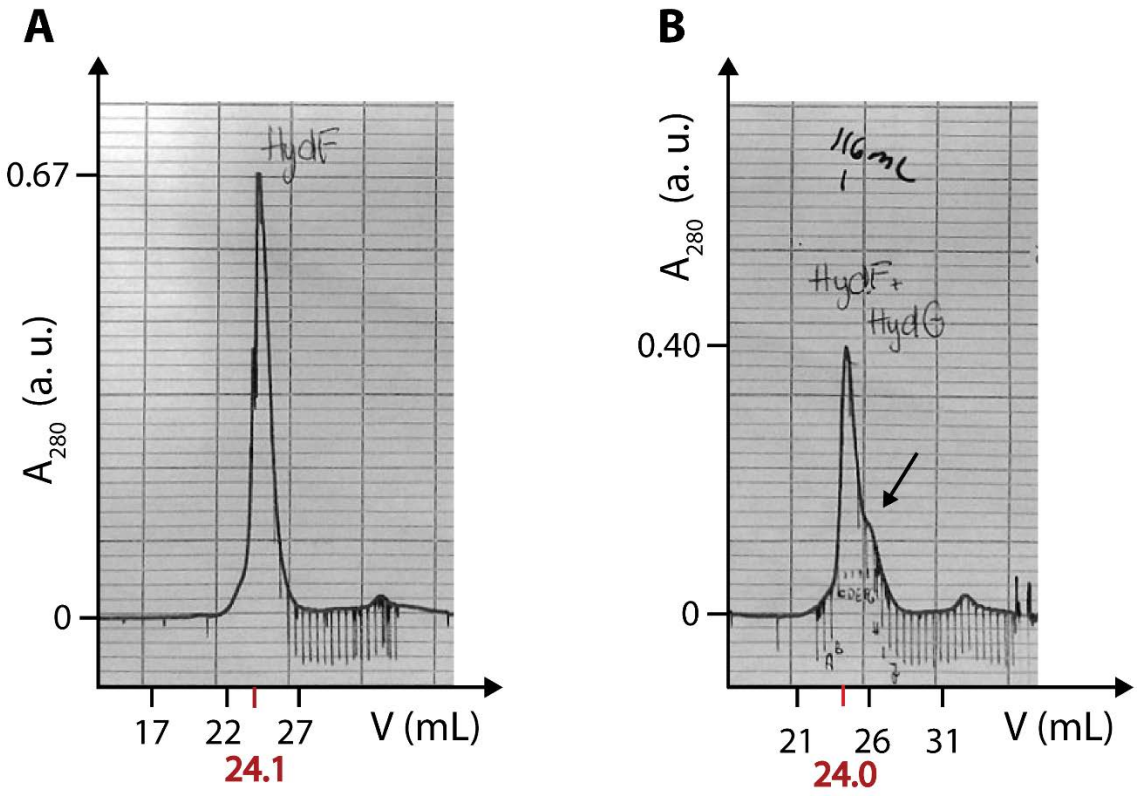

Figure 5.5: Gel filtration chromatogram of 300 µL of 400 µM reconstituted HydF (A) and a mixture of 200 µM reconstituted HydF and HydG (B).

The calculated molecular weight from the retention volume of the HydF peak and the shoulder are similar to the already reported values for the reconstituted HydF and HydG protein alone (Table 5.4) with only a slight increase for the mass of HydG pointing towards no complex formation.

Table 5.4: Retention volumes V_e, theoretical molecular weights and calculated molecular weights of the analyzed HydF and the HydF + HydG mixture elution profile.

Enzyme	V_e/mL	V_e/V_0	M/kDa	calc. M/ kDa
Recon. HydF	24.1	1.34	47.5	111
Recon. HydG	27.1	1.51	55	50
Recon. HydG + Recon. HydF	24.0	1.33	-	116
HydG shoulder	26.5	1.44	-	66

Furthermore, the resultant SDS-PAGE analysis of fractions collected from the analytical gel filtration column (Figure 5.6) also supports the assumption that HydF and HydG eluted separately from one another and no proof for complex formation could be obtained. However, the first three fractions (A-C) contained small amounts of HydG which might be due to overlapping peaks or real protein interactions.

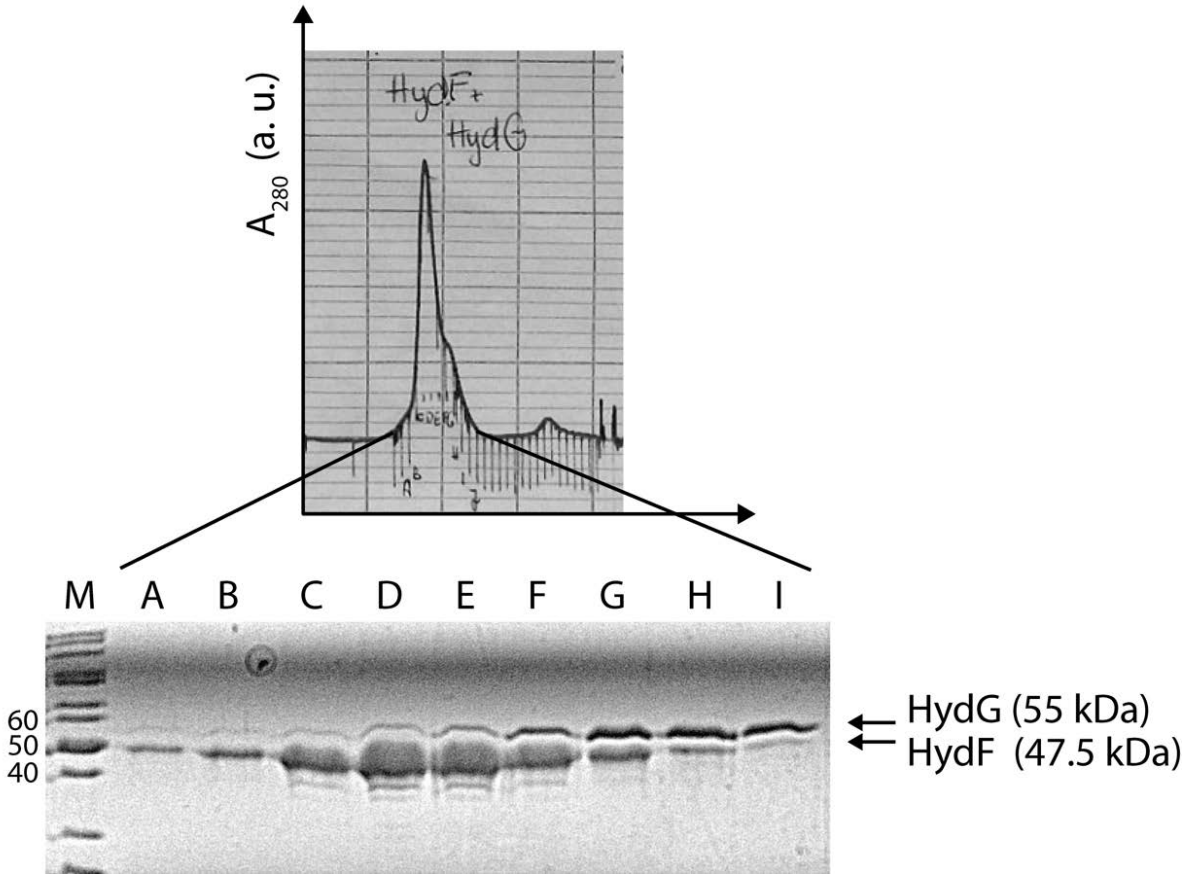

Figure 5.6: Elution profile from the analytical gel filtration of the HydF and HydG mixture and the corresponding SDS-PAGE of the 0.5 mL fraction taken during the elution.

Furthermore, the concentration of both proteins seems to have been different, as the HydF protein bands appear to be much thicker than the detected HydG protein bands (Figure 5.6), which might be due to the fact that HydF is a dimer. Because no obvious protein-protein interaction could be detected, the addition of a substrate might be needed to induce conformational changes or recognition that enable interaction and binding.

As it is very time- and material- consuming to test different conditions for protein-protein binding with gel filtration chromatography another strategy was explored herein. By taking advantage of the different affinity-tags of StrepHydF and the His_6-tagged HydG and HydE proteins pull-down assays were carried out to screen for protein-protein binding.

5.6 Pull-down assays

The principle of pull-down assays rely on the selective affinity of one binding partner to a specific resin, similar to affinity chromatography, whereas, the second binding partner does not bind to the specific resin and is free to interact with the resin-bound binding partner. Therefore, it is an excellent *in vitro* tool to determine the physical interaction between two or three proteins and to screen for optimal conditions.[397]

A schematic set-up of the pull-down assays carried out for this thesis is represented in Figure 5.7.

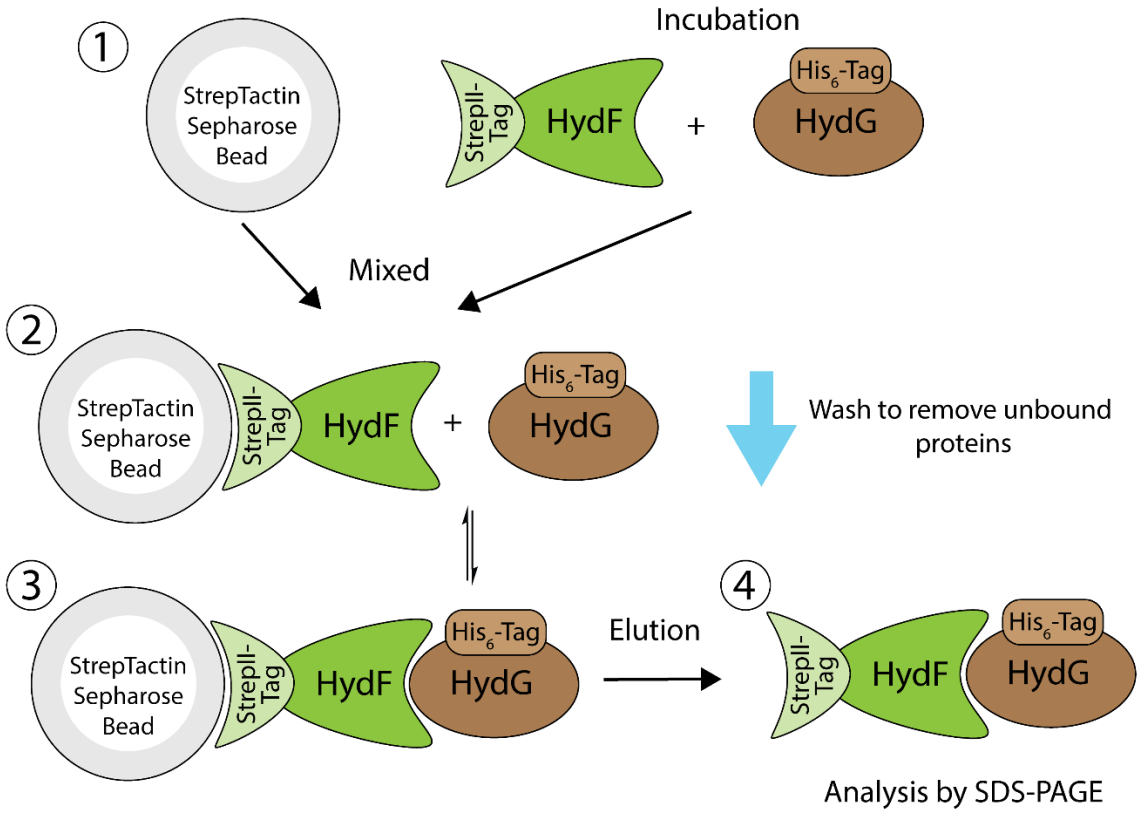

Figure 5.7: Schematic description of the pull-down assay used herein. 1. His_6HydG was added to a solution of StrepHydF and incubated for 1h, subsequently the reaction mixture was mixed with equilibrated StrepTactin sepharose beads and incubated for 10 min; 2. After incubation, the resin was washed with buffer to remove unbound proteins and molecules; 3. Potentially bound StrepHydF to His_6HydG was co-eluted by addition of a desthiobiotin containing buffer and analyzed *via* SDS-PAGE.

The StrepII-Tag of HydF possesses a high affinity for the StrepTactin sepharose and, prior to mixing with the resin, StrepThitHydF was incubated with its potential partner enzyme His_6ThitHydG to ensure complex formation independent from affinity binding to the resin. In the following step, the incubated solution of HydF and HydG was mixed with the StrepTactin resin and unbound molecules and proteins were removed by

washing with equilibration buffer. To elute the complex from the resin, elution buffer with D-desthiobiotin was added. The resulting solution containing StrepHydF and possibly His_6HydG was analyzed *via* SDS-PAGE.

To adapt the pull-down assay for the [FeFe]-hydrogenase maturation proteins HydE, HydG and HydF, the affinity-tag of HydE was modified from Strep- to His_6-Tag (Chapter 2, Section 2.4.1).

5.6.1 Initial screen for HydF-HydG binding

The experimental procedure for the pull-down assays was inspired by binding studies of the iron-sulfur cluster scaffold Isu protein with the chaperon Jac1 protein and cysteine desulfurase Nfs1.[398,399] Based on these studies a protocol was designed, which is schematically shown in Figure 5.8.

In preparation for the pull-down assays, 0.8 mL columns were filled with 100 μL high-capacity StrepTactin resin (200 μL 50% suspension) with a binding capacity of 7 mg protein/mL resin according to the manufacturer.[400] Protein concentrations loaded onto the resin ranged between 40-100 μM and the volume remained constant at 50 μL, corresponding to 1-4 mg protein/mL (or 0.1-0.4 mg/100 μL of resin) of resin.

The resin-filled columns were transferred into the glovebox and pre-equilibrated with 1 mL HydF buffer (25 mM HEPES, 300 mM KCl, 5% glycerol, 1 mM DTT, pH 8.0) (Figure 5.8, Step 1).

To allow and ensure complex formation between StrepThitHydF and His_6ThitHydG or His_6ThitHydE1265/His_6ThitHydE1675, the proteins were mixed together in varying ratios. Furthermore, different compounds and/or substrates that were candidates to improve the binding interactions were also added. These mixtures were incubated for 1 h at 18 °C inside the glovebox (Figure 5.8, Step 2).

Subsequently 50 μL of the incubated mixture was applied on the equilibrated StrepTactin resin and left to incubate for 10 min. Unbound components were removed by washing with the equilibration buffer (3 x 250 μL) (Figure 5.8, Step 3).

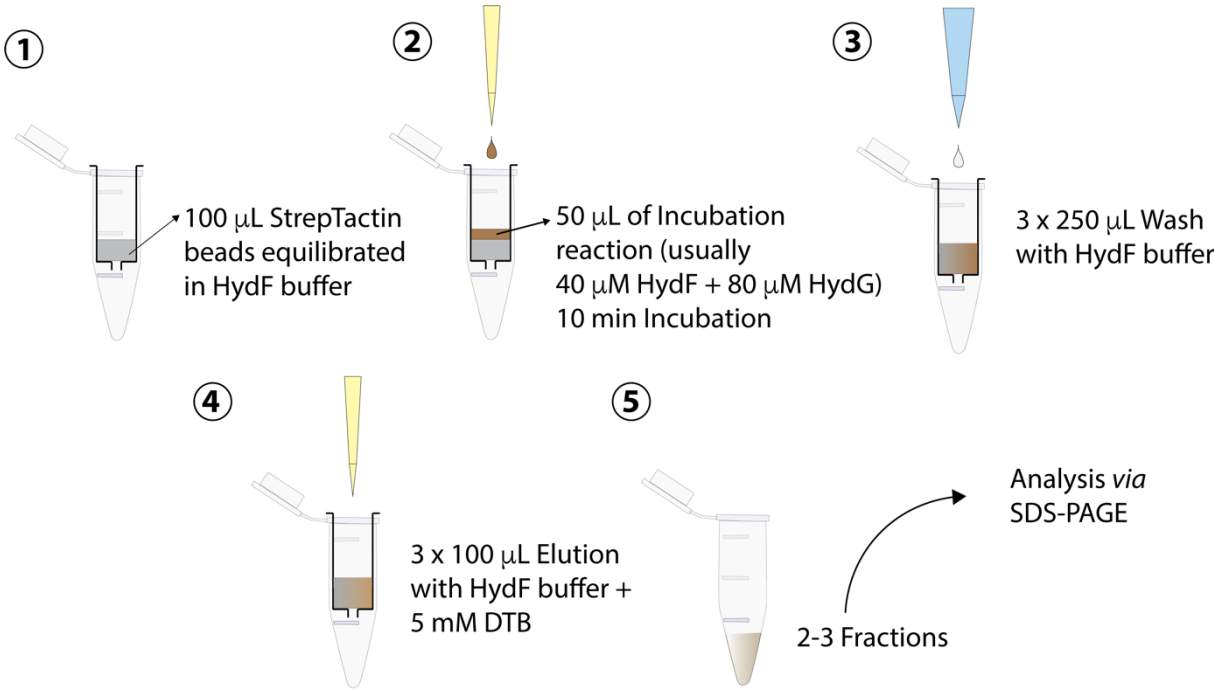

Figure 5.8: Experimental procedure of the pull-down assays carried out with StrepThitHydF and His_6ThitHydG or His_6ThitHydE1265/His_6ThitHydE1265. 1. Equilibration of StrepTactin Resin; 2. Reaction mixture loading and incubation for 10 min; 3. Wash with HydF buffer; 4. Elution with 5 mM D-desthiobiotin; 5. Eluted protein fractions analyzed with SDS-PAGE.

The next step (Step 4) described in Figure 5.8 is the elution with the equilibration buffer supplemented with 5 mM D-desthiobiotin. Either three 100 µL fractions were collected or one 200 µL plus a 100 µL fraction. Obtained fractions were analyzed using SDS-PAGE and the thickness of protein bands analyzed by densitometry with the program Image J. The corresponding protein bands are visualized as peaks and the integrals measured. The resulting percentage of protein bound, which is shown in the following Figure 5.9 relates to the amount of HydG (or BSA, or HydE) compared to HydF after eluting from the column.

The first experiments carried out in the context of the pull-down assays were simple mixtures of StrepThitHydF and His_6ThitHydG with no further additives, similar to the gel filtration experiments in Section 5.4.2. However, as observed before, no interaction could be detected, even if HydG was added in a 2-fold excess. Subsequent experiments included compounds to improve complex formation.

The following compounds were added to a mixture of 40 μM StrepThitHydF and 40 μM His_6ThitHydG: 5 mM L-tyrosine, 3 mM L-cysteine, 80 μM $FeCl_2$, 1 mM sodium dithionite. Furthermore, assays were carried out where one of the compounds was omitted to test their influence on the complex formation. Because the solubility of tyrosine is limited in water, a 20 mM L-tyrosine stock is prepared from a 25.71 mM tyrosine in 200 mM HCl. To the 25.71 mM tyrosine solution in 200 mM HCl, 20 μL buffer and 80 μL 1 M NaOH are added to obtain a pH of around 8.0.

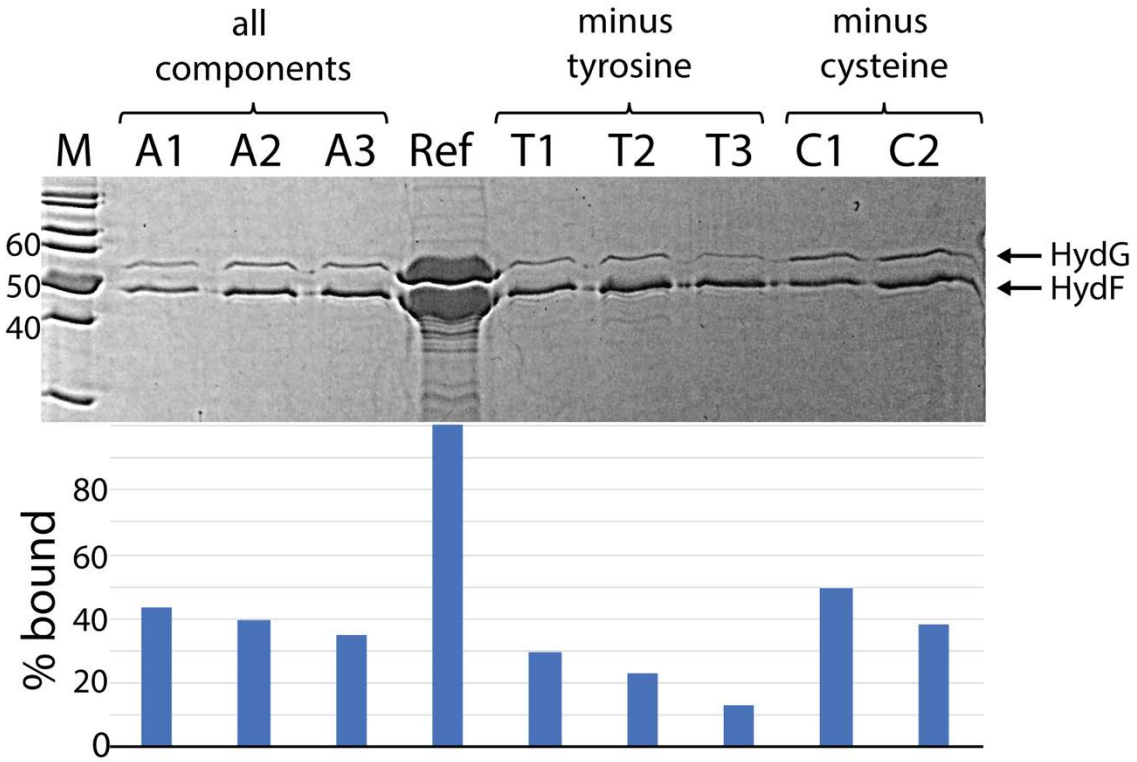

Figure 5.9: SDS-PAGE and bar-chart analyzing the pull-down assay carried out with 40 μM HydF (47.5 kDa) and 40 μM HydG (55 kDa). All components are 5 mM tyrosine, 3 mM cysteine, 80 μM $FeCl_2$ and 1 mM dithionite. A1-A3: Elution fractions resulting from the experiment will all additives. Ref: 40 μM HydF + 40 μM HydG. T1-T3: Elution fractions resulting from the experiment where tyrosine was omitted. C1-C3: Elution fractions resulting from the experiment where cysteine was omitted. Continues as Figure 5.10.

Three elution fractions (1-3) were collected of each pull-down assay and loaded onto a SDS-PAGE, the corresponding results are shown in Figure 5.9 and 5.10. With ImageJ, analysis of protein band intensity revealed that if all components are added, circa 40 % of HydG remains bound to HydF. Depleting tyrosine from the complex had a negative effect on the percentage remaining bound, whereas omitting cysteine or iron slightly increased the percentage bound to around 50-60%. Removing dithionite from the complex formation mixture resulted in a higher percentage of circa 70% HydG

remaining bound to HydF. Based on these results, dithionite was left out for the subsequent complex formation reactions.

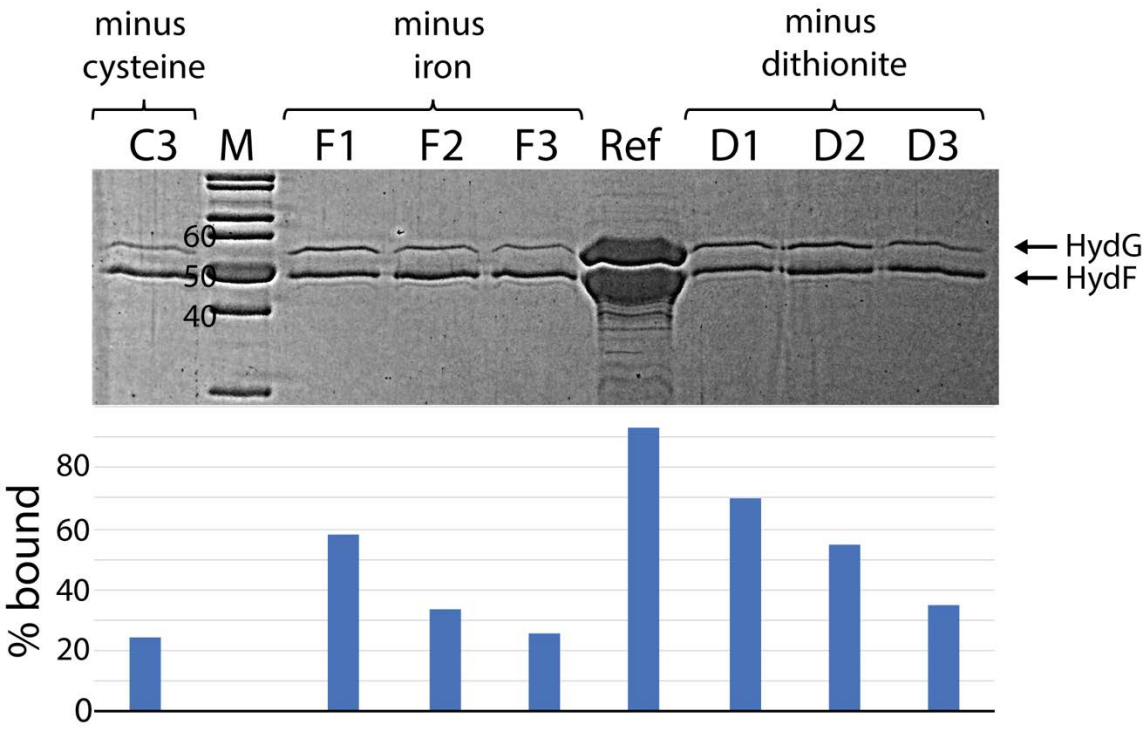

Figure 5.10: SDS-PAGE and bar-chart analyzing the pull-down assay carried out with 40 μM HydF and 40 μM HydG. All components are 5 mM tyrosine, 3 mM cysteine, 80 μM $FeCl_2$ and 1 mM dithionite. C1-C3: Elution fractions resulting from the experiment where cysteine was omitted. Ref: 40 μM HydF + 40 μM HydG. F1-F3: Elution fractions resulting from the experiment where $FeCl_2$ was omitted. D1-D3: Elution fractions resulting from the experiment where dithionite was omitted.

5.6.2 Effect of the buffer on HydF-HydG binding

To investigate if the buffer composition has an effect on the HydF-HydG binding, three different buffers were tested (Figure 5.11, Table 5.5). Initially, the standard high salt HydF buffer used for the Strep-purification (A+, 25 mM HEPES, 300 mM KCl, 5% glycerol, 1 mM DTT, pH 8.0). Later, a lower salt concentration was chosen, in an effort to maintain ionic interactions between the two proteins studied (A, 25 mM HEPES, 30 mM KCl, 5% glycerol, 1 mM DTT, pH 8.0). The third buffer included the extra components in the buffer (A*, 25 mM HEPES, 30 mM KCl, 5% glycerol, 1 mM DTT, 5 mM tyrosine, 3 mM cysteine, 80 μM $FeCl_2$, pH 8.0) to guarantee constant concentrations of the compounds during the whole experiment. Additionally, omitting tyrosine or cysteine from the mixture was tested once more as well as the addition of GTP (3 mM), known to be a substrate of HydF.[51] To include a control measurement

the experiment has been carried out for BSA as well, as a replacement for HydG (Figure 5.12). For these experiments, the HydG concentration was raised to 72 μM to increase the chance of the binding event and- the same was done for the control reaction with BSA (72 μM).

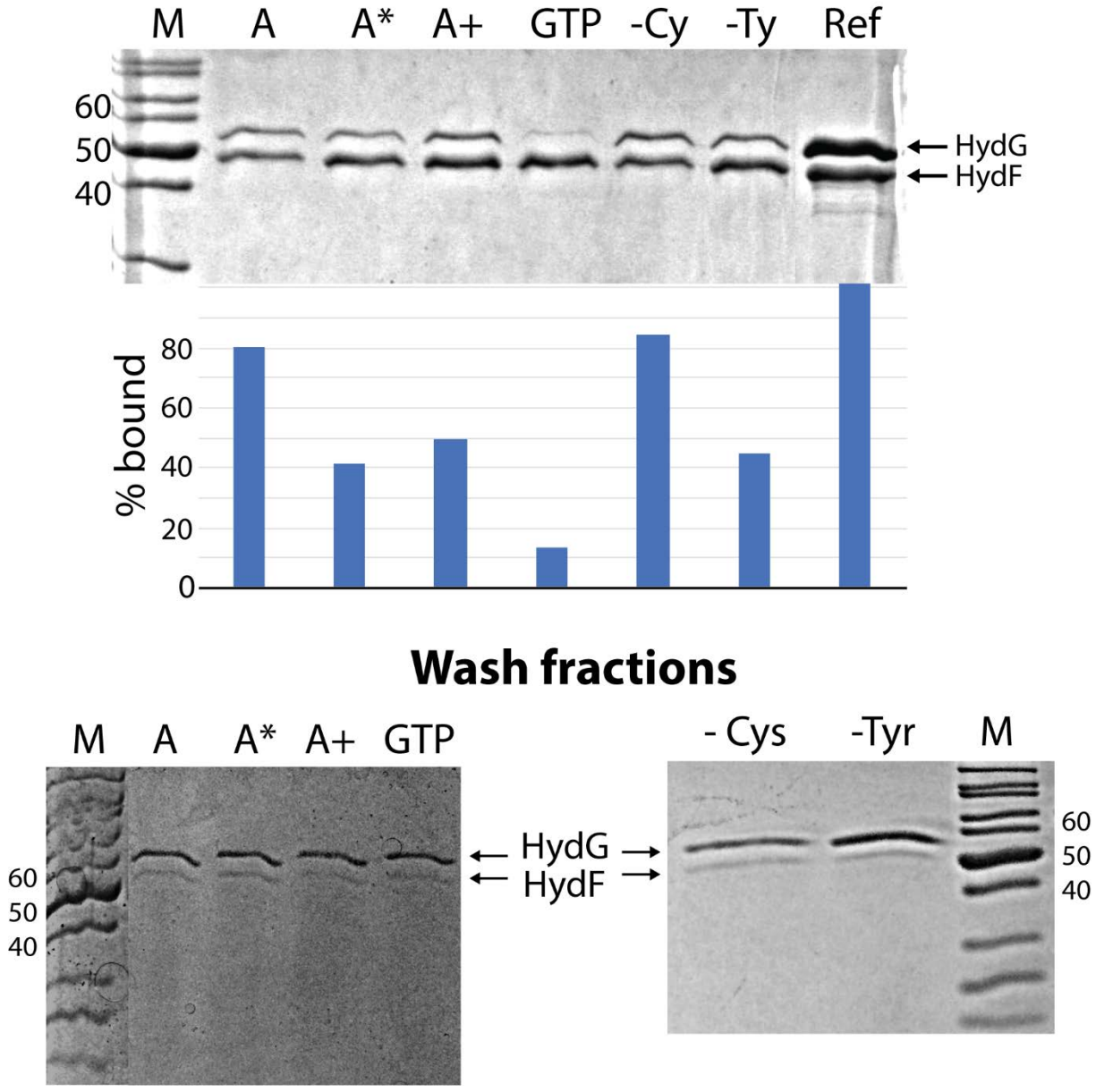

Figure 5.11: SDS-PAGEs and bar-chart analyzing the pull-down assay carried out with 40 μM HydF and 72 μM HydG. Top: Elution fractions. Bottom: Wash fractions A: First elution fraction with the low salt HydF buffer and the additives 5 mM tyrosine, 3 mM cysteine, 80 mM $FeCl_2$. All lanes represent first elution fractions except Ref: 40 μM HydF + 40 μM HydG. A*: Assay with the low salt buffer with supplements and the same additives as in A. A+: Assay with the high salt HydF buffer and the same additives as in A. GTP: Assay in low salt buffer and with GTP added to the additives in A. -Cy: Assay with omitted cysteine. -Ty: Assay with omitted tyrosine.

Table 5.5: Buffer compositions used for pull-down assays.

	A	A*	A+
HEPES (mM)	25	25	25
Glycerol (% w/v)	5	5%	5
DTT (mM)	1	1	1
pH	8.0	8.0	8.0
KCl (mM)	30	30	300
Tyrosine (mM)	-	5	-
Cysteine (mM)	-	3	-
$FeCl_2$ (μM)	-	80	-

The results from the SDS-PAGE analysis (Figure 5.11) with different buffers suggested that the low salt buffer seems to give the optimal conditions for HydF-HydG binding to occur, with 80% HydG bound. Moreover, addition of GTP significantly decreases the occurrence of binding, which has been reported before in binding studies where GTP induced the dissociation of HydF binding partners.[253] Also, omitting tyrosine from the complex forming reaction decreased the extent of HydG binding, which might mean that tyrosine is essential for the binding of HydG to HydF. Depleting cysteine had almost no effect on the binding. The corresponding wash fractions (Figure 5.11 bottom) clearly show a higher amount of HydG passing through the column without binding to the resin. Especially the wash fraction corresponding to the assay with removed tyrosine shows a very thick band of HydG (-Tyr).

Regarding the control experiment with BSA, binding to HydF has been observed up to 40%, which means HydF interacts with BSA to a significant degree. Reasons for this might lie in the open configuration of the HydF dimer in solution with exposed residues and the fact that HydF appears to have a protein binding surface that may have limited selectivity. Therefore, care is required in interpreting these results and as a rule of thumb, only interactions above 40% will be taken into account as real/strong interactions with HydF.

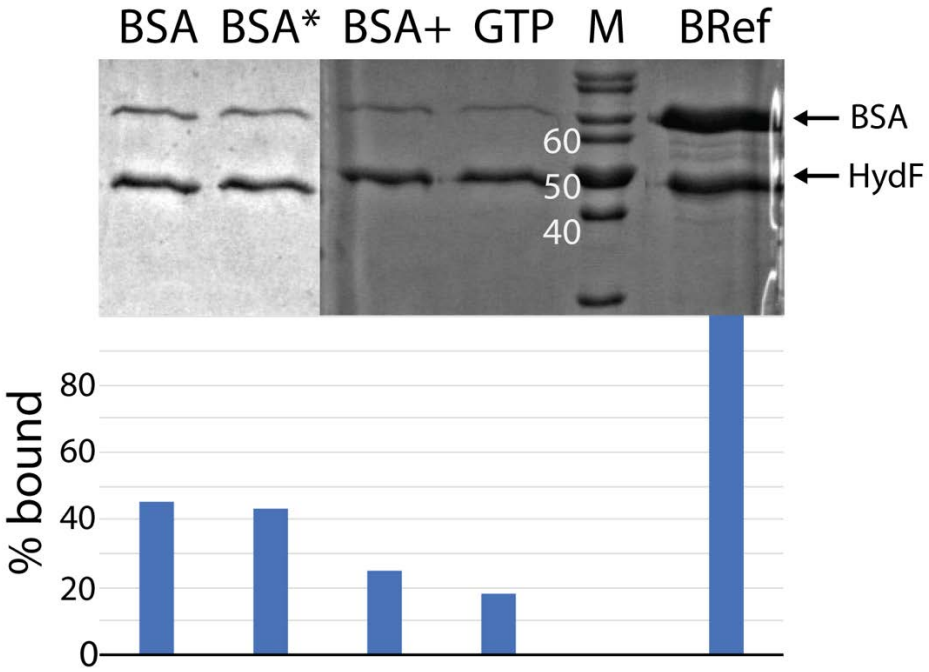

Figure 5.12: SDS-PAGE and bar-chart analyzing the pull-down assay carried out with 40 μM HydF and 72 μM BSA (66 kDa). BSA: Experiment in low salt buffer, BSA*: Experiment with compounds added in the buffer plus the general additives of the assay. BSA+: Assay in the high salt buffer. GTP: GTP added to an assay with BSA in low salt buffer and the core additives (5 mM tyrosine, 3 mM cysteine and 80 mM $FeCl_2$. BRef: 40 μM HydF plus 72 μM BSA.

5.6.3 Different ratio of HydF to HydG

To obtain data for the plotting of a binding curve, different ratios of HydG were incubated with 40 μM HydF in the low salt HydF buffer and with the core reagents 5 mM L-tyrosine, 3 mM cysteine and 80 μM $FeCl_2$. ImageJ analysis (Figure 5.13) revealed that a ratio of 1:1.8 HydF:HydG is necessary to obtain a complete complex of HydF and HydG.

Therefore, this ratio was kept for the following pull-down assays.

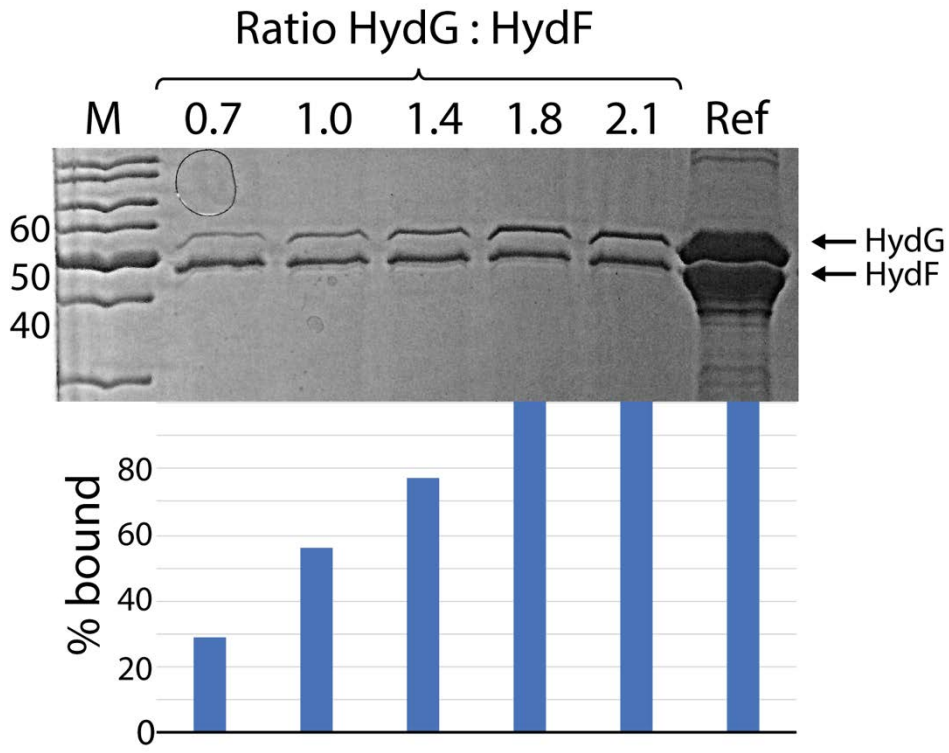

Figure 5.13: SDS-PAGE and bar-chart analyzing the pull-down assay carried out with 40 μM HydF and different ratios of HydG (as indicated). Ref: 40 μM HydF + 40 μM HydG.

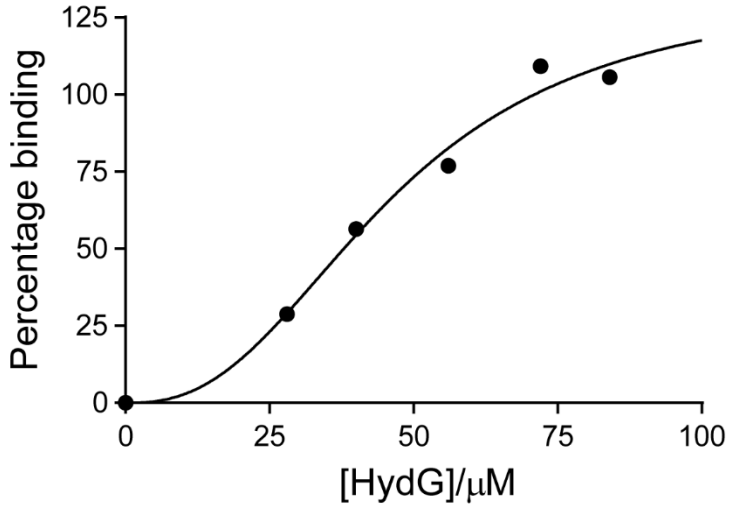

Figure 5.14: Binding curve representing the binding of HydG to HydF. The curve was fitted to specific binding with a Hill slope using GraphPad.[401]

Table 5.6: List of parameters for the fitting of the data to a specific binding with a Hill slope (Figure 5.14).

Protein: Protein	B_{max}/ %	Hill slope h	K_d/ μM	R^2
HydF:HydG	134.8 ± 29.4	2.5 ± 0.8	46.7 ± 10.0	0.99

The obtained data from the HydG:HydF binding with different HydG ratios has been plotted and fitted to a specific binding curve with a Hill slope (Figure 5.14). Resultant parameters from the fitting are summarized in Table 5.6, including a K_d of 46.7 μM, which is greater than the previously reported K_d of 1.3 μM[253]. The Hill slope h of 2.5 indicates the presence of multiple binding sites with positive cooperativity, whereas B_{max} gives the maximum specific binding at 135 %.[401]

Adapting the assay on the basis of these results (Figure 5.13 and 5.14), the subsequent assays were carried out with the necessary HydG concentration to obtain the complete complex formation (100% bound at 72 μM, 1.8 ratio).

Since depletion of cysteine from the complex forming reaction mix did not decrease the amount of complex formed, it was removed from the core reactants. Besides BSA, *Burholderia pseudomallei* TrmD (kindly provided by Josh Prince) was used as a control for complex formation. The high salt in comparison to the low salt buffer was tested once more. Addition of cysteine or GTP to the core reagent mix was assessed for influencing the complex formation as well as depletion of tyrosine or $FeCl_2$. GTP (3 mM) was also added to the control reactions with BSA and TrmD, to evaluate if it generally induces dissociation. Resultant SDS-PAGE and analysis with Image J is shown in Figure 5.15 and 5.16.

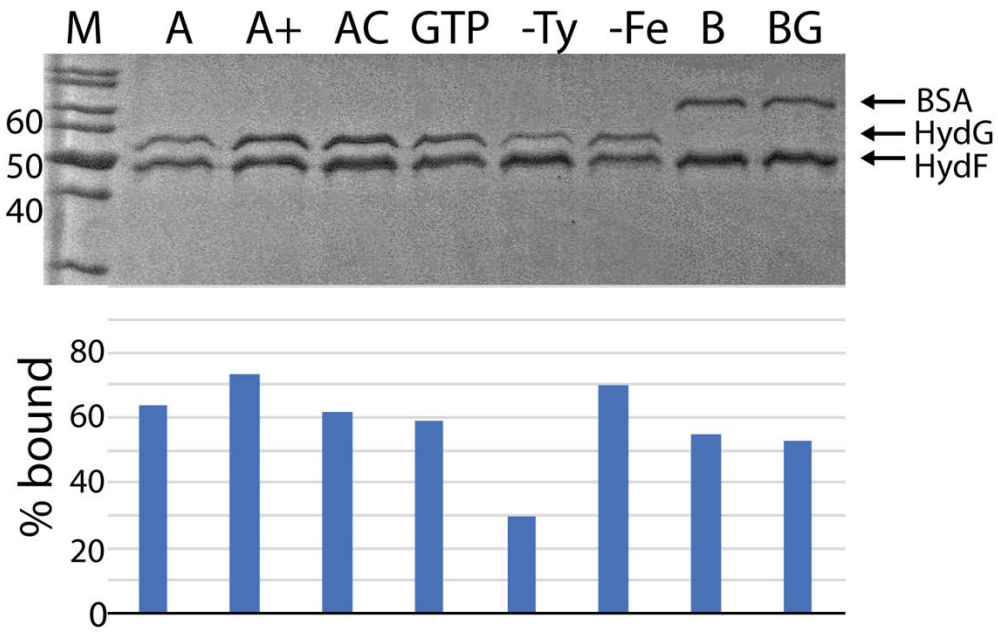

Figure 5.15: SDS-PAGE and bar-chart analyzing the pull-down assay carried out with 40 μM HydF and 72 μM HydG or BSA. A: Assay with low salt buffer; A+: Assay in high salt buffer. AC: Assay with 3 mM cysteine added in the reaction; GTP: Assay with 3 mM GTP added; -Tyr: Assay without tyrosine; -Fe: Assay without added iron; B: BSA control assay, BG: BSA control assay with added GTP.

Highest complex formation was achieved in the assay with the standard high salt buffer, indicating that the salt content of the buffer does not influence the complex formation, since previously the low salt buffer seemed to increase the chance of binding. As reported earlier (Figure 5.9, 5.10 and 5.11), addition or depletion of cysteine does not have an effect on the protein-protein binding. Surprisingly, in this set of assays with higher concentration of the binding partner GTP did not promote dissociation of the complex, neither for HydG, BSA or TrmD (Figure 5.14 and 5.15). Another negative point is the amount of BSA or TrmD bound to HydF. Around 50% of the proteins BSA and TrmD remain bound to HydF after elution from the Strep column. This could suggest unselective binding of HydF to a variety of proteins, due to its open dimeric form or to the unreliability of the pull-down assay, deriving from insufficient washing or binding of BSA and TrmD to the Strep-resin. Alternatively, the obtained results could mean that HydF has a tendency to participate in non-specific protein-protein interactions, which needs to be investigated further in the future.

To evaluate how tightly or specifically HydE binds to HydF another pull-down assay with His_6ThitHydE1265 (E1) and His_6ThitHydE1675 (E2) was carried out. This time SAM and different thiols were added to a mixture of HydF and HydE and incubated for 1 h before loaded onto the StrepTactin resin. The different thiols included cysteine, glutathione as well as a 1:1 mixture of glyoxylate and cysteine, each were added to an end concentration of 3 mM. Following a recent study on HydE[70] the 1:1 mix of glyoxylate and cysteine was tested to possibly enhance complex formation. In this study HydE was shown to bind the molecule (2*R*,4*R*)-TDA ((2*R*,4*R*)-1,3-thiazolidine-2,4-dicarboxylic acid), which is prepared by mixing cysteine and glyoxylate in a 1:1 ratio.

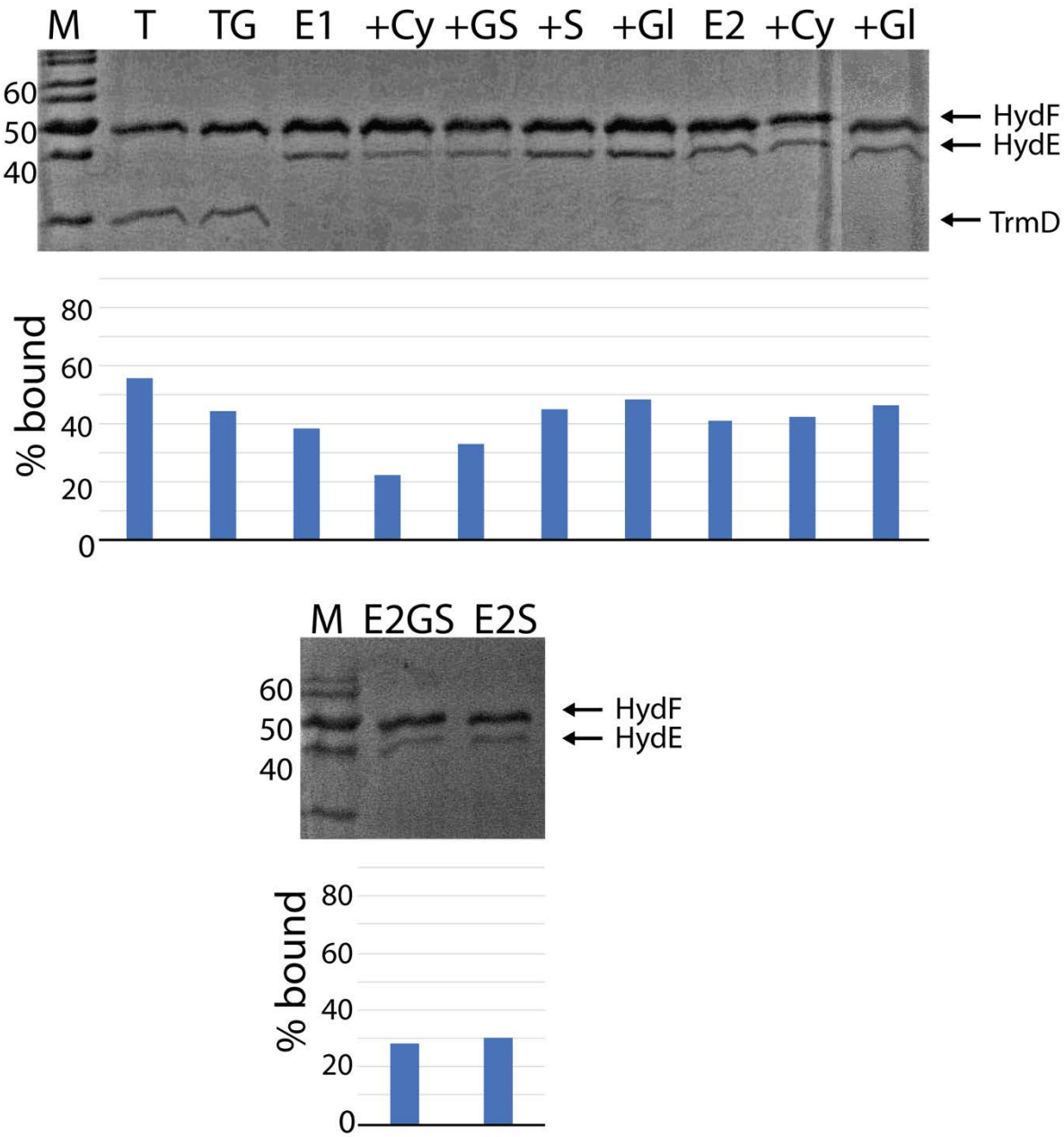

Figure 5.16: SDS-PAGE and bar-chart analyzing the pull-down assay carried out with 40 μM HydF and 72 μM HydE1265 (E1), HydE1675 (E2) or TrmD (T). Lanes described from left to right. T: Same assay conditions as standard HydF/HydG assay with TrmD replacing HydG as a control; TG: Same as T with added GTP; E1: Assay with HydF and HydE1265 without any additives; +Cy: Same as E1 with added cysteine; +GS: Same as E1 with added glutathione. +S: Same as E1 with added SAM; +Gl: Same as E1 with added 1:1 mixture of glyoxylate and cysteine; E2: Assay with HydF and HydE1675 without any additives; +Cy: Same as E2 with added cysteine; +Gl: Same as E2 with added 1:1 mixture of glyoxylate and cysteine. Bottom: E2GS: Same as E2 with added glutathione; E2S: Same as E2 with added SAM.

The resultant SDS-PAGEs in Figure 5.16 show a relatively low extent of complex formation (40-50%) between StrepHydF and the His_6ThitHydE constructs. Basically, the binding between StrepHydF and His_6BpTrmD is of the same scale as the binding with HydE, suggesting the affinity of HydE is roughly the same as a non-specific

binding partner TrmD and therefore making it difficult to draw any deeper conclusions. However, the main trend for binding with HydE1 seems to be enhanced when SAM or (2*R*,4*R*)-TDA is present, whereas for HydE2 cysteine and (2*R*,4*R*)-TDA gave the best results.

5.6.4 The pH dependent binding of HydF to HydG

An important observation was made when the solutions used to prepare the tyrosine stock were changed and freshly prepared. Tyrosine was dissolved in 200 mM HCl (350 μL) and neutralized with 1 M NaOH. By using the fresh tyrosine stock the extent of complex formation between StrepHydF and His_6HydG dropped drastically.

In order to assess this observation, assays were been carried out with varying pH of the tyrosine stock (Table 5.7), to evaluate the effect of the pH on the binding event. The same assay conditions as previously were used, except with higher concentration of HydG, meaning 40 μM HydF was mixed with 80 μM HydG, 5 mM tyrosine and 80 μM $FeCl_2$ in low salt HydF buffer.

Table 5.7: Amounts of 1 M NaOH and buffer added to 350 μL of the tyrosine stock in 200 μM HCl and the resultant pH of the neutralized Tyr stock and the assay mixture.

Add. 1 M NaOH	Add. buffer	pH (20 mM Tyr stock)	pH (assay mixture)
65	35	8	8
70	30	9	8
75	25	10	9
80	20	11	9
85	15	12	10
90	10	13	11
95	5	14	11

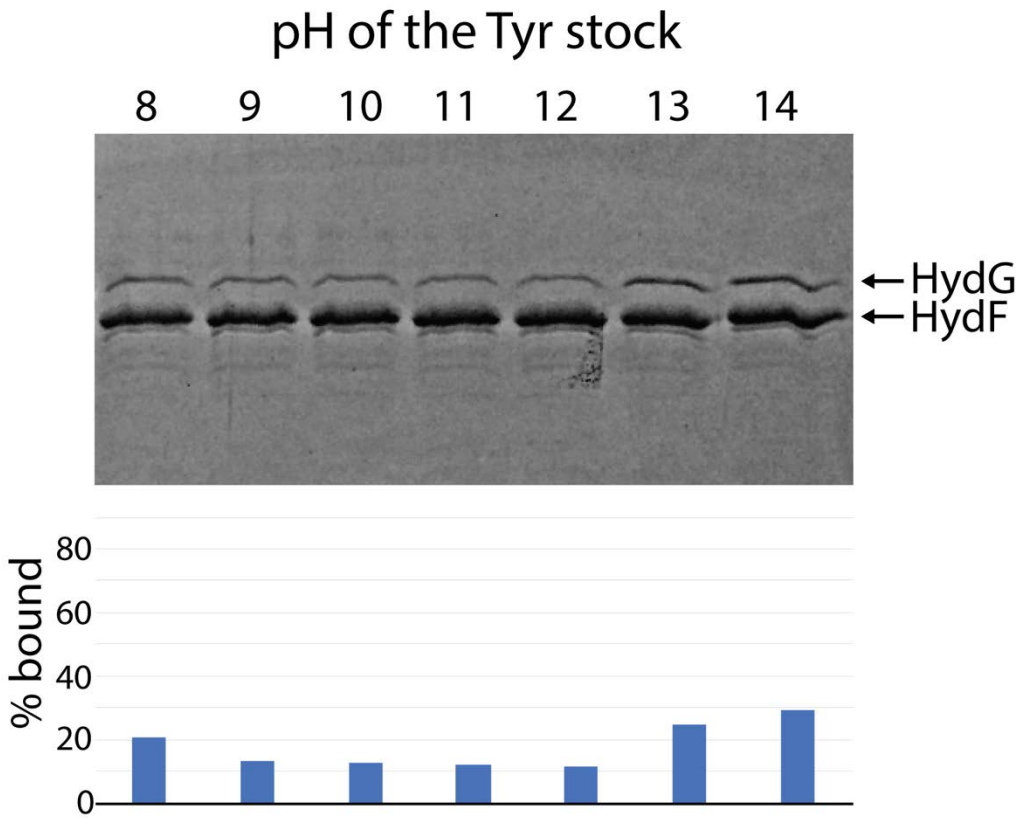

Figure 5.17: SDS-PAGE and bar-chart analyzing the pull-down assay carried out with 40 μM HydF and 80 μM HydG with varying pH of the tyrosine stock (25 μL to 100 μL reaction) added.

What can be observed from the SDS-PAGE in Figure 5.17 is the fact that the higher the pH of the tyrosine stock the higher the apparent binding of HydG to HydF. Nevertheless, the amount remained bound (30%) is extremely low in comparison to earlier studies (Figures 5.9 to 5.16).

The SDS-PAGE in Figure 5.18 supports these observations from Figure 5.17, where the assay with the highest pH of 11 gave the highest binding between HydF and HydG. It was expected that a pH in the physiological range (around pH 7) would give the best conditions for binding, as the proteins are presumably evolved to operate in an approximately neutral bacterial cytoplasm. Interestingly, two lyases expressed from *Thermoanaerobacter italicus* Ab9 exhibited an optimal activity above physiological range at a pH of 9.[402] Nonetheless, since in the previous chapter 3 both the activity assays of HydF (Section 4.4.1, Figure 4.19 and 4.20) as well as HydG (Section 4.3.3 to 4.3.5, Figure 4.7 to 4.15) and HydE (Section 4.3.3 to 4.3.5, Figure 4.7 to 4.14) were measured at a pH of 7.4 (HydG and HydE) or pH 8.0 (HydF), having similar activities

to previously reported [FeFe]-hydrogenase maturation enzymes it is unlikely that a pH of 11 is optimal for the enzymes.

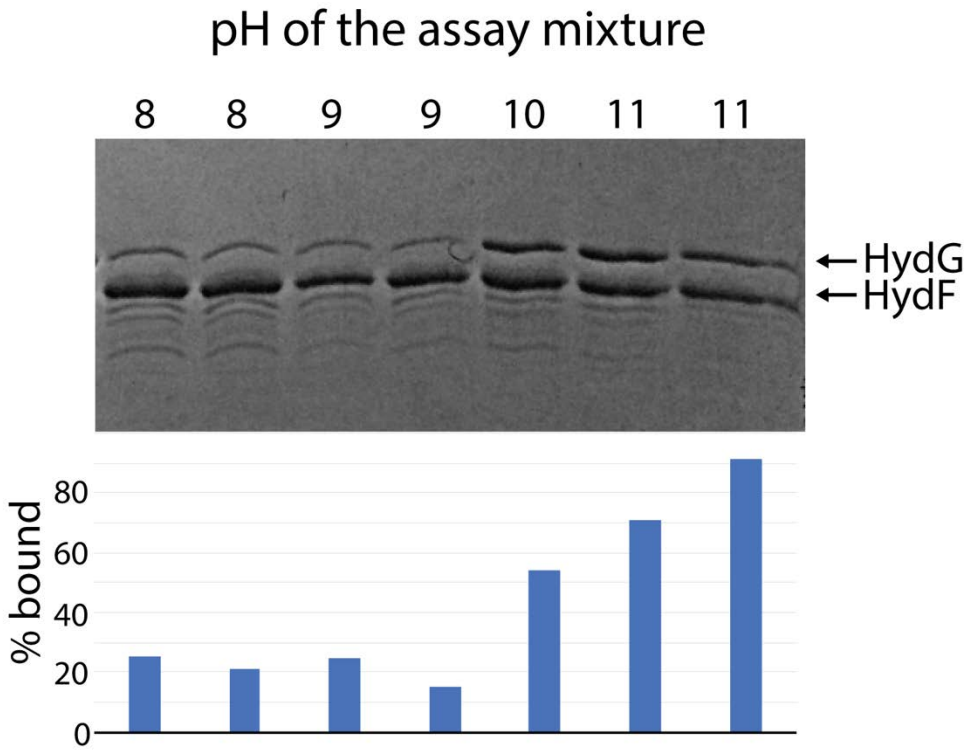

Figure 5.18: SDS-PAGE and bar-chart analyzing the pull-down assay carried out with 40 μM HydF and 80 μM HydG in varying pH conditions.

Assays that were measured at a pH of 7.0 or 8.0 were not showing more than 30% binding of HydG to HydF (Figure 5.18). Interestingly, the previously assigned requirement of tyrosine for HydF:HydF complex formation might have been interpreted wrongly, since the tyrosine solution most likely increased the pH which might have caused better binding outcomes according to Fig. 5.18.

5.6.5 Pull-down assay with all maturases

Nonetheless, a final assay experiment with all [FeFe]-hydrogenase maturation enzymes was tested in a 1:1:1 ratio, each at a concentration of 80 μM. Additives were 1 mM tyrosine, 1 mM SAM, 1 mM $FeCl_2$ for all reactions. Variations in the supplements are summarized in Table 5.8.

Table 5.8: Composition of pull-down assays represented in Figure 5.19.

Lane	HydE1 or HydE2	Cys or GSH (1 mM)	Dithionite or TCEP (1 mM)
1	HydE1	Cys	-
2	HydE2	Cys	-
3	HydE1	GSH	-
4	HydE2	GSH	-
5	HydE1	Cys	Dithionite
6	HydE2	Cys	TCEP
7	HydE1	Cys	Dithionite

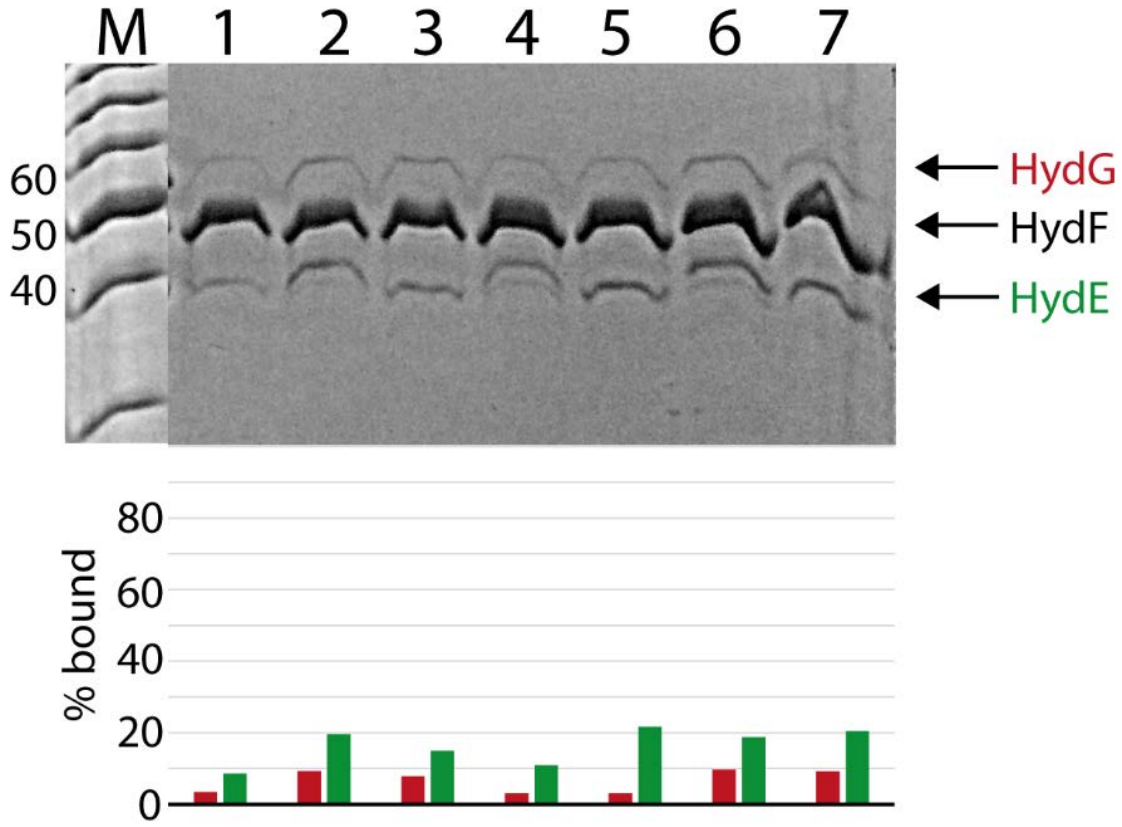

Figure 5.19: SDS-PAGE and bar-chart analyzing the pull-down assay carried out with 80 μM HydF, 80 μM HydG and 80 μM HydE (HydE1265 or HydE1675). Each assay was prepared in low salt HydF buffer and with added 1 mM tyrosine, 1 mM SAM and 1 mM $FeCl_2$. Further additions can be either 1 mM cysteine or glutathione and 1 mM dithionite or TCEP.

Even though the resultant binding between HydF and HydG and/or HydE was very low (maximum 20%), a clear trend could be observed. The binding between HydF and HydE seems to be favored, possibly with higher affinity, than binding to HydG. This observation is in accord with the binding affinities reported for the SPR experiments of StrepCaHydF with His_6CaHydG and His_6CaHydE which reported lower K_d values for

the binding of HydF to HydE than for HydG.[253] Addition of a reducing agent (lane 5-7) had a positive effect on the formation of an HydF-HydE complex.

5.6.6 Pull-down assay after turnover

In context of the activity assays, described in Chapter 4.6, a large scale reaction (500 μL) was prepared and applied to a small StrepTactin column (100 μL of resin) used for the pull-down assays. The hypothesis was that a higher degree of binding HydG or HydE to HydF might occur after multiple turnovers. An overview of the components of each reaction is summarized in Table 5.9. In this case the reaction was analyzed only qualitatively (SDS-PAGE, Figure 5.20) to investigate if the partner enzymes remained bound after the activity assay.

Table 5.9: Components of activity assays loaded onto StrepTactin resin to carry out a pull-down assay.

	R1	**R2**	**R3**	**R4**
HydF (μM)	25	50	50	50
HydE (μM)	25	25	25	25
HydG (μM)	25	150	150	75
SAM (μM)	500	500	500	500
Tyr (mM)	1	1	1	1
Cys (μM)	200	200	200	200
Fe (μM)	200	200	200	200
GTP (mM)	2	2	2	2
DTH (mM)	1	1	1	1
DTT (μM)		300	300	-
PLP (μM)		500	500	-
S (μM)		200	200	-
GSH (μM)		200	200	-

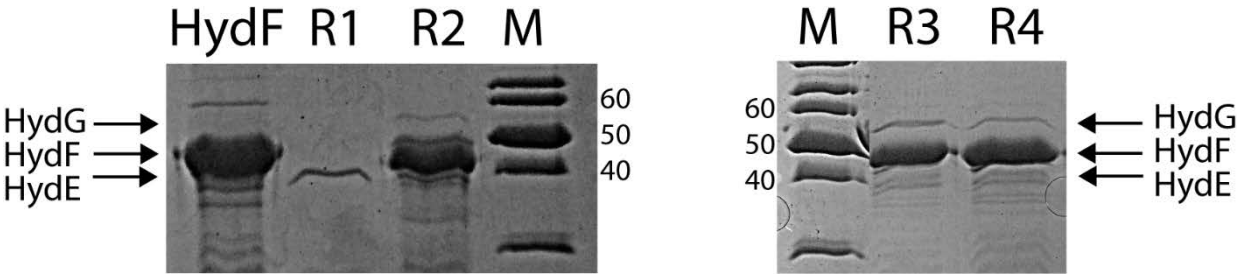

Figure 5.20: SDS-PAGES analyzing the pull-down assay carried out with the activity reactions summarized in Table 5.9.

The resultant SDS-PAGE (Figure 5.20) of the pull-down assay from the activity reactions, shows surprisingly only HydE for reaction 1 (R1), which might be due to a mistake with the elution buffer, since HydE does carry a His_6-tag and shouldn't bind to the StrepTactin resin. The remaining three reactions (R2-R4) share a similar outcome, very little HydG seemed to be bound after the reaction, even if added in a 3-fold excess. Detecting HydE on the SDS-PAGE is difficult since it is very close to the intense HydF protein band. However, in R2 (Figure 5.20) the HydE band is stronger than the HydG band, which corresponds to the observation made for the pull-down assay where HydE had a higher affinity to HydF than HydG (Section 5.6.4). For lane R3 and R4 both the HydE and HydG protein band are very weak and almost not visible. To summarize, for the conditions tested, both enzymes HydG and HydE seem to dissociate from HydF after the enzyme reaction.

5.7 Protein crystallization experiments with HydF and HydG

5.7.1 Crystallization experiments for *holo*-HydF and for the hetero-complex HydF:HydG

Due to the fact that until May 2017[244] only an *apo*-crystal structure of HydF had been reported,[243] the first attempts at crystallization were with reconstituted HydF with or without the substrate GTP or pdt-mimic. After the production of a sufficient amount of HydF, as described in Chapter 2 (Section 2.3.3), HydF could be concentrated to concentrations of up to 2 mM. Additionally, to obtain crystals of a HydF:HydG hetero-complex different conditions, additives and ratios of HydF to HydG were also screened.

The first conditions tested are summarized in Table 5.10. These conditions were tested with the commercial broad screen Hampton PEGRx in sitting drips (with varying polymers, polymer molecular weights, pH and secondary reagents.). The three different sitting drops represent varying conditions for the crystallization of HydF, one without any additives (Drop 1), the following with the HydF substrate GTP (Drop 2) and the third drop containing additionally to GTP the partner maturase HydG and the HydG substrate SAM (Drop 3).

Table 5.10: Initial screening conditions tested for crystal growth in a 96-well sitting drop plate.

Stocks	**Drop 1**	**Drop 2**	**Drop 3**
HydF (400 μM)	400 μM	360 μM	300 μM
GTP (50 mM)		2.5 mM	2.5 mM
HydG (2 mM)			300 μM
SAM (80 mM)			4 mM

HydF and HydG stocks were in the following buffer tabulated in Table 5.11.

Table 5.11: Buffer components of HydF and HydG storage buffers.

	HydF	**HydG**
HEPES (mM)	25	20
Salt (mM)	300	500
DTT (mM)	1	5
Glycerol (% w/v)	5	10
pH	8.0	7.4

Unfortunately, only colorless crystals were obtained (Figure 5.21), which were first suspected to possibly correspond to GTP or to a protein structure missing iron-sulfur cluster but turned out to be unidentified salt crystals when tested at the Diamond Light Source. An exemplary diffraction pattern of a protein in comparison to a salt crystal is shown in (Figure 5.22). Both diffraction patterns differ in the occurrence and symmetry of diffraction spots, with many spots across all resolution levels (low, mid and high) for protein crystals and sporadic spots at mid high resolution for salt crystals.[403]

Figure 5.21: Colorless crystals observed for the HydF + GTP condition (Drop 2) in the Hampton PEGRx screen.

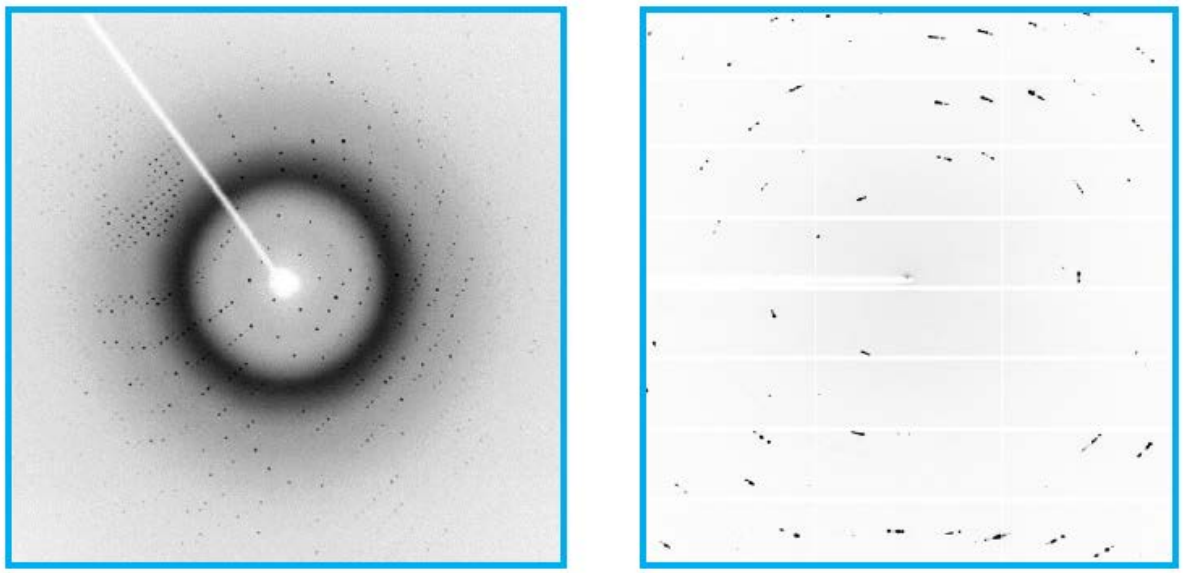

Figure 5.22: X-Ray diffraction pattern of a protein crystal (left) and a salt crystal (right). From [404].

Another screening experiment for crystallizing HydF in its *holo*-form or in complex with the H-cluster pdt-mimic was attempted, this time using four different commercial screens, Hampton PEGRx, Molecular Dimensions JCSG+ (different salt and PEG conditions), PACT premier (different anions and cations, pH using PEG as precipitant) and Midas (optimized for complexes, different polymer precipitants, physiological pH and salt concentrations). The corresponding conditions, screened are listed in Table 5.12. For these crystallization conditions the HydF buffer was depleted of DTT to ensure that the pdt-mimic is able to coordinate the [4Fe4S] cluster of HydF.

Table 5.12: Crystallization conditions for obtaining holo-HydF and GTP or pdt-mimic bound HydF.

Stocks	Drop 1	Drop 2	Drop 3
HydF (1 mM)	1 mM	900 μM	920 μM
GTP (50 mM)		5 mM	-
Mimic (50 mM)			2 mM

Conditions that gave potentially promising particles, but not identified as HydF crystals at this stage, (Figure 5.23), were tested at Diamond Light Source with no positive result for diffraction. Attempts to reproduce the potential crystals under similar conditions did not result in crystal formation.

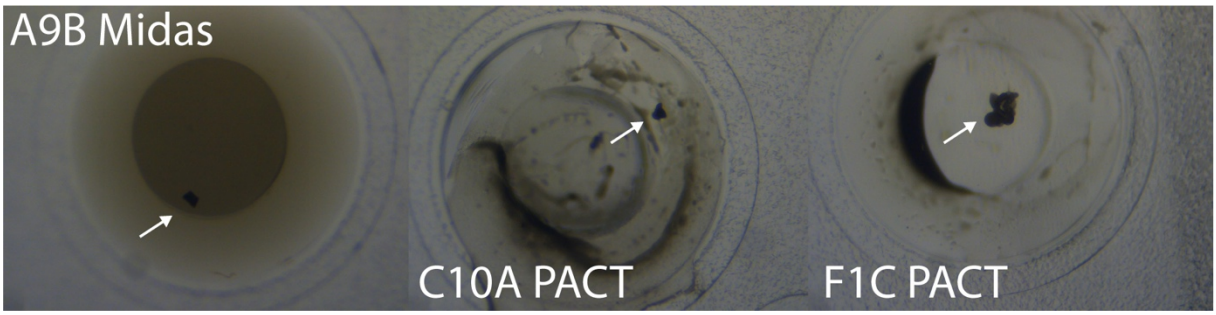

Figure 5.23: Promising crystallization conditions for HydF. A9B Midas: Drop B conditions in 0.1 M MES, 25% (v/v) pentaerythritol (5/4 PO/OH), pH 6.0. C10A PACT: Drop A conditions in 0.2 M Magnesium chloride, 0.1 M HEPES, 20% (w/v) PEG 6000, pH 7.0. F1C PACT: Drop C conditions in 0.2 M Sodium fluoride, 0.1 M Bis-Tris-propane, 20% (w/v) PEG 3350 pH 6.5.

After obtaining the results of the pull-down assays, and thus with the knowledge that tyrosine might be crucial for hetero complex formation of HydF:HydG, another set of crystallization experiments were carried out. Conditions are summarized in Table 5.13 and 5.14.

In addition to tyrosine, SAM was added to the conditions and for drop 2 and 3 also a reducing agent (TCEP or dithionite) to induce the reaction.

Table 5.13: Crystallization conditions to obtain a crystal structure of the hetero complex HydF:HydG in 1:1.7 ratio.

Stocks	Drop 1	Drop 2	Drop 3
HydF (1.5 mM)	350 μM	350 μM	350 μM
HydG (1 mM)	580 μM	580 μM	580 μM
SAM (80 mM)	5 mM	5 mM	5 mM
Tyrosine (20 mM)	2.5 mM	2.5 mM	2.5 mM
TCEP/dithionite (100 mM)	-	2 mM TCEP	2 mM dithionite

To provide a simple analogue of the iron synthon that might potentially bind to the auxiliary cluster in HydF, the conditions in Table 5.13 were supplemented with Fe^{2+} and cysteine (Table 5.14).

Table 5.14: Modified crystallization conditions to obtain a crystal structure of the hetero complex HydF:HydG in 1:2 ratio.

Stocks	Drop 1	Drop 2	Drop 3
HydF (1.3 mM)	1.3 μM	340 μM	340 μM
HydG (1.3 mM)		680 μM	680 μM
Mimic (50 mM)	5 mM	-	-
SAM (80 mM)		5 mM	5 mM
Fe^{2+} (100 mM)		1 mM	1 mM
Cysteine (100 mM)		1 mM	1 mM
Tyrosine (20 mM)		2.5 mM	2.5 mM
TCEP/dithionite (100 mM)	-	2 mM TCEP	2 mM dithionite

Despite all the efforts and tested conditions no protein crystal growth was observed. Potential reasons for the lack of success with these crystallization screening experiments are numerous. One reason might be in the handling and preparation of the 96-well sitting-drop plates, such as too long exposure of the tiny drops in the glovebox atmosphere that might have caused drying, or not properly sealed crystallization plates, that might have caused evaporation outside the well/plate. Another potential reason could have been the atmosphere of the glove box, which might have caused oxidative damage of the anaerobic proteins, depending on the sensitivity of the clusters. Non-optimal protein concentrations, inhomogeneous protein samples or incomplete reconstitutions are other possible factors, although protein concentrations were kept above 10 mg/mL, which is often regarded as a reasonable concentration for crystallization screening.

5.8 Investigating the binding constant between HydF and HydG with ITC

An important method to determine binding constants is isothermal titration calorimetry as described in 5.2. Before starting to study the binding constants on the formation of a hetero complex of HydF:HydG, a preliminary study of GTP binding to HydF was evaluated to establish the ITC method inside the glovebox. Since a K_d value of HydF binding to GTPγS is already known,[252] as shown in Table 5.15, this is a good model system to evaluate the method in the glove box. To obtain a realistic value of the dissociation constants, the experiments need to be carried out in an anaerobic environment, such as in a glovebox, because the iron-sulfur cluster cofactors of HydF and HydG are extremely sensitive to oxygen.

Table 5.15: ITC experiment at 25°C in 25 mM Tris-HCl pH 8.0, 200 mM KCl, 1mM $MgCl_2$. A 500 mM stock of GTPγS was titrated into protein solution of 75 μM. Data taken from Galazzo *et al.*[252]

Sample	titrant	n	ΔH (cal mol^{-1})	ΔS (cal mol^{-1} deg^{-1})	K_d (μM)
HydF	GTPγS	0.594	-2873 ± 28.36	17.9	0.96 ± 0.09[252]

For the protein concentration, 50 μM was chosen for HydF and GTP concentrations were ranging between 0.6-60 mM.

As a general rule of thumb the protein concentration in the sample cell should be at least 10 times higher than the expected K_d.[405] Most commonly, concentrations between 30-60 μM are used for the protein. The concentration of the titrant is usually 10-20 fold higher than the protein concentration, to ensure a 2:1 or 4:1 titrant: sample cell ratio in the end. It is particularly important for ITC experiments that the titrant is in the exact same buffer and pH as the sample cell solution (i.e. the buffers at 'matched'), to minimize heating effects that occur upon mixing differing buffers.

In Figure 5.24 and 5.25 exemplary outcomes of the ITC experiments are shown. For the buffer DTT was removed as it causes erratic baselines and possibly alters the activity of the protein. The standard HydF buffer (25 mM HEPES, 300 mM KCl, 5% (w/v) glycerol, pH 8.0) was used for all solutions required for the ITC measurements.

Noise corrected spectra were re-analyzed with the online application AffinityMeter[406,407] using a 1:1 binding model (result sheets in the appendix 5.1). Two different concentrations for HydF were analyzed, once with the concentration of the whole monomer (50 μM) and the other with the concentration of the dimer HydF (25 μM). Therefore, a model for N = 1 and N = 0.5 was generated. However, due to high noise and defective data, the resultant calculated thermodynamic parameters have a very high error and it is not possible to draw any conclusion from this data.

Despite several attempts the titrations were always accompanied by high levels of background noise in the enthalpy output of each addition of titrant. Reasons for this might lie in not adequately degassed buffers; however, buffers were stirred in the glove box overnight, prior to the ITC experiment. Since HydF is expected to be hydrolyzing GTP to GDP under non-reducing conditions, the reaction might have taken place when the substrate was added to HydF producing an enthalpy that influenced the binding enthalpy and therefore it was not possible to measure the binding event itself. Another observation made was when the pressure of the glove box changed by touching one glove or by opening the door the titration peak went into positive enthalpy values instead of negative, which might mean that oxygen diffused into the box if the pressure changed. Other possible reasons for noisy spectra might be the iron-sulfur cluster causing unexpected signals by oxidative damage. Furthermore, a dirty reaction cell with possible deposits might be responsible for the noise obtained, although thorough cleaning was carried out before the experiment. The interaction in Figure 5.25 might not be in the detectable range of the instrument.

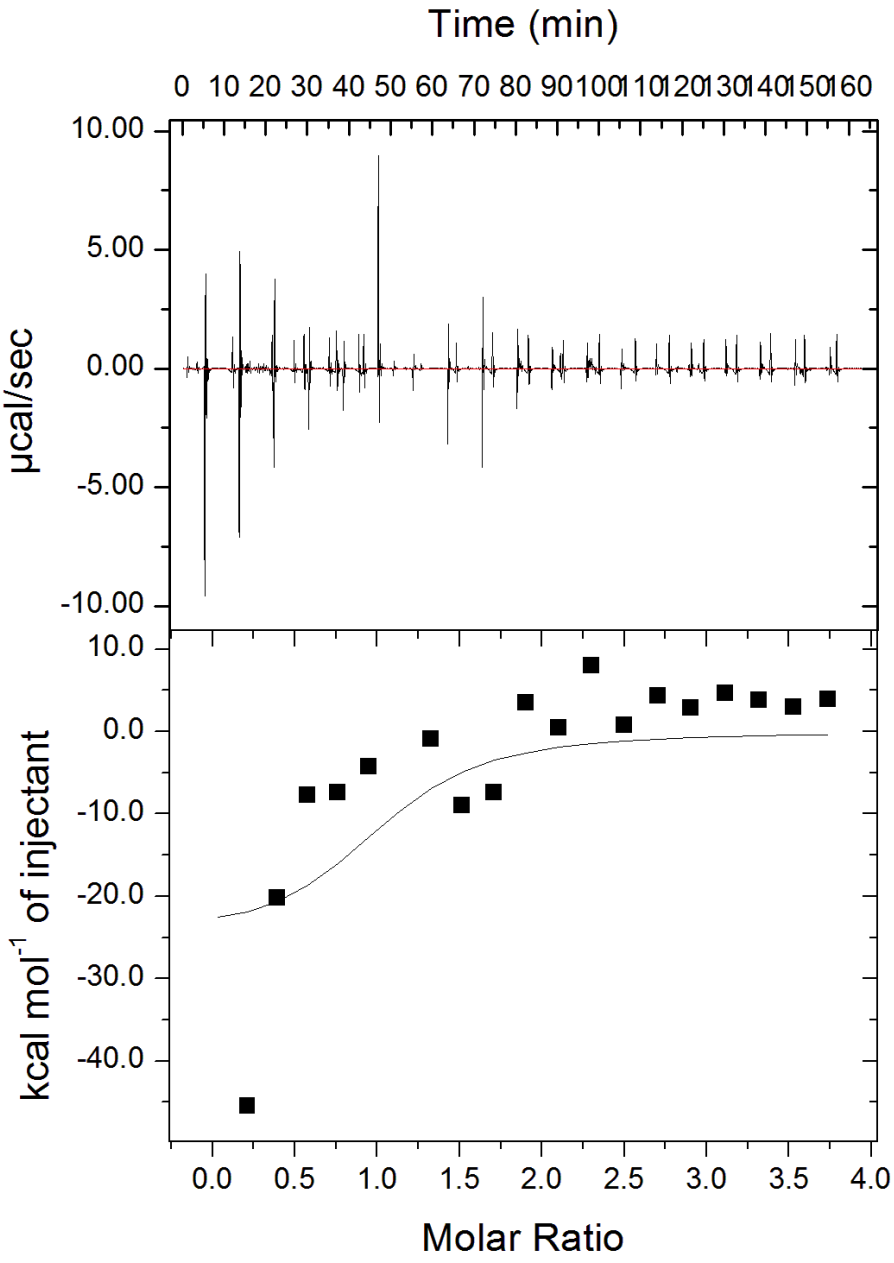

Figure 5.24: Uncorrected raw data of the ITC experiment 300617: 900 µM GTP (Titrant), 50 µM HydF (Sample).

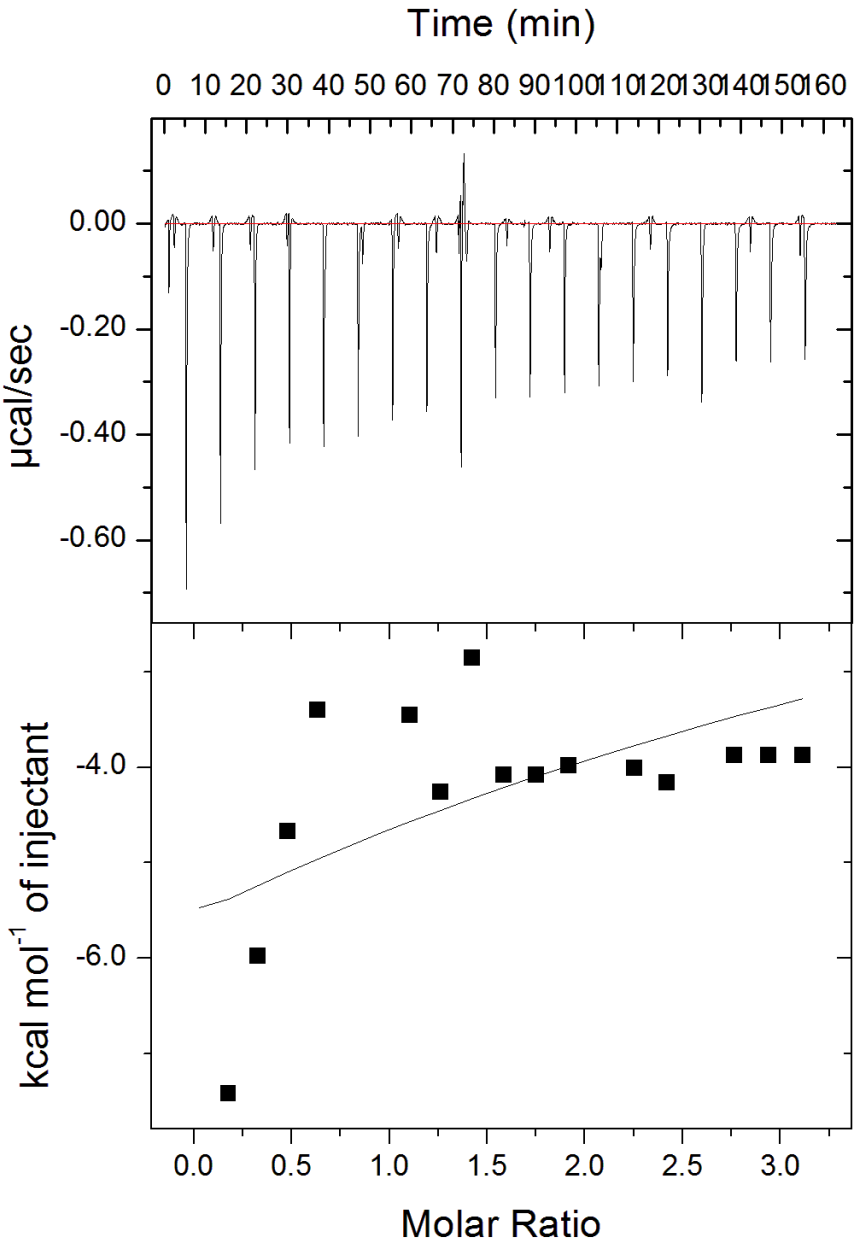

Figure 5.25: Uncorrected raw data of the ITC experiment 060717: 750 µM GTP (Titrant), 50 µM HydF (Sample).

5.9 Summary and conclusions

In this chapter the interaction of the [FeFe]-hydrogenase maturation proteins HydE, HydG and HydF from *Thermoanaerobacter italicus* has been studied with size-exclusion chromatography, pull-down assays, isothermal titration calorimetry and with the attempts to grow crystals of *holo*-HydF and a hetero HydF:HydG complex.

The multimeric state of reconstituted and freshly purified HydF and with reconstituted HydG was studied in solution *via* size exclusion chromatography. Whereas, un- and reconstituted HydF is known to form a dimer in solution,[244] reconstituted HydG persists as a monomer in solution.[269] Mixing reconstituted HydF and HydG together with incubation did not lead to the formation of a HydF:HydG complex eluting from the size exclusion column as estimated by the chromatogram and SDS-PAGE. This might indicate that specific substrates or special buffer adjustments are necessary for HydG to form a complex with HydF.

To study the effects of compounds and/or conditions on complex formation, pull-down assays have been assessed as a possible method for quick screening. Initially components were added to HydF and HydG that were known to bind to either enzymes or affect their enzyme activity. These compounds included tyrosine, iron(II), cysteine and dithionite (Chapter 4). An assay mixture containing all these components plus the appropriate enzymes HydF and HydG was evaluated as well as assay mixtures with one missing component. Omitting dithionite increased resultant binding whereas deleting tyrosine decreased the binding outcome between HydF and HydG. Tyrosine seems to play an important role for the interaction between HydG and HydF, possibly by inducing conformational changes in HydG and might be crucial for complex formation. Changing the salt composition of the buffer did not have a great influence on binding, however to ensure electrostatic interactions were not perturbed, the salt content was lowered from 300 mM to 30 mM. Addition of GTP to the pull-down assay seemed to have decreased the yield of the HydF:HydG complex, but unfortunately not consistently. Furthermore, experiments replacing HydG with BSA or TrmD as a control assay resulted in a comparable amount of HydF complexed with BSA or TrmD, which might suggest that HydF is binding unspecifically to these enzymes. Indeed, the HydF dimer exhibits an open protein structure with a lot of surface exposed to the solvent for possible interactions.[243] Since there are no studies on the binding-selectivity of HydF,

it might be possible that HydF has a tendency to form non-specific protein-protein complexes.

The pull-down assays were extended to the second HydF interaction partner HydE (ThitHydE1265 and ThitHydE1675) with and without additives that might influence the binding between the two enzymes. Chosen additives were SAM, L-cysteine, reduced glutathione and a 1:1 mixture of glyoxylate and L-cysteine based on previous studies with HydE.[70,65] No clear trend could be observed in dependence of the additives, if compared to an assay without any additives and with the control reaction with BSA and TrmD. Nonetheless, this might indicate that the thiol-containing substrate of HydE is not required for the binding between HydF and HydE.

Changing the solutions to make up the tyrosine stock revealed an important pH dependence of the binding event. Higher pH seemed to have increased the likelihood of HydF binding to HydG, BSA and TrmD. Carrying out the assay at physiological pH range dropped the formation of a HydF:HydG hetero complex significantly. Assays carried out before this observation, probably had a higher pH than 8. Further optimization is need to obtain better complex formation in the physiological pH range.

To investigate which of the radical SAM enzymes HydG or HydE binds tighter to HydF, an assay with all three [FeFe]-hydrogenase maturation proteins at physiological pH was set up. Additives included L-tyrosine, SAM and $FeCl_2$ for all reactions. Interestingly, HydE seemed to be binding with higher affinity to HydF than HydG (up to 20% binding), as has been reported before.[253]

Increasing the scale of the pull-down assay could have a positive effect on the consistency of the results, as the error caused by small amounts transferred with the pipette might decrease. Furthermore, using another affinity-tag (such as GST) or additionally NiNTA-affinity resin for the His_6-tagged proteins, could help elucidate the main trends in [FeFe]-hydrogenase maturases even further.

Trials to grow crystals of holo-HydF or a HydF:HydG hetero complex were unsuccessful. Even though four different broad screens were tested (384 conditions in total) for varying protein conditions, only colorless salt crystals or dark protein aggregates were obtained. Three HydF crystal structures are reported in the literature, which were either obtained in *apo*-form (TnHydF, 3QQ5[243] and TmHydF, 5LAD[244]) or in *holo*-form (TmeHydF, 5KH0[244]). Both crystal structures in *apo*-form obtained hits

in the PGA screen (poly-γ-glutamic acid polymer (PGA), Molecular Dimensions) and TnHydF crystals were also observed in the PACT screen (Molecular Dimensions).[243,244] On the other hand, crystal growth of HydF in *holo*-form was detected in the PEGRx 1 screen (Hampton Research) and manually optimized further.[244] The PACT and PEGRx1 screen were also tested for ThitHydF but did not gave any hits. Reasons for not obtaining protein crystals can have very different sources including oxidative damage of the iron-sulfur cluster, insufficient reconstitution, to low protein concentrations, unsealed crystallization plates, slow setting up of crystallization plates, wrong protein-protein ratios, inadequate concentrations of additives, unfavorable pH, missing or slow-acting nucleation or very long crystal growth times. A thorough purification using size-exclusion chromatography with S200 Superdex resin instead of gel filtration with G25 Sephadex resin of reconstituted HydF could improve the outcome of the crystallization, as it was carried out for the previously reported HydF structures.[243,244] Nevertheless, an optimized buffer system for the separation between reconstituted HydF and FeS-colloid-bound HydF is needed.

An easy, quick and sensitive tool to estimate binding constants is ITC. To assess this method for anaerobic enzymes in the glovebox, the binding of HydF to its substrate GTP was measured. Unfortunately, the data obtained was very high in noise and estimation of the dissociation constant was not possible. Possible factors that influence the outcome of the ITC experiment are pressure changes during the experiment, inappropriate buffer, HydF hydrolyzing GTP during the titration and bubbles in the sample cell or syringe. A glovebox with constant pressure settings, exclusively used for ITC could provide a better system to measure binding constants of anaerobic proteins.

Overall, first efforts towards elucidating the interactions between the [FeFe]-hydrogenase maturation proteins HydE, HydG and HydF from *Thermoanaerobacter italicus* were undertaken with size-exclusion chromatography and pull-down assays, revealing crucial factors that influence binding. However, these methods need further optimization to selectively achieve complex formation between HydF and HydG or HydE. The correct approach for screening crucial compounds for the binding between the maturases was determined, by taking different influences into account, such as pH, buffer compositions and protein:protein ratios but must be expanded to additional methods that can be carried out in an anaerobic atmosphere. Useful techniques to

directly detect an [FeFe]-hydrogenase maturase complex and determine the stoichiometry of the complex could be scattering methods like SAXS (Small angle X-Ray scattering) or MALS (Multiangle light scattering), however a specialized set-up is needed for anaerobic proteins. To determine binding constants, an anaerobic set-up of SPR, ITC or MST (Microscale thermophoresis) would be beneficial to obtain thermodynamic data. Furthermore, NMR spectroscopy could give detailed information about the interacting residues and the dynamics of the complex. Mass spectrometry could provide a further tool to study the appearance of complexes, such as non-denaturing native mass spectrometry or IMMS (Ion mobility mass spectrometry). Another possibility to study protein-protein interactions between the [FeFe]-hydrogenase maturation proteins could be cross-linking the proteins using chemical reagents and following analysis by the above mentioned methods.

Chapter 6

Conclusions and Future Work

This thesis focused on spectroscopic, enzymatic and protein interaction studies of the [FeFe]-hydrogenase maturation enzymes from *Thermoanaerobacter italicus* HydF, HydE and HydG. In the following section, the observed results are summarized, conclusions are drawn and suggestions for future experiments are given.

6.1 Conclusion and future work concerning the expression of [FeFe]-hydrogenase maturation enzymes

Expression with pBAD vector unsuccessful for StrepHydF and StrepHydE

Prior to investigating the [FeFe]-hydrogenase maturation enzymes from *Thermoanaerobacter italicus* HydF, HydE and HydG, a sufficient amount of each enzyme was required for characterization and possible crystallization experiments. Since His_6ThitHydG has been already successfully produced and crystallized from a pBAD expression system including the ISC cluster machinery, the same system was assessed for the production of ThitHydF and ThitHydE, by introducing the genes of ThitHydF, ThitHydE1 or ThitHydE2 into the pBAD vector backbone *via* molecular cloning. However, instead of a His_6-Tag a Strep-Tag was chosen, in order to avoid conditions that might strip off the iron-sulfur cluster bound to the proteins, possibly caused by high concentrations of imidazole or by excessive iron-sulfur cluster coordination from the multi-histidine tag.

Despite a thorough optimization process including changing variables such as temperatures, induction times, variation of additives and using an optimized *E. coli* BL21 strain (Δ*iscR*) for iron-sulfur cluster production for the pBAD expression, the protein yield of StrepThitHydF did not exceed 12 mg/L of expression culture. The same was observed for the two HydE proteins StrepThitHydE1265 and StrepThitHydE1675, which either did not express or expressed with an even lower yield. Reasons for these low expression levels might lie in the fact that during the pBAD expression mixed cultures of induced and un-induced cells are produced, resulting in an inhomogeneous expression culture and causing insufficient protein production.

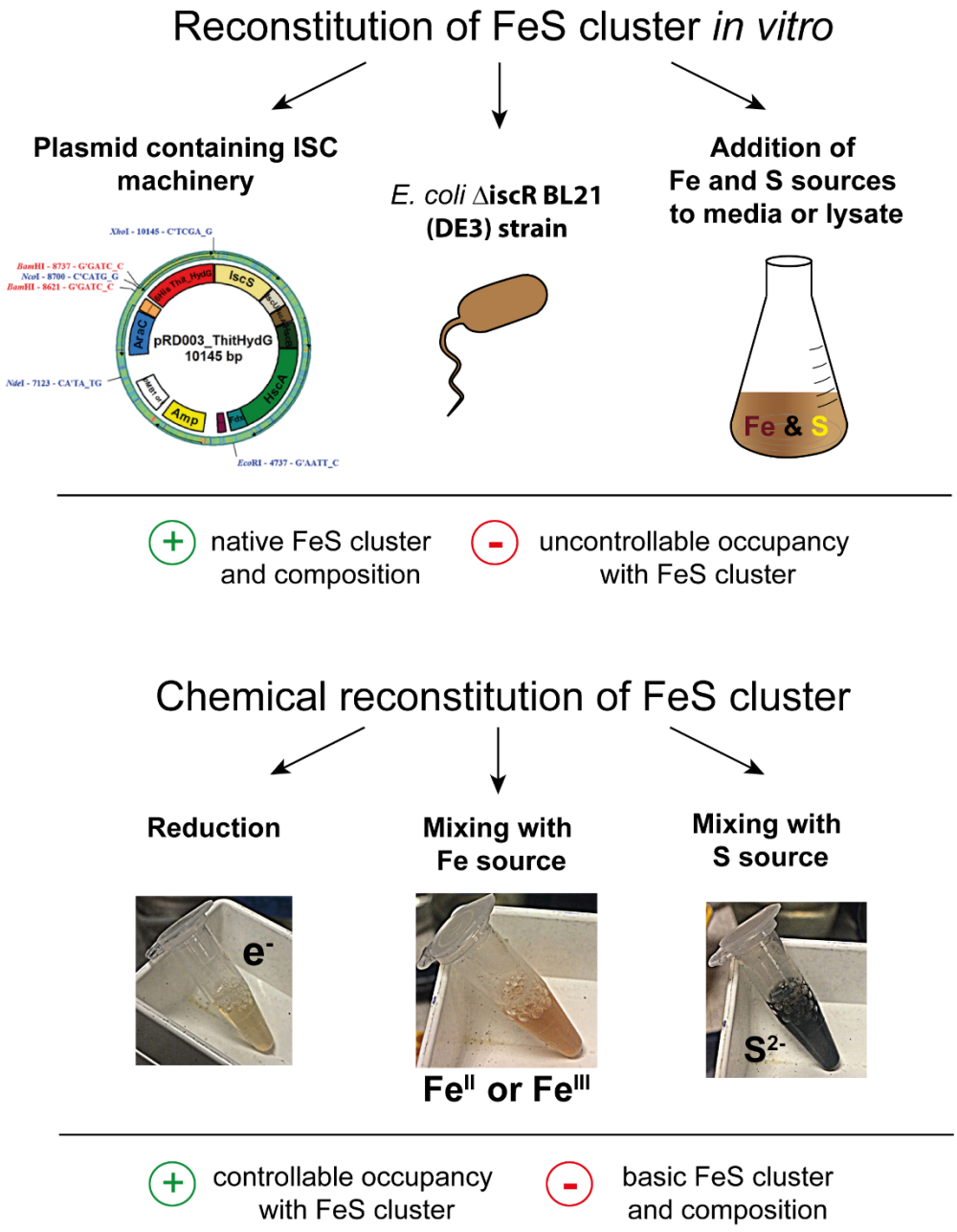

Figure 6.1: Different strategies used for iron-sulfur cluster reconstitutions: *In vitro* reconstitution and chemical reconstitution with advantages and disadvantages

Autoinduction expression with pCDuet vector lead to high yields of StrepHydF, StrepHydE and His_6HydE

As an alternative to the pBAD promoter system, the widely used T7-promotor expression system was evaluated using the pCDuet vector. In preparation of the pCDuet plasmids containing either StrepThitHydF, StrepThitHydE1 or StrepThitHydE2 genes as well as a co-expression construct with both StrepHydF and untagged HydE, the corresponding vector (pCDuet) and the synthesized plasmid containing the [FeFe]-hydrogenase maturation enzyme were digested with the same restriction enzymes. Purified fragments of interest were ligated with the T4 ligase to result in the new plasmid with the desired maturase gene. The isolated purified plasmid DNA of colonies carrying the correct plasmid was transformed into the optimized *E. coli* expression strain for overproducing iron-sulfur cluster (BL21 (DE3) Δ*iscR*). Different strategies were employed for obtaining a reconstituted protein after purification, which are summarized in Figure 6.1.

Small and medium scale expression studies revealed insufficient yields of StrepHydF with IPTG induction, whereas autoinduction seemed to be the optimal inducting method to obtain a high yield of Strep-tagged HydF and HydE of up to 30 mg of protein/L of culture (Chapter 2, Figure 2.25, 2.28 and 2.29 and Table 2.11 and 2.12). The yield could be further improved by supplementing the corresponding expression media with sources of iron and sulfur, iron(III) ammonium citrate and L-cysteine respectively. Not only did this improve protein yields of up to 38 mg of HydF per liter of culture (Chapter 2, Table 2.11), it also increased the stability and [4Fe4S]-cluster content (measured by UV-Vis spectroscopy) of HydF. A summarizing flow-chart describing the production of StrepThitHydF is shown in Figure 6.2. Co-expression of StrepHydF with untagged HydE did not yield a complex of HydF:HydE during the purification of StrepHydF.

In preparation for further pull-down interaction and biochemical studies, the affinity-tags of HydG and HydE were successfully modified *via* site-directed ligase independent mutagenesis (SLIM) resulting in His_6-tagged HydE and Strep-tagged HydG. For these constructs, the protein yield of the His_6HydE (in pCDuet vector) was very high with up to 100 mg/ L of culture. The yield of StrepHydG (in pBAD vector) was remarkably low with 0.4 mg protein per liter culture (Chapter 2, Figure 2.38 and Table 2.18). The reason behind this low yield of HydG is unknown.

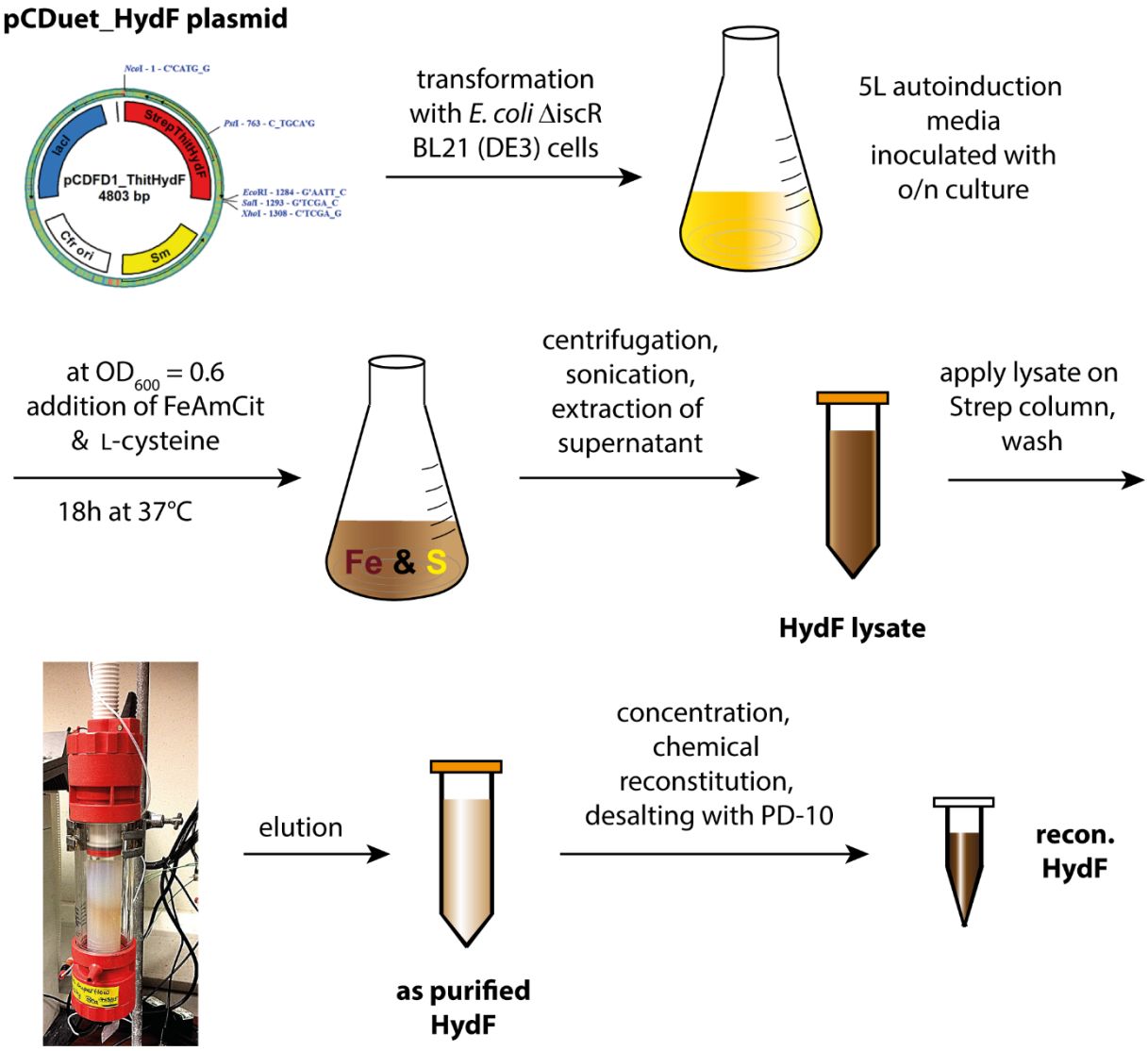

Figure 6.2: Flow chart of the StrepThiHydF production, isolation and reconstitution.

Future work

In regard to the protein yield of all [FeFe]-hydrogenase maturation enzyme constructs, a total protein yield of over 100 mg was achieved for pCDuet constructs with autoinduction. The total yield for the Strep-tagged constructs cloned into the pBAD vector was less than 58 mg and did not provide a sufficient amount of stable protein. Optimization of the pBAD expression protocol is needed for these constructs, which could be achieved by addition of L-arabinose in the early exponential phase (OD = 0.4-0.6), increasing the arabinose concentrations even higher, or addition of supplements to improve protein stability.

Concerning the cluster reconstitution state after expression of the [FeFe]-hydrogenase maturation enzymes, the maximum uptake of [4Fe4S]-cluster achieved was 23% by addition of an iron and sulfur source to the expression media. However, to obtain better uptake an iron and sulfur source could be added to the lysis buffer as well (Figure 6.1). Additionally, the autoinduction expression could be carried out in the fermenter to facilitate the formation of iron-sulfur cluster under reduced oxygen.

6.2 Conclusion and future work concerning the spectroscopy of [FeFe]-hydrogenase maturation enzymes

Glutathione optimally stabilized reconstituted HydF

The purified [FeFe]-hydrogenase maturation enzymes that were obtained in a sufficient yield but were lacking iron-sulfur clusters were chemically reconstituted and characterized by different spectroscopy methods. An absorption spectroscopy method that provides assessment of the type and amount of iron-sulfur cluster bound is UV-Vis spectroscopy and was used herein to estimate the concentration of [4Fe4S]-cluster bound in the appropriate reconstituted protein sample of HydF, HydG or HydE.

Furthermore, [4Fe4S]-cluster reconstitution of HydF was optimized towards stability by testing different reducing agents that improve the outcome of the reconstitution after gel filtration with a PD-10 column. Under the reducing agents tested glutathione showed the best uptake and stability of [4Fe4S]-cluster after reconstitution. Glutathione might coordinate or bind the [4Fe4S]-cluster and shield it from solvent in the open structure of the HydF.

The proposed function of the scaffold protein HydF is the transfer of the H-cluster precursor onto HydA; to evaluate the factors that influence cluster transfer, HydF was reconstituted with a pdt-mimic of the H-cluster. Different factors such as incubation time and addition of GTP were tested to investigate whether these altered the amount of pdt-mimic bound to HydF. The incorporation of the pdt-mimic was quantified by UV-Vis spectroscopy and quantification of the iron content by the method of FISH[318] (Section 3.3.2). The addition of GTP did not influence the uptake of pdt-mimic, and incubation times between 1h and overnight were giving similar concentrations of mimic remaining bound. A sufficient incorporation of pdt-mimic onto HydF was achieved for the sample lacking GTP, but no more than 0.4 equivalents remained bound.

For HydE and HydG constructs the reducing agent dithithreitol (DTT) was used for reconstitution of [4Fe4S]-cluster, since the iron-sulfur cluster is embedded inside the protein structure (TIM-barrel) and well isolated from the solvent. Measurements with HydG have confirmed it binds two [4Fe4S]-clusters, in comparison HydE1265 which is also suspected to bind two [4Fe4S]-cluster (Section 3.3.3), as suggested from the concentrations measured by the intensity of the 410 nm absorption band in the corresponding UV-Vis spectrum, characteristic for [4Fe4S]-clusters.

ThitHydG auxiliary cluster shows S = 5/2 signal and coordination by cysteine

Further studies on the iron-suflur cluster states of the [FeFe]-hydrogenase maturation enzymes were conducted with EPR spectroscopy to confirm the presence of [4Fe4S]-cluster in each enzyme and to confirm the auxiliary cluster state of HydG which contains an [4Fe4S] [FeS] cluster that gives an S = 5/2 spin signal in the EPR spectrum (Scheme 6.1). All studied [FeFe]-hydrogenase maturation enzymes carry at least one [4Fe4S]-cluster, with the typical S = ½ rhombic EPR signal that was simulated using the program Easyspin. The EPR spectrum of the radical SAM enzyme clusters of HydE and HydG are influenced by SAM binding and change the shape of the signal if SAM is present. In comparison, in HydF, addition of GTP did not have an influence on the shape of its [4Fe4S]-cluster signal. In order to detect the 5th iron of the reduced HydG auxiliary cluster high and low power EPR spectra were recorded with SAM and L-cysteine added to the sample to stabilize the 5th iron (Section 3.5.3). Recorded EPR spectra revealed the existence of the high spin 5th iron with *g*-values at 9.15 and 5.18 for a S = 5/2 and S = 3/2 spin, respectively (Table 6.1). The resultant signals indicate iron coordination by L-cysteine, since the signals were not present in the absence of L-cysteine. Simulating the S = 5/2 EPR signal turned out to be difficult. However, a good fit could be achieved with the sum of a S = 5/2 and S = 3/2 function at a g-value of 2.0 if zero-field splitting was taken into account.

FT-IR spectroscopy confirmed ThitHydGs activity to form CO and CN ligands

FT-IR spectroscopy was used to carry out functional studies on HydG and to confirm the incorporation of the pdt-mimic of the H-cluster onto HydF. The FT-IR spectrum of HydF reconstituted with pdt-mimic contained all signals which were reported previously of HydF containing the pdt-mimic[27,244] (Figure 6.3), however two additional signals appeared which might correspond to a unspecific 'FeCN' species (Section 3.6.1), that dissociated from the cluster.

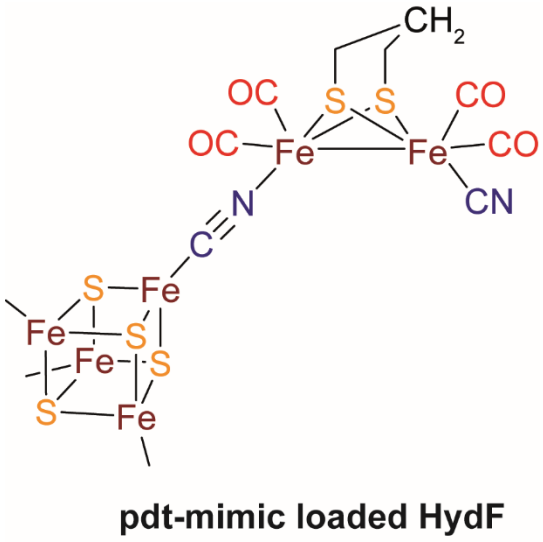

Figure 6.3: Proposed molecular structure of the iron-sulfur cluster of HydF loaded with the H-cluster pdt-mimic.

Activity studies on HydG were carried out by Dr. Pedro Dinis and preliminary data analysis by Dr. Philip Ash. Efforts to repeat the exact experiment did not succeed due to long exposure to dry ice. Detailed analysis of the peaks obtained from the studies of Dr. P. Dinis were carried out herein. The time progression (0-80 min) of the peak areas was analyzed in order to determine if the appropriate CO or CN^- signals are forming within the first 3 min or after 3 min (Section 3.6.2). Since complex A (Fe(CO)(CN)) is forming within the first 3 min according to studies of Britt *et al.*[61] peak areas that were quickly saturating or decreasing with time were assigned to complex A. On the other hand if the peak area progression went slowly or started to increase at a later time point the corresponding peaks were tentatively assigned to complex B ($Fe(CO)_2(CN)$). As the resultant peaks exceeded the stoichiometry expected, additional peaks might have derived from dissociated free CO, non-specific FeCN species or dissociated complex B (released synthon). However, it could be confirmed

that ThitHydG is able to produce complex A and complex B on the auxiliary cluster (Tabe 6.1), as it had been reported for SoHydG before[59,61].

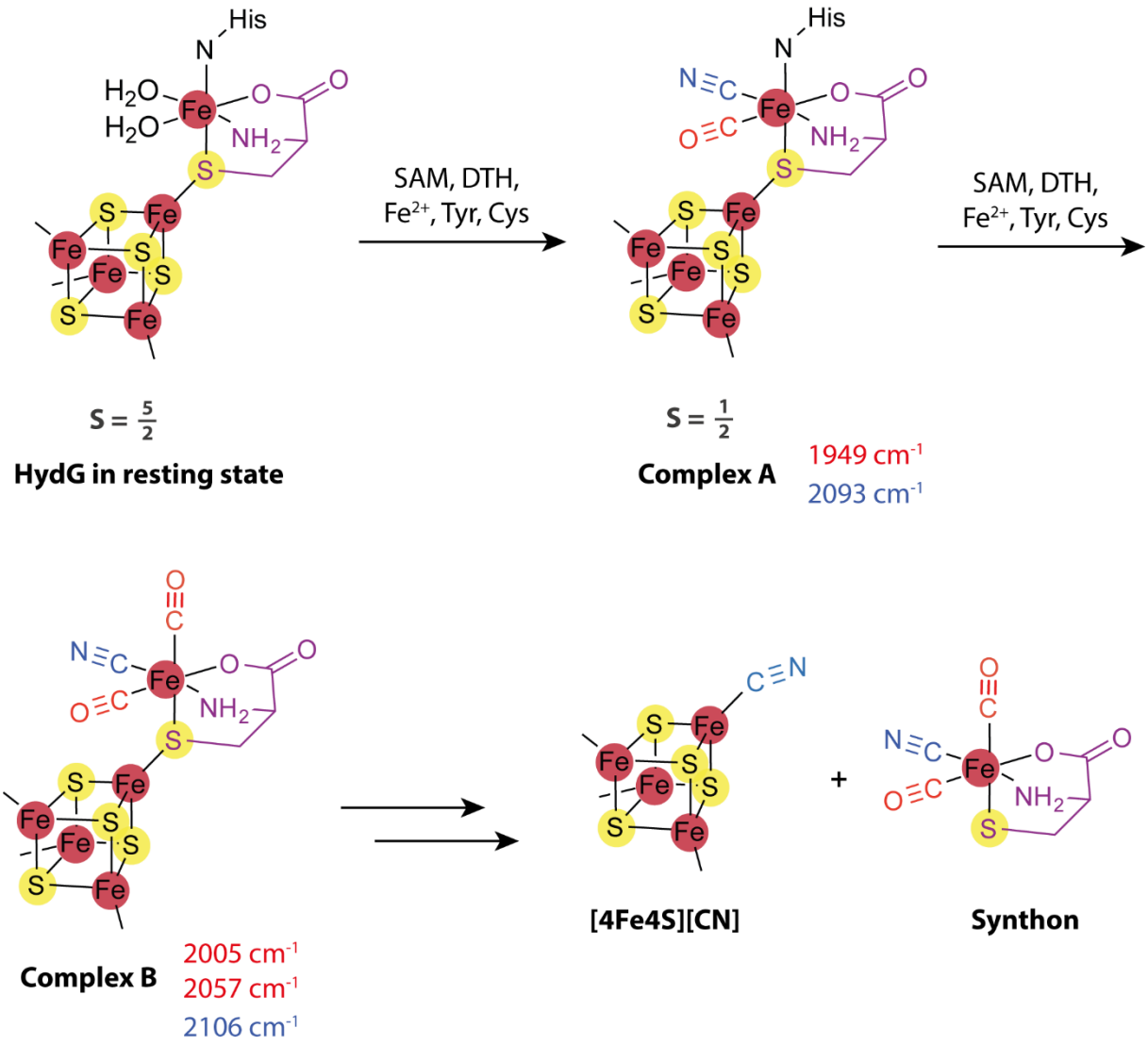

Scheme 6.1: States of the auxiliary cluster of HydG including the resting state, and the active states of complex A, complex B with corresponding wavenumber detected by FT-IR spectroscopy and the synthon.

Table 6.1: Comparison of the spectroscopic properties of SoHydG and ThitHydG.

Spectroscopy	SoHydG	ThitHydG
EPR S = 5/2 and 3/2 signal, *g*-values	9.5, 4.7, 4.1, 3.8[66]	9.2, 5.2, (4.3)
FT-IR band complex A in cm^{-1}	1949 (CO) 2093 (CN^-)[61]	1963 (CO) 2097 (CN^-)
FT-IR band complex B in cm^{-1}	2005, 2057 (CO) 2106 (CN^-)[61]	2004, 2036, 2047 (CO) 2074, (2097) (CN^-)

Future work

To continue with the spectroscopic studies on the reconstitution of HydF, different approaches could be tested to understand how glutathione is contributing to the stability of the iron-sulfur cluster of HydF. To help understand which part of the molecule is in contact with the iron-sulfur cluster EPR studies with labelled glutathione would be useful to obtain hyperfine constants that reveal a coordination of the appropriate group. To find out if glutathione is directly binding to HydF, ITC experiments could reveal any interaction. Furthermore size exclusion chromatography after HydF reconstitution could result in isolated dimeric and/or tetrameric forms of the enzyme and could also be a method to test the stability of the iron-sulfur cluster after reconstitution with either glutathione or DTT.

In regard to the EPR studies of HydF, EPR relaxation profiles at different temperatures could reveal if a second [2Fe2S]-cluster is present in StrepThitHydF. A triple alanine mutant of the [4Fe4S]-cluster binding site cysteine could show if another cluster other than the [4Fe4S]-cluster is present. Furthermore, mutagenesis of iron-sulfur cluster ligands would be also beneficial for ThitHydE1265 which only showed weak evidence of a second cluster which has not been confirmed yet.

Additional EPR spectroscopic studies for characterization of HydG could include the study of a HydG mutant lacking the radical SAM cluster, to better assign the signals and record EPR spectra at different temperature to obtain exact zero-field splitting parameters. Moreover, recent EPR studies of HydG show the EPR spectra of the active state of the auxiliary cluster after circa 40 s, known as complex A with a CO and CN ligand attached to the 5th iron and resulting in an additional S = ½ low spin signal.[71] This could be repeated for ThitHydG to confirm the same behavior over HydG from different organisms.

Further characterization of this active HydG state would be possible with FT-IR spectroscopy by testing factors that increased the rate of CO and CN formation. One of these factors might be GTP which was shown in chapter 4 to increase the SAM and L-tyrosine cleavage activity of HydG. Exact assignment of the CO and CN ligands would be enabled by using selectively labelled samples of L-tyrosine. To elucidate the mechanism between the two partner maturation enzymes HydE and HydF with HydG, FT-IR spectroscopy could help to investigate on which enzyme the synthon is

transferred, by carrying out the HydG reaction in the presence of one of the partner enzymes and isolating HydG directly after from the reaction mixture, by either affinity or size-exclusion chromatography.

6.3 Conclusion and future work concerning the activity of [FeFe]-hydrogenase maturation enzymes

Time-dependent activity assays revealed independent activity of HydG and HydE

For the full characterization of enzymes, in this case the [FeFe]-hydrogenase maturation enzymes, their activities needed to be evaluated on their own and in context/interplay with the partner maturation enzymes.
Time-dependent assays of the SAM and L-tyrosine cleavage activity of HydG and HydE revealed comparable values of turnover rates to already reported values[52,65,269] (Section 4.3.3). Nevertheless, since the second substrate of HydE is unknown and under investigation, the reactions were only supplemented with SAM, L-tyrosine, iron(II), dithionite and the potential substrate L-cysteine in a 8-fold excess. Nonetheless, the SAM cleavage activity of HydE was very small in comparison to HydG (around 80% less). A coupled assay containing HydG and HydE did not show any dependence on HydE or an increase in the resulting DOA and *p*-cresol formation (above the sum of the levels of DOA produced by the independent enzymes), so no enhancement of SAM cleavage activity was observed.

Screening for compounds that enhance HydG or HydE activity revealed the stimulating effect of GTP

In order to assess which compound could enhance the activity of either HydG or HydE, a mixture of all [FeFe]-hydrogenase maturation enzymes (HydG plus HydE1 plus HydE2 and HydF) was supplemented with core reagents and with potential compounds that could enhance the activity, according to previous experiments by Kuchenreuther *et al.*[47-50] (Section 4.3.4) Belonging to the list of potential compounds are sulfide, dithiothreitol, glutathione, PLP, GTP and *E. coli* cell extract (Figure 6.4).

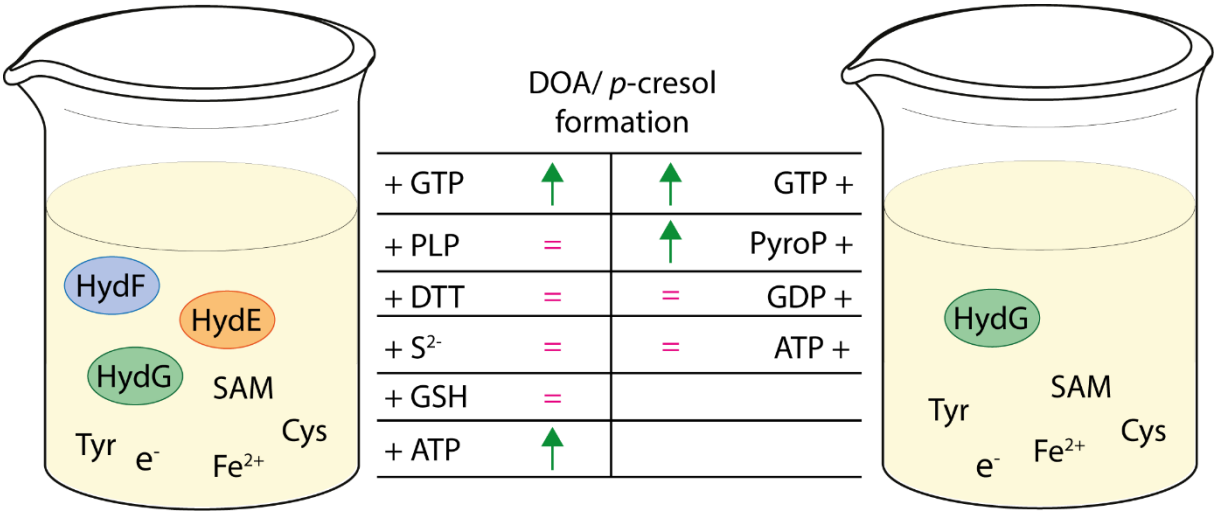

Figure 6.4: Composition of activity assays with compounds influencing the DOA and p-cresol formation of HydE and HydG.

Surprisingly, the only compound that seemed to have an effect on the activity of the maturation enzymes, was the nucleotide GTP, known as the substrate of the GTPase HydF. To find out on which specific enzyme GTP had an effect different combinations of the [FeFe]-hydrogenase maturation enzymes were assessed at two different incubation times 35 and 65 min, revealing HydG's activity as being stimulated by the addition of GTP, having a consistent increasing effect on the activity from 0-65 min. To evaluate the selectivity of HydG for GTP, similar compounds were added to HydG to test for a similar effect, these compounds included GDP, ATP and pyro-phosphate (Section 4.3.5). In summary, the result for ATP was inconclusive, GDP clearly did not show any effect and pyro-phosphate enhanced the activity of HydG in the same magnitude as GTP (Figure 6.4). These results potentially indicate a role of the (pyro)phosphates for HydG.

GTP might coordinate HydGs synthon

Since GTP is the substrate of HydF, GTPase activity assays of HydF were carried out as well, resulting in expectant values for the hydrolysis of GTP[246]. Addition of the partner maturation enzyme HydG to HydF did not have a significant effect on the GTPase activity of HydF, whereas adding all of the partner maturation enzymes slowed down HydF significantly. To address the question if HydG is converting GTP during

turnover, a GTPase assay was also carried out with HydG alone, but did not show any hydrolysis activity, no newly formed GDP was detected (Section 4.4.2). As a potential role, the phosphates of GTP could coordinate the synthon iron complex of HydG and transport the synthon onto HydF where GTP is recognized as a substrate (Scheme 6.2).

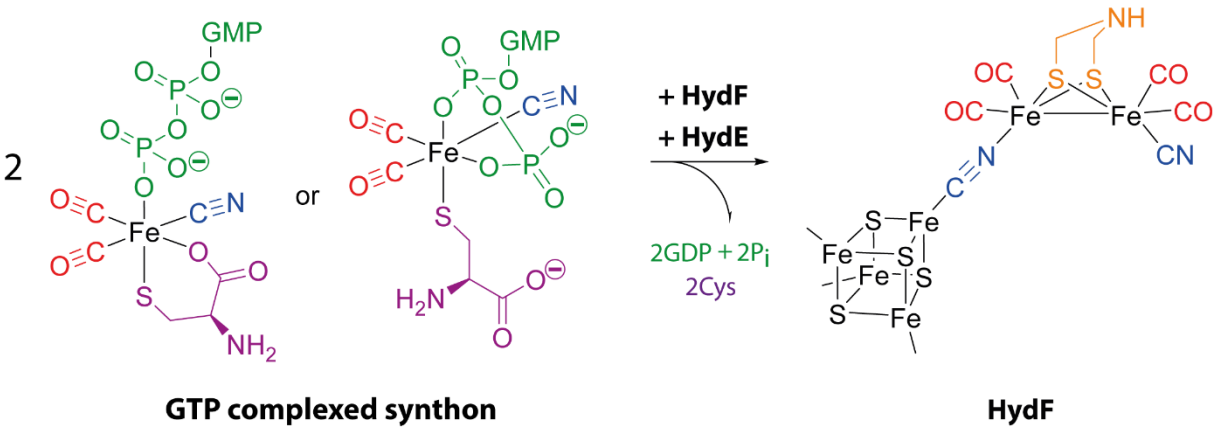

Scheme 6.2: Hypothetical mechanism of the transport of 2 equivalents of GTP complexed synthon onto HydF and following dithiomethylamine synthesis by HydE to form the H-cluster precursor on HydF.

Alternatively, there may be another cellular factor (protein or small molecule) that normally coordinates and transports the synthon onto HydF, but in the assays, where this unknown factor is missing, GTP is standing in for it.

Future work

This hypothesis could be studied with further activity assays, such as a GTPase HydF assay with varying concentrations of HydG to check if HydG sequesters (or even binds) GTP. Another interesting GTPase assay experiment could involve the pdt-mimic loaded HydF construct, in order to check if it has any influence on the GTP hydrolysis activity (i.e. when the H-cluster is already built). Also HydG cyanide and carbonmonoxide formation assays should be assessed for GTPs enhancing effect. Further to that, it could be possible to isolate the GTP-synthon complex by HPLC and potentially characterize the corresponding fraction using LCMS or IR spectroscopy. Spectroscopic techniques could provide excellent tools to study the effect of GTP on HydG, by assessing the coordination of GTP/phosphates with the synthon iron with

EPR spectroscopy, there should be a clear shift or extra signals visible if GTP is interacting with the synthon. Also FT-IR spectroscopy could confirm if the formation of CO and CN ligands is also enhanced by the addition of GTP. Potentially the iron-phosphate complex could be detectable by ATR-FTIR, which has been shown to absorb IR at wavelengths between 900-1200 cm^{-1}.[408]

6.4 Conclusion and future work concerning interactions of [FeFe]-hydrogenase maturation enzymes

Size-exclusion chromatography revealed multimeric HydF and HydG state and no spontaneous complex formation

Crucial for an estimation of maturation events leading to an active [FeFe] hydrogenase are interaction studies of the [FeFe]-hydrogenase maturation enzymes. Efforts towards obtaining information about the interactions were made with size-exclusion chromatography, pull-down assays, isothermal calorimetry titration and anaerobic crystallography studies.

Size-exclusion experiments helped to estimate the multimeric states of reconstituted HydG and HydF. HydF is forming a dimer in solution as reported before[248], whereas HydG stays in its monomeric state. Initial tests for spontaneous complex formation between HydG and HydF, by simply incubating the enzymes together and analyzing the mixture by SEC revealed that HydF did not form a complex with HydG under standard conditions.

Pull-down assays suggest a crucial pH-dependent effect of tyrosine

A less material-consuming and quicker method to test and screen for complex formation between two or three proteins is pull-down assays. Selective affinity of one protein to a specific resin, which is lacking for the partner proteins, enables the pull-down assays. As observed for the SEC, simple mixtures of HydF and HydG did not lead to complex formation. Hence, different compounds and compound mixtures were added to HydF and HydG to identify components causing an increase in complex formation. A compound mixture containing tyrosine, iron, cysteine and dithionite was tested first, containing molecules likely to bind to HydG but not initiating turnover. The

amount of complex detected was greatly enhanced by the compound mixture and omitting one of each compound from the incubation reaction revealed the importance for complex formation. In the first instance removing dithionite from the reaction mixture increased complex formation, whereas omitting tyrosine clearly decreased the amount of HydF:HydG complex detected, leading to the tentative hypothesis of a role of tyrosine for the formation of the complex (Section 5.6.1). To explore this further, dithionite was removed from the incubation mixture for future experiments. In addition, GTP was added to the mixture and seemingly decreased the amount of complex formed, but this was not observed for every experiment.

Different buffer conditions were screened which contained either the standard salt concentration (300 mM) or less salt (30 mM) to enhance the chance of ionic interactions or an additional composition including the compounds of the incubation mixture (tyrosine, cysteine, iron(II) in order to keep the concentrations in the assay mixture constant. Best results were mostly achieved with the reduced salt buffer, which was used from then on.

Control experiments were carried out by replacing HydG with BSA or TrmD, however the amount of complex formed with HydF seemed to be in the same scale as with HydG, suggesting HydF binds unselectively to other enzymes not related to the [FeFe]-hydrogenase, which might be facilitated by its open dimeric structure. Previously published interaction studies did not provide control experiments with other enzymes other than [FeFe]-hydrogenase maturation enzymes.[253] Testing HydE1 and HydE2 complex formation with HydF revealed no significant influence by any of the compounds added to the incubation mixture (SAM, cysteine, glutathione or a 1:1 mixture of pyruvate:cysteine).

The interaction between HydF and HydG is hugely dependent on the pH of the incubation mixture as observed when tyrosine stock solutions were remade (Section 5.6.4). Higher pH, above 8.0, seemed to increase the amount of complex formed between HydF and HydG, BSA or TrmD. Forcing the assay conditions to a near physiological pH of 8.0 dropped the amounts of complexes detected significantly.

Despite little interaction between HydF and HydG, a pull-down assay containing all three [FeFe]-hydrogenase maturation enzymes (HydF + HydG + HydE1 or HydE2) was carried out. It could be clearly seen that the amount of HydE remaining bound was higher than HydG (Figure 5.19, Section 5.6.5), which has been confirmed before by SPR studies[253].

Overall crucial compounds for the binding between the maturases were determined (L-tyrosine), by taking different influences into account, such as pH, buffer compositions and protein:protein ratios

Crystallization and ITC experiments

Efforts to anaerobically grow crystals of *holo*-HydF and/or an HydF:HydG hetero-complex were unsuccessful. Despite several batches and different mixtures of protein, substrates or cofactors tested with four different crystallization broad screens did not yield in protein crystals.
Measuring interactions quantitatively with ITC to obtain information about the interaction of HydF with GTP and HydF with HydG did not yield analyzable data. The resultant data was noisy possible due to pressure changes during the experiment resulting from the glovebox gloves, bubbles in the syringe or cell, or a contaminated syringe or reaction cell.

Future work

To improve the outcome of the pull-down assays, tight control of pH, concentrations and volumes are needed to further optimize the protocol. Increasing the scale of the assay amounts (from 100 µL to 500 µL) could lead to an improvement of the consistency of the results, and minimizing the amount of samples assayed in one day could lower the error resulting from pipetting. Furthermore, different compounds and conditions could be evaluated, by changing the incubation temperatures, times and by addition of different combinations of substrates and cofactors.
Furthermore, additional methods could be carried out to detect or quantify complex formation in an anaerobic atmosphere. Beneficial techniques to directly detect an [FeFe]-hydrogenase maturase complex and determine the stoichiometry of the complex could be scattering methods like SAXS (Small angle X-Ray scattering) or MALS (Multiangle light scattering). Determination of binding constants and thermodynamic data could be achieved with SPR, ITC or MST (Microscale thermophoresis). Moreover, detailed information of interacting amino acid residues in the protein-protein complex could be provided by NMR spectroscopy.

6.5 Overall contribution of this work

The PhD work presented herein provides insights into approaches to study complex mechanisms between anaerobic proteins. Production and isolation of anaerobic proteins can be challenging, as the oxidation sensitive cofactors (iron-sulfur clusters for example) are labile and easily degradable. Methods to keep the iron-sulfur-clusters intact and the protein fully occupied with cofactors were applied and evaluated by their outcome. Satisfactory results were achieved by using an optimized bacterial strain for iron-sulfur-cluster synthesis and supplementing expression media with external iron and sulfur sources. Furthermore, for the improvement of the protein yield it was necessary to change the expression vector and the induction system, pointing out that alternative systems can provide solution strategies if optimization of one system is not leading to better results.

Once a sufficient yield of protein was established, the occupancy of cofactors was still less than 50%, despite expression with optimized bacterial strains and addition of iron and sulfur sources during expression. In these cases, a chemical reconstitution with iron-sulfur-clusters was necessary. After chemical reconstitution, spectroscopic techniques served as the best methods to quantitatively and qualitatively assign the amount and type of iron-sulfur-clusters bound to the specific enzyme. Hereby it is noted that UV-Vis spectroscopy is used for the quantification of the iron-sulfur cluster concentration (specifically [4Fe4S] cluster) and EPR-spectroscopy mostly for qualitative assignment of the type of iron-sulfur-cluster. A unique type of cluster has been previously detected in the crystal structure of HydG[64] and the binding mode or associated ligands can be studied with EPR spectroscopy. The results obtained with EPR build an optimal platform to future studies, as the S = 5/2 signal confirms the presence of the 5th iron in the [5Fe5S] cluster and monitors any changes in the ligand sphere. This enables a strategy to estimate the reconstitution efficiency and to observe different ligands that bind to the 5th iron. The unique CO and CN ligands produced by HydG are detectable by FT-IR spectroscopy and sample preparation and storage (cardice diffuses into samples) is key for obtaining good results.

Once the reconstitution state of each [FeFe]-hydrogenase maturation enzyme has been characterized, the enzymes have been assessed for their activity to cleave SAM, tyrosine or to hydrolyze GTP. So far, the activities of these enzymes have not been studied in dependence of the partner enzymes in a mixture, even though it is known that these enzymes work together to form the H-cluster precursor. The outcome of the activity studies revealed that the activities of the radical SAM enzymes HydG and HydE are uncoupled, whereas the activity of HydF dropped if both HydG and HydE were present. Moreover, different compounds that might increase the overall SAM cleavage activity of the maturation enzymes were examined; surprisingly GTP had a stimulating effect on the SAM and tyrosine cleavage activity of HydG. This new discovery led to the hypothesis that GTP might be responsible for the transport of the synthon complex from HydG onto HydF, which is recognizing GTP as its substrate. Two synthon molecules could form the [2Fe]-subcluster precursor of the H-cluster. This hypothesis opens up many future experimental studies with GTP, whereby spectroscopic methods could reveal the exact binding mode of GTP to HydG or HydF. Further activity studies could gain insights if HydG induces a chemical change in GTP or sequesters the nucleotide. Additionally, GTP derivatives could reveal the mechanism leading to the stimulation of activity. The possible directing role of GTP might influence the hydrogen production ability of the maturation product (the H-cluster) and therefore might be important for the efficiency of the biofuel generation by the [FeFe]-hydrogenase.

Efforts to study the interactions between the anaerobic [FeFe]-hydrogenase maturation enzymes, did not yield the desired results. However, it is to be noted that pull-down assays could provide a comprehensive tool to investigate the interactions between anaerobic proteins, but some important considerations such as pH, protein reconstitution and concentrations and compound stock concentration need to be taken to account to keep the assays at consistent conditions. Thermodynamic studies with ITC resulted in mostly noisy data, however this might have been due to the usage of the actual substrate of the HydF protein and the following reaction initiation. To obtain better analyzable results non-hydrolysable or non-reducible substrate derivatives are required instead. Crystallization and Co-crystallization trials did not gave any hits for the [FeFe]-hydrogenase maturation enzymes HydF and HydG. Since the crystallization plates were prepared by hand, pipetting errors or long exposure time might have caused drying or inappropriate concentrations of proteins. A major reason

that might have caused the lack of crystal growth for HydF is the fact that the last purification step included a desalting column instead of a size-exclusion column. The desalting column does not differentiate the multimeric forms of a protein and a mixture of monomer, dimer and tetramer might have eluted together. Furthermore, iron sulfur aggregates were possibly still present after the desalting step. For future crystallographic studies, these factors need to be considered.

Overall, important contributions and insights on the characterization of anaerobic metalloproteins and the mechanisms between these proteins were gained. This information will be critical for future scientific investigations.

Chapter 7

Experimental

7.1 Materials

General reagent grade chemicals were purchased from Sigma Aldrich or Fisher Scientific if not otherwise stated. Bacto-tryptone, yeast extract and bacto-agar were bought from Oxoid and Fisher Scientific. DTT, IPTG and antibiotics were obtained from Melford Laboratories Ltd. Polyacrylamide-bis polyacrylamide (30% w/v, 37:5:1) was purchased from Fisher Scientific.

Consumable Wizard® Plus SV Miniprep Plasmid DNA purification system kits were purchased from Promega. GeneRuler 1kb DNA ladder and EZ-Run protein ladder were obtained from Fisher Scientific. Falcon tubes of 15 and 50 mL volume were also bought from Fisher Scientific. Nancy-520 nucleotide dye, Bradford reagent and Antifoam 204 were purchased from Sigma Aldrich. EDTA-free protease inhibitor tablets were acquired from Roche. GE Healthcare was the supplier for pre-packed Nap-10 and PD10 columns and for Superdex 75 and 200 resin. PES based membranes, 10-30kDa MWCO were either purchased from Millipore or Sartorius Stedim Biotech. Sterile 0.22 or 0.45 μm syringe filters were obtained from Millipore. EPR tubes (Wilmad Quartz (CFQ), 4mm OD) were acquired from Sigma Aldrich. Analytical HPLC columns were bought from Phenomenex. Crystallization plates and microplates (24 and 96 well) were purchased from Greiner Bio-One.
Benzonase and BSA enzyme were obtained from Sigma Aldrich. All restriction enzymes were either purchased from New England Biolabs or Thermo Fisher Scientic. Thermo Fisher Scientific is also the supplier for the Phusion DNA polymerase.

Synthesized DNA plasmids pMA_ThitStrepHydF, pMA_StrepThitHydE1265 and pMA-RQ_StrepThitHydE1675 were made by GeneArt at Life Technologies (now Thermo Fisher Scientific).

7.2 Equipment

Microbiology

PCR reactions to amplify DNA were carried out in an Eppendorf Mastercycler gradient. An electrophoresis apparatus (BioRad) was used to run agarose gels or SDS-PAGEs and the SynGene GeneGenius Bio Imaging System to collect the gel images. The gels were visualized with the UV transilluminator or white light and analysed with the program GeneTools. To quantify bands on resultant gels the program Image J was used. DNA quantification was carried out in the Nanodrop ND-1000 spectrophotometer.

Bacterial Growth

Solutions for bacterial growth or deionised water were sterilized in an Astell AMA260BT autoclave at 121°C for 25 min. Glucose, lactose, arabinose, IPTG and antibiotic solutions were filter sterilized through 0.22-0.45 µm syringe filters. Bacterial cultures were incubated and shaken in an Innova 4230 Incubator Shaker (≤ 200 mL, New Brunswick Scientific), Innova 4400 Incubator Shaker (5 L, New Brunswick Scientific) or a BioFlo® 110 fermentor with a 7.5 L vessel (Eppendorf UK Ltd.). Agarose plates containing bacterial colonies were incubated in a Function Line Incubator (Hereaus®). Cells were harvested by centrifugation (Sorvall Lynx 6000, ThermoFisher Scientific) using the F9-6x1000 LEX rotor. Small volume centrifugations (≤ 1.5 mL) were carried out in a bench top micro centrifuge (5415D, Eppendorf) at RT.

pH Determination

Measurements to determine the pH of a solution were carried out with a Mettler Detla 340 pH meter and the corresponding Mettler Toledo Inlab 413 Combination Electrode calibrated at pH 4.0, pH 7.0, pH 10.0 when required and stored in 3 M potassium chloride.

Anaerobic purification

Experiments with oxygen sensitive proteins were carried out inside an anaerobic glovebox (Belle Technology, O_2 < 2 ppm, 20°C) equipped with a Pharmacia Acta FPLC (GE Healtcare) and a VC 130 Sonicator (Sonics and Materials). Cell lysates were

cleared by centrifugation in 50 mL centrifuge bottles (Sorval Lynx 6000, F21-8x50y rotor). Purification buffers and solutions were deoxygenated overnight inside the glovebox, and the purification itself was carried out with Pharmacia XK columns or BioRad columns. Protein solutions were concentrated using an Amicon stirred ultrafiltration pressure-cell (>1 mL) or spin filters (<1 mL).

UV-Vis spectroscopy

Aerobic absorbance readings were recorded on a Biomate 3 (Thermo Scientifc) spectrometer or a Tecan Safire^2 microplate reader. Anaerobic absorbance spectra were recorded in UV quartz cuvettes with an USB2000 spectrophotometer (Ocean Optics) equipped with a Mini-D2-GS light source and QP400-2-SR-BX fibres.

HPLC analysis

Liquid chromatographic separation of compounds was achieved on a workstation (Gilson 321 Pump H1 Heads and a Gilson 234 Autoinjector) connected to a dual wavelength Gilson-UV-Vis-155 detector and a Shimadzu RF-10AXL fluorimeter. Analysis of the obtained chromatograms was carried out using the Gilson Unipoint Software (5.11).

EPR spectroscopy

EPR measurements were carried out using an X/Q-band Bruker Elexsys E580 Spectrometer (Bruker BioSpin GmbH, Germany) equipped with a closed-cycle cryostat (Cryogenic Ltd, UK). Temperature calibration was accomplished with an external Cernox thermometer. A Bruker strong pitch sample (g = 2.0028), was used to calibrate the magnetic field at room temperature. Measurements were carried out either using an X-band split-ring resonator module with 2 mm sample access (ER4118X-MS2) or the dielectric resonator (ER4118X-MD5) for 4 mm tubes, both operated in continuous-wave (CW) mode. The resonators differ in the conversion factor of the microwave power, the ER4118X-MS2 has 8G/W factor and the ER4118X-MD5 operating at 9.8 GHz has a conversion factor of 1.48 G/W. All spectra presented in this thesis were baseline-subtracted.

FT-IR spectroscopy

Transmission FT-IR measurements were carried out on a Bruker Vertex 80 spectrometer equipped with a liquid-nitrogen cooled HgCdTe detector housed in an anaerobic, dry glovebox (Glove Box Technology Ltd, <1 ppm O_2, dewpoint <85 C°. Spectra were recorded at glovebox temperature (around 25 °C) in a vacuum-tight transmission cell with CaF_2 windows and a 25 μm optical path length (Specac). Reactions were either initiated by mixing with a sodium dithionite solution (100 mM stock) in a 500 μL micro centrifuge tube and injecting or directly injecting (around 30 μL) into the transmission cell using a gas-tight syringe. This gave an experimental 'dead-time' of approximately one-two minutes. Spectra were recorded continuously as an average of 256 interferrograms with a collection time of around 2 minutes per spectrum.

Reference water or buffer spectra were subtracted from the obtained spectrum and baseline corrected in cases where stated. Spectral analysis was performed using the Origin software.

Crystallography

Crystal trays were manually prepared inside the glovebox (Belle Technology) and monitored with a Mejii EMZ-13TR microscope connected to an infinity 1 camera situated inside glovebox. Images were taken using the corresponding Infinity Capture or Infinity Analyse software.

7.3 General microbiology methods

Media

Compositions of liquid growth media are summarized in Table 7.1.

Table 7.1: Composition of media.

	Quantity for		
Component	2YT medium	LB medium	Autoinduction
Bacto-Tryptone	16 g	10 g	20 g
Bacto-Yeast Extract	10 g	5 g	5 g
NaCl	5 g	10 g	5 g
Phosphate buffer (pH 7.2)	-	-	6 g (Na_2HPO_4) 3 g (KH_2PO_4)
Adjust to 1 L with deionised water and autoclave.			

Antibiotic stock solutions were prepared in sterile water or ethanol and were added to growth media. The appropriate concentrations are listed in Table 7.2.

Table 7.2: Concentrations of antibiotic solutions.

Antibiotic	Stock concentration (mg/mL)	Concentration in media (µg/mL)
Ampicillin	100	100
Kanamycin	50	50
Streptomycin	50	50
Chloramphenicol	34 (in EtOH)	34 (in EtOH)

Medium for agar plates was prepared by adding 15 g/L bacto agar to 2YT medium, which was subsequently autoclaved and transferred into a microbiological safety cabinet. At a temperature of 50°C the antibiotic stock solution was added. The resulting solution was poured into petri dishes, dried, and cooled at 4°C until further use.

Method 1 Preparation of competent *E. coli* cells

The rubidium chloride method by Hanahan[409] was used to prepare competent *Escherichia coli* XL10 GOLD, JM109, BL21 (DE3) or Δ*iscR* BL21 (DE3) cells. To inoculate 10 mL of 2 YT media with antibiotic, a glycerol freeze smear of the required *E. coli* cells was added and incubated overnight at 37°C, 180 rpm. The resulting culture

(1 mL) was added to 100 mL of fresh 2YT medium with antibiotic and grown at 37°C, 180 rpm until the OD_{600} reached 0.6-0.7. Immediately the culture was chilled on ice for 10 min. Cells were collected by centrifugation (2 x 50 mL, Heraeus Stratos Centrifuge, 6000 rpm, 4 °C, 10 min). After discarding the supernatant the pellet was resuspended in 10 mL ice cold TFBI buffer and centrifuged for further 10 min. The supernatant was discarded and the cells were resuspended in 1.5 mL TFBII buffer and subsequently divided into 100 µL aliquots and flash frozen in liquid nitrogen. Cells were stored at -80 °C until further use.

Table 7.3: Buffer composition for the preparation of competent cells.

Buffer	Component	Quantity in g	End concentration
TFBI	$RbCl_2$	12.1	100 mM
	$MnCl_2$	9.9	50 mM
	KOAc	2.9	30 mM
	$CaCl_2$	1.1	10 mM
	Glycerol	150	15% (w/v)
Adjust to pH 5.8 with acetic acid and 1 L volume with deionized water. Filter sterilize.			
TFBII	MOPS	2.1	10 mM
	RbCl	1.2	10 mM
	$CaCl_2$	8.3	75 mM
	Glycerol	150	15% (w/v)
Adjust to pH 6.8 with sodium hydroxide and filter sterilize. Storage at -80 °C for both.			

Method 2 Transformation with competent *E. coli* cells

A 100 µL aliquot of competent *E. coli* cells was thawed on ice for 10 min before addition of 1-2 µL purified plasmid DNA or 10-20 µL for ligation reactions. The cells were kept on ice for further 30 min and then heat-shocked at 42 °C for 40 sec. Immediately after, the cells were returned to ice for 2 minutes and mixed with 250 µL SOC medium. Resulting cell suspensions were incubated at 37 °C while shaking (180 rpm) for 1 h. Inside a MSC the cell suspension was plated onto 2YT agar plates containing the appropriate antibiotic. Prepared agar plates were incubated at 37 °C overnight. Plates with grown colonies were stored at 4 °C until further use. A control transformation without plasmid DNA was carried out at the same conditions alongside.

Table 7.4: Composition of SOC medium.

Component	Quantity
Bacto-Tryptone	20 g
Bacto-Yeast Extract	5 g
NaCl	0.5 g
Glucose (1 M)	20 mL
$MgCl_2$	5 mL
Deionised water	To a final volume of 1 L

Method 3 Glycerol Stock Preparation

Single well-isolated colonies were picked from agar plates with a sterile tip and cultured in 10 mL 2YT medium including the appropriate antibiotic. To 600 µL cell culture 600 µL sterile glycerol (50% (v/v)) was added, mixed, flash frozen in liquid nitrogen and stored at -80 °C.

Method 4 DNA plasmid isolation

Overnight cultures of *E. coli* cells (10 mL) were harvested by centrifugation (6000 rpm, 10 min, 4 °C) and the plasmid DNA was purified and isolated according to the manufacturer's instructions of the Wizard® Plus SV Miniprep Plasmid DNA Purification System Kit. To elute the purified plasmid DNA the purification column was incubated with 100 µL deionized nuclease-free water and centrifuged (13200 rpm, 1 min, RT). The plasmid solution was stored at -20 °C.

Method 5 Determination of DNA concentration

The Nanodrop photometer ND-1000 from PEQLab was used to determine the DNA concentration of a plasmid solution. For the concentration measurement, a 1.5 µL drop of the sample was measured at a wavelength of 260 nm against a deionized water blank.

Method 6 Analytical and preparative digest

The size and accuracy of purified plasmids was analysed by a single or double digest with restriction enzymes. Digests in a preparative scale were used to purify plasmid fragments for cloning or mutagenesis. Purified plasmid DNA was digested with one or two restriction enzymes according to optimal enzyme conditions (NEBbuffer and presence or absence of BSA) provided by NEB. The composition of the reaction mixture is summarized in Table 7.5. Reactions were incubated at 37 °C for 2 h (analytical digest) or 4h (preparative digest).

Finished digests were analysed by 1% agarose gel containing the Nancy520 dye for DNA visualization under UV light. The visualized fragments for preparative digests were cut out under UV light using a scalpel. Obtained fragments were purified with a gel extraction kit (E. Z. N. A. Gel Extraction Kit from VWR Omega Bio-Tek or Pure Link™ Quick Gel Extraction Kit from Invitrogen).

Table 7.5: Typical composition of DNA digest reaction mixtures.

	Quantity in	
Reagent	**Analytical digest**	**Preparative digest**
Plasmid DNA (50-100 ng/µL)	5 µL	40 µL
NEB buffer (10x)	1 µL	5 µL
BSA (1 mg/mL)	1 µL	5 µL
Restriction enzyme 1	0.5 µL	1.5 µL
Restriction enzyme 2	0.5 µL	1.5 µL
Deionized water	2 µL	-

Method 7 Ligation of DNA fragments

Two digested DNA fragments (Insert DNA and vector backbone DNA) were combined to form a circular plasmid via ligation with the T4 DNA ligase enzyme. The ligase is able to from phosphodiester linkages between the digested DNA fragments. All components listed in Table 7.6 were mixed together, except the ligase which was added last and kept cool on ice. The ligation reaction was incubated at RT for 20 min and subsequently heat deactivated at 60 °C for 10 min. After the mixture reached RT it was transformed with competent *E. coli* XL10 GOLD or JM109.

Table 7.6: Ligation mixture for a 3:1 insert to vector ratio.

Reagent	Quantity for pBAD (8500 bp) constructs	Quantity for pCDuet (3500 bp) constructs
Vector DNA	75 ng	25 ng
Insert DNA (~1000 bp)	25 ng	28 ng
T4 Ligase buffer	2 µL	2 µL
T4 Ligase	1 µL	1 µL
Deionized water	Ad to 20 µL	Ad to 20 µL

Method 8 Agarose gel electrophoresis

For the preparation of an 1% (w/v) agarose gel, the appropriate amount of agarose was added to 1x Tris-Acetate-EDTA (TAE) buffer (Table 7.7) and heated in the microwave until the agarose was dissolved. After the agarose mixture cooled down to about 50 °C the DNA dye Nancy520 was added (2 µL per 50 mL), mixed and poured into the gel chamber. Each sample was mixed with 6x Gel loading buffer (from Thermo Fisher) and filled into the gel pocket. The gel was run in 1x TAE buffer at a constant voltage of 70-90 V for 35 min – 2 h and immediately visualized under UV light.

Table 7.7: TAE buffer contents.

Component	Quantity
TrisBase	242 g
Acetic Acid	57.1 mL
500 mM EDTA, pH 8.0	100 mL
Deionized water	Adjust to 1 L

7.4 Preparation of DNA plasmids

The genes of the StrepThitHydF, StrepThitHydE1265 and StrepThitHydE1675 proteins have been purchased from GeneArt (Life Technologies). The genes were inserted in the commercial vectors of the company, the corresponding plasmid maps of pMA-RQ_StrepThitHydF, pMA_StrepThitHydE1265 and pMA_StrepThitHydE1675 are shown in the Appendix A 2.1.

Method 9 Cloning: Restriction digest and Ligation

The desired vector (pCDuet or pBAD_ISC) and the gene (*hydF*, *hydE* or *hydG*) that will be cloned into the vector backbone were digested with the same two restriction enzymes producing compatible sticky ends. The typical contents of the digest mixture are summarized in Table 7.5. Products of the digest were loaded onto an agarose gel, and the fragments separated by electrophoresis at 70 V for 1-2 h. Resulted fragments were visualized by UV-Vis, cut out with a scalpel and extracted and purified with a gel extraction kit (E. Z. N. A. Gel Extraction Kit from VWR Omega Bio-Tek or Pure Link^{TM} Quick Gel Extraction Kit from Invitrogen).

The purified DNA fragments (vector backbone and insert) were linked together by ligation with the T4 DNA ligase (see Method 7). After the ligation reaction, the mixture has been transformed with *E. coli* JM109 or XL10 Gold cells (see Method 2). The resultant purified plasmids from overnight cultures of single colonies from solid selective 2 YT media, were tested for the presence of the inserted gene *via* an analytical digest. If the analytical digest has shown the desired digest products, plasmids were sent for sequencing to confirm the accuracy of the inserted gene.

Method 10 Site-directed ligase independent mutagenesis (SLIM)

The site-directed ligase independent mutagenesis (SLIM) method was first described by Chiu and is reliable and efficient method to insert, delete and mutate DNA.[410.411]

The SLIM reaction requires a set of four primers, two forward and two reverse primers. One primer in each primer pair carries an overhang sequence, which contains the mutation and which minimal length is 18 bp. Each primer pair is complementary to

each other except the overhang sequence. The complementary sequence of the primer pairs is flanking the target sequence that will be mutated. To amplify the whole plasmid with an overhang, for each primer pair (with and without overhang) a PCR reaction is carried out. The typical contents of the PCR reaction are shown in Table 7.8 and the PCR program in Table 7.9. The result of the PCR are two different products that contain the mutation sequence (overhang) on two different ends. During a hybridisation reaction (contents and program in Table 7.10 and 7.11) in 5x Hybridisation buffer (750 mM NaCl, 125 mM Tris, 100 mM EDTA, pH 8.0) of the two DNA molecules, a hybrid between the single strands of the two PCR products is formed. Since the two overlapping overhangs on the different ends are complementary to themselves they hybridize together to form a complete plasmid including the new mutation. The two complete single strands are repaired by the hosting *E. coli* cell after transformation.

Table 7.8: Composition of a SLIM PCR reaction.

Component	Volume/ µL
Template DNA	0.5
DMSO	1.25
dNTP-Mix (2 mM)	6.25
Forward Primer	1.25
Reverse Primer	1.25
Phusion DNA polymerase	0.25
HF buffer	5.0
Deionised water	Add up to 25 µL

Table 7.9: SLIM PCR program.

PCR program	For pRD003_StrepHydG		For pCDuet_His_6HydEs	
	Temperature/ °C	Time/ s	Temperature/ °C	Time/ s
Initial Denaturation	98	15	98	15
35 cycles of				
Annealing(± 3 °C)	58	30	60	30
Elongation	72	324	72	150
Final Elongation	72	300	72	300

Table 7.10: Composition of a SLIM hybridisation reaction.

Components	Volume/ µL
PCR 1 product	10
PCR 2 product	10
5 x Hybridisation buffer	10
Deionised Water	Add up to 50 µL

Table 7.11: SLIM hybridisation program.

Temperature/ °C	Time/ min
98	3
3 cycles of	
65	5
30	30

7.5 Protein expression and purification

Method 11 Small scale protein expression studies

Small scale protein expression studies were carried out in order to optimise the conditions for improved protein solubility and yield. Tested conditions included different inducer concentrations, variable inducing times (depending on the OD_{600nm}) and changes in temperature and duration of the growth after induction. An BL21 (DE3) or Δ*iscR* BL21 (DE3)::*kan E. coli* overnight culture was added as an 1% inoculum to 100 mL or 1.25 L of autoclaved 2YT media (Table 7.1) including the required antibiotic (Table 7.2). Cells were grown at 37 °C and 180 rpm until the culture reached the mid-log phase (OD_{600nm}=0.6-0.9), monitored by optical density at 600 nm. The small cultures were induced with varying concentrations of IPTG (pCDuet vector) or L-arabinose (pBAD vector). Growth temperatures between 16 °C and 37 °C (180 rpm) and durations between 4h and overnight were probed. Resulted cells were collected by centrifugation (6000 rpm, 10 min, 4 °C) and stored at -80 °C until further use.

For the analysis of the cell pellet and amount of soluble protein, the cell pellet was suspended in cold lysis buffer (appropriate protein purification buffer including x mg lysozyme per x mL buffer and a protease inhibitor tablet) and incubated on ice for 30 min. To extract the soluble protein inside the cell wall, the suspended and lysed cells were sonicated with 1 sec on 1 sec off bursts for 1 min. A sample of the resulted

lysate was kept for the SDS-PAGE. Centrifugation (13200 rpm, 10 min, RT) led to the soluble clear lysate and the insoluble pellet, which were also used for the SDS-PAGE. The SDS-PAGE with loaded lysate, clear lysate and cell pellet gave insight to what extent the desired protein was expressed and if it is in the soluble fraction or the insoluble.

Method 12 Large scale protein expression in flasks

An BL21 (DE3) or Δ*iscR* BL21 (DE3)::*kan E. coli* overnight culture containing the plasmid for the expression of the desired protein (ThitHydF, ThitHydE1265, ThitHydE1675 or ThitHydG) was added (1% inoculum) to 4 x 1.25 L autoclaved 2YT media in flasks (4 L) including the required antibiotic (Table 7.2). Cells were grown at 37 °C and 180 rpm until the culture reached the mid-log phase (OD_{600nm}=0.6-0.9). At this time point the culture was induced either with 0.5-1 mM end concentration of IPTG (pCDuet plasmid) or 250 mL of 20% (w/v) L–arabinose (pBAD plasmid). Depending on the protein the culture was grown overnight (16-25°C) or for 5-6 h (25-37°C) at 180 rpm. Cells were harvested by centrifugation (8000 rpm, 20 min, 4 °C). Harvested cells were frozen at -80 °C until further use.

Method 13 Large scale protein expression in a fermenter

A fermenter unit containing 5 L sterilized 2YT media (Table 7.1) was equilibrated at 37 °C overnight. On the following day the media was supplemented with ampicillin (Table 7.2) , antifoam (0.1 mg/mL) and 50 mL overnight culture of BL21 (DE3) or Δ*iscR* BL21 (DE3)::*kan E. coli* containing the pBAD derived plasmid of pRD003_ThitHydG, pBMW001_ThitHydF, pBMW002_ThitHydE1265 or pBMW003_ThitHydE1675. The cell culture was incubated at 37 °C and the agitation ranged from 50-250 rpm, depending on the oxygen level in the media. Optimal oxygen levels were set to 40% compared to full aeration (100%) equilibrated before addition of the supplements. Cells were grown until the optical density reached a value of OD_{600nm}=0.7-0.8 at which point they were induced by addition of filter sterilized 20% (w/v) arabinose (50 mL/L). To express the desired protein the cells were further incubated at 27 °C for 6 hours. Cells were pelleted by centrifugation (8000 rpm, 4 °C, 20 min) and the resulting cell paste was stored at -80 °C until further use.

Method 14 Large scale protein expression *via* autoinduction

Autoinduction media in flasks (4 x 1.25 L) was sterilized with an autoclave and each flask supplemented with 12.5 mL of filter-sterilized 60% (v/v) glycerol solution, 6.25 mL of filter-sterilized 10% (w/v) glucose solution and 31.25 mL of filter-sterilized 8% (w/v) lactose solution. Right after, streptomycin (Table 7.2) was added and the media inoculated with an overnight culture of Δ*iscR* BL21 (DE3)::*kan E. coli* containing the pCDuet plasmid with ThitHydF, ThitHydF+ThitHydE1265, ThitHydE1265 or ThitHydE1675. The auto-induced expression was incubated at 37 °C and 180 rpm overnight. On the following day the cells were collected by centrifugation (8000 rpm, 4 °C, 20 min) and stored at -80 °C until further use.

Method 15 Anaerobic purification of His_6-tagged enzymes

Inside an anaerobic glovebox crushed frozen cell pellet of a His_6ThitHydG or His_6ThitHydE expression was resuspended in buffer A (3 mL/g of pellet). Buffer A was supplemented with lysozyme (1mg/g of pellet) and EDTA-free protease inhibitor tablet (1 tablet per 50 mL) and the suspension was stirred in a ice cooled-water bath for 45 min. Cells were lysed by sonication (6 x 10 min, 1 s bursts, 20 W) and cleared by centrifugation (18000 rpm, 4 °C, 45 min). Clear supernatant was loaded with 10 mL/min onto a NiNTA column (Ni Sepharose Fast Flow resin, 50 mL, XK50, internal diameter 50 mm) equilibrated with buffer A. Absorbance at 280 nm indicated the presence and quantity of proteins eluting from the column. The column was washed with buffer A until all unbound proteins eluted from the column and the absorbance reached baseline level. A linear gradient to 60% buffer B was applied to the column within 60 mL to elute the target protein. Fractions that showed a brownish colour, hence the desired protein, were combined and concentrated to 30 mL using a stirred ultrafiltration cell (10-30 kDa cut-off filter). To remove imidazole the protein solution was loaded with 3 mL/min onto a S75 gel filtration column (50 mL, XK26, internal diameter 26 mm) equilibrated with buffer C, for buffer exchange. Collected brown fractions were combined and chemically reconstituted. After reconstitution, the sample was concentrated to 3 mL by a stirred ultrafiltration cell and subsequently loaded onto a size exclusion S200 column (300 mL, XK26, internal diameter 26 mm). The Size-Exclusion column allowed the separation between FeS-protein aggregates, which eluted first as a black solution and pure protein, which eluted immediately after as a golden-brown fraction. Golden-brown

fractions were pooled, chemically re-reconstituted and concentrated to around 1 mM of protein concentration. Directly after, the protein was separated into 100-300 µL aliquots and stored at -80 °C until further use.

Table 7.12: Composition of His_6ThitHydG purification buffers.

HydG buffer A	HydG buffer B	HydG buffer C
25 mM HEPES	25 mM HEPES	25 mM HEPES
500 mM NaCl	500 mM NaCl	500 mM NaCl
10% (w/v) glycerol	10% (w/v) glycerol	10% (w/v) glycerol
20 mM Imidazole	500 mM Imidazole	-
-	-	5 mM DTT
pH 7.4	pH 7.4	pH 7.4

Table 7.13: Composition of His_6ThitHydE1265 and His_6ThitHydE1265 purification buffers.

HydE buffer A	HydE buffer B	HydE buffer C
50 mM Tris	50 mM Tris	50 mM Tris
250 mM KCl	250 mM KCl	250 mM KCl
10% (w/v) glycerol	10% (w/v) glycerol	10% (w/v) glycerol
20 mM Imidazole	500 mM Imidazole	-
-	-	5 mM DTT
pH 8.0	pH 8.0	pH 8.0

Method 16 Anaerobic purification of StrepII-tagged enzymes

Under anaerobic conditions in the glovebox, the beige cell pellet from a StrepThitHydF, StrepThitHydG or StrepThitHydE expression was resuspended in buffer SA (3 mL/g of pellet). Buffer SA was supplemented with lysozyme (1 mg/g of pellet) and EDTA-free protease inhibitor tablet (1 tablet per 50 mL) and the suspension was stirred in a ice cooled-water bath for 45 min. Sonication was used to lyse the cells for 60 min (6 x 10 min, 1 s bursts, 20 W) and centrifugation for separating the soluble from insoluble proteins (18000 rpm, 4 °C, 45 min). Clear supernatant was loaded with 3 mL/min onto a Strep-Tactin® column (Strep-Tactin® Superflow® high capacity resin, 50 mL, XK26, internal diameter 26 mm) equilibrated with buffer SB. After loading the clear lysate and washing the column with buffer SB until the 280 nm absorbance returned to baseline

level, the desired protein was eluted with a linear gradient to 100% buffer SC within 60 mL. Slightly brown fractions that contained the protein according to the absorbance at 280 nm were combined and concentrated using a stirred ultrafiltration cell (10-30 kDa cut-off filter). The protein solution was concentrated up to a protein concentration of 1.2 mM. Subsequently, the protein solution was divided into 100-300 µL aliquots, flash frozen in liquid nitrogen and kept at -80 °C until further use.

Table 7.14: Composition of StrepII-tagged protein purification buffers for HydF and HydE.

HydF buffer SA=SB	HydE buffer SA=SB
25 mM HEPES	50 mM Tris
300 mM KCl	250 mM KCl
5% glycerol (w/v)	10% glycerol (w/v)
1 mM DTT	1 mM DTT
pH 8.0	pH 8.0
for SC buffer	**for SC buffer**
+ 5 mM D-desthiobiotin	+ 5 mM D-desthiobiotin

Table 7.15: Composition of StrepII-tagged protein purification buffers for HydG.

HydG buffer SA	HydG buffer SB	HydG buffer SC
25 mM HEPES	25 mM HEPES	25 mM HEPES
500 mM NaCl	500 mM NaCl	500 mM NaCl
10% glycerol (w/v)	10% glycerol (w/v)	10% glycerol (w/v)
-	1 mM TCEP	0.5 mM TCEP
-	-	5 mM D-desthiobiotin
pH 7.4	pH 7.4	pH 7.4

Method 17 Analytical Gelfiltration

Samples of affinity purified and reconstituted StrepThitHydF and His_6ThitHydG were individually or loaded together with 0.5 mL/min onto an S200 Econo Column with Flow Adapter (Bio Rad, 1.5 cm x 50 cm, 75 mL) equilibrated in HydF buffer SA (Table 7.14). Cytochrome C (12.4 kDa), carbonic anhydrase (29 kDa), bovine albumine (66 kDa), alcohol dehydrogenase (150 kDa) and β-Amylase (200 kDa) from a Sigma-Aldrich Kit were used as standards to calibrate the column. The void volume (V_0 = 18 mL) of the column matches the retention volume of a loaded blue dextran (2000 kDa, 1 mg/mL) sample. The retention time and elution volume V_e of the protein samples was

monitored by absorbance at 280 nm. A calibration curve (Figure 7.1) was used to estimate the molecular weight and/or multimeric state of [FeFe]-hydrogenase maturation proteins or protein complexes, after recording their retention time.

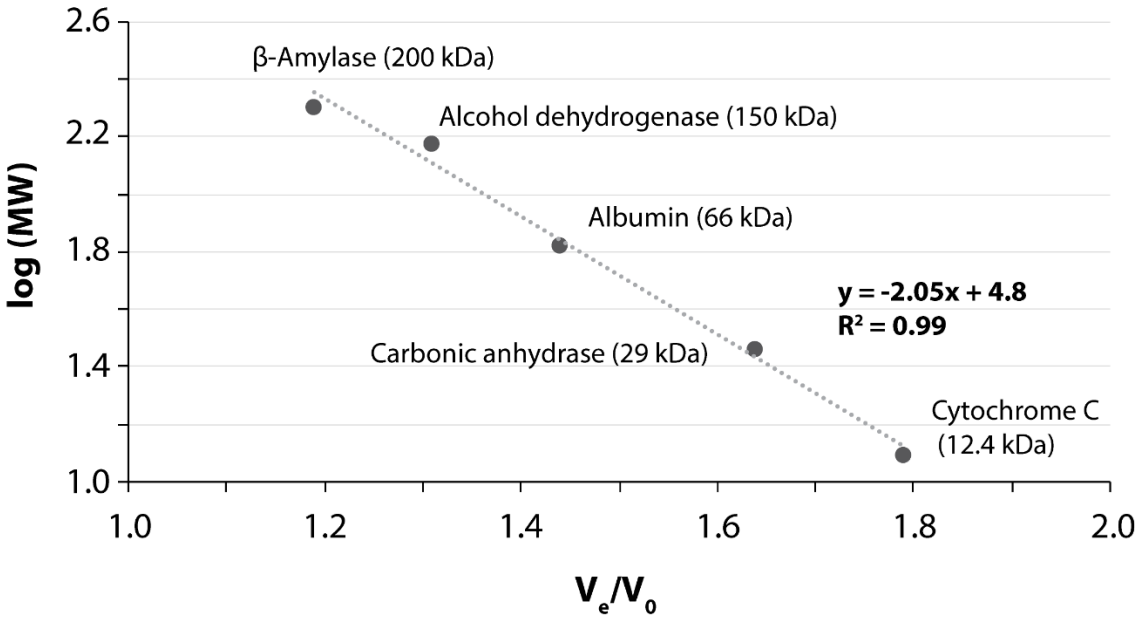

Figure 7.1: Calibration graph of the analytical gel filtration column.

Method 18 Protein concentration determination by Bradford assay

Protein concentrations in solution were determined using the Bradford[277] protein assay, a spectroscopical procedure using the principle of protein-dye binding. In a clear 96-well half-area microplate 10 µL of protein samples were mixed with 100 µL of Bradford reagent. The absorbance of the solution at 595 nm was recorded with a microplate reader. Solutions with defined BSA concentrations were used for calibration (Table 7.16).

Table 7.16: BSA calibration solutions for the Bradford assay.

BSA stock (1 mg/mL)/ µL	dH_2O/ µL	Final concentration/ mg/mL
0.000	10.000	0.000
1.250	8.750	0.125
2.500	7.500	0.250
5.000	5.000	0.500
10.000	0.000	1.000

Method 19 SDS-PAGE analysis

SDS-PAGE analysis was used for the determination of protein sizes and quantities. Components listed in Table 7.17 were mixed together for four 15% resolving polyacrylamide gel and filled between two glass plates (BioRad, 5 mL each double plate). Isopropanol was added on the top of the gel to ensure a plane surface and the gel left to polymerize for 45 mi at RT. Subsequently isopropanol was removed and the stacking gel mix applied onto the top, a teflon comb inserted and left for further 45 min at RT. After the comb was removed the wells were washed with dH_2O. Gels were stored at 4 °C until further use.

Table 7.17: Components of a 15% polyacrylamide gel.

	Resolving gel	Stacking gel
Component	**Quantity**	
Deionised water	4.6 mL	5.5 mL
30% (w/v) Acrylamide	10 mL	1.3 mL
1.5 M Tris (pH 8.8)	5 mL	-
1 M Tris (pH 6.8)	-	1 mL
10% (w/v) SDS	200 μL	80 μL
10% (w/v) APS (fresh)	200 μL	80 μL
TEMED	8 μL	8 μL

Diluted protein samples (10-20 μL, 1-2 mg/mL) were mixed with 2x SDS-PAGE loading buffer (10-20 μL, Table 7.18) and heated at 95 °C in a PCR cycler. Samples were loaded onto the gel and separated by electrophoresis at 200 V (~45 min) in 1x SDS-PAGE running buffer (Table 7.18). Gels were stained by heating in Coomassie Brilliant Blue R250 stain (Table 7.19) in the microwave for 60 sec and cooling on a rocker for 5 min. Gels were left to destain for several hours in destain buffer (Table 7.19) and imaged afterwards.

Table 7.18: Composition of the 2x SDS-PAGE loading and 1x SDS-PAGE running buffer.

Component	Quantity	Final concentration
2x SDS-PAGE loading buffer		
400 mM Tris·HCl, pH 6.8	25 mL	100 mM
Bromophenol Blue	0.2 g	0.2% (w/v)
SDS	4 g	4% (w/v)
Glycerol	20 g	20% (w/v)
DTT*		200 mM
Adjust to 100 mL with dH_2O, store at RT.		
* Add DTT (31 mg) shortly before use to 1 mL buffer.		
1x SDS-PAGE running buffer		
TrisBase	15.1 g	125 mM
Glycine	94 g	1.25 M
10% (w/v) SDS	5 g	3.5 mM
Adjust to 5 L with dH_2O.		

Table 7.19: Composition of SDS-PAGE imaging solutions.

Component	Quantity	Final concentration
SDS-PAGE stain solution		
Acetic acid	100 mL	10% (v/v)
MeOH	100 mL	10% (v/v)
Coomassie Brilliant Blue R250	2.5 g	0.25% (w/v)
Adjust to 1 L with deionised water.		
SDS-PAGE destain solution		
Acetic Acid	375 mL	7.5 % (v/v)
Methanol	250 mL	5 % (v/v)
Adjust to 1 L with deionised water.		

7.6 Protein reconstitution and activity assays

Method 20 Chemical reconstitution of iron-sulfur cluster enzymes

Purified [FeFe]-hydrogenase maturation proteins required chemical reconstitution of their iron-sulfur clusters, since the expression in *E. coli* BL21 (DE3) or even *E. coli* ΔiscR BL21 (DE3) resulted in an insufficient loading of iron-sulfur cluster cofactors. Reconstitution of the proteins were carried out under strictly anaerobic conditions in the glovebox.

His_6-tagged HydG and HydE proteins were reconstituted after Ni-NTA purification including buffer exchange. Initially the protein solution was reduced by addition of 5 mM DTT (200 mM stock in dH_2O) and incubation for 30 min. Depending on the cluster binding sites HydG and HydE1265 (2x iron-sulfur cluster binding sites) were loaded with 10 molar equivalents of $FeCl_3$ and HydE1675 (1x iron-sulfur cluster binding sites) with 5 molar equivalents of $FeCl_3$ by the dropwise addition of a $FeCl_3$ solution. The molar equivalents were added in respect to the protein concentration. After an incubation period of 30–60 min another 10 molar equivalents of $Na_2S{\cdot}9H_2O$ for HydG and HydE1265 or 5 molar equivalents of $Na_2S{\cdot}9H_2O$ for HydE1675 were added drop by drop and left to incubate for 2 h or overnight. Precipitated protein and excess FeS were removed by centrifugation (18000 rpm, 15 min, 4 °C). Subsequently after the purification by size exclusion chromatography the protein solution was re-reconstituted with 5 mM DTT, 5 molar equivalents of $FeCl_3$ and $Na_2S{\cdot}9H_2O$ (HydG and HydE1265) or 3 equivalents of $FeCl_3$ and $Na_2S{\cdot}9H_2O$ (HydE1675) following the previously described protocol. Fully reconstituted protein solutions were aliquoted, concentrated to around 1 mM, flash frozen in liquid N_2 and stored at -80 °C until further use.

Strep-tagged HydF was reconstituted after Strep purification. Frozen aliquots (100 μL) of unreconstituted HydF were thawed, 5 mM of GSH (200 mM stock in dH_2O) was added and incubated for 30 min. Subsequently, 5 to 8 molar equivalents of $FeCl_3$ (50 mM stock) were added and left to incubate for 1 h. Precipitated iron salts were dissolved by mixing the protein solution with a pipette. Immediately after, 5 to 8 molar equivalents of $Na_2S{\cdot}9H_2O$ were added and incubated for 2 h. To remove excess FeS the reconstituted HydF solution was passed through a PD-10 desalting column and concentrated using 10 kDa cut-off spin filters. Reconstituted HydF was stored in aliquots at -80 °C until further use.

Method 21 Chemical insertion of H-cluster Mimic into recon. HydF

The method of chemical insertion of the pdt-Mimic into recon. HydF is adapted from Fontecave *et al.*.[244] For the insertion, a solution of reconstituted HydF (500 μL) was applied onto a PD-10 column for buffer exchange into 25 mM HEPES, 300 mM KCl, 5% glycerol (w/v) pH 8.0, to remove any excess of DTT, which might decompose the organometallic compound. Subsequently, 50 μM of recon. HydF was incubated with 10 molar equivalents of the pdt-Mimic in deionized water (500 μM) for 1 h or overnight at 18 °. After incubation, the unbound pdt-mimic molecules were removed with a PD-10 column equilibrated in the same buffer as HydF. The resulted pdt-Mimic loaded recon. HydF solution was concentrated and stored at -80°C until further use. Incorporation of the pdt-mimic complex was analysed by UV-Vis spectroscopy (Method 24), FISH assay (Method 21) and FT-IR spectroscopy (Method 26).

Method 22 Quantification of iron equivalents – the FISH assay

Reconstituted and unreconstituted protein samples (concentrations between 10-100 μM) in 500 μL were tested for their iron content using a modified version of the colorimetric FISH assay[318]. An iron calibration curve was prepared by measuring different dilutions of an $FeCl_3 \cdot 7H_2O$ stock (50 μg/mL in dH_2O). The corresponding iron contents for the calibration curve are summarized in Table 7.20.

Table 7.20: Dilution series for the Fe^{3+} calibration curve.

(50 μg/mL) Fe^{3+} stock/ μL	dH_2O/ μL	n Fe^{3+}/ nmol
400	600	74
350	650	64.75
300	700	55.5
250	750	46.25
200	800	37
150	850	27.75
100	900	18.5
50	950	9.25
30	970	5.55
10	990	1.85
0	1000	0

A freshly prepared solution of reagent A (0.142 M $KMnO_4$ in 0.6 M HCl, 500 µL) was added to all the samples (500 µL volume) and incubated for 2 h at 60°C in a water bath. In the meantime, 12 mL of reagent B was prepared containing ascorbic acid (2 M), ammonium acetate (5 M), ferrozine (6.5 mM) and neocuproine (13.1 M). As soon as the samples were cooled down to room temperature, 100 µL of the yellow reagent B was mixed with the samples by shaking or vortexing turning the sample to a pinkish colour. Following 10 min incubation at room temperature the absorbance at 562 nm was measured with an UV-Vis spectrometer. The amount of iron was estimated with the iron calibration curve (Table 7.20 and Figure 7.2).

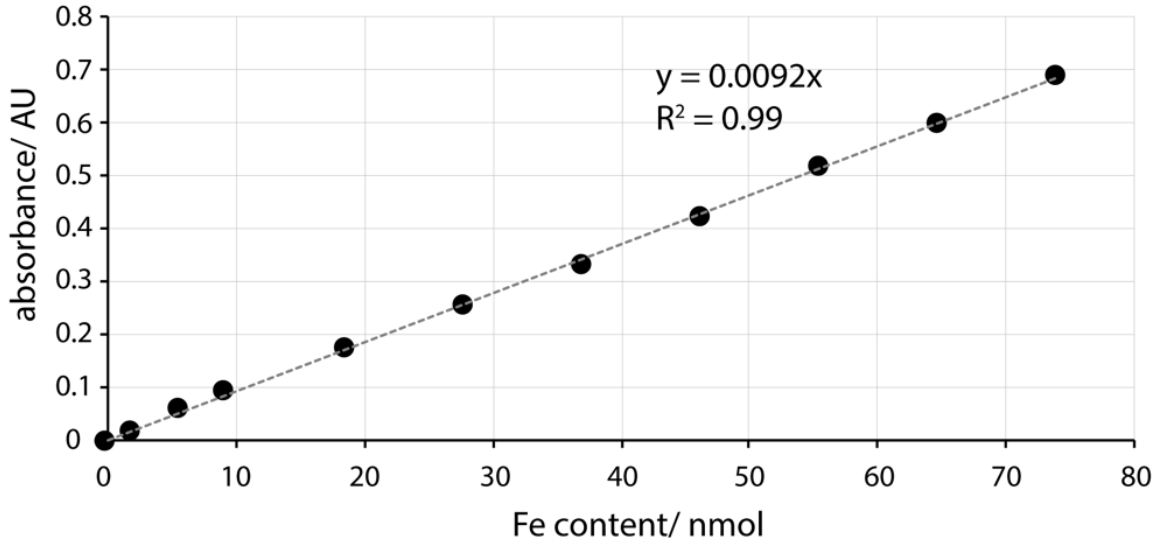

Figure 7.2: Typical Fe content calibration curve with slope.

Method 23 GTPase activity assay

Under an anaerobic atmosphere, assays containing a total volume of 200 µL were prepared with 40 µM HydF, 2 mM $MgCl_2$, 2 mM GTP in the absence and presence of HydG, HydE1265 and HydE1675 (40 µM) in buffer HydF buffer SA (25 mM HEPES, 300 mM KCl, 5% glycerol, 1 mM DTT, pH 8.0). In a waterbath outside the glovebox the assay mixtures were pre-equilibrated at 37°C for 5 min and then further incubated for 4 or 20 min. By using small spin filters (10 kDa cut-off) the protein was separated from the assay solutions. Assay mixtures were subsequently analysed by HPLC or stored at -80°C until further analysis.

Method 24 Coupled and uncoupled HydG and HydE activity assays

Assay solutions were mixed under an anaerobic atmosphere inside a glovebox. All assay compound stock solutions were prepared freshly. To obtain a 20 mM Tyrosine stock solution, 350 μL of a 25.71 mM Tyrosine solution (5.5 mg in 1180 μL) in 200 mM HCl were added to 20 μL buffer and 80 μL 1 M NaOH. All other solutions and assay mixtures were made in assay buffer (50 mM HEPES, 500 mM KCl, pH 7.4). Frozen reconstituted enzymes (HydG, HydE1265, HydE1675 and HydF) were thawed and the concentration in each assay mixture is 25 μM. Assays (230 μL) were prepared in duplicates, if not other stated, in 1.5 mL Eppendorf tubes. A full coupled assay contained 25 μM HydG, 500 μM SAM, 200 μM cysteine, 200 μM $FeCl_2$ which was added in the stated order and left for 20 min, to ensure the incorporation of the 5th iron on the HydG auxiliary cluster. This was followed by the addition of 1 mM Tyr, 25 μM HydE1265, 25 μM HydE1675, 25 μM HydF and 1 mM DTH. Additional supplements were 2 mM GTP, 500 μM PLP, 300 μM DTT, 200 μM $Na_2S{\cdot}9H_2O$, 200 μM GSH, 20% (v/v) clear lysate of a *E. coli* ΔiscR BL21 (DE3) culture (4 mg/mL) or 40% (v/v) PD-10 desalted clear lysate of a *E. coli* ΔiscR BL21 (DE3) culture (2 mg/mL). The samples were immediately transferred to a water bath outside the glovebox and pre-equilibrated at 37 °C for 5 min, followed either by incubations at selected time points or for a 60 min incubation. Reactions were stopped by addition of 17.25 μL 20% perchloric acid. Precipitated protein and compounds were removed by centrifugation (13200 rpm, 10 min, RT) and the cleared assays were divided into 10 μL aliquots for the glyoxylate assay and 100 μL aliquots for the HPLC analysis of the SAM assay, which were subsequently flash frozen in liquid nitrogen and stored at -80 °C until HPLC analysis.

7.7 Protein spectroscopy

Method 25 UV-Vis spectroscopy

UV-Vis spectra of proteins were recorded inside the glovebox under anaerobic conditions. A Mini-D2 lightsource with DT-Mini-2B or Mini-D2-GS light bulb and USB2000 spectrometer are outside the glovebox connected through QP400-2-SR-BX fibres to the cuvette holder inside the glovebox. Either a 1 cm or 1 mm cuvette was used to analyse protein or cofactor solutions. Integration times between 300-600 ms were used for data acquisition. For quantification of iron-sulfur cluster incorporation, the absorption at the appropriate wavelength was subtracted from the background at 880 nm (the end of the spectrum). UV-Vis spectroscopy was used for the protein concentration determination at 280 nm, by using the theoretical protein extinction coefficient estimated with the tool ProtParam. For reconstitution studies, only protein concentration measured with UV-Vis spectroscopy were used for [4Fe4S]-content determination.

Method 26 EPR spectroscopy

For the EPR experiments carried out with the small resonator (ER4118X-MS2), reconstituted protein aliquots of His_6HydG, StrepHydE1265 and StrepHydF (400 μM each) or premixed samples of His_6HydG and StrepHydE1265 with 3 mM SAM or StrepHydF with 10 mM GTP were thawed inside a Braun UniLab-plus glovebox at room temperature. A 100 mM stock of sodium dithionite in water was added to the sample to give an end concentration of 10 mM. Immediately after, the sample (10 μL) was transferred into a WG-222T-RB Q Band Suprasil EPR tube (OD = 2 mm), frozen in a cold trap containing ethanol, cooled from outside the glovebox with a dry ice/acetone bath and then stored in liquid nitrogen until analysis by EPR.

The EPR experiments for ThitHydG experiments were adapted from studies carried out by Britt *et al.*[66] including additional samples of StrepHydE1265 and StrepHydF. These samples were measured in the large resonator (ER4118X-MD5) and prepared inside a Braun UniLab-plus glovebox (see Table 7.21). For that, reconstituted protein aliquots were thawed inside a glovebox and the appropriate supplements were added in the same order as presented in Table 7.21. All compound stocks were prepared freshly (30 mM SAM, 30 mM L-Cys, 30 mM $FeCl_2$, 100 mM DTH, 100 mM GTP) in

HydG C buffer (25 mM HEPES, 500mM NaCl, 10% glycerol (w/v), 5 mM DTT at pH 7.4).

Subsequently, after everything was added to the protein solution, it was transferred into Wilmad Quartz (CFQ) tubes (4 mm OD) and immediately frozen in liquid nitrogen and analyzed.

The EPR sample preparation and measurements were carried out with the help of Prof. Maxie Roessler, Dr. Enrico Salvadori and John Wright at Queen-Mary University London.

Table 7.21: EPR sample composition for the large resonator experiments.

Sample	Sample contents
1	450 uM HydG
2	450 uM HydG, 10 mM DTH
3	450 uM HydG, 10 mM DTH, 3 mM SAM
4	450 uM HydG, 10 mM DTH, 3 mM SAM, 3 mM Fe
5	450 uM HydG, 10 mM DTH, 3 mM SAM, 3 mM L-Cys
6	450 uM HydG, 10 mM DTH, 3 mM SAM, 3 mM L-Cys, 3 mM Fe
7	300 uM HydF, 20 mM DTH
8	300 uM HydF, 20 mM DTH, 10 mM GTP
9	300 uM HydE1265, 10 mM DTH, 3 mM SAM

First derivatives of the EPR spectra were baseline corrected by Dr. Enrico Salvador and plotted with Microsoft Excel. EPR data with high noise was smoothed using the exponential smoothing tool of Microsoft excel with a damping factor of 0.9. Simulations of the EPR spectra were generated with the EasySpin[(350)] software in combination with MATLAB.

Method 27 FT-IR spectroscopy

The HydG activity experiment for the FT-IR measurement has been carried out by Dr. Pedro Dinis and preliminary analysis by Dr. Philip Ash. In this thesis the detailed analysis of the results is provided by myself. In the following the experimental procedure fulfilled by Dr. Pedro Dinis is described. In preparation of the transmission FT-IR experiments, stock solutions of SAM (50 mM), L-cysteine (30 mM) and L-tyrosine (20 mM) were freshly prepared in HydG C buffer (25 mM HEPES, 500mM NaCl, 10% glycerol (w/v), 5 mM DTT at pH 7.4) inside a glovebox. Tyrosine stock solutions were prepared as described in Method 23. Reconstituted ThitHydG (only reconstituted with

5 eq. of Fe and S, see Chapter 2.2.3) was supplemented with the components of the prepared stock solutions (Table 7.22). Subsequently, the reactions were initiated by mixing HydG with the dithionite stock (100 mM). The time between addition of dithionite and measuring the first spectra was about 1-2 minutes. Moreover, the sample containing recon. HydF loaded with the pdt-Mimic was thawed and directly measured, without any additions.

Table 7.22: Contents of the HydG reaction mix, prepared for FT-IR measurements.

Solution (concentration)	HydG reaction mix	Final concentration
Recon. HydG (1000 μM)	50 μL	500 μM
SAM (30 mM)	10 μL	3 mM
Cys (30 mM)	10 μL	3 mM
Tyr (20 mM)	15 μL	20 mM
Buffer	5 μL	-
DTH (100 mM)	10 μL	10 mM
Total volume	100 μL	-

7.8 Protein-protein interaction assays

Method 28 Pull-down assays

In preparation for pull-down assays little columns (volume 0.7 mL) fitting in 1.5 mL Eppendorf tubes were filled with 100 μL StrepTactin high capacity resin and transferred into the glovebox. The resin was equilibrated with 2 x 500 μL E-buffer, which was either low salt HydF buffer (25 mM HEPES, 30 mM KCl, 5% glycerol (w/v) pH 8.0) or HydF buffer (25 mM HEPES, 300 mM KCl, 5% glycerol (w/v) pH 8.0).

For the interaction mixture, reconstituted protein aliquots of StrepHydF and His_6-tagged HydG or HydE were thawed or freshly reconstituted protein was diluted in the equilibration buffer (E-buffer) to a concentration between 40-100 μM. Freshly prepared stocks of tyrosine (as described in method 23, 20 mM), DTH (100 mM), SAM (80 mM), cysteine (100 mM), $FeCl_2$ (100 mM), GTP (50 mM), GSH (50 mM), Gly/Cys Mix (20 mM) were added to different end concentrations. As a control StrepHydF and BSA or TrmD were mixed together with the same additives as the HydG or HydE partner

enzyme. The resulted interaction mix was incubated for 1 h at 18 °C inside the glovebox.

After the incubation period the interaction mixture (50 μL) was applied onto the equilibrated StrepTaction resin and incubated for further 10 min. Subsequently the column was washed with E-buffer (3 x 500 μL). StrepHydF and the corresponding bound protein were incubated for 10 min and eluted with E-buffer + 5 mM d–Dethio-biotin with either 1 x 200 μL plus 1 x 100 μL or with 3x100 μL. The elution and wash fractions were analysed by SDS-PAGE. Quantification of protein bands was carried out with the program ImageJ[412].

7.9 HPLC methods

Method 29 Quantification of GTP and GDP

To quantify GTP and GDP resulted from the GTPase activity assay with HydF a modified HPLC method was used. To remove excess particles the assay mixture was centrifuged (5 min, 13.2 krpm, RT) and directly applied to a Gemini C_{18} reverse phase HPLC column (4.6 82 x 150 mm, 5 µm, 150 Å) equilibrated with 85 % solvent A (5% MeOH, 15 mM N,N- dimethylhexylamine (DMHA) adjusted to pH 7.0 with acetic acid), 0.8 mL/min. Subsequently after injection the program was starting by applying 85% solvent A for 5 min, followed by a gradient to 90 % solvent B (80% MeOH, 15 mM DHMA, adjusted to pH 7.0 with acetic acid) within 28 min. Moreover, an isocratic phase over 5 min was applied to the column and finished with return to 15 % solvent B over 1 min. As a preparation for the next measurement, the column was re-equilibrated with 85 % solvent A for 10 min. GTP and GDP were detected at an absorbance wavelength of 260 nm. The amounts of GDP (RT = 21.1 ± 2 min) and GTP (RT = 27.4 ± 2 min) (see Figure 7.3) were calculated relative to the GTP and GDP (2, 1.5, 1, 0.5, 0.25 mM standards) calibration standards shown in Figure 7.4.

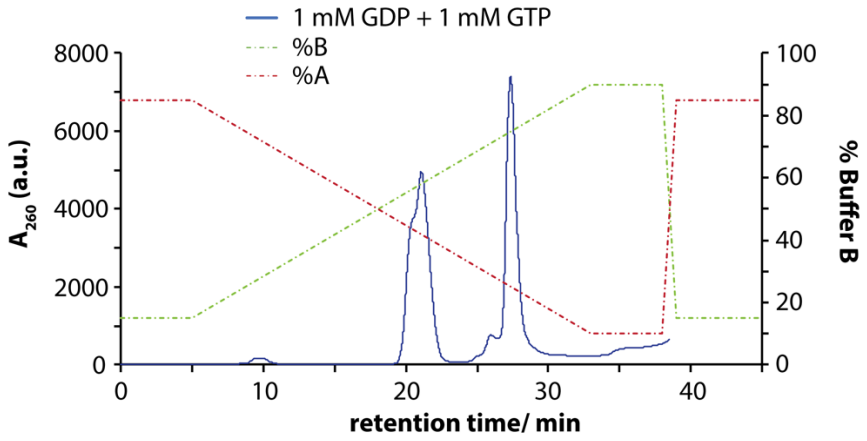

Figure 7.3: Elution profile of the GTP assay HPLC trace containing a mixture of 1mM GTP and 1 mM GDP.

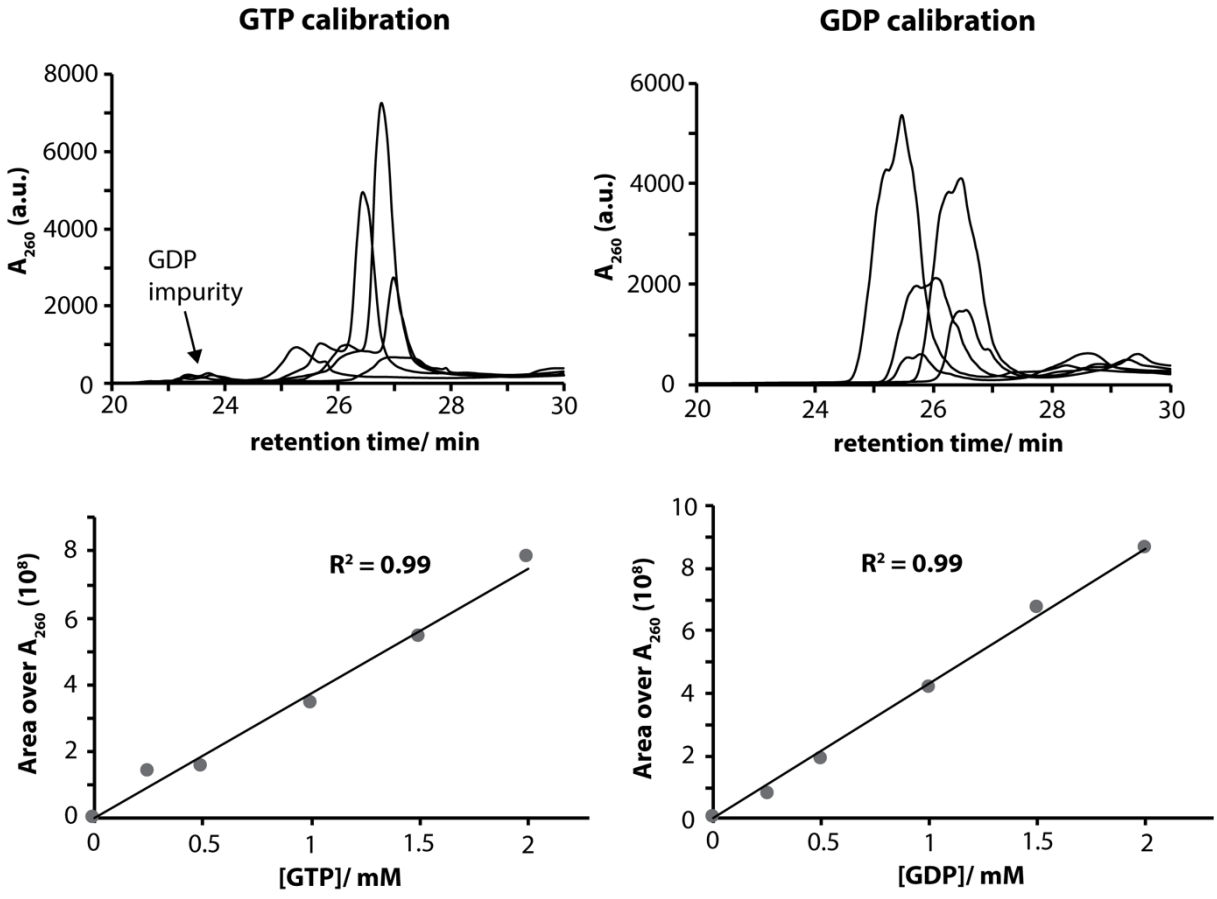

Figure 7.4: Calibration standards of GTP and GDP analysed by HPLC, the integrated areas of the resulting peaks were plotted against the respective concentration.

Method 30 Quantification of DOA and *p*-cresol

To analyse and quantify the products of the coupled and uncoupled HydG and HydE activity assay a modified HPLC method has been applied. To remove any precipitation the assay mixture was centrifuged (5 min, 13.2 krpm, RT) and directly applied to a Gemini C_{18} reverse phase HPLC column (4.6 82 x 150 mm, 5 µm, 150 Å) which was equilibrated with 100% solvent A (0.1% (v/v) acetic acid in water, 0.8 mL/min). After injection (40 µL), the column was further washed with 100% solvent A for 8 min and followed by a gradient to 50% solvent B (0.1% (v/v) acetic acid in acetonitrile) over 32 min. For a period of 3 min the gradient was further increased to 100% solvent B and held isocratically for 5 min, when returned to 100% solvent A within 0.5 min. Prior to the next injection, the column was re-equilibrated with 100% solvent A for 10 min. The complete HPLC run took 60 min. Reaction products were monitored with a dual wavelength UV-Vis detector set at an absorbance wavelength of 254 nm for detection of 5'-dAH and 280 nm for L-tyrosine. Whereas, the cleavage product *p*-cresol (and L-tyrosine) was observed via a fluorescence detector set at λ_{ex} = 274 nm and λ_{em} = 312 nm. Amounts of 5'-dAH (RT = 18 min), *p*-cresol (RT = 41 min), SAM (RT = 2.2 min) and L-tyrosine (RT = 7 min) were quantified by consulting a calibration curve of synthetic standards (Figure 7.5).

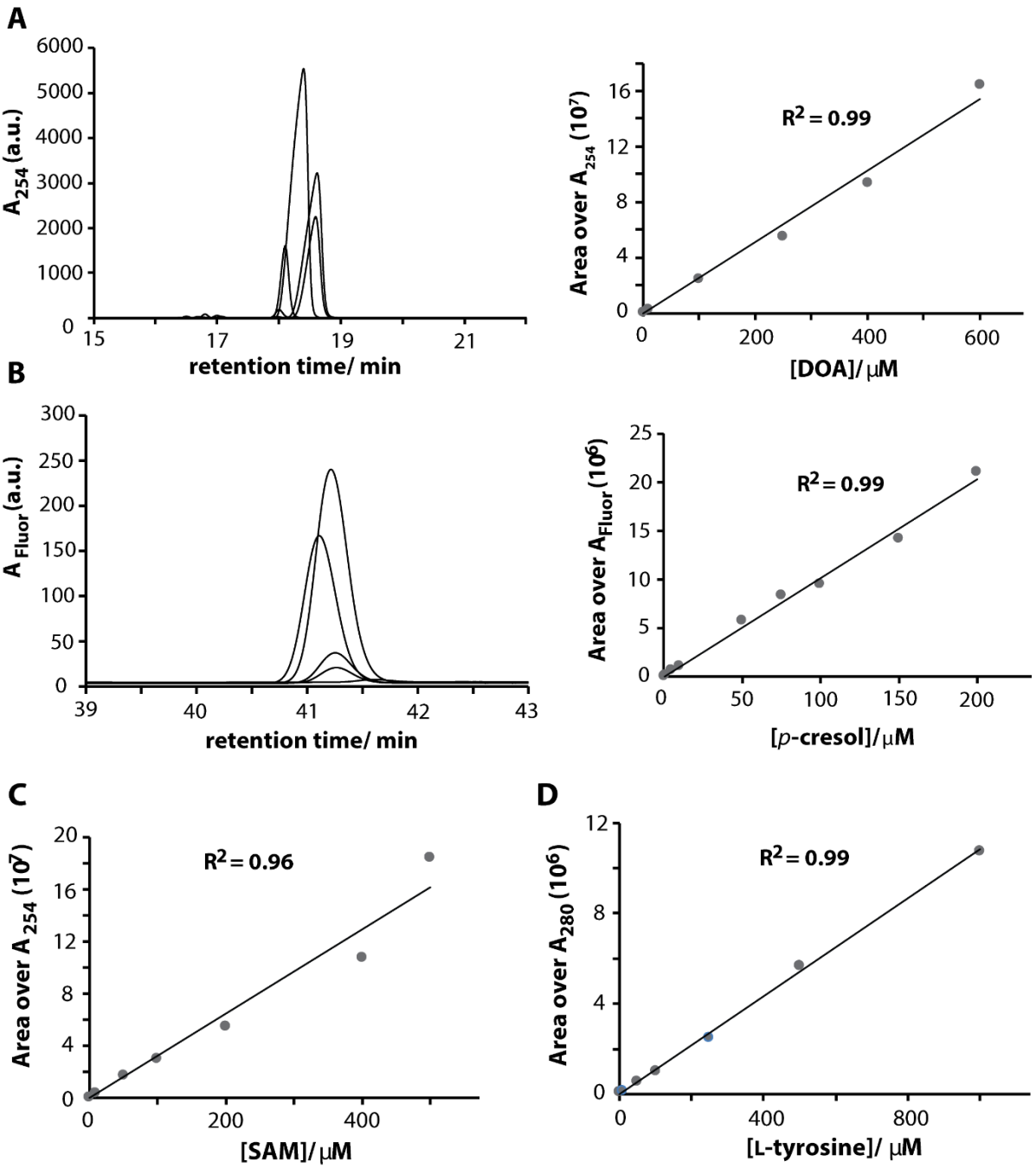

Figure 7.5: Calibration standards of DOA (A), *p*-cresol (B), SAM (C) and L-tyrosine (D) analysed by HPLC, the integrated areas of the resulting peaks were plotted against the respective concentration.

Method 31 Quantification of glyoxylate

The quantification of glyoxylate was carried out after the derivatisation reaction with *o*-phenyl diamine resulting in the formation of the fluorescent soluble compound 2-quinoxalinol which is detectable with fluorescent HPLC. The protocol for the derivatisation was adapted from Driesener *et al.*[60] and described here after. Cleared assay supernatants (Method 23) were diluted with 50 mM HEPES, pH 7.5 to 50 µL, and acidified after with 0.5 M HCl (100 µL) as well as supplemented with *o*-phenyl diamine in 0.5 M HCl (10 mg/ml, 50 µL). All samples were incubated at 25 °C for 1 min, heated at 95 °C for 10 min, then returned to 25 °C for 10 min, in a PCR machine. Subsequently, 1.25 M NaOH (120 µL) was added and incubated at 5 °C for 5 min in a temperature controlled room. Samples were directly stored at -80 °C and thawed only shortly before HPLC analysis. The reaction mixture (40 µL) was applied on a Gemini C_{18} reverse phase HPLC column (4.6 82 x 150 mm, 5 µm, 150 Å) equilibrated with 85% solvent A (100 mM ammonium bicarbonate, 0.8 mL/min). Following the injection, the column was washed with 85% solvent A for 5 min, and a gradient to 50% solvent B (100% acetonitrile) was applied over 15 min. For a 1 min period the gradient was further increased to 100% solvent B, hold isocratically for 4 min and returned to 85% solvent A over 1 min. The column was re-equilibrated with 85% solvent B for 10 min, before the next injection. A fluorescence detector set at λ_{ex} = 350 nm and λ_{em} = 420 nm, monitored the elution of 2-quinoxalinol (R = 8.5 min). Due to high background caused by dithionite, which was added to the assay mixtures, the calibration curve of the synthetic 2-quinoxalinol standards (Figure 7.6) were measured in the presence of dithionite (1 mM) and were treated the same as control assays mixtures lacking the enzymes.

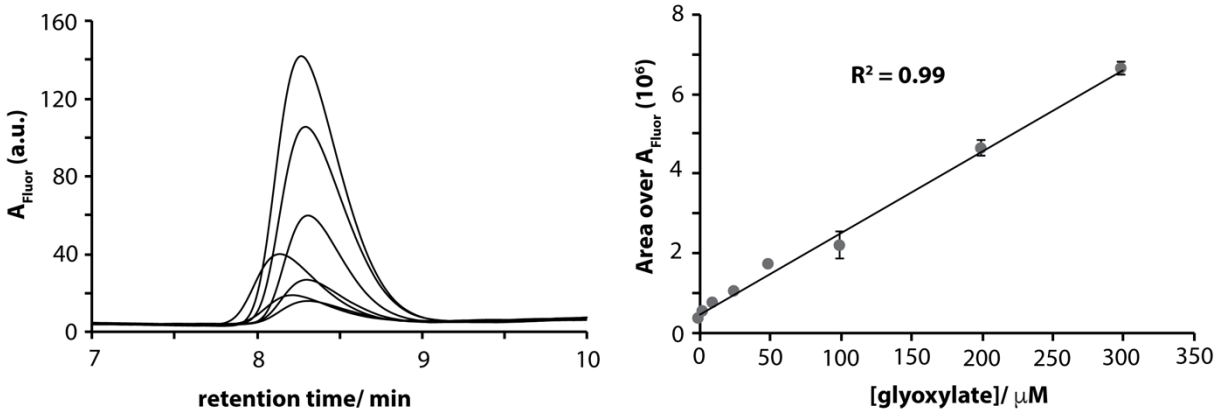

Figure 7.6: Calibration standards of derivatized glyoxylate analysed by HPLC, the integrated areas of the resulting peaks were plotted against the respective concentration.

7.10 Protein crystallography

[FeFe]-hydrogenase maturation (Hyd) proteins were prepared in the appropriate protein buffer either in HydF buffer (25 mM, HEPES, 300 mM KCl, 5% glycerol (w/v), pH 8.0) or in HydG buffer (20 mM HEPES, 500 mM NaCl, 10% (w/v) glycerol, pH 7.4). For crystal trays containing both HydF and HydG, HydF buffer was used to prepare small compound stock solutions. L-tyrosine stocks were prepared as described before (Method 23).

Final protein concentrations were always above 300 μM. Crystallisation processes was monitored with a microscope inside the glovebox, initially every second day, then every week.

Method 32 Preparation of 96-well sitting-drop crystallization plates

The appropriate 96-well sitting-drop crystallization plates were purged with nitrogen in the big port of the glovebox for 10 min, before being placed inside the glovebox 24 h before requirement. Mixtures of proteins and substrates (at least 130 μL) were prepared in 1.6 mL Eppendorf tubes using stocks of at least 1 mM freshly reconstituted HydF or freshly thawed HydG, as well as freshly prepared stocks of 80 mM SAM, 20 mM tyrosine, 100 mM cysteine, 100 mM $Fe^{2+}Cl_2$, 1 mM pdt-mimic, 100 mM GTP, 100 mM TCEP and 100 mM dithionite. With the help of a multichannel pipette, commercial screening buffers (50 μL) were transferred into the 96 main reservoir wells. Subsequently, the appropriate protein-substrate mixture was filled into PCR tubes (lid-cut, 12 x 10.5 mL). Quickly after, three different protein-protein-substrate or protein-

substrate mixtures (1 μL) were placed with a multichannel pipette from the PCR tubes into the three sub-wells and the reservoir solution (1 μL) was placed onto the protein mixture drop immediately, resulting in a 1:1 mixture of protein and precipitant solution. To avoid any evaporation the plate was directly covered with a transparent adhesive film and incubated at 18-20°C inside the glovebox.

Method 33 Crystal freezing

Objects that appeared to be a protein crystal were selected and tested at the Diamond or ESRF light source. To avoid crystal damage by transportation or radiation and ensure better quality data, the potential protein crystals were frozen prior to the measurement. For the crystal freezing the appropriate 96-well sitting-drop plate was removed from the glovebox. To isolate the crystal of interest the transparent adhesive film was cut precisely with a scalpel at the well where the crystal was spotted. In order to avoid water crystals, the protein crystal was cryo-protected by addition of 1 μL of 100% (w/v) glycerol. A cleaned CryoLoop in a matching size of the protein crystal was used to carefully remove the crystal and was subsequently flash frozen in liquid nitrogen. The frozen protein crystals in the CryoLoops were stored inside a dewar filled with liquid nitrogen until analysis at Diamond in Didcot, UK or ESRF in Grenoble, France.

7.11 ITC measurements

Method 34 General procedure for ITC experiments

ITC measurements on [FeFe]-hydrogenase maturation enzymes have been carried out on a Microcal ITC_{200}, inside the glovebox. All solutions and buffers used for ITC were made in HydF buffer lacking DTT (25 mM HEPES, 300 mM KCl, 5% (w/v) glycerol, pH 8.0).

Before starting the experiment, a thorough cleaning procedure has been carried out including washing the syringe and cell three times manually with desalted water followed by the automatic ‘cell water rinse’, ‘cell buffer rinse’ and ‘cell and syringe wash’. After the cleaning procedure the reaction cell and the corresponding reference cell were filled with the protein solution (each 250 μL). Subsequently, the syringe

needle was filled with the titrant (substrate or protein, 200 μL provided, 40 μL filled) and placed inside the centre cell. In the experimental design the total number of injections is set to 20 times 2 μL, and the temperature at 30°C. The syringe speed was set to 750 rpm, due to a cricked type of syringe. The first injection is unique and only 0.4 μL of the titrant solution is added to the cell. After setting up the experimental parameters the measurement is started. Analysis of ITC data was carried out with the MicroCal ITC-Origin Analysis software or with the online tool AffinityMeter[406,407].

Appendix

A 2.1 Plasmid maps, corresponding gene and protein sequences

pBMW001_StrepThitHydF

E.coli optimized gene sequence of StrepThitHydF

```
8698 ATG
8701 GCCGGGTCGT GGTCGCATCC GCAGTTCGAG AAGAACATGT CATCGGGGGT
8751 GATGAATACC ACACCGGTTA GCAGCCGTCT GCATATTGCA ATTTTTGGTC
8801 GTCGTAATGC AGGTAAAAGC AGCCTGATTA ATGCACTGAC CAATCAAGAA
8851 GTTGCACTGG TTTCAGACGT CGCAGGCACC ACCACCGATC CGGTGAGCAA
8901 AGCAATGGAA ATTCTGCCGA TTGGTCCGGT TGTTATTATT GATACCGCAG
8951 GTCTGGATGA TACCGGTGAA CTGGGCGAAC TGCGTGTGAA AAAAACCTAT
9001 GAAGTTCTGA ATCGTACCGA TCTGGCAATT CTGGTTATTG ATGGCACCAT
9051 TGGTCTGAGC GAATTTGAAG AAAACGTTCT GAAAGTGATC CGCGATAAAA
9101 ACATTCCGGT TGTGGGTGTG ATCAACAAAA AAGATCTGAG CCAGTATAGC
9151 GAAGAGGATA AACGTAAATG GGAAGAACGT CTGAAACTGG AACTGATTGA
9201 AGTTAGCGCA CTGAAAAAAC ATGGTATCGA AGCCCTGAAA ATGATGCTGA
9251 TCAAAAAAGC ACCGTATGAT GATCGTGAAC TGAGCATTGT TGGTGATCTG
9301 ATTAAACCGG GTGATTTTGT TGTTCTGGTG ATCCCGATTG ATAAAGCAGC
9351 ACCGAAAGGT CGTCTGATTC TGCCGCAGCA GCAGACCATT CGTGATATTC
9401 TGGATAATGA TGCAATGGCC ATCGTGACCA AAGAACATGA ACTGAAAGAA
9451 ACCCTGCAGA ACCTGGGTAA AAAACCGAGC CTGGTTATTA CCGATAGCCA
9501 GGCATTTCTG AAAGTTAGTG CAGATACCCC GAAAGATATT CCGCTGACCA
9551 GCTTTAGCAT TCTGTTTGCG CGCTATAAAG GCGATCTGGA AGAACTGGTT
9601 CGTGGTGTTA AAGCAATCAA AAAACTGAAA CCTGGCGACA AAGTTCTGAT
9651 TGCAGAAGGT TGTACCCATC ATCGTCAGCC GGATGATATT GGTAAAGTTA
9701 AAATTCCGCG TTGGATTCGT CAGATTGTTG GCGGTGATAT TCAGTTCGAA
9751 TGGTCAAGCG GTATTACCTT TCCGGATAAC CTGGAAGAAT ATAGCCTGAT
9801 TGTGCACTGT GGCGCCTGTA TGCTGAATCG TCGTGAAATG ATGTATCGTA
9851 TCAGCTACGC AAAAAGCAAA AATATCCCGA TCGTGAATTA TGGCATTCTG
9901 ATCGCCTATG TTCAGGGTCT GATGCCTCGT GCAATTGAAA TGTTTCCGCT
9951 GGCAAAAATG GTGTATGAAG AAGAGTAG
```

Plasmid map of pBMW001_StrepThitHydF

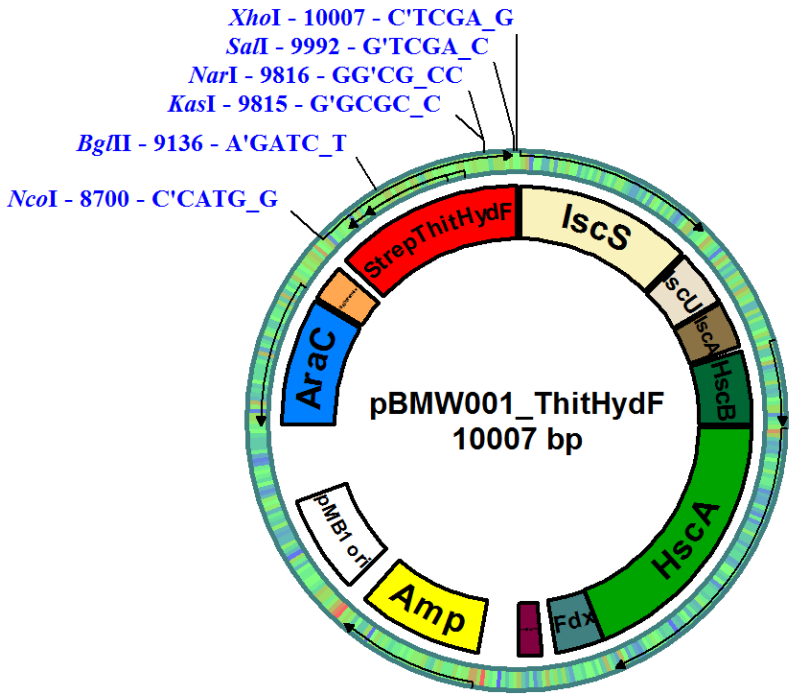

Amino acid sequence of StrepThitHydF

StrepThitHydF (47.54 kDa)

```
MAGSWSHPQF EKNMSSGVMN TTPVSSRLHI AIFGRRNAGK SSLINALTNQ 50
EVALVSDVAG TTTDPVSKAM EILPIGPVVI IDTAGLDDTG ELGELRVKKT 100
YEVLNRTDLA ILVIDGTIGL SEFEENVLKV IRDKNIPVVG VINKKDLSQY 150
SEEDKRKWEE RLKLELIEVS ALKKHGIEAL KMMLIKKAPY DDRELSIVGD 200
LIKPGDFVVL VIPIDKAAPK GRLILPQQQT IRDILDNDAM AIVTKEHELK 250
ETLQNLGKKP SLVITDSQAF LKVSADTPKD IPLTSFSILF ARYKGDLEEL 300
VRGVKAIKKL KPGDKVLIAE GCTHHRQPDD IGKVKIPRWI RQIVGGDIQF 350
EWSSGITFPD NLEEYSLIVH CGACMLNRRE MMYRISYAKS KNIPIVNYGI 400
LIAYVQGLMP RAIEMFPLAK MVYEEE 437
```

pBMW002_StrepThitHydE1265

E.coli optimized gene sequence of StrepThitHydE1265

```
8703 ATGGCCGG GTCGTGGTCG CATCCGCAGT TCGAGAAGCA TATGTCGGGG
8751 GTGATGCTGG AACTGATCAA AAAAGCCGAA GAAACCCATA CCCTGACCAA
8801 AAAAGAAATT GTGGAACTGC TGAAAGACGA CCAGTATAAC GATGAACTGT
8851 TTAAAGCAGC AGATCGCGTT CGCAAAAAAT ACGTTGGTGA TGAAGTGCAC
8901 CTGCGTGGCC TGATTGAATT TAGCAATATT TGCAAACAGA ACTGCCTGTA
8951 TTGTGGTCTG CGTCGTGATA ACAAAAACAT TAAACGTTAT CGCCTGAAAC
9001 CTGAGCAGAT TATCAATTTT GCCAAAAATG CGCGCAATCT GGGTTATCGT
9051 ACCGTTGTTC TGCAGAGCGG TGAAGATGAT TTTTTCAATG TTGAACGCAT
9101 GACCAAAATC ATCAAAAGCA TCAAAGAACT GGATGTGGCA ATTACCCTGA
9151 GCATTGGTGA AAAAACCCGT GAAGAATACA AAGCCTATAA AGAAGCAGGC
9201 GCCGATCGTT ATCTGCTGCG TATTGAAACC ACCGATAAAG AACTGTATGA
9251 AAAACTGGAC CCGAACATGA GCCATGAAAA TCGTAAACGT TGCCTGAAAG
9301 ATCTGAAAGA GCTGGGTTAC GAAGTTGGTA CCGGTTGTCT GATTGGTCTG
9351 CCTGGTCAGA CCATTGAAAG CATTGCAGAT GATATCCTGT TCTTCAAAGA
9401 AATCGATGCC GATATGATTG GTGTGGGTCC GTTTATTCCG AATCCGGATA
9451 CACCGCTGAA AAATGAAAAA GGTGGTACAT TTGAACTGAG CCTGAAAGTT
9501 ATGGCCATTA CCCGTCTGCT GATGCCGGAT ATTAACATTC CGGCAACCAC
9551 CGCAATGGAA AGCCTGAATA TTAACGGTCG CCTGATTGCA CTGCGTAGCG
9601 GTGCAAACGT TGTTATGCCG AATGTTACCG AAGGTGAATA TCGCAAACTG
9651 TATGCACTGT ATCCGGGTAA AATTTGCATC AATGATACAC CGGCACATTG
9701 CTTTAGCTGT ATTACCGGCA AAATTAATAG CATTGGTCGT CCGATTGCAA
9751 AAGATTATGG TTACCGTAAA AAAGTGATGA GCAAAAAATA A
```

Plasmid map of pBMW002_StrepThitHydE1265

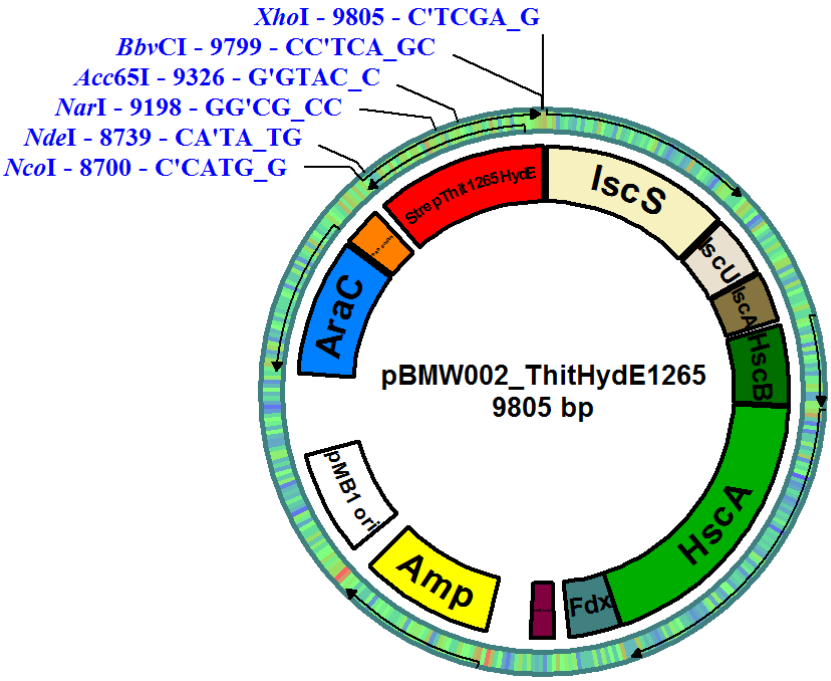

Amino acid sequence of StrepThitHydE1265

StrepThitHydE1265 (41.21 kDa)

```
MAGSWSHPQF EKHMSGVMLE LIKKAEETHT LTKKEIVELL KDDQYNDELF 50
KAADRVRKKY VGDEVHLRGL IEFSNICKQN CLYCGLRRDN KNIKRYRLKP 100
EQIINFAKNA RNLGYRTVVL QSGEDDFFNV ERMTKIIKSI KELDVAITLS 150
IGEKTREEYK AYKEAGADRY LLRIETTDKE LYEKLDPNMS HENRKRCLKD 200
LKELGYEVGT GCLIGLPGQT IESIADDILF FKEIDADMIG VGPFIPNPDT 250
PLKNEKGGTF ELSLKVMAIT RLLMPDINIP ATTAMESLNI NGRLIALRSG 300
ANVVMPNVTE GEYRKLYALY PGKICINDTP AHCFSCITGK INSIGRPIAK 350
DYGYRKKVMS KK 362
```

pBMW003_StrepThitHydE1675

E.coli optimized gene sequence of StrepThitHydE1675

```
8703 ATGGCCGG GTCGTGGTCG CATCCGCAGT TCGAGAAGCA TATGTCGGGG
8751 GTGATGATCA ACGAGAAAGA TAACGATGTG CTGATCGAAA AACTGGAAAC
8801 CCAGCATGAT ATCGATAAAG AAGAGGTTGT TATGCTGCTG GCACTGAAAG
8851 ATCCGAGCAA ACTGTATCAG GCAGCAGATC GTGTTCGTCG TAAATATGTT
8901 GGTGATGATG TGCACCTGCG TGGCCTGATT GAATTTAGCA ATTATTGTAA
8951 CAATACCTGC TTTTATTGCG GTCTGCGTGG TCCGAATCGT ACCATTAAAC
9001 GTTATCGTAT GGAACCGGAA GAAATTATTC AGTGCGCAAA ATATGGTGCA
9051 GCAGCAGGTC TGAAAACCAT TGTTCTGCAG AGCGGTGAGG ATAAATACTT
9101 CAAAATTAAC ACCCTGTGCA AAATCATCGA AGAAATCAAA AAACTGGATA
9151 TCGCCGTTAC CCTGAGCATT GGTGAACTGA GCACCAAAGA TTATGCCGAA
9201 CTGAAAAAAG CCGGCGCAGA TCGCTATCTG CTGCGTATTG AAACCACCAA
9251 TAAAGAGCTG TATCAGAAAC TGCATCCGGG TATGAGCTAT GAAAATCGTG
9301 TGCGTTGTCT GATGGATCTG CGTGAACTGG GTTATGAAGT TGGCACCGGT
9351 AGCCTGGTTG GTCTGCCTGG TCAGACCCTG GAAATGCTGG CAGATGATCT
9401 GATCTTCTTC AAAAAAATCG ATGCCGATAT GCTGGGTATT GGTCCGTTTA
9451 TTCCGTGTGA AAATACACCG CTGGAACGTG AAAAAGGTGG TAATGTTGAA
9501 ATCGTGCTGA AAATGCTGGC CCTGAGCCGT CTGCTGCTGC CGGATATTAA
9551 TATTCCGGCA ACCACCGCAC TGGCAGTTAA AGATAAAGCA GGTTATATCA
9601 AAGGCCTGAA ATGTGGCGCC AACGTTATCA TGCCGAACAT TGGTATCGAC
9651 GAATACAAAA AACTGTATAA ACTGTACCCT GGCAAAGTTC CGGATAATCC
9701 GAGCGAAGCA GTTAATAGCC TGGAAAACAT CAAAAAACTG ATCCTGAGCC
9751 AGAATCGCAC CATTGGTAAA GACAAAGGTT ACCGGAAAAA AATCCTGAAT
9801 TAA
```

Plasmid map of pBMW003_StrepThitHydE1675

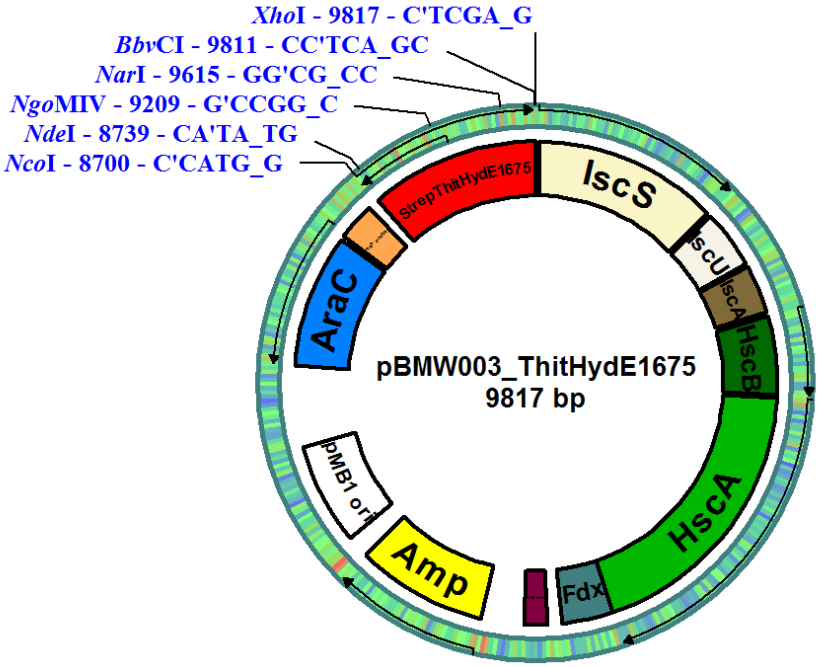

Amino acid sequence of StrepThitHydE1675

StrepThitHydE1675 (41.27 kDa)

```
MAGSWSHPQF  EKHMSGVMIN  EKDNDVLIEK LETQHDIDKE  EVVMLLALKD   50
PSKLYQAADR  VRRKYVGDDV  HLRGLIEFSN YCNNTCFYCG  LRGPNRTIKR  100
YRMEPEEIIQ  CAKYGAAAGL  KTIVLQSGED KYFKINTLCK  IIEEIKKLDI  150
AVTLSIGELS  TKDYAELKKA  GADRYLLRIE TTNKELYQKL  HPGMSYENRV  200
RCLMDLRELG  YEVGTGSLVG  LPGQTLEMLA DDLIFFKKID  ADMLGIGPFI  250
PCENTPLERE  KGGNVEIVLK  MLALSRLLLP DINIPATTAL  AVKDKAGYIK  300
GLKCGANVIM  PNIGIDEYKK  LYKLYPGKVP DNPSEAVNSL  ENIKKLILSQ  350
NRTIGKDKGY  RKKILN 366
```

pBMW004_StrepThitHydG

E.coli optimized gene sequence of StrepThitHydG

```
8702  ATGGGCAGC AGCTGGTCGC ATCCGCAGTT CGAGAAGAGC CAGGATCCGA
8751  TGGTTAAAGA AAAAGCCGAT TTCATCAACG ACGAAAAAAT TCGTCAGGAT
8801  CTGGAAAAAG CCAAAAAAGC AACCAGCAAA GATGCCCTGG AAATTATCGA
8851  GAAAGCGAAA AATCTGAAAG GCATCACACC GGAAGAAGCA GCAGTTCTGC
8901  TGAATGTTGA AGATGAAGAT CTGCTGAACG AGATGTTTAA AGTTGCCCGT
8951  TATATCAAAG AAGAGATCTA CGGTAATCGC ATCGTTATTT TTGCACCGCT
9001  GTATGTGAGC AATTATTGCG TGAATAATTG CCGCTATTGC GGTTATCGTC
9051  ATAGCAATGA ACAGCAGCGT AAAAAACTGA CAATGGAAGA AGTTCGTCGC
9101  GAAGTTGAAA TTCTGGAAGA AATGGGTCAT AAACGTCTGG CAGTTGAAGC
9151  CGGTGAAGAT CCGGTTAATT GTCCGATTGA TTATATCGTG GATGTGATCA
9201  AAACCATCTA CGATACCAAA CTGAAAAATG GTAGCATTCG TCGCGTGAAT
9251  GTTAATATTG CAGCAACCAC CGTGGAAAAC TACAAAAAAC TGAAAAAAGT
9301  GGGCATCGGC ACCTATGTTC TGTTTCAAGA AACCTATCAT CGTCCGACCT
9351  ATGAATATAT GCATCCGCAG GGTCCGAAAC ACGATTATGA TTATCATCTG
9401  ACCGCAATGG ATCGTGCAAT GGAAGCAGGT ATTGATGATG TTGGTCTGGG
9451  TGTTCTGTAT GGTCTGTATG ATTACAAATA TGAAACCGTG GCCATGCTGT
9501  ATCATGCAAA TCATCTGGAA GAGAAATTTG GTGTTGGTCC GCATACCATT
9551  AGCGTTCCGC GTCTGCGTCC GGCACTGAAT ATTAGCATTG ATAAATTTCC
9601  GTACATCGTG AGCGATAAAG ATTTCAAAAA ACTGGTTGCC GTTATTCGTA
9651  TGGCAGTTCC GTATACCGGC ATGATTCTGA GCACCCGTGA AAAACCTAAA
9701  TTTCGCGAAG AAGTGATTAG CATCGGTATT AGCCAGATTA GCGCAGGTAG
9751  CTGTACCGGT GTTGGTGGTT ATCATGAAGA AATTAGCAAA AAAGGTGGTA
9801  GCAAACCGCA GTTTGAAGTG GAAGATAAAC GTAGCCCGAA CGAAATTCTG
9851  CGTACCCTGT GTGAACAGGG TTATCTGCCG AGCTATTGTA CCGCATGTTA
9901  TCGTATGGGT CGTACCGGTG ATCGTTTTAT GAGCTTTGCA AAAAGTGGCC
9951  AGATCCATAA CTTTTGTCTG CCGAATGCAA TCCTGACCTT CAAAGAATTT
10001 CTGATCGATT ATGGTGATGA GAAAACCAAA AAAATCGGCG AAAAAGCGAT
10051 TGCCGTTAAC CTGGAAAAAA TCCCGAGCCG TACCGTTCGT GAAGAAACCA
10101 AACGTCGTCT GACCCGTATT GAAAATGGTG AACGTGATCT GTACTTTTA
10151 C
```

Plasmid map of pBMW004_StrepThitHydG

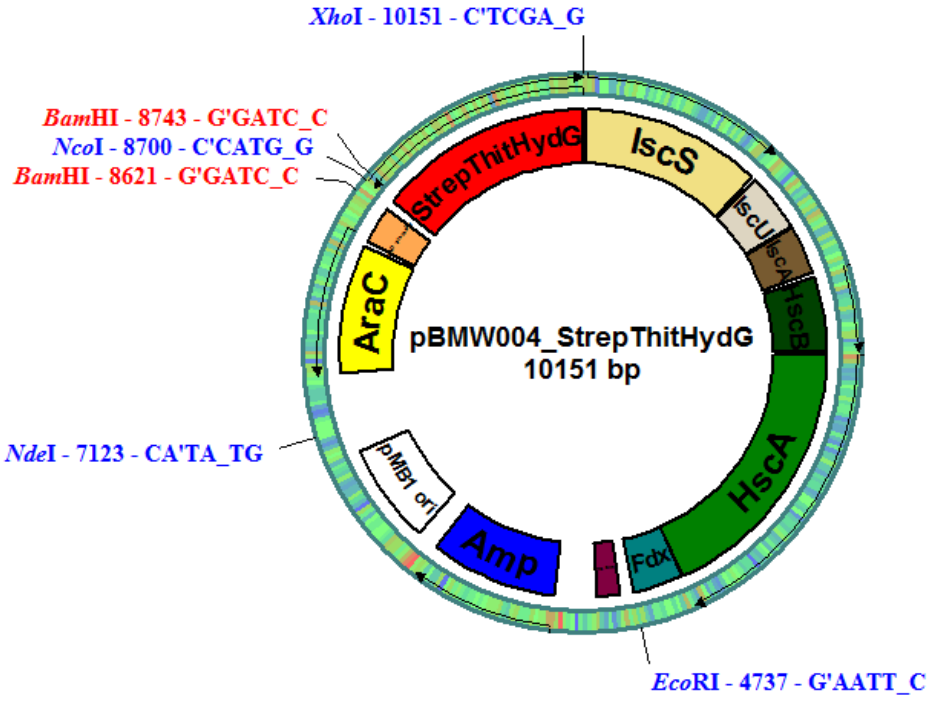

Amino acid sequence of StrepThitHydG

StrepThitHydG (55.35 kDa)

```
MGSSWSHPQF EKSQDPMVKE KADFINDEKI RQDLEKAKKA TSKDALEIIE 50
KAKNLKGITP EEAAVLLNVE DEDLLNEMFK VARYIKEEIY GNRIVIFAPL 100
YVSNYCVNNC RYCGYRHSNE QQRKKLTMEE VRREVEILEE MGHKRLAVEA 150
GEDPVNCPID YIVDVIKTIY DTKLKNGSIR RVNVNIAATT VENYKKLKKV 200
GIGTYVLFQE TYHRPTYEYM HPQGPKHDYD YHLTAMDRAM EAGIDDVGLG 250
VLYGLYDYKY ETVAMLYHAN HLEEKFGVGP HTISVPRLRP ALNISIDKFP 300
YIVSDKDFKK LVAVIRMAVP YTGMILSTRE KPKFREEVIS IGISQISAGS 350
CTGVGGYHEE ISKKGGSKPQ FEVEDKRSPN EILRTLCEQG YLPSYCTACY 400
RMGRTGDRFM SFAKSGQIHN FCLPNAILTF KEFLIDYGDE KTKKIGEKAI 450
AVNLEKIPSR TVREETKRRL TRIENGERDL YF 482
```

pCDuet_StrepThitHydF

Plasmid map of pCDuet_StrepThitHydF

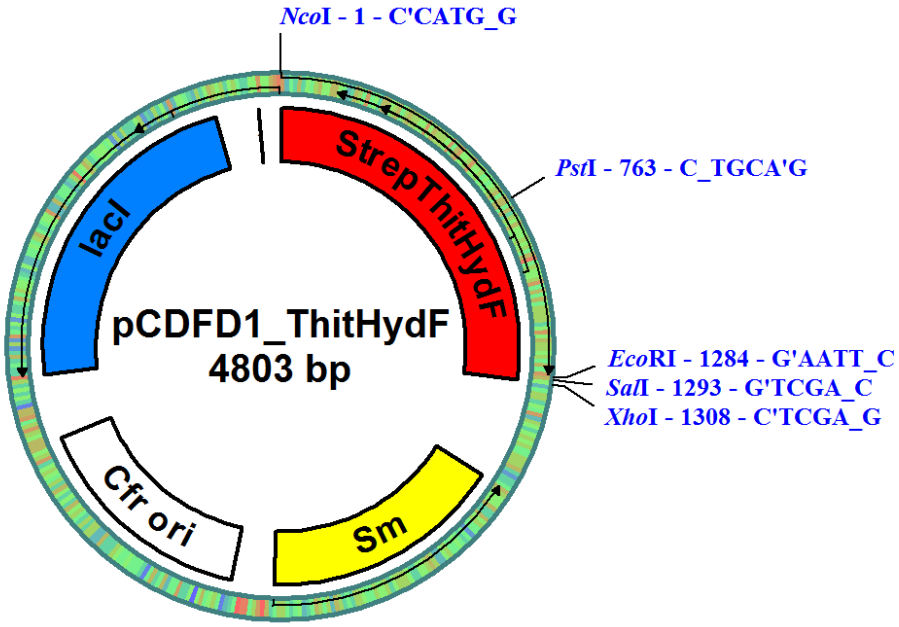

pCDuet_StrepThitHydE1265

Plasmid map of pCDuet_StrepThitHydE1265

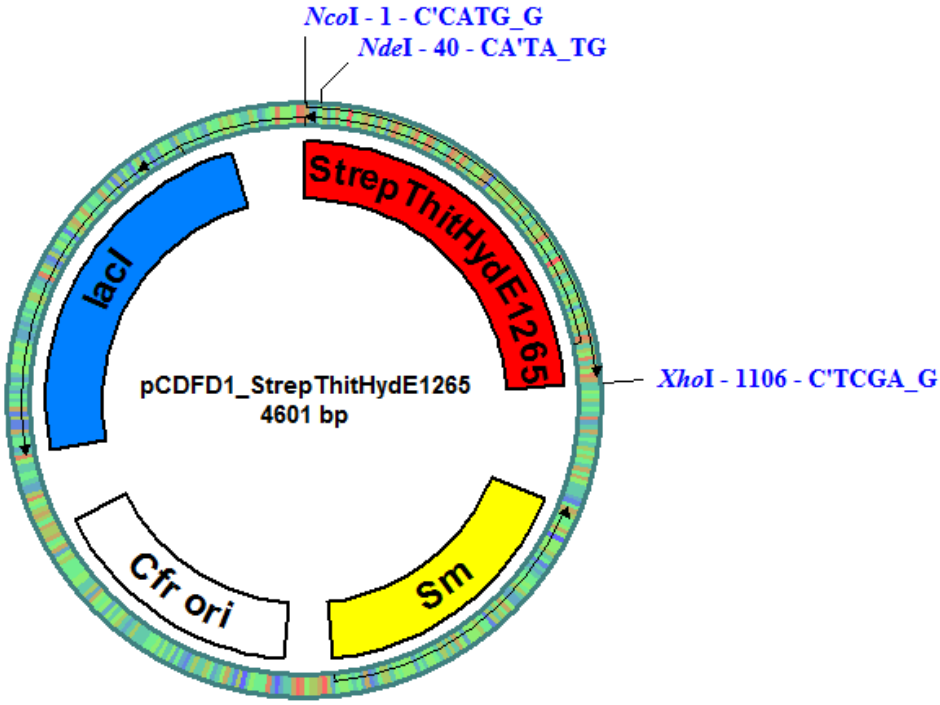

pCDuet_His$_6$ThitHydE1265

E.coli optimized gene sequence of His$_6$ThitHydE1265

```
3     ATGGCCGG GTCGCATCAC CATCATCACC ACCATATGTC GGGGGTGATG
51    CTGGAACTGA TCAAAAAAGC CGAAGAAACC CATACCCTGA CCAAAAAAGA
101   AATTGTGGAA CTGCTGAAAG ACGACCAGTA TAACGATGAA CTGTTTAAAG
151   CAGCAGATCG CGTTCGCAAA AAATACGTTG GTGATGAAGT GCACCTGCGT
201   GGCCTGATTG AATTTAGCAA TATTTGCAAA CAGAACTGCC TGTATTGTGG
251   TCTGCGTCGT GATAACAAAA ACATTAAACG TTATCGCCTG AAACCTGAGC
301   AGATTATCAA TTTTGCCAAA AATGCGCGCA ATCTGGGTTA TCGTACCGTT
351   GTTCTGCAGA GCGGTGAAGA TGATTTTTTC AATGTTGAAC GCATGACCAA
401   AATCATCAAA AGCATCAAAG AACTGGATGT GGCAATTACC CTGAGCATTG
451   GTGAAAAAAC CCGTGAAGAA TACAAAGCCT ATAAAGAAGC AGGCGCCGAT
501   CGTTATCTGC TGCGTATTGA AACCACCGAT AAAGAACTGT ATGAAAAACT
551   GGACCCGAAC ATGAGCCATG AAAATCGTAA ACGTTGCCTG AAAGATCTGA
601   AAGAGCTGGG TTACGAAGTT GGTACCGGTT GTCTGATTGG TCTGCCTGGT
651   CAGACCATTG AAAGCATTGC AGATGATATC CTGTTCTTCA AAGAAATCGA
701   TGCCGATATG ATTGGTGTGG GTCCGTTTAT TCCGAATCCG GATACACCGC
751   TGAAAAATGA AAAAGGTGGT ACATTTGAAC TGAGCCTGAA AGTTATGGCC
801   ATTACCCGTC TGCTGATGCC GGATATTAAC ATTCCGGCAA CCACCGCAAT
851   GGAAAGCCTG AATATTAACG GTCGCCTGAT TGCACTGCGT AGCGGTGCAA
901   ACGTTGTTAT GCCGAATGTT ACCGAAGGTG AATATCGCAA ACTGTATGCA
951   CTGTATCCGG GTAAAATTTG CATCAATGAT ACACCGGCAC ATTGCTTTAG
1001  CTGTATTACC GGCAAAATTA ATAGCATTGG TCGTCCGATT GCAAAAGATT
1051  ATGGTTACCG TAAAAAAGTG ATGAGCAAAA AATAA
```

Plasmid map of pCDuet_His$_6$ThitHydE1265

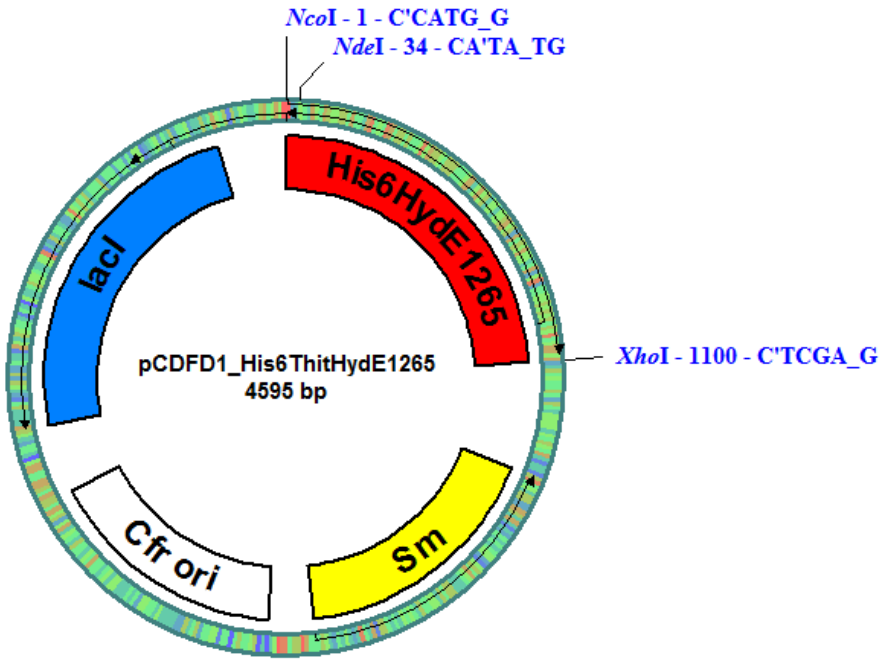

Amino acid sequence of His_6ThitHydE1265

His_6ThitHydE1265 (41.00 kDa)

```
MAGSHHHHHH HMSGVMLELI KKAEETHTLT KKEIVELLKD DQYNDELFKA 50
ADRVRKKYVG DEVHLRGLIE FSNICKQNCL YCGLRRDNKN IKRYRLKPEQ 100
IINFAKNARN LGYRTVVLQS GEDDFFNVER MTKIIKSIKE LDVAITLSIG 150
EKTREEYKAY KEAGADRYLL RIETTDKELY EKLDPNMSHE NRKRCLKDLK 200
ELGYEVGTGC LIGLPGQTIE SIADDILFFK EIDADMIGVG PFIPNPDTPL 250
KNEKGGTFEL SLKVMAITRL LMPDINIPAT TAMESLNING RLIALRSGAN 300
VVMPNVTEGE YRKLYALYPG KICINDTPAH CFSCITGKIN SIGRPIAKDY 350
GYRKKVMSKK 360
```

pCDuet_StrepThitHydE1675

Plasmid map of pCDuet_StrepThitHydE1265

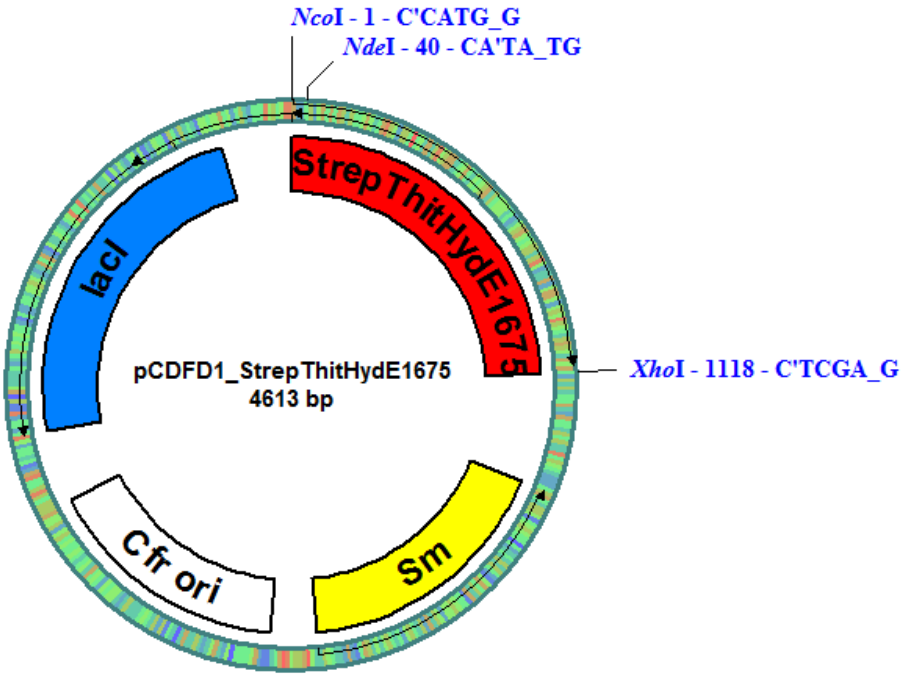

pCDuet_His$_6$ThitHydE1675

E.coli optimized gene sequence of His$_6$ThitHydE1675

```
3    ATGGCCGG GTCGCATCAC CATCATCACC ACCATATGTC GGGGGTGATG
51   ATCAACGAGA AAGATAACGA TGTGCTGATC GAAAAACTGG AAACCCAGCA
101  TGATATCGAT AAAGAAGAGG TTGTTATGCT GCTGGCACTG AAAGATCCGA
151  GCAAACTGTA TCAGGCAGCA GATCGTGTTC GTCGTAAATA TGTTGGTGAT
201  GATGTGCACC TGCGTGGCCT GATTGAATTT AGCAATTATT GTAACAATAC
251  CTGCTTTTAT TGCGGTCTGC GTGGTCCGAA TCGTACCATT AAACGTTATC
301  GTATGGAACC GGAAGAAATT ATTCAGTGCG CAAAATATGG TGCAGCAGCA
351  GGTCTGAAAA CCATTGTTCT GCAGAGCGGT GAGGATAAAT ACTTCAAAAT
401  TAACACCCTG TGCAAAATCA TCGAAGAAAT CAAAAAACTG GATATCGCCG
451  TTACCCTGAG CATTGGTGAA CTGAGCACCA AAGATTATGC CGAACTGAAA
501  AAAGCCGGCG CAGATCGCTA TCTGCTGCGT ATTGAAACCA CCAATAAAGA
551  GCTGTATCAG AAACTGCATC CGGGTATGAG CTATGAAAAT CGTGTGCGTT
601  GTCTGATGGA TCTGCGTGAA CTGGGTTATG AAGTTGGCAC CGGTAGCCTG
651  GTTGGTCTGC CTGGTCAGAC CCTGGAAATG CTGGCAGATG ATCTGATCTT
701  CTTCAAAAAA ATCGATGCCG ATATGCTGGG TATTGGTCCG TTTATTCCGT
751  GTGAAAATAC ACCGCTGGAA CGTGAAAAAG GTGGTAATGT TGAAATCGTG
801  CTGAAAATGC TGGCCCTGAG CCGTCTGCTG CTGCCGGATA TTAATATTCC
851  GGCAACCACC GCACTGGCAG TTAAAGATAA AGCAGGTTAT ATCAAAGGCC
901  TGAAATGTGG CGCCAACGTT ATCATGCCGA ACATTGGTAT CGACGAATAC
951  AAAAAACTGT ATAAACTGTA CCCTGGCAAA GTTCCGGATA ATCCGAGCGA
1001 AGCAGTTAAT AGCCTGGAAA ACATCAAAAA ACTGATCCTG AGCCAGAATC
1051 GCACCATTGG TAAAGACAAA GGTTACCGGA AAAAAATCCT GAATTAA
```

Plasmid map of pCDuet_His$_6$ThitHydE1675

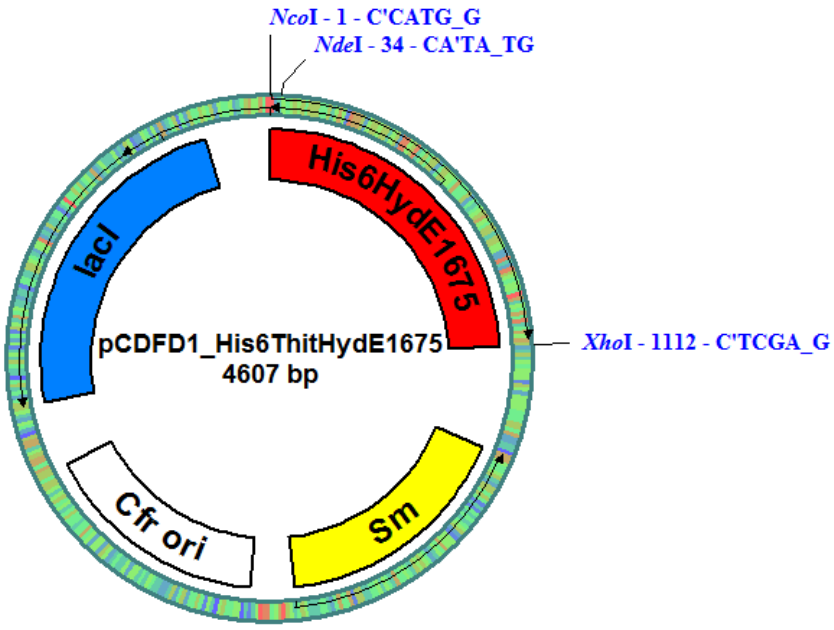

Amino acid sequence of His_6ThitHydE1675

His_6ThitHydE1675 (41.05 kDa)

```
MAGSHHHHHH HMSGVMINEK DNDVLIEKLE TQHDIDKEEV VMLLALKDPS 50
KLYQAADRVR RKYVGDDVHL RGLIEFSNYC NNTCFYCGLR GPNRTIKRYR 100
MEPEEIIQCA KYGAAAGLKT IVLQSGEDKY FKINTLCKII EEIKKLDIAV 150
TLSIGELSTK DYAELKKAGA DRYLLRIETT NKELYQKLHP GMSYENRVRC 200
LMDLRELGYE VGTGSLVGLP GQTLEMLADD LIFFKKIDAD MLGIGPFIPC 250
ENTPLEREKG GNVEIVLKML ALSRLLLPDI NIPATTALAV KDKAGYIKGL 300
KCGANVIMPN IGIDEYKKLY KLYPGKVPDN PSEAVNSLEN IKKLILSQNR 350
TIGKDKGYRK KILN 364
```

pCDuet_StrepThitHydF+HydE1265

E.coli optimized gene sequence of untagged ThitHydE1265

```
4954 ATGTCGG GGGTGATGCT GGAACTGATC AAAAAAGCCG AAGAAACCCA
5001 TACCCTGACC AAAAAAGAAA TTGTGGAACT GCTGAAAGAC GACCAGTATA
5051 ACGATGAACT GTTTAAAGCA GCAGATCGCG TTCGCAAAAA ATACGTTGGT
5101 GATGAAGTGC ACCTGCGTGG CCTGATTGAA TTTAGCAATA TTTGCAAACA
5151 GAACTGCCTG TATTGTGGTC TGCGTCGTGA TAACAAAAAC ATTAAACGTT
5201 ATCGCCTGAA ACCTGAGCAG ATTATCAATT TTGCCAAAAA TGCGCGCAAT
5251 CTGGGTTATC GTACCGTTGT TCTGCAGAGC GGTGAAGATG ATTTTTTCAA
5301 TGTTGAACGC ATGACCAAAA TCATCAAAAG CATCAAAGAA CTGGATGTGG
5351 CAATTACCCT GAGCATTGGT GAAAAAACCC GTGAAGAATA CAAAGCCTAT
5401 AAAGAAGCAG GCGCCGATCG TTATCTGCTG CGTATTGAAA CCACCGATAA
5451 AGAACTGTAT GAAAAACTGG ACCCGAACAT GAGCCATGAA AATCGTAAAC
5501 GTTGCCTGAA AGATCTGAAA GAGCTGGGTT ACGAAGTTGG TACCGGTTGT
5551 CTGATTGGTC TGCCTGGTCA GACCATTGAA AGCATTGCAG ATGATATCCT
5601 GTTCTTCAAA GAAATCGATG CCGATATGAT TGGTGTGGGT CCGTTTATTC
5651 CGAATCCGGA TACACCGCTG AAAAATGAAA AAGGTGGTAC ATTTGAACTG
5701 AGCCTGAAAG TTATGGCCAT TACCCGTCTG CTGATGCCGG ATATTAACAT
5751 TCCGGCAACC ACCGCAATGG AAAGCCTGAA TATTAACGGT CGCCTGATTG
5801 CACTGCGTAG CGGTGCAAAC GTTGTTATGC CGAATGTTAC CGAAGGTGAA
5851 TATCGCAAAC TGTATGCACT GTATCCGGGT AAAATTTGCA TCAATGATAC
5901 ACCGGCACAT TGCTTTAGCT GTATTACCGG CAAAATTAAT AGCATTGGTC
5951 GTCCGATTGC AAAAGATTAT GGTTACCGTA AAAAAGTGAT GAGCAAAAAA
6001 TGA
```

Plasmid map of pCDuet_StrepThitHydF + ThitHydE1265

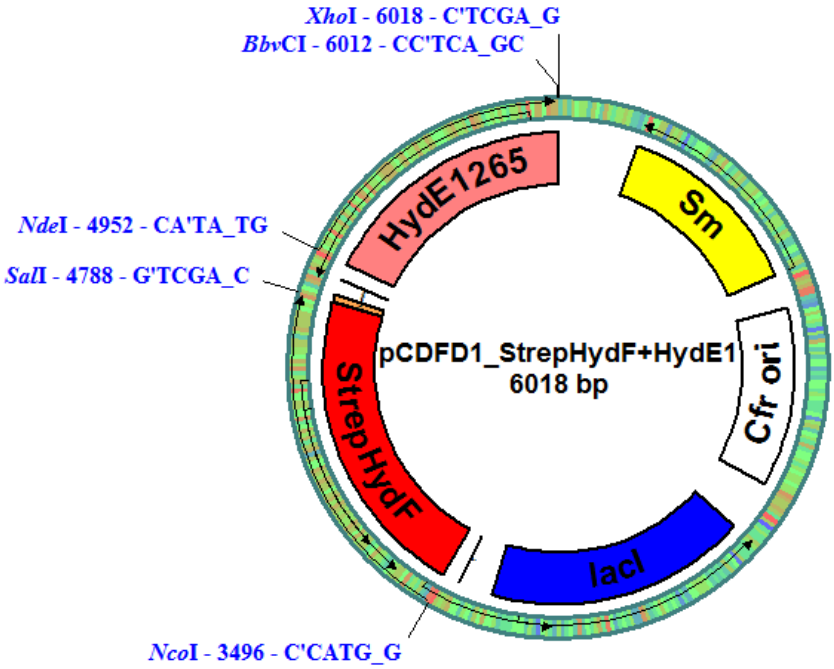

Amino acid sequence of untagged ThitHydE1265

Untagged ThitHydE1265 (39.69 kDa)

```
MSGVMLELIK KAEETHTLTK KEIVELLKDD QYNDELFKAA DRVRKKYVGD 50
EVHLRGLIEF SNICKQNCLY CGLRRDNKNI KRYRLKPEQI INFAKNARNL 100
GYRTVVLQSG EDDFFNVERM TKIIKSIKEL DVAITLSIGE KTREEYKAYK 150
EAGADRYLLR IETTDKELYE KLDPNMSHEN RKRCLKDLKE LGYEVGTGCL 200
IGLPGQTIES IADDILFFKE IDADMIGVGP FIPNPDTPLK NEKGGTFELS 250
LKVMAITRLL MPDINIPATT AMESLNINGR LIALRSGANV VMPNVTEGEY 300
RKLYALYPGK ICINDTPAHC FSCITGKINS IGRPIAKDYG YRKKVMSKK 349
```

A 2.2 Sequencing results for His_6ThitHydE1265, His_6ThitHydE1675 and StrepThitHydG

Sequencing of His_6ThitHydE1265 (First 100 bp, His_6-Tag highlighted in *red*)

```
CATGGCCGGG TCGCATCACC ATCATCACCA CCATATGTCG GGGGTGATGC 50
TGGAACTGAT CAAAAAAGCC GAAGAAACCC ATACCCTGAC CAAAAAAGAA 100
```

Alignment of the sequencing result with the His_6ThitHydE1265 gene sequence (First 50 bp)

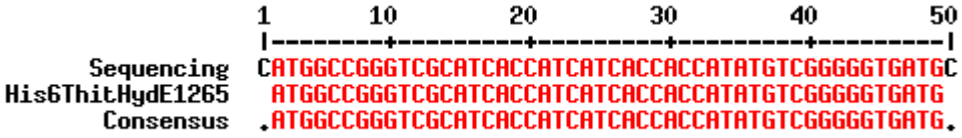

Sequencing of His_6ThitHydE1675 (First 100 bp, His_6-tag highlighted in *red*)

```
CCATGGCCGG GTCGCATCAC CATCATCACC ACCATATGTC GGGGGTGATG 50
ATCAACGAGA AAGATAACGA TGTGCTGATC GAAAAACTGG AAACCCAGCA 100
```

Alignment of the sequencing result with the His_6ThitHydE1675 gene sequence (First 50 bp)

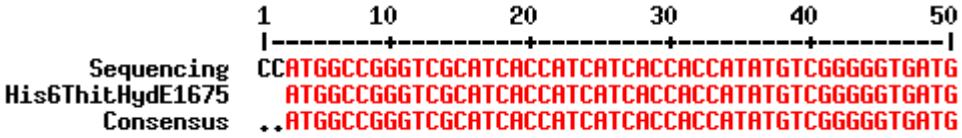

Sequencing of StrepThitHydG (First 100 bp, Strep-tag highlighted in *red*)

```
CATGGGCAGC AGCTGGTCGC ATCCGCAGTT CGAGAAGAGC CAGGATCCGA 50
TGGTTAAAGA AAAAGCCGAT TTCATCAACG ACGAAAAAAT TCGTCAGGAT 100
```

Alignment of the sequencing result with the StrepThitHydG gene sequence (First 50 bp)

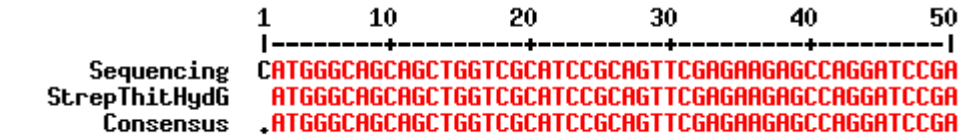

A 3.1 Mass spectrometry of the pdt H-cluster mimic

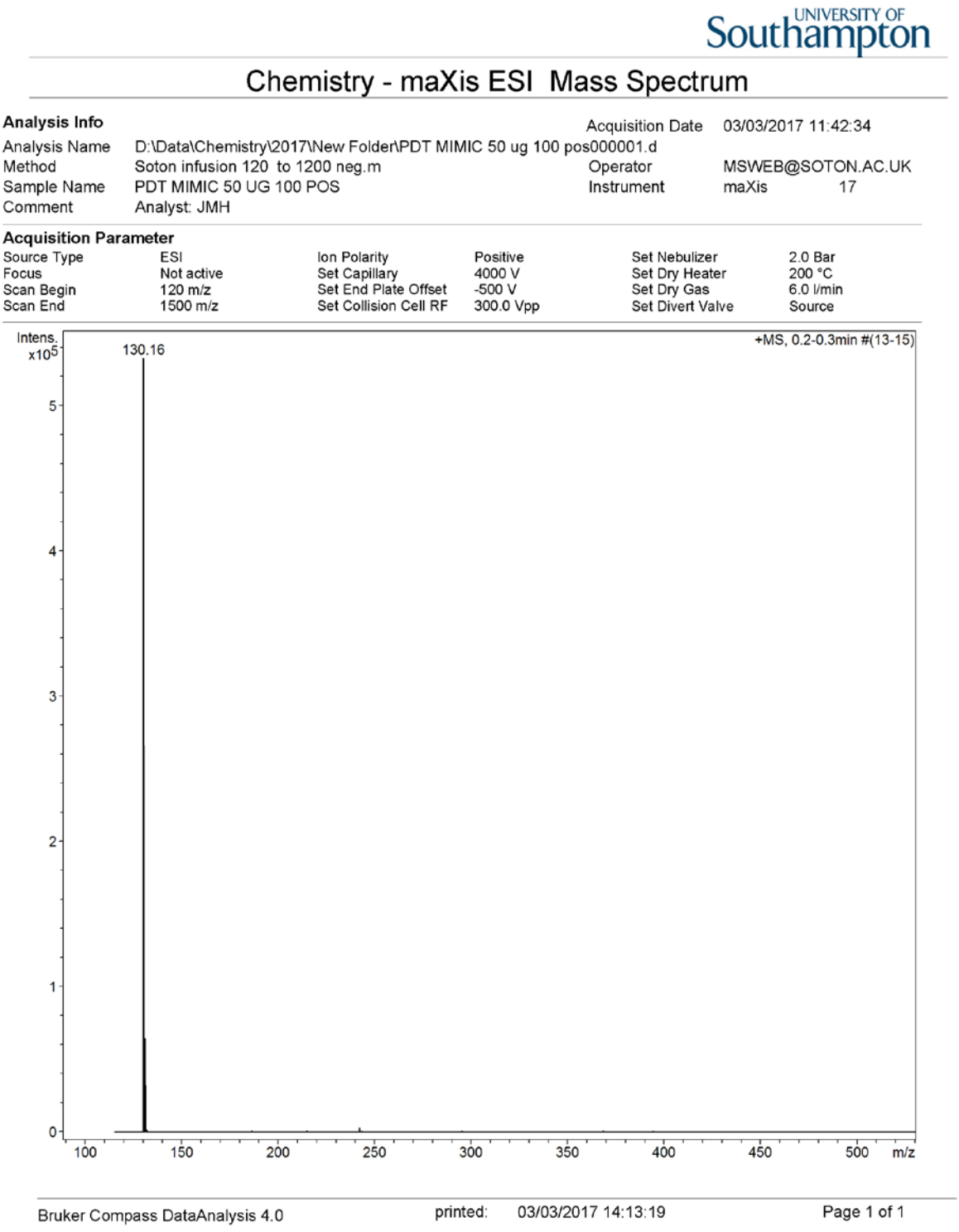

ESI (+) mode in 100 % ACN:

Found 130.16 m/z corresponding to the tetraethylammonium counterion Et_4N^+

UNIVERSITY OF Southampton

Chemistry - maXis ESI Mass Spectrum

Analysis Info

Analysis Name	D:\Data\Chemistry\2017\New Folder\PDT MIMIC 50 ug 5050 NEG B000001.d	Acquisition Date	03/03/2017 11:33:07
Method	Soton infusion 120 to 1200 neg.m	Operator	MSWEB@SOTON.AC.UK
Sample Name	PDT MIMIC 50 UG 5050 neg B	Instrument	maXis 17
Comment	Analyst: JMH		

Acquisition Parameter

Source Type	ESI	Ion Polarity	Negative	Set Nebulizer	2.0 Bar
Focus	Not active	Set Capillary	4000 V	Set Dry Heater	200 °C
Scan Begin	120 m/z	Set End Plate Offset	-500 V	Set Dry Gas	6.0 l/min
Scan End	1500 m/z	Set Collision Cell RF	300.0 Vpp	Set Divert Valve	Source

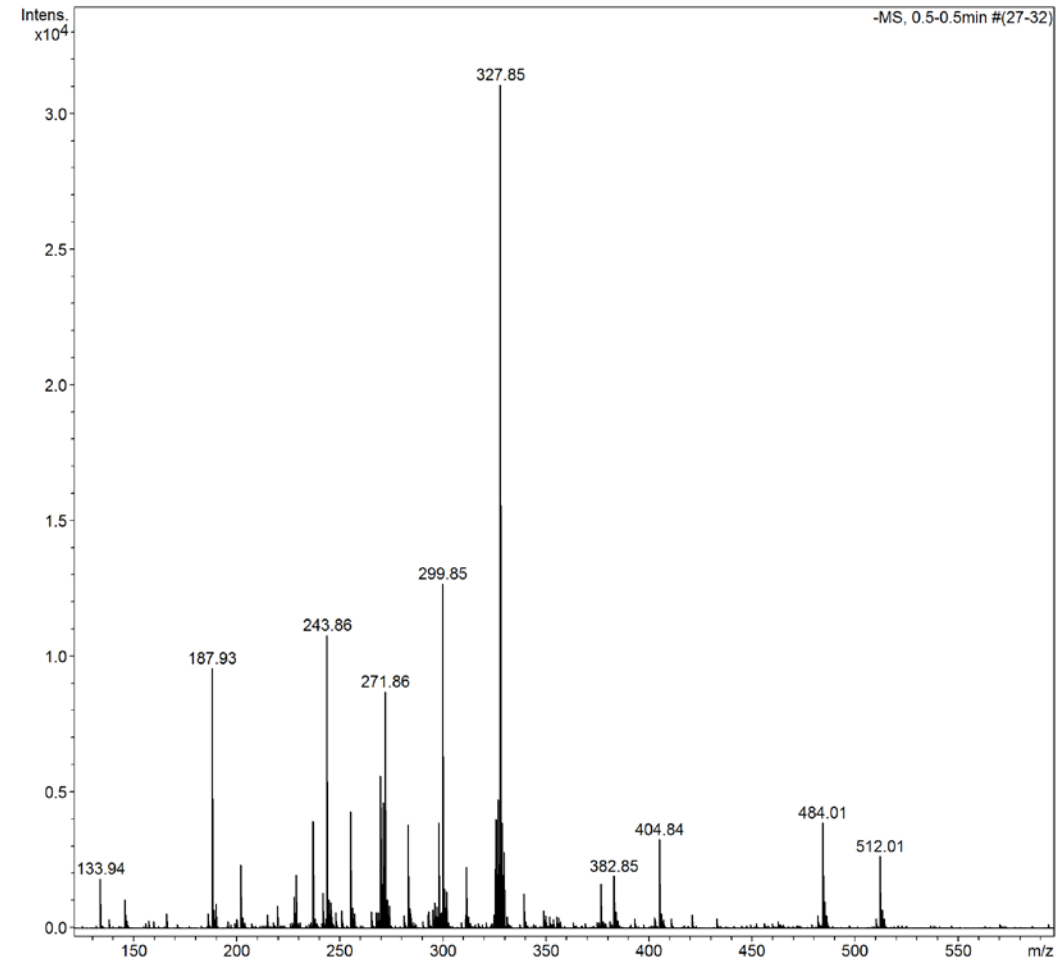

Bruker Compass DataAnalysis 4.0 printed: 03/03/2017 14:06:31 Page 1 of 1

ESI (-) mode in 50 % ACN (acetonitrile) and 50% water:

Expected: $Fe2C9H6S2O4N2$ $(Fe2(pdt)(CO)4(CN)2)^{2-}$ = 381.846774 m/z

Found: 327.85 m/z corresponding to $Fe2C7H6S2O3N1$ $(Fe2(pdt)(CO)3(CN)1)^{-1}$

A 3.2 EPR simulations: Easyspin script for MatLab

Simulation for StrepHydE1265 (small resonator, Figure 3.16)

```
Sys.S=1/2;
Sys.g = [1.90 2.04];
Sys.gStrain = [0.06 0.05];
Sys.lwpp = 0.5;
Vary.g = [0.05 0.05 0.01];
Exp.mwFreq = 9.496;
Exp.Range = [300 400]
Exp.Temperature = 15;
Exp.ModAmp = 1;
pepper(Sys,Exp, Vary);
```

Simulation for StrepHydE1265 (large resonator, Figure 3.17)

```
Sys.S=1/2;
Sys.g = [1.83 1.88 2.004];
Sys.gStrain = [0.035 0.015 0.01];
Sys.lwpp = 0.5;
Vary.g = [0.05 0.05 0.01];
Exp.mwFreq = 9.67;
Exp.Range = [300 400]
Exp.Temperature = 10;
Exp.ModAmp = 1;
pepper(Sys,Exp, Vary);
```

Simulation for StrepHydF (large resonator, Figure 3.18)

```
Sys.S=1/2;
Sys.g = [1.86 2.05];
Sys.gStrain = [0.06 0.04];
Sys.lwpp = 0.5;
Vary.g = [0.05 0.05 0.01];
Exp.mwFreq = 9.68;
Exp.Range = [300 400]
Exp.Temperature = 10;
Exp.ModAmp = 1;
pepper(Sys,Exp, Vary);
```

Simulation for His_6HydG (small resonator, Figure 3.19)

```
Sys.S=1/2;
Sys.g = [1.874 1.914 2.033];
Sys.gStrain = [0.024 0.026 0.016];
Sys.lwpp = 0.5;
Vary.g = [0.05 0.05 0.01];
Exp.mwFreq = 9.50;
Exp.Range = [300 400]
Exp.Temperature = 10;
Exp.ModAmp = 1;
pepper(Sys,Exp, Vary);
```

Simulation for His_6HydG (large resonator, Figure 3.23B)

```
Sys.S=1/2;
Sys.g = [1.860 2.00];
Sys.gStrain = [0.055 0.04];
Sys.lwpp = 0.5;
Vary.g = [0.05 0.05 0.01];
Exp.mwFreq = 9.68;
Exp.Range = [300 400]
Exp.Temperature = 10;
Exp.ModAmp = 1;
pepper(Sys,Exp, Vary);
```

Simulation for His_6HydG, high spin signal (large resonator, Figure 3.23A and Figure 3.25)

```
Sys.S = [5/2];
Sys.g = [2.0];
Sys.gStrain = [0.2 0.2 0.3];
D = 135000; E = 27350;
Sys.D = [-1,-1,2]/3*D + [1,-1,0]*E
Sys.HStrain = [10 10 10];       % 10 MHz Gaussian FWHM broadening in all directions
Sys.lwpp = 0.5;
Vary.g = [0.05];
Exp.mwFreq = 9.7;
Exp.Range = [25 250]
Exp.Temperature = 10;
Exp.ModAmp = 1
pepper(Sys,Exp,Vary);
```

```
Sys.S = [3/2];
Sys.g = [2.0];
Sys.gStrain = [0.25 0.2 0.1];
D = 125000; E = 36250;
Sys.D = [-1,-1,2]/3*D + [1,-1,0]*E
Sys.HStrain = [10 10 10];       % 10 MHz Gaussian FWHM broadening in all directions
Sys.lwpp = 0.5;
Vary.g = [0.05];
Exp.mwFreq = 9.7;
Exp.Range = [25 250]
Exp.Temperature = 10;
Exp.ModAmp = 1
pepper(Sys,Exp,Vary);
```

A 4.1 Alignments (active sites)

Sequence alignment of HydEs from *Thermoanaerobacter italicus* and in comparison to PylB from *Methanosarcina barkeri* and BioB from *Escherichia coli*. The alignment was generated with ClustalW(α,β).

```
ThitHydE1265      ---------MLELIKKAEETHTLTKKEIVELLKD--DQYNDELFKAADRVRKKYVGDEVH
ThitHydE1675      ---MINEKDNDVLIEKLETQHDIDKEEVVMLLAL--KDP-SKLYQAADRVRRKYVGDDVH
MbPylB            MIQKMALDEFDSLGDKVIEGYQLTDNDLRTLLSLESKEGLERLYSAARKVRDHYFGNRVF
EcoliBioB         ----------------MAHRPRWTLSQVTELFEK---PLLDLLFEAQQVHRQHFDPRQVQ
                                  .::  *:        . *:.*    * ::    *

ThitHydE1265      LRGLIEFSN-ICKQNCLYCG--LRRDNKNIKRYRLKPEQIINFAKNARNLGYRTVVLQSG
ThitHydE1675      LRGLIEFSN-YCNNTCFYCG--LRGPNRTIKRYRMEPEEIIQCAKYGAAAGLKTIVLQSG
MbPylB            LNCFIYFST-YCKNQCSFCY--YNCRN-EINRYRLTMEEIKETCKTLKGAGFHMVDLTMG
EcoliBioB         VSTLLSIKTGACPEDCKYCPQSSRYKTGLEAERLMEVEQVLESARKAKAAGSTRFCMGAA
                  :  :: :..  * : * :*    .  .    .  :  *:: : .:     *   . :  .

ThitHydE1265      EDDFFNVER---MTKIIKSIKELDVAITLSIGEKTREEYKAYKEAGADRYLLRIETTDKE
ThitHydE1675      EDKYFKINT---LCKIIEEIKKLDIAVTLSIGELSTKDYAELKKAGADRYLLRIETTNKE
MbPylB            EDPYYYEDPNRFVELVQIVKEELGLPIMISPGLMDNATLLKAREKGANFLALYQETYDTE
EcoliBioB         WKNPHERDMP-YLEQMVQGVKAMGLEACMTLGTLSESQAQRLANAGLDYYNHNLDTS-PE
                   .  .  :    :  :    : :.:   :: *          : * :      :*   *

ThitHydE1265      LYEKLDPNMSHENRKRCLKDLKELGYEVGTGCLIGLPGQTIESIADDILFFKEIDA-DMI
ThitHydE1675      LYQKLHPGMSYENRVRCLMDLRELGYEVGTGSLVGLPGQTLEMLADDLIFFKKIDA-DML
MbPylB            LYRKLRVGQSFDGRVNARRFAKQQGYCVEDGILTGVG-NDIESTILSLRGMSTNDP-DMV
EcoliBioB         FYGNIITTRTYQERLDTLEKVRDAGIKVCSGGIVGLGETVKDRAGLLLQLANLPTPPESV
                  :* ::    :.: *       :: *  *  * : *:     :     :   .   . : :

ThitHydE1265      GVGPFIPNPDTPLKNEKGGTFELSLKVMAITRLLMPDINIPATTAMESLNINGRLIALRS
ThitHydE1675      GIGPFIPCENTPLEREKGGNVEIVLKMLALSRLLLPDINIPATTALAVKDKAGYIKGLKC
MbPylB            RVMTFLPQEGTPLEGFRDKSNLSELKIISVLRLMFPKRLIPAS--LDLEGIDGMVLRLNA
EcoliBioB         PINMLVKVKGTPLADNDDVDAFDFIRTIAVARIMMPTSYVRLSAGREQMNEQTQAMCFMA
                   :  ::   .***    .      :: ::: *:::*   :  :      .       : .

ThitHydE1265      GAN------VVMPNVTEGEYRKLYALYPGKICIN-DTPAHCFSCITGKINSIGRPIAKDY
ThitHydE1675      GAN------VIMPNIGIDEYKKLYKLYPGKVPDNPSEAVNSLENIKKLILSQNRTIGKDK
MbPylB            GAN------IVTSILPPDSQLEGVANYDRDLEER----DRDIKSVVRRLEIMGMKPARQA
EcoliBioB         GANSIFYGCKLLTTPNPEEDKDLQLFRKLGLNPQQTAVLAGDNEQQQRLEQALMTPDTDE
                  ***       : .     .  .        :  .        .     :        :

ThitHydE1265      GYRKKVMSKK
ThitHydE1675      GYRKKILN--
MbPylB            DFEAVLGC--
EcoliBioB         YYNAAAL---
                   :.
```

Sequence alignment of HydG from *Thermoanaerobacter italicus* in comparison to ThiH from *Escherichia coli* and NosL from *Streptomyces actuosus*. The alignment was generated with ClustalW(α,β).

```
ThitHydG        -----MVKEKADFINDEKIRQDLEKAKKATSKDALEIIEKAKNLKGITPEEAAVLLNVED
EcoliThiH       ----------MKTFSDRWRQLDWDDIRLRINGKTAADVERALNASQLTRDDMMALLSPAA
SaNosL          MTQNSQAMTSHAMTGDFVLPELEDVRAEAATVDTRAVLALAEGEEPAESRAAVALALWED
                             .*      :     . .:   :  * . .       .*

ThitHydG        EDLLNEMFKVARYIKEEIYGNRIVIFAPLYVSNYCVNNCRYCGYRHSNE-QQRKKLTMEE
EcoliThiH       SGYLEQLAQRAQRLTRQRFGNTVSFYVPLYLSNLCANDCTYCGFSMSNR-IKRKTLDEAD
SaNosL          RSIGTAELQAAAEARCGARRPRLHTFVPLYTTNYCDSECKMCSMRKGNHRLDRKFSGRKE
                 .     : *          :  :.*** :* * .:*  *.   .*.  .**     :

ThitHydG        VRREVEILEEMG-HKRLAVEAGEDPVNCPIDYIVDVIKTIYDTKLKNGSIRRVNVNIAAT
EcoliThiH       IARESAAIREMG-FEHLLLVTGEHQAKVGMDYFRRHLPALREQFSS------LQMEVQPL
SaNosL          ITEQLEILYHHEGVRGVGFLTGEYEDKHTRLASAFRIGWAIRTALDLGFERVYFNIGSME
                : .:   : .    . : . :**   :         :        .

ThitHydG        TVENYKKLKKVG---IGTYVLFQETYHRPTYEYMHPQG----PKHDYDYHLTAMDRAMEA
EcoliThiH       AETEYAELKQLG---LDGVMVYQETYHEATYARHHLKG----KKQDFFWRLETPDRLGRA
SaNosL          QDEIDVLGEWIGREDPVTMCVFQESYDRETYRRFMGKTSVGVPKADFDRRVVSFDRWLDA
                       : :*        ::**:*.. **     :      * *:  :: : **   *

ThitHydG        GIDDVGLGVLYGLYD-YKYETVAMLYHANHLEEKFGVGPHTISVPRLRPALNISIDKFPY
EcoliThiH       GIDKIGLGALIGLSDNWRVDSYMVAEHLLWLQQHYWQSRYSVSFPRLRPCTGG--IEPAS
SaNosL          GYRYVNPGVLVGLHDDLSAELVSLVAHGDHLRSRG--ATADLSVPRMRPAMKS---RDTT
                *   :. *.* ** *    :   :  *   *..:   .   :*.**:**.      . .

ThitHydG        IVSDKDFKKLVAVIRMAVPYTGMILSTREKPKFREEVISIGISQISAGSCTGVGGYHEEI
EcoliThiH       IMDERQLVQTICAFRLLAPEIELSLSTRESPWFRDRVIPLAINNVSAFSKTQPGGYADNH
SaNosL          RVGDDDYLRLMSVVAFTCPEQRLVLTTREPQEFQDVALGLAG-VISPGSPDVAPYRAGCE
                 :.: :  : :... :  *   : *:***   *:: .: :.   :*. *

ThitHydG        SKKGGSKPQFEVEDKRSPNEILRTLCEQGYLPSYCTACYRMGRTGDRFMSFAKSGQIHNF
EcoliThiH       P----ELEQFSPHDDRRPEAVAAALTAQGLQPVWKDWDSYLGRASQRL------------
SaNosL          ARNDEKSSQFLVADLRRPRHILGRIEASGTP--VDHFVNPAGEASRAV------------
                .    .  **   * * *. :   :  .*           *.:.  .

ThitHydG        CLPNAILTFKEFLIDYGDEKTKKIGEKAIAVNLEKIPSRTVREETKRRLTRIENGERDLY
EcoliThiH       ------------------------------------------------------------
SaNosL          ------------------------------------------------------------


ThitHydG        F
EcoliThiH       -
SaNosL          -
```

Sequence alignment of HydF from *Thermoanaerobacter italicus* and *Clostridium acetobutylicum*, as well as homologous GTPases MnmE from *Fervidicola ferrireducens* and EngA from *Clostridioides difficile*. The alignment was generated with ClustalW(α,β).

```
ThitHydF        -----MNTTPVSSRLHIAIFGRRNAGKSSLINALTNQEVALVSDVAGTTTDPVSKAMEIL
FefeMnmE        MQKASLNETPTASRLHIAIFGRRNAGKSSLINAITNQDIALVSPVAGTTTDPVFKAMELL
CaHydF          --MNELNSTPKGERLHIALFGKTNVGKSSVINALTSQEIALVSNVKGTTTDPVYKAMELL
ClodiEngA       ---MSLNSTPQSVRVHIGLFGKRNAGKSSIINAITNQSAAIVSDIAGTTTDPVFRPMEIL
                     :* ** . *:**.:**: *.****:***:*.*. *:** : ******* :.**:*

ThitHydF        PIGPVVIIDTAGLDDTGELGELRVKKTYEVLNRTDLAILVIDGTIGLSEFEENVLKVIRD
FefeMnmE        PIGPVVIIDTAGIDDEGELGELRVKKTYQVLNKTDLAVLIIDGMTGVTDYDLEILGRIRE
CaHydF          PLGPVMLIDTAGLDDISDLGELRRGKTLEVLSKTDVAILVFDVESGITEYDKNIYSLLLE
ClodiEngA       PIGPCVLIDTAGLDDVGELGELRIGKSLDVLEKTDIALLVVDCQIGISQEDLSLIEKFND
                *:** ::*****:** .:*****  *: :**.:**:*:*:.*   *::: : .:   : :

ThitHydF        KNIPVVGVINKKDLSQYSEEDKRKWEERLKLELIEVSALKKHGIEALKMMLIKKAPYDDR
FefeMnmE        KNIPVVGVVNKCDVAGYTPEDKKNWEKRLNINLIEVSALKRQGIEELKREIINKAPSSIS
CaHydF          KKIPLIGVLNKIDKKDYKLED---YTSQFKIPIVPISALNNKGINNLKDELIRLAPENDD
ClodiEngA       KNIPHILTLNKIDTIKNQSEILNLTKNKVKCPVVSVSSTDKIGIENLKNEIIKVLPKDST
                *:** : .:** *      *      .:.:  :: :*: .. **: **  :*.  * .

ThitHydF        ELSIVGDLIKPGDFVVLVIPIDKAAPKGRLILPQQQTIRDILDNDAMAIVTKEHELKETL
FefeMnmE        EHPLIGDLISPGDIVVLVVPIDKAAPKGRLILPQQQTIRDVLDHNAIAVVTKETELKNTL
CaHydF          KFKIVGDLLSPGDIAVLVTPIDKAAPKGRLILPQQQTIRDILESDAIAMVTKEFELRETL
ClodiEngA       EFKLVSDLIEPNDLVVLVVPIDKAAPKGRLILPQQQVIRDILDSGAISIVTKEDSLKETL
                :  ::.**:.*.*:.*** *****************.***:*: .*:::**** .*::**

ThitHydF        QNLGKKPSLVITDSQAFLKVSADTPKDIPLTSFSILFARYKGDLEELVRGVKAIKKLKPG
FefeMnmE        SSLARKPRIVVTDSQAFARVAQDTPRDIPMTSFSILFARYKGDLAQLVEGVKAIKNLKPG
CaHydF          DSLRKKPKIVITDSQVFLKVAADTPKDILMTSFSILMARHKGDLIELARGARAIEDLKDG
ClodiEngA       SNLGKKPKLVITDSQVFPQVDKDTPKDIPLTSFSILFARQKGDLKELINGAYALENLKDG
                ..* :** :*:****.* :*  ***:** :******:** **** :* .*. *::.** *

ThitHydF        DKVLIAEGCTHHRQPDDIGKVKIPRWIRQIVGGDIQFEWSSGITFPDNLEEYSLIVHCGA
FefeMnmE        DRVLIAEACTHHRQEDDIGTVKIPRWLRQILGFDVQFEWSSGFGFPENLEDFKLVIHCGG
CaHydF          DKILIAEACTHHRQSDDIGKVKIPRWLRQKTGKKLEFDFSSGFSFPPNIEDYALIVHCAG
ClodiEngA       DKILMAEGCTHHRQTDDIGTVKIPNMIRKKTGKNITFEFSSGVSFTEDINKYALVVHCGA
                *::*:**.****** ****.****. :*:  * .: *::***. *. ::::: *::**..

ThitHydF        CMLNRREMMYRISYAKSKNIPIVNYGILIAYVQGLMPRAIEMFPLAKMVYEEE---
FefeMnmE        CMINRKEMLYRLSLLKRRNIPVVNYGVFIAYALGILERALEPIPEAALLFSSES--
CaHydF          CMLNRRSMLHRIESSVKKQIPIVNYGVLIAYVQGILPRALKPFPYADRIFNQSSRN
ClodiEngA       CMMNRAGMLSRIEKAKSFNVPIVNYGILIAYVKGILERSLELFNY----------
                **:**  *: *:.     ::*:****::***. *:: *::: :
```

A 5.1 ITC

Noise corrected spectra (Figure 5.24 and 5.25) were re-analyzed with the online application AffinityMeter. Two different concentrations for HydF were analyzed, once with the concentration of the whole dimer (25 μM) and the other with the concentration of the monomer HydF (50 μM). Therefore a model for N = 1 and N = 0.5 was generated. However, due to noisy data the errors are very high, and the calculated kinetic parameters are giving just an idea of the magnitude of interaction.

Table A.1: With AffinityMeter calculated binding constants and enthalpies.

Conc. (HydF)	Conc. (GTP)	K_D	ΔH
25 μM	900 μM	(3.5734 ± 2.1997)e-04	(-8.0558 ± 8.3106)e+05
50 μM	900 μM	(3.1462 ± 2.9881)e-04	(-1.2506 ± 1.0211)e+06
25 μM	750 μM	(0.2297 ± 2.0173)e-07	(-8.5764 ± 1.8441)e+02
50 μM	750 μM	(0.5381 ± 4.6800)e-07	(-2.7106 ± 1.1596)e+03

References

(1) Sachs J. D., Clean energy benefits the climate, the economy and our health (**2016**), *Bull World Health Organ.*, **94(7)**, 489-490.

(2) Waheed R., Chang D., Sarwar S., Chen W., Forest, agriculture, renewable energy, and CO_2 emission (**2018**), *J Clean Prod*, **172**, 4231-4238.

(3) Turner J. A., Sustainable hydrogen production (**2004**), *Science*, **305(5686)**, 972-974.

(4) Show K. Y., Yan Y., Ling M., Ye G., Li T., Lee D. J., Hydrogen production from algal biomass- Advances, challenges and prospects (**2018**), *Bioresour Technol.*, **257**, 290-300.

(5) Zannoni D., De Philippis R., Microbail BioEnergy: Hydrogen Production (**2014**), *Springer*, **38 Advances in Photosynthesis and Respiration**, ISBN 9401785546.

(6) Lubitz W., Ogata H., Rüdiger O., Reijerse E., Hydrogenases (**2014**), *Chem Rev.*, **114(8)**, 4081-4148.

(7) Stephenson M., Stickland L. H., Hydrogenase: a bacterial enzyme activating molecular hydrogen (**1931**), *Biochem J.*, **25(1)**, 205-214.

(8) Vignais P. M., Billoud B., Meyer J., Classification and phylogeny of hydrogenases (**2001**), *FEMS Microbiol Rev.*, **25(4)**, 455-501.

(9) Mulder D. W., Shepard E. M., Meuser J. E., Joshi N., King P. W., Posewitz M. C., Broderick J. B., Peters J. W., Insights into [FeFe]-Hydrogenase Structure, Mechanism, and Maturation (**2011**), *Structure*, **19**, 1038-1052.

(10) Shima S., Ermler U., Structure and Function of [Fe]-Hydrogenase and its Iron-Guanylpyridinol (FeGP) Cofactor (**2010**), *Eur J Inorg Chem.*, **2011**, 963-972.

(11) Shima S., Thauer R. K., A third type of hydrogenase catalyzing H2 activation (**2007**), *Chem Rec.*, **7(1)**, 37-46.

(12) Winkler M., Esselborn J., Happe T., Molecular basis of [FeFe]-hydrogenase function: an insight into the complex interplay between protein and catalytic cofactor (**2013**), *Biochim Biophys Acta.*, **1827(8-9)**, 974-985.

(13) Tard C., Pickett C. J., Structural and Functional Analogues of the Active Sites of the [Fe]-, [NiFe]-, [FeFe]-Hydrogenases (**2009**), *Chem Rev.*, **109**, 2245-2274.

(14) Pierik A. J., Roseboom W., Happe R.P., Bagley K.A., Albracht S. P. J., Carbon Monoxide and Cyanide as Intrinsic Ligans to Iron in the Active Site of [NiFe]-Hydrogenases (**1999**), *J Biol Chem.*, **274(6)**, 3331-3337.

(15) Peters J. W., Schut G. J., Boyd E. S., Mulder D. W., Shepard E. M., Broderick J. B., King P. W., Adams M. W., [FeFe]- and [NiFe]-hydrogenase diversity, mechanism and maturation (**2015**), *Biochim Biophys Acta.*, **1853(6)**, 1350-1369.

(16) Tang H., Hall M. B., Biomimetics of [NiFe]-Hydrogenase: Nickel- or Iron-Centered Proton Reduction Catalysis? (**2017**), *J Am Chem Soc.*, **139(49)**, 18065-18070.

(17) Ogata H., Lubitz W., Higuchi Y., Structure and function of [NiFe] hydrogenases (**2016**), *J Biochem.*, **160(5)**, 251-258.

(18) Artz J. H., Mulder D. W., Ratzloff M. W., Lubner C. E., Zadvornyy O. A., LeVan A. X., Williams S. G., Adams M. W. W., Jones A. K., King P. W., Peters J. W., Reduction Potentials of [FeFe]-Hydrogenase Accessory Iron-Sulfur Clusters Provide Insights into the Energetics of Proton Reduction Catalysis (**2017**), *J Am Chem Soc.*, **139(28)**, 9544-9550.

(19) Hatchikian E. C., Forget N., Fernández V. M., Williams R., Cammack R., Furhter characterization of the [Fe]-hydrogenase from Desulfovibrio desulfuricans ATCC 7757 (**1992**), *Eur J Biochem.*, **209(1)**, 357-365.

(20) Peters J. W., Lanzilotta W. N., Lemon B. J., Seefeldt L. C., X-ray crystal structure of the Fe-only hydrogenase (CpI) from Clostridium pasteurianum to 1.8 angstrom resolution (**1998**), *Science*, **282(5395)**, 1853-1858.

(21) Nicolet Y., Piras C., Legrand P., Hatchikian C. E., Fontecilla-Camps J. C., Desulfovibro desulfuricans iron hydrogenase: the structure shows unusual coordination to an active site Fe binuclear center (**1999**), *Structure*, **7(1)**, 13-23.

(22) Dinis P., Wieckowski B. M., Roach P. L., Metallocofactor assembly for [FeFe]-hydrogenases (**2016**), *Curr Opin Struct Biol.*, **41**, 90-97.

(23) Morra S., Maurelli S., Chiesa M., Mulder D. W., Ratzloff M. W., Giamello E., King P. W., Gilardi G., Valetti F., The effect of a C298D mutation in CaHydA [FeFe]-hydrogenase: Insights into the protein-metal cluster interaction by EPR and FTIR spectroscopic investigation (**2016**), *Biochim Biophys Acta*, **1857(1)**, 98-106.

(24) Van der Spek T. M., Arendsen A. F., Happe R. P., Yun S., Bagley K. A., Stufkens D. J., Hagen W. R., Albracht S. P., Similarities in the architecture of the active sites of Ni-hydrogenases and Fe-hydrogenases detected by means of infrared spectroscopy (**1996**), *Eur J Biochem.*, **237(3)**, 629-634.

(25) Pierik A. J., Hulstein M., Hagen W. R., Albracht S. P., A low-spin iron with CN and CO as intrinsic ligands forms the core of the active site in [Fe]-hydrogenases (**1998**), *Eur J Biochem*., **258(2)**, 572-578.

(26) Ryde U., Greco C., De Gioia L., Quantum refinement of [FeFe] hydrogenase indicates a dithiomethylamine ligand (**2010**), *J Am Chem Soc.*, **132(13)**, 4512-4513.

(27) Berggren G., Adamska A., Lambertz C., Simmons T. R., Esselborn J., Atta M., Gambarelli S., Mouesca J. M., Reijerse E., Lubitz W., Happe T., Artrero V. Fontecave M. Biomimetic assembly and activation of [FeFe]-hydrogenases (**2013**), *Nature*, **499**, 66-69.

(28) Esselborn J., Lambertz C., Adamska-Venlatesh A., Simmons T., Berggren G., Noth J., Siebel J., Hemschemeier A., Artreo V., Reijerse E., Fontecave M., Lubitz W., Happe T., Spontaneous activation of [FeFe]-hydrogenases by an inorganic [2Fe] active site mimic (**2013**), *Nat Chem Biol*, **9(10)**, 607-609.

(29) Schilter D., Rauchfuss T. B., And the winner is...azadithiolate: an amine proton relay in the [FeFe] hydrogenases (**2013**), *Angew Chem Int Ed Engl*., **52(51)**, 13518-13530.

(30) Vignais P M., Billoud B., Occurrence, classification and biological function of hydrogenases: an overview (**2007**), *Chem Rev.*, **107**, 4206-4272.

(31) Mulder D. W., Boyd E. S., Sarma R., Lange R. K., Endrizzi J. A., Broderick J. B., Peters J. W., Stepwise [FeFe]-hydrogenase H-cluster assembly revealed in the structure of HydA (DeltaEFG) (**2010**), *Nature*, **465(7295)**, 248-251.

(32) Winkler M., Heil B., Happe T., Isolation and molecular characterization of the [Fe]-hydrogenase from the unicellular green alga *Chlorella fusca* (**2002**), *Biochim Biophy Acta*, **1576**, 330-334.

(33) Gauquelin C., Baffert C., Richaud P., Kamionka E., Etienne E., Guieysse D., Girbal L., Fourmond V., André I., Guigliarelli D., Léger C., Soucaille P., Meynial-Salles I., Roles of the F-domain in [FeFe] hydrogenase (**2018**), *Biochim Biophys Acta*, **1859(2)**, 69-77.

(34) Voordouw G., Hagen W. R., Krüse-Wolters K. M., van Berkel-Arts A., Veeger C., Purification and characterization of Desulfovibrio vulgaris (Hildenborough) hydrogenase expressed in Escherichia coli (**1987**), *Eur J Biochem.*, **162**, 31-36.

(35) Mulder D. W., Ortillo D. O., Gardenghi D. J., Naumov A. V., Ruebush S. S., Szilagyi R. K., Huynh B., Broderick J. B., Peters J. W., Activation of HydA(DeltaEFG) requires a preformed [4Fe-4S] cluster (**2009**), *Biochemistry*, **48(26)**, 6240-6248.

(36) Barras F., Loiseau L., Py B., How *Escherichia coli* and *Saccharomyces cerevisiae* build Fe/S proteins (**2005**), *Adv Microb Physiol.*, **50**, 41-101.

(37) Caserta G., Pecqueur L., Papini C., Fontecave M., FeFe-Hydrogenase Assembly (**2017**), *Encycl Inorg Bioinorg Chem.*, John Wiley & Sons Ltd.

(38) Suess D. L. M., Kuchenreuther J. M., De La Paz L., Swartz J. R., Britt R. D., Biosynthesis of the [FeFe] Hydrogenase H Cluster: A Central Role for the Radical SAM Enzyme HydG (**2016**), *Inorg Chem.*, **55(2)**, 478-487.

(39) Peters J. W., Szilagyi R. K., Naumov A., Douglas T., A radical solution for the biosynthesis of the H-cluster of hydrogenase (**2006**), *FEBS Lett.*, **580(2)**, 363-367.

(40) Posewitz M. C., King P. W., Smolinski S. L., Zhang L., Seibert M., Ghirardi M. L., Discovery of two novel radical S-adenosylmethionine proteins required for the assembly of an active [Fe] hydrogenase (**2004**), *J Biol Chem*, **279(24)**, 25711-25720.

(41) Posewitz M. C., King P.W., Smolinski S. L., Smith R. D., Ginley A. R., Ghirardi M. L., Seibert M., Identification of genes required for hydrogenase activity in Chlamydomonas reinhardtii (**2005**), *Biochem Soc Trans.*, **33(Pt1)**, 102-104.

(42) King P. W., Posewitz M. C., Ghirardi M. L., Seibert M., Functional studies of [FeFe] hydrogenase maturation in an Escherichia coli biosynthetic system (**2006**), *J Bacteriol.*, **188(6)**, 2163-2172.

(43) Czech I., Silakov A., Lubitz W., Happe T., The [FeFe]-hydrogenase maturase HydF from Clostridium acetobutylicum contains a CO and CN^- ligated iron cofactor (**2010**), *FEBS Lett.*, **584(3)**, 638-642.

(44) Sybirna K., Antoine T., Lindberg P., Fourmond V., Rousset M., M**é**jean V., Bottin H., Shewanella oneidensis: a new and efficient System for Expression and Maturation of heterologous [Fe-Fe] Hydrogenase from Chlamydomonas reinhardtii (**2008**), *BMC Biotechnol.*, **8:73**, 1-8.

(45) McGlynn S. E., Ruebush S. S., Naumov A., Nagy L. E., Dubini A., King P. W., Broderick J. B., Posewitz M. C., Peters J. W., In vitro activation of [FeFe] hydrogenase: new insights into hydrogenase maturation (**2007**), *J Biol Inorg Chem.*, **12(4)**, 443-447.

(46) Boyer M. E., Stapleton J. A., Kuchenreuther J. M., Wang C. W., Swartz J. R., Cell-free synthesis and maturation of [FeFe] hydrogenases (**2008**), *Biotechnol Bioeng.*, **99(1)**, 59-67.

(47) Kuchenreuther J. M., Stapleton J. A., Swartz J. R., Tyrosine, cysteine, and S-adenosyl methionine stimulate in vitro [FeFe] hydrogenase activation (**2009**), *PLoS One*, **4(10)**:e7565.

(48) Kuchenreuther J. M., Grady-Smith C. S., Bingham A. S., George S. J., Cramer S. P., Swartz J. R., High-yield expression of heterologous [FeFe] hydrogenases in Escherichia coli (**2010**), *PLoS One*, **5(11)**:e15491.

(49) Kuchenreuther J. M., George S. J., Grady-Smith C. S., Cramer S. P., Swartz J. R., Cell-free H-cluster synthesis and [FeFe] hydrogenase activation: all five CO and CN^- ligands derive from tyrosine (**2011**), *PLoS One*, **6(5)**:e20346.

(50) Kuchenreuther J. M., Britt R. D., Swartz J. R., New insights into [FeFe] hydrogenase activation and maturase function (**2012**), *PLoS One*, **7(9)**, e45850.

(51) Brazzolotto X., Rubach J. K., Gaillard J., Gambarelli S., Atta M., Fontecave M., The [Fe-Fe]-hydrogenase maturation protein HydF from *Thermotoga maritima* is a GTPase with an iron-sulfur cluster (**2006**), *J Biol Chem.*, **281(2)**, 769-774.

(52) Rubach J. K., Brazzolotto X., Gaillard J., Fontecave M., Biochemical characterization of the HydE and HydG iron-only hydrogenase maturation enzymes from *Thermatoga maritima* (**2005**), *FEBS Lett.*, **579(22)**, 5055-5060.

(53) Nicolet Y., Rubach J. K., Posewitz M. C., Amara P., Mathevon C., Atta M., Fontecave M., Fontecilla-Camps J. C., X-ray structure of the [FeFe]-hydrogenase maturase HydE from *Thermotoga maritima* (**2008**), *J Biol Chem.*, **283(27)**, 18861-18872.

(54) Pilet E., Nicolet Y., Mathevon C., Douki T., Fontecilla-Camps J. C., Fontecave M., The role of the maturase HydG in [FeFe]-hydrogenase active site synthesis and assembly (**2009**), *FEBS Lett.*, **583(3)**, 506-511.

(55) Driesener R. C., Challand M. R., McGlynn S. E., Shepard E. M., Boyd E. S., Broderick J. B., Peters J. W., Roach P. L., [FeFe]-hydrogenase cyanide ligands derived from *S*-adenosylmethionine-dependent cleavage of tyrosine (**2010**), *Angew Chem Int Ed Engl.*, **49(9)**, 1687-90.

(56) Shepard E. M., Duffus B. R., George S. J., McGlynn S. E., Challand M. R., Swanson K. D., Roach P. L., Cramer S. P., Peters J. W., Broderick J. B., [FeFe]-hydrogenase maturation: HydG-catalyzed synthesis of carbon monoxide (**2010**), *J Am Chem Soc.*, **132(27)**, 9247-9249.

(57) Nicolet Y., Martin L., Tron C., Fontecilla-Camps J. C., A glycyl free radical as the precursor in the synthesis of carbon monoxide and cyanide by the [FeFe]-hydrogenase maturase HydG (**2010**), *FEBS Lett.*, **584(19)**, 4197-4202.

(58) Nicolet Y., Rohac R., Martin L., Fontecilla-Camps J. C., X-ray snapshots of possible intermediates in the time course of synthesis and degradation of protein-bound Fe4S4 clusters (**2013**), *Proc Natl Acad Sci USA*., **110(18)**, 7188-7192.

(59) Kuchenreuther J. M., Myers W. K., Stich T. A., George S. J., Nejatyjahromy Y., Swartz J. R., Britt R. D., A radical intermediate in tyrosine scission to the CO and CN-ligands of FeFe hydrogenase (**2013**), *Science*, **342(6157)**, 472-475.

(60) Driesener R. C., Duffus B. R., Shepard E. M., Bruzas I. R., Duschene K. S., Coleman N. J., Marrison A. P., Salvadori E., Kay C. W., Peters J. W., Broderick J. B. Roach P. L., Biochemical and kinetic characterization of radical S-adenosyl-L-methionine enzyme HydG (**2013**), *Biochemistry*, **52(48)**, 8696-8707.

(61) Kuchenreuther J. M., Myers W. K., Suess D. L., Stich T. A., Pelmenschikov V., Shiigi S. A., Cramer S. P., Swartz J. R., Britt R. D., George S. J., The HydG enzyme generates an Fe(CO)2(CN) synthon in assembly of the FeFe hydrogenase H-cluster (**2014**), *Science*, **343(6169)**, 424-427.

(62) Duffus B. R., Ghose S., Peters J. W., Broderick J. B., Reversible H atom abstraction catalyzed by the radical S-adenosylmethionine enzyme HydG (**2014**), *J Am Chem Soc.*, **136(38)**, 13086-13089.

(63) Nicolet Y., Pagnier A., Zeppieri L., Martin L., Amara P., Fontecilla-Camps J. C., Crystal structure of HydG from *Carboxydothermus hydrogenoformans*: a trifunctional [FeFe]-hydrogenase maturase (**2015**), *Chembiochem.*, **16(3)**, 397-402.

(64) Dinis P., Suess D. L., Fox S. J., Harmer J. E., Driesener R. C., De La Paz L., Swartz J. R., Essex J. W., Britt R. D., Roach P. L., X-ray crystallographic and EPR spectroscopic analysis of HydG a maturase in [FeFe]-hydrogenase H-cluster assembly (**2015**), *Proc Natl Acad Sci USA*, **112(5)**, 1362-1367.

(65) Betz J. N., Bosewell N. W., Fugate C. J., Holliday G. L., Akiva E., Scott A. G., Babbitt P. C., Peters J. W., Shepard E. M., Broderick J. B., [FeFe]-hydrogenase maturation: insights into the role HydE plays in dithiomethylamine biosynthesis (**2015**), *Biochemistry*, **54(9)**, 1807-1818.

(66) Suess D. L., Bürstel I., De La Paz L., Kuchenreuther J. M., Pham C. C., Cramer S. P., Swartz J. R., Britt R. D., Cysteine as a ligand platform in the biosynthesis of the FeFe hydrogenase H cluster (**2015**), *Proc Natl Acad Sci USA*, **112(37)**, 11455-11460.

(67) Suess D. L., Britt R. D., EPR Spectroscopic Studies of [FeFe]-Hydrogenase Maturation (**2015**), *Catal Letters*, **58(12)**, 699-707.

(68) Pagnier A., Martin L., Zeppieri L., Nicolet Y., Fontecilla-Camps J. C., CO and CN- syntheses by [FeFe]-hydrogenase maturase HydG are catalytically differentiated events (**2016**) *Proc Natl Acad Sci USA*, **113(1)**, 104-109.

(69) Suess D. L., Pham C. C., Bürstel I., Swartz J. R., Cramer S. P., Britt R. D., The Radical SAM Enzyme HydG Requires Cysteine and a Dangler Iron for Generation an Organometallic Precursor to the [FeFe]-Hydrogenase H-Cluster (**2016**), *J Am Chem Soc.*, **138(4)**, 1146-1149.

(70) Rohac R., Amara P., Benjdia A., Martin L., Ruffié P., Favier A., Berteau O., Mouesca J. M., Fontecilla-Camps J. C., Nicolet Y., Carbon-sulfur bond-forming reaction catalysed by the radical SAM enzyme HydE (**2016**), *Nat Chem.*, **8(5)**, 491-500.

(71) Rao G., Tao L., Suess D. L. M., Britt R. D., A [4Fe-4S]-Fe(CO)(CN)-L-cysteine intermediate is the first organometallic precursor in [FeFe] hydrogenase H-cluster bioassembly (**2018**), *Nat Chem.*, **10(5)**, 555-560.

(72) Fan H. J., Hall M. B., A capable bridging ligand for Fe-only hydrogenase: density functional calculations of a low-energy route for heterolytic cleavage and formation of dihydrogen (**2001**), *J Am Chem Soc.*, **123(16)**, 3828-3829.

(73) Adams M. W. W., The structure and mechanism of iron-hydrogenases (**1990**), *Biochim Biophys Acta*, **1020**, 115-145.

(74) Popescu C. V., Münck E., Electronic structure of the H cluster in [Fe]-hydrogenases (**1999**), *J Am Chem Soc.*, **121**, 7877-7884.

(75) Cao Z., Hall M. B., Modeling the active sites in metalloenzymes. 3. Density function calculation on models for [Fe]-hydrogenase: structures and vibrational frequencies of the observed redox forms and the reaction mechanism at the Diiron Active centre (**2001**), *J Am Chem Soc.*, **123**, 3734-3742.

(76) Pereira A. S., Tavares P., Moura I., Moura J. J. G., Huynh B. H., Mössbauer characterization of the iron-sulfur clusters in *Desulfovibrio vulgaris* hydrogenase (**2001**), *J Am Chem Soc.*, **123**, 2771-2782.

(77) Kubas G. J., Fundamentals of H_2 binding and reactivity on transition metals underlying hydrogenase function and H_2 production and storage (**2007**), *Chem Rev.*, **107**, 4152-4205.

(78) Lemon B. J., Peters J. W., Binding of exogenously added carbon monoxide at the active site of the iron-only hydrogenase (CpI) from Clostridium pasteurianum (**1999**), *Biochemistry*, **38**, 12969-12973.

(79) Nicolet Y., Lemon B. J., Fontecilla-Camps J. C., Peters J. W., A novel FeS cluster in Fe-only hydrogenases (**2000**), *Trends Biochem Sci.*, **25**, 138-143.

(80) Nicolet Y., de Lacey A. L., Vernède X., Fernandez V. M., Hatchikian E. C., Fontecilla-Camps J. C., Crystallographic and FTIR spectroscopic evidence of changes in Fe coordination upon reduction of the active site of the Fe-only hydrogenase from Desulfovibrio desulfuricans (**2001**), *J Am Chem Soc.*, **123**, 1596-1601.

(81) Silakov A., Reijerse E. J., Albracht S. P. J., Hatchikian E. C., Lubitz W., The electronic structure of the H-cluster in the [FeFe]-hydrogenase from Desulfovibrio desulfuricans: a Q-band 57Fe-ENDOR and HYSCORE study (**2007**), *J Am Chem Soc.*, **129**, 11447-11458.

(82) Fan H.-J., Hall M. B., A capable bridging ligand for Fe-only hydrogenase: a density functional calculations of a Low-energy route for heterolytic cleavage and formation of dihydrogen (**2001**), *J Am Chem Soc.*, **123**, 3928-3829.

(83) Schilter D., Camara J. M., Huynh M. T., Hammes-Schiffer S., Rauchfuss T. B., Hydrogenase Enzymes and Their Synthetic Models: The Role of Metal Hydrides (**2016**), *Chem Rev.*, **116(15)**, 8693-8749.

(84) Winkler M., Senger M., Duan J., Esselborn J., Wittkamp F., Hofmann E., Apfel U. P., Stripp S. T., Happe T., Accumulating the hydride state in the catalytic cycle of [FeFe]-hydrogenases (**2017**), *Nat Commun.*, **8**:16115.

(85) Knörzer P., Silakov A., Foster C. E., Armstrong F. A., Lubitz W., Happe T., Importance of the Protein Framework for Catalytic Activity of [FeFe]-Hydrogenases (**2012**), *J Biol Chem.*, **287(2)**, 1489-1499.

(86) Hong G., Cornish A. J., Hegg E. L., Pachter R., On understanding proton transfer to the biocatalytic [Fe-Fe] H sub-cluster in [Fe-Fe]H2ases: QM/MM MD simulations (**2011**), *Biochim Biophys Acta.*, **1807(5)**, 510-517.

(87) Cornish A. J., Gärtner K., Yang H., Peters J. W., Hegg E. L., Mechanism of proton transfer in [FeFe]-hydrogenase from Clostridium pasteurianum (**2011**), *J Biol Chem.*, **286(44)**, 38341-38347.

(88) Ginovska-Pangovska B., Ho M. H., Linehan J. C., Cheng Y., Dupuis M., Raugei S., Shaw W. J., Molecular dynamics study of the proposed proton transport pathways in [FeFe]-hydrogenase (**2014**), *Biochim Biophys Acta.*, **1837(1)**, 131-138.

(89) Long H., King P. W., Chang C. H., Proton transport in Clostridium pasteurianum [FeFe] hydrogenase I: a computantional study (**2014**), *J Phys Chem B.*, **118(4)**, 890-900.

(90) Mulder D. W., Guo Y., Ratzloff M. W., King P. W., Identification of a Catalytic Iron-Hydride at the H-cluster of [FeFe]-hydrogenase (**2017**), *J Am Chem Soc.*, **139(1)**, 83-86.

(91) Winkler M., Senger M., Duan J., Esselborn J., Wittkamp F., Hofmann E., Apfel U. P., Stripp S. T., Happe T., Accumulating the hydride state in the catalytic cycle of [FeFe]-hydrogenases (**2017**), *Nat Commun.*, **8**:16115.

(92) Pelmenschikov V., Birrell J. A., Pham C. C., Mishra N., Wang H., Sommer C., Reijerse E., Richers C. P., Tamasaku K., Yoda Y., Rauchfuss T. B., Lubitz W., Cramer S. P., Reaction Coordinate Leading to H_2 Production in [FeFe]-Hydrogenase Identified by Nuclear Resonance Vibrational Spectroscopy and Density Functional Theory (**2017**), *J Am Chem Soc.*, **139(46)**, 16894-16902.

(93) Rumpel S., Sommer C., Reijerse E., Farès C., Lubitz W., Direct Detection of the Terminal Hydride Intermediate in [FeFe] Hydrogenase by NMR spectroscopy (**2018**), *J Am Chem Soc.*, **140(11)**, 3863-3866.

(94) Sommer C., Richers C. P., Lubitz W., Rauchfuss T. B., Reijerse E. J., A [RuRu] Analogue of an [FeFe]-Hydrogenase Traps the Key Hydride Intermediate of the Catalytic Cycle (**2018**), *Angew Chem Int Ed Engl.*, **57(19)**, 5429-5432.

(95) Akiva E., Brown S., Almonacid D. E., Barber A. E. 2nd, Custer A. F., Hicks M. A., Huang C. C., Lauck F., Mashiyama S. T., Meng E. C., Mischel D., Morris J. H., Ojha S., Schnoes A. M., Stryke D., Yunes J. M., Ferrin T. E., Holliday G. L., Babbitt P. C., The Structure-Function Linkage Database (**2014**), *Nucleic Acids Res.*, **42** (Database issue), D521-D530.

(96) Sofia H. J., Chen G., Hetzler B. G., Reyes-Spindola J. F., Miller N. E., Radical SAM, a novel protein superfamily linking unresolved steps in familiar biosynthetic pathways with radical mechanisms: functional characterization using new analysis and information visualization methods (**2001**), *Nucleic Acids Res.*, **29(5)**, 1097-1106.

(97) Benjdia A., Balty C., Berteau O., Radical SAM Enzymes in the Biosynthesis of Ribosomally Synthesized and Post-translationally Modified Peptides (RiPPs) (**2017**), *Front Chem.*, **5**:87.

(98) Broderick J. B., Duffus B. R., Duschene K. S., Shepard E. M., Radical *S*-Adenosylmethionine Enzymes (**2014**), *Chem Rev.*, **114(8)**, 4229-4317.

(99) Chatterjee A., Li Y., Zhang Y., Grove T. L., Lee M., Krebs C., Booker S. J., Begley T. P., Ealick S. E., Reconstitution of ThiC in thiamine pyrimidine biosynthesis expands the radical SAM superfamily (**2008**), *Nat Chem Biol.*, **4(12)**, 758-765.

(100) McGlynn S. E., Boyd E. S., Shepard E. M., Lange R. K., Gerlach R., Broderick J. B., Peters J. W., Identification and characterization of a novel member of the radical AdoMet enzyme superfamily and implications for the biosynthesis of the Hmd hydrogenase active site cofactor (**2010**), *J Bacteriol.*, **192(2)**, 595-598.

(101) Dowling D. P., Bruender N. A., Young A. P., McCarty R. M., Bandarian V., Drennan C. L., Radical SAM enzyme QueE defines a new minimal core fold and metal-dependent mechanism (**2014**), *Nat Chem Biol.*, **10(2)**, 106-112.

(102) Fugate C. J., Jarrett J. T., Biotin synthase: insights into radical-mediated carbon-sulfur bond formation (**2012**), *Biochim Biophys Acta.*, **1824(11)**, 1213-1222.

(103) Douglas P., Kriek M., Bryant P., Roach P. L., Lipoyl synthase inserts sulfur atoms into an octanoyl substrate in a stepwise manner (**2006**), *Angew Chem Int Ed Engl.*, **45(31)**, 5197-5199.

(104) Forouhar F., Arragain S., Atta M., Gambarelli S., Mouesca J. M., Hussain M., Xiao R., Kieffer-Jaquinod S., Seetharaman J., Acton T. B., Montelione G. T., Mulliez E., Hunt J. F., Fontecave M., Two Fe-S clusters catalyze sulfur insertion by radical-SAM methylthiotransferases (**2013**), *Nat Chem Biol.*, **9(5)**, 333-338.

(105) Lawhorn B. G., Mehl R. A., Begley T. P., Biosynthesis of the thiamin pyrimidine: the reconstitution of a remarkable rearrangement reaction (**2004**), *Org Biomol Chem.*, **2**, 2538-2546.

(106) Hover B. M., Tonthat N. K., Schuhmacher M. A., Yokoyama K., Mechanism of pyranopterin ring formation in molybdenum cofactor biosynthesis (**2015**), *Proc Natl Acad Sci USA*, **112(20)**, 6347-6352.

(107) Mehta A. P., Abdelwahed S. H., Mahanta N., Fedoseyenko D., Philmus B., Cooper L. E., Liu Y., Jhulki I., Ealick S. E., Begley T. P., Radical *S*-Adenosylmethionine (SAM) Enzymes in Cofactor Biosynthesis: A Treasure Trove of Complex Organic Radical Rearrangment Reactions (**2015**), *J Biol Chem.*, **290(7)**, 3980-3986.

(108) Liu W. Q., Amara P., Mouesca J. M., Ji X., Renoux O., Martin L., Zhang C., Zhang Q., Nicolet Y., 1,2-Diol Dehydration by the Radical SAM Enzyme AprD4: A Matter of Proton Circulation and Substrate Flexibility (**2018**), *J Am Chem Soc.*, **140(4)**, 1365-1371.

(109) Thweatt J. L., Ferlez B. H., Golbeck J. H., Bryant D. A., BciD is a Radical *S*-Adenosyl-L-methionine (SAM) Enzyme That Completes Bacteriochlorophyllide e Biosynthesis by Oxidizing a Methyl Group into a Formyl Group at C-7 (**2017**), *J Biol Chem.*, **292(4)**, 1361-1373.

(110) Bruender N. A., Bandarian V., The radical S-adenosyl-L-methionine enzyme MftC catalyzes an oxidative decarboxylation of the C-terminus of the MftA peptide (**2016**), *Biochemistry*, **55(20)**, 2813-2816.

(111) Feng J., Wu J., Dai N., Lin S., Xu H. H., Deng Z., He X., Discovery and characterization of BlsE, a radical S-adenosyl-L-methionine decarboxylase involved in the blasticidin S biosynthetic pathway (**2013**), *PLoS One*, **8(7)**, e68545.

(112) Kühner M., Schweyen P., Hoffmann M., Ramos J. V., Reijerse E. J., Lubitz W., Bröring M., Layer G., The auxiliary [4Fe-4S] cluster of the Radical SAM heme synthase from Methanosarcina barkeri is involved in electron transfer (**2016**), *Chem Sci.*, **7**, 4633-4643.

(113) Berteau O., Benjdia A., DNA Repari by the Radical SAM Enzyme Spore Photoproduct Lyase: From Biochemistry to Structural Investigations (**2017**), *Photochem Photobiol.*, **93(1)**, 67-77.

(114) Yan F., LaMarre J. M., Röhrich R., Wiesner J., Jomaa H., Mankin A. S., Fujimori D. G., RlmN and Cfr are Radical SAM Enzymes Involved in Methylation of Ribosomal RNA (**2010**), *J Am Chem Soc.*, **132(11)**, 3953-3964.

(115) Hänzelmann P., Schindelin H., Crystal Structure of the *S*-adenosylmethionine-dependent enzyme MoaA and its implications for molybdenum cofactor deficiency in humans (**2004**), *Proc Natl Acad Sci USA*, **101**, 12870-12875.

(116) Byer A. S., Shepard E. M., Peters J. W., Broderick J. B., Radical *S*-Adenosyl-L-methionine Chemistry in the Synthesis of Hydrogenase and Nitrogenase Metal Cofactors (**2015**), *J Biol Chem.*, **290(7)**, 3987-3994.

(117) Walsby C. J., Ortillo D., Broderick W. E., Broderick J. B., Hoffman B. M., An anchoring role for FeS clusters: chelation of the amino acid moiety of S-adenosylmethionine to the unique iron site of the [4Fe-4S] center of pyruvate fromate-lyase activating enzyme (**2002**), *J Am Chem Soc.*, **124**, 11270-11271.

(118) Chen D., Walsby C., Hoffman B. M., Frey P. A., Coordination and mechanism of reversible cleavage of S-adenosylmethionine by the [4Fe-4S] centre in lysine 2,3-aminomutase (**2003**), *J Am Chem Soc.*, **125**, 11788-11789.

(119) Duschene K. S., Broderick J. B., The antiviral protein viperin is a radical SAM enzyme (**2010**), *FEBS Lett.*, **584(6)**, 1263-1267.

(120) Cosper N. J., Booker S. J., Ruzicka F., Frey P. A., Scott R. A., Direct FeS cluster involvement in generation of a radical in lysine 2,3-aminomutase (**2000**), *Biochemistry*, **39(51)**, 15668-15673.

(121) Vey J. L., Drennan C. L., Structural Insights into Radical Generation by the Radical SAM Superfamily (**2011**), *Chem Rev.*, **111(4)**, 2487-2506.

(122) Nicolet Y., Amara P., Mouesca J.-M., Fontecilla-Camps J. C., Unexpected electron transfer mechanism upon AdoMet cleavage in radical SAM proteins (**2009**), *Proc Natl Acad Sci USA*, **106(35)**, 14867-14871.

(123) Dey A., Peng Y., Broderick W. E., Hedman B., Hodgson K. O., Broderick J. B., Solomon E. I., S K-edge XAS and DFT Calculations on SAM Dependent Pyruvate Formate-Lyase Activating Enzyme: Nature of Interaction between the Fe_4S_4 Cluster and SAM and its Role in Reactivity (**2012**), *J Am Chem Soc.*, **133(46)**, 18656-18662.

(124) Jarrett J. T., Farrar C. E., Radical S-Adenosylmethionine (SAM) Superfamily (**2014**), In: eLS. *John Wiley & Sons*, Ltd: Chichester.

(125) Imlay J. A., Iron-sulphur clusters and the problem with oxygen (**2006**), *Mol Microbiol.*, **59(4)**, 1073-1082.

(126) Walsby C. J., Hong W., Broderick W. E., Cheek J., Ortillo D., Broderick J. B., Hoffman B. M., Electron-nuclear double resonance spectroscopic evidence that S-adenosylmethionine bind in contact the catalytically active [4Fe-4S](+) cluster of pyruvate formate-lyase activating enzyme (**2002**), *J Am Chem Soc.*, **124(12)**, 3143-3151.

(127) Horitani M., Byer A. S., Shisler K. A., Chandra T., Broderick J. B., Hoffman B. M., Why Nature Uses Radical SAM Enzymes so Widely: Electron Nuclear Double Resonance Studies of Lysine 2,3-Aminomutase Show the 5'-dAdo• "Free Radical" is Never Free (**2015**), *J Am Chem Soc.*, **137(22)**, 7111-7121.

(128) Suzuki Y., Noma A., Suzuki T., Senda M., Senda T., Ishitani R., Nureki O., Crystal structure of the radical SAM enzyme catalyzing tricyclic modified base formation in tRNA (**2007**), *J Mol Biol.*, **372(5)**, 1204-1214.

(129) Magnusson O. T., Reed G. H., Frey P. A., Characterization of an allylic analogue of the 5'-deoxyadenosyl radical: an intermediate in the reaction of lysine 2,3-aminomutase (**2001**), *Biochemistry*, **40(26)**, 7773-7782.

(130) Wagner A. F., Frey M., Neugebauer F. A., Schäfer W., Knappe J., The free radical in pyruvate formate-lyase is located on glycine-734 (**1992**), *Proc Natl Acad Sci USA*, **89(3)**, 996-1000.

(131) Wang S. C., Frey P. A., *S*-adenosylmethionine as an oxidant: the radical SAM superfamily (**2007**), *Trends Biochem Sci.*, **32(3)**, 101-110.

(132) Challand M. R., Driesener R. C., Roach P. L., Radical *S*-adenosylmethionine enzymes: Mechanism, control and function (**2011**), *Nat Prod Rep.*, **28**, 1696-1721.

(133) Qianzhu H., Ji W., Ji X., Chu L., Guo C., Lu W., Ding W., Gao J., Zhang Q., Reactivity of the nitrogen-centered tryptophanyl radical in the catalysis by the radical SAM enzyme NosL (**2016**), *Chem Commun (Camb).*, **53(2)**, 344-347.

(134) Yan F., Fujimori D. G., RNA methylation by Radical SAM enzymes RlmN and Cfr proceeds via methylene transfer and hydride shift (**2011**), *Proc Natl Acad Sci USA.*, **108(10)**, 3930-3934.

(135) Lanz N. D., Booker S. J., Identification of auxiliary iron-sulfur clusters in radical SAM enzymes (**2012**), *Biochim Biophys Acta.*, **1824(11)**, 1196-1212.

(136) Colichman E. L., Love D. L., Polarography of sulfonium salts (**1953**), *J Org Chem.*, **18(1)**, 40-46.

(137) Saeva F. D., Morgan B. P., Mechanism of one-electron electrochemical reductive cleavage reactions of sulfonium salts (**1984**), *J Am Chem Soc.*, **106(15)**, 4121-4125.

(138) Wang S. C., Frey P. A., Binding energy in the one-electron reductive cleavage of *S*-adenosylmethionine in lysine 2,3-aminomutase, a radical SAM enzyme (**2007**), *Biochemistry*, **46(45)**, 12889-12895.

(139) S. Klimašauskas, G. Lukinavičius, AdoMet-Dependent Methyltransferases (**2008**), *Wiley Encyclopedia of Chemical Biology*, John Wiley & Sons, Inc., 1-10.

(140) Broderick J. B., Biochemistry: A radically different enzyme (**2010**), *Nature*, **465(7300)**, 877-878.

(141) Kampmeier J. A., Regioselectivety in the Homolytic Cleavage of *S*-Adenosylmethionine (**2010**), *Biochemistry*, **49(51)**, 10770-10772.

(142) Layer G., Moser J., Heinz D. W., Jahn D., Schubert W. D., Crystal structure of coproporphyrinogen III oxidase reveals cofactor geometry of Radical SAM enzymes (**2003**), *EMBO J.*, **22(23)**, 6214-6224.

(143) Berkovitch F., Nicolet Y., Wan J. T., Jarrett J. T., Drennan C. L., Crystal structure of biotin synthase, an S-adenosylmethionine dependent radical enzyme (**2004**), *Science*, **303(5654)**, 76-79.

(144) Demick J. M., Lanzilotta W. N., Radical SAM activation of the B12-independent glycerol dehydratase results in formation of 5'-deoxy-5'-(methylthio)adenosine and not 5'-deoxyadenosine (**2011**), *Biochemistry*, **50(4)**, 440-442.

(145) Zhang Y., Zhu X., Torelli A. T., Lee M., Dzikovski B., Koralewski R. M., Wang E., Freed J., Krebs C., Ealick S. E., Lin H., Diphthamide biosynthesis requires an Fe-S enzyme-generated organic radical (**2010**), *Nature*, **465(7300)**, 891-896.

(146) Dong M., Zhang Y., Lin H., Noncanonical Radical SAM Enzyme Chemistry Learned from Diphthamide Biosynthesis (**2018**), *Biochemistry*, **57(25)**, 3454-3459.

(147) Vey J. L., Yang J., Li M., Broderick W. E., Broderick J. B., Drennan C. L., Structural basis for glycyl radical formation by pyruvate formate-lyase activating enzyme (**2008**), *Proc Natl Acad Sci USA*, **105**, 16137-16141.

(148) Shibata N., Toraya T., Molecular architectures and functions of radical enzymes and their (re)activating proteins (**2015**), *J Biochem.*, **158(4)**, 271-292.

(149) Wierenga R. K., The TIM-barrel fold: a versatile framework for efficient enzymes (**2001**), *FEBS Lett.*, **492(3)**, 193-198.

(150) Nicolet Y., Zeppieri L., Amara P., Fontecilla-Camps J. C., Crystal structure of tryptophane lyase (NosL): evidence for radical formation at the amino group of tryptophan (**2014**), *Angew Chem Int Ed Engl.*, **53**, 11840-11844.

(151) Quitterer F., List A., Eisenreich W., Bacher A., Groll M., Crystal structure of methylornithine synthase (PylB): insights into the pyrrolysine biosynthesis (**2012**), *Angew Chem Int Ed Engl.*, **51**, 1339-1342.

(152) Lepore B. W., Ruzicka F. J., Frey P. A., Ringe D., The X-ray crystal structure of lysine-2,3-aminomutase from *Clostridium subterminale* (**2005**), *Proc Natl Acad Sci USA*, **102**, 13819-13824.

(153) Goldman P. J., Grove T. L., Booker S. J., Drennan C. L., X-ray analysis of butirosin biosynthetic enzyme BtrN redefines structural motifs for AdoMet radical chemistry (**2013**), *Proc Natl Acad Sci USA*, **110**, 15949-15954.

(154) Wang J., Woldring R. P., Román-Meléndez G. D., McClain A. M., Alzua B. R., Marsh E. N., Recent advances in radical SAM enzymology: new structures and mechanisms (**2014**), *ACS Chem Biol.*, **9(9)**, 1929-1938.

(155) Fenwick M. K., Mehta A. P., Zhang Y., Abdelwahed S. H., Begley T. P., Ealick S. E., Non-canonical active site architecture of the radical SAM thiamin pyrimidine synthase (**2015**), *Nat Commun.*, **6**:6480.

(156) Zhu X., Dzikovski B., Su X., Torelli A. T., Zhang Y., Ealick S. E., Freed J. H., Lin H., Mechanistic understanding of Pyrococcus horikoshii Dph2, a [4Fe-4S] enzyme required for diphthamide biosynthesis (**2011**), *Mol Biosyst.*, **7(1)**, 74-81.

(157) Dong M., Horitani M., Dzikovski B., Pandelia M. E., Krebs C., Freed J. H., Hoffman B. M., Lin H., Organometallic Complex Formed by an Unconventional Radical *S*-Adenosylmethionine Enzyme (**2016**), *J Am Chem Soc.*, **138(31)**, 9755-9758.

(158) Dong M., Horitani M., Dzikovski B., Freed J. H., Ealick S. E., Hoffman B. M., Lin H., Substrate-Dependent Cleavage Site Selection by Unconventional Radical *S*-Adenosylmethionine Enzymes in Diphthamide Biosynthesis (**2017**), *J Am Chem Soc.*, **139(16)**, 5680-5683.

(159) Dong M., Kathiresan V., Fenwick M. K., Torelli A. T., Zhang Y., Caranto J. D., Dzikovski B., Sharma A., Lancaster K. M., Freed J. H., Ealick S. E., Hoffman B. M., Lin H., Organometallic and radical intermediates reveal mechanism of diphthamide biosynthesis (**2018**), *Science*, **359(6381)**, 1247-1250.

(160) Nicolet Y., Drennan C. L., AdoMet radical proteins—from structure to evolution—alignment of divergent protein sequences reveals strong secondary structure element conservation (**2004**), *Nucleic Acids Res.*, **32(13)**, 4015-4025.

(161) Dowling D. P., Vey J. L., Croft A. K., Drennan C. L., Structural diversity in the AdoMet Radical Enzyme Superfamily (**2012**), *Biochim Biophys Acta.*, **1824(11)**, 1178-1195.

(162) Farrar C. E., Jarrett J. T., Protein residues that control the reaction trajectory in S-adenosylmethionine radical enzymes: mutagenesis of asparagine 153 and aspartate 155 in Escherichia coli biotin synthase (**2009**), *Biochemistry*, **48(11)**, 2448-2458.

(163) McCarty R. M., Somogyi Á., Guangxin L., Jacobsen N. E., Bandarian V., The deazapurine biosynthetic pathway revealed: In vitro enzymatic synthesis of preQ$_0$ from guanosine-5'-triphosphate in four steps (**2009**), *Biochemistry*, **48(18)**, 3847-3852.

(164) McCarty R. M., Krebs C., Bandarian V., Spectroscopic, steady-state kinetic, and mechanistic characterization of the radical SAM enzyme QueE, which catalyzes a complex cyclization reaction in the biosynthesis of 7-deazapurines (**2013**), *Biochemistry*, **52(1)**, 188-198.

(165) Jäger C. M., Croft A. K., Radical Reaction Control in the AdoMet Radical Enzyme CDG Synthase (QueE): Consolidate, Destabilize, Accelerate (**2017**), *Chemistry*, **23(4)**, 953-962.

(166) Bruender N., Grell T. A. J., Dowling D. P., McCarty R. M., Drennan C. L., Bandarian V., 7-Carboxy-7-deazaguanine Synthase: A Radical S-Adenosyl-L-methionine Enzyme with Polar Tendencies (**2017**), *J Am Chem Soc.*, **139(5)**, 1912-1920.

(167) Wilcoxen J., Bruender N. A., Bandarian V., Britt R. D., A Radical Intermediate in Bacillus subtilis QueE during Turnover with the Substrate Analogue 6-Carboxypterin (**2018**), *J Am Chem Soc.*, **140(5)**, 1753-1759.

(168) Lanz N. D., Booker S. J., Auxiliary iron-sulfur cofactors in radical SAM enzymes (**2015**), *Biochim Biophys Acta*, **1853(6)**, 1316-1334.

(169) Harmer J. E., Hiscox M. J., Dinis P. C., Fox S. J., Iliopoulos A., Hussey J. E., Sandy J., Van Beek F. T., Essex J. W., Roach P. L., Structures of lipoyl synthase reveal a compact active site for controlling sequential sulfur insertion reactions (**2014**), *Biochem J.*, **464(1)**, 123-133.

(170) Goldman P. J., Grove T. L., Sites L. A., McLaughlin M. I., Booker S. J., Drennan C. L., X-ray structure of an AdoMet radical activase reveals an anaerobic solution for formylglycine posttranslational modification (**2013**), *Proc Natl Acad Sci USA*, **110(21)**, 8519-8524.

(171) Flühe L., Knappe T. A., Gattner M. J., Schäfer A., Burghaus O., Linne U., Marahiel M. A., The radical SAM enzyme AlbA catalyzes thioether bond formation in subtilosin A (**2012**), *Nat Chem Biol.*, **8**, 350-357.

(172) Khaliullin B., Aggarwal P., Bubas M., Eaton G. R., Eaton S. S., Latham J. A., Myocofactocin biosynthesis: modification of the peptide MftA by the radical S-adenosylmethionine protein MftC (**2016**), *FEBS Lett.*, **590**, 2538-2548.

(173) Barr I., Stich T. A., Gizzi A. S., Grove T. L., Bonanno J. B., Latham J. A., Chung T., Wilmot C. M., Britt R. D., Almo S. C., Klinman J. P., X-ray and EPR Characterization of the Auxiliary Fe-S Clusters in the Radical SAM enzyme PqqE (**2018**), *Biochemistry*, **57**, 1306-1315.

(174) Marquet A., Bui B. T., Florentin D., Biosynthesis of biotin and lipoic acid (**2001**), *Vitam Horm.*, **61**, 51-101.

(175) Marquet A., Florentin D., Ploux O., Tse Sum Bui B., In vivo formation of C-S bonds in biotin. An example of radical chemistry under reducing conditions (**1998**), *J Phys Org Chem.*, **11**, 529-535.

(176) Miller J. R., Busby R. W., Jordan S. W., Cheek J., Henshaw T. F., Ashley G. W., Broderick J. B., Cronan J. E. Jr., Marletta M. A., Escherichia coli LipA is a lipoyl synthase: in vitro biosynthesis of lipoylated pyruvate dehydrogenase somplex from octanoyl-acyl carrier protein (**2000**), *Biochemistry*, **39(49)**, 15166-15178.

(177) Cicchillo R. M., Booker S. J., Mechanistic investigations of lipoic acid biosynthesis in Escherichia coli: both sulfur atoms in lipoic acid are contributed by the same lipoyl synthase polypeptide (**2005**), *J Am Chem Soc.*, **127(9)**, 2860-2861.

(178) Zhao X., Miller J. R., Jiang Y., Marletta M. A., Cronan J. E., Assembly of the covalent linkage between lipoic acid and its cognate enzymes (**2003**), *Chem Biol.*, **10(12)**, 1293-1302.

(179) Haft D. H., Bioinformatic evidence for a widely distributed, ribosomally produced electron carrier precursor, its maturation proteins, and its nicotinoprotein redox partners (**2011**), *BMC genomics*, **11**, 12:21.

(180) Haft D. H., Basu M. K., Biological systems discovery in silico: radical S-adenosylmethionine protein families and their target peptides for posttranslational modification (**2011**), *J Bacteriol.*, **193(11)**, 2745-2755.

(181) Grell T. A. J., Goldman P. J. Drennan C. L., SPASM and Twitch Domains in *S*-Adenosylmethionine (SAM) Radical Enzymes (**2015**), *J Biol Chem.*, **290(7)**, 3464-3971.

(182) Benjdia A., Subramanian S., Leprince J., Vaudry H., Johnson M. K., Berteau O., Anaerobic Sulfatase-Maturating Enzyme: A Mechanistic Link with Glycyl Activating Enzymes? (**2011**), *FEBS J.*, **277(8)**, 1906-1920.

(183) Grove T. L., Lee K.-H., Clair J. S., Krebs C., Booker S. J., In Vitro Characterization of AtsB, a Radical SAM Formylglycine-Generating Enzyme That Contains Three [4Fe-4S] Clusters (**2008**), *Biochemistry*, **47(28)**, 7523-7538.

(184) Grove T. L., Ahlum J. H., Qin R. M., Lanz N. D., Radle M. I., Krebs C., Booker S. J., Further characterization of Cys-type and Ser-type anaerobic sulfatase maturating enzymes suggests a commonality in the mechanism of catalysis (**2013**), Biochemistry, **52(17)**, 2874-2887.

(185) Yokoyama K., Numakura M., Kudo F., Ohmori D. Eguchi T., Characterization and mechanistic study of a radical SAM dehydrogenase in the biosynthesis of butirosin (**2007**), *J Am Chem Soc.*, **129(49)**, 15147-15155.

(186) Yokoyama K., Ohmori D., Kudo F., Eguchi T., Mechanistic study on the reaction of a radical SAM dehydrogenase BtrN by electron paramagnetic resonance spectroscopy (**2008**), *Biochemistry*, **47(34)**, 8950-8960.

(187) Grove T. L., Ahlum J. H., Sharma P., Krebs C., Booker S. J., A consensus mechanism for Radical SAM-dependent dehydrogenation? BtrN contains two [4Fe-4S] clusters (**2010**), *Biochemistry*, **49(18)**, 3783-3785.

(188) Menéndez C., Siebert D., Brandsch R., MoaA of Arthrobacter nicotinovorans pAO1 involved in Mo-pterin cofactor synthesis is an Fe-S protein (**1996**), *FEBS Lett.*, **391(1-2)**, 101-103.

(189) Mehta A. P., Hanes J. W., Abdelwahed S. H., Hilmey D. G., Hänzelmann P., Begley T. P., Catalysis of a new ribose carbon-insertion reaction by the molybdenum cofactor biosynthetic enzyme MoaA (**2013**), Biochemistry, **52(7)**, 1134-1136.

(190) Mehta A. P., Abdelwahed S. H., Begley T. P., Molybdopterin biosynthesis: trapping an unusual purine ribose adduct in the MoaA-catalyzed reaction (**2013**), *J Am Chem Soc.*, **135(30)**, 10883-10885.

(191) Mehta A. P., Abdelwahed S. H., Xu H., Begley T. P., Molybdopterin biosynthesis: trapping of intermediates for the MoaA-catalyzed reaction using 2'-deoxyGTP and 2'-chloroGTP as substrate analogues (**2014**), *J Am Chem Soc.*, **136(30)**, 10609-10614.

(192) Mehta A. P., Abdelwahed S. H., Begley T. P., Molybdopterin biosynthesis-Mechanistic studies on a novel MoaA catalyzed insertion of a purine carbon into the ribose of GTP (**2015**), *Biochim Biophys Acta.*, **1854(9)**, 1073-1077.

(193) Hänzelmann P., Schindelin H., Binding of 5'-GTP to the C-terminal FeS cluster of the radical S-adenosylmethionine enzyme MoaA provides insights into its mechanism (**2006**), *Proc Natl Acad Sci USA*, **103(18)**, 6829-6834.

(194) Lees N. S., Hänzelmann P., Hernandez H. L., Subramanian S., Schindelin H., Johnson M. K., Hoffman B. M., ENDOR spectroscopy shows that guanine N1 binds to [4Fe-4S] cluster II of the S-adensoylmethionine-dependent enzyme MoaA: mechanistic implication (**2009**), *J Am Chem Soc.*, **131(26)**, 9184-9185.

(195) Eklund H., Fontecave M., Glycyl radical enzyme: a conservative structural basis for radicals (**1999**), *Structure*, **7(11)**, 257-262.

(196) Fontecave M., Ribonucleotide reductases and radical reactions (**1998**), *Cell Mol Life Sci.*, **54(7)**, 684-695.

(197) Sawers G., Watson G., A glycyl radical solution: oxygen-dependent interconversion of pyruvate formate-lyase (**1998**), *Mol Microbiol.*, **29(4)**, 945-954.

(198) Selmer T., Pierik A. J.,Heider J., New glycyl radical enzymes catalyzing key metabolic steps in anaerobic bacteria (**2005**), *Biol Chem.*, **386(10)**, 981-988.

(199) Noma A., Kirino Y., Ikeuchi Y., Suzuki T., Biosynthesis of wybutosine, a hyper-modified nucleoside in eukaryotic phenylalanine tRNA (**2006**), *EMBO J.*, **25(10)**, 2142-2154.

(200) Rodriguez V., Vasudevan S., Noma A., Carlson B. A., Green J. E., Suzuki T., Chandrasekharappa S. C., Structure-function analysis of human TYW2 enzyme required for the biosynthesis of a highly modified Wybutosine (yW) base in phenylalanine-tRNA (**2012**), *PLoS One*, **7(6)**:e39297.

(201) Kriek M., Martins F., Challand M. R., Croft A., Roach P. L., Thiamine biosynthesis in *Escherichia coli*: identification of the intermediate and by-product derived from tyrosine (**2007**), *Angew Chem Int Ed Engl.*, **46(48)**, 9223-9226.

(202) Adamska-Venkatesh A., Roy S., Siebel J. F., Simmons T. R., Fontecave M., Artero V., Reijerse E., Lubitz W., Spectroscopic Characterization of the Bridging Amine in the Active Site of [FeFe] Hydrogenase Using Isotopologues of the H-cluster (**2015**), *J Am Chem Soc.*, **137(40)**, 12744-12747.

(203) Scheffzek K., Ahmadian M. R., GTPase activating proteins: structural and functional insights 18 years after discovery (**2005**), *Cell Mol Life Sci.*, **62**, 3014-3038.
(204) Rodnina M. V., Visualizing the protein synthesis machinery: New focus on the translational GTPase elongation factor Tu (**2009**), *Proc Natl Acad Sci USA*, **106(4)**, 969-970.

(205) Kolanczyk M., Pech M., Zemojtel T., Yamamoto H., Mikula I., Calvaruso M. A., van den Brand M., Richter R., Fischer B., Ritz A., Kossler N., Thurisch B., Spoerle R., Smeitink J., Kornak U., Chan D., Vingron M., Martasek P., Lightowlers R. N., Nijtmans L., Schuelke M., Nierhaus K. H., Mundlos S., NOA1 is an essential GTPase required for mitochondrial protein synthesis (**2011**), Mol Biol Cell., **22(1)**, 1-11.

(206) Brand A. C., Morrison E., Milne S., Gonia S., Gale C. A., Gow N. A. R., Cdc42 GTPase dynamics control directional growth responses (**2014**), *Proc Natl Acad Sci USA*, **111(2)**, 811-816.

(207) Yang H., Gong R., Xu Y., Control of cell growth: Rag GTPases in activation of TORC1 (**2013**), *Cell Mol Life Sci.*, **70(16)**, 2873-2885.

(208) Pucéat M., Travo P., Quinn M. T., Fort P., A Dual Role of the GTPase Rac in Cardiac Differentiation of Stem Cells (**2003**), *Mol Biol Cell.*, **14(7)**, 2781-2792.

(209) Coisy-Quivy M., Sanguesa-Ferrer J., Weill M., Johnson D. S., Donnay J. M., Hipskind R., Fort P., Philips A., Identification of Rho GTPases implicated in terminal differentiation of muscle cell in ascidia (**2006**), *Biol Cell*, **98**, 577-588.

(210) Symons M., Rusk N., Control of vesicular trafficking by Rho GTPases (**2003**), *Curr Biol.*, **13(10)**, R409-418.

(211) Hutagalung A. H., Novick P. J., Role of Rab GTPases in Membrane Traffic and Cell Physiology (**2011**), *Physiol Rev.*, **91(1)**, 119-149.

(212) Exton J. H., Small GTPases minireview series (**1998**), *J Biol Chem.*, **273(32)**:19923.

(213) Cherfils J., Zeghouf M., Regulation of small GTPases by GEFs, GAPs and GDIs (**2013**), *Physiol Rev.*, **93**, 269-309.

(214) Gilman A. G., G proteins: transducers of receptor-generated signals (**1987**), *Annu Rev Biochem.*, **56**, 615-649.

(215) Bourne H. R., Wrischnik L., Kenyon C., Ras proteins. Some signal developments (**1990**), *Nature*, **348(6303)**, 678-679.

(216) Vögler O., Barceló J. M., Ribas C., Escribá P. V., Membrane interactions of G proteins and other related proteins (**2008**), *Biochim Biophys Acta.*, **1778(7-8)**, 1640-1652.

(217) Yang Z., Small GTPases: versatile signaling switches in plants (**2002**), *Plant Cell*, **14**, S375-S388.

(218) Marlovits T. C., Haase W., Herrmann C., Aller S. G., Unger V. M., The membrane protein FeoB contains an intramolecular G protein essential for Fe(II) uptake in bacteria (**2002**), *Proc Natl Acad Sci USA*., **99(25)**, 16243-16248.

(219) Ash M. R., Guilfoyle A., Clarke R. J., Guss J. M., Maher M. J., Jormakka M., Potassium-activated GTPase reaction in the G-protein coupled ferrous iron transporter B (**2010**), *J Biol Chem.*, **285(19)**, 14594-14602.

(220) Rafay A., Majumdar S., Prakash B., Exploring potassium-dependent GTP hydrolysis in TEES family GTPases (**2012**), *FEBS Open Bio*, **2**, 173-177.

(221) Smith A. T., Sestok A. E., Expression and purification of functionally active ferrous iron transporter FeoB from Klebsiella pneumoniae (**2018**), *Protein Expr Purif.*, **142**, 1-7.

(222) Maier T., Jacobi A., Sauter M., Böck A., The product of the hypB gene, which is required for nickel incorporation into hydrogenase, is a novel guanine nucleotide-binding protein (**1993**), *J Bacteriol.*, **175(3)**, 630-635.

(223) Maier T., Lottspeich F., Böck A., GTP hydrolysis by HypB is essential for nickel insertion into hydrogenases of Escherichia coli (**1995**), *Eur J Biochem.*, **230(1)**, 133-138.

(224) Leach M. R., Sandal S., Sun H., Zamble D. B., Metal binding activity of the Escherichia coli hydrogenase maturation factor HypB (**2005**), *Biochemistry*, **44(36)**, 12229-12238.

(225) Sydor A. M., Liu J., Zamble D. B., Effects of Metal on the Biochemical Properties of Heliobacter pylori HypB, a Maturation Factor of [NiFe]-Hydrogenase and Urease (**2011**), *J Bacteriol.*, **193(6)**, 1359-1368.

(226) Xia W., Li H., Yang X., Wong K. B., Sun H., Metallo-GTPase HypB from Helicobacter pylori and its interaction with nickel chaperone protein HypA (**2012**), *J Biol Chem.*, **287(9)**, 6753-6763.

(227) Chan K. H., Lee K. M., Wong K. B., Interaction between hydrogenase maturation factors HypA and HypB is required for [NiFe]-hydrogenase maturation (**2012**), *PLoS One*, **7(2)**, e32592.

(228) Lacasse M. J., Douglas C. D., Zamble D. B., Mechanism of Selective Nickel Transfer from HypB to HypA, Escherichia coli [NiFe]-Hydrogenase Accessory Proteins (**2016**), *Biochemistry*, **55(49)**, 6821-6831.

(229) Zambelli B., Stola M., Musiani F., De Vriendt K., Samyn B., Devreese B., Van Beeumen J., Turano P., Dikiy A., Bryant D. A., Ciurli S., UreG, a chaperone in the urease assembly process, is an intrinsically unstructured GTPase that specifically binds Zn2+ (**2005**), *J Biol Chem.*, **280(6)**, 4684-4695.

(230) Hausinger R. P., Nickel enzymes in microbes (**1994**), *Sci Total Environ.*, **148(2-3)**, 157-166.

(231) Boer J. L., Quiroz-Valenzuela S., Anderson K. L., Hausinger R. P., Mutagenesis of Klebsiella aerogenes UreG to probe nickel binding and interactions with other urease-related proteins (**2010**), *Biochemistry*, **49(28)**, 5859-5869.

(232) Zambelli B., Turano P., Musiani F., Neyroz P., Ciurli S., Zn2+-linked dimerization of UreG from Helicobacter pylori, a chaperone involved in nickel trafficking and urease activation (**2009**), *Proteins*, **74(1)**, 222-239.

(233) Musiani F., Ippoliti E., Micheletti C., Carloni P., Ciurli S., Conformational fluctuations of UreG, an intrinsically disordered enzyme (**2013**), *Biochemistry*, **52(17)**, 2949-2954.

(234) Yuen M. H., Fong Y. H., Nim Y. S., Lau P. H., Wong K. B., Structural insights into how GTP-dependent conformational changes in ametallochaperone UreG facilitate urease maturation (**2017**), *Proc Natl Acad Sci USA*, **114(51)**, E10890-10898.

(235) Padovani D., Labunska T., Banerjee R., Energetics of interaction between the G-protein chaperone, MeaB, and B_{12}-dependent methylmalonyl-CoA mutase (**2006**), *J Biol Chem.*, **281(26)**, 17838-17844.

(236) Padovani D., Banerjee R., Assembly and Protection of the Radical Enzyme, Methylmalonyl-CoA Mutase, by Its Chaperone (**2006**), *Biochemistry*, **45(30)**, 9300-9306.

(237) Hubbard P. A., Padovani D., Labunska T., Mahlstedt S. A., Banerjee R., Drennan C. L., Crystal structure and mutagenesis of the metallochaperone MeaB: insight into the causes of methylmalonic aciduria (**2007**), *J Biol Chem.*, **282(43)**, 31308-31316.

(238) Campanello G. C., Lofgren M., Yokom A. L., Southworth D. R., Banerjee R., Switch I-dependent allosteric signaling in a G-protein chaperone-B_{12} enzyme complex (**2017**), *J Biol Chem.*, **292(43)**, 17617-17625.

(239) Berto P., Di Valentin M., Cendron L., Vallese F. Albertini M., Salvadori E., Giacometti G. M., Carbonera D., Costantini P., The [4Fe-4S]-cluster coordination of [FeFe]-hydrogenase maturation protein HydF as revealed by EPR and HYSCORE spectroscopies (**2012**), *Biochim Biophys Acta.*, **1817(12)**, 2149-2157.

(240) Joshi N., Shepard E. M., Byer A. S., Swanson K. D., Broderick J. B., Peters J. W., Iron-sulfur cluster coordination in the [FeFe]-hydrogenase H cluster biosynthetic factor HydF (**2012**), *FEBS Lett.*, **586(22)**, 3939-3943.

(241) Berggren G., Garcia-Serres R., Brazzolotto X., Clemancey M., Gambarelli S., Atta M., Latour J. M., Hernández H. L., Subramanian S., Johnson M .K., Fontecave M., An EPR/HYSCORE, *M*össbauer, and resonance Raman study of the hydrogenase maturation enzyme HydF: a model for N-coordination to [4Fe-4S] clusters (**2014**), *J Biol Inorg Chem*., **19(1)**, 75-84.

(242) Swanson K. D., Ratzloff M. W., Mulder D. W., Artz J. H., Ghose S., Hoffman A., White S., Zadvornyy O. A., Broderick J. B., Bothner B., King P. W., Peters J. W., Probing the Solvent Accessibility of the [4Fe-4S] Cluster of the Hydrogenase Maturation Protein HydF from Thermotoga neapolitana by HYSCORE and 3p-ESEEM (**2015**), *J Phys Chem B.*, **119(43)**, 13680-13689.

(243) Cendron L., Berto P., D'Adamo S., Vallese F., Govoni C., Posewitz M. C., Giacometti G. M., Costantini P., Zanotti G., Crystal structure of HydF scaffold protein provides insights into [FeFe]-hydrogenase maturation (**2011**), *J Biol Chem.*, **286(51)**, 43944-43950.

(244) Caserta G., Pecqueur L., Adamska-Venkatesh A., Papini C., Roy S., Artero V., Atta M., Reijerse E., Lubitz W., Fontecave M., Structural and functional characterization of the hydrogenase-maturation HydF protein (**2017**), *Nat Chem Biol.*, **13(7)**, 779-784.

(245) McGlynn S. E., Shepard E. M., Winslow M. A., Naumov A. V., Duschene K. S., Posewitz M. C., Broderick W. E., Broderick J. B., Peters J. W., HydF as a scaffold protein in [FeFe] hydrogenase H-cluster biosynthesis (**2008**), *FEBS Lett.*, **582(15)**, 2183-2187.

(246) Shepard E. M., McGlynn S. E., Bueling A. L., Grady-Smith C. S., George S. J., Winslow M. A., Cramer S. P., Peters J. W., Synthesis of the 2Fe subcluster of the [FeFe]-hydrogenase H cluster on the HydF scaffold (**2010**), *Proc Natl Acad Sci USA*, **107(23)**, 10448-10453.

(247) Czech I., Stripp S., Sanganas O., Leidel N., Happe T., Haumann M., The [FeFe]-hydrogenase maturation protein HydF contains a H-cluster like [4Fe4S]-2Fe site (**2011**), *FEBS Lett.*, **585(1)**, 225-230.

(248) Shepard E. M., Byer A. S., Betz J. N., Peters J. W., Broderick J. B., A redox active [2Fe-2S] cluster on the hydrogenase maturase HydF (**2016**), *Biochemistry*, **55(25)**, 3514-3527.

(249) Shepard E. M., Byer A. S., Aggarwal P., Betz J. N., Scott A. G., Shisler K. A., Usselman R. J., Eaton G. R., Eaton S. S., Broderick J. B., Electron Spin Relaxation and Biochemical Characterization of the Hydrogenase Maturase HydF: Insights into [2Fe-2S] and [4Fe-4S] Cluster Communication and Hydrogenase Activation (**2017**), *Biochemistry*, **56(25)**, 3234-3247.

(250) Shepard E. M., Byer A. S., Broderick J. B., Iron-Sulfur Cluster States of the Hydrogenase Maturase HydF (**2017**), *Biochemistry*, **56(36)**, 4733-4734.

(251) Scrima A., Wittinghofer A., Dimerisation-dependent GTPase reaction of MnmE: how potassium acts as GTPase-activating element (**2006**), *EMBO J.*, **25(12)**, 2940-2951.

(252) Galazzo L., Maso L., De Rosa E., Bortolus M., Doni D., Acquasaliente L., De Filippis V., Costantini P., Carbonera D., Identifiying conformational changes with site-directed spin labeling reveals that the GTPase domain of HydF is a molecular switch (**2017**), *Sci Rep.*, **7(1)**, 1714.

(253) Vallese F., Berto P., Ruzzene M., Cendron L., Sarno S., De Rosa E., Giacometti G. M., Costantini P., Biochemical analysis of the interactions between the proteins involved in the [FeFe]-hydrogenase maturation process (**2012**), *J Biol Chem.*, **287(43)**, 36544-36555.

(254) Larkin M. A., Blackshields G., Brown N. P., Chenna R., McGettigan P. A., McWilliam H., Valentin F., Wallace I. M., Wilm A., Lopez R., Thompson J. D., Gibson T. J., Higgins D. G., Clustal W and Clustal X version 2.0 (**2007**), *Bioinformatics*, *23(21)*, 2947-2948.

(255) Goujon M., McWilliam H., Li W., Valentin F., Squizzato S., Paern J., Lopez R., A new bioinformatics analysis tools framework at EMBL-EBI (**2010**), *Nucleic Acids Research*, **38**, W695-699.

(256) Waterhouse A. M., Procter J. B., Martin D. M. A., Clamp M., Barton G. J., Jalview Version 2 - a multiple sequence alignment editor and analysis workbench (**2009**), *Bioinformatics*, **25**, 1189-1191.

(257) Akhtar M. K., Jones P. R., Delestion of iscR stimulates recombinant clostridial Fe-Fe hydrogenase and H_2-accumulation in Escherichia coli BL21 (DE3) (**2008**), *Appl Microbiol Biotechnol*, **78**, 853-862.

(258) Guzman L. M., Belin D., Carson M. J., Beckwith J., Tight regulation, modulation, and high-level expression by vectors containing the arabinose PBAD promotor (**1995**), *J Bacteriol.*, **177(14)**, 4121-4130.

(259) Lee N. L., Gielow W. O., Wallace R. G., Mechnaism of araC autoregulation and the domains of two overlapping promotors, Pc and PBAD, in the L-arabinose regulatory region of Escherichia coli (**1981**), *Proc Natl Acad Sci U S A*, **78(2)**, 752-756.

(260) Hahn S., Hendrickson W., Schleif R., Transcription of Escherichia coli ara in vitro. The cyclic AMP receptor protein requirement for PBAD induction that depends on the presence and orientation of the araO2 site (**1986**), *J Mol Biol.*, **188(3)**, 355-367.

(261) Lobell R. B., Schleif R. F., DNA looping and unlooping by AraC protein (**1990**), *Science*, **250(4980)**, 528-532.

(262) Schleif R., AraC protein, regulation of the l-arabinose operon in Escherichia coli, and the light switch mechanism of AraC action (**2010**), *FEMS Microbiol Rev.*, **34(5)**, 779-796.

(263) Robinson A. S., Production of Membrane Proteins: Strategies for Expression and Isolation (**2011**), *Wiley-VCH*, 19.

(264) Balzer S., Kucharova V., Megerle J., Lale R., Brautaset T., Valla S., A comparative analysis of the properties of regulated promoter systems commonly used for recombinant gene expression in *Escherichia coli* (**2013**), *Microb Cell Fact.*, **12**: 26.

(265) Miyada C. G., Stoltzfus L., Wilcox G., Regulation of the araC gene of *Escherichia coli*: catabolite repression, autoregulation, and effect on araBAD expression (**1984**), *Proc Natl Acad Sci U S A*, **81(13)**, 4120-4124.

(266) Pundir S., Martin M. J., O'Donovan C., UniProt Protein Knowledgebase (**2017**), *Methods Mol. Biol.*, **1558**, 41-55.

(267) NCBI Resource Coordinators, Database resources of the National Centre for Biotechnology Information (**2016**), *Nucleid Acid Res.*, **44**, D7-D19.

(268) Lucas S., Copeland A., Lapidus A., Cheng J.-F., Bruce D., Goodwin L., Pitluck S., Chertkov O., Detter J. C., Han C., Tapia R., Land M., Hauser L., Kyrpides N., Mikhailova N., Hemme C. L., Woyke T., Complete sequence of *Thermoanaerobacter italicus Ab9* (**2010**), US DOE Joint Genome Institute.

(269) Driesener R. C., Mechanistic and structural characterisation of HydG catalysed L-tyrosine cleavage (**2014**), *PhD thesis*, University of Southampton.

(270) Kambampati R., Lauthon C. T., IscS is a sulfurtransferase for the in vitro biosynthesis of 4-thiouridine in *Escherichia coli* tRNA (**1999**), *Biochemistry*, **38(50)**, 16561-16568.

(271) Adinolfi S., Rizzo F., Masino L., Nair M., Martin S. R., Pastore A., Temussi P. A., Bacterial IscU is a well folded and functional single domain protein (**2004**), *Eur. J. Biochem.*, **271**, 2093-2100.

(272) Popovic M., Pastore A., Chemical shift assignment of the alternative scaffold protein IscA (**2016**), *Biomol NMR Assign.*, **10**, 227-231.

(273) Markley J. L., Kim J. H., Dai Z., Bothe J. R., Cai K., Frederick R. O., Tonelli M., Metamorphoric protein IscU alternates conformations in the course of ist role as the scaffold protein for iron-sulfur cluster biosynthesis and delivery (**2013**), *FEBS Letters*, **587(8)**, 1172-1179.

(274) Silberg J. J., Tapley T. L., Hoff K. G., Vickery L. E., Regulation of the HscA ATPase reaction cycle by the co-chaperone HscB and the iron-sulfur cluster assembly protein IscU (**2004**), *J Biol Chem.*, **279(52)**, 53924-53931.

(275) Blanc B., Gerez C., Ollagnier de Choudens S., Assembly of Fe/S proteins in bacterial systems: Biochemistry of the bacterial ISC system (**2015**), *Biochim Biophys Acta.*, **1853(6)**, 1436-1447.

(276) Dinis P. C. E. G., Structural analysis of proteins from the radical SAM superfamily (**2015**), *PhD thesis*, University of Southampton.

(277) Bradford M. M., A rapid and sensitive method for the quantification of microgram quantities of protein utilizing the principle of protein-dye binding (**1976**), *Anal Biochem.*, **72**, 248-254.

(278) Pardee A. B., Jacob F., Monod J., The genetic control of cytoplasmic expression of "inducibility" in the synthesis of b-galactosidase by E. coli (**1959**), *J. Mol. Biol.*, **1**, 165-178.

(279) Jacob F., Monod J., Genetic regulatory mechanisms in the synthesis of proteins (**1961**), *J. Mol. Biol.*, **3(3)**, 318-356.

(280) Beckwith J. R., Regulation of the Lac Operon (**1967**), *Science*, **156(3775)**, 597-604.

(281) Golomb M., Chamberlin M., Characterization of T7-specfiic ribonucleic acid polymerase. IV. Resolution of the major in vitro transcripts by gel electrophoresis (**1974**), *J Biol Chem.*, **249(9)**, 2858-2863.

(282) Gilbert W., Müller-Hill B., Isolation of the Lac repressor (**1966**), *Proc. Nat. Acad. Sci. USA*, **56(6)**, 1891-1898.

(283) Gilbert W., Maxam A., The Nucleotide Sequence of the *lac* Operator (**1973**), *Proc. Nat. Acad. Sci. USA*, **70(12)**, 3581-3584.

(284) Lewis M. Chang G., Horton N. C., Kercher M. A., Pace H. C., Schumacher M. A., Brennan R. G., Lu P., Crystal structure of the lactose operon repressor and its complexes with DNA and inducer (**1996**), *Science*, **271(5253)**, 1247-1254.

(285) Fernandez-Castane A., Vine C. E., Caminal G., Lopez-Santin J., Evidencing the role of lactose permease in IPTG uptake by Escherichia coli in fed-batch high density cultures (**2011**), *J Biotechnol.*, **8**, 391-398.

(286) Fernandez-Castane A., Caminal G., Lopez-Santin J., Direct measurements of IPTG enable analysis of the induction behavior of E. coli in high density cultures (**2012**), *Microb Cell Fact.*, **8**, 58.

(287) Studier F. W., Protein production by auto-induction in high density shaking cultures (**2005**), *Protein Expr Purif.*, **41(1)**, 207-234.

(288) Blommel P. G., Backer K. J., Duvnjak P., Fox B. G., Enhanced Bacterial Protein Expression During Autio-induction Obtained by Alteration of Lac Repressor Dosage and Medium Composition (**2007**), *Biotechnol Prog.*, **23(3)**, 585-598.

(289) Fox B. G., Blommel P. G., Autoinduction of Protein Expression (**2009**), *Curr Protoc Protein Sci.*, **5**, 5.23.

(290) Studier F. W., Stable expression clones and auto-induction for protein production in E. coli (**2014**), *Methods Mol Biol.*, **1091**, 17-32.

(291) Inada T., Kimata K., Aiba H., Mechanism responsible for glucose-lactose diauxie in Escherichia coli: challenge to the cAMP model (**1996**), *Genes Cells.*, **1(3)**, 293-301.

(292) Hogema B. M., Arents J. C., Bader R., Ejikemans K., Inada T., Aiba H., Postma P. W., Inducer eclusion by glucose 6-phosphate in Escherichia coli (**1998**), *Mol Microbiol.*, **28(4)**, 755-765.

(293) Briand L., Marcion G., Kriznik A., Heydel J. M., Artur Y., Garrido C., Seigneuric R., Neiers F., A self-inducible heterologous protein expression system in Escherichia coli (**2016**), *Sci Rep.*, **6**, 33037.

(294) Sweeney W. V., Rabinowitz J., C., Proteins containing 4Fe-4S clusters - an overview (**1980**), *Ann. Rev. Biochem*., **49**, 139-161.

(295) Wai Y., Measurement of Thiol Ligands bound to the [5Fe5S] Cluster of StrepThitHydG using Fluorescent Derivatization and HPLC Analysis (**2017**), Chemistry Reasearch Project dissertation, University of Southampton.

(296) Ferreira-Rajabi L., Hill B. C., Characterization of reductant-induced, tryptophan fluorescence changes in cytochrome oxidase (**1989**), *Biochemistry*, **28(20)**, 8028-8032.

(297) Shafiee F., Moazen F., Rabbani M., Sadeghi H. M. M., Optimization of the Expression of Reteplase in Escherichia coli TOP10 using Arabinose Promoter (**2015**), *Jundishapur J Nat Pharm Prod.*, **10(1)**, e16676.

(298) Khlebnikov A., Datsenko K. A., Skaug T., Wanner B. L., Keasling J. D., Homogeneous expression of the P(BAD) promoter in Escherichia coli by constitutive expression of the low-affinity high-capacity AraE transporter (**2001**), *Microbiology*, **147(Pt 12)**, 3241-3247.

(299) Baneyx F., Recombinant protein expression in Escherichia coli (**1999**), *Curr Opin Biotechnol.*, **10(5)**, 411-421.

(300) Beinert H., Kennedy M. C., Stout C. D., Aconitase as iron-sulfur protein, enzyme, and iron-regulatory protein (**1996**), *Chem Rev.*, **96**, 2335-2374.

(301) Kennedy M. C., Werst M., Telser J., Emptage M. H., Beinert H., Hoffman B. M., Mode of substrate carboxyl binding to the [4Fe-4S]$^{+}$ cluster of reduced acotinase as studied by ^{17}O and ^{13}C electron-nuclear double resonance spectroscopy (**1987**), *Proc. Natl. Acad. Sci. USA*, **84**, 8854-8858.

(302) Aliverti A., Hagen W.R., Zanetti G., Direct electrochemistry and EPR spectroscopy of spinach ferredoxin mutants with modified electron transfer properties (**1995**), *FEBS Lett.*, **368(2)**, 220-224.

(303) Vollmer S. J., Switzer R. L., Debrunner P. G., Oxidation-reduction properties of the iron-sulfur cluster in *Bacillus subtilis* glutamine phosphoribosylpyrophosphate amindotransferase (**1983**), *J Biol Chem.*, **258(23)**, 14284-14293.

(304) Agarwalla S., Stroud R. M., Gaffney B. J., Redox Reactions of the Iron-Sulfur Cluster in a Ribosomal RNA Methyltransferase, Rum A (**2004**), *J Biol Chem*., **279(33)**, 34123-34129.

(305) Kiley P. J., Beinert H., Oxygen sensing by the global regulator, FNR: the role of the iron-sulfur cluster (**1998**), *FEMS Microbiol Rev.*, **22(5)**, 341-352.

(306) Crack J. C., Green J., Thomson A. J., Le Brun N. E., Iron-sulfur clusters as biological sensors: the chemistry of reactions with molecular oxygen and nitric oxide (**2014**), *Acc Chem Res.*, **47(10)**, 3196-3205.

(307) Gnandt E., Dörner K., Strampraad M. F. J., de Vries S., Friedrich T., The multitude of iron-sulfur clusters in respiratory complex I (**2016**), *Biochim Biophys Acta*, **1857(8)**, 1068-1072.

(308) Mettert E. L., Kiley P. J., Fe-S proteins that regulate gene expression (**2015**), *Biochim Biophys Acta*, **1853(6)**, 1284-1293.

(309) Dos Santos P. C., Johnson D. C., Raagle B. E., Unciuleac M. C., Dean D. R., Controlled expression of nif and isc iron-sulfur protein maturation components reveals target specificity and limited functional replacement between the two systems (**2007**), *J Bacteriol.*, **189(7)**, 2854-2862.

(310) Sandmann G., Malkin R., Iron-Sulfur Centers and activities of the photosynthetic electron transport chain in iron-deficient cultures of the blue-green alga Aphanocapsa (**1983**), *Plant Physiol.*, **73(3)**, 724-728.

(311) Bruska M. K., Stiebritz M. T., Reiher M., Analysis of differences in oxygen sensitivity of Fe-S clusters (**2013**), *Dalton Trans.*, **42(24)**, 8729-8735.

(312) Gault V. A., McClenaghan N. H., Understanding Bioanalytical Chemistry: Principles and Applications (**2009**), *Wiley-Blackwell*, 105-113.

(313) Owen T., Fundamentals of modern UV-Vis spectroscopy (**2000**), *Agilent Technologies*, 37.

(314) Nakamaru-Ogiso E., Yano T., Ohnishi T., Yagi T., Characterization of the iron-sulfur cluster coordinated by a cysteine cluster motif ($CXXCXXXCX_{27}C$) in the Nqo3 subunit in the proton-translocating NADH-quinone oxidoreductase (NDH-1) of *Thermus thermophiles* HB-8 (**2002**), *J Biol Chem*., **277(3)**, 1680-1688.

(315) Ugulava N. B., Gibney B. R., Jarrett J. T., Biotin synthase contains two distinct iron-sulfur cluster binding sites: Chemical and spectroelectrochemical analysis of iron-sulfur cluster interconversions (**2001**), *Biochemistry*, **40(28)**, 8343-8351.

(316) Hoppe A., Pandelia M.-E., Gärtner W., Lubitz W., [Fe_4S_4]- and [Fe_3S_4]-cluster formation in synthetic peptides (**2011**), *Biochim Biophys Acta.*, **1807(11)**, 1414-1422.

(317) Qian L., Zheng C., Liu J., Characterization of iron-sulfur cluster assembly protein IscA from Acidithiobacillus ferrooxidans (**2013**), *Biochemistry (Mosc).*, **78(3)**, 244-251.

(318) Fish W. W., Rapid colorimetric micromethod for the quantification of complexed iron in biological samples (**1988**), *Methods Enzymol.*, **158**, 357-364.

(319) Rashid M. H., Mandal T. K., Templateless Synthesis of Polygonal Gold Nanoparticles: An Unsupported and Reusable Catalyst with Superior Activity (**2008**), *Adv Funct Mater.*, **18(15)**, 2261-2271.

(320) David S. S., Fe-S Cluster Enzymes Part B (**2018**), *Methods Enzymol.*, **599**, 205-206.

(321) Saichana N., Tanizawa K., Ueno H., Pechoušek J., Novák P., Frébortová J., Characterization of auxiliary iron-sulfur clusters in a radical *S*-adenosylmethionine enzyme PqqE from *Methylobacterium extorquens* AM1 (**2017**), *FEBS Open Bio*, **7(12)**, 1864-1879.

(322) Khoroshilova N., Popescu C., Münck E., Beinert H., Kiley P. J., Iron-sulfur cluster disassembly in the FNR protein of Escherichia coli O_2: [4Fe-4S] to [2Fe-2S] conversion with loss of biological activity (**1997**), *Proc Natl Acad Sci USA*, **94**, 6087-6092.

(323) Parent A., Benjdia A., Guilot A., Kubiak X., Balty C., Lefranc B., Leprince J., Berteau O., Mechanistic Investigations of PoyD, a Radical *S*-Adenosyl-L-methionine Enzyme Catalyzing Iterative and Directional Epimerizations in Polytheonamide A Biosynthesis (**2018**), J Am Chem Soc., **140(7)**, 2469-2477.

(324) Ruszczycky M. W., Choi S.-h., Liu H.-w., Stoichiometry of the Redox Neutral Deamination and Oidative Dehydrogenation Reactions Catalyzed by the Radical SAM Enzyme DesII (**2011**), *J Am Chem Soc.*, **132(7)**, 2359-2369.

(325) Sugiura Y., Ishizu K., Kimura T., Tanaka H., Dithiol-sulfur and selenium complexes: A comparison with iron sulfur proteins (**1975**), *Bioinorg Chem.*, 4(4), 291-302.

(326) Mühlenhoff U, Richhardt N., Gerber J., Lill R., Characterization of iron-sulfur protein assembly in isolated mitochondria (**2002**), *J Biol Chem.,* **277(33)**, 29810-29816.

(327) Gloaguen F., Lawrence J. D., Schmidt M., Wilson S. R., Rauchfuss T. B., Synthetic and Structural Studies on $[Fe_2(SR)_2(CN)_x(CO)_{6-x}]^{x-}$ as Active Site Models for Fe-Only Hydrogenases (**2001**), *J Am Chem Soc.*, **123(50)**, 12518-12527.

(328) Contakes S. M., Hsu S. C. N., Rauchfuss T. B., Wilson S. R., Preparative and Structural Studies on the Carbonyl Cyanides of Iron, Manganese, and Ruthenium: Fundamentals Relevant to the Hydrogenases (**2002**), *Inorg Chem.*, **41**, 1670-1678.

(329) Eaton G. R., Eaton S. S., Barr D. P., Weber R. T., Quantitative EPR (**2010**), *Springer Science & Business Media*, 185 pages.

(330) Roat-Malone R. M., Bioinorganic Chemistry: A Short Course (**2007**), *John Wiley & Sons*, 528 pages.

(331) Junk M. J. N., Assessing the Functional Structure of Molecular Transporters by EPR Spectroscopy (**2012**), *Springer Science & Business Media*, 212 pages.

(332) Hagen W. R., Biomolecular EPR Spectroscopy (**2008**), *CRC Press*, 248 pages.

(333) Ohnishi T., Iron-sulfur clusters/semiquinones in complex I (**1998**), *Biochim Biophys Acta*, **1364(2)**, 186-206.

(334) Murphy D. M., EPR (Electron Paramagnetic Resonance) Spectroscopy of Polycrystalline Oxide Systems (**2008**), *Wiley-VCH*, Weinheim, Germany.

(335) Duin E., Electron Paramagnetic Resonance Theory, EPR manuals, Auburn University.

(336) Hagen W. R., Broadband Transmission EPR Spectroscopy (**2013**), *PLOS ONE*, **8(3)**, e59874.

(337) Lund A., Shiotani M., EPR of Free Radicals in Solids I: Trends in Methods and Applications (**2012**), *Springer Science & Business Media*, 414 pages.

(338) Kaupp M., Bühl M., Malkin V. G., Calculation of NMR and EPR paramters (**2004**), *Wiley-VCH*, Weinheim, Germany.

(339) Davies M. J., Gilbert B. C., McLauchlan K. A., Electron Paramagnetic Resonance (**2000**), *Royal Society of Chemistry*, 346 pages.

(340) Weil J. A., Bolton J. R., Electron Paramagnetic Resonance: Elementary Theory and Practical Applications (**2007**), *John Wiley & Sons*, 688 pages.

(341) Odom B., Hanneke D., D'Urso B., Gabrielse G., New Measurement of the Electron Magnetic Moment Using a One-Electron Quantum Cyclotron (**2006**), *Phys Rev Lett.*, **97**, 030801.

(342) G. Jeschke, EPR techniques for studying radical enzymes (**2005**), *Biochim Biophys Acta*, **1707(1)**, 91-102.

(343) Goldfarb D., Stoll S., EPR Spectroscopy: Fundamentals and Methods (**2018**), *John Wiley & Sons*, 648 pages.

(344) Cammack R., EPR, Methods (**1999**), *Encyclopedia of Spectroscopy and Spectrometry*, 457-469.

(345) Roessler M. M., Salvadori E., Principles and applications of EPR spectroscopy in chemical sciences (**2018**), *Chem Soc Rev.*, **47**, 2534.

(346) Hanson G., Berliner L., Metals in Biology: Applications of High-Resolution EPR (**2001**), Springer Science + Buisness Media.

(347) Zhang Y., Yang C., Dancis A., Nakamaru-Ogiso E., EPR studies of wild type and mutant Dre2 identify essential [2Fe--2S] and [4Fe--4S] clusters and their cysteine ligands (**2017**), *J Biochem*., **161(1)**, 67-78.

(348) Liu A., Gräslund A., Electron paramagnetic resonance evidence for a novel interconversion of [3Fe-4S](+) and [4Fe-4S](+) clusters with endogenous iron and sulfide in anaerobic ribonucleotide reductase activase in vitro (**2000**), *J Biol Chem.*, **275(17)**, 12367-12373.

(349) Priem A. H., Klaassen A. A., Reijerse E. J., Meyer T. E., Luchinat C., Capozzi F., Dunham W. R., Hagen W. R., EPR analysis of multiple forms of [3Fe-4S](+) clusters in HiPIPs (**2005**), *J Biol Inorg Chem*, **10(4)**, 417-424.

(350) Stoll S., Schweiger A., EasySpin, a comprehensive software package for spectral simulation and analysis in EPR (**2006**), *J Magn Reson.*, **178(1)**, 42-55.

(351) Fadeeva M. S., Bertsova Y. V., Verkhovsky M. I., Bogachev A. V., Site-directed mutagenesis of conserved cysteine residues in NqrD and NqrE subunits Na^+-translocating NADH:quinone oxidoreductase (**2008**), *Biochemistry (Mosc)*, **73(2)**, 123-129.

(352) Kennedy M. C., Kent T. A., Emptage M., Merkle H., Beinert H., Münch E., Evidence for the formation of a linear [3Fe-4S] cluster in partially unfolded aconitase (**1984**), *J Biol Chem.*, **259(23)**, 14463-14471.

(353) Atkins P., Friedman R., Molecular Quantum Mechanics (**2005**), *Oxford University Press*, 357-359.

(354) Markovich R. J., Pidgeon C., Introduction to Fourier transform infrared spectroscopy and applications in the pharmaceutical sciences (**1991**), *Pharm Res.*, **8(6)**, 663-675.

(355) J. Li, Noll B. C., Schulz C. E., Scheidt W. R., Comparison of CN^- and CO as Ligands in Iron(II) Porphyrinates (**2010**), *Angew Chem Int Ed Engl.*, **48(27)**, 5010-5013.

(356) Kaval A., Rauchfuss T. B., Protonation studies of the new iron carbonyl cyanide trans-[Fe(CO)3(CN)2]2-: implications with respect to hydrogenases (**2003**), *Inorg Chem.*, 42(17), 5046-5048.

(357) Fidai I., Wachnowsky C., Cowan J. A., Glutathione-complexed [2Fe-2S] clusters function in Fe-S cluster storage and trafficking (**2016**), *J Biol Inorg Chem.*, **21(7)**, 887-901.

(358) Yokoyama K., Lilla E. A., C-C bond forming radical SAM enzymes involved in the construction of carbon skeletons of cofactors and natural products (**2018**), *Nat Prod Rep.*, 35(7), 660-694.

(359) Rudack T., Xia F., Schlitter J., Köttling C., Gerwert K., The Role of Magnesium for Geometry and Charge in GTP Hydrolysis, Revealed by Quantum Mechanisc/Molecular Mechanics Simulations (**2012**), *Biophys J.*, **103(2)**, 293-302.

(360) Zhang B., Zhang Y., Wang Z.-x., Zheng Y., The Role of Mg^{2+} Cofactor in the Guanine Nucleotide Exchange and GTP Hydrolysis Reactions of Rho Family GTP-binding Proteins (**2000**), *J Biol Chem.*, **275(33)**, 25299-25307.

(361) Fersht A., Enzyme Structure and Mechanism (**1984**), *W.H Freeman and Company Ltd*, 2.

(362) Atkins P., De Paula J., Physical Chemistry (**2006**), *OUP Oxford*, 8.

(363) Michaelis L., Menten M. L., Die Kinetik der Invertinwirkung (**1913**), *Biochem Z.*, **49**, 333-369.

(364) Briggs G. E., Haldane J. B., A Note on the Kinetics of Enzyme Action (**1925**), *Biochem J.*, **19**, 338-339.

(365) Li H., Rauchfuss T. B., Iron carbonyl sulfides, formaldehyde, and amines condense to give the proposed azadithiolate cofactor of the Fe-only hydrogenases (**2002**), *J Am Chem Soc.*, **124(5)**, 726-727.

(366) Farrar C. E., Siu K. K. W., Howell P. L., Jarrett J. T., Biotin Synthase Exhibits Burst Kinetics and Multiple Turnovers in the Absence of Inhibition by Products and Product-Related Biomolecules (**2010**), *Biochemistry*, **49**, 9985-9996.

(367) Mann S., Ploux O., Pyridoxal-5'-phosphate-dependent enzymes involved in biotin biosynthesis: Structure, reaction mechanism and inhibition (**2011**), *Biochim Biophys Acta.*, **1814(11)**,1459-1466.

(368) Bhandari D. M., Fedoseyenko D., Begley T. P., Mechanistic Studies on Tryptophan Lyase (NosL): Identification of Cyanide as a Reaction Product (**2018**), *J Am Chem Soc*, **140(2)**, 542-545.

(369) L. A. McNeill, L. Bethge, K., Hewitson K. S., Schofield C. J., A fluorescence-based assay for 2-oxoglutarate-dependent oxygenases (**2005**), *Anal Biochem.*, **336(1)**, 125-131.

(370) Wu X., Diao Y., Sun C., Yang J., Wang Y., Sun S., Fluorimetric determination of ascorbic acid with o-phenylenediamine (**2003**), *Talanta*, **59(1)**, 95-99.

(371) Patchornik G., Goldshleger R., Karlish S. J., The complex ATP-Fe(2+) serves as a specific cleavage reagent in ATP-Mg(2+) sites of Na,K,-ATPase: altered ligation of Fe(2+) (Mg(2+)) ions accompanies the E(1)→E(2) conformational change (**2000**), *Proc Natl Acad Sci USA*, **97(22)**, 11954-19959.

(372) El-Mahdaoui L., Tajmir-Riahi H. A., A comparative study of ATP and GTP complexation with trivalent Al, Ga and Fe cations. Determination of cation binding site and nucleotide conformation by FTIR difference spectroscopy (**1995**), *J Biomol Struct Dyn.*, **13(1)**, 69-86.

(373) Weaver K. D., Gabričević M., Anderson D. S., Adhikari P., Mietzner T. A., Crumbliss A.L., The role of citrate and phosphate anions in the mechanism of iron(III) sequestration by ferric binding protein: Kinetic studies of holoprotein formation of wild type and engineered mutants of FbpA (**2010**), *Biochemistry*, **49(29)**, 6021-6032.

(374) Amutha B., Gordon D. M., Gu Y., Lyver E. R., Dancis A., Pain D., GTP is required for iron-sulfur cluster biogenesis in mitochondria (**2008**), *J Biol Chem.*, **283(3)**, 1362-1371.

(375) Saraste M., Sibbald P. R., Wittinghofer A., The P-loop--a common motif in ATP- and GTP-binding proteins (**1990**), *Trends Biochem Sci.*, **15(11)**, 430-434.

(376) Vetter I. R., Wittinghofer A., The guanine nucleotide-binding switch in three dimensions (**2001**), *Science*, **294(5545)**, 1299-1304.

(377) Colicelli J., Human RAS superfamily proteins and related GTPases (**2004**), *Sci STKE*, **2004(250)**, RE13.

(378) Kuhle B., Ficner R., A monovalent cation acts as structural and catalytic cofactor in translational GTPases (**2014**), *EMBO J.*, **33(21)**, 2547-2563.

(379) David S. S., Approaches to Interrogate the Role of Nucleotide Hydrolysis by Metal Trafficking NTPases: The Nbp35-Cfd1 Iron-Sulfur Cluster Scaffold as a Case Study (**2018**), *Methods Enzymol.*, **599**, 294-321.

(380) Fong Y. H., Wong H. C., Yuen M. H., Lau P. H., Chen Y. W., Wong K. B., Structure of UreG/UreF/UreH complex reveals how urease accessory proteins facilitate maturation of Helicobacter pylori (**2013**), *PLoS Biol.*, **11(10)**, e1001678.

(381) Padovani D., Banerjee R., A G-protein editor gates coenzyme B12 loading and is corrupted in methylmalonic aciduria (**2009**), *Proc Natl Acad Sci USA*, **106(51)**, 21567-21572.

(382) Kastritis P. L., Bonvin A. M. J. J., On the binding affinity of macromolecular interactions: daring to ask why proteins interact (**2013**), *J R Soc Interface*, **10**, 20120835.

(383) Bronowska A. K., Thermodynamics of Ligand-Protein Interactions: Implications for Molecular Design, Thermodynamics – Interaction Studies – Solids, Liquids and Gases (**2011**), *Dr. Juan Carlos Moreno Pirajan (Ed.)*, **ISBN: 978-953-307-563-1**, 1-48.

(384) Du X., Li Y., Xia Y. L., Ai S. M., Liang J., Sang P., Ji X. L., Liu S. Q., Insights into Protein-Ligand Interactions: Mechanisms, Models, and Methods (**2016**), *Int J Mol Sci.*, **17(2)**, E144.

(385) Lodish H., Berk A., Zipursky S. L., Section 2.2 Noncovalent Bonds (**2000**), *Molecular Cell Biology. 4th edition*, New York, W. H. Freeman.

(386) D. J., McClements D. J., Non-covalent interactions between proteins and polysaccharides (**2006**), *Biotechnol Adv.*, **24(6)**, 621-625.

(387) Pace C. N., Scholtz J. M., Grimsley G. R., Forces Stabilizing Proteins (**2014**), *FEBS Lett.*, **588(14)**, 2177-2184.

(388) Veselovsky A. V., Ivanov Y. D., Ivanov A. S., Archakov A. I., Lewi P., Janssen P., Protein-protein interactions: mechanisms and modification by drugs (**2002**), *J. Mol. Recognit.*, **15**, 405-422.

(389) Malvern Pananalytical. https://www.malvernpanalytical.com/en/products/technology/microcalorimetry/isotheriso-titration-calorimetry. Opened 09/04/2018.

(390) Matte A., Kozlov G., Trempe J.-F., Currie M. A., Burk D., Jia Z., Gehring K., Ekiel I., Berghuis A. M., Cygler M., Preparation and characterization of bacterial protein complexes for structural analysis (**2009**), *Adv Protein Chem Struct Biol*, **76**, 1-42.

(391) Dessau M. A., Modis Y., Protein Crystallization for X-Ray Crystallography (**2011**), *J Vis Exp.*, **47**, 2285.

(392) McPherson A., Gavira J. A., Introduction to protein crystallization (**2014**), *Acta Crystallogr F Struct Biol Commun*, **70(Pt 1)**, 2-20.

(393) J. R. Luft, Newman J., Snell E. H., Crystallization screening: the influence of history on current practice (**2014**), *Acta Crystallogr F Struct Biol Commun*, **70(Pt 7)**, 835-853.

(394) Hong P., Koza S., Bouvier E. S. P., Size-Exclusion Chromatography for the Analysis of Protein Biotherapeutics and their Aggregates (**2012**), *J Lig Chromatogr Relat Technol.*, **35(20)**, 2923-2950.

(395) Hagel L., Gel-filtration chromatography (**2001**), *Curr Protoc Mol Biol.*, **Chapter 10**, Unit 10.9.

(396) Hagel L., Haneskog L., Size-exclusion chromatography (**2010**), *Encyclopedia of Life Sciences (ELS)*, John Wiley & Sons, Ltd: Chichester.

(397) Louche A., Salcedo S. P., Bigot S., Protein-Protein Interactions: Pull-Down Assays (**2017**), In: *Journet L., Cascales E. (eds) Bacterial Protein Secretion Systems. Methods in Molecular Biology*, vol **1615**. Humana Press, New York, NY.

(398) Majewska J., Ciesielski S. J., Schilke B., Kominek J., Blenska A., Delewski W., Song J. Y., Marszalek J., Craig E. A., Dutkiewicz R., Binding of the chaperone Jac1 protein and cysteine desulfurase Nfs1 of the iron-sulfur cluster scaffold Isu protein is mutually exclusive (**2013**), *J Biol Chem*, **288(40)**, 29134-29142.

(399) Ciesielski S. J., Schilke B. A., Osipiuk J., Bigelow L., Mulligan R., Majewska J., Joachimiak A., Marszalek J., Craig E. A., Dutkiewicz R., Interaction of J-protein co-chaperone Jac1 with Fe-S scaffold Isu is indispensable in vivo and conserved in evolution (**2012**), *J Mol Biol*, **417(1-2)**,1-12.

(400) IBA Lifesciences, Goettingen, Germany. https://www.iba-lifesciences.com/details/product/51.html. Retrieved 27/04/2018.

(401) Analysis: Specific binding with Hill slope was performed using GraphPad Prims version 7.00 for Windows, GraphPad Software, La Jolla California USA, www.graphpad.com.

(402) Kozianowski G., Canganella F., Rainey F. A., Hippe H., Antranikian G., Purification and characterization of thermostable pectate-lyases from a newly isolated thermophilic bacterium, Thermoanaerobacter italicus sp. nov. (**1997**), *Extremophiles*, **1(4)**, 171-182.

(403) Guttman C., Crystallography for beginners – part 5 – monitoring and evaluating crystallization experiments results (**13/04/2013**). https://benchwise.wordpress.com/2013/04/13/crystallography-for-beginners-part-5-monitoring-and-evaluating-crystallization-experiments-results/. Retrieved on 28/04/2018.

(404) Hampton Research – Solutions for Crystal Growth, Salt or Protein Crystals? – Crystal Growth 101 (**2016**), 1-2.

(405) User's Manual iTC_{200} Microcalorimeter MAU 501460 RevD, MicroCal Northampton, USA.

(406) Burnouf D., Ennifar E., Guedich S., Puffer B., Hoffmann G., Bec G., Disdier F., Baltzinger M., Dumas P., kinITC: A new method for obtaining joint thermodynamic and kinetic data by isothermal titration calorimetry (**2012**), *J Am Chem Soc*., **134(1)**, 559-565.

(407) Dumas P., Ennifar E., Da Veiga C., Bec G., Palau W., Di Primo C., Piñeiro A., Sabin J., Muñoz E., Rial J., Chapter Seven – Extending ITC to kinetics with kinITC (**2016**), *Methods Enzymol.*, **567**, 157-180.

(408) Arai Y., Sparks D. L., ATR-FTIR Spectroscopic Investigation on Phosphate Adsorption Mechanisms ath the Ferrihydrite-Water Interace (**2001**), *J Colloid Interface Sci.*, **241**, 317-326.

(409) Hanahan D., Studies on transformation of Escherichia coli with plasmids (**1983**). *J. Mol. Biol.*, **166**, 557-580.

(410) J. Chiu, P. E. March, R. Lee, D. Tillett, Site-directed, Ligase-Independent Mutagenesis (SLIM): a single-tube methodology approaching 100% efficiency in 4h (**2004**). *Nuc. Acids Res.*, **32(21)**, e174.

(411) J. Chiu, D. Tillett, I.W. Dawes, P.E. March, Site-directed, Ligase-Independent Mutagenesis (SLIM) for highly efficient mutagenesis of plasmids greater than 8kb (**2008**). *Microbiol Met.*, **73**, 195-198.

(412) Schneider C. A., Rasband W. S., Eliceiri K. W., NIH Image to Image J: 25 years of image analysis (**2012**), *Nature Methods*, **9(7)**, 671-675.